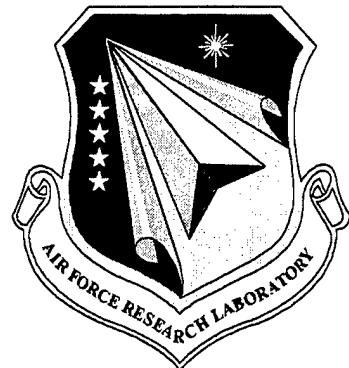


AFRL-ML-WP-TR-1998-4127

ENHANCED LASER GENERATED ULTRASOUND



**JAMES M. NELSON
RAYMOND D. REMPT
STANLEY M. SORSCHER
WAYNE E. WOODMANSEE
WILLIAM B. SHEPHERD
ROBERT L. NERENBERG
MARC CHOQUET (NATIONAL RESEARCH COUNCIL)
JEAN-PIERRE MONCHALIN (NATIONAL RESEARCH COUNCIL)**

**BOEING INFORMATION, SPACE & DEFENSE SYSTEMS
P.O. BOX 3999
SEATTLE, WA 98124**

DATE: 8 JULY 1998

FINAL REPORT FOR DECEMBER 1996 THROUGH FEBRUARY 1998

19980929 101

APPROVED FOR PUBLIC RELEASE: DISTRIBUTION IS UNLIMITED

DTIC QUALITY INSPECTED 8

**Materials & Manufacturing Directorate
Air Force Research Laboratory
Air Force Materiel Command
Wright-Patterson AFB, OH 45433-7734**

NOTICE

WHEN GOVERNMENT DRAWINGS, SPECIFICATIONS, OR OTHER DATA ARE USED FOR ANY PURPOSE OTHER THAN IN CONNECTION WITH A DEFINITELY GOVERNMENT-RELATED PROCUREMENT, THE UNITED STATES GOVERNMENT INCURS NO RESPONSIBILITY OR ANY OBLIGATION WHATSOEVER. THE FACT THAT THE GOVERNMENT MAY HAVE FORMULATED OR IN ANY WAY SUPPLIED THE SAID DRAWINGS, SPECIFICATIONS, OR OTHER DATA, IS NOT TO BE REGARDED BY IMPLICATION OR OTHERWISE IN ANY MANNER CONSTRUED, AS LICENSING THE HOLDER OR ANY OTHER PERSON OR CORPORATION, OR AS CONVEYING ANY RIGHTS OR PERMISSION TO MANUFACTURE, USE, OR SELL ANY PATENTED INVENTION THAT MAY IN ANY WAY BE RELATED THERETO.

THIS REPORT IS RELEASABLE TO THE NATIONAL TECHNICAL INFORMATION SERVICE (NTIS). AT NTIS, IT WILL BE AVAILABLE TO THE GENERAL PUBLIC, INCLUDING FOREIGN NATIONS.

THIS TECHNICAL REPORT HAS BEEN REVIEWED AND IS APPROVED FOR PUBLICATION.



CURTIS J. FIEDLER, Project Engineer
Nondestructive Evaluations Branch
Metals, Ceramics & NDE Division



TOBEY M. CORDELL, Chief
Nondestructive Evaluations Branch
Metals, Ceramics & NDE Division



GERALD J. PETRAK, Acting Asst Chief
Metals, Ceramics & NDE Division
Materials & Manufacturing Directorate

IF YOUR ADDRESS HAS CHANGED, IF YOU WISH TO BE REMOVED FROM OUR MAILING LIST, OR IF THE ADDRESSEE IS NO LONGER EMPLOYED BY YOUR ORGANIZATION, PLEASE NOTIFY, AFRL/MLLP, WRIGHT-PATTERSON AFB OH 45433-7817 AT 59819 TO HELP US MAINTAIN A CURRENT MAILING LIST.

COPIES OF THIS REPORT SHOULD NOT BE RETURNED UNLESS RETURN IS REQUIRED BY SECURITY CONSIDERATIONS, CONTRACTUAL OBLIGATIONS, OR NOTICE ON A SPECIFIC DOCUMENT.

REPORT DOCUMENTATION PAGE

 FORM APPROVED
 OMB NO. 0704-0188

Public reporting burden for this collection of information is estimated to average 1 hour per response, including the time for reviewing instructions, searching existing data sources, gathering and maintaining the data needed, and completing and reviewing the collection of information. Send comments regarding this burden estimate or any other aspect of this collection of information, including suggestions for reducing this burden, to Washington Headquarters Services, Directorate for Information Operations and Reports, 1215 Jefferson Davis Highway, Suite 1204, Arlington, VA 22202-4302 and to the Office of Management and Budget, Paperwork Reduction Project (0704-0188), Washington, DC 20503.

| | | | |
|---|---|---|---|
| 1. AGENCY USE ONLY (Leave blank) | | 2. REPORT DATE 8 JULY 1998 | 3. REPORT TYPE AND DATES COVERED FINAL DECEMBER 1996-FEBRUARY 1998 |
| 4. TITLE AND SUBTITLE ENHANCED LASER GENERATED ULTRASOUND | | 5. FUNDING NUMBERS C - F33615-96-C-5268 PE - 63112F PR - 3153 TA - 00 WU - 17 | |
| 6. AUTHOR(S) James M. Nelson, Raymond D. Rempt, Stanley M. Sorscher, Wayne E. Woodmansee William B. Shepherd, Robert Nerenberg; and Marc Choquet (National Research Council) and Jean-Pierre Monchalin (National Research Council) | | 8. PERFORMING ORGANIZATION REPORT NUMBER D950-10322-1 | |
| 7. PERFORMING ORGANIZATION NAMES(ES) AND ADDRESS(ES) BOEING INFORMATION, SPACE & DEFENSE SYSTEMS P O BOX 3999 SEATTLE WA 98124 | | 9. SPONSORING/MONITORING AGENCY NAMES(ES) AND ADDRESS(ES) Materials & Manufacturing Directorate Air Force Research Laboratory Air Force Materiel Command Wright-Patterson AFB, OH 45433-7734 POC: Feildler, AFRL/MLP, 937-255-9797 | |
| 10. SPONSORING/MONITORING AGENCY REPORT NUMBER AFRL-ML-WP-TR-1998-4127 | | | |
| 11. SUPPLEMENTARY NOTES | | | |
| 12a. DISTRIBUTION/AVAILABILITY STATEMENT APPROVED FOR PUBLIC RELEASE: DISTRIBUTION IS UNLIMITED | | 12b. DISTRIBUTION CODE | |
| 13. ABSTRACT (Maximum 200 words) A Laser Based Ultrasound (LBU) inspection system at McClellan AFB, CA was used to understand actual LBU capabilities and to evaluate its performance versus conventional systems. The effort identified particular classes of aircraft and aerospace parts for which LBU inspection is superior to conventional ultrasonic systems inspection. The evaluation also identified the best procedures for use of the McClellan AFB LBU system and identified shortcomings and potential improvements of the system. Briefly, the evaluation found that the McClellan AFB LBU system provided excellent flexibility in the wide range of part types and shapes that can be inspected. This LBU system demonstrated the ability for automated inspection of complex shapes that are usually inspected manually, at greater cost. The LBU system was generally not competitive on simple parts where conventional systems have been optimized for inspections. The results of that evaluation are reported in this document. | | | |
| 14. SUBJECT TERMS laser based ultrasound, laser ultrasonic inspection system, nondestructive evaluation | | 15. NUMBER OF PAGES 307 | 16. PRICE CODE |
| 17. SECURITY CLASSIFICATION OF REPORT Unclassified | 18. SECURITY CLASSIFICATION OF THIS PAGE Unclassified | 19. SECURITY CLASSIFICATION OF ABSTRACT Unclassified | 20. LIMITATION OF ABSTRACT SAR |

NSN 7540-01-280-5500

COMPUTER GENERATED

 STANDARD FORM 298 (Rev. 2-89)
 Prescribed by ANSI Std. Z39-18
 298-102

TABLE OF CONTENTS

| | <u>Page</u> |
|---|-------------|
| Abstract | xxi |
| Key Words | xxi |
| Acknowledgments | xxii |
| Table of Contents | iii |
| List of Figures | vi |
| List of Tables | xx |
| Executive Summary | 1 |
| 1.0 Introduction | 3 |
| 2.0 Equipment Description | 7 |
| 3.0 Test Process Description | 16 |
| 4.0 Data Analysis Processes Description | 23 |
| 4.1 LUIS Signal Processing | 23 |
| 4.2 Optimized Data Processing | 24 |
| 5.0 Analysis of Parts Data | 43 |
| 5.1 Commercial Aircraft Composite Parts | 43 |
| 5.1.1 Graphite Composite Skin Panel Standard - 1-A | 43 |
| 5.1.2 Graphite Composite Skin Panel Standard - 2-A | 51 |
| 5.1.3 Graphite Composite Skin Panel Standard -3-A | 57 |
| 5.1.4 7J7 Graphite Composite Test Panel | 68 |
| 5.1.5 Graphite Composite Rib Containing Foreign Materials | 74 |
| 5.1.6 Graphite Composite Vertical Fin Panel 181 | 79 |
| 5.1.7 Graphite Composite I-Stiffener | 83 |
| 5.1.8 Leading Edge of Graphite Composite Aileron | 86 |
| 5.1.9 Graphite Composite Honeycomb Repair Panel R-10 | 89 |
| 5.1.10 Horizontal Stabilizer Skin Panel 459 | 97 |
| 5.1.11 Complex Graphite Composite Component | 102 |
| 5.1.12 Graphite Composite Angle Test Standards | 106 |
| 5.1.13 Porosity Standards | 118 |

TABLE OF CONTENTS (Continued)

| | <u>Page</u> |
|--|-------------|
| 5.2 Military Aircraft Composite Parts | 125 |
| 5.2.1 A-6 Ply Drop Standard | 125 |
| 5.2.2 A-6 Near/Far Surface Resolution Panel | 129 |
| 5.2.3 Foreign Material Panel #3 | 141 |
| 5.2.4 Impact Test Panel | 144 |
| 5.2.5 F-22 Radius Standards | 147 |
| 5.2.6 Acute External Angle | 151 |
| 5.2.7 F-22 Ply Drop Standard | 153 |
| 5.2.8 B-2 Stiffened Wing Panels | 161 |
| 5.2.9 Titanium Stiffened Composite "T" Section | 164 |
| 5.2.10 "Hat" Stiffened Panel | 167 |
| 5.2.11 Seven Ply composite Repair Test Standard | 168 |
| 5.2.12 Aluminum Honeycomb Repair Panel K1 | 171 |
| 5.2.13 Aluminum Honeycomb Repair Panel K2 | 173 |
| 5.2.14 Composite Repair Calibration Standard for Skin-To-Core Disbonds | 175 |
| 5.2.15 Honeycomb Cored Composite Repair Standard Matrix | 177 |
| 5.2.16 Composite Flywheel | 183 |
| 5.2.17 Sine Wave Spar | 185 |
| 5.2.18 F-22 Fuselage Bulkhead | 188 |
| 5.2.19 Composite "Crow's Foot" Section | 192 |
| 5.2.20 One Piece Wing Box | 195 |
| 5.2.21 F-22 Landing Gear Door | 199 |
| 5.2.22 Foam Filled AWACS Instrument Panel Section | 203 |
| 5.2.23 MILSTAR Radome Sample | 206 |
| 5.2.24 Three Stage Cured Repair on Stiffened Solid Laminate Panel | 210 |
| 5.2.25 Fiberglass/Honeycomb Repair Panel K-4 | 213 |
| 5.3 Miscellaneous LUIS Data | 215 |
| 6.0 Special Studies | 224 |

TABLE OF CONTENTS (Continued)

| | <u>Page</u> |
|--|-------------|
| 6.1 LUIS System Variability | 224 |
| 6.2 Determination of Modulation Transfer Function for LUIS | 232 |
| 6.3 Production Testing Simulation | 234 |
| 6.3.1 Time Evaluation | 234 |
| 6.3.2 Repeatability Evaluation | 235 |
| 6.4 Inspection of Metal Parts | 248 |
| 6.5 Paint Study | 251 |
| 7.0 Conclusions | 254 |
| 7.1 Notable Successes | 254 |
| 7.2 Notable Limitations | 255 |
| 7.3 Specific Positive and Negative Factors | 255 |
| 7.3.1 Data Files | 255 |
| 7.3.2 Resolution | 256 |
| 7.3.3 Scan Size and Ranging | 257 |
| 7.3.4 Preparation and Setup | 261 |
| 7.3.5 Detection Depth | 264 |
| 7.3.6 Speed | 265 |
| 7.3.7 Data Processing | 266 |
| 7.4 LBU Benefit Analysis | 267 |
| 7.4.1 Customized Conventional System | 267 |
| 7.4.2 Flexible conventional System | 270 |
| 7.4.3 System Scanning Comparisons | 272 |
| 7.4.4 Best LBU Applications | 274 |
| 7.4.5 Economic Analysis | 275 |
| 7.5 Recommendations | 277 |
| 7.5.1 Short Term | 277 |
| 7.5.2 Long Term | 279 |
| Appendix A. Table of Scans | A1 |

LIST OF FIGURES

| | | <u>Page</u> |
|---------------|--|-------------|
| Figure 1-1 | Conventional Bubbler Installation at Boeing | 4 |
| Figure 1-2 | Bubbler Clasp | 4 |
| Figure 2-1 | Laser Gantry and Workbay | 7 |
| Figure 2-2 | Laser Gantry Extended | 8 |
| Figure 2-3 | Samples in Workbay and Laser Tracking Spot | 10 |
| Figure 2-4 | Rotating Mirror and Yoke | 11 |
| Figure 2-5 | Detection Unit | 12 |
| Figure 2-6 | Control Unit | 15 |
| Figure 3-1 | LUIS Inspection Plan Record | 17 |
| Figure 3-2 | Technician Communicating Laser Power Setting Information to Control Room | 19 |
| Figure 4.2-1 | Example initial amplitude C-scan image | 26 |
| Figure 4.2-2 | Example initial time of flight C-scan image | 27 |
| Figure 4.2-3 | Example horizontal B-scan image | 28 |
| Figure 4.2-4 | Example vertical B-scan image | 28 |
| Figure 4.2-5 | Waveform at thickest section of part | 29 |
| Figure 4.2-6 | Amplitude C-scan image | 30 |
| Figure 4.2-7 | Time of flight C-scan image | 31 |
| Figure 4.2-8 | Saturation in amplitude C-scan | 32 |
| Figure 4.2-9 | Saturation in waveform | 32 |
| Figure 4.2-10 | Near surface defect in TOF C-scan | 32 |
| Figure 4.2-11 | Waveform for near surface defect | 32 |
| Figure 4.2-12 | Near surface defect seen in vertical B-scan | 33 |
| Figure 4.2-13 | Time of flight C-scan image | 33 |
| Figure 4.2-14 | Waveform at position marked by x-cursor in figure 4.2-13 | 33 |
| Figure 4.2-15 | Waveform with ringing from paint layer | 34 |
| Figure 4.2-16 | Power spectrum of waveform in Figure 4.2-15 | 34 |
| Figure 4.2-17 | Waveform with non-flat baseline | 36 |

| | | |
|-----------------|---|----|
| Figure 4.2-18 | Waveform filtered with sharp cutoff | 36 |
| Figure 4.2-19 | Waveform filtered with slow cutoff | 36 |
| Figure 4.2-20 | Amplitude C-scan image after filtering | 37 |
| Figure 4.2-21 | Time of C-scan image after filtering | 37 |
| Figure 4.2-22 | Exponential decay ion waveform | 38 |
| Figure 4.2-23 | Correction of waveform with numerical DAC | 38 |
| Figure 4.2-24 | Amplitude C-scan image after filtering, DAC correction and normalization | 39 |
| Figure 4.2-25 | TOF C-scan image after filtering, DAC correction and normalization | 40 |
| Figure 4.2-26 | Position of cross section for B-scan views | 41 |
| Figure 4.2-27 | Horizontal B-scan | 41 |
| Figure 4.2-28 | Vertical B-scan | 41 |
| Figure 4.2-29 | Typical waveform from thick sample (A-6 near/far panel) | 42 |
| Figure 4.2-30 | Waveform from thick sample after spatial averaging (a-6 near/far panel) | 42 |
| Figure 5.1.1-1 | Skin Panel Standard 1-A | 44 |
| Figure 5.1.1-2 | Photograph of standard 777-1-A | 45 |
| Figure 5.1.1-3. | 3.5 MHz Bubbler peak amplitude pulse echo image of standard 1-A. Toolside scan | 46 |
| Figure 5.1.1-4 | LUIS peak amplitude image of standard 1-A. Toolside scan after painting. | 47 |
| Figure 5.1.1-5 | 3.5 MHz Bubbler time of flight image of standard 1-A. Toolside scan. | 47 |
| Figure 5.1.1-6 | LUIS time of flight image of standard 1-A. Palette enhanced image of 22 ply section. Tool side scan after painting. | 48 |
| Figure 5.1.1-7 | LUIS time of flight image of standard 1-A. Palette enhanced image of 15 ply section. Tool side scan after painting. | 49 |
| Figure 5.1.1-8 | LUIS time of flight image of standard 1-A. Palette enhanced image of 9 ply section. Tool side scan after painting. | 49 |

| | | |
|----------------|---|----|
| Figure 5.1.1-9 | LUIS time of flight image of standard 1-A. Palette enhanced image of 12 and 18 ply bond lines. Tool side scan after painting. | 50 |
| Figure 5.1.2-1 | Drawing of standard 777-2-A | 52 |
| Figure 5.1.2-2 | 3.5 MHz Bubbler peak amplitude pulse echo image of standard 2-A, toolside scan | 54 |
| Figure 5.1.2-3 | LUIS peak amplitude image of standard 2-A, toolside scan after painting. | 55 |
| Figure 5.1.2-4 | 3.5 MHz Bubbler time of flight image of standard 2-A, toolside scan. | 55 |
| Figure 5.1.2-5 | LUIS time of flight data standard 2-A. Palette enhanced data from thickest section. | 56 |
| Figure 5.1.2-6 | LUIS time of flight data standard 2-A. Palette enhanced data from thinnest section | 56 |
| Figure 5.1.3-1 | Drawing of standard 777-3-A | 58 |
| Figure 5.1.3-2 | 3.5 MHz Bubbler peak amplitude pulse echo image of standard 3-A, toolside scan | 62 |
| Figure 5.1.3-3 | LUIS peak amplitude image of standard 3-A. Toolside scan after painting. | 62 |
| Figure 5.1.3-4 | 3.5 MHz Bubbler time of flight image of standard 3-A, toolside scan. | 63 |
| Figure 5.1.3-5 | LUIS time of flight image of standard 3-A. Toolside scan after painting. | 63 |
| Figure 5.1.3-6 | LUIS peak amplitude image of standard 3-A. Toolside scan after painting. | 64 |
| Figure 5.1.3-7 | LUIS time of flight image of standard 3-A. Toolside scan after painting | 64 |
| Figure 5.1.3-8 | 3.5 MHz Bubbler TOF data from stringer over 74 ply laminate. Thickness increment 0.54" to 0.58". | 65 |
| Figure 5.1.3-9 | 3.5 MHz Bubbler TOF data from stringer over 110 ply | 65 |

| | | |
|-----------------|---|----|
| | laminate. Thickness increment 0.80" to 0.84". | |
| Figure 5.1.3-10 | LUIS B-Scan image of standard 3-A from 62 to 130 plies. Bond line echo at 74 plies is circled. Release ply F insert 2 plies above stiffener bond line and centered on web. | 66 |
| Figure 5.1.3-11 | LUIS B-scan image of standard 3-A from 62 to 130 plies. Bond line echo at 74 plies is circled. Release ply F insert 2 plies above bond line under right flange of stiffener. | 66 |
| Figure 5.1.3-12 | LUIS B-Scan image of standard 3-A from 62 ply to 130 plies. Echo from release ply F at 85 plies is circled. | 67 |
| Figure 5.1.4-1 | Photograph of bagside of 7J7 test panel | 70 |
| Figure 5.1.4-2 | Toolside of 7J7 panel | 71 |
| Figure 5.1.4-3 | 3.5 MHz Bubbler peak amplitude image of 7J7 test panel | 71 |
| Figure 5.1.4-4 | 3.5 MHz Bubbler time of flight image of 7J7 test panel | 72 |
| Figure 5.1.4-5 | Initial LUIS peak amplitude image of unpainted toolside of 7J7 panel | 72 |
| Figure 5.1.4-6 | LUIS peak amplitude image of 7J7 panel after toolside surface painted | 73 |
| Figure 5.1.4-7 | LUIS pulse echo time of flight image of 7J7 panel after toolside surface painted | 73 |
| Figure 5.1.5-1 | Photograph of 777 graphite composite rib with foreign materials | 76 |
| Figure 5.1.5-2 | TTU water jet image at 1 Mhz of graphite composite rib. | 76 |
| Figure 5.1.5-3 | Graphite composite rib with foreign material. 1 Mhz TTU water jet scan. | 77 |
| Figure 5.1.5-4 | LUIS peak amplitude image of composite rib with foreign material | 77 |
| Figure 5.1.5-5 | Time of flight image of 777 graphite composite rib | 78 |
| Figure 5.1.5-6 | LUIS amplitude image of rib (web-radius-flange). Left flange with foreign material at 5 mm depth. | 78 |
| Figure 5.1.5-7 | LUIS time of flight image of rib (web-radius-flange). Left | 78 |

| | | |
|----------------|---|----|
| | flange with foreign material at 5 mm depth. | |
| Figure 5.1.6-1 | 3.5 MHz pulse echo peak amplitude bubbler array scan of I-stiffened composite vertical fin panel | 81 |
| Figure 5.1.6-2 | 3.5 MHz pulse echo time of flight bubbler array scan of I-stiffened composite vertical fin panel | 81 |
| Figure 5.1.6-3 | LUIS peak amplitude scan of flawed portion of I-stiffened composite vertical fin panel | 83 |
| Figure 5.1.7-1 | Photograph of I Stiffener | 83 |
| Figure 5.1.7-2 | LUIS peak amplitude image of upper cap and lower flange of graphite composite I-stiffener. | 85 |
| Figure 5.1.7-3 | LUIS peak amplitude image of low flange of graphite composite I-stiffener. | 85 |
| Figure 5.1.8-1 | Photograph of leading edge of a short segment of a composite aileron. | 87 |
| Figure 5.1.8-2 | LUIS peak amplitude image from curved leading edge laminate of composite aileron segment. | 88 |
| Figure 5.1.8-3 | LUIS time of flight image from curved leading edge of composite aileron segment | 88 |
| Figure 5.1.9-1 | Drawing of repair panel | 90 |
| Figure 5.1.9-2 | 1 MHz TTU image of honeycomb composite repair panel R-10 | 91 |
| Figure 5.1.9-3 | 3.5 MHz bubbler pulse echo peak amplitude image of honeycomb repair panel R-10. Gating inserts nearer to toolside surface. | 92 |
| Figure 5.1.9-4 | 3.5 MHz bubbler pulse echo peak amplitude image of honeycomb repair panel R-10. Gating inserts farther from tool side surface. | 92 |
| Figure 5.1.9-5 | LUIS pulse echo peak amplitude image of honeycomb repair panel R-10. Inserts from 2 to 8 plies beneath the tool side are lighter indications. The insert that is 1 ply beneath the tool side is a dark indication at 3 o'clock from panel center. | 93 |

| | | |
|-----------------|--|-----|
| Figure 5.1.9-6 | LUIS pulse time of flight image of honeycomb repair panel R-10. Inserts that are from 1 to 8 plies beneath the tool side are visible. The blue indication at 3 o'clock from panel center is from a one inch diameter graphite insert 1 ply below the toolside surface. | 94 |
| Figure 5.1.9-7 | LUIS time of flight image of honeycomb repair panel R-10. Inserts that are from 5 to 11 plies beneath the tool side surface are visible. | 95 |
| Figure 5.1.9-8 | LUIS pulse time of flight image of honeycomb repair panel R-10. The insert 11 plies beneath the tool side is the orange circle at top center. The red indication to the right and slightly above this is 10 plies down from the tool side surface. | 95 |
| Figure 5.1.10-1 | Photograph of tool side surface of horizontal stabilizer skin panel 459 | 99 |
| Figure 5.1.10-2 | Photograph of painted tool side surface of horizontal stabilizer skin panel | 99 |
| Figure 5.1.10-3 | Peak amplitude image of horizontal skin panel 4590. 3.5 MHz pulse echo bubbler scan with 8-element array. | 100 |
| Figure 5.1.10-4 | Time of flight image of horizontal skin panel. 3.5 MHz pulse echo bubbler scan with 8-element. | 100 |
| Figure 5.1.10-5 | LUIS peak amplitude, high resolution image of skin panel | 101 |
| Figure 5.1.10-6 | LUIS peak amplitude, reduced resolution image of skin panel 459 | 101 |
| Figure 5.1.11-1 | Photograph of convex surface | 103 |
| Figure 5.1.11-2 | Photograph of concave surface | 103 |
| Figure 5.1.11-3 | 3 MHz water jet through transmission ultrasonic image of "chainguard" | 104 |
| Figure 5.1.11-4 | LUIS peak amplitude image from complex composite part | 105 |
| Figure 5.1.11-5 | LUIS time of flight image from complex composite part | 105 |
| Figure 5.1.12-1 | Photograph of angle standards | 107 |

| | | |
|------------------|---|-----|
| Figure 5.1.12-2 | Drawing of standard 8A | 108 |
| Figure 5.1.12-3 | Drawing of standard 24A | 109 |
| Figure 5.1.12-4 | Drawing of standard 25A | 110 |
| Figure 5.1.12-5 | Drawing of standard 28A | 111 |
| Figure 5.1.12-6 | Drawing of standard 29A | 112 |
| Figure 5.1.12-7 | LUIS Time of flight images of angle standard 25-A | 113 |
| Figure 5.1.12-8 | 5 MHz Water jet through transmission ultrasonic test of angle standard 25-A | 113 |
| Figure 5.1.12-9 | LUIS peak amplitude image of angle standard 24-A | 114 |
| Figure 5.1.12-10 | Water jet 5 MHz through transmission image on angle standard 24-A. Gray scale range 14 db | 114 |
| Figure 5.1.12-11 | LUIS peak amplitude image of angle standard 28-A | 115 |
| Figure 5.1.12-12 | 5 MHz water jet through transmission image of angle standard 28-A | 115 |
| Figure 5.1.12-13 | LUIS peak amplitude (upper) and time of flight (lower) images of angle standard 29-A | 115 |
| Figure 5.1.12-14 | 5 MHz water jet through transmission image of angle standard 29-A | 116 |
| Figure 5.1.12-15 | LUIS peak amplitude image of angle standard 8A | 116 |
| Figure 5.1.12-16 | LUIS time of flight image of angle standard 8A | 116 |
| Figure 5.1.12-17 | LUIS peak amplitude image of angle standard 8A of radius and adjacent flanges | 117 |
| Figure 5.1.12-18 | 3 MHz through transmission ultrasonic image of standard 8A | 117 |
| Figure 5.1.13-1 | Porosity Standards | 118 |
| Figure 5.1.13-2 | LUIS image using the full filtered waveform bandwidth | 119 |
| Figure 5.1.13-3 | LUIS image filtered to 3 MHz center frequency | 120 |
| Figure 5.1.13-4 | Conventional pulse-echo C-scan image taken at 3.25 MHz. | 120 |
| Figure 5.1.13-5 | LUIS image of porosity samples and histogram of values in the center panel | 121 |
| Figure 5.1.13-6 | Conventional pulse-echo image and histogram of values in the | 121 |

| | | |
|-----------------|---|-----|
| | center panel | |
| Figure 5.1.13-7 | Signal levels for 24-ply thick composite panels with varying levels of porosity | 123 |
| Figure 5.1.13-8 | Signal levels for 32-ply thick composite panels with varying levels of porosity | 124 |
| Figure 5.2.1-1 | A-6 Ply Drop Standard | 126 |
| Figure 5.2.1-2 | LUIS bag side amplitude C-scan | 126 |
| Figure 5.2.1-3 | LUIS TOF bag side image | 126 |
| Figure 5.2.1-4 | Boeing production amplitude C-scan of bag side | 127 |
| Figure 5.2.1-5 | Production TOF image of bag side | 127 |
| Figure 5.2.1-6 | Toolside LUIS amplitude C-scan image | 127 |
| Figure 5.2.1-7 | LUIS TOF of tool side | 127 |
| Figure 5.2.1-8 | Toolside production amplitude C-scan | 128 |
| Figure 5.2.1-9 | Production TOF image of tool side | 128 |
| Figure 5.2.2-1 | A-6 near/far resolution panel | 129 |
| Figure 5.2.2-2 | Amplitude C-scan taken by Boeing production scanner | 131 |
| Figure 5.2.2-3 | Amplitude C-scan taken with LUIS | 131 |
| Figure 5.2.2-4 | TOF images taken with Boeing scanner | 132 |
| Figure 5.2.2-5 | TOF images taken with LUIS | 132 |
| Figure 5.2.2-6 | B-scan of A6 near/far surface resolution panel taken with LUIS | 133 |
| Figure 5.2.2-7 | Amplitude C-scan gated to near the front surface taken with high resolution | 137 |
| Figure 5.2.2-8 | Amplitude C-scan gated to near the front surface taken at reduced resolution | 137 |
| Figure 5.2.2-9 | Time-of-Flight C-scan gated to near the back surface, taken with high resolution | 138 |
| Figure 5.2.2-10 | Time-of-Flight C-scan gated to near the back surface, taken with reduced resolution | 138 |
| Figure 5.2.2-11 | Short gated amplitude C-scan taken from tool side | 139 |
| Figure 5.2.2-12 | Short gated amplitude C-scan from bag side | 139 |

| | | |
|-----------------|---|-----|
| Figure 5.2.3-1 | A-6 Foreign Material Standard | 141 |
| Figure 5.2.3-2 | LUIS TOF scan | 142 |
| Figure 5.2.3-3 | Production amplitude C- scan | 143 |
| Figure 5.2.4-1 | Impact panel | 144 |
| Figure 5.2.4-2 | Backside of impact panel | 145 |
| Figure 5.2.4-3 | LUIS TOF scan | 146 |
| Figure 5.2.4-4 | LUIS amplitude scan | 146 |
| Figure 5.2.5-1 | Photograph of F-22 angle standards | 148 |
| Figure 5.2.5-2 | LUIS amplitude C-scan of angle standards | 149 |
| Figure 5.2.5-3 | LUIS TOF scan of angle standards | 150 |
| Figure 5.2.6-1 | Angle Standard | 151 |
| Figure 5.2.6-2 | LUIS amplitude C-scan of 80 degree standard | 151 |
| Figure 5.2.6-3 | LUIS TOF Scan of 80 degree standard | 152 |
| Figure 5.2.6-4 | LUIS TOF scan of 110 degree standard | 152 |
| Figure 5.2.7-1 | Photo of F-22 ply drop standard from bag side, showing plateaus and transitions | 153 |
| Figure 5.2.7-2 | Close up of F-22 ply drop standard bag side, mounted for LUIS scanning | 153 |
| Figure 5.2.7-3 | Plan drawing of the panel | 155 |
| Figure 5.2.7-4 | Amplitude C-scans taken from tool side by LUIS | 155 |
| Figure 5.2.7-5 | Conventional amplitude C-scan taken from tool side | 155 |
| Figure 5.2.7-6 | Time-of-flight C-scans taken with LUIS | 156 |
| Figure 5.2.7-7 | Time-of-flight C-scan taken at Boeing | 156 |
| Figure 5.2.7-8 | Boeing production Ultra image IV amplitude C-scan of tool side standard | 157 |
| Figure 5.2.7-9 | Bag side C-scans taken with the LUIS: Amplitude | 158 |
| Figure 5.2.7-10 | Bag side C-scans taken with the LUIS: Time-of-Flight | 159 |
| Figure 5.2.7-11 | LUIS B-scans taken from bag side | 159 |
| Figure 5.2.7-12 | LUIS B-scans taken from tool side | 160 |
| Figure 5.2.7-13 | LUIS B-scan | 160 |

| | | |
|-----------------|---|-----|
| Figure 5.2.8-1 | B-2 Wing panel tool side. | 161 |
| Figure 5.2.8-2 | B-2 wing panel bag side and stiffener | 162 |
| Figure 5.2.8-3 | LUIS amplitude scan | 162 |
| Figure 5.2.8-4 | LUIS TOF scan | 162 |
| Figure 5.2.8-5 | Boeing 5 MHz bubbler amplitude C-scan | 163 |
| Figure 5.2.9-1 | Photograph of stiffened "T" section | 164 |
| Figure 5.2.9-2 | LUIS amplitude C-scan | 165 |
| Figure 5.2.9-3 | LUIS TOF scan | 166 |
| Figure 5.2.10-1 | Hat stiffened panel | 167 |
| Figure 5.2.10-2 | LUIS amplitude C-scan of hit stiffened panel | 167 |
| Figure 5.2.11-1 | Photograph of repair standard | 168 |
| Figure 5.2.11-2 | LUIS amplitude C-scan of repair standard | 169 |
| Figure 5.2.11-3 | LUIS TOF scan of repair standard | 169 |
| Figure 5.2.11-4 | Conventional TTU scan | 170 |
| Figure 5.2.11-5 | LUIS TOF scan of repair standard | 170 |
| Figure 5.2.12-1 | Photograph of panel K1 | 171 |
| Figure 5.2.12-2 | LUIS amplitude C-scan image of panel K1 | 172 |
| Figure 5.2.12-3 | LUIS TOF image of panel K1 | 172 |
| Figure 5.2.12-4 | Conventional TTU image of panel K1 | 172 |
| Figure 5.2.13-1 | Photograph of panel K2 | 173 |
| Figure 5.2.13-2 | LUIS TOF scan image of panel K2 | 174 |
| Figure 5.2.13-3 | Conventional TTU scan of panel K2 | 174 |
| Figure 5.2.14-1 | LUIS B-scan of composite repair calibration standard | 175 |
| Figure 5.2.14-2 | LUIS amplitude C-scan of composite repair calibration standard | 175 |
| Figure 5.2.14-3 | LUIS TOF scan image | 176 |
| Figure 5.2.15-1 | Photograph of standards | 177 |
| Figure 5.2.15-2 | LUIS TOF image of matrix composite standards showing graphite inserts | 178 |
| Figure 5.2.15-3 | LUIS B scan of composite standard for potting with air voids | 179 |

| | | |
|-----------------|--|-----|
| Figure 5.2.15-5 | Boeing pulse echo amplitude C-scan | 181 |
| Figure 5.2.15-6 | Boeing production TTU scan | 182 |
| Figure 5.2.16-1 | Composite Flywheel | 183 |
| Figure 5.2.16-2 | Flywheel amplitude C-scan | 184 |
| Figure 5.2.17-1 | Photograph of sine wave spar | 185 |
| Figure 5.2.17-2 | LUIS C-scan | 186 |
| Figure 5.2.17-3 | LUIS C-scan | 186 |
| Figure 5.2.17-4 | LUIS TOF scan | 187 |
| Figure 5.2.17-5 | LUIS TOF scan | 187 |
| Figure 5.2.17-6 | LUIS amplitude scan along sine wave phase | 187 |
| Figure 5.2.17-7 | LUIS amplitude scan across sine wave phase | 187 |
| Figure 5.2.18-1 | F-22 Fuselage Bulkhead | 188 |
| Figure 5.2.18-2 | Amplitude C-scan with flaw indicated | 189 |
| Figure 5.2.18-3 | TOF scan of left side of part | 190 |
| Figure 5.2.18-4 | Amplitude C-scan of upper right side of part | 191 |
| Figure 5.2.19-1 | A section of a larger prototype structure for the F-22 program | 192 |
| Figure 5.2.19-2 | Amplitude C-scan front side | 193 |
| Figure 5.2.19-3 | Amplitude C-scan backside | 194 |
| Figure 5.2.20-1 | Integral wing box prototype | 195 |
| Figure 5.2.20-2 | Close up of wing box corner | 196 |
| Figure 5.2.20-3 | Wing box corner painted | 197 |
| Figure 5.2.20-4 | Amplitude scan of wing box corner | 198 |
| Figure 5.2.20-5 | TOF image of wing box corner | 198 |
| Figure 5.2.21-1 | F-22 landing gear door bag side view | 199 |
| Figure 5.2.21-2 | F22 landing door mounted for tool side scan | 200 |
| Figure 5.2.21-3 | LUIS amplitude C-scan | 201 |
| Figure 5.2.21-4 | Boeing amplitude C-scan | 201 |
| Figure 5.2.21-5 | LUIS TOF image | 202 |
| Figure 5.2.21-6 | Boeing production TOF image | 202 |
| Figure 5.2.22-1 | LUIS amplitude image | 203 |

| | | |
|-----------------|--|-----|
| Figure 5.2.22-1 | LUIS amplitude image | 203 |
| Figure 5.2.22-2 | LUIS TOF image | 204 |
| Figure 5.2.22-3 | TOF image | 205 |
| Figure 5.2.22-4 | Production TTU scan | 205 |
| Figure 5.2.23-1 | LUIS amplitude C-scan | 206 |
| Figure 5.2.23-2 | Boeing production amplitude C-scan | 206 |
| Figure 5.2.23-3 | LUIS B-scan tangent to bottom of upper feature | 207 |
| Figure 5.2.23-4 | LUIS B-scan one line up form scan in Figure 2 | 208 |
| Figure 5.2.23-5 | LUIS B-scan near center of upper feature | 208 |
| Figure 5.2.23-6 | LUIS B-scan near center of hammer glow | 209 |
| Figure 5.2.24-1 | LUIS amplitude C-scan | 210 |
| Figure 5.2.24-2 | Boeing production amplitude C-scan processed from full wave data | 211 |
| Figure 5.2.24-3 | LUIS TOF image | 212 |
| Figure 5.2.24-4 | Boeing production TTU image | 212 |
| Figure 5.2.25-1 | Repair Panel K-4 | 213 |
| Figure 5.2.25-2 | Boeing TTU scan | 214 |
| Figure 5.2.25-3 | LUIS amplitude C-scan of panel K-4 | 214 |
| Figures 5.3-1 | Edge view of panel SHM-8 | 215 |
| Figures 5.3-2 | Backside of Panel SHM-8 | 216 |
| Figures 5.3-3 | Front side of Panel SHM-8 | 216 |
| Figures 5.3-4 | Conventional C-scan of Panel SHM-8 | 218 |
| Figures 5.3-5 | Air Scan of Panel SHM-8 | 219 |
| Figures 5.3-6 | Rockwell Science Center LBU C-scan of Panel SHM-8 | 220 |
| Figures 5.3-7 | LUIS 747 C-scan of Panel SHM-8 | 221 |
| Figures 5.3-8 | LUIS 747 C-scan of C-17 part | 222 |
| Figures 5.3-9 | AV-8 stabilizer collage C-scan and scan plan | 223 |
| Figure 6.1-1 | Signals Variability Test Panels | 225 |
| Figure 6.1-2 | Signal Shape Factor Definition | 225 |
| Figure 6.1-3 | Spatial Variation of Pulse Amplitude | 227 |

| | | |
|----------------|---|-----|
| Figure 6.1-4 | Spatial Variation of Shape Factor | 227 |
| Figure 6.1-5 | Pulse Shape Variability | 228 |
| Figure 6.1-6 | Pulse Amplitude Variability | 229 |
| Figure 6.2-1 | C scan views of gated echo amplitude at each of four steps in graphite step wedge | 232 |
| Figure 6.2-2 | LUIS ultrasonic edge response from back face echo | 233 |
| Figure 6.2-3 | Modulation Transfer Function for each of four steps | 233 |
| Figure 6.3-1 | First Scan | 236 |
| Figure 6.3-2 | Second Scan | 236 |
| Figure 6.3-3 | Third Scan | 237 |
| Figure 6.3-4 | Fourth Scan | 237 |
| Figure 6.3-5 | Fifth Scan | 238 |
| Figure 6.3-6 | Histogram of Pixel Gray Scales for Figures 6.3-1 through 6.3-5 | 239 |
| Figure 6.3-7 | Pixel Gray Scale Differences between Figures 6.3-1 and 6.3-2 | 240 |
| Figure 6.3-8 | Pixel Gray Scale Differences between Figures 6.3-1 and 6.3-3 | 240 |
| Figure 6.3-9 | Pixel Gray Scale Differences between Figures 6.3-1 and 6.3-4 | 241 |
| Figure 6.3-10 | Pixel Gray Scale Differences between Figures 6.3-1 and 6.3-5 | 241 |
| Figure 6.3-11 | Pixel Gray Scale Differences between Figures 6.3-2 and 6.3-3 | 241 |
| Figure 6.3-12 | Pixel Gray Scale Differences between Figures 6.3-2 and 6.3-4 | 242 |
| Figure 6.3-13 | Pixel Gray Scale Differences between Figures 6.3-2 and 6.3-5 | 242 |
| Figure 6.3-14 | Pixel Gray Scale Differences between Figures 6.3-3 and 6.3-4 | 242 |
| Figure 6.3-15 | Pixel Gray Scale Differences between Figures 6.3-3 and 6.3-5 | 243 |
| Figure 6.3-16 | Pixel Gray Scale Differences between Figures 6.3-34 and 6.3-5 | 243 |
| Figure 6.3-17 | Histogram of Pixel Gray Scale Differences | 245 |
| Figure 6.3-18 | Contrast Comparison Feature | 246 |
| Figure 6.4-1 | Rocket Nozzle Photograph and LUIS Scan | 248 |
| Figure 6.4-2 | Rockwell Science Center LBU scan of rocket nozzle | 249 |
| Figure 6.4-3 | F-22 Titanium Seal | 250 |
| Figure 6.4-4 | F-22 Titanium Seal Thickness Mapping | 250 |
| Figure 7.3.3-1 | LUIS Auto Ranging Data | 259 |

| | | |
|----------------|--|-----|
| Figure 7.3.3-2 | LUIS Auto Ranging and Time of Flight Data Combined | 259 |
| Figure 7.3.4-1 | 7J7 Panel LUIS Data Without Paint | 263 |
| Figure 7.3.4-2 | 7J7 Panel LUIS Data With Paint | 264 |
| Figure 7.4.2-1 | AUSS | 271 |
| Figure 7.4.2-2 | AUSS Close up | 271 |
| Figure 7.4.5-1 | F-22 Rib Post | 277 |

LIST OF TABLES

| | | <u>Page</u> |
|---------------|---|-------------|
| Table 2-1 | Specifications for Generation Laser | 9 |
| Table 2-2 | Specifications for Detection Laser | 14 |
| Table 2-3 | Specifications for Control System | 14 |
| Table 5.2.2-1 | Flaws detected with 3.5 MHz bubbler (Toolside scan) (Bag side view) | 134 |
| Table 5.2.2-2 | Flaws detected with LUIS (Composite of bag side & tool side views) | 135 |
| Table 5.2.2-3 | Flaws detected with LUIS (bag side scan) (bag side view) | 136 |
| Table 6.1-1 | Listing of Data Files and Conditions for Variability Study | 230 |
| Table 6.3-1 | Gray Level Ranges for LUIS Images | 239 |
| Table 6.3-2 | Gray Level Ranges for Differences between LUIS Images | 244 |
| Table 6.3-3 | Average Gray Scale Values | 246 |
| Table 7.4.3-1 | System Comparisons | 272 |

ABSTRACT

As composite parts become more widely used in aerospace vehicles, there is a greater need for thorough, fast, nondestructive evaluation (NDE) of such parts. Relatively simple, flat composite parts are generally easily inspectable with modern conventional ultrasonic systems. Composite parts of complex shapes are much more difficult. Laser based ultrasonic (LBU) inspection systems should benefit from several theoretical advantages over conventional ultrasonic systems for inspecting composites. To understand actual LBU capabilities, a specific LBU system at McClellan AFB, CA was exercised to evaluate its performance versus conventional systems. The results of that evaluation are reported in this document. The effort was intended to identify particular classes of aircraft and aerospace parts for which LBU inspection is superior to conventional ultrasonic system inspection. The evaluation was also intended to identify the best procedures for use of the McClellan AFB LBU system and to identify shortcomings and potential improvements of the system. Briefly, the evaluation found that the specific LBU system provides excellent flexibility in the wide range of part types and shapes that can be inspected. This flexibility does require a degree of complexity in the LBU hardware and software. The LBU system demonstrated the ability for automated inspection of complex shapes that are usually inspected manually, at greater cost. The LBU system was generally not competitive on simple parts where conventional systems have been optimized for inspections.

Key Words

laser based ultrasound
laser ultrasonic inspection system
nondestructive evaluation
NDE

Acknowledgments

The authors wish to acknowledge the contributions of several people who provided technical support and assistance.

Air Force employees Tom Ducharme and Joe Kwan operated the LUIS at Sacramento ALC and provided day to day logistical support. Christian Padoleau of the National Research Council of Canada provided technical support for the operation of the LUIS. Air Force employees Wes Frazier, Gordon Hendrickson, Mike Mattos and Don Bailey provided managerial and logistical support for the activities at McClellan AFB. Andy McKie from the Rockwell Science Center provided technical advice and assistance. Kathleen O'Connor from Boeing's Reusable Space Systems group in Downey, CA provided comparison data from earlier LUIS work. Jeff Kollgaard and Rick Krizanich of Boeing Commercial Airplane Group - MR&D, and Marty Freet of Boeing Information, Space and Defense Systems - QA provided conventional UT data for comparison to LUIS results. Mark Vogel in St. Louis provided information on the AV-8 data. Teri Nelson and Vonnie Fisher compiled and edited this document.

EXECUTIVE SUMMARY

The work reported in this document answers questions about a Laser Based Ultrasound (LBU) system installed by the U.S. Air Force at McClellan AFB, CA. The LBU system studied is a Laser Ultrasonic Inspection System (Luis) model 747 manufactured by UltraOptec, Inc. of Boucherville, Quebec. In this contracted study data from the Luis 747 was compared to data from conventional ultrasonic systems in order to identify advantages and disadvantages of the Luis 747 for the inspection of aerospace parts. The contract also evaluated Luis 747 signal variability, identified optimum data processing steps and identified possible enhancements to the Luis 747. In performing these evaluations, Boeing noted which potential LBU benefits actually accrued in the operation of the Luis 747.

The Luis 747 is an impressive system that embodies many of the positive features of LBU technology in a very robust package compatible with production areas. Since it was built to specifications that are not universal and since technology has advanced since it was built, it can not be expected to perform every possible ultrasonic inspection in an optimum manner. Still, it was able to handle a very wide range of part types and sizes with at least some beneficial results.

Boeing found that the Luis 747 provided detection advantages compared to current inspection methods for thin, composite parts with surfaces containing small radii and complex curvatures. This enables better detection of disbonds and delaminations, which could potentially cause failures, in areas that are difficult to inspect conventionally. The Luis 747 also offers a unique 3D geometry capture feature which could be used for metrology, reverse engineering and visualization of ultrasonic data in 3D projections of parts.

An LBU system such as the Luis 747 is ideal in supporting rapid prototyping of composite parts with a wide variety of complicated shapes and geometries. It offers the capability to quickly inspect parts of almost any shape without the necessity to build unique fixturing or fabricate complicated transducer arrays and their associated contact preserving apparatus.

Boeing found the LUIS 747 to be at a disadvantage compared to conventional systems for composite parts that are thick or for parts that are relatively flat, and parts that must be inspected from the toolside. The LUIS 747 was judged to be slower, less sensitive, more costly or requiring more preparation than conventional systems for these types of parts. The initial capital cost of the LUIS 747 system and limited advantages compared to conventional ultrasonic systems are the largest impediments to encouraging further use of LBU technology on a large scale.

Shot to shot and scan to scan variability was shown to be a minor issue in LUIS 747 operation, the optimum steps for signal processing were generated and several possible enhancements to the LUIS 747 were identified.

The LUIS 747 is clearly an asset to development of new LBU systems or exploration of LBU inspection of new composite parts. However, because of the impending transfer of ownership of the LUIS 747 to Sacramento County, Boeing recommends that no U.S. Government money be spent to upgrade or enhance the LUIS. The Air Force should encourage use of the LUIS 747 as a testbed for experiments and further LBU development. If the Air Force wishes to encourage continued development of LBU technology, then Boeing recommends that the Air Force assist the following short term and long term developments.

Short term development should focus on the fielding of a low cost system in a high inspection volume environment to demonstrate that the potential benefits of LBU can be realized at competitive cost. Also, with what appear to be relatively minor changes in the software, the LUIS 747 can be useful in support of rapid prototyping of composite parts of almost arbitrary shape.

Long term work should focus on development of new laser and detector technologies that will reduce the complexity, size and price of LBU systems, while increasing their speed.

1.0 INTRODUCTION

Ultrasonic inspection provides valuable information about the presence or absence of defects in aerospace parts. A typical conventional system couples the ultrasonic signal from a transducer to the part via liquid couplant. These systems work well with simple, fairly flat geometry parts. Complex shapes are more difficult to inspect since the transducer(s) must introduce ultrasound normal to the inspection surface to provide good detection of ultrasonic energy in the test article. Complex parts may require long set-up times to program the transducer to follow difficult curvatures. Elaborate fixturing may be needed to maintain proper orientation of water jets for systems that use one water jet for excitation and a second water jet on the opposite side of the test specimen for acquisition of the signal. Such systems are limited when geometry prevents easy access to a back surface. These squirter systems are also limited by the speed of the mechanical motion of transducers across the inspection surface. Scanning complex geometries is slow because it is necessary to control 3 degrees of translation and 3 degrees of angular orientation while keeping two transducers oriented normal to the part surface and pointed at each other. Setup time to program the scan path and precisely fix parts can be long. Other configurations are also representative of conventional ultrasonic inspection technology. These include so-called bubbler systems in which the water is confined and minimized, as well as immersion systems using a tank of water to support the transmission of ultrasound. A typical bubbler system is shown in Figures 1-1 and 1-2.

Bubbler systems and immersion systems overcome some of the limitations of squirters, but in turn have their own limitations. For example, immersion systems cannot be used with parts that cannot be covered with water. Conventional systems have benefited from years of development and do offer many real advantages. To be embraced by the Non-Destructive Inspection community, competing technologies such as LBU must overcome conventional limitations while replicating successful traits to be considered as viable alternatives. Conventional systems are generally low in cost and provide high speed throughput by use of arrays of transducers customized for particular shapes.

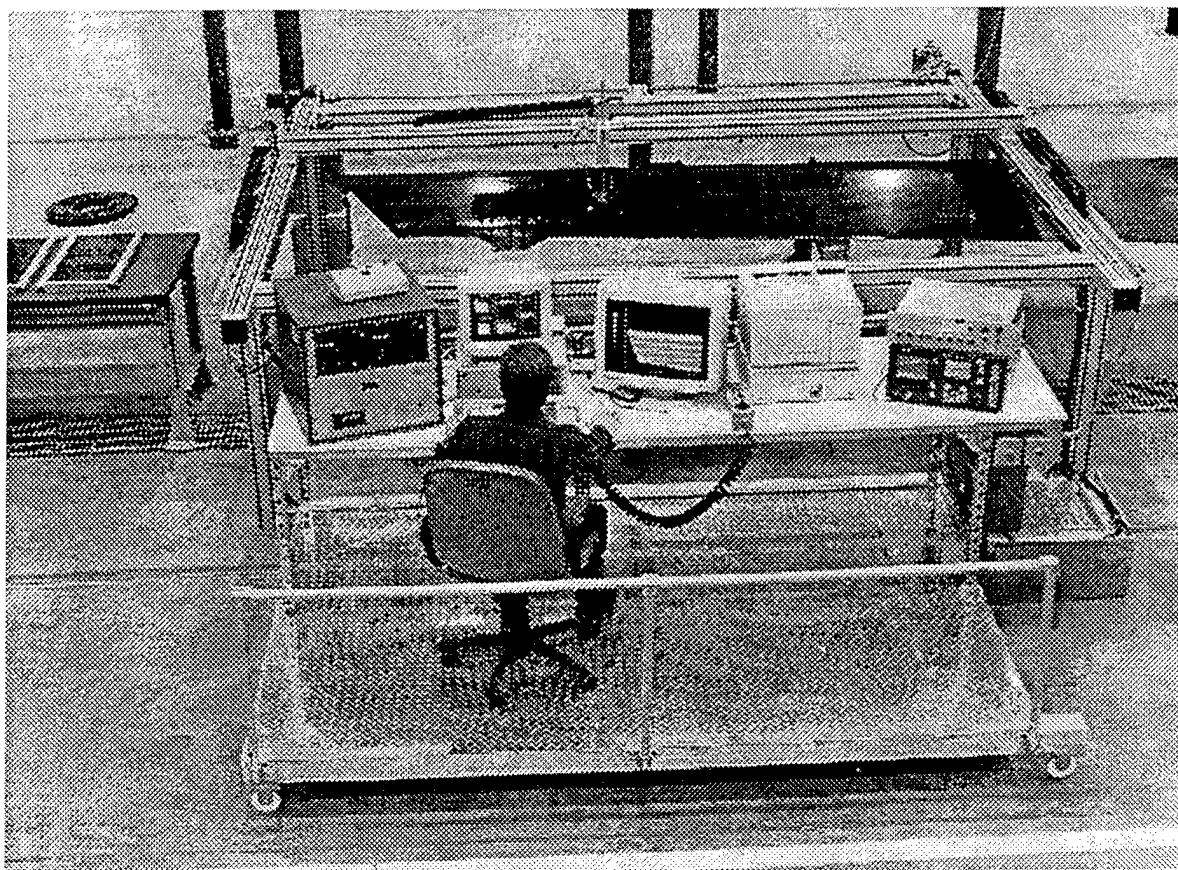


Figure 1-1. Conventional Bubbler Installation at Boeing

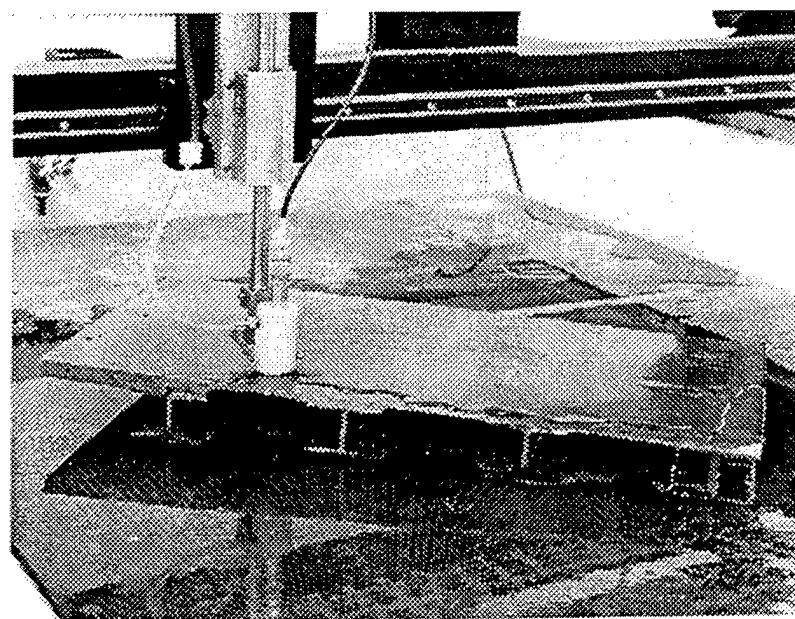


Figure 1-2. Bubbler Closeup

Laser based ultrasound (LBU) pulse echo systems may overcome some limitations of conventional systems. In a typical LBU setup, a generation laser rapidly heats a spot on the surface of the part to be inspected. The generation laser beam is absorbed in a small volume near the surface that acts as an ultrasonic transducer coplanar to the surface. Because the material expands as it is heated very rapidly, the pressure in the absorption volume increases. This pressure is relieved by a release acoustic wave originating at the free surface of the material. The ultrasound propagates normal to the surface, independent of the laser beam angle of incidence. This eliminates the need for difficult scan plans and complex fixturing to maintain the inspection beam normal to the surface. It should make inspection of complex shapes easier since normality is not a strict requirement. The free surface velocity is measured by detecting the Doppler shift of a second laser beam. The Doppler shift is typically detected using a Farbry-Perot interferometer to monitor returning ultrasonic echoes, which contain information about the internal structure of the part.

This type of LBU system works in pulse echo mode. Pulse echo mode and non-normal laser beam incidence should allow LBU to easily inspect complex shapes that may be extremely difficult for conventional systems. LBU may increase the speed of inspection since laser beams can be quickly scanned across a surface by the small movements of a mirror, instead of mechanical motion of water jets or transducers. LBU systems may also be preferred in cases where the test part cannot be exposed to water or other liquid couplants. LBU also offers the possibility of inspecting parts in environmental chambers while replicating operating conditions such as vacuum or extreme temperatures. Where potential cost savings or inspection advantages can be realized in practice, LBU will be a very valuable inspection technique. This contract addressed the realization of these benefits for a particular system.

In 1996, the U.S. Air Force purchased a Laser Ultrasonic Inspection System (L UIS) model 747 from UltraOptec, Inc. of Boucherville, Quebec. The L UIS was installed at Sacramento Air Logistics Center (ALC), McClellan AFB, CA., which was designated as the Air Force center for composite development and repair. To assess the real benefits of the L UIS, the Materials

Directorate of the Air Force Research Laboratory contracted with Boeing to evaluate system performance using ultrasonic test standards and actual aerospace parts. The results of that evaluation are discussed in this document.

To evaluate the LUIS, a program of scanning typical aircraft and aerospace part types was executed by the NDE Physics group from Boeing Information, Space and Defense Systems Group in Kent, WA with the assistance of the NDE research group from Boeing Commercial Aircraft Group in Renton, WA. Personnel from the National Research Council of Canada who are former employees of UltraOptec and experienced in the engineering, operation and maintenance of the LUIS 747 supplied system expertise. On-site support was provided by Air Force NDE technicians and engineering personnel at McClellan AFB.

The LUIS 747 was designed principally for inspection of bare graphite epoxy composites. Composite parts with complex geometries or cores such as honeycomb are important aerospace structures. The wavelength of the generation laser is not appropriate for efficient generation of longitudinal ultrasonic waves in bare metals. Metal parts can be painted to permit inspection and some specialized metal parts were inspected. However, the main focus of the test program was on composite part types from various military and commercial aircraft.

2.0 EQUIPMENT DESCRIPTION

The LUIS 747 is made up of three units: the generation unit, the detection unit and the control console. The generation unit consists of a generation laser beam source and an optical scanner assembly with associated optics. The generation unit is mounted on a computer controlled robot system, which gives it the capability to move in 3 linear axes and 1 rotation axis in a large volume and inspect large components. The gantry is contained in a large bay capable of handling parts up to 40 feet long and 11.5 feet high. Figure 2-1 shows an overall view of the gantry system and work bay. Figure 2-2 shows the robot arm extended.

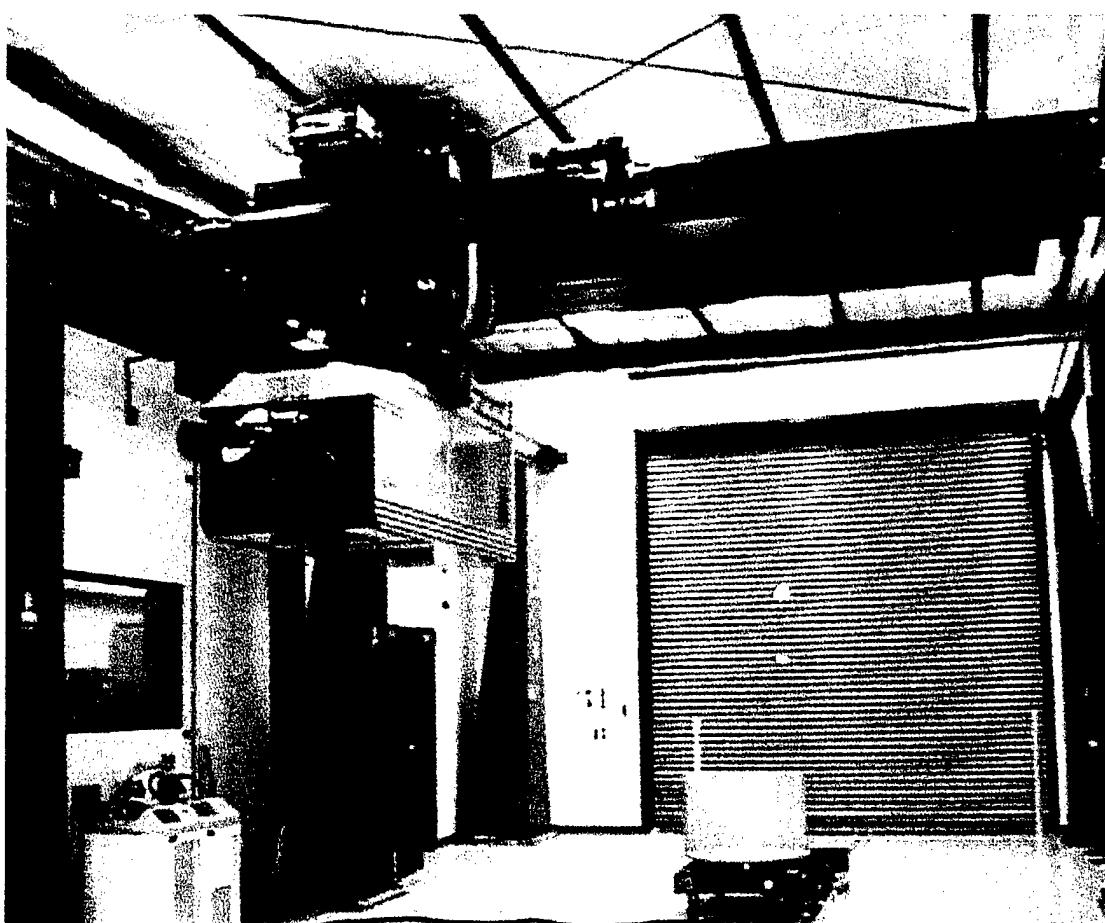


Figure 2-1. Laser Gantry and Work Bay

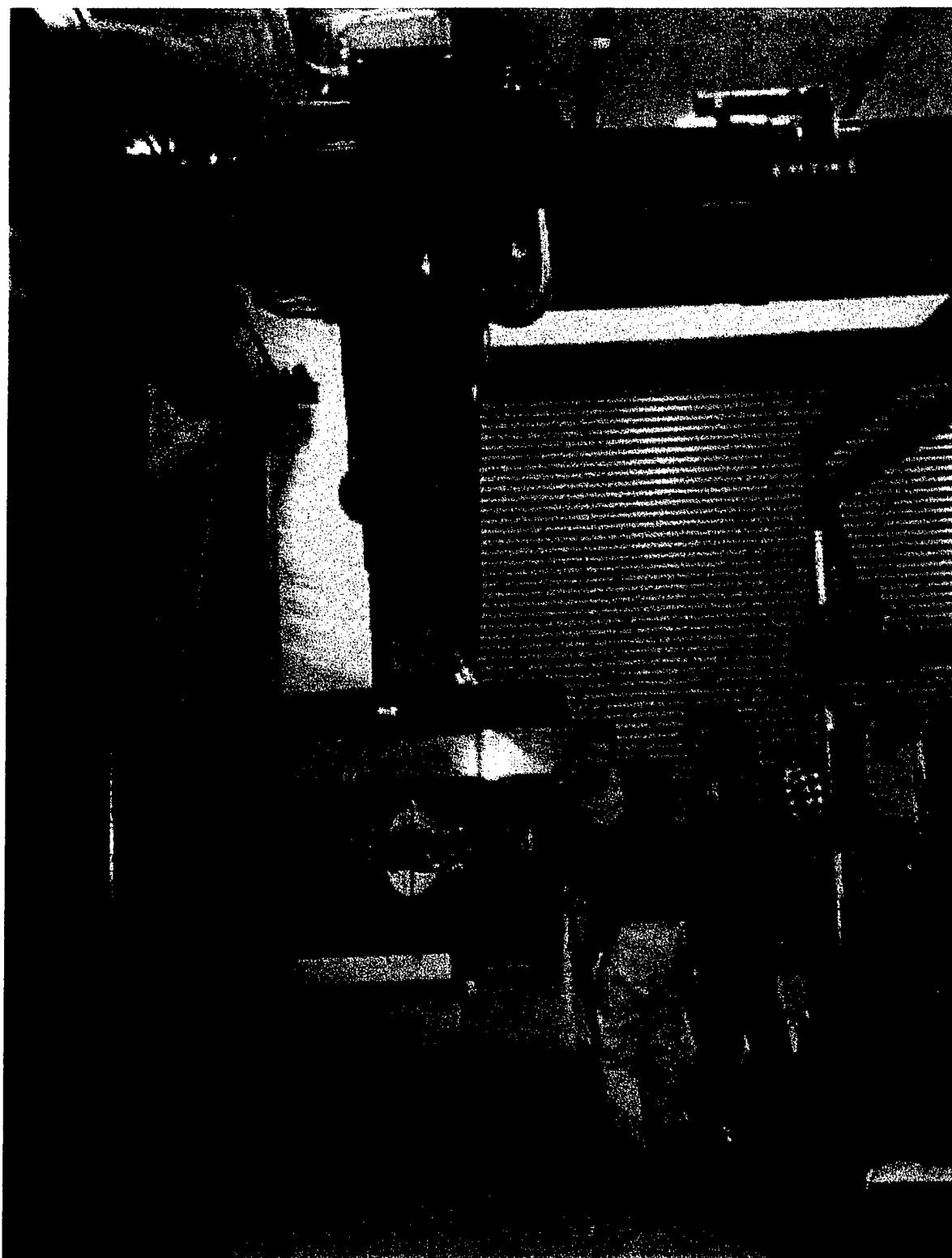


Figure 2-2. Laser Gantry Extended

The LUIS 747 generation laser is an industrial, commercial CO₂ laser with a custom gas mixture

D950-10322-1

to maximize the generation of ultrasonic waves. The specifications of the laser are shown in Table 2-1.

Table 2-1. Specifications for Generation Laser

| | |
|------------------------|-----------------|
| Wavelength (optical): | 10.6 μ m |
| Repetition Rate: | 100 Hz |
| Pulse duration (FWHM): | 130 \pm 20 ns |
| Output power: | >150 mJ |

The LUIS 747 has an optical aperture system, which limits the spot sizes of the generation and detection lasers to either 0.2" or 0.1" in diameter. The spot sizes of the generation and detection lasers are selected by the operator and are controlled by the automatic focusing subsystem. The generation and detection laser spots as well as the spot of a visible He-Ne tracer beam are superimposed and focused to the same spot size onto the surface of the component. Figure 2-3 shows several samples in the workbay being held in place by the sample stabilization hardware. The red dot in the photograph is the He-Ne tracking beam spot. The photograph appears yellow due to the filtering properties of the control room window.

The scanner mechanism is a single elliptical mirror with a major axis of 18 inches and a minor axis of 8.25 inches. The mirror rotates independently around 2 mechanical axes. This gives the system a total of 6 degrees of freedom. The primary scanning axis of the mirror mount allows back and forth motion of the mirror in a range of $\pm 31^\circ$. When the smaller axis is vertical, the laser beam scans in a horizontal plane parallel to the ground. The orientation of the mirror primary axis is controlled by the rotation of a yoke that holds the mirror mount. The yoke rotates around a horizontal line and can orient the mirror primary axis anywhere between vertical and horizontal. Figure 2-4 shows the mirror from the backside with the smaller axis in a vertical position. The rotating yoke can be seen on the left side of the photograph. The scanning mechanism has an angular resolution of $.01^\circ$ for both axes. The mechanical scanning system allows scanning an area of up to 6 x 6 feet at a work distance of 5 feet from the scanner for a single scan. Larger areas require additional lateral translation of the generation unit.

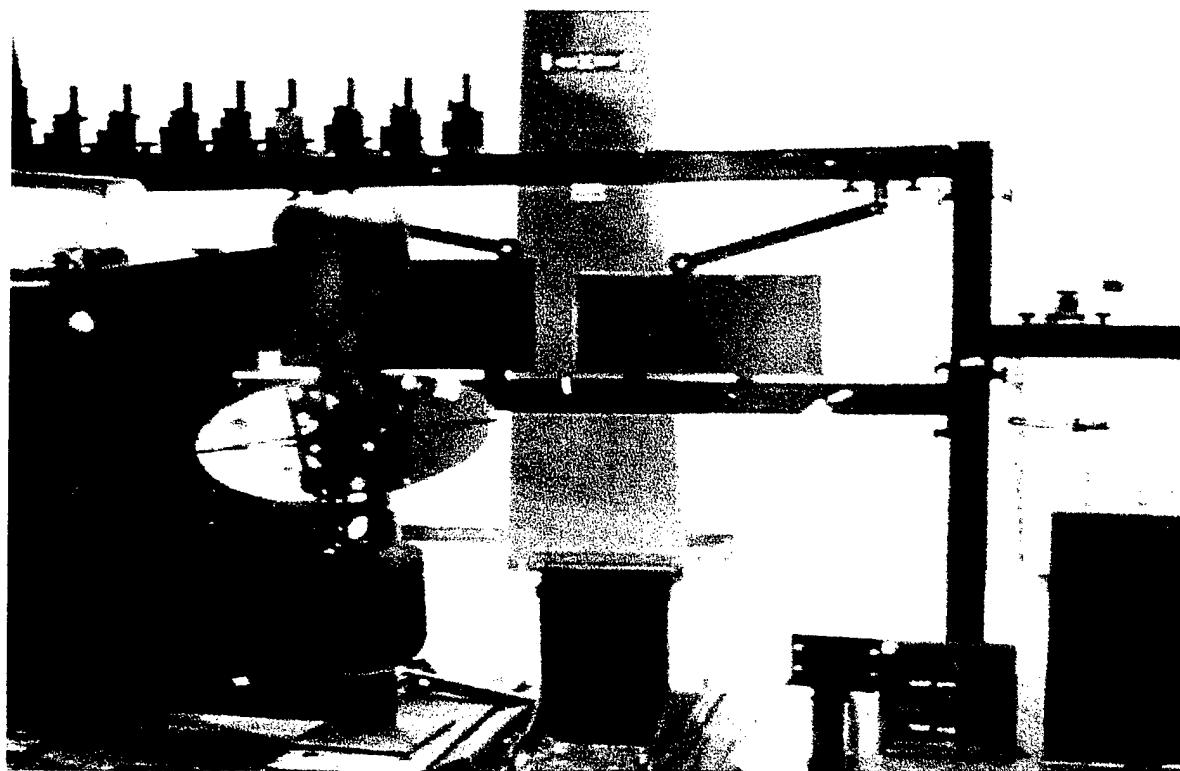


Figure 2-3. Samples in Workbay and Laser Tracking Spot

The detection unit, located in the control room and connected to the scanning head via fiber optics, contains a detection laser beam source and an optical demodulator system. The detection unit is fixed but the detection laser beam is routed via an optical fiber link to the robot gantry and the optical scanner assembly for transmission to the inspection sample. The detection unit is shown in figure 2-5. The detection unit is housed in a rectangular enclosure mounted on a vibration-isolated table resting on a movable carriage. It includes the detection laser and the confocal Fabry-Perot interferometer and its detector assembly.

The confocal Fabry-Perot is 1 meter long with 85% reflectivity mirrors for demodulation of the laser detection light. The -6dB low frequency cut-off is at 2 MHz and a high frequency cut-off is at 15.6 MHz. The peak responsivity of the LUIS 747 detection system is at 5.5 MHz.

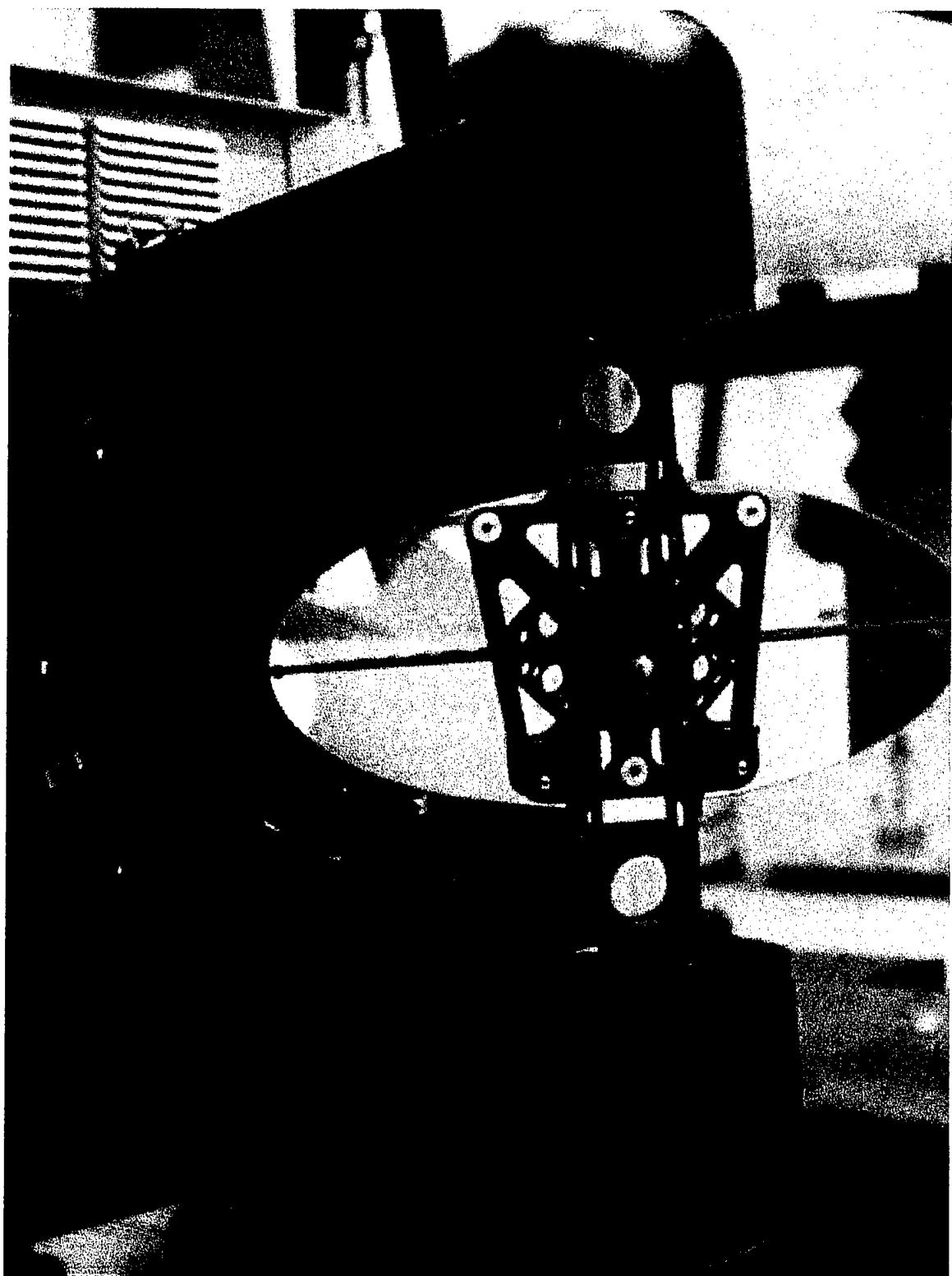


Figure 2-4. Rotating Mirror and Yoke

D950-10322-1

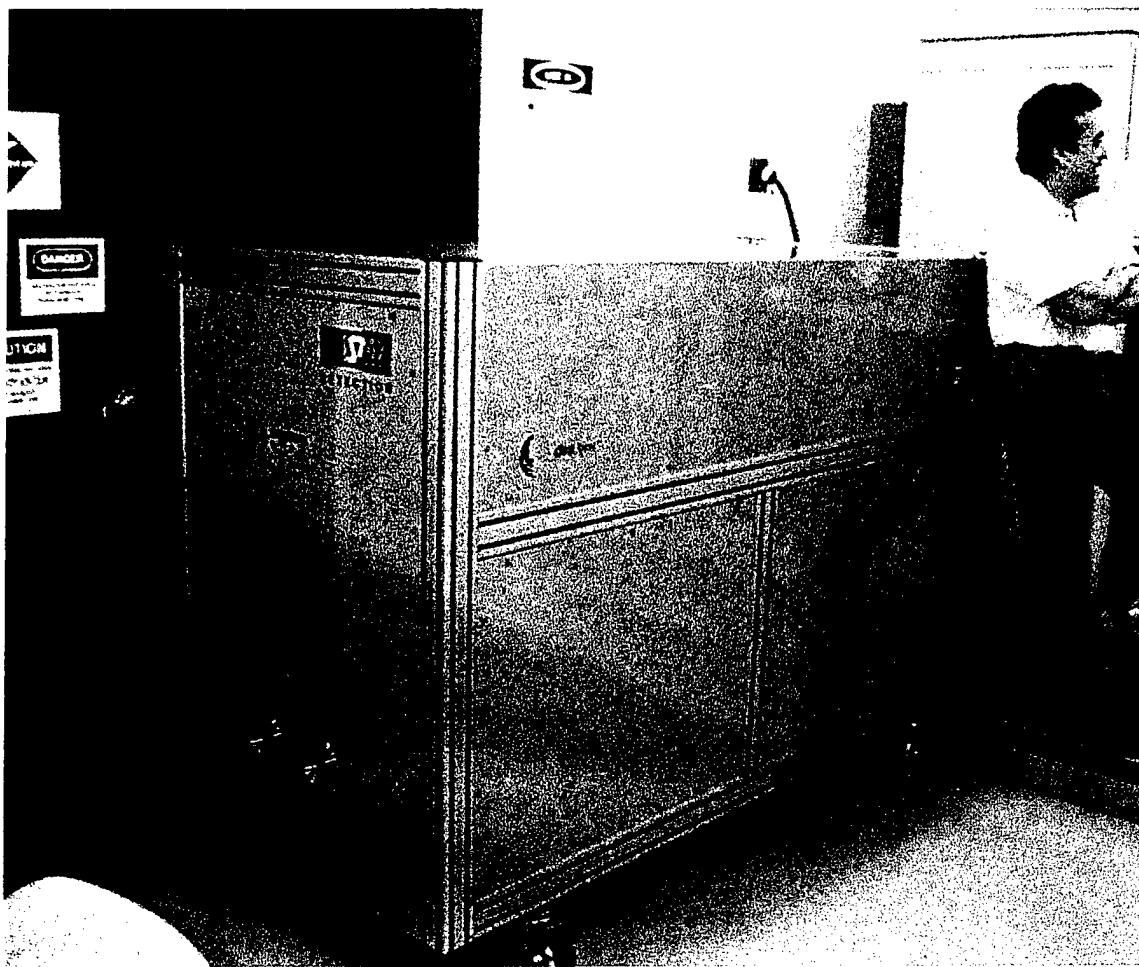


Figure 2-5. Detection Unit

The LUIS 747 is equipped with a range finding system, which enables it to measure the shape of the component being inspected. The shape data may be used to produce a 3D image of the component with the ultrasonic information mapped onto it. The ranging system is mounted on the scanner. The ranging system measures the distance by laser triangulation. The detection laser is focused onto the surface of a component. The scattered light is collected by a single lens and imaged onto a plane behind the lens. As the surface of the component is shifted along the probe beam axis, the position of the image behind the lens follows a line slightly tilted with respect to the normal to the optical axis of the lens. By placing a line camera along the image displacement axis, a precise measurement of the component's surface is obtained. The ranging system provides a typical accuracy of ± 0.2 inch at a distance of 5 feet from the center of the scanner.

The optical assembly superimposes the generation laser beam with the detection laser beam from the detection unit, focuses the beams onto the inspected part with a spot of approximately constant size, and collects scattered light of the detection laser and focuses it into a large-core receiving fiber which transmits it to the detection unit for demodulation.

The arrival of a reflected ultrasonic pulse at the inspected surface is detected by a frequency stabilized laser focused at the point of inspection. The motion of the surface induces a phase change on the beam reflected from the inspected surface. This phase change produces an amplitude variation of the light output from the Fabry-Perot interferometer. The incident detection laser beam possesses good stability in the frequency range of the ultrasonic pulses to prevent masking of the ultrasonic signal due to frequency variation in the laser beam.

To attain high stability, the detection laser is built around a stabilized seed laser that is amplified to obtain a high output detection beam. The seed laser is amplified through a flashlamp pumped Nd:YAG system, providing peak output power above 500 W at the wavelength of $1.06\mu\text{m}$.

Variations in the reflectivity of the surface are compensated for by a power output controller at the output of the detection laser. The system is controlled by a feedback loop sensing the light incident at the interferometer. Variations in surface reflectivity are handled by changing the output power of the detection laser. The receiving laser assembly includes a visible tracer He-Ne laser beam that is coincident with the Nd-YAG beam. The visible tracer beam is focused into the illuminating Nd-YAG fiber and produces a visible spot exactly superimposed on the detecting spot on the surface of the part.

The LUIS 747 detection laser specifications are shown in Table 2- 2.

Table 2-2. Specifications for Detection Laser

| | |
|---------------------------|----------------|
| Wavelength (optical): | 1.06 μ m |
| Repetition rate: | 100 Hz |
| Pulse duration (FWHM): | 55 μ s |
| Peak power: | >500 W |
| Attenuator dynamic range: | 30 dB (1/1000) |

The control unit is composed of control electronics and the primary computer workstation. Complete control of the LUIS 747 is obtained through the primary workstation, a Silicon Graphics Indigo 2 computer. A number of microprocessor-controlled subsystems handle specific functions. These include the Data Acquisition Control Computer, the Scanner Control Computer for mirror control, the RFCC for control of measurement data and the autofocus system, a robot gantry controller and the system security and control module. These offload some work from the primary workstation allowing it to display inspection data during the scan. A second Indigo 2 is connected to provide offline processing of data captured. Control specifications for the LUIS 747 follow in Table 2-3.

Table 2-3. Specifications for Control System

| | |
|-------------------------------------|---|
| Inspection step size: | 0.05 inch at distance of 5 feet |
| Scanner envelope: | 6 x 6 feet at a distance of 5 feet |
| Scan rate: | 100 points/second |
| Spot size: | 0.2 inch and 0.1inch diameters |
| Total envelope in a vertical plane: | 40 x 11.5 feet |
| Working range: | 4 - 8 feet |
| Ranging System: | \pm 0.2 inch at 5 feet from the scanner |
| Points per waveform: | up to 2048 |
| Digitization rate: | from 12.5 MHz to 100 MHz |
| Analog-to-Digital conversion: | 8 bits |

Figure 2-6 shows the control console and workstation.

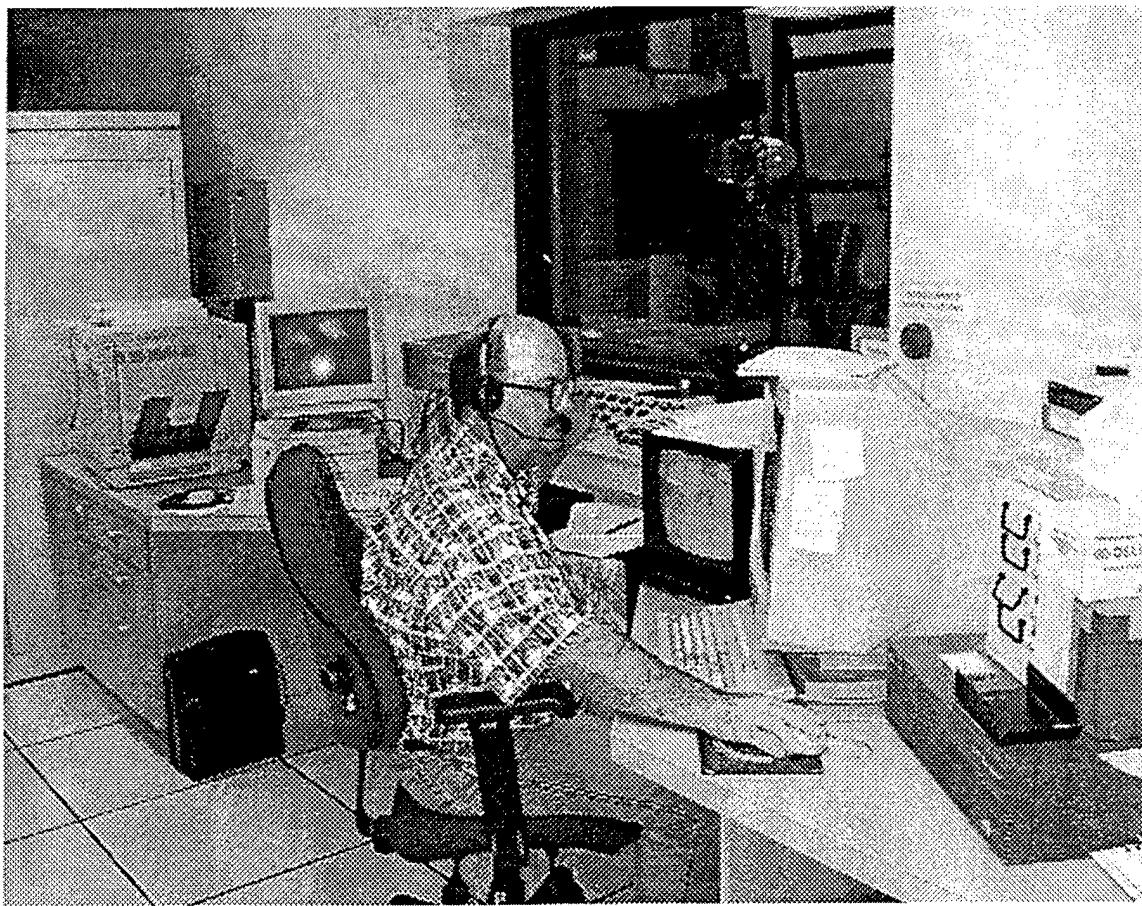


Figure 2-6. Control Unit

D950-10322-1

3.0 TEST PROCESS

The test program was driven by the intent to evaluate the LUIS for sensitivity to typical defects in composite parts. The plan was to inspect a wide variety of actual parts with known defects and well characterized standards with simulated defects. Composite part samples from major aircraft programs were selected for use. Consideration was given to composite parts from the 777, the Navy A-6 composite re-wing, F-22, B-2, JSF, 757 and 747. In addition, several ultrasonic test standards used for calibration of conventional NDE systems were inspected. Since the contracted effort intended to identify possible applications for the LUIS, consideration was also given to other part types. Various painted samples from E-3 AWACS and commercial aircraft were tested to evaluate the possibility of precision paint thickness measurement. An F-22 titanium seal was inspected to evaluate LUIS use for thickness monitoring of machining processes. A metal alloy Rocketdyne thruster nozzle was tested to evaluate LUIS resolution of small features in metallic parts.

The parts were chosen to test the ability of the LUIS to detect various characteristics in various part types. Once the parts arrived at McClellan AFB, they were mounted in the stabilizing hardware racks shown in Figure 2-3. Parts were positioned to present an area of interest to the optical assembly on the robot gantry arm. Air Force technicians responsible for operating the equipment set up an inspection plan for the equipment to automatically follow. The inspection plan defines a step size and a rectangular area, which delineates a section of the test part to be inspected.

The LUIS was designed for use in a production environment, which was conceptualized as allowing fast, easy, repetitive inspections of identical aircraft parts after initial setup. To achieve this objective, the LUIS makes extensive use of a database to store and retrieve all the information required for the inspection of a given type of part. Once the inspection information is stored in the system database, an inspection of a known part requires only the setting of a reference point on the part. This reference point is previously identified during the setup of the database inspection plan record.

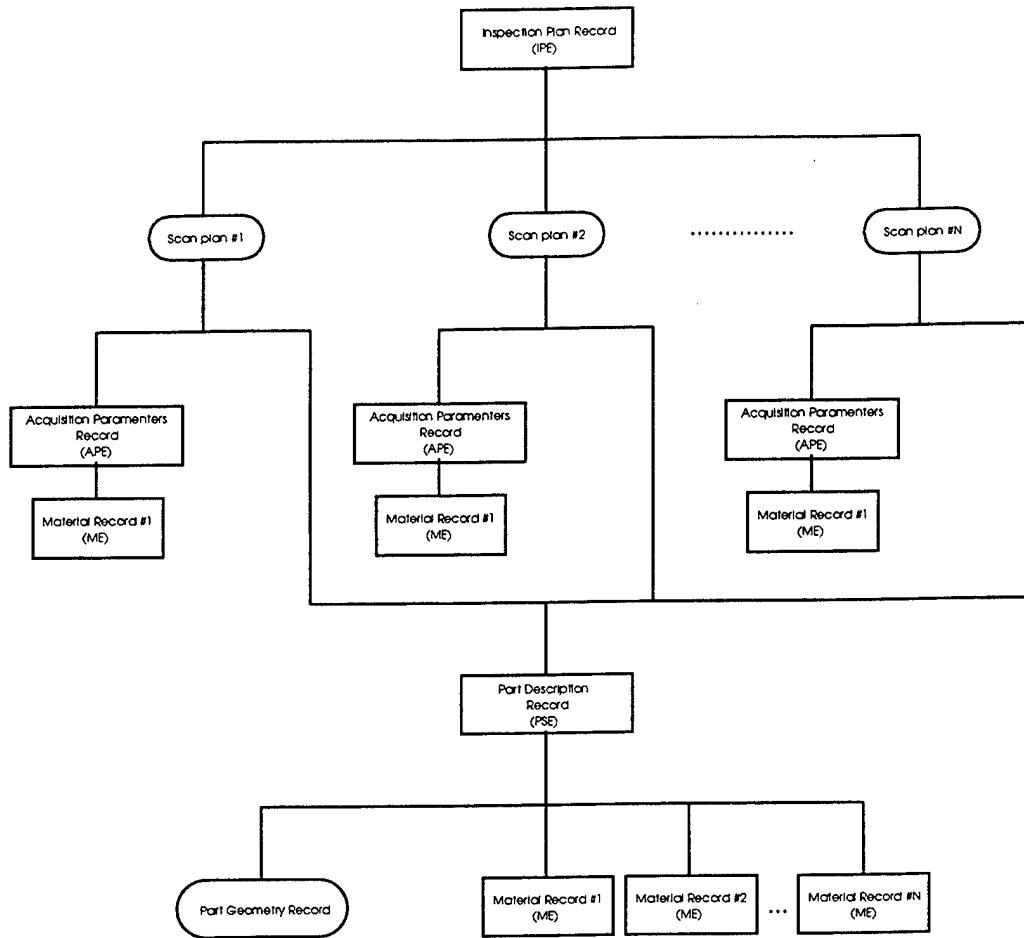


Figure 3-1. LUIS Inspection Plan Record

The database record structure for each type of part is shown in figure 3-1. At the top level, there is the inspection plan record that contains all the information needed to inspect a given type of part, e.g., an F-22 landing gear door. The inspection plan record is composed of a number of scan plan records. All the scan plans of the inspection plan record will be automatically executed in a sequence when the given inspection plan is selected. The scan plans are defined with the help of the part geometry, which is an area defined by the operator that completely contains the inspected part. The coordinates of the scan plans are given in relation to an origin defined in the part's geometry. The acquisition parameter record in each scan plan uses the material description to limit the maximum usable laser power settings, as set during the damage threshold assessment procedure. A part description record may have more than one material since a part can be made of more than one material.

The drawback to the use of this extensive database is that there is no fast way to inspect a new part unknown to the database. A detailed setup process must first take place. The procedure to setup a new part in the database is as follows:

1. Damage threshold determination of the surface materials of the part and output laser settings.

For each type of material unknown to the database on the inspected part, a damage threshold assessment must be made. The procedure involves determining the maximum power of the generation and detection lasers that can be used without damaging the surface of the material. In preparation for testing the operator watches for smoke, a flash, or surface discoloration on the test surface while increasing the output of the generation laser in 5% steps. If all of the materials of the part are known to the database, this step can be skipped. The laser power selection process of the LUIS essentially involves determining the laser damage threshold of the materials of the inspected parts. In most cases, the LUIS power levels will be set at 80 to 95% of damage threshold power in order to get the maximum signal to noise ratio. If the damage threshold of the material is known, setting up the laser power levels takes only a few minutes.

To determine the laser damage threshold, an operator must be inside the inspection bay in order to closely watch the part's surface. The damage threshold assessment is presently impeded by the inability of the operator inside the inspection bay to control the firing of the LUIS lasers. A second operator in the control room must fire the laser while the first operator looks for any laser damage from inside the inspection bay. Figure 3-2 shows a technician inside the inspection bay provide feedback on test firing of the laser.

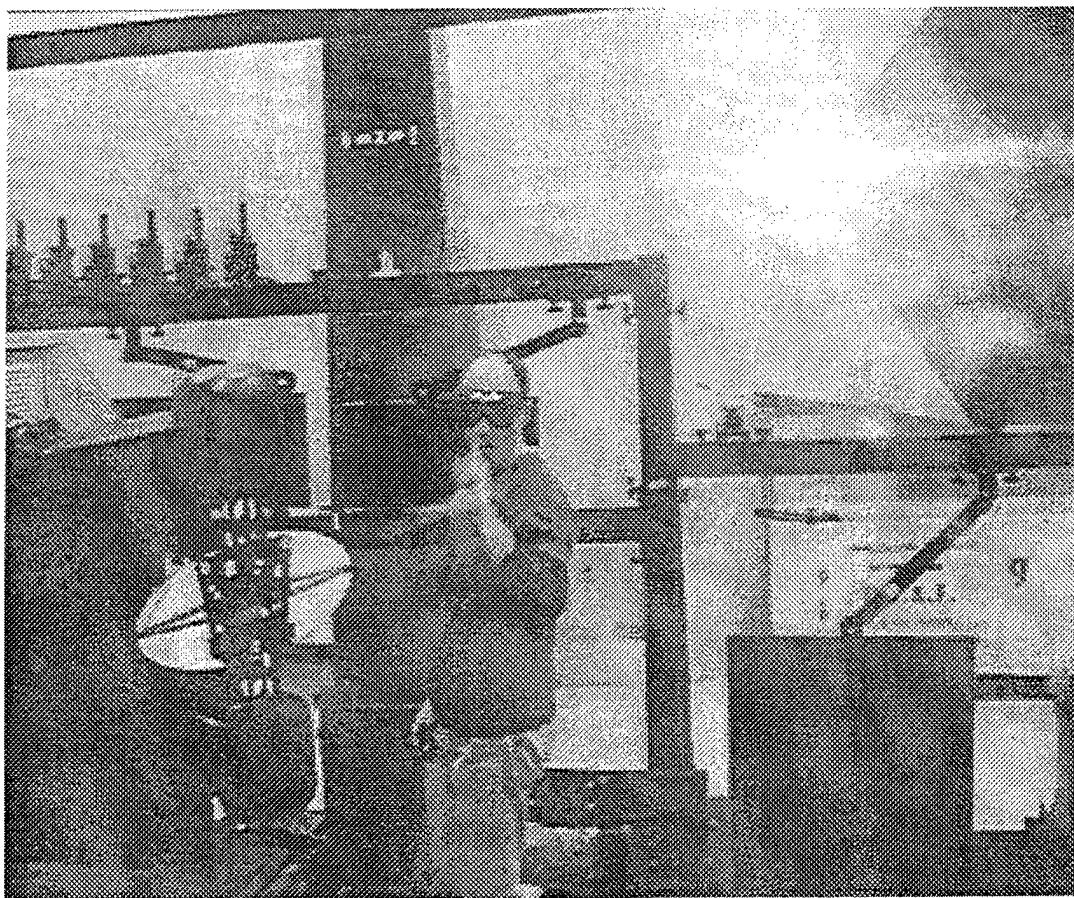


Figure 3-2. Technician Communicating Laser Power Setting Information to Control Room

The communication between both operators was initially done by hand signals, which could cause misinterpretations. A simple intercom system to provide better communications between the operators and simplify the damage assessment procedure was put into place during the testing. The procedure could be speeded up even more if the operator in the inspection bay could have a direct control on the firing of the lasers. This could be done by interfacing the LUIS control system with a portable industrial PC. A single operator could then make the full laser damage assessment of the LUIS laser.

Notice that the laser damage threshold assessment is not required for a new part but only for a new material. If a coupon of the materials is available, the damage threshold can be done on this coupon for all of the parts using this material. However, this requires that a

material list of every inspected part be supplied to the LUIS operators.

2. Define the part geometry

The second step consists of defining in the database an outline of the part's shape as seen by the scanner of the generation unit. This is done to allow the system to recognize the physical limits of the part. It will be used by the operator to set up the individual scanned areas of the part. In the part geometry definition, fiduciary points may also be identified. The scanned area need not cover the entire part.

3. Definition of inspection plan of the part.

The inspection plan defines how the part will be inspected i.e., number of scan plans, size of each scan plan, position of the scan plan and resolution of the scan. In a given inspection plan, an area can be scanned more than once. For example, the operator can set up a low resolution scan of the whole part and a high resolution scan over a small section of the part. For each scan plan in the inspection plan, an acquisition parameter record is used. In most circumstances, the acquisition parameter record will be the same for all of the scan plans of a given inspection plan. The acquisition parameter record for a new part is set in this step.

4. Pre-scan of the part.

Once the inspection plan of the new part has been made, a low resolution inspection of the part is then made using the newly created scan plans. This will allow the setup operator to determine any problems in the scan setups such as improper orientation of the part or low detection light return from some areas of the part.

5. Modifications to the inspection plan.

If any problems are discovered during the pre-scan, the inspection plan is modified. If these modifications are extensive, a second pre-scan may be needed.

6. Final inspection of the part at the appropriate resolution.

For parts with simple geometry, the pre-scan may not be required. In such cases, the operator only needs to check the signal-to-noise ratio obtained with the current settings at the extremities of the parts (i.e., at the point with the highest laser beam angle of incidence

to the surface for each material type of the part). If the signal to noise ratio is appropriate at these points, then the inspection of the part can be made directly.

Depending on the proficiency of the setup operators, the setup time for a new part should take between 20 to 60 minutes for parts smaller than 6 ft x 6 ft. This does not include the mounting of the part on the inspection cart. Most of the setup time is composed of the time required for the pre-scan of the part. For larger part, the setup time is increased by the setup of more scan plans in the inspection plan and of the time required for the pre-scan. Once the information is in the database, the scan of a known part should proceed quickly. It involves only identifying a reference point on the part, which takes a few minutes and then executing the pre-stored scan plan. The setup time is longer than that needed for custom conventional systems that are optimized for a single part shape, but shorter than the setup time for a complex part in a flexible conventional system such as an immersion tank.

During the inspection sessions at McClellan AFB, some delays in the setup of new parts were caused by a current software bug in the acquisition parameter editor (APE). In some circumstances, the APE will produce a corrupted acquisition parameter record. This corrupted record will only be noticed when it produces a shutdown of the generation and detection lasers during an inspection. When this happens each parameter record in the inspection plan must be manually reset and the corrupted record deleted. As an example, the sine wave spar took more than one hour to set for a very small scan area. A full database crash took the operators more than 45 minutes to recover from. This bug can be corrected easily and should be.

Scans are limited to a rectangular area. To completely scan irregular parts requires scanning empty space. When the optical auto-ranging system senses an object beyond edge of the part, but within the dynamic range of the ranging system, some undesirable variations occur as the lasers come back onto the part. The ability to restrict scanning to irregular areas would save time, reduce data file sizes, and avoid confusing the auto-ranging system when the beam runs off a part.

Appendix A contains a table listing the test identification numbers and descriptions of parts that were inspected at the LUIS. Some parts are shown as having been scanned multiple times. Some

of these multiple scans are due to dividing large parts up into 2 or more scan sections, scanning from both sides of a part, scanning before and after application of paint and redundant scans to recover from data errors.

4.0 Data Analysis Processes Description

Once data are captured, they must be processed to extract the information present. The LUIS digitizes the full detected waveform and displays real time C-scan and B-scan images on the control console. Since there are no available functions to process the real time images on the control console, data processing relies on off-line post-processing using proprietary software. Some hardware is available on the LUIS to reproduce the post-processing procedures on subsequent scans of the same part. An expanded use of hardware processing would eliminate almost all of the post-processing currently done off-line. The signal processing and data comparison methods used with the present equipment are discussed in this section.

4.1 LUIS Signal Processing

Steps in a generalized process for analyzing LUIS data are listed here.

1. Make a general C-scan of the data file with the back-wall ultrasonic echo or recall C-scan images produced during the acquisition of the data if such images are available. This would produce two C-scan images, an amplitude and time of flight C-scan. These images allow us to determine the internal features of the parts and can also allow identification of suspicious areas where defects might be. Significant drop in amplitude of the back-wall echo may indicate the presence of porosity or of semi-transparent inclusions.
2. Check with B-scan or full wave form (A-scan) of suspicious areas to determine the origin of suspicious areas in the C-scan.
3. If needed, use signal processing to increase contrast of suspicious areas. Signal processing functions such as filtering, distance amplitude correction (DAC) for part with varying thickness, and normalization to correct for variation in the laser shot-to-shot pulse energy may be useful. Generally, by looking at the frequency distribution of the back-wall ultrasonic echo or of the echo from the defects, a filter to remove the signal outside of the spectral range of the ultrasonic echo can be found. It should be noted that post-acquisition signal processing is required only if a detailed analysis of the defects is required. For simple identification of the presence of defects, signal processing may not

be needed, especially if hardware processing is used.

4. Flip through the B-scans or Z-scans and look for echo “in the bulk” of the parts (i.e., between the surface signal and the back-wall echo). These echoes could originate from inclusion or delamination defects in the bulk of the material.
5. Check to see if the “defects” found in step 4 are not structural items. This can be done by looking at the full wave form at the suspicious positions and/or drawings of the inner structure of the part.
6. Flip through the B-scans and look for breaks in the back-wall ultrasonic echo. Breaks in the back-wall ultrasonic echo may be caused by the “shadow” of a near surface defect or semi-transparent bulk defect, and by the presence of porosity in the bulk of the parts.
7. Check to see if the “defects” of step 6 are caused by structural items.
8. Generate new C-scan images with appropriate gates to isolate the “defects” identified in steps 5 or 7.
9. Note the actual defects after confirmation with C-scans.
10. Although this approach has some systematic features, it is based primarily on the experience of analysts trained on the LUIS 747. As with other NDT methods, the experience of the operator will have an important impact on the number of defects identified and in the number of false calls.

4.2 Optimized Data Processing

In this section, an optimized step-by-step procedure for generating C-scan images using the LUIS data visualization software WinImag is demonstrated. The objective of this procedure is to maximize the contrast of features of interest in an inspected part. For this demonstration, the features are inclusions in an inspection standard. These inclusions simulate defects such as delaminations and foreign materials. This procedure assumes that the operator does not have any prior knowledge on the internal shape of the part and that the part was scanned for the first time. It is assumed that no prior ultrasonic image of the part is available for comparison. It should be noted that these conditions are not generally encountered in a production environment, but will allow demonstration of the normal procedure for tackling a new part with the LUIS data.

During daily operation in a depot environment, since the procedure to identify defects within a part would have been previously determined, such an extensive approach would not be needed. However, when a new part is inspected for the first time with the LUIS, this procedure must be used to determine the optimal conditions for defect detection. This procedure would, for example, determine the different gate position to allow the operator to find defects using the real-time image. The optimization procedure would also be very important if hardware signal processing such a broader bank of analog filter and an analog DAC is added to the LUIS. The procedure allows the operator to determine the parameters that must be used for a given part to optimize the real-time image produced by the LUIS.

This demonstration uses a part with some difficulties, namely a wide range of thickness throughout the part. The part does have a relatively good signal-to-noise ratio. The demonstration addresses, at the end of the section, the available signal processing tools to work in conditions of low to poor signal to noise ratio of the acquired waveforms. The part chosen is the F-22 ply-drop standard that is described in section 5.2.7. The file to be processed in this demonstration is file #0058d001 that corresponds to the inspection id 1421 in the LUIS system database for this contract. The part was scanned on the tool side that was covered with a thin layer of peelable paint prior to inspection with the LUIS, in order to enhance the generation and detection efficiency of the laser-ultrasonic system.

The first step when approaching the analysis of the data from an unknown part is to make two C-scan images (one time-of-flight C-scan image and one amplitude C-scan image) of the part. This is in order to get a quick understanding (“feel”) of the internal structure of the part. These images can be used to determine the thickest and thinnest sections of the part. To determine these section thicknesses, the operator could use the C-scan images produced during the acquisition of the data for the part (in this example the 0058d001.ga1 and 0058d001.ga2 files). Unfortunately, since the internal structure is generally unknown at the acquisition time, the selected C-scan gates used during the acquisition of the waveform may not render an appropriate image of the part. It should be noted that if the part’s internal structure is known or if the part has been analyzed previously, the appropriate gates and signal processing could have been setup and used during the acquisition

of the data. Then, the storage of the full waveform may not be needed.

Using the control A-scan window, the operator sets a quick gate (box) and “flips through” the waveform until fairly certain that the gate includes most of the back wall echo (ultrasonic reflection from the back wall of the part) throughout the part. The objective is to get a “quick and dirty” image of the part to determine, in the next step, the thickest and thinnest sections of the part. The gate can be adjusted using the cursor to control the position (width and height) of the gate. The gate can also be modified using the C-scan control menu prior to the calculation of the image. Two images are generally made: an amplitude C-scan, where the maximum amplitude of the waveform within the gate is color coded and mapped, and a time-of-flight C-scan, where the time of arrival of the maximum of the waveform within the gate is color coded and mapped. The figures 4.2-1 and 4.2-2 show respectively the amplitude and time-of-flight C-scan images obtained.

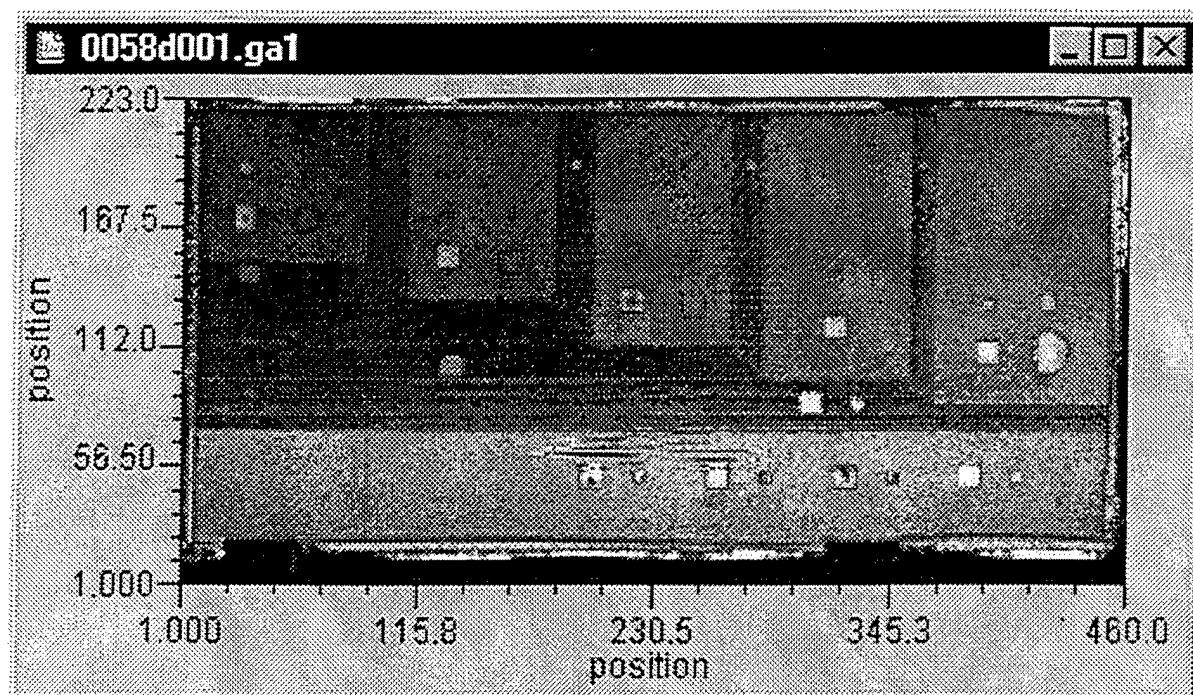


Figure 4.2-1. Example initial amplitude C-scan image

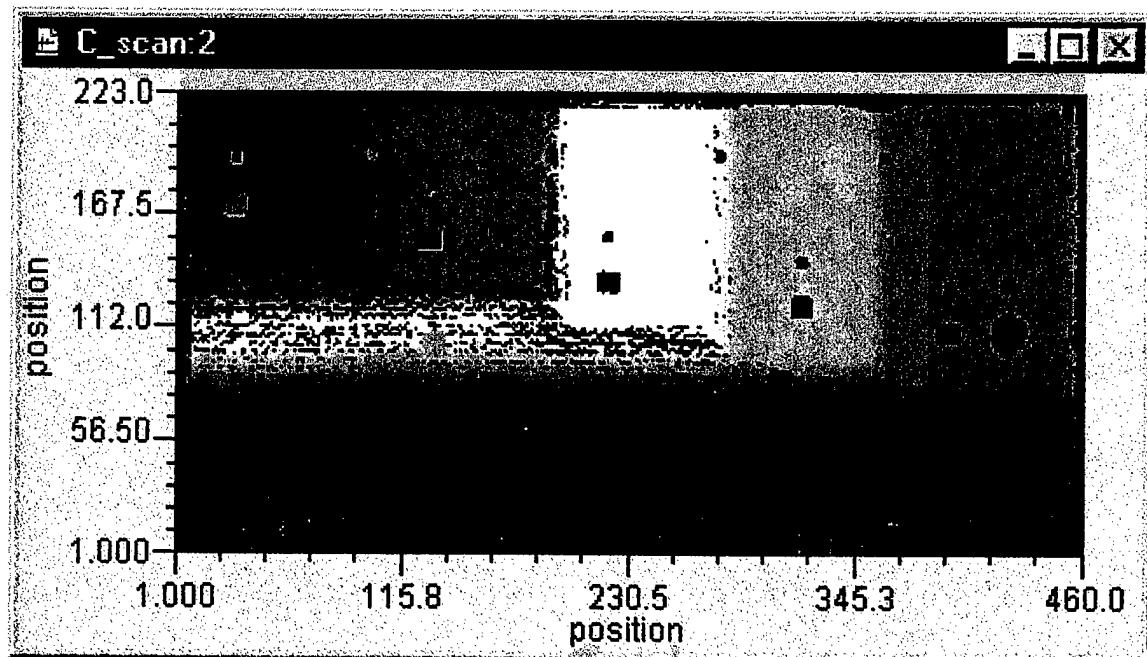


Figure 4.2-2. Example initial time-of-flight C-scan image

Using these two C-scan images, the operator can determine the thickest and thinnest sections of the part: the thickest section will appear in the amplitude C-scan image as darker areas and "blue" area in the time-of-flight C-scan, while the thinnest section will appear as lighter areas in the amplitude C-scan and "yellow" areas in the time-of-flight.

Notice that all of the figures shown in this section are captured directly from the screen display obtained with the WinImag software. Only the text appearing in the images has been added.

Using the cursor, the operator can view cross-sections through the part thickness using B-scans. Figure 4.2-3 and figure 4.2-4 show the B-scans along both horizontal and vertical axes. The thickest section of the part can then be clearly identified.

Using the cursor in one of the B-scan images, the operator can display in the control waveform window, a waveform from the thickest section of the part. The operator then sets the time gate (horizontal axis of the gate box) to include the full back wall echo, as can be seen in figure 4.2-5. The gate is also set to be as close as possible to the surface signal (large amplitude signal on the

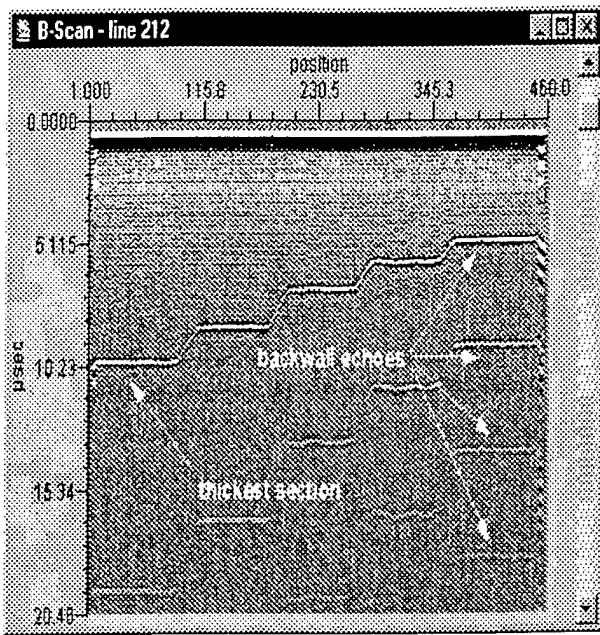


Figure 4.2-3. Example horizontal B-scan image

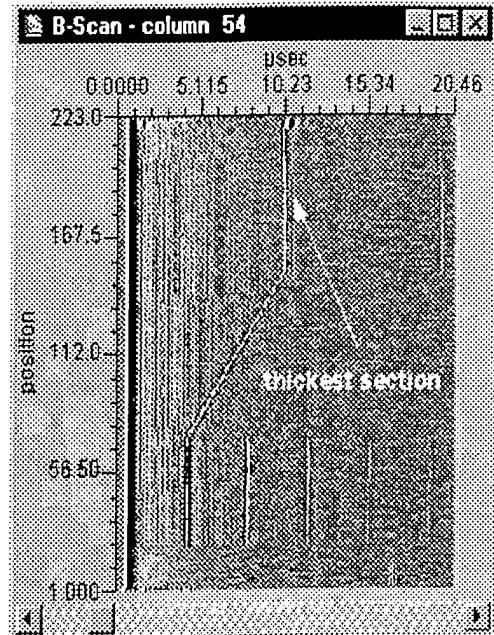


Figure 4.2-4. Example vertical B-scan image

left in figure 4.2-5). The surface signal is caused by the initial thermal expansion of the part's surface when the generation laser beam is absorbed. Notice that the surface signal does not hold any ultrasonic information of the bulk of the part but does indicate the start of the ultrasonic waveform, i.e., the surface of the part.

The height of the gate (maximum amplitude) is generally set to be full scale at this stage. This ensures that no saturation (strong white areas) in the amplitude image will be added by the gate extraction procedure. If the height of the gate is too high for the waveform collected, the operator will notice an overall gray image for the amplitude C-scan. Also, the image will have an overall low contrast for the different details in the image. To correct this, the operator would determine the areas of maximum amplitude of the waveform in the part by selecting, with the cursor, the area of brightest color (nearest to white) in the amplitude C-scan. Using this selected waveform, the operator could then reset the amplitude of the gate to match the maximum amplitude observed in the waveforms of the data file.

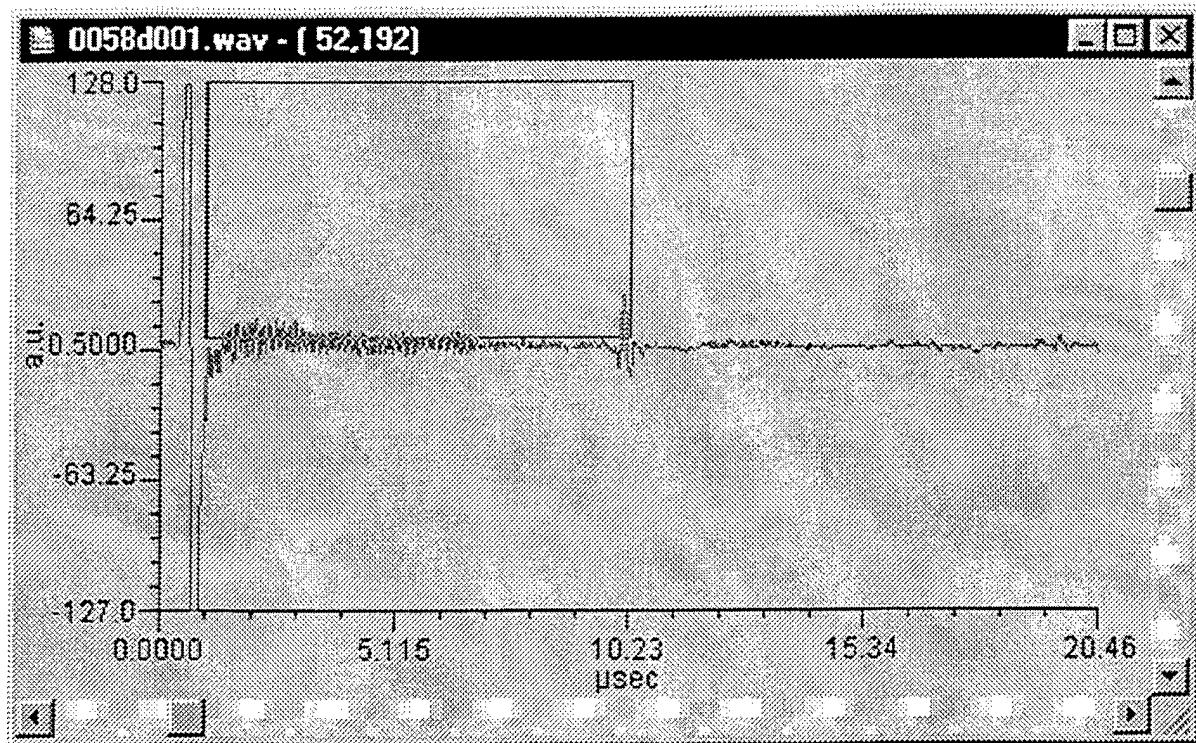


Figure 4.2-5. Waveform at thickest section of part

The bottom of the gate (minimum amplitude of the gate) is set to be slightly above the noise level in a typical waveform. The noise level can be determined by using the signal amplitude before the surface signal, i.e., before the laser generation of the ultrasounds. This will provide the level of background electronic noise. For highly scattering materials, the background signal level can be used to set the bottom threshold of the gate. By setting the bottom of the gate above the noise level, defects can be detected by observing the lack of back wall echo when the time gate is set near the time of arrival of the back wall echo. This is particularly important for time-of-flight C-scan images. If no ultrasonic echo is present within the gate and the bottom of the gate is set too low as to pick up noise, then the time-of-flight image will show an erroneous time of arrival (more or less random) for low amplitude back wall echoes. If the gate is set above the noise level and no echo is present within the gate, the time-of-flight C-scan image will display "black" pixels at these positions, as it should.

Notice that the previous procedure applies only for the production of maximum amplitude C-scan images. In some cases where the ultrasonic echoes are inverted, minimum amplitude C-scan

images are used and the same procedure is applied but with inverted values (e.g. set minimum of gate to full scale instead maximum of gate to full scale).

Notice, in figure 4.2-5, the presence of a high frequency signal near the surface signal. This signal is caused by the presence of a thin layer of paint on the surface of the sample. The signal is the ultrasonic reverberation of the paint layer. The paint layer was added to enhance the laser generation and detection efficiency of the part's surface. This signal does not contain any ultrasonic information on the bulk of the part and may impede the observation of inclusions within the part.

With the new gate shown in figure 4.2-5, there are now two new C-scan images shown in figures 4.2-6 and 4.2-7. Notice that, since the gate has been more appropriately set, there is a better dynamic range for the time-of-flight C-scan image.

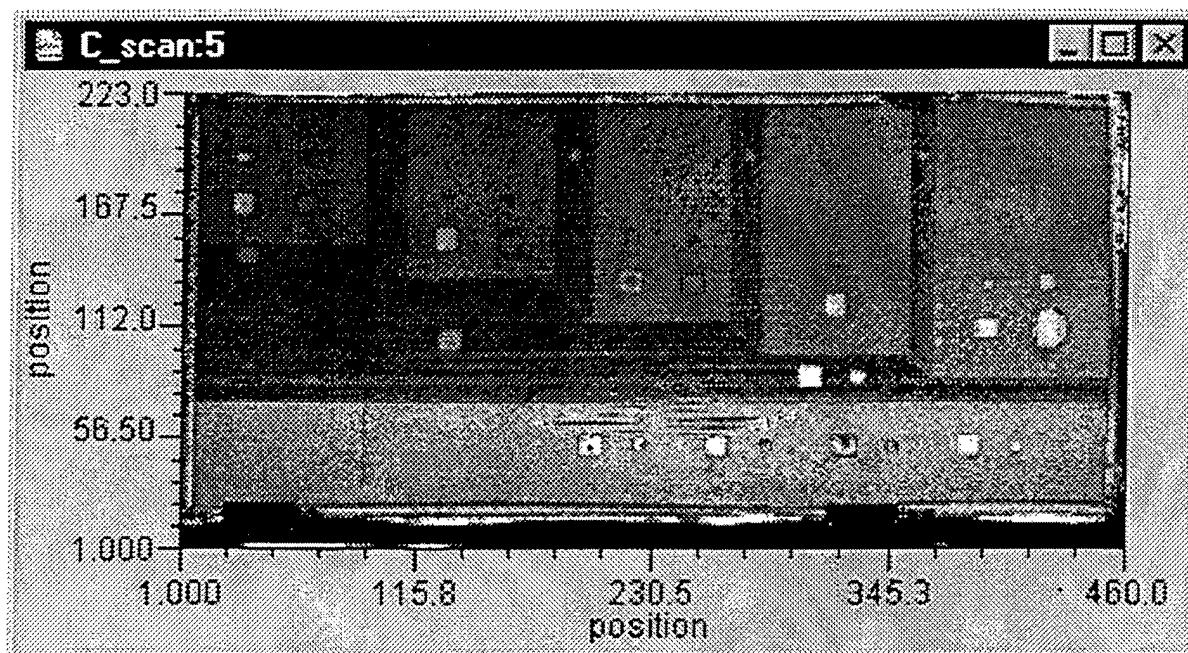


Figure 4.2-6. amplitude C-scan image

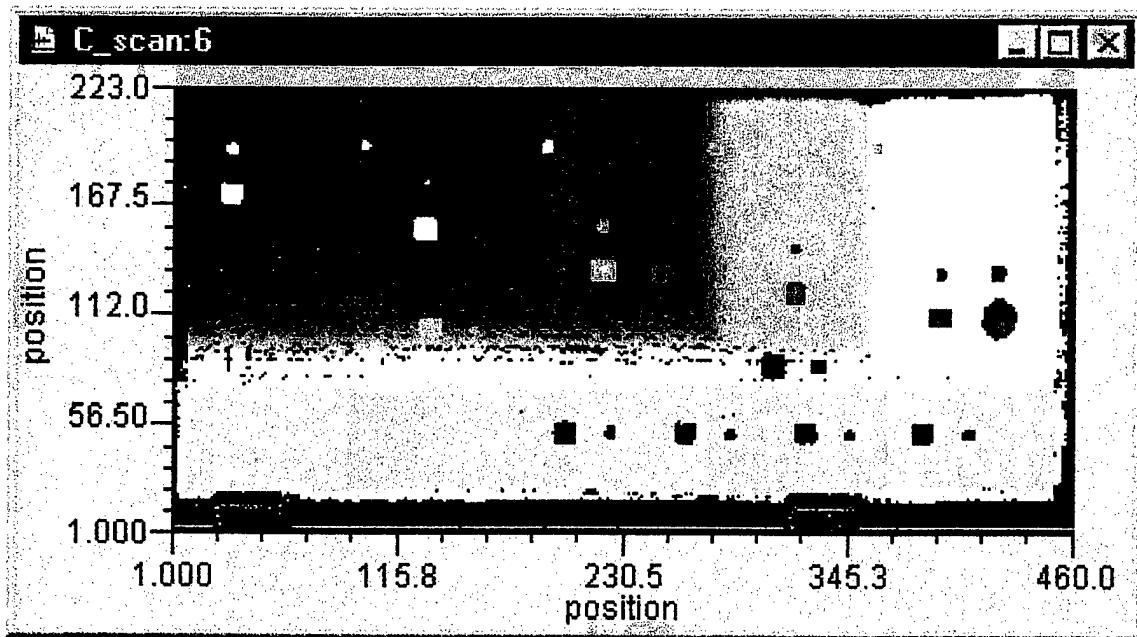


Figure 4.2-7. time-of-flight C-scan image

Note that, even at full scale, the amplitude of the C-scan image (gray scale image) is saturated. The saturation, shown as white pixels, occurs for inclusion defects near the surface of the part. The saturation occurred during the acquisition of the data, as shown in figure 4.2-9. Unfortunately, no signal processing can be used to retrieve the information lost by saturation. If the information is needed (e.g., for attenuation measurements), the part would have to be re-scanned with the LUIS with either lower generation laser power output or with a higher digitizer scale. Note that lowering the generation laser output power could reduce significantly the signal-to-noise of the acquired waveforms and could lead to difficulty in the detection of the ultrasonic echoes in the thickest sections of the part. Also, increasing the scale setting of the digitizer would reduce the sensitivity of the inspection. At this point, the operator would have to choose, given the objective of the inspection, between saturation of the signal at some points or reduced sensitivity. It should be noted that increasing the dynamic range of the LUIS' digitizer could eliminate much of this problem. Changing the digitizer from an 8 bit A/D to a 12 bit A/d would significantly increase the dynamic range of the system. The operator would then have access to both sensitivity and dynamic range.

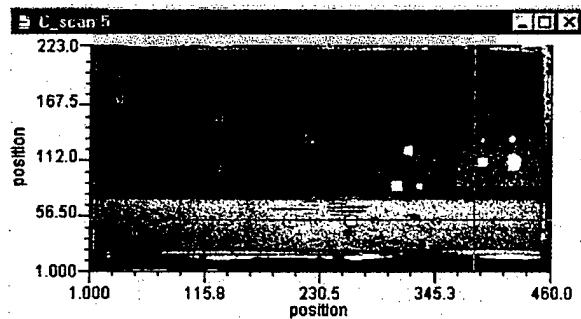


Figure 4.2-8. saturation in amplitude C-scan

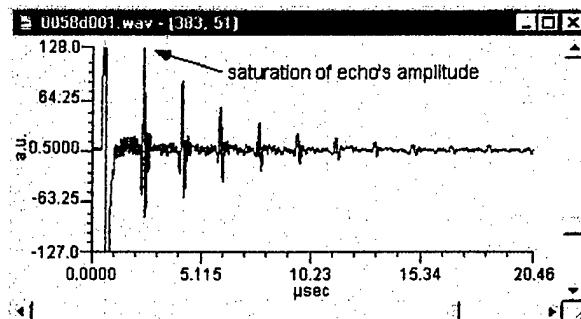


Figure 4.2-9. saturation in waveform

In the time-of-flight C-scan image there are some “black zones”. By using the cursor, the operator can identify that these zones correspond to inclusions near the surface of the part (see figure 4.2-10 and 4.2-11). The exact depth of the defect cannot be determined from the waveform since the arrival of the first echoes is lost in the initial surface signal, as can be seen in the B-scan of figure 4.2-12. Note however that the depth of the defect could still be determined using the frequency spectrum of the waveform. The surface signal causes a “dead zone” for which no ultrasonic echoes can be observed. For the near surface defects of the inspected part, the reverberation between the inclusions and the surface of the part is strong enough to be seen after this “dead zone”. It is difficult to reduce the “dead zone” with signal processing as it is caused by both the physical process of the surface signal and the electronic analog filters used during the acquisition of the waveform by the LUIS. To reduce its impact would require changes to the acquisition hardware of the present LUIS system. Other optical demodulators, such as the novel photorefractive device developed at the National Research Council of Canada, does not require as much electronic filtering and thus has a much more reduced “dead zone”.

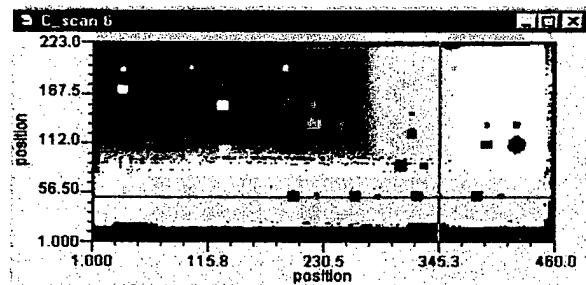


Figure 4.2-10. Near surface defect in TOF C-scan

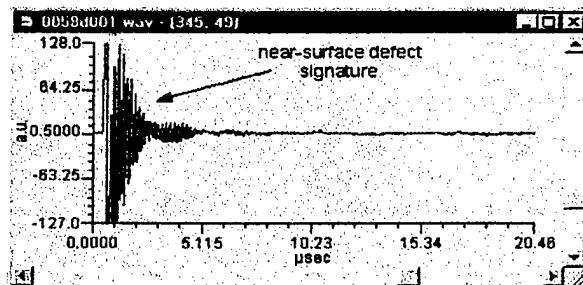


Figure 4.2-11. Waveform for near surface defect

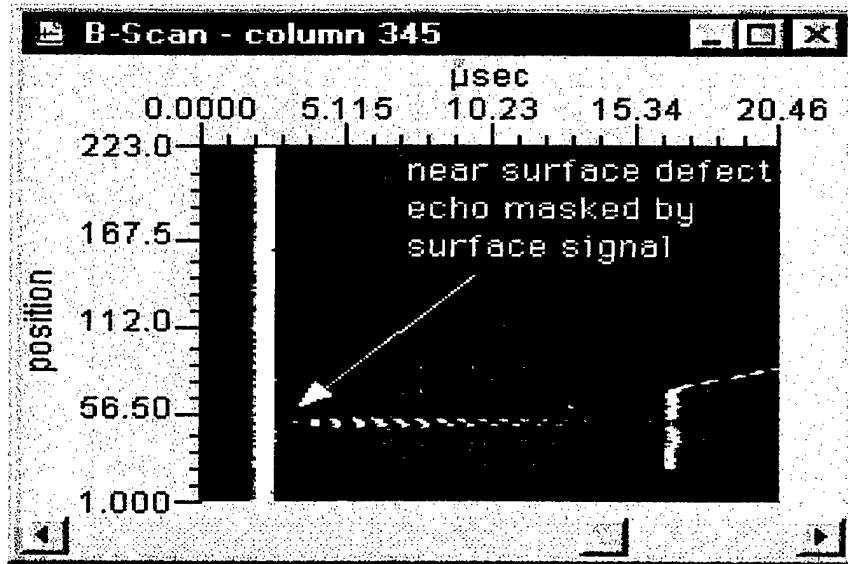


Figure 4.2-12. Near surface defect seen in vertical B-scan

In the time-of-flight C-scan image, “brownish” zones are visible that mark a distinct break from the slow color variation surrounding these zones (see cursor position in figure 4.2-13). These zones correspond to areas where the back wall echo has a lower amplitude than the signal from the paint layer, as can be seen in figure 4.2-14. Hence for these zones, the time-of-flight C-scan image records the time of arrival of the signal from the paint layer instead of the arrival of the back wall echoes. Some signal processing is needed to eliminate these artifacts in the C-scan image, since the ultrasonic information is available. The back wall echo can clearly be seen in figure 4.2-14, but is masked by the paint layer signal.

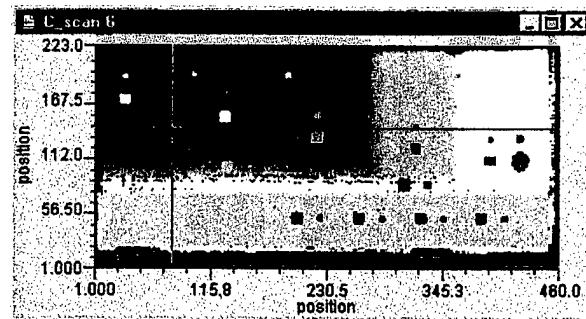


Figure 4.2-13. time-of-flight C-scan image

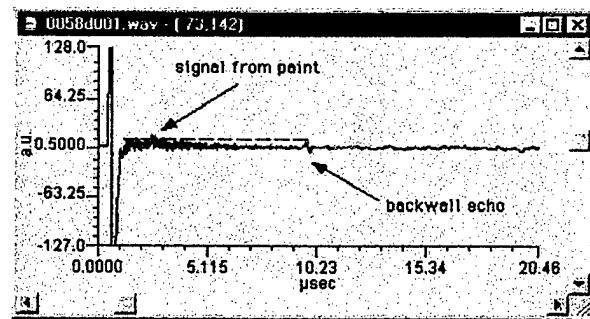


Figure 4.2-14. waveform at position marked by x-cursor in figure 4.2-13

The next step in the processing of the LUIS data is to do some numerical filtering. Filtering is generally needed for two reasons: first to eliminate low frequency fluctuation in the waveform caused by the detection laser, and second to eliminate high frequency noise, generally electronic noise.

Filtering may sometimes be needed to remove the low frequency fluctuation resulting from the slow variation in the amplitude of the pulse detection laser. Filtering may also be needed to remove high frequency noise, which can originate from the environment. The environment at McClellan AFB has not been shown to produce a lot of such high frequency noise. However, the use of a thin paint layer to enhance the generation and detection efficiencies of the LUIS may create, depending on the layer's thickness, a high frequency signal due to the "ringing" of the ultrasound in the paint's layer. A typical waveform and its corresponding power spectrum for a painted surface are shown in figures 4.2-15 and 4.2-16. The sharp spike near 5.5 MHz is caused by the presence of the paint. This signal can produce errors in the time-of-flight C-scan images obtained.

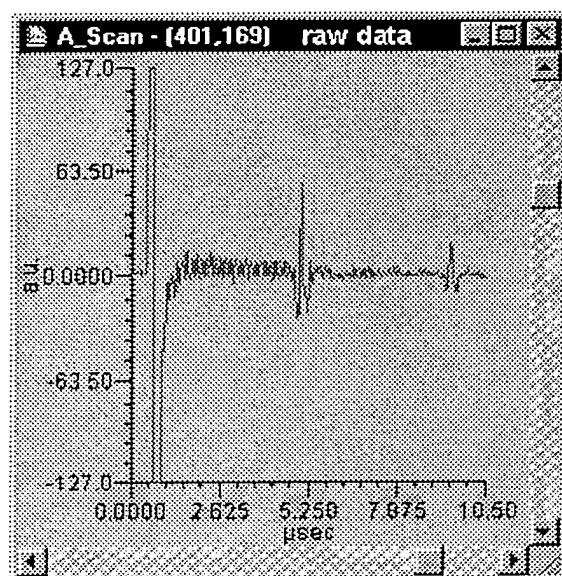


Figure 4.2-15 -Waveform with ringing from paint layer

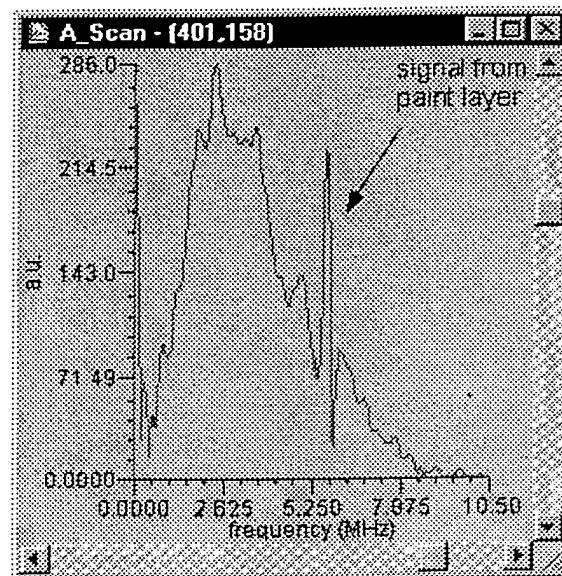


Figure 4.2-16 -Power spectrum of waveform in figure 4.2-14

Generally, a band pass filter is used for processing the waveform. The low pass cut-off frequency is chosen as to be as high as possible in order to conserve the largest possible bandwidth (and hence the maximum depth resolution), while still eliminating the paint “ringing” in the waveform. The results of a low pass filter with a low cut-off frequency of 5 MHz is shown in figure 4.2-17.

When using a low pass filter only (i.e., band-pass filter with high pass cut-off at 0 MHz), the lower frequency fluctuation appears as a non-flat baseline in the waveform. A flat baseline in the waveform allows for a better dynamic range in the amplitude since the bottom of the gate can be set at its lowest level. A flat baseline may also be needed for attenuation measurement, such as for porosity detection. These low frequency fluctuation can also cause the same kind of “marking” problems as do the “ringing” signal from the paint layer in the time-of-flight C-scan images. To eliminate these fluctuation, a band pass filter is used with a typical high-pass cut-off frequency of 500 kHz to 1Mhz, depending on the level of fluctuations. Note that using a sharp band pass filter, i.e. a low value of cut-off slope such as 1 MHz^{-1} , will increase the size of the “dead zone” by producing a sharp rise or “bump” in the waveform near the surface signal, as can be seen in figure 4.2-18. This bump is the tail section of the surface signal. To reduce this impact, a high value of cut-off slope, typical 3 MHz^{-1} , is used instead. The resulting waveform, shown in figure 4.2-19, has a flat baseline, no ringing signal from the paint, and a “dead zone” nearly equal to the un-filtered “dead zone”.

Although it may be time consuming, it is a good practice to make new C-scan images, both amplitude and time-of-flight, with the same gate after each addition of a new signal processing step, in order to see the enhancement (if any) in the images obtained. The new C-scan images are shown in figure 4.2-20 and 4.2-21. The new amplitude C-scan image does not have major changes as compared to the earlier image (figure 4.2-12) but some defects in the slope of the thickest section are clearly more visible. The net gain by the filtering can be seen in the time-of-flight C-scan image. The zone of erroneous time of arrival (“brownish” zone) have been significantly reduced. The next step in the signal processing procedure is to correct for the ultrasonic attenuation of the material of the part. This is particularly useful for a part, such as this one, which has varying thickness. The process of correcting for attenuation, called distance amplitude

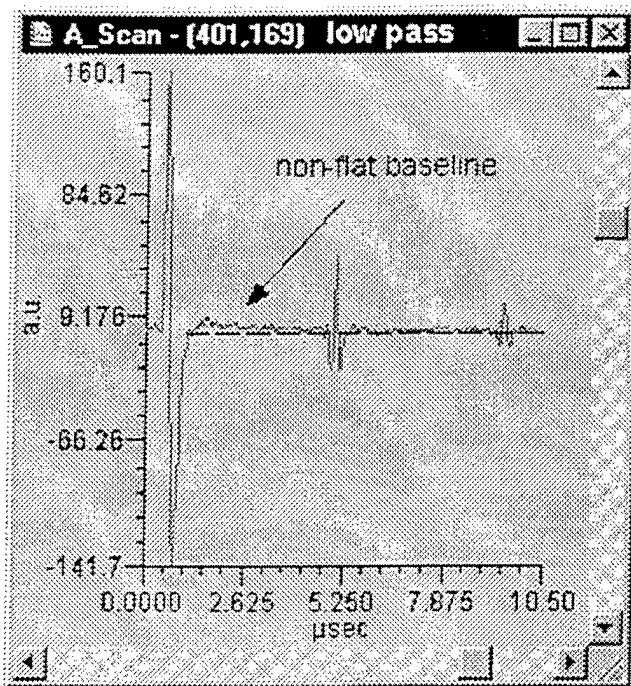


Figure 4.2-17. Waveform with non-flat baseline

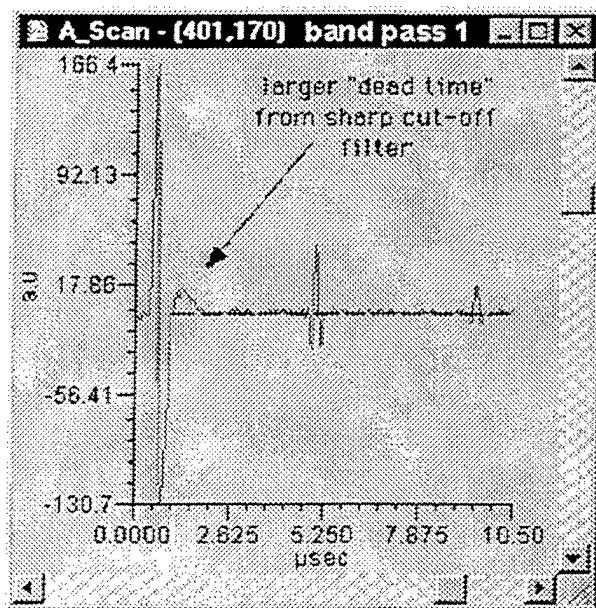


Figure 4.2-18. Waveform filtered with sharp cut-off

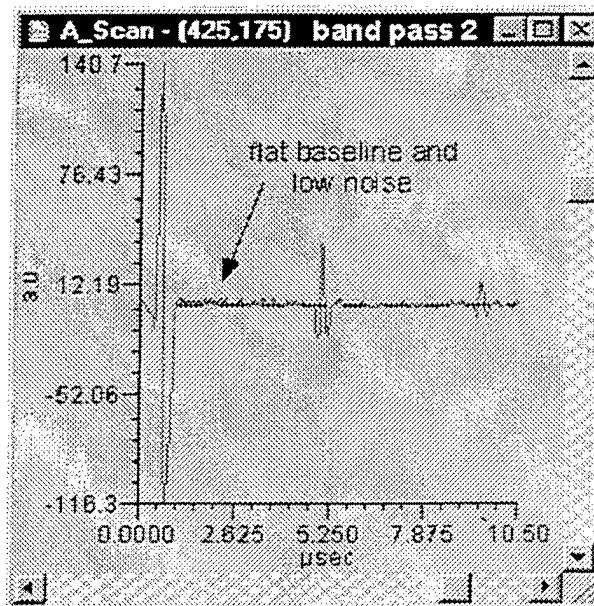


Figure 4.2-19. Waveform filtered with slow cut-off

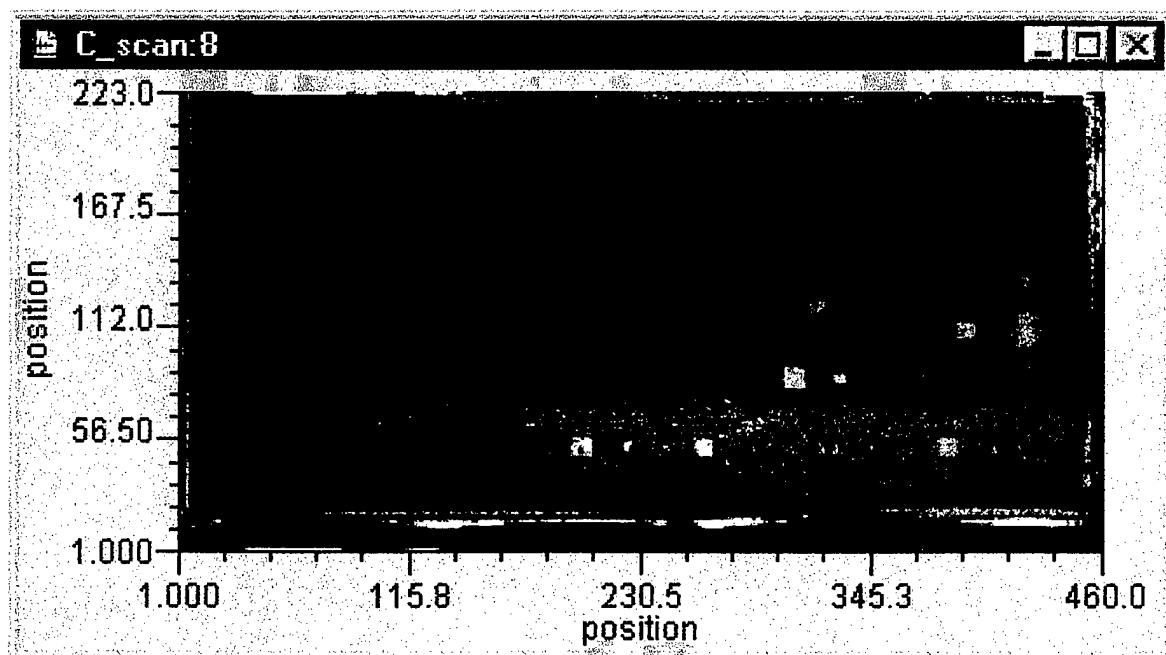


Figure 4.2-20. Amplitude C-scan image after filtering

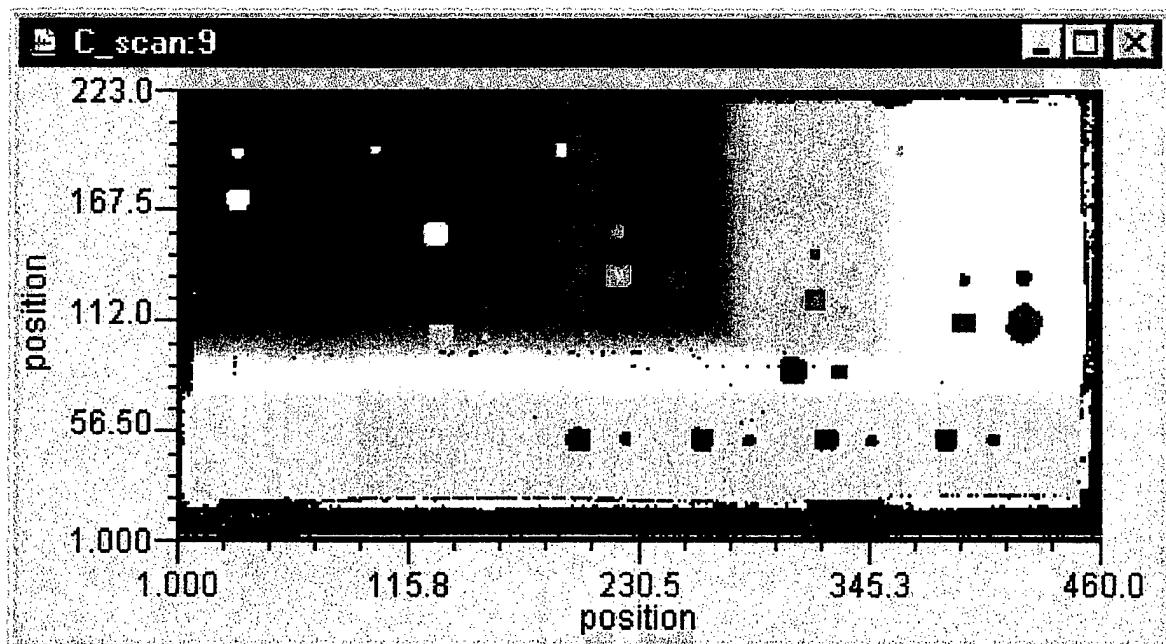


Figure 4.2-21. Time-of-flight C-scan image after filtering

correction (DAC), is done by multiplying the waveform by an inverse exponential function whose parameters are set by the operator. The objective is to find the values corresponding to the exponential decay observed in the waveform (see figure 4.2-22) in order to remove this

attenuation from the waveform. The DAC is set with two values: the start position of the correction function and the maximum amplification scale at the end of the waveform. Notice that this approach in parameters allows the use of exponential, linear or parabolic type functions for corrections (all three are available with the imaging software). The start point is generally set at the beginning of the gate, since there is no point in correcting the data outside of the gate. The maximum scaling factor is adjusted to have the multiple echoes from the back wall having nearly the same amplitude once corrected. Notice that the parameters are adjusted to have a slight residual linear decrease in the amplitude of the multiple echoes, as shown in figure 4.2-23. The residual decrease is left so that the gate selects the first echo of the series for the mapping of the time-of-flight C-scan images. The objective of the DAC correction is not to totally eliminate the effect of attenuation but to increase the contrast in the detection of defect in the thickest section of the part.

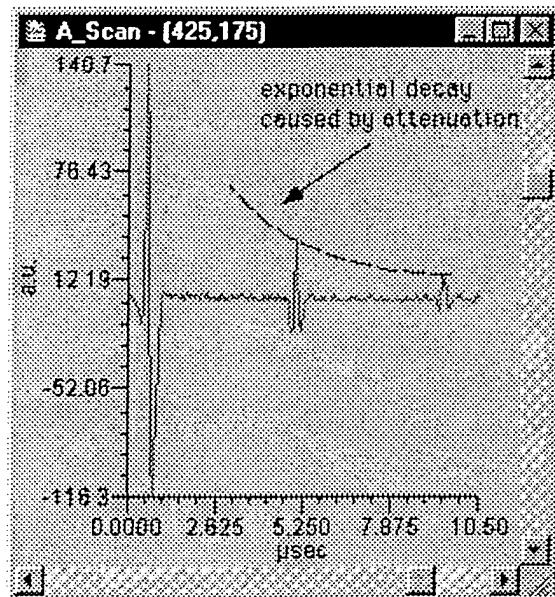


Figure 4.2-22. Exponential decay in waveform

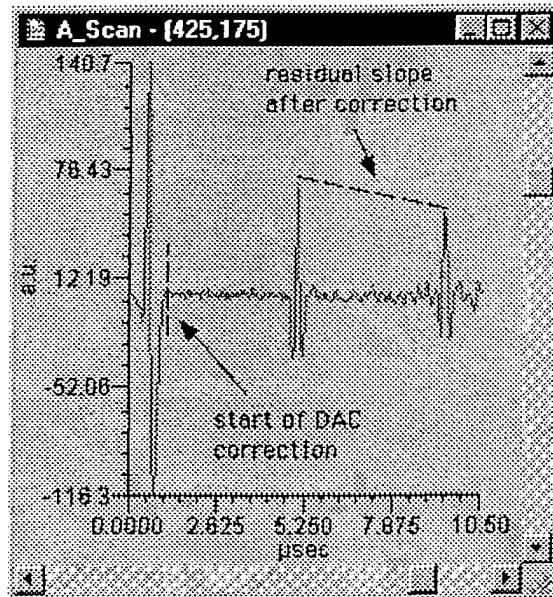


Figure 4.2-23. Correction of waveform with numerical DAC

The next step in the signal processing is to normalize the waveform. The LUIS generation and detection lasers are both pulsed lasers that have some shot-to-shot variation in the output power. These shot-to-shot variations can lead to variations in the amplitude of the generated and detected

ultrasonic signal. Also, surface variation such as point-to-point changes in surface finish or in paint thickness, can cause the same type of variations in the amplitude of the acquired waveform. A simple method to correct some of the variations is to use the amplitude of the surface signal as a reference value. The imaging software allows the operator to “re-scale” each waveform so that the amplitude inside a given gate, generally around the surface signal, as a set value given by the operator. This approach is a crude method to correct for the point-to-point variation and does not take into account the possible saturation of the surface signal. It has been shown to be useful, however, particularly for V-shaped parts.

The results of the DAC correction and normalization are shown in figure 4.2-24 and 4.2-25. The new time-of-flight C-scan image is almost completely void of “brownish” zones. Also, the different steps of the parts shown in the amplitude C-scan images now have the same background intensity. The angled sections, however, still do have a darker background. For these sections, the attenuation in the amplitude of the waveform is caused by the lack of reflection of the ultrasonic echo to the surface of the part, where the signal is acquired. Since the back wall is at an angle,

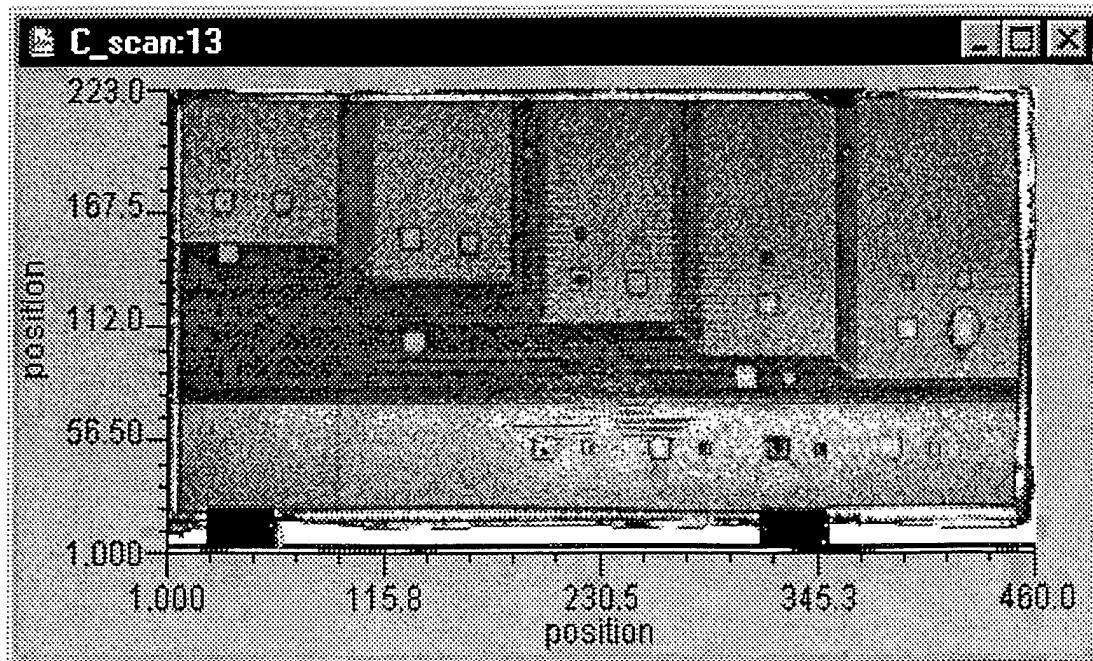


Figure 4.2-24. Amplitude C-scan image after filtering, DAC correction and normalization

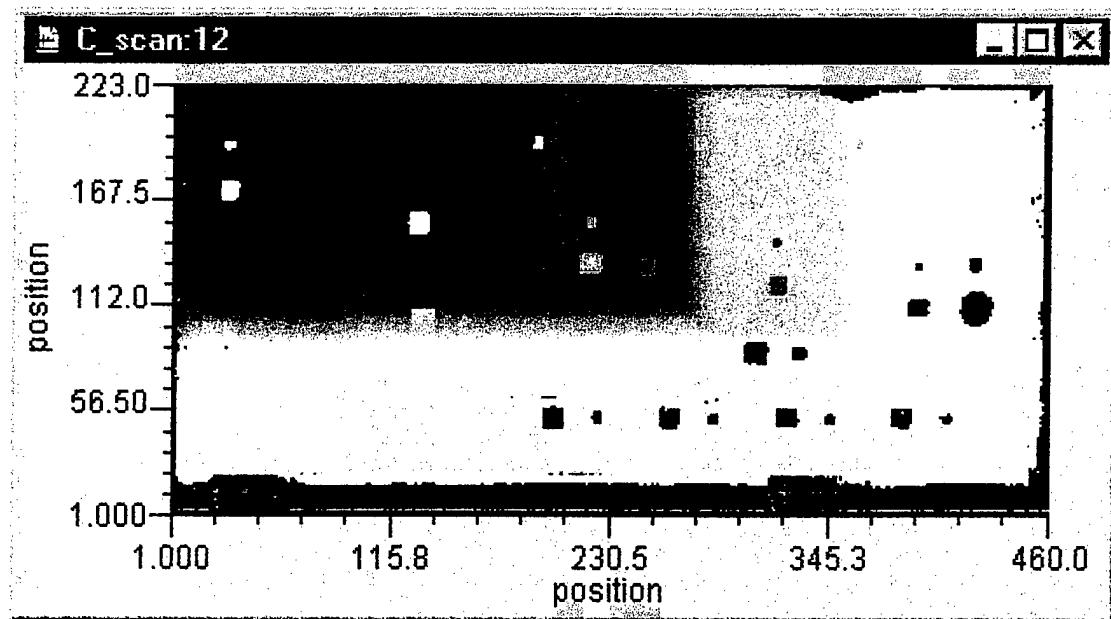


Figure 4.2-25. TOF C-scan image after filtering, DAC correction and normalization

with respect to the surface, most of the ultrasonic energy is also deflected at an angle, away from the detection position. Hence, the amplitude of the back wall echo is significantly reduced. In most cases, the signal processing procedure would end at this point. In the majority of the images produced in the study, only these three steps were used, i.e. band-pass filtering, DAC correction and normalization. Unfortunately, even with the signal processing, some inclusions can only be clearly seen on the B-scan images, not on the C-scan images. For example, some of the inclusions in the angled sections of the part only show up in the C-scan images as faint variation in the amplitude C-scans. However, these same inclusions can clearly be detected in the B-scan, both in the bulk of the material, as can be seen in figure 4.2-27, and near the back surface of the angled part, as can be seen in figure 4.2-28.

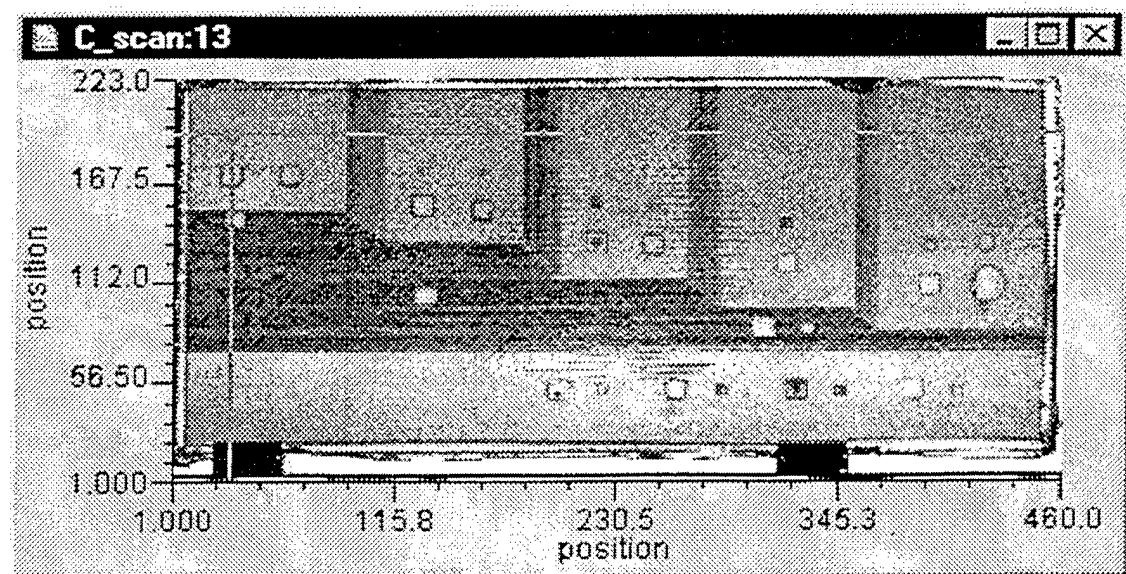


Figure 4.2-26. Position of cross-section for B-scan views

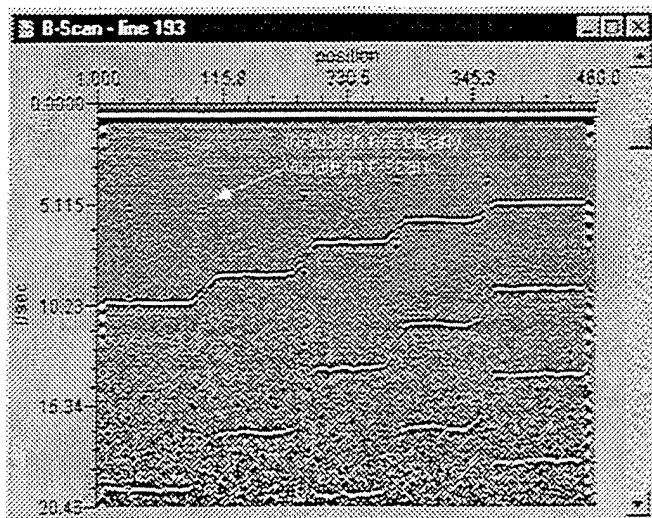


Figure 4.2-27. Horizontal B-scan

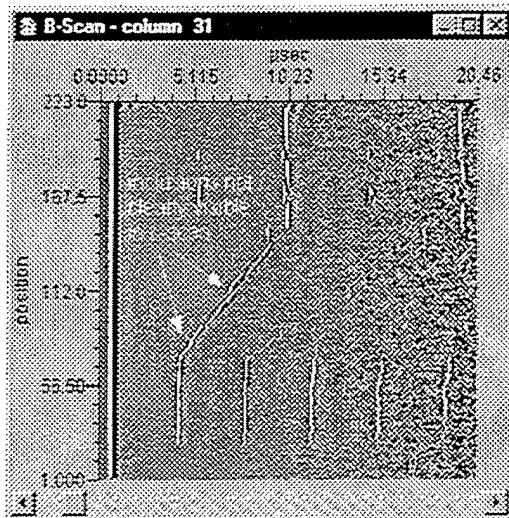


Figure 4.2-28. Vertical B-scan

Finally, when the initial signal-to-noise ratio is low, spatial averaging can be used. The imaging software allows the operator to calculate, at each position in the map, the average value of the waveforms of the N nearest neighbor to the selected position. This is particularly useful for thick samples where the signal to noise ratio is known to be low. Figure 4.2-29 and 4.2-30 shows the same waveform before and after spatial averaging. By adding the waveforms for the N nearest

neighbors, the signal-to-noise is generally increased by a factor of $(N+1)^{1/2}$. The procedure is highly efficient but reduces the spatial resolution and significantly increases the time to produce an image, in particular if numerical filtering is used. The procedure would be more efficient if such spatial averaging would be possible during the acquisition of the data. Typically, for an average size scan (250 MB of data), using spatial averaging will increase the processing time by a factor of 60, from 2 minutes to 2 hours !

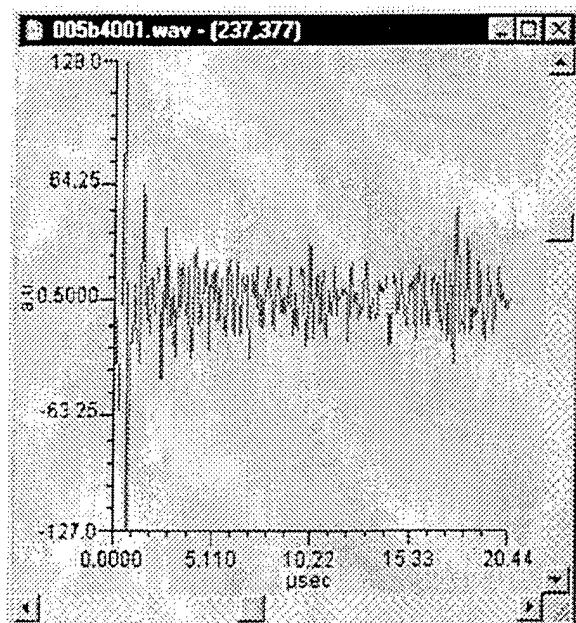


Figure 4.2-29. Typical waveform from thick sample (A6 near/far test sample)

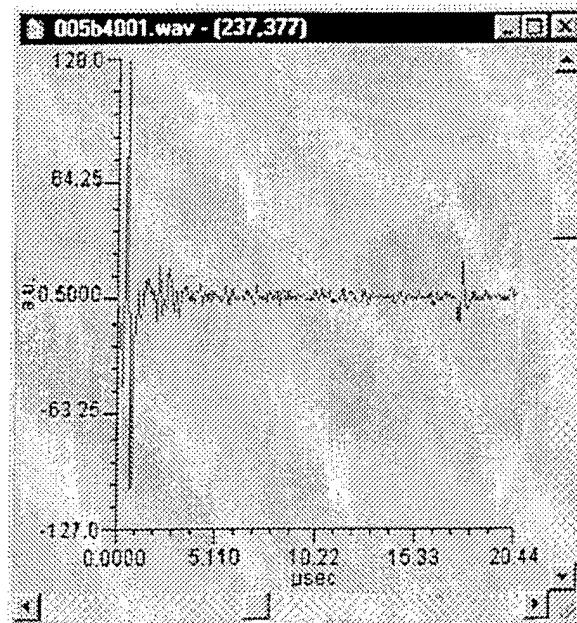


Figure 4.2-30. Waveform from thick sample after spatial averaging (A6 near/far test sample)

5.0 ANALYSIS OF PARTS DATA

This section contains data from LUIS inspection of various parts. In cases where it was possible to generate conventional data for comparison, the conventional data are presented. Some of the parts inspected with the LUIS are not inspectable by any conventional method and no comparisons are possible.

5.1 Commercial Aircraft Composite Parts

The parts shown in this section were borrowed from Boeing Commercial Airplane Group. Many of the conventional ultrasonic images shown in comparison were developed on production hardware like that shown in Figure 1-1. Such inspection systems have been optimized for high volume production applications at the lowest possible hardware cost.

5.1.1 Graphite Composite Skin Panel Standard -1-A

This is the thinnest (9 to 22 plies) of three standards prepared to represent the materials and ply stacking sequences in the empennage skin panels of the 777. A drawing of this panel may be found in Figure 5.1.1-1 and a photograph is shown in Figure 5.1.1-2. Inserts prepared from three different foreign materials were placed in these standards. The inserts were brass foil (0.001" thick), Release ply F, and a tape. The brass foils were easy to detect. The Release ply F was moderately difficult to find and the tape was more challenging to detect, particularly at greater depths or when it was in or adjacent to a bond line. The brass inserts were placed in the upper third of the panel. Release ply F inserts were placed in the middle section and tape in the lower third. The sizes of the inserts were either 0.25" x 0.25" or 0.5" x 0.5" for the brass or tape. The Release ply F inserts were 0.7" x 0.7". Sections of I-stiffeners were cobonded to the laminate at two locations. Trimming of both of the upper and lower panel edges caused inserts to be located adjacent to all of the outer laminate edges. As the brass inserts are rather easily detected, the indications from the tape and Release ply F inserts are a better test of the relative sensitivity of the conventional and LUIS tests.

NOTES:

1. THIS IS NOT A CONTROLLED
2. BREAK ALL SHARP EDGES AND CORNERS EXCEPT
3. TOLERANCE: DECIMAL: .XX= .
.XX= .
ANGULAR = .5
4. MATERIAL IS BMS 8-276 TAPE / BMS 8-245 GRADE 05 (FOR BONDING OF
5. SPACING BETWEEN THE INSERTS IS
6. TEXT NEAR INSERT DENOTES ITS PLY
THE TOOLSIDE SURFACE.
= BRASS FOIL INSERT
= TAPE AB-6782 INSERT
= RELEASE PLY F INSERT
7. AFTER TRIM, ALL EXPOSED INSERT EDGES MUST
8. PROCESS PER BAC 5578 PSD 6-4 (150 PSI CURE
9. USE OF EXISTING STRINGER EXCESS IS
HOWEVER, NO INDICATION GREATER
ATTENUATION IS
(1.5dB PER BAC 5980 PSD 6-6

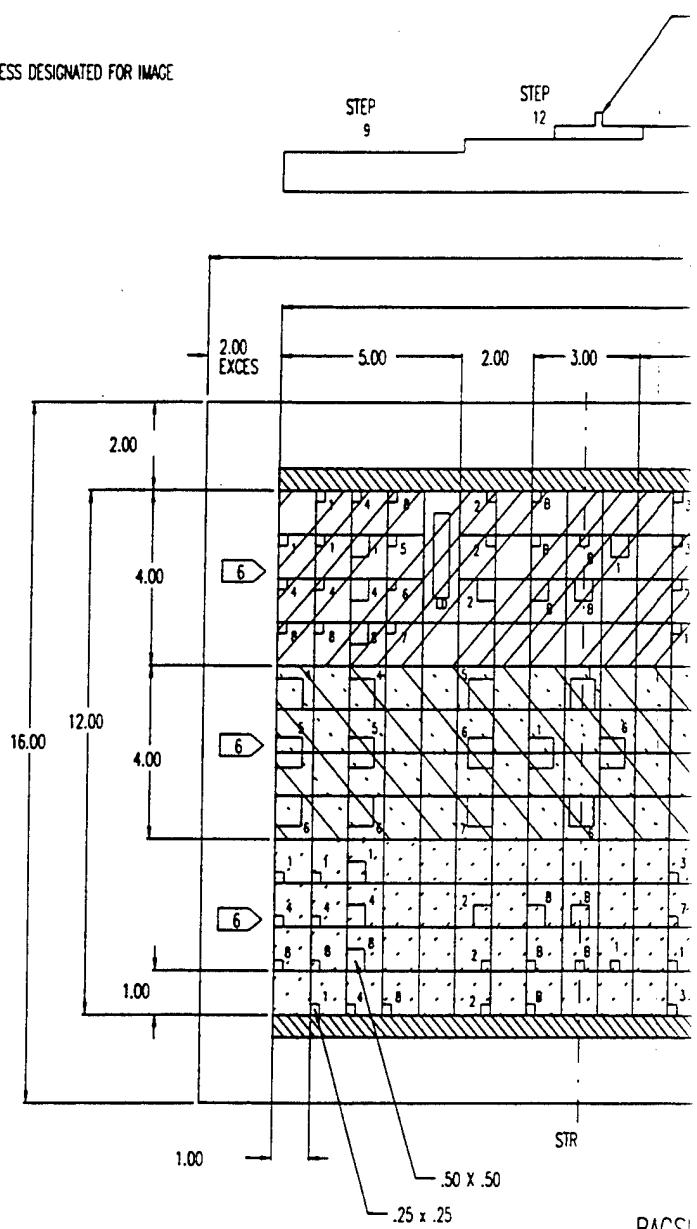
PLY TABLES

| PLY | DIRECTION |
|-----|-----------|
| 1 | 0 |
| 2 | +45 |
| 3 | -45 |
| 4 | 90 |
| 5 | 0 |
| 6 | 90 |
| 7 | -45 |
| 8 | +45 |
| 9 | 0 |
| 10 | -45 |
| 11 | +45 |
| 12 | 0 |
| 13 | -45 |
| 14 | +45 |
| 15 | 0 |
| 16 | -45 |
| 17 | +45 |
| 18 | 0 |
| 19 | 90 |
| 20 | -45 |
| 21 | +45 |
| 22 | 0 |

10. PLY BY PLY COMPACTION IS
(MINIMUM OF 1 MINUTE AT 25° TO
11. STIFFENER WEB TO BE .25" TO .50" HIGH
RADIUS ON WEB
12. ALPHA DESIGNATOR SHALL BE ASSIGNED FOR
NO CURRENT OR FUTURE STANDARD FABRICATED PER
WILL DUPLICATE THE ALPHA

TOTAL # OF

 = EXCESS DESIGNATED FOR IMAGE



| | |
|---------|--------|
| TOLERAN | 5 |
| SCALE: | BOEING |

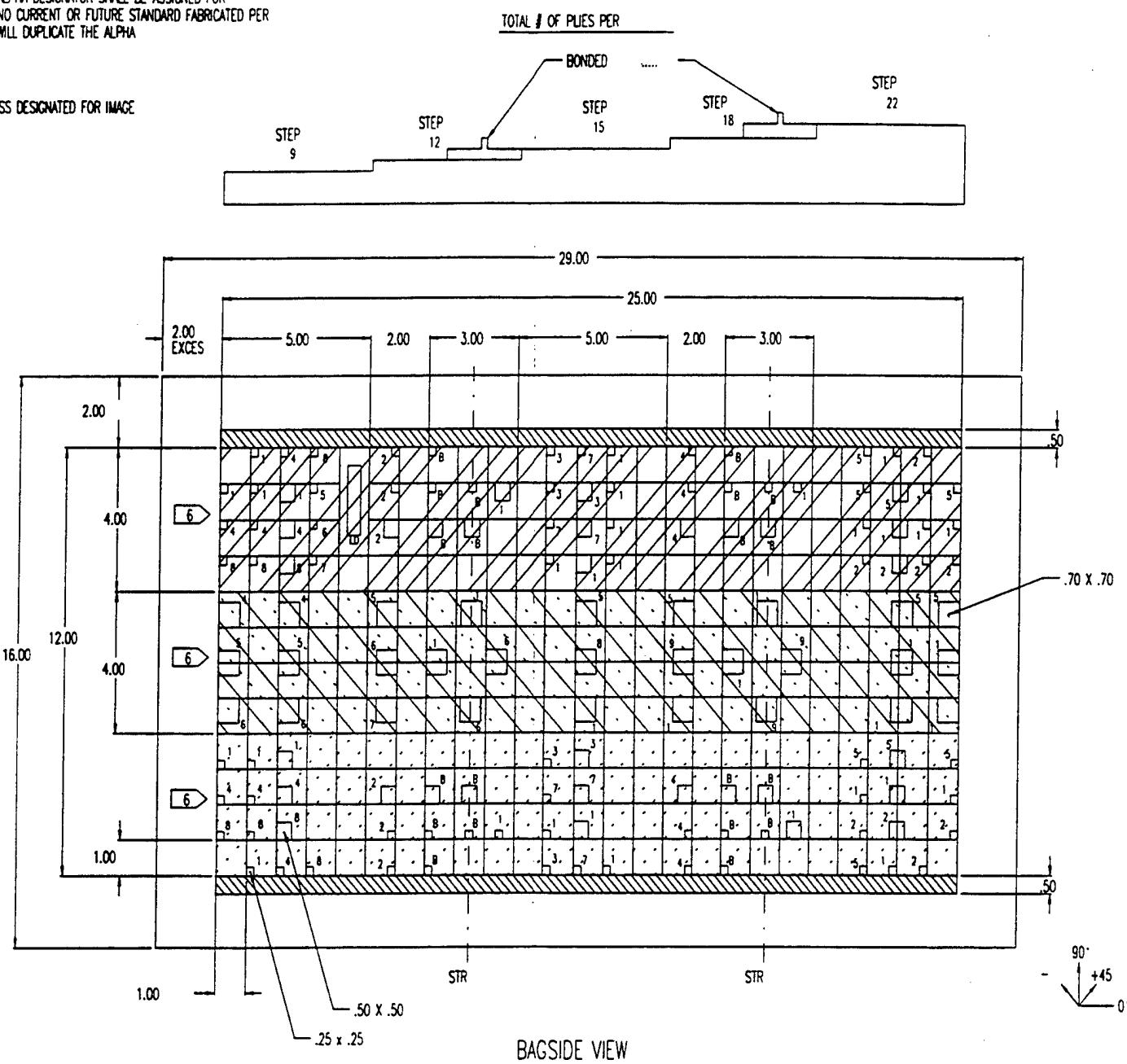
Figure 5.1.1-1 Skin Panel Standard 1-A

PLY BY PLY COMPACTION IS
(MINIMUM OF 1 MINUTE AT 25° TO

STIFFENER WEB TO BE .25" TO .50" HIGH
RADIUS ON WEB

> ALPHA DESIGNATOR SHALL BE ASSIGNED FOR
NO CURRENT OR FUTURE STANDARD FABRICATED PER
WILL DUPLICATE THE ALPHA

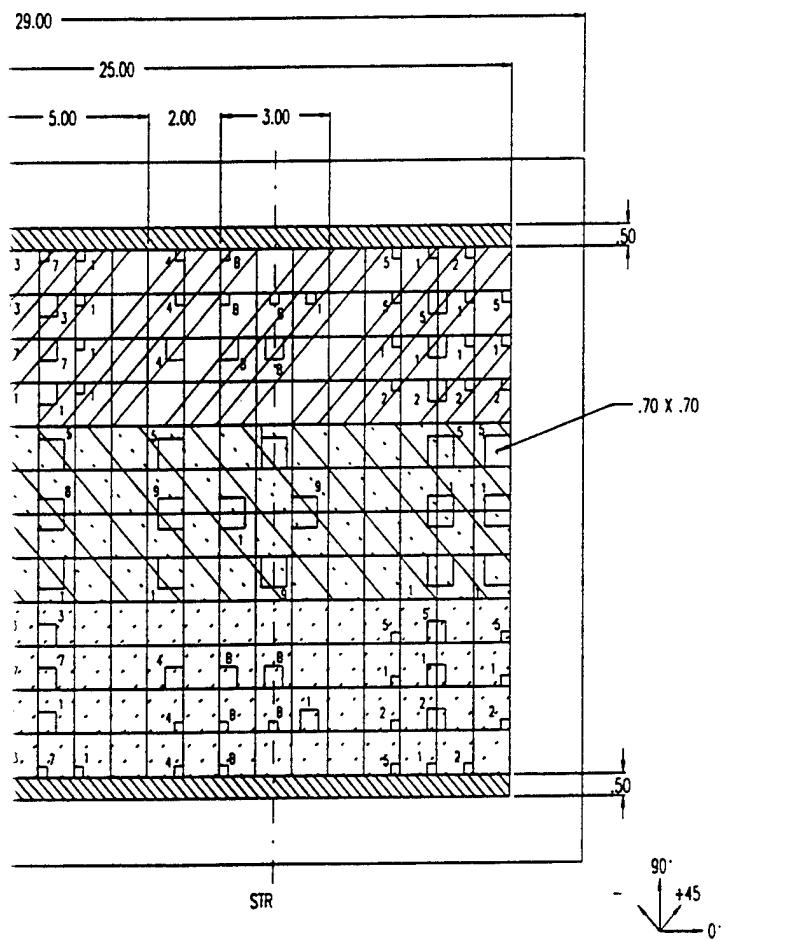
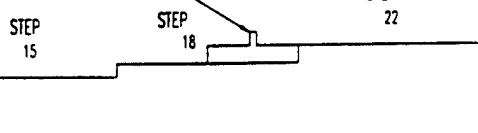
CESS DESIGNATED FOR IMAGE



| | | | | | | |
|--------------|--------|--|--|----------|---------|--------------|
| TOLERAN 5 | BOEING | DAT 12-7- C.MARE CHK. STICKNE ENGR | TITL 777-30- 12 STANDARD STEP BLOCK | SIZ D | SH 1 | 1 OF 1 |
| SCALE: | | | | | NO. | SK77730 |

F PLIES PER

- BONDED



SIDE VIEW

| | DAT | TITL | SLZ | SH | 1 |
|-------------|------|---------------------|-----|-----|--------|
| DWN C.MARE | 12-7 | 777-30- 12 | | 1 | OF 1 |
| CHK STICKNE | | | | | |
| ENGR | | STANDARD STEP BLOCK | D | NO. | SK7773 |

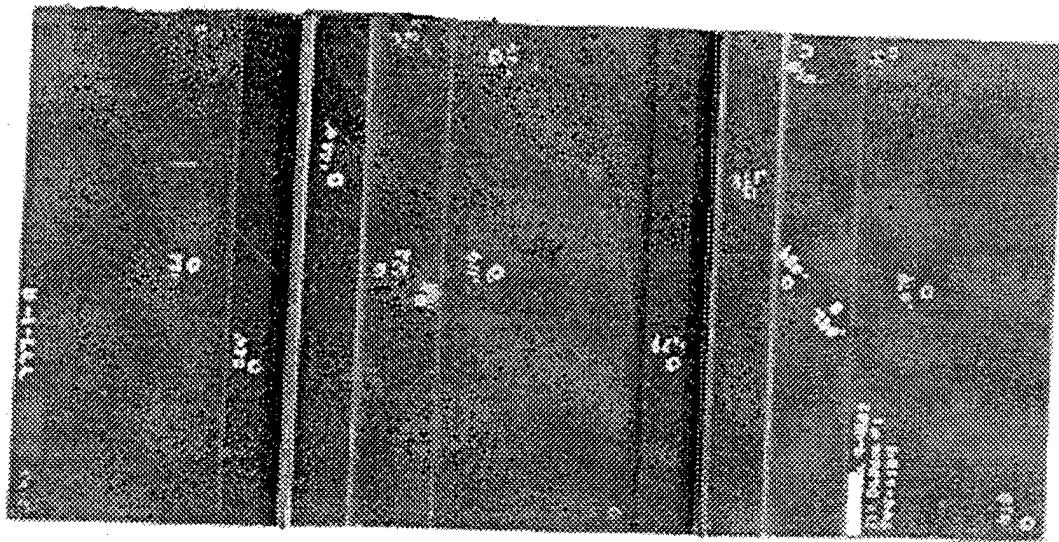


Figure 5.1.1-2. Photograph of standard 777-1-A

Conventional Test Results

The skins were scanned with a 3.5 MHz focused transducer mounted in a bubbler which traveled on the tool-side surface of the standard. The test frequency was selected based upon measurements on a variety of foreign materials placed at different depths in several test parts. Detection and correct sizing of foreign materials was required throughout complex parts which varied in thickness from about 0.1" to nearly 1.0." The standards were scanned parallel to the stringers as this was the direction to be used for the full-scale skin panels. The data sampling interval was 0.080" and the index increment was 0.120." The somewhat coarse data sampling, particularly in the index direction, was chosen to help meet the inspection rate requirements of 42 skin panels per month.

A peak amplitude image of the pulse echo data from standard 1-A is shown in Figure 5.1.1-3. The simultaneously collected time of flight (TOF) image is shown in Figure 5.1.1-5. The bubbler allowed scanning to within approximately 0.5" of each of the edges of the standard. The smaller inserts at the left and right edges as well as those at the top and bottom edges of the drawings are thus not detectable by the bubbler technique. For production inspection of these parts a separate edge scan is used to cover the outer 2" of the parts. This ensures overlap with the automated

bubbler scan which travels to within 1" of the outer trim border of the parts. The brass inserts in the upper third of the standard are effective reflectors, and they often result in stronger echoes than the back surface echoes at each thickness. This produces the light colored indications seen with many of the brass inserts in the upper third of the panel. The majority of the Release ply F inserts in the middle portion of the panel were seen easily. The Release ply F inserts two plies below the bond line of the stiffener in the 12 ply region were faintly visible in both the amplitude and time of flight images. The Release ply F inserts two plies below the bond line in the 18 ply region were detectable, but less obvious. Additional high resolution TOF images of this data clearly showed the Release ply F inserts two plies from the two bond lines. The tape inserts at both stiffener bond lines were not detected.

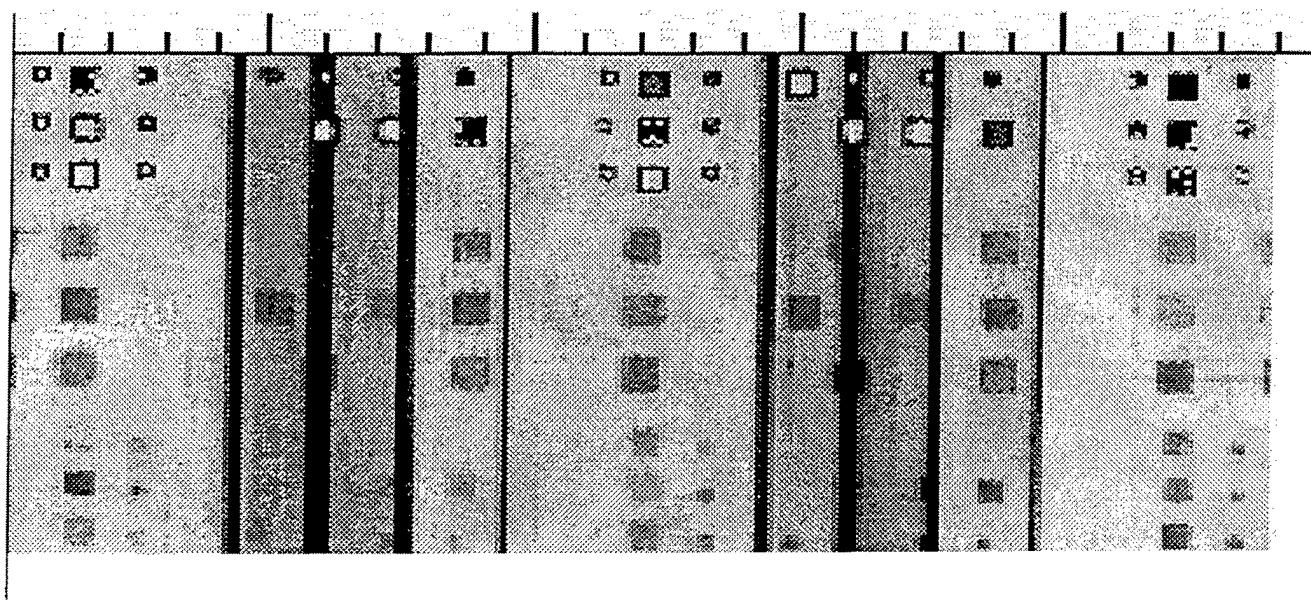
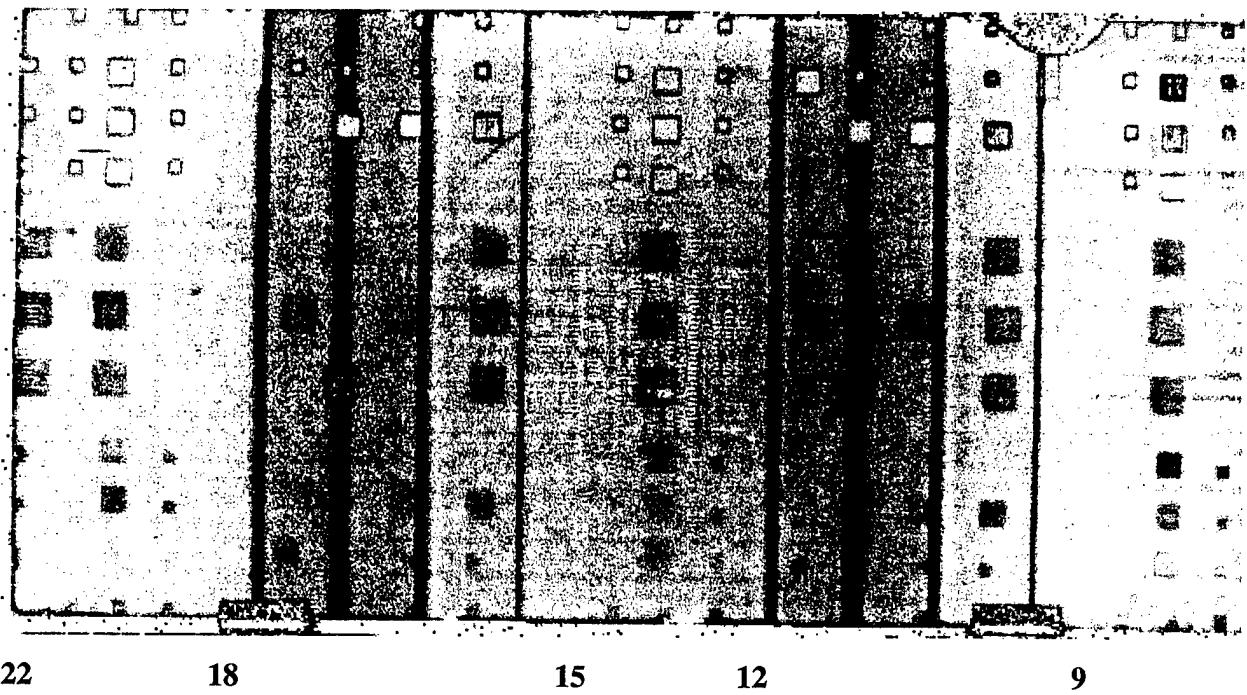
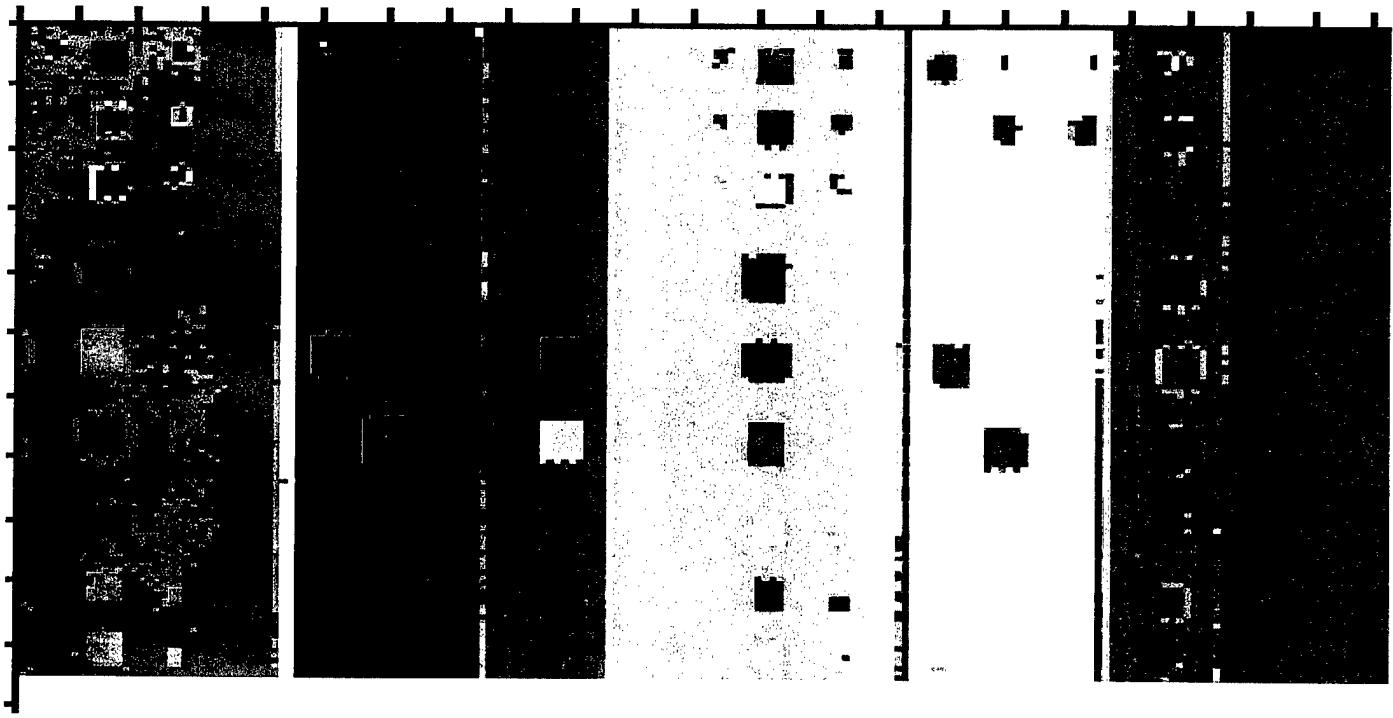


Figure 5.1.1-3. 3.5 MHz Bubbler peak amplitude pulse echo image of standard 1-A. Tool-side scan.



Plies 22 18 15 12 9

Figure 5.1.1-4. LUIS peak amplitude image of standard 1-A.



Plies 22 18 15 12 9

Figure 5.1.1-5. 3.5 MHz Bubbler time of flight image of standard 1-A. Tool-side scan.

LUIS Test Results

The LUIS signals obtained on standard 1-A. A peak amplitude image of this part may be seen in Figure 5.1.1-4. Three TOF images from the same data file may be seen in Figures 5.1.1-6, 5.1.1-7 and 5.1.1-8. The ability to scan the panel completely enabled detection of inserts at all of the edges of the standard. The higher data density (0.05" sample and index increments) also resulted in better definition in the ultrasonic indications from the edges of the inserts. In the peak amplitude image the indications from the Release ply F in the 15 ply portion of the panel are less obvious than those in the 9 and 22 ply regions. The TOF images were made with separate color palette settings to enhance indications in the 9, 15, and 22 ply portions of the panel. The tape inserts within two plies of the 12 ply and 18 ply stringer bond lines were detectable in the TOF image in Figure 5.1.1-9. The Release ply F inserts at the stiffener bond lines were not detected.

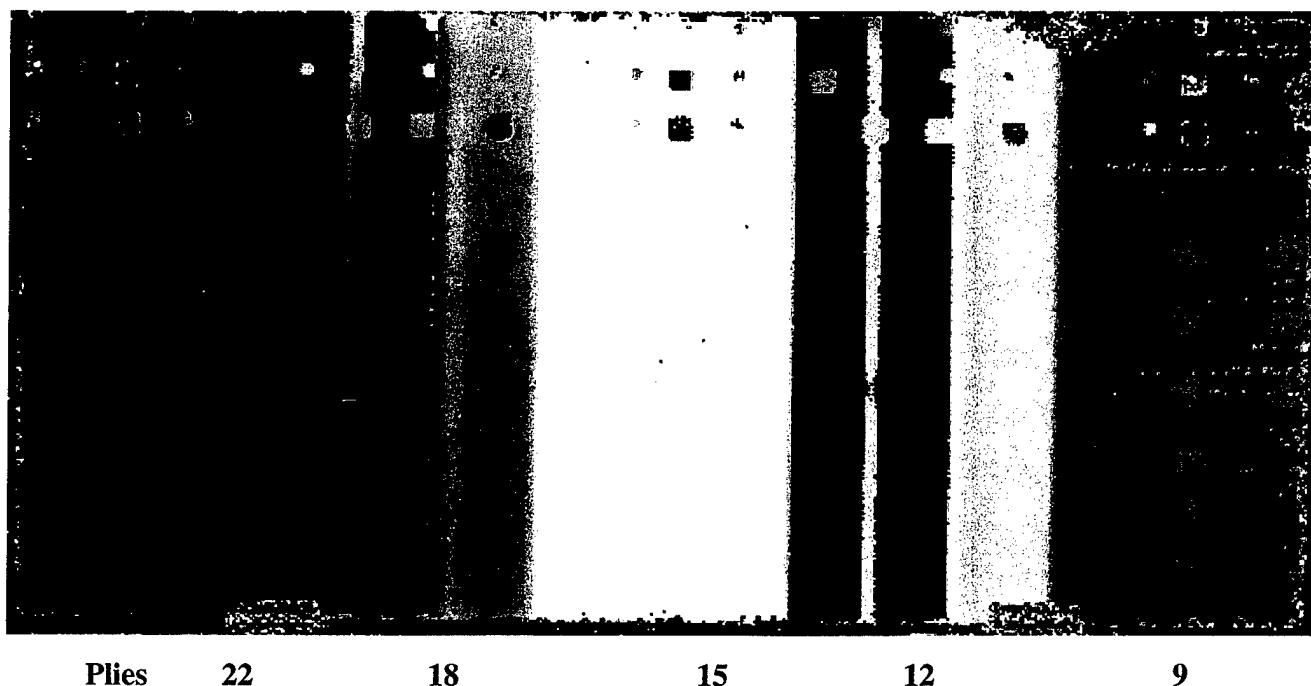
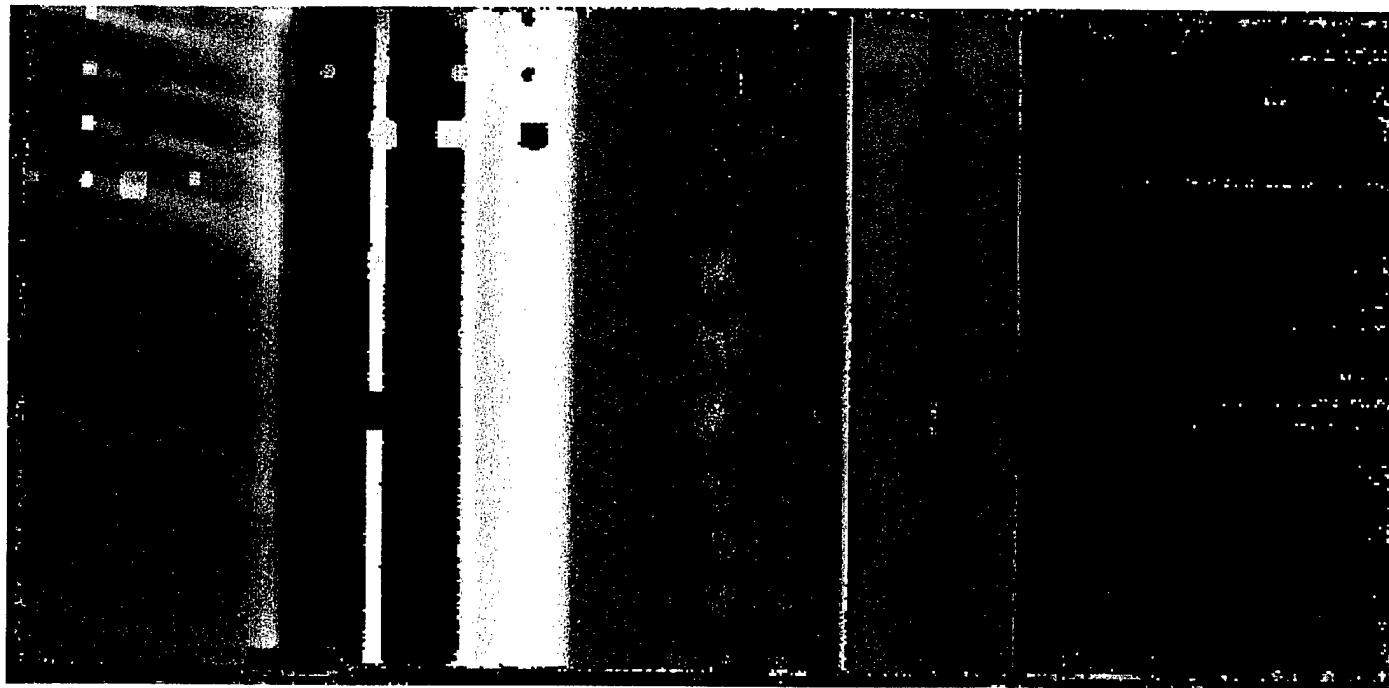
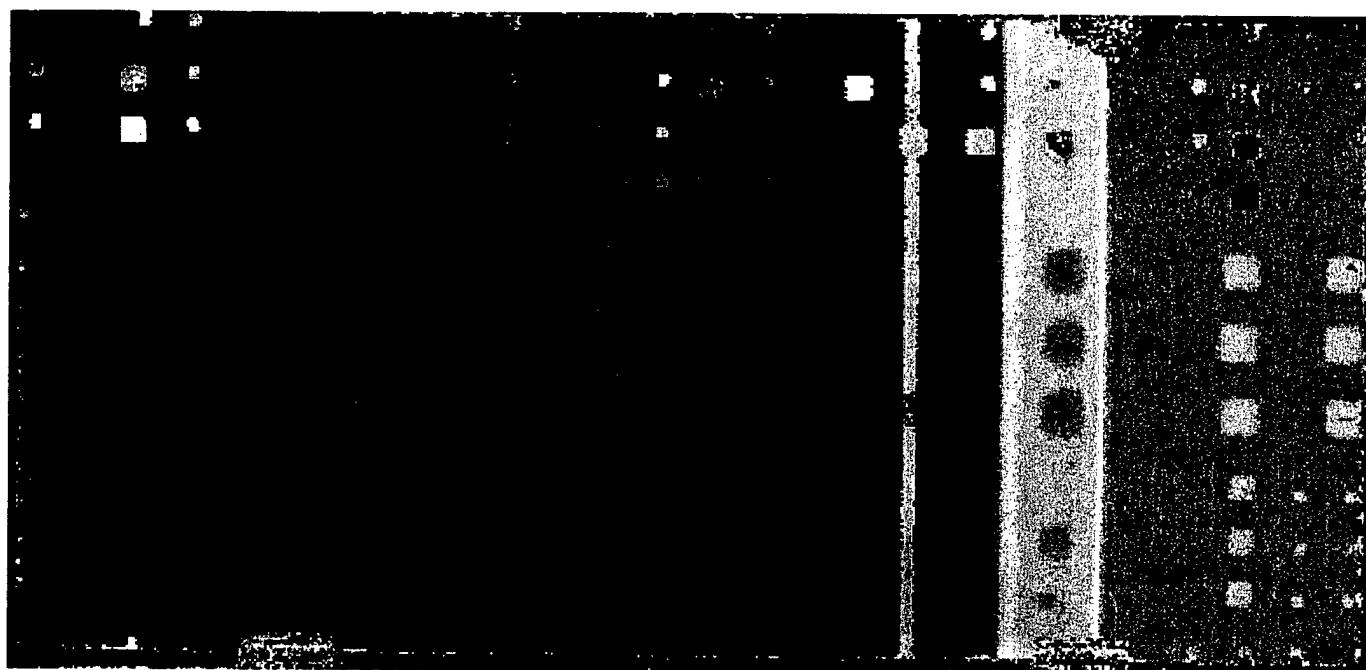


Figure 5.1.1-6. LUIS time of flight image of standard 1-A. Palette enhanced image of 22-ply section



Plies 22 18 15 12 9

Figure 5.1.1-7. LUIS time of flight image of standard 1-A. Palette enhanced image of 15-ply section



Plies 22 18 15 12 9

Figure 5.1.1-8. LUIS time of flight image of standard 1-A. Palette enhanced image of 9-ply section

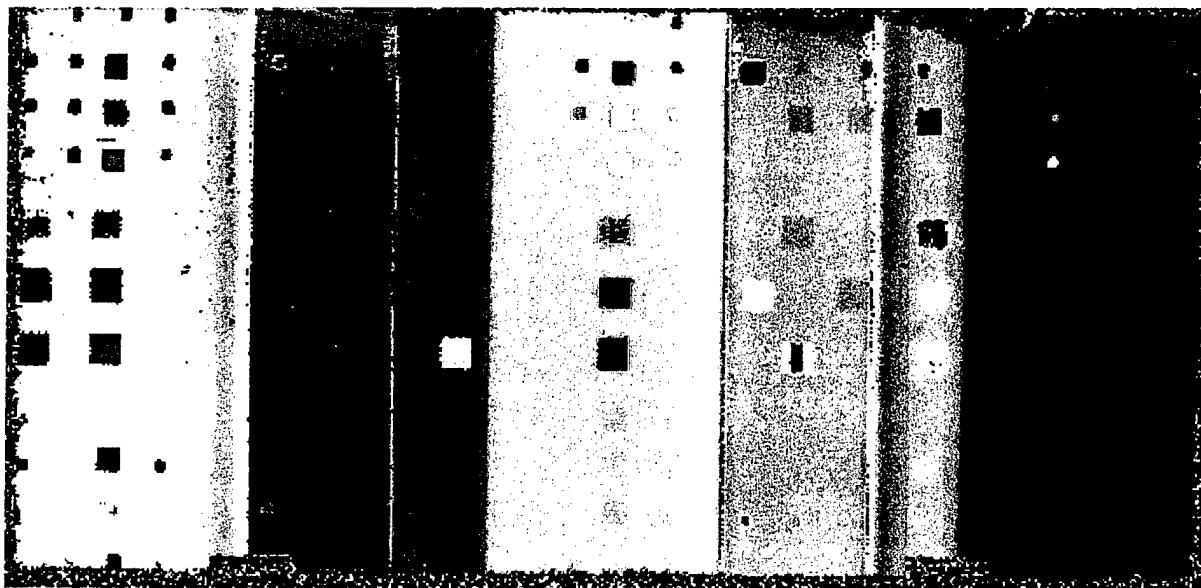


Figure 5.1.1-9. LUIS time of flight image 777-1-A. Enhanced image of 12 and 18-ply bond lines

Evaluation of Test Results

The ability to scan to the part edges is clearly an advantage of the LUIS system. While the surface-riding bubbler is a fast means of inspecting large skin areas, its use requires a separate test technique for the skin panel edges. The sensitivity obtained with the LUIS ultrasound to the inserts built into this standard was very similar to that obtained with the 3.5 MHz pulse echo bubbler. The number of inserts in standard 1-A detected with the bubbler and LUIS were essentially the same. The LUIS full wave detection of ultrasonic signals and the ability to test different gate positions would be valuable in investigating suspect areas in a test article. With the bubbler system suspect areas are evaluated by a separate full wave scan over a limited area encompassing the possible fault indication. The electronic distance amplitude correction (DAC) used to collect the bubbler data gave a uniform response with different numbers of plies. Software DAC equalization was more difficult to achieve in analyzing the LUIS data. It would be possible to use the electronic DAC with the LUIS since its output signal is equivalent to that from a conventional transducer. Hardware DAC would be beneficial for the LUIS. As an example, the use of hardware DAC in a USIP-20 would be familiar to many ultrasonic technicians.

In terms of cost, speed, and convenience for production testing of large, slightly contoured, composite laminate parts, the conventional ultrasonic technique would be preferred.

5.1.2 Graphite Composite Skin Panel Standard -2-A

This is the second (26 to 52 plies) of three standards prepared to represent the materials and ply stacking sequences in the empennage skin panels of the 777. A drawing of this panel may be found in Figure 5.1.2-1. Inserts prepared from three different foreign materials were placed in these standards. The inserts were brass foil (0.001" thick), Release ply F, and a tape. The brass foils were easy to detect. The release ply F was moderately difficult to find and the tape was more challenging to detect, particularly at greater depths or when it was in or adjacent to a bond line. The brass inserts were placed in the upper third of the panel. Pieces of Release ply F were placed in the middle section and tape inserts in the lower third. The sizes of the inserts were either 0.25" x 0.25" or 0.5" x 0.5" for the brass or tape. All of the Release ply F inserts were 0.7" x 0.7" Sections of I-stiffeners were cobonded to the laminate at two locations. Trimming of both of the upper and lower edges caused inserts to be located adjacent to all of the outer edges. As the brass inserts are rather easily detected, the indications from the tape and release ply F inserts are a better test of the relative sensitivity of the conventional and LUIS tests.

Conventional Test Results

The skins were scanned with a 3.5 MHz focused transducer mounted in a bubbler which traveled on the tool-side surface of the standard. The test frequency was selected based upon measurements on a variety of foreign materials placed at different depths in several different test parts. Detection and correct sizing of foreign materials was required throughout complex parts which varied in thickness from about 0.1" to nearly 1.0." The standard was scanned parallel to the stringers as this was the direction to be used for the full-scale skin panels. The data sampling interval was 0.080" and the index increment was 0.120." The somewhat coarse data sampling, particularly in the index direction, was chosen to help meet the expected inspection rate requirement of 42 skin panels per month.

A peak amplitude image of the pulse echo data from standard 2-A is shown in Figure 5.1.2-2. The simultaneously collected time of flight image is shown in Figure 5.1.2-4. The bubbler allowed scanning to within approximately 0.5" of each of the edges of the standard. The smaller inserts at the left and right edges as well as those at the top and bottom edges of the drawings are

NOTES:

1. THIS IS NOT A CONTROLLED DRAWING(S)
2. BREAK ALL SHARP EDGES AND CORNERS EXCEPT AS NOTED
3. TOLERANCE: DECIMAL: $XXX = \pm .010$
 $XX = \pm .02$
 ANGULAR: $= \pm .5$ ANGULAR: $= \pm .5$
4. MATERIAL IS BMS 8-276 TAPE / BMS 8-245 GRADE 05 (FOR BONDING OF STRINGERS).
5. SPACING BETWEEN THE INSERTS IS GENERALLY 0.5".
6. TEXT NEAR INSERT DENOTES ITS PLY DEPTH FROM THE TOOLSIDE SURFACE.
 - = BRASS FOIL INSERT ZONE
 - = TAPE AB-6782 INSERT ZONE
 - = RELEASE PLY F INSERT ZONE
7. AFTER TRIM, ALL EXPOSED INSERT EDGES MUST BE SEALED.
8. PROCESS PER BAC 5578 POS 6-4 (150 PSI CURE PRESSURE).
9. USE OF EXISTING STRINGER EXCESS IS ALLOWED; HOWEVER, NO INDICATION GREATER THAN 1.568 ATTENUATION IS PERMITTED.
 (1.568 PER BAC 5980 PSD 6-6 SECTION 2.2).

PLY TABLES

| PLY # | DIRECTION |
|-------|-----------|
| 1 | 0 |
| 2 | 0 |
| 3 | +45 |
| 4 | -45 |
| 5 | 0 |
| 6 | 90 |
| 7 | 0 |
| 8 | +45 |
| 9 | -45 |
| 10 | 0 |
| 11 | +45 |
| 12 | -45 |
| 13 | +45 |
| 14 | 0 |
| 15 | -45 |
| 16 | +45 |
| 17 | -45 |
| 18 | 0 |
| 19 | +45 |
| 20 | -45 |
| 21 | 0 |
| 22 | 90 |
| 23 | 0 |
| 24 | +45 |
| 25 | -45 |
| 26 | 0 |

| PLY # | DIRECTION |
|-------|-----------|
| 27 | +45 |
| 28 | 90 |
| 29 | -45 |
| 30 | 0 |
| 31 | +45 |
| 32 | -45 |
| 33 | 0 |
| 34 | +45 |
| 35 | -45 |
| 36 | 0 |
| 37 | +45 |
| 38 | 0 |
| 39 | -45 |
| 40 | 90 |
| 41 | +45 |
| 42 | 0 |
| 43 | -45 |
| 44 | 0 |
| 45 | +45 |
| 46 | 0 |
| 47 | -45 |
| 48 | 90 |
| 49 | +45 |
| 50 | 0 |
| 51 | -45 |
| 52 | 0 |

10. PLY BY PLY COMPACTION IS REQUIRED (MINIMUM OF 1 MINUTE AT 25° TO 30° HG).
11. STIFFENER WEB TO BE .25" TO .50" HIGH WITH .12" RADIUS ON WEB CORNER.
12. ALPHA DESIGNATOR SHALL BE ASSIGNED FOR UNIQUE IDENTITY. NO CURRENT OR FUTURE STANDARD FABRICATED PER THIS DWG WILL DUPLICATE THE ALPHA DESIGNATOR.

= EXCESS DESIGNATED FOR IMAGE ANALYSIS

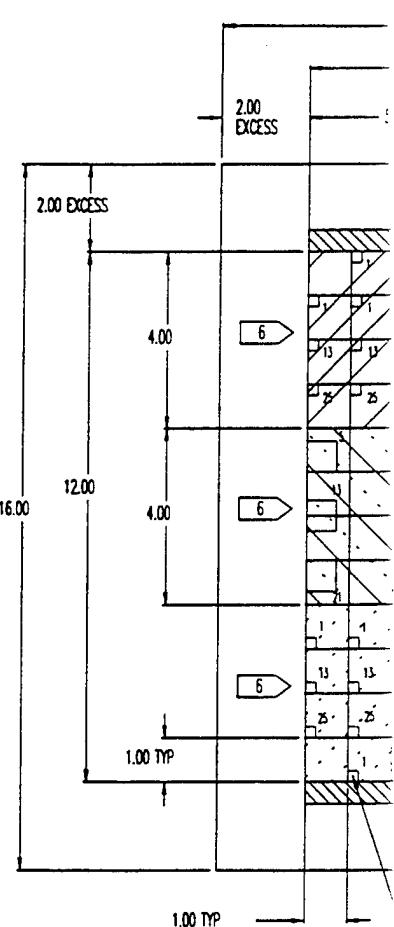


Figure 5.1.2-1 Skin Panel Standard

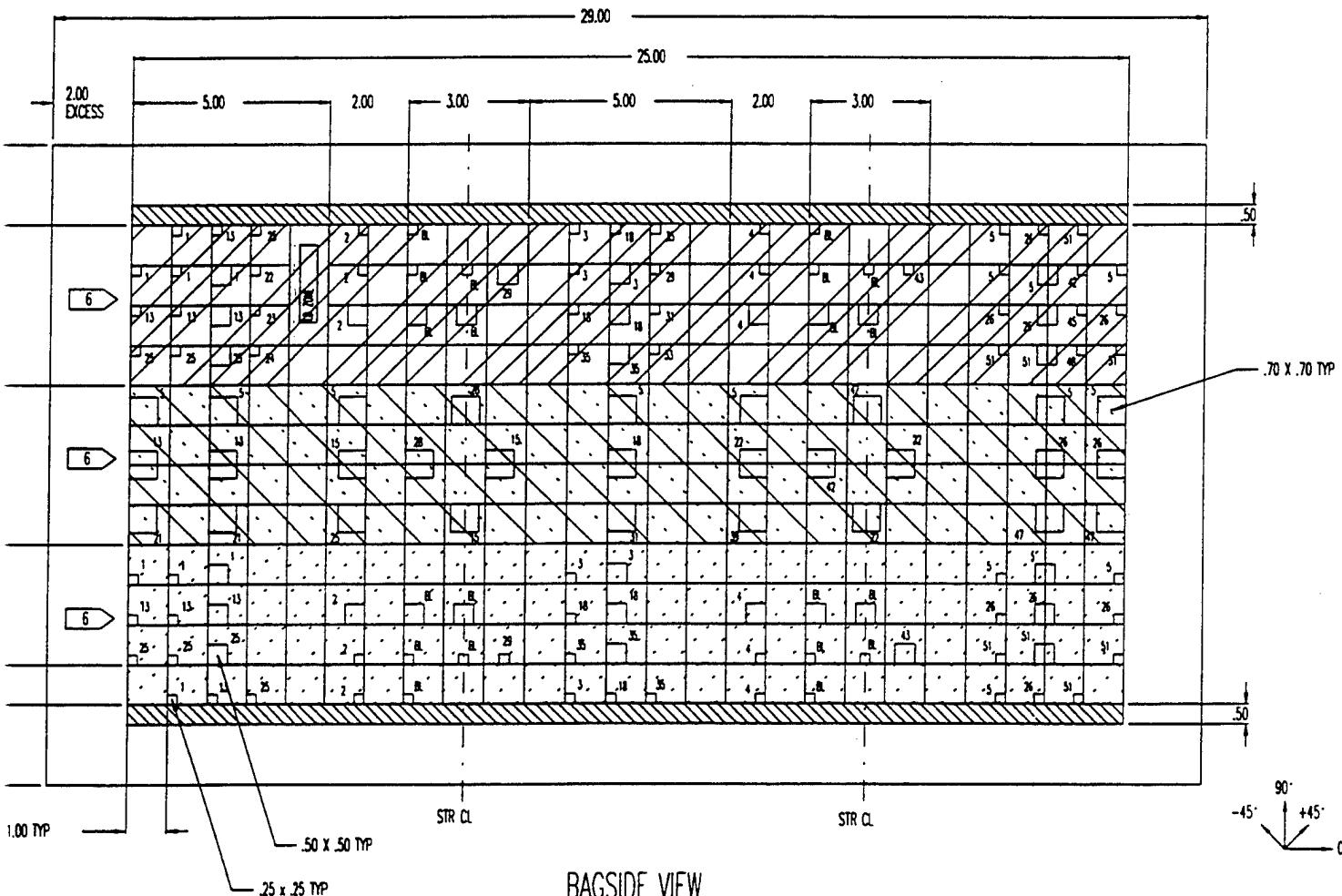
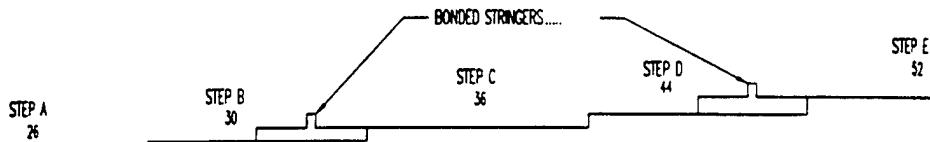
(1)

RED
10 30° Hg).

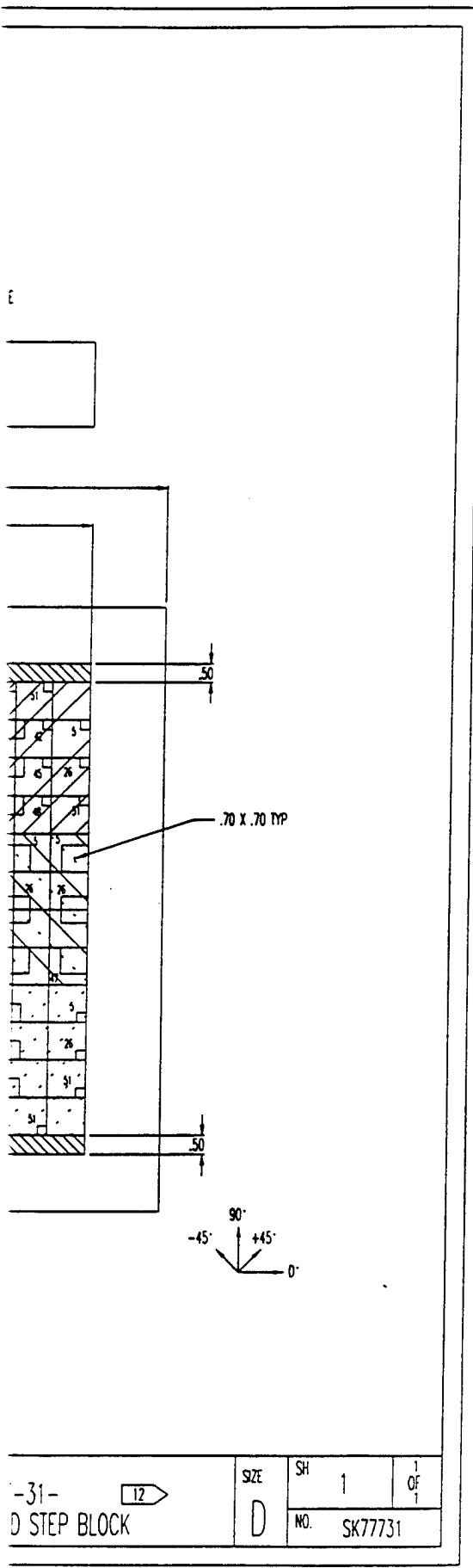
"HIGH WITH .12"

SIGNED FOR UNIQUE IDENTITY.
WHO FABRICATED PER THIS DWG
CHATOR.

TOTAL # OF PUES PER STEP



| | | | | | | |
|---|--------|---------------------|------|---|--|------------------|
| TOLERANCE  3 | BOEING | C. MARES 12-7-51 | DATE | TITLE 777-31- STANDARD STEP BLOCK | SIZE  D | SH 1 NO. SK77 |
| SCALE: 1/1 | | STICKNEY | | | | |
| | | DICK | | | | |



Y4.0 FILE: SK77731.PRT

(3)

thus not detectable by this technique. For production inspection of these parts a separate edge scan is used to cover the outer 2" of the parts. This ensures overlap with the automated bubbler scan which travels to within 1" of the outer trim border of the parts. The brass inserts in the upper third of the standard are effective reflectors and they often produce stronger echoes than the back surface echoes at each thickness. This results in the light colored indications seen with many of the brass inserts. The Release ply F inserts in the middle portion of the panel were seen easily with the exception of two that were each two plies below the bond lines of the two stiffeners (30 and 44 plies). Faint amplitude indications of the Release ply F inserts two plies from the bond lines were seen. Higher resolution TOF images of the bond lines clearly showed these inserts. The tape inserts at the stiffener bond lines were not detected, although inserts at ply 29 (above 30-ply bond line) and ply 43 (above 44-ply bond line) were easily seen.

LUIS Test Results

Application of a white, strippable paint improved the signals obtained on standard 2-A. A peak amplitude image of this part may be seen in Figure 5.1.2-3. Two time-of-flight (TOF) images from the same data file may be seen in Figures 5.1.2-5 and 5.1.2-6. The ability to scan the panel completely enabled detection of inserts at the edges of the standard. The higher data density (0.05" sample and index increments) of the LUIS scans resulted in better definition in the ultrasonic indications from the edges of the inserts. In the amplitude image the Release ply F inserts two plies above the bond lines at 30 and 44 plies were not detected. The TOF image in Figure 5.1.2-5, however, had distinct indications for the inserts two plies from both of the bond lines. In the amplitude image the indications from the release ply F in the 26, 36, and 52 ply portions of the panel were visible. The TOF images also yielded clear indications of both the Release ply F and tape in the 26 and 52 ply portions of the panel. These images gave clear indications of the release ply F inserts in both the thickest and thinnest areas of this panel, although the tape inserts 2 plies from the bond lines in the 30 and 44 ply regions were not detected.

Evaluation of Test Results

The ability to scan to the part edges is clearly an advantage of the LUIS system. While the surface-riding bubbler is a fast means of inspecting large skin areas, its use requires a separate test technique for the skin panel edges. The sensitivity obtained with the LUIS ultrasound to the inserts built into this standard was very similar to that obtained with the 3.5 MHz pulse echo bubbler. The number of inserts in standard 2-A detected with the bubbler and LUIS was essentially the same. The necessity to paint the test surface to improve the LUIS ultrasonic signal strength would be a drawback of this method in a production environment. The LUIS full wave detection of ultrasonic signals and the ability to test different gate positions would be valuable in investigating suspect areas in a test article. With the bubbler system suspect areas are evaluated by a separate full wave scan over a limited area encompassing the possible fault indication. The electronic distance amplitude correction (DAC) used to collect the bubbler data gave a uniform response with different numbers of plies. Software DAC equalization was more difficult to achieve in analyzing the LUIS data.

In terms of cost, speed, and convenience for testing large, slightly contoured, composite laminate parts, the conventional ultrasonic technique would be preferred.

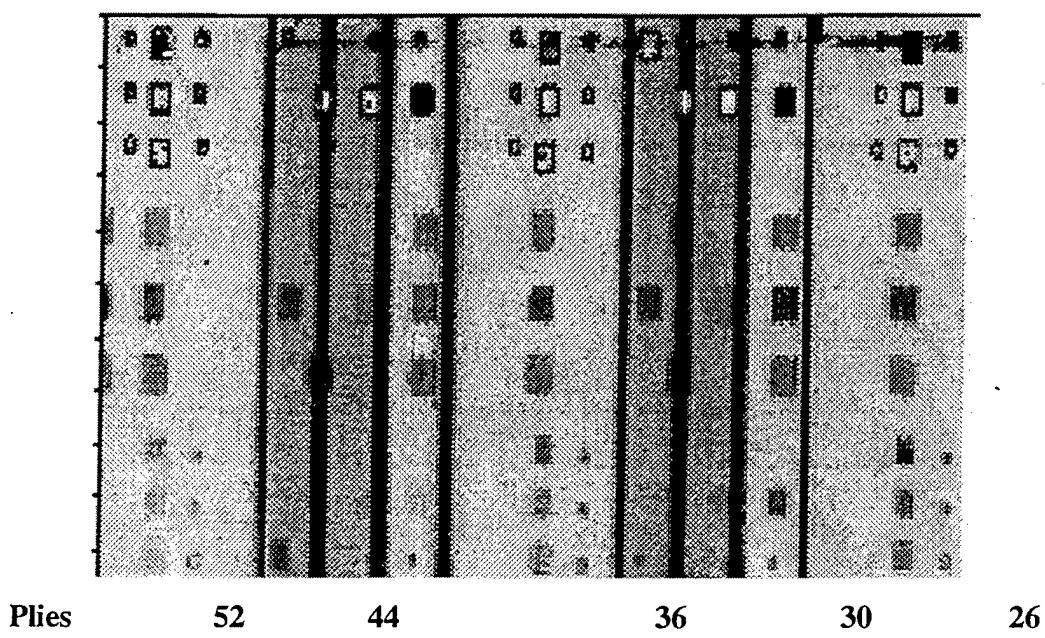
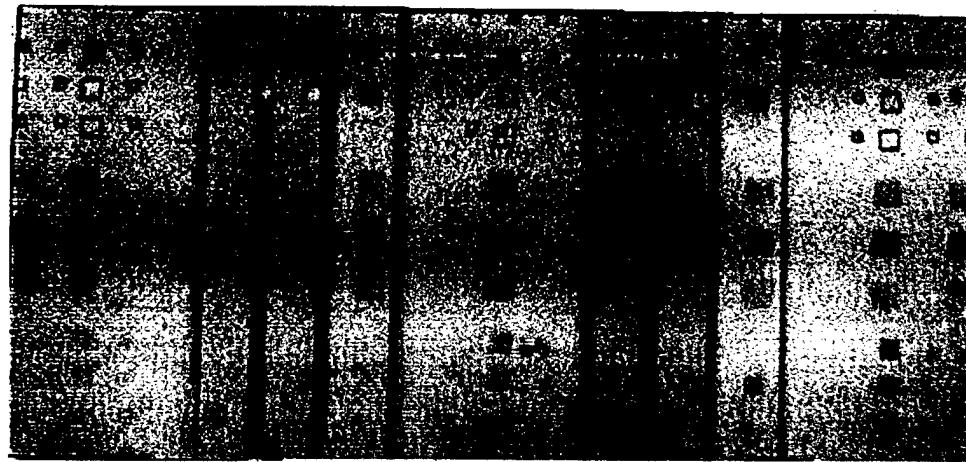


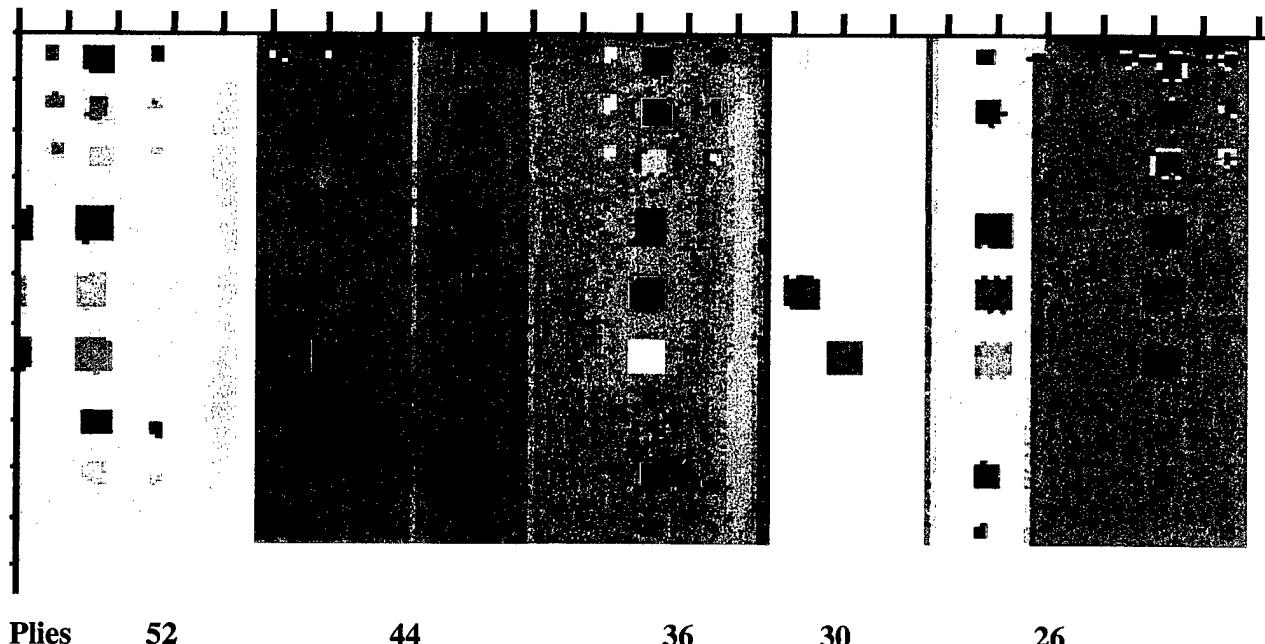
Figure 5.1.2-2. 3.5 MHz Bubbler peak amplitude pulse echo image, 777- 2-A, tool-side scan

D950-10322-1



Plies 52 44 36 30 26

Figure 5.1.2-3. LUIS peak amplitude image of standard 2-A, tool-side scan after painting



Plies 52 44 36 30 26

Figure 5.1.2-4. 3.5 MHz Bubbler time of flight image of standard 2-A, tool-side scan

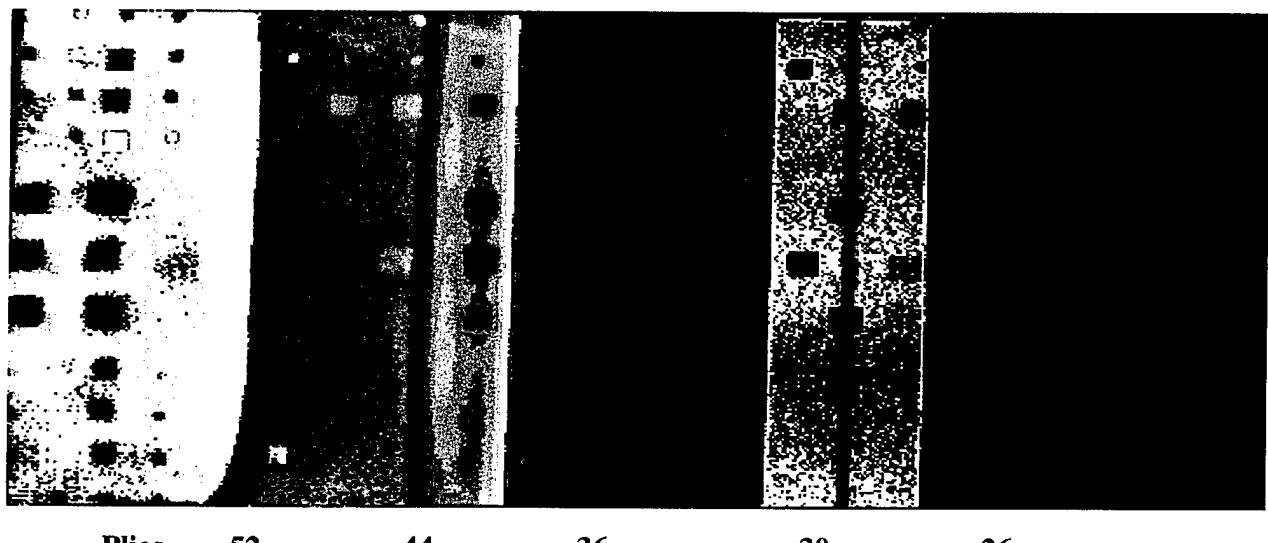


Figure 5.1.2-5. LUIS time of flight data standard 2-A. Palette enhanced data from thickest section.

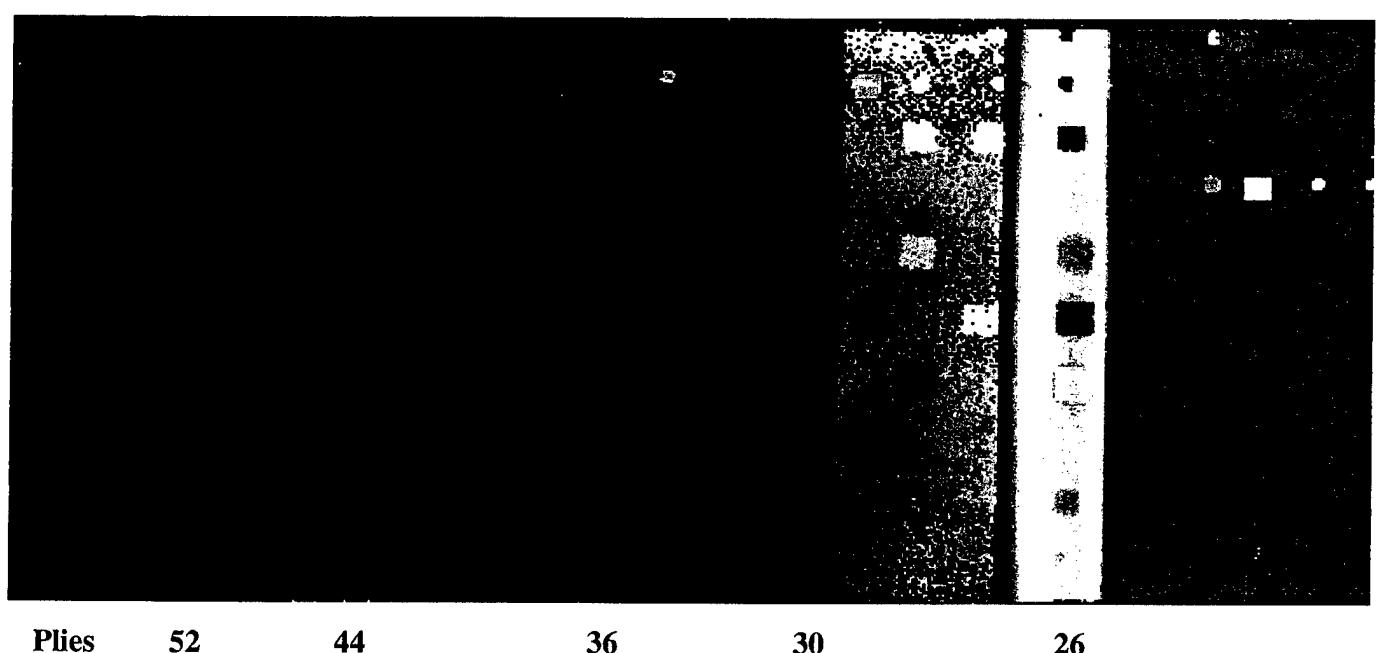


Figure 5.1.2-6. LUIS time of flight data standard 2-A. Palette enhanced data from thinnest section.

5.1.3 Graphite Composite Skin Panel Standard -3-A

This is the thickest (62 to 130 plies) of three standards prepared to represent the materials and ply stacking sequences to be encountered in the empennage skin panels of the 777. A drawing of this panel may be found in Figure 5.1.3-1. Inserts prepared from three different foreign materials were placed in these standards. The inserts were brass foil (0.001" thick), Release ply F, and a tape. The brass foils were easy to detect. The release ply F was moderately difficult to find and the tape was more challenging to detect, particularly at greater depths or when it was in or adjacent to a bond line. The brass inserts were placed in the upper third of the panel. Release ply F inserts were placed in the middle section and tape inserts in the lower third. The sizes of the inserts were either 0.25" x 0.25" or 0.5" x 0.5" for the brass or tape. The Release ply F inserts were 0.7" x 0.7" I-stiffeners were cobonded to the laminate at two locations. Trimming of both the upper and lower edges resulted in inserts located adjacent to all of the outer laminate edges. The bubbler and LUIS pulse echo indications from only the Release ply F inserts in the middle portion of the 74, 90, and 110 ply regions will be evaluated to compare the relative sensitivity of the conventional and LUIS tests on this panel.

Conventional Test Results

The skins were scanned with a 3.5 MHz focused transducer mounted in a bubbler that traveled on the tool-side surface of the standard. The test frequency was selected based upon measurements on a variety of foreign materials placed at different depths in several different test parts. Detection and correct sizing of foreign materials was required throughout complex parts which varied in thickness from about 0.1" to nearly 1.0." The standard was scanned parallel to the stringers as this was the direction to be used for the full-scale skin panels. The data sampling interval was 0.080" and the index increment was 0.120." The somewhat coarse data sampling, particularly in the index direction, was chosen to help meet the expected inspection rate requirement of 42 skin panels per month.

A peak amplitude image of the pulse echo data from standard 3-A is shown in Figure 5.1.3-2. The simultaneously collected time of flight image (TOF) is shown in Figure 5.1.3-4. The bubbler

NOTES:

1. THIS IS NOT A CONTROLLED DRAWING(S).
2. BREAK ALL SHARP EDGES AND CORNERS EXCEPT AS NOTED.
3. TOLERANCE: DECIMAL: $XXX = \pm .010$
 $XX = \pm .02$
 ANGULAR: $= \pm .5$ ANGULAR: $= \pm .1$
4. MATERIAL IS BMS 8-276 TAPE / BMS 8-245 GRADE D5 (FOR BONDING OF STRINGERS).
5. SPACING BETWEEN THE INSERTS IS GENERALLY 0.5".
6. TEXT NEAR INSERT DENOTES ITS PLY DEPTH FROM THE TOOLSIDE SURFACE.
 = BRASS FOIL INSERT ZONE
 = TAPE AB-6782 INSERT ZONE
 = RELEASE PLY F INSERT ZONE
7. AFTER TRIM, ALL EXPOSED INSERT EDGES MUST BE SEALED.
8. PROCESS PER BAC 5578 PSD 6-4 (150 PSI CURE PRESSURE).
9. USE OF EXISTING STRINGER EXCESS IS ALLOWED;
 HOWEVER: NO INDICATION GREATER THAN 1.508 ATTENUATION IS PERMITTED.
 (1.508 PER BAC 5880 PSD 6-6 SECTION 22).

10. PLY BY PLY COMPACTION IS REQUIRED
 (MINIMUM OF 1 MINUTE AT 25° TO 30° HG).
11. STIFFENER WEB TO BE .25" TO .50" HIGH WITH .12" RADIUS ON WEB CORNER.
12. ALPHA DESIGNATOR SHALL BE ASSIGNED FOR UNIQUE IDENTITY.
 NO CURRENT OR FUTURE STANDARD FABRICATED PER THIS Dwg WILL DUPLICATE THE ALPHA DESIGNATOR.

= EXCESS DESIGNATED FOR IMAGE ANALYSIS

STEP A
62

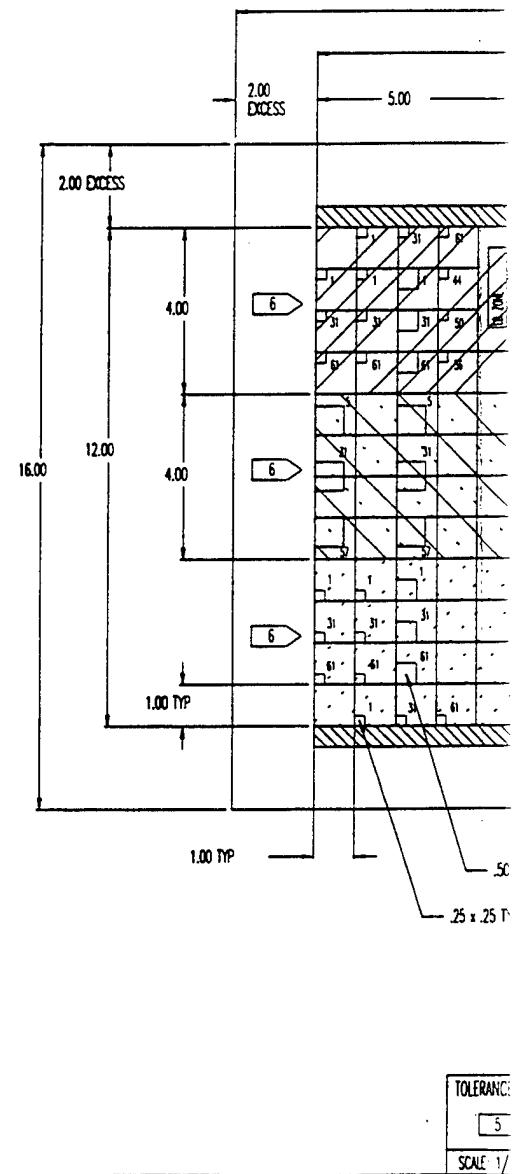
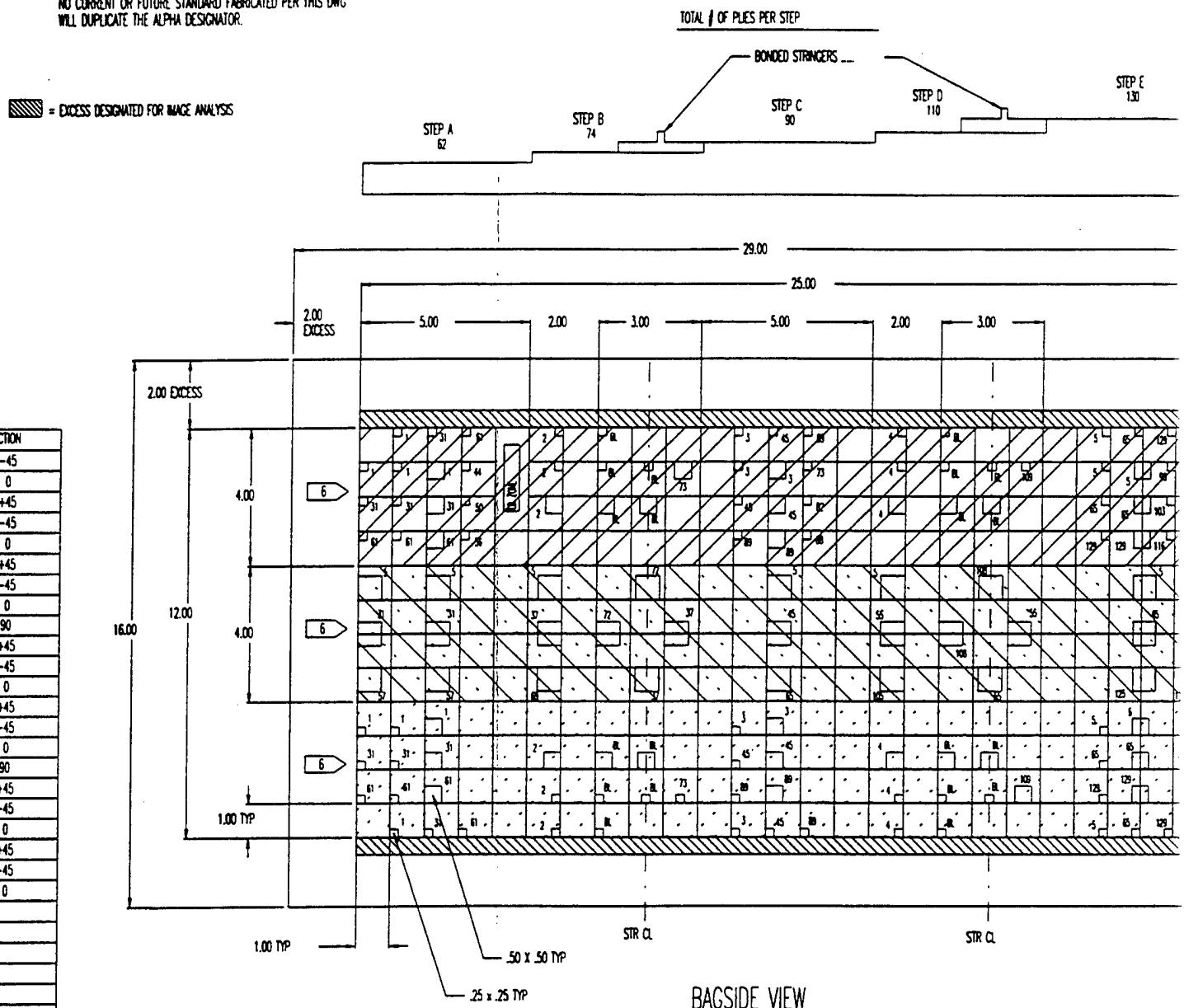


Figure 5.1.3-1 Skin Panel Standard

10. PLY BY PLY COMPACTION IS REQUIRED
(MINIMUM OF 1 MINUTE AT 25° TO 30° Hz).

11. STIFFENER WEB TO BE .25" TO .50" HIGH WITH .12" RADIUS ON WEB CORNER.

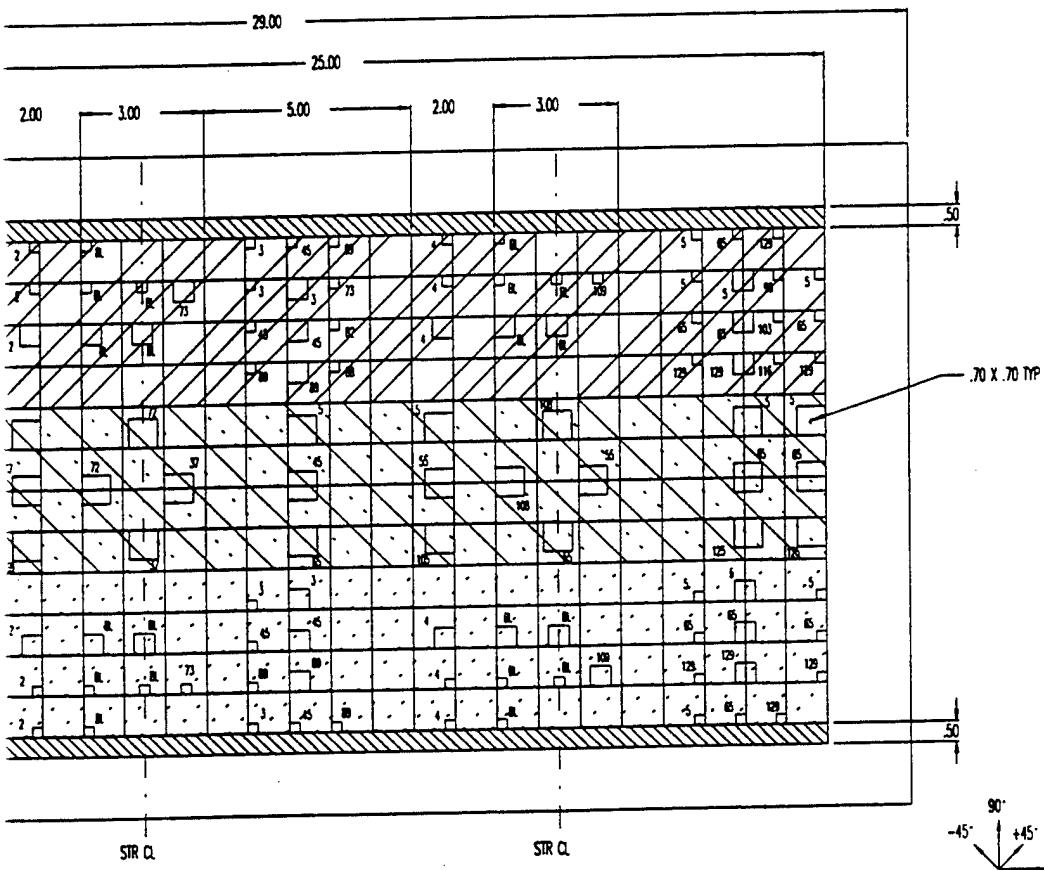
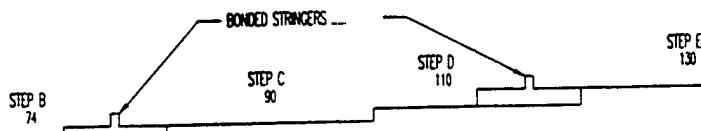
12. ALPHA DESIGNATOR SHALL BE ASSIGNED FOR UNIQUE IDENTITY. NO CURRENT OR FUTURE STANDARD FABRICATED PER THIS DWG WILL DUPLICATE THE ALPHA DESIGNATOR.



| | | |
|----------------|--------------|-----------------|
| TOLERANCE 5 | BOEING | DATE 10-7-83 |
| SCALE: 1/1 | CRW C.MARES | 777-32- |
| | CRW STICKNEY | STANDARD SITE |
| | ENGR | |

Figure 5.1.3-1 Skin Panel Standard 3-A

TOTAL # OF PLIES PER STEP



BAGSIDE VIEW

| | | | | | |
|--------|--|-------------------------------------|---|-----------|----------------|
| BOEING | | DATE 12-7-83 | TITLE 777-32- STANDARD STEP BLOCK | SIZE D | SH 1 1 OF 1 |
| | | DRW C.MARES COK STICKNEY ENGR | | | NO. SK77732 |

allowed scanning to within approximately 0.5" of each of the edges of the standard. The smaller inserts at the left and right edges as well as those at the top and bottom edges of the drawings are thus not detectable by this technique. For production inspection of these areas a separate edge scan is used to cover the outer 2" of the parts. This ensures overlap with the automated bubbler scan which travels to within 1" of the outer trim border of the parts. The brass inserts in the upper third of the standard are effective reflectors, and they often produce stronger echoes than the back surface echoes at each thickness. This results in the light colored indications seen with many of the brass inserts. In the 74 ply region the Release ply F inserts at 5, 37, and 69 plies (to the right of the stiffener) were visible in the enhanced contrast peak amplitude image in Figure 5.1.3-2. The inserts 5, 45, and 85 plies from the tool-side surface in the 90 ply portion and those at 5, 55, and 105 plies in the 110 ply region (to the right of the stiffener) were less obvious but still visible. Above both of the stiffeners there were inserts at one-half the laminate thickness. These were all easily detected in the TOF image in Figure 5.1.3-4. The Release ply F inserts two plies above the stiffener bond lines in the 74 ply and 110 ply regions were more difficult to find. High resolution images of the TOF data in Figures 5.1.3-8 and 5.1.3-9, however, clearly show these inserts.

LUIS Test Results

Application of a white, strippable paint improved the signals obtained on standard 3-A. A peak amplitude image of this part may be seen in Figure 5.1.3-3 (without DAC) and Figure 5.1.3-6 (with DAC). A TOF image from the same data file may be seen in Figures 5.1.3-5 (without DAC) and Figure 5.1.3-7 (with DAC). The ability to scan the panel completely enabled detection of inserts at the edges of the standard. The higher data density (0.05" sample and index increments) of the LUIS scans resulted in better definition in the ultrasonic indications from the edges of the inserts.

The Release ply F inserts in the 74 ply region (to the right of the stringer) were at depths of 5, 37, and 69 plies from the tool-side in the area without the stringer. Those at 5 and 37 plies were easily seen in both the amplitude and TOF images created without DAC corrections. The insert at 69 plies was readily seen in the TOF image with DAC correction. The two inserts at 37 plies beneath the tool-side in the 74 ply region to which the stringer was bonded were both seen easily in the

images without DAC correction. The two inserts at 72 plies (two plies from the bond line) were more difficult to detect. In the DAC corrected image in Figure 5.1.3-7 there are very faint indications from these inserts near the 74 ply bond line. B-scan images of this panel were also prepared to evaluate these indications. The Release ply F insert centered over the web and two plies above the 74 ply bond line shows a slight broadening of the B-scan bond line indication in Figure 5.1.3-10, but it would be difficult to detect in an unknown sample. The second insert two plies above the 74 ply bond line was above the right stiffener flange. There is again a slight broadening of the associated B-Scan indication in Figure 5.1.3-11, but detection of the Release ply F inserts at bond line depths of 74 plies or greater would be marginal in a production environment.

In the central 90 ply region, the inserts were 5, 45, and 85 plies beneath the tool-side. There was no stringer in this region. The inserts at 5 and 45 plies were easily seen in both the amplitude and TOF images without DAC correction. The insert at 85 plies below the tool-side was only marginally detectable in the DAC corrected TOF image in Figure 5.1.3-7. A B-scan made aligned with the center of the insert at 85 plies shows a faint indication in Figure 5.1.3-12. Detection of the Release ply F insert at depths of 85 plies or greater beneath the tool-side in this material would be very marginal.

In the 110 ply region to the right of the stringer the inserts at 5 and 55 plies were seen easily in the peak amplitude image without DAC correction and in both TOF images. The insert at 105 plies was not detected. The inserts above the stringer at 55 plies were readily seen in the same images. No indications were seen in any of the LUIS images of the inserts at ply 108 or two plies above the 110 ply bond line.

Evaluation of Test Results

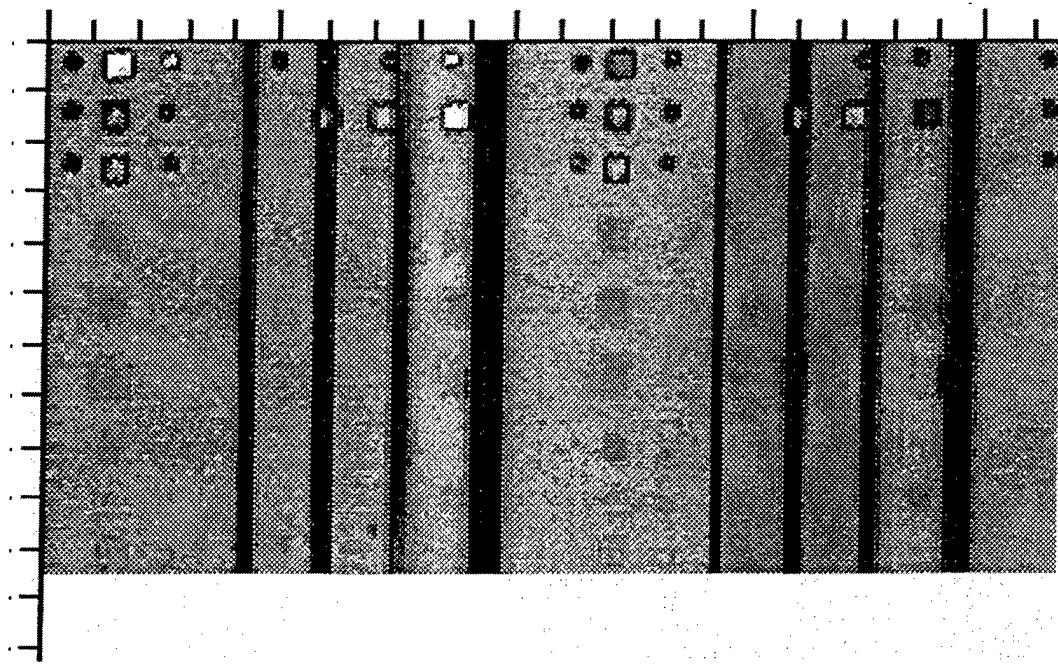
The results obtained on standard 3-A showed the LUIS to be less sensitive than the conventional pulse echo test to Release ply F inserts at depths of 85 plies or greater in laminates of the 777 empennage graphite material and stacking sequence. These same inserts within two plies of a bond line at depths of 74 plies or more were marginally detectable in the LUIS results, but they

were quite obvious in the bubbler TOF data. The bubbler pulse echo data also allowed detection of the inserts at 105 plies (110 ply laminate) and at 125 plies (130 ply laminate). The bubbler pulse echo system also detected both inserts at 108 plies above the 110 ply bond line.

The electronic distance amplitude correction (DAC) used to collect the bubbler pulse echo data produced a uniform response with different numbers of plies. DAC equalization was more difficult to achieve via software in analyzing the LUIS data from standard 3-A. The comparatively strong and repeatable signals obtained with piezoelectric transducers make it easier to detect small variations in the ultrasonic signals. There appears to be greater variation in the signals detected with LUIS compared with conventional pulse echo systems. This will make it more difficult to detect weak reflectors, particularly those deep within a laminate. The 3.5 MHz frequency of the bubbler transducer was chosen to allow detection of materials over a broad range of thickness. The LUIS center frequency is more typically at 5-6 MHz. While excellent response is seen with flaws at moderate depths, the greater attenuation at the higher frequencies generated by the LUIS will also reduce the response to foreign materials in thicker parts. The high power and low frequencies available from piezoelectric transducers have an advantage in thick parts.

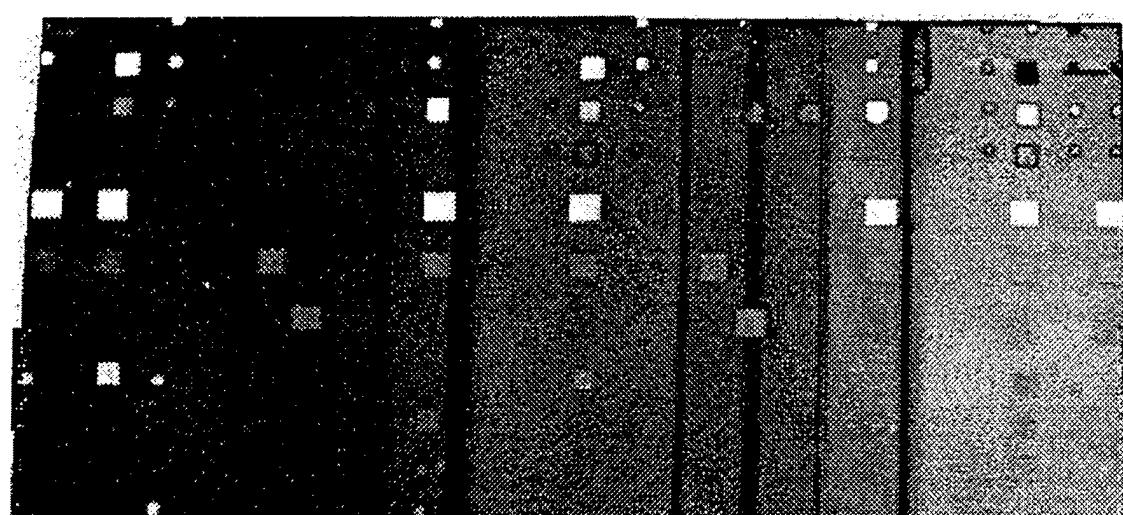
The necessity to paint the test surface to improve the LUIS ultrasonic signal strength would be a drawback of this method in a production environment. The LUIS full wave detection of ultrasonic signals and the ability to test different gate positions would be valuable in investigating suspect areas in a test article. With the bubbler system suspect areas are evaluated by a separate full wave scan over a limited area encompassing the possible fault indication. Use of the LUIS full wave capability only in limited suspect areas would save the time and expense of generating large full wave data files that cover the entire part.

In terms of cost, speed, convenience for testing large, slightly contoured, composite laminate parts, and sensitivity through composite laminates of 85 plies or more, the conventional ultrasonic technique would be preferred. It is comparatively inexpensive to build bubbler systems with multiple element linear arrays and achieve inspection rates of nearly 200 square feet per hour for these types of panels.



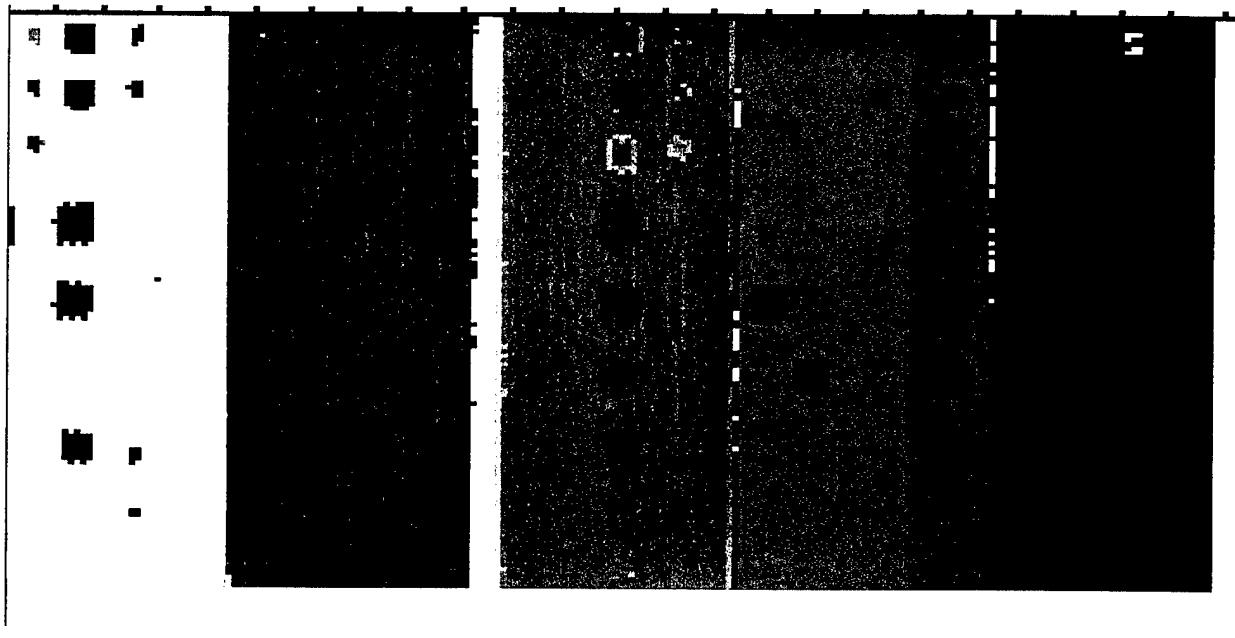
Plies 130 110 90 74 62

Figure 5.1.3-2. 3.5 MHz Bubbler peak amplitude pulse echo image of standard 3-A.
Tool-side scan.



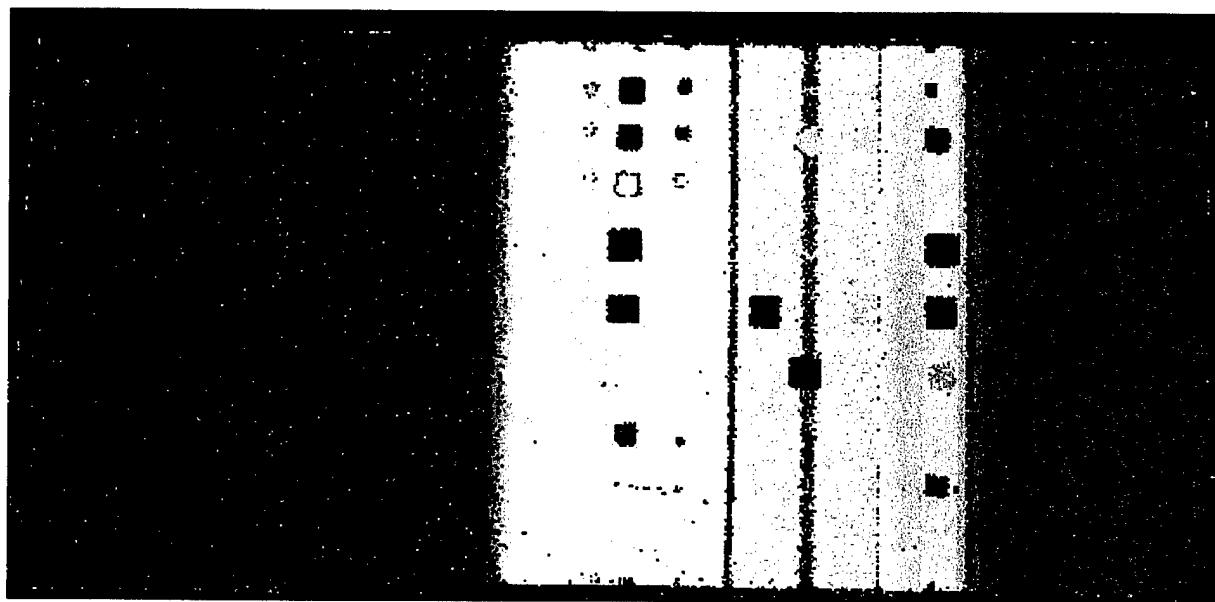
Plies 130 110 90 74 62

Figure 5.1.3-3. LUIS peak amplitude image of standard 3-A. Tool-side scan after painting.



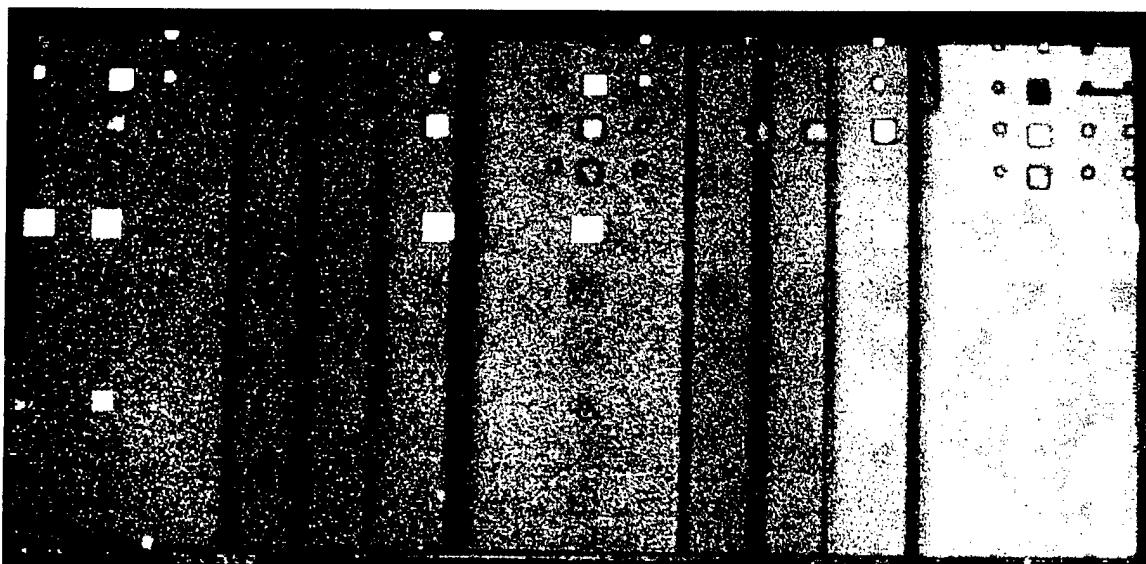
Plies 130 110 90 74 62

Figure 5.1.3-4. 3.5 MHz Bubbler time of flight image of standard 3-A. Tool-side scan.



Plies 130 110 90 74 62

Figure 5.1.3-5. LUIS time of flight image of standard 3-A. Tool-side scan after painting.



Plies 130

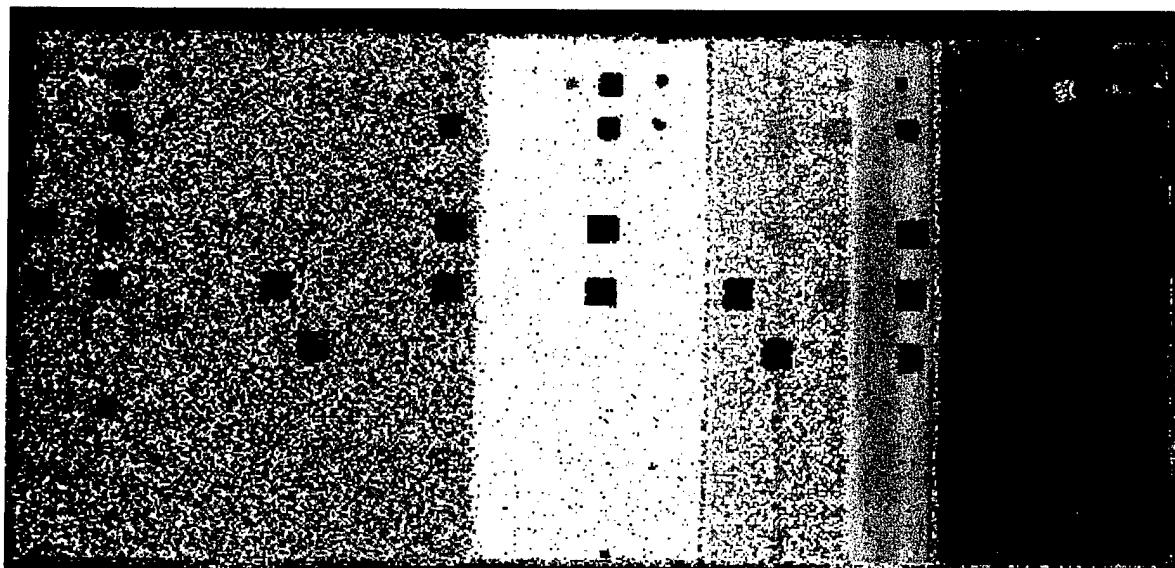
110

90

74

62

Figure 5.1.3-6. LUIS peak amplitude image of standard 3-A. Tool-side scan after painting.



Plies 130

110

90

74

62

Figure 5.1.3-7. LUIS time of flight image of standard 3-A. Tool-side scan after painting.

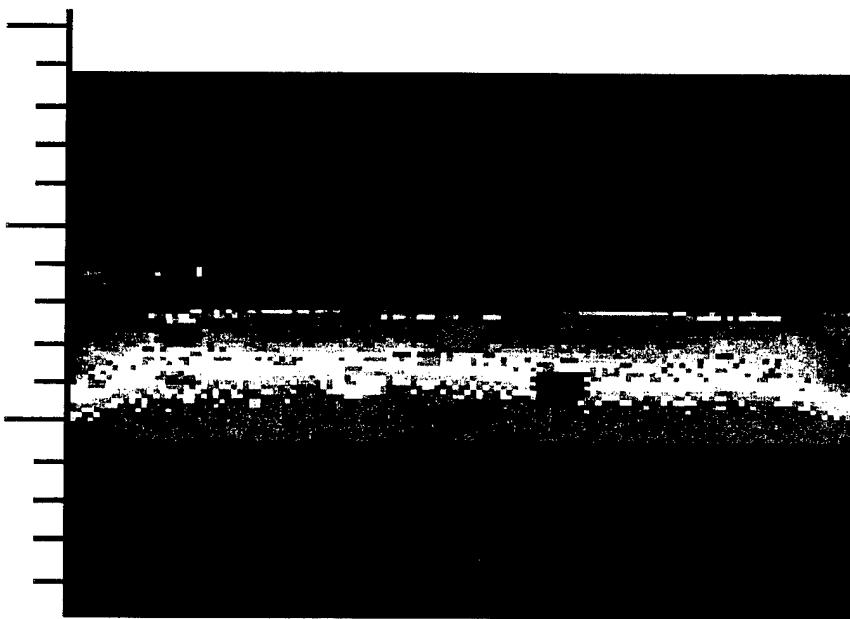


Figure 5.1.3-8. 3.5 MHz Bubbler TOF data from stringer over 74 ply laminate. Thickness increment 0.54" to 0.58".

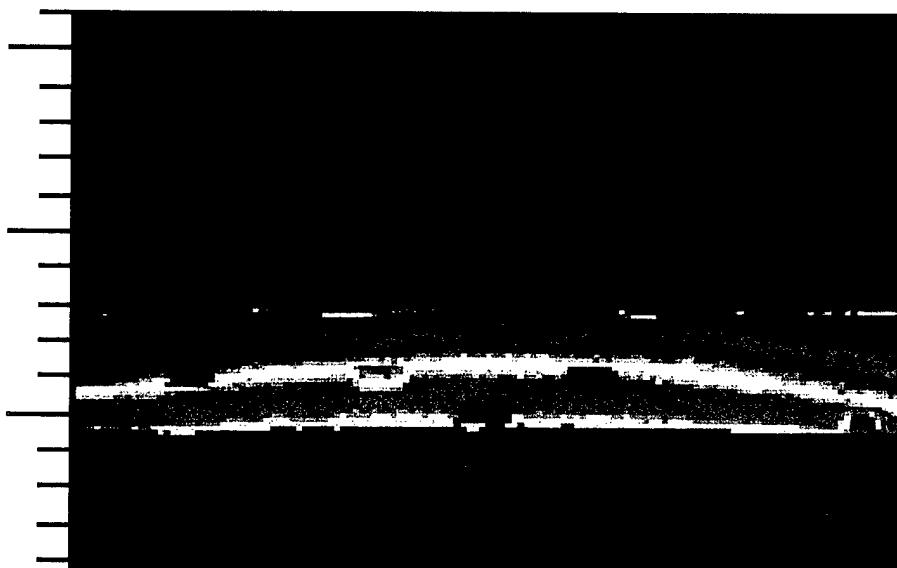
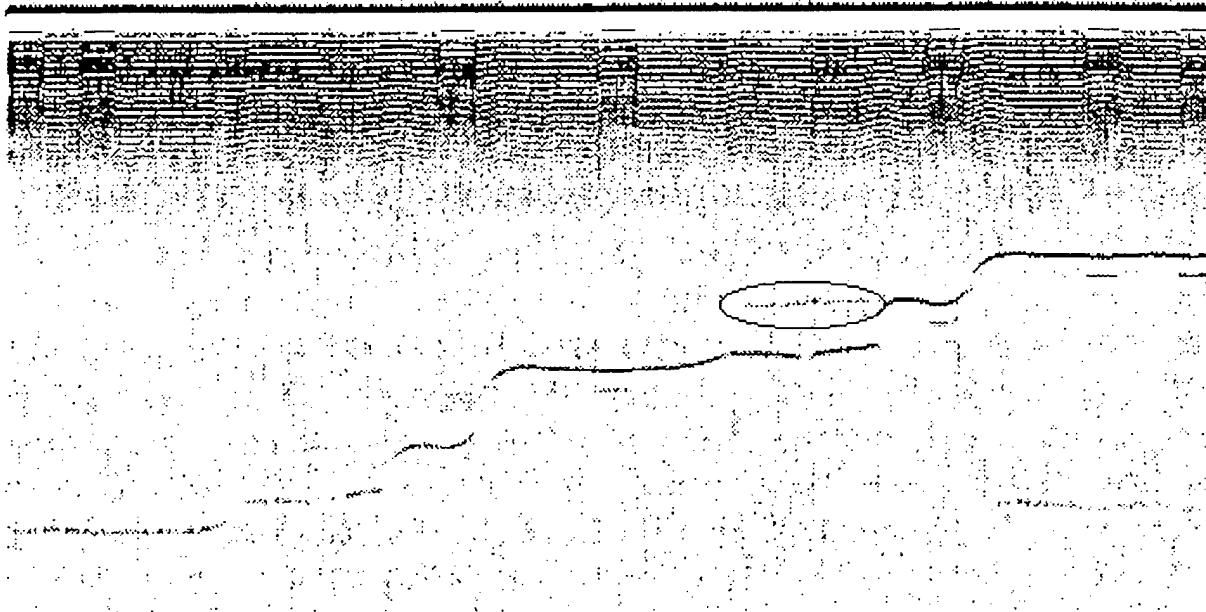
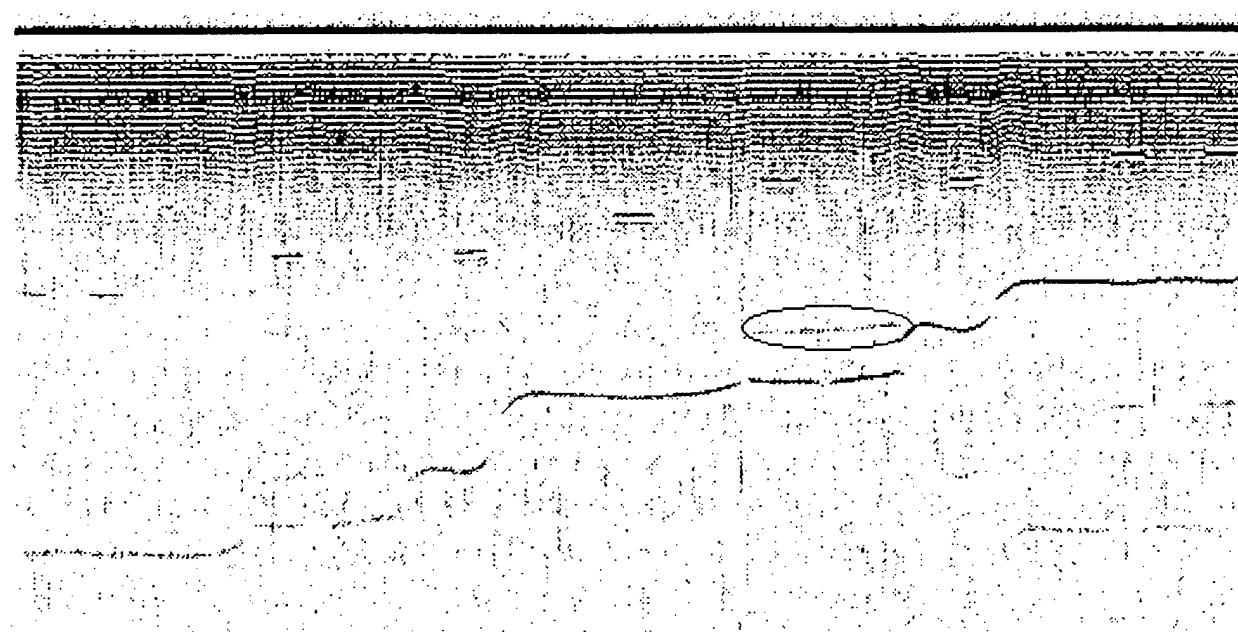


Figure 5.1.3-9. 3.5 MHz Bubbler TOF data from stringer over 110 ply laminate. Thickness increment 0.80" to 0.84".



| | | | | | |
|--------------|------------|------------|-----------|-----------|-----------|
| Plies | 130 | 110 | 90 | 74 | 62 |
|--------------|------------|------------|-----------|-----------|-----------|

Figure 5.1.3-10. LUIS B-Scan image of standard 3-A from 62 to 130 plies. Bond line echo at 74 plies is circled. Release ply F insert 2 plies above stiffener bond line and centered on web.



| | | | | | |
|--------------|------------|------------|-----------|-----------|-----------|
| Plies | 130 | 110 | 90 | 74 | 62 |
|--------------|------------|------------|-----------|-----------|-----------|

Figure 5.1.3-11. LUIS B-Scan image of standard 3-A from 62 to 130 plies. Bond line echo at 74 plies is circled. Release ply F insert 2 plies above bond line under right flange of stiffener.

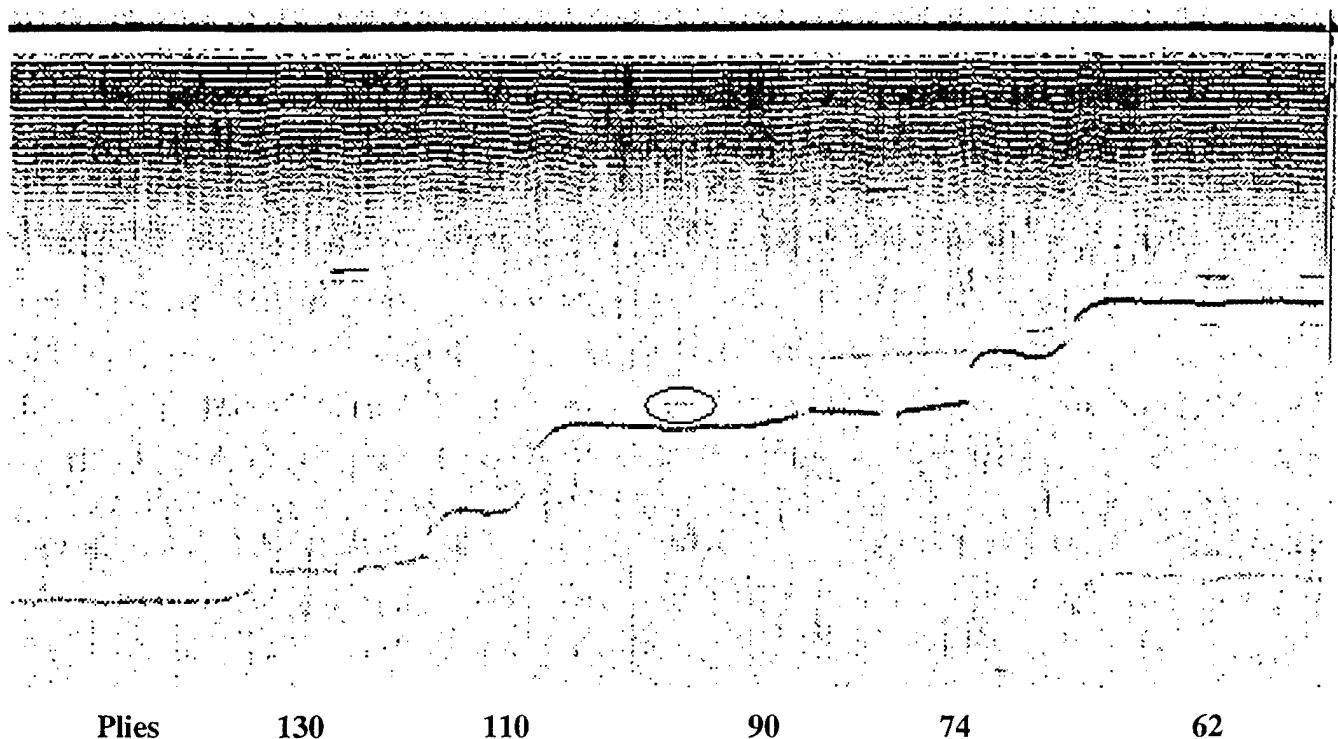


Figure 5.1.3-12. LUIS B-Scan image of standard 3-A from 62 ply to 130 plies. Echo from Release ply F at 85 plies is circled.

5.1.4 7J7 Graphite composite Test Panel

This is a test article for the 7J7, a conceptual airplane that was not manufactured. This panel was prepared during development of the manufacturing process for skin panels for the proposed vertical fin, which was to be made from graphite composites. A photograph of the bag-side of the test panel may be seen in figure 5.1.4-1. Three composite I-stiffeners may be seen bonded to the bag-side surface of the panel. The tool-side of this part may be seen in figure 5.1.4-2. The tool-side surface had a Fiberglas-copper mesh layer on the periphery for lightning strike protection. Several ply drops were made in the skin laminate with the result that the outer edges and the tip were thicker (0.3") than the central portion of the panel (0.1"). Small samples of foreign materials were inserted at different depths within both the laminate skin and in the flanges of the stiffeners. The skin inserts were 0.5" x 0.5" while those in the stiffener flanges were either 0.125" x 0.5" or 0.25" x 0.5".

Conventional Test Results.

The panel was scanned from the tool-side surface with a surface-riding bubbler containing a focused 3.5 MHz transducer. Total scan time was 38 minutes. Figure 5.1.4-3 contains a peak detected amplitude image using a gate commencing just after the front surface echo and extending to cover the maximum thickness of the panel. As the probe rides on the surface and follows its contour, the scan does not reach the outermost edge of the test panel. A separate test was envisioned for the outermost inch of the panel periphery. The darker area around the outer edge of the skin was caused by the Fiberglass-copper mesh material that resulted in a reduction of the back echo amplitude. At the right edge of the image two elongated dark indications may be seen where there were overlaps in the lightning protection material. The footprints of the stiffener flanges are easily seen as are the dark indications from the stiffener webs owing to the absence of echoes returning from these areas. The inserts built into the stiffener flanges were easily seen including some that extended into the radius between the flange and web. A number of naturally occurring indications were also seen in the area of the uppermost stringer in the image.

Numerous ply drops may be seen at the right end of the skin and along the lower edge of the panel. Several of the inserts built into the laminate resulted in a reduction in the peak amplitude

signal within the gate. These are seen as darker indications. Other inserts gave strong reflections that were seen as dark outlines with a light indication from the central portion of the insert. The latter were also easily detected in the time of flight image for this panel as seen in Figure 5.1.4-4. Two rows of 6 inserts were placed between the bottom and middle stringers. Only one of these rows is seen in the peak amplitude image, however, the time of flight image shows all of them. The row of inserts missing in the amplitude image is located close to the tool-side surface, and they produced very small echoes. The echoes were, however, sufficient to allow the inserts to be seen with the time of flight gate that uses a trigger threshold of 10% of full scale in order to detect weakly reflecting foreign materials.

LUIS Inspection Results

The initial scan of the 7J7 panel with the LUIS was made without painting the tool-side surface. While the data obtained on the periphery of the panel was quite comparable to the bubbler scan data, the signals from the unpainted central area were too low to obtain a useful image. The data from this initial test may be seen in Figure 5.1.4-5. The panel was scanned with the LUIS system in two separate rectangular segments. One of the principal reasons for this is the size of the data files generated. The data file for the left portion of the 7J7 panel, for example, was 425 Mbytes. The processing times for these large files were so long that there was a reluctance to scan images of the full size that LUIS could generate. Of course, in a "production" mode, full waveforms would not be digitized for every part of the same type and files would be smaller.

The panel was rescanned following tool-side application of a strippable white paint. The peak amplitude image obtained after painting may be seen in Figure 5.1.4-6. The scan time for the left segment of this panel was 59 minutes. The time of flight image generated may be seen in Figure 5.1.4-7. Considerable time was spent in attempting to obtain images of the upper row of inserts between the bottom and middle stringers in this panel. While some of the inserts could be detected, the combinations of gate, DAC, and filter settings resulted in increased noise in other portions of the image. As noted above, the echoes from these inserts were weak and close to the tool-side surface.

Evaluation of Test Results

There is excellent agreement between the peak amplitude images obtained by both the LUIS and pulse echo bubbler technique. Equivalent amplitude responses were seen by both methods to the natural and artificial faults in this test part. The LUIS also covered the entire area of the test panel while the bubbler was unable to scan the outermost inch of the part. It was disappointing that we could not obtain a time of flight image with the LUIS data that showed all of the inserts in the laminate. Detecting the weak reflectors close to the tool-side surface with the LUIS was difficult. By manipulating the filter settings it was possible to image some of the inserts, but this was only achieved by knowing that the inserts were present. Greater effort to tailor the setup for weak reflectors close to the surface may have improved these results.

Owing to higher inspection rates achievable by multi-transducer conventional pulse-echo tests with comparable sensitivity, the bubbler tests would be the preferred inspection method for these parts. The LUIS required 106 minutes to scan the part versus 38 minutes with the bubbler for the part (excluding the outermost 1 inch). The bubbler scan used a single transducer. In a production environment, this rate may be improved 5 to 6 fold by use of linear array transducers. The LUIS would have a possible advantage in a part like this since it could inspect the skin panel and the stiffeners in one scan. In current practice, the stiffeners are cured separately and inspected before they are bonded to the skin.

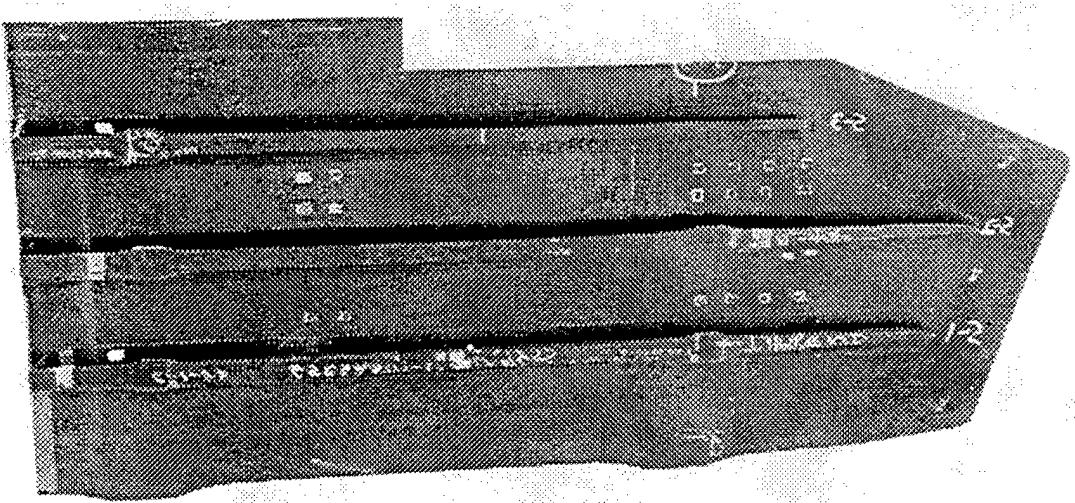


Figure 5.1.4-1. Photograph of bag-side of 7J7 test panel

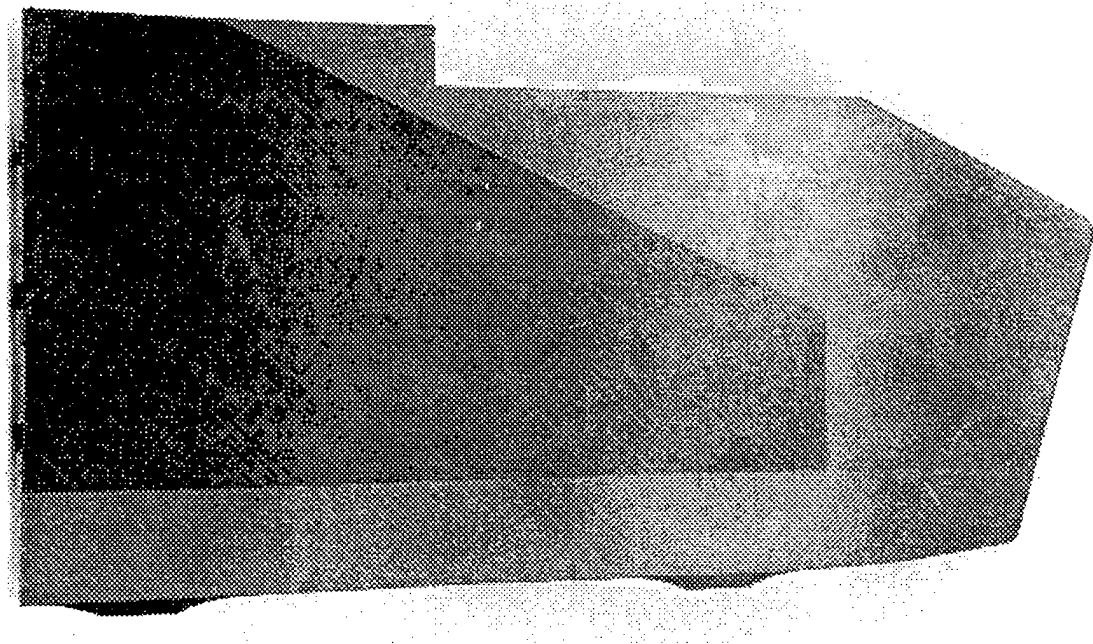


Figure 5.1.4-2. Tool-side of 7J7 panel

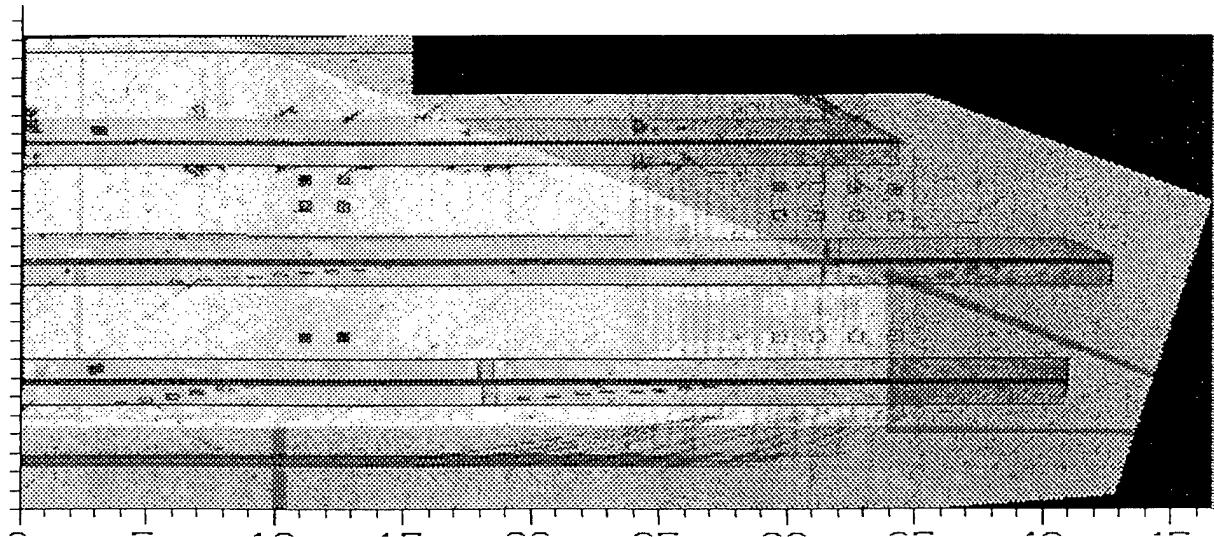


Figure 5.1.4-3. 3.5 Mhz Bubbler Peak Amplitude image of 7J7 Test Panel

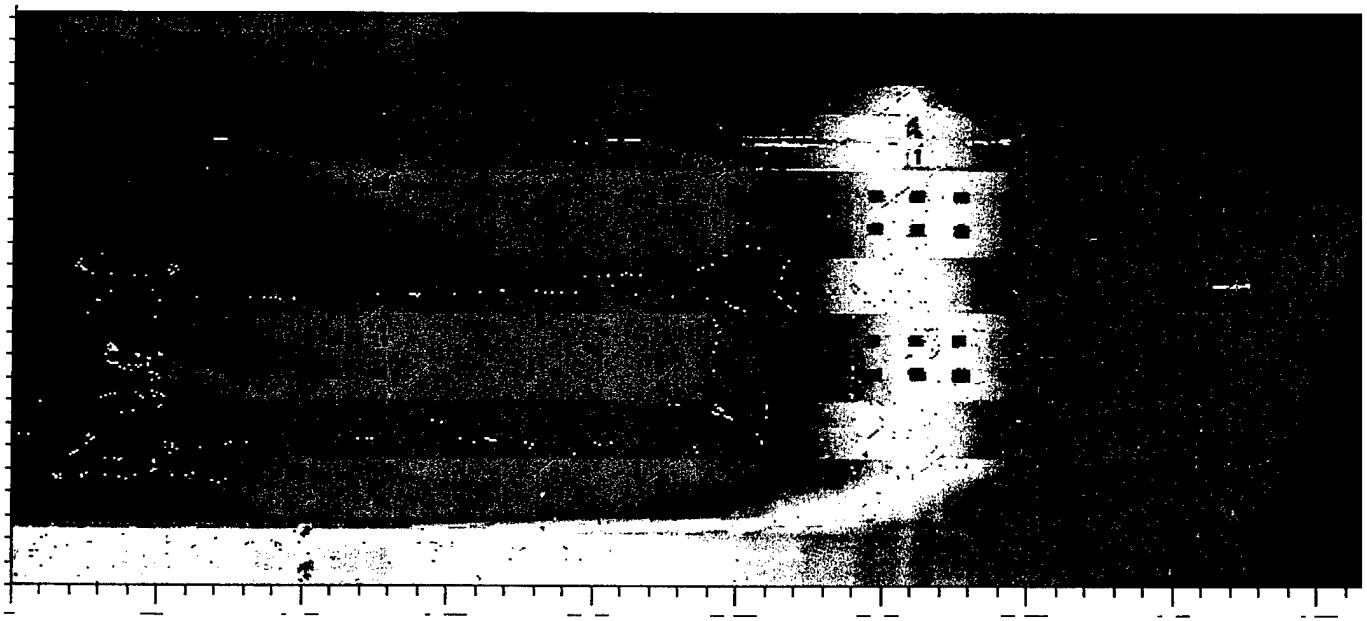


Figure 5.1.4-4. 3.5 Mhz Bubbler time of flight image of 7J7 Test Panel

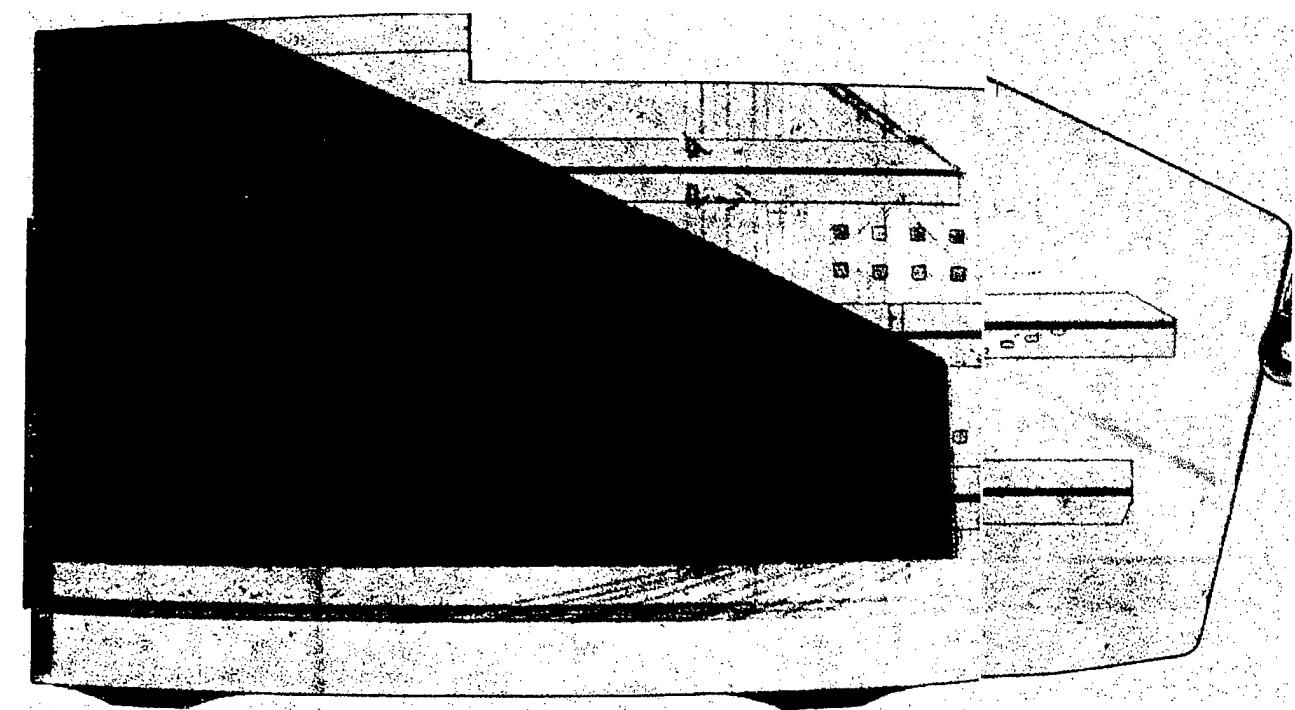


Figure 5.1.4-5. Initial LUIS peak amplitude image of unpainted tool-side of 7J7 panel

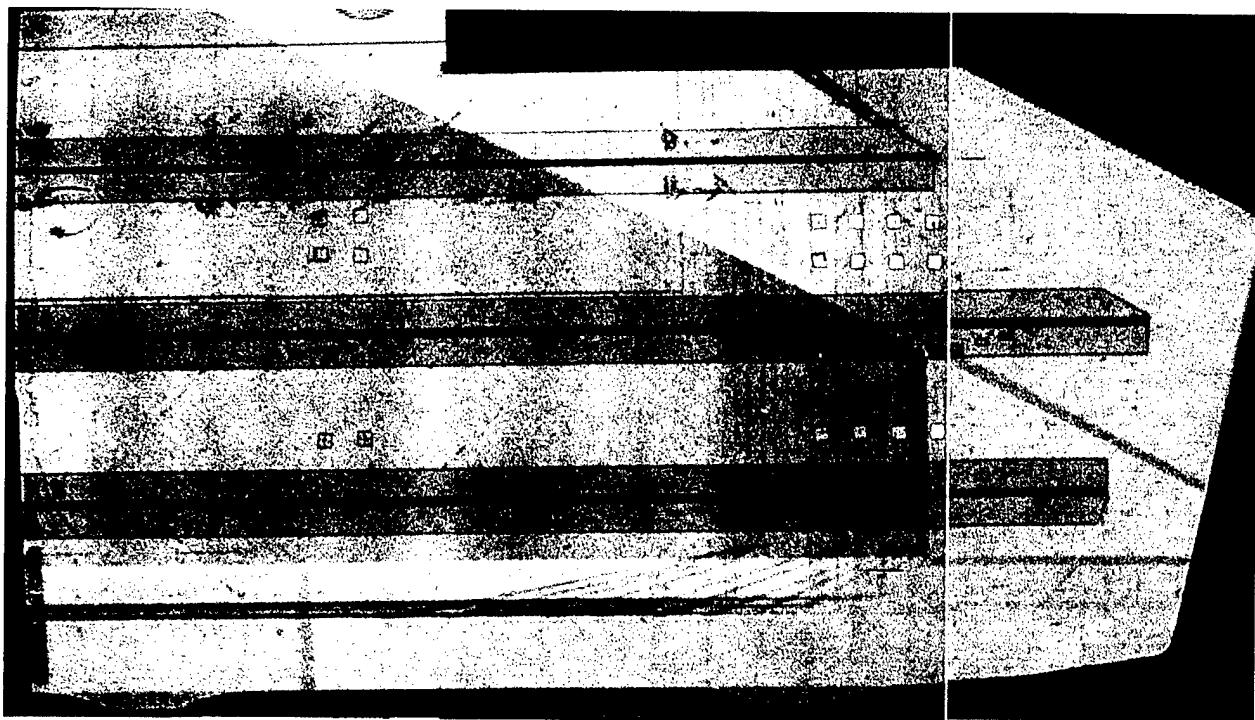


Figure 5.1.4-6. LUIS peak amplitude image of 7J7 panel after tool-side surface painted

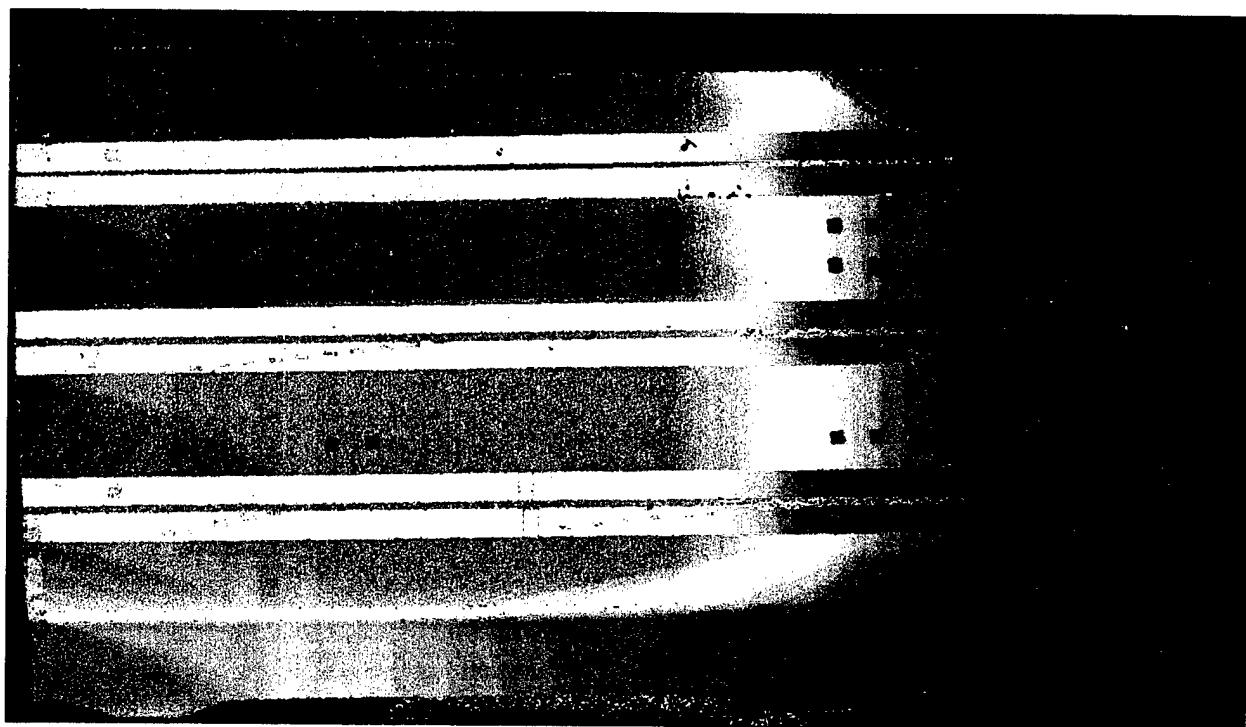


Figure 5.1.4-7. LUIS Pulse Echo Time of Flight Image of 7J7 Panel after tool-side surface painted

5.1.5 Graphite Composite Rib Containing Foreign Materials

A photograph of the rib may be seen in Figure 5.1.5-1. This rib contained foreign materials, most probably ply backing materials, in the web and extending into two flanges. The depths of the foreign materials could be located by examining the upper edges of the rib flanges where they were clearly visible. The foreign material on the left edge was 5 mm below the tool-side surface and 3 mm below the tool-side surface on the right side.

Conventional Test Results

The conventional inspection of these ribs involves two separate immersion through-transmission ultrasonic tests. The solid laminate flanges and radius are scanned at 5 MHz and the rib web that contains honeycomb is tested at 1 MHz. Both the web and flange inspections are performed with arrays of discrete transducers in order to meet inspection rate requirements. The conventional tests readily found the foreign materials although the through-transmission tests do not yield information about the depth of the faults. As noted above, the foreign materials could be seen in the flange edges in this instance.

A single channel, water jet through-transmission ultrasonic test image at 1 MHz of a portion of the rib web may be seen in Figure 5.1.5-2. A color image may be seen in Figure 5.1.5-3. The scan time required was 19 minutes. The foreign materials in the web are seen as areas of increased attenuation (darker indications) at the left and right of the image. The unwanted materials extend from the edge of the honeycomb into the solid laminate flanges on both sides of the panel. The increased attenuation owing to the foreign material was 40 to 50 dB when compared with web areas with similar construction.

LUIS Inspection results.

The rib was scanned from the tool-side surface with the lasers roughly normal to the web. A peak amplitude image from the web may be seen in Figure 5.1.5-4 and a time of flight image may be seen in Figure 5.1.5-5. These pulse echo images reveal the rather complex ply lay-up of the region scanned and they clearly show the depth of the foreign material relative to the

honeycomb core segment, which is in the central portion of the panel. The foreign material on the left is below the honeycomb layer and the material on the right edge is above the honeycomb.

A second angled scan was made of the left edge of the panel so that both the upright flange and the web tool-side surface could be combined in a single image. The peak amplitude and time of flight images may be seen in figures 5.1.5-6, and 5.1.5-7. The foreign material is readily detected in both images. This illustrates the ability of the laser ultrasound to perform inspections within corners with the laser beam off normal to the majority of the test surface.

Evaluation of test results

Both conventional through-transmission (immersion and water jet) readily found the foreign materials. The LUIS data clearly showed the relative depth of the foreign material by virtue of the pulse echo test. The greater inspection rate available with multi-transducer conventional techniques dictate their use for production applications. The LUIS would be valuable as an evaluation tool after the foreign material is detected. The LUIS ability to image in radius areas and the adjacent web and rib flanges is quite useful to develop a single overall image of the extent and location of the foreign material. This is more cumbersome to do with conventional methods in which separate images of the web, radius, and flanges would have to be combined. Typically current Boeing production inspection methods use bubbler systems for flat panels and immersion systems for beams.



Figure 5.1.5-1. Photograph of 777 graphite composite rib with foreign materials



Figure 5.1.5-2. TTU water jet image at 1 MHz of graphite composite rib

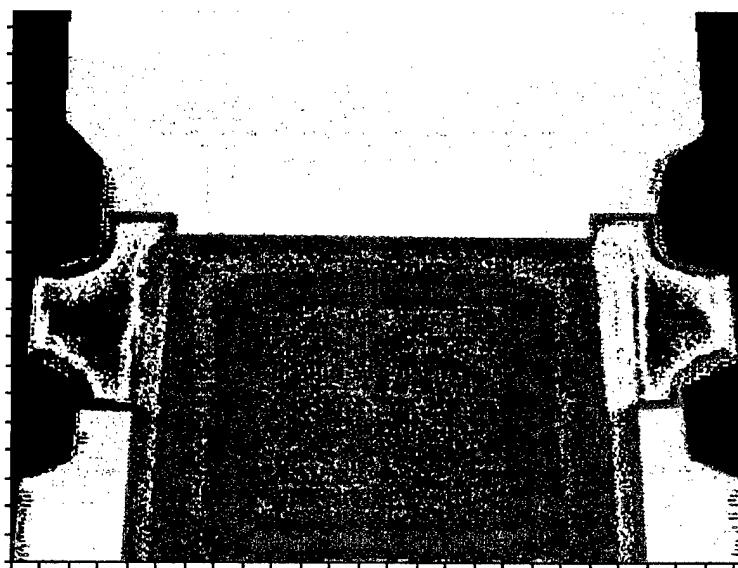


Figure 5.1.5-3. Graphite Composite Rib with foreign material. 1 MHz TTU water jet scan

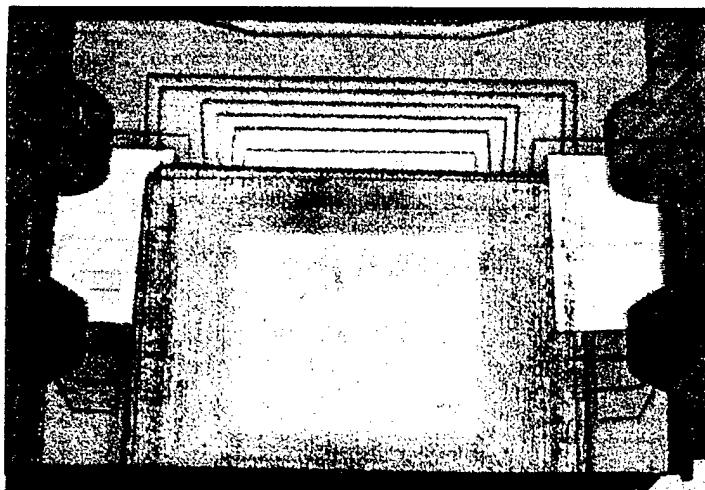


Figure 5.1.5-4. LUIS Peak Amplitude Image of Composite Rib with Foreign Material

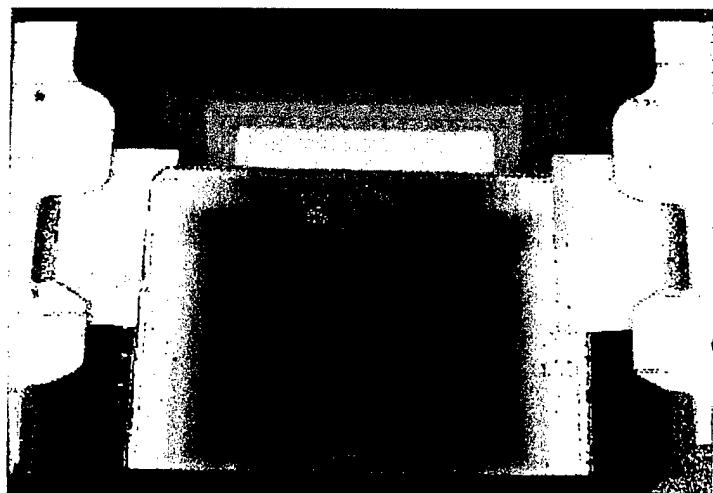


Figure 5.1.5-5. Time of flight image of 777 graphite composite rib



Figure 5.1.5-6. LUIS amplitude image of rib (web-radius-flange). Left flange with foreign material at 5-mm depth.

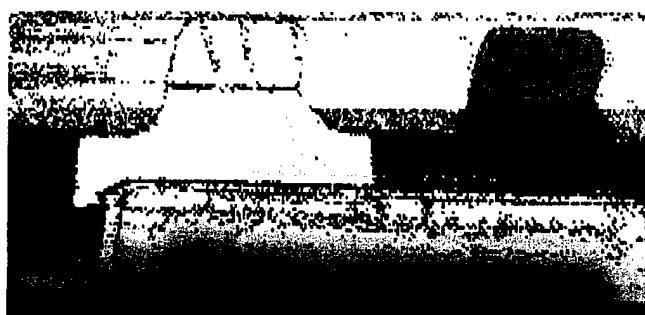


Figure 5.1.5-7. LUIS time of flight image of rib (web-radius-flange). Left flange with foreign material at 5-mm depth.

5.1.6 Graphite Composite Vertical Fin Panel 181

During the autoclave cure process for this skin, a break developed in the bagging material which surrounds the precured composite I-stiffeners and the underlying uncured, laminate material. The bag must remain intact in order for the stiffener to bond properly to the laminate, for the resin to flow within the laminate plies, and for the laminate plies to be properly compacted. The damage sustained by the bag breakage caused this panel to be rejected. As these I-stiffened skins are approximately 50' long, shipping the complete skin to the LUIS was not feasible. A section 14.5" wide and 58" long that contained some of the most extensive damage beneath two stiffeners was cut from the scrapped skin.

Conventional Test Results

The production pulse echo scan of these skins is performed using a surface-riding bubbler in which an eight-element line-focus linear array is mounted. The bubbler is held by gimbals attached to a vertical slider to enable the probe to follow the contour of the tool-side surface of the skin panels. The bubbler transmit signals are generated by separate pulsers coupled to individual piezo elements. The receive signals are sequentially detected by a USIP-20 instrument which provides distance amplitude correction and separate gate outputs for the peak amplitude and time of flight for the first echo exceeding a 10% threshold level. Data sampling takes place at 0.08" intervals in the scan direction (horizontal in the image) and the array element spacing of 0.12" sets the index increment.

A peak amplitude production image of the skin is shown in Figure 5.1.6-1. An overlay is superimposed on the ultrasonic image to show the location of laminate ply drops, stiffener ply drops, rib centerlines, and the footprints of the stiffener flanges. Total scan time for this portion of the overall skin was 20 minutes. A white rectangular box denoted as WARD-1 surrounds the approximate area, which was cut from the skin for scanning by the LUIS. The principal features causing the rejection of this skin were the unfilled ply gaps beneath the stiffener and in the areas adjacent to the stiffeners (dark indications at $\pm 45^\circ$ to the length of the panel) and the large dark areas which resulted from multi-level, intermittent separations within the laminate.

Time of flight data for the overall skin segment is shown in Figure 5.1.6-2. As the threshold for the time of flight measurements is set to be 10% of full-scale on the ultrasonic instrument, in normal areas this image shows the part thickness. As it detects the comparatively weak bond-line echo beneath the stiffeners, the time of flight image shows the bond-line depth rather than the total thickness including the stiffener flanges. In damaged areas the time of flight often yields a white indication since no significant echoes were returned over the total measured depth. The unfilled ply gaps and the areas of multi-level separations appear white in this time of flight image.

LUIS Test Results

The rectangular test article cut from the vertical skin panel was scanned with the LUIS in three portions. Each was about 19" long and covered the panel width. The separate LUIS peak amplitude images are joined together and may be seen in Figure 5.1.6-3. The higher resolution LUIS scan (0.05" sample and index intervals) yielded very clear images of the unfilled ply gaps. The areas of multilevel intermittent separations also agree very well with the production inspection amplitude image. A subtle indication unrelated to the flaws is the approximately 1" wide vertical stripe at the right edge of the middle figure. This is an area of overlap of the Fiberglas that is the first ply placed on the lay-up tool during the process of manufacturing the skins. One minor difficulty encountered with the LUIS optical detection system is illustrated with the left portion of the image in Figure 5.1.6-3. The white indication near the center of this image bounded by a circular edge at the left and bottom is an artifact. This can occur when the laser beams are normal to the test surface, and the intensity of the reflected detection laser exceeds the dynamic range of the LUIS detection system. This problem was generally overcome by ensuring that parts were tilted slightly relative to the laser beam.

Evaluation of Test Results

The sensitivity and resolution of the LUIS data in imaging the flaw conditions in these parts were better than the data from the bubbler production scan. The greater density of data sampling is probably a partial answer. The flaws were imaged very clearly and convincingly. For a high rate production application, however, the bubbler array transducer technique is significantly faster and much less costly. This is another instance in which a reasonably priced laser-based field test

system, which could remotely test aircraft structures, would be very attractive in assessing damage.

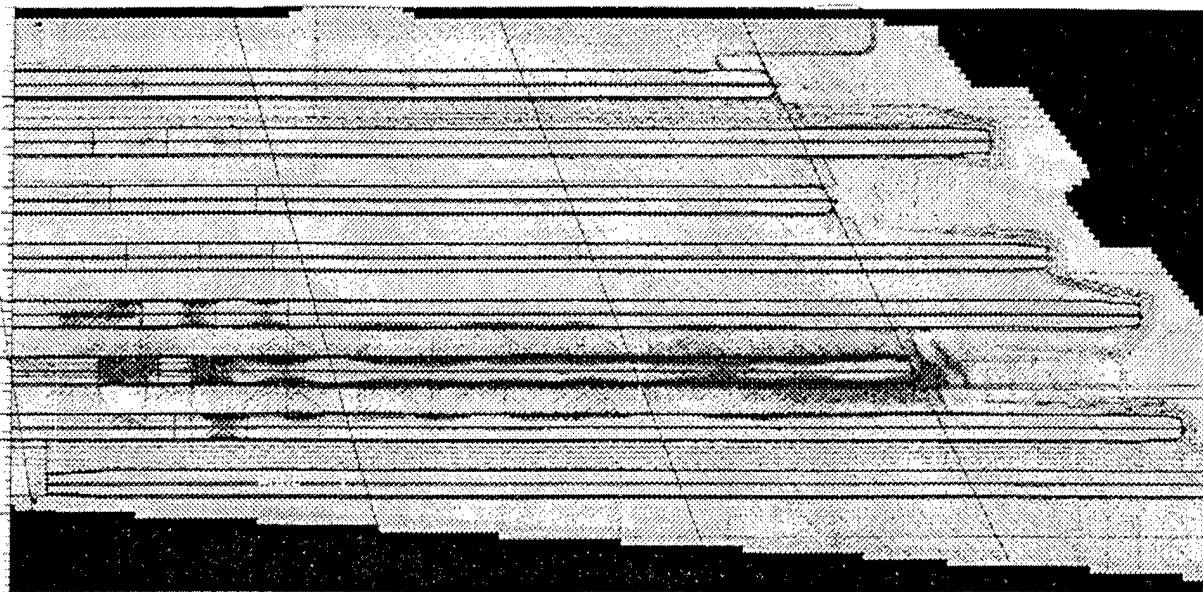


Figure 5.1.6-1. 3.5 MHz Pulse echo peak amplitude bubbler array scans of I-stiffened composite vertical fin panel.

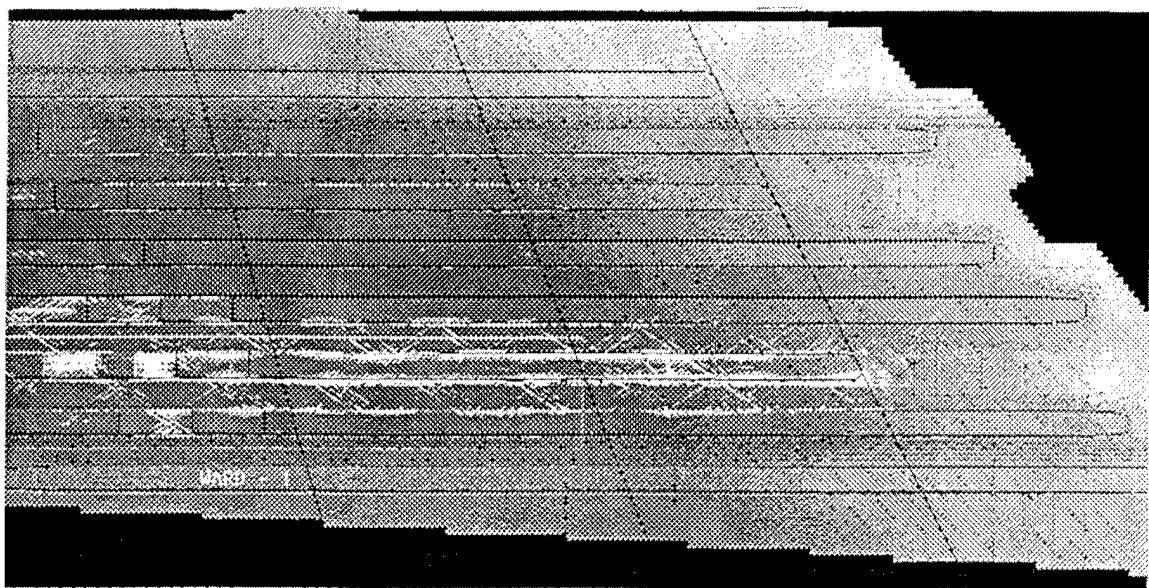


Figure 5.1.6-2. 3.5 MHz pulse echo time of flight bubbler array scan of I-stiffened composite vertical fin panel.

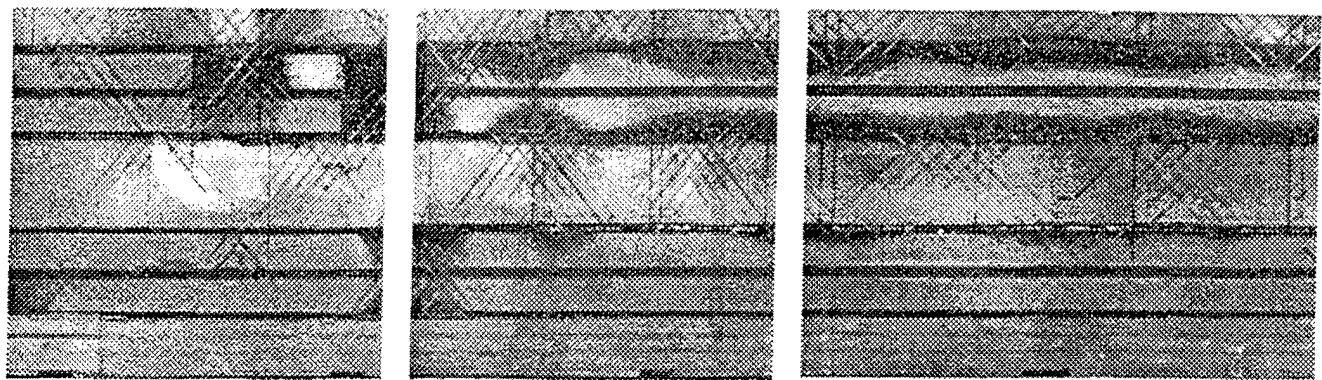


Figure 5.1.6-3. LUIS peaks amplitude scan of flawed portion of I-stiffened composite vertical fin panel.

5.1.7 Graphite Composite I-Stiffener

The part is pictured in Figure 5.1.7-1. Precured graphite composite stiffeners are cobonded to complex laminates to form the main structural components of the 777 empennage. The stiffeners are prepared and inspected prior to bonding to the skin materials. The stiffener used for this work was apparently damaged during handling which created a delamination in one of the lower flanges. This was an obvious fault, but the scrapped stiffener was an attractive geometry to use with laser ultrasound owing to the flexibility of this means of inspection. The stiffener was not painted for the LUIS tests.

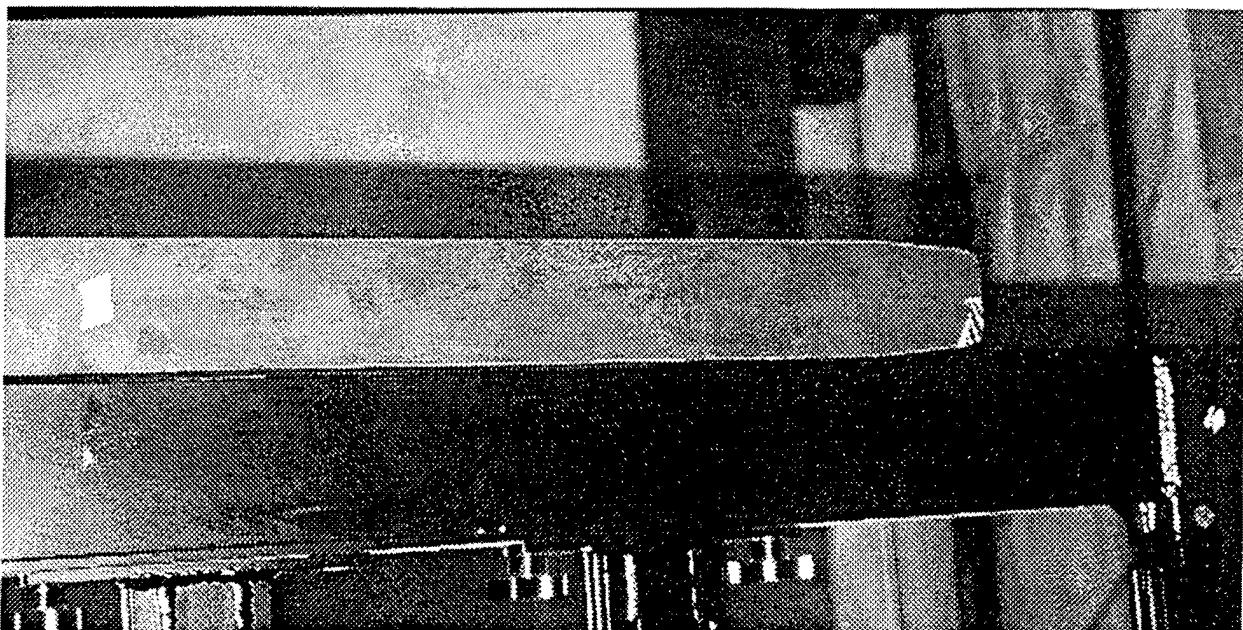


Figure 5.1.7-1. Photograph of I Stiffener

Conventional Test Results

The stiffeners are inspected in production by means of a "pass-through" system containing a large number of transducers, which perform through transmission ultrasonic tests on the upper cap, the web, the lower flanges, and the radius areas where the web joins the cap and lower flanges. In one pass through the inspection zone all of the regions of interest are tested by 49 pairs of 5 MHz transducers. In this case the damaged zone at the end of the lower flange was detectable by visual examination, and a recording from the pass-through system was not available.

LUIS Test Results

Two scans were made of the scrapped stiffener. The first scan was of a 24" portion of the stiffener upper cap. At the same time the portion of the lower flanges, which were not shadowed by the upper cap, were imaged. The peak amplitude image of this data may be seen in Figure 5.1.7-2. The sound loss into the upper edge of the web caused the dark central indication. The delamination is seen in the upper left end of the image as a darkened indication at the edge of the flange. The broad, dark bands at the left and right ends of the image are associated with a ply of Fiberglas that is the outermost layer of the upper surface of the cap and lower flanges. The white markings at the right end of the image identified the stiffener as being scrapped. A view of the lower flanges may be seen in Figure 5.1.7-3. The delamination was detected on the lower left corner of the lower flange. The lower edge of the web is seen as the dark central line. The edges of the delamination are better defined in this view from the lower surface of the stiffener. No additional faults were seen in these images.

Evaluation of Test Results

The existing multi-transducer method affords a rapid and thorough means of inspecting composite stringers in production. The principal drawback of the present method is that if design changes are introduced (such as a tapered web at the ends of stringers), the transducer arrays, holding fixtures, electronics, and software would have to be modified to accommodate a new part geometry. The LUIS system could be adapted more easily to these changes since the stiffener is not contacted by this inspection. In order to demonstrate complete inspection of these stiffeners with LUIS, however, it would be necessary to demonstrate that the pulse echo technique is effective in the radius areas. This demonstration was not accomplished in the present contract, but it would be a useful investigation for furthering applications of LUIS.

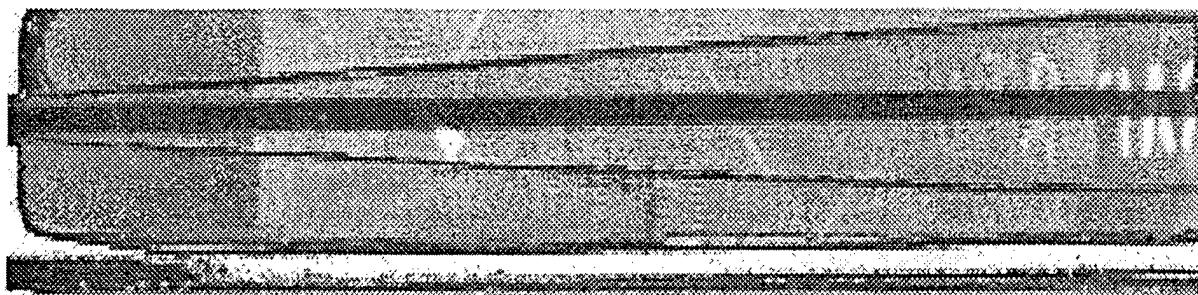


Figure 5.1.7-2. LUIS Peak amplitude images of upper cap and lower flange of graphite composite I-stiffener

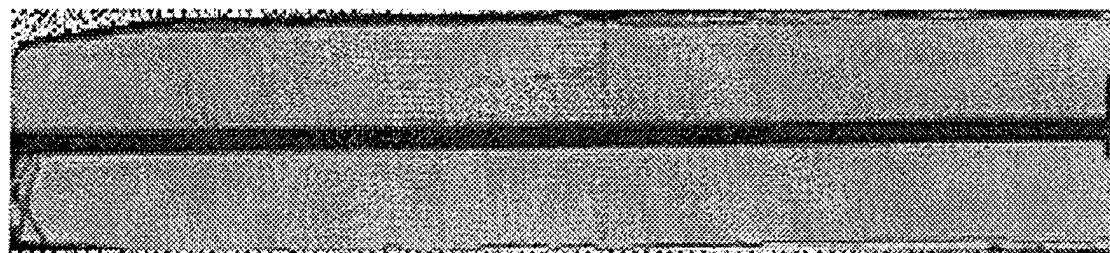


Figure 5.1.7-3. LUIS Peak amplitude image of lower flange of graphite composite I-stiffener

5.1.8 Leading Edge of Graphite Composite Aileron

The leading edge of composite ailerons, flaps, and other control surfaces often are comprised of a C-shaped spar to which are bonded the upper and lower skins of the component. The skins are often curved at the leading edge for aerodynamic purposes. The spacing between the upper and lower surfaces together with hinge fittings on the forward edge of the spar often preclude use of automated water jet through transmission ultrasonics. This test article was the leading edge of a short section of a composite aileron pictured in Figure 5.1.8-1. This part is manually inspected by a hand-held yoke fitted with small water jets. The manual inspection does not produce a record. These manual tests are very difficult to perform thoroughly and consistently over a lengthy control surface.

Conventional Test Results

The conventional inspection of this part is with a hand-held yoke. No image is available for comparison.

Luis Inspection Results

There were no known faults in the aileron section scanned. The curved leading edge was scanned without painting the test surface. The Luis amplitude and time of flight images from the aileron leading edge may be seen in Figures 5.1.8-2 and 5.1.8-3. A clearance cutout in the upper edge of the near skin is seen as a white rectangular indication at the upper edge of the peak amplitude image in Figure 5.1.8-2. The dark spot to the right of center in both images is from a hole drilled in this portion of the upper skin.

Evaluation of Test Results

There were no conventional results available to compare with the Luis images. The Luis would be a convenient means of performing tests of leading edge portions of control surfaces that are presently inspected by manual tests. The complete aileron is substantially longer than the segment tested for this demonstration. The manual tests on these ailerons are difficult, time-consuming, and less reliable than automated inspections as demonstrated with Luis.

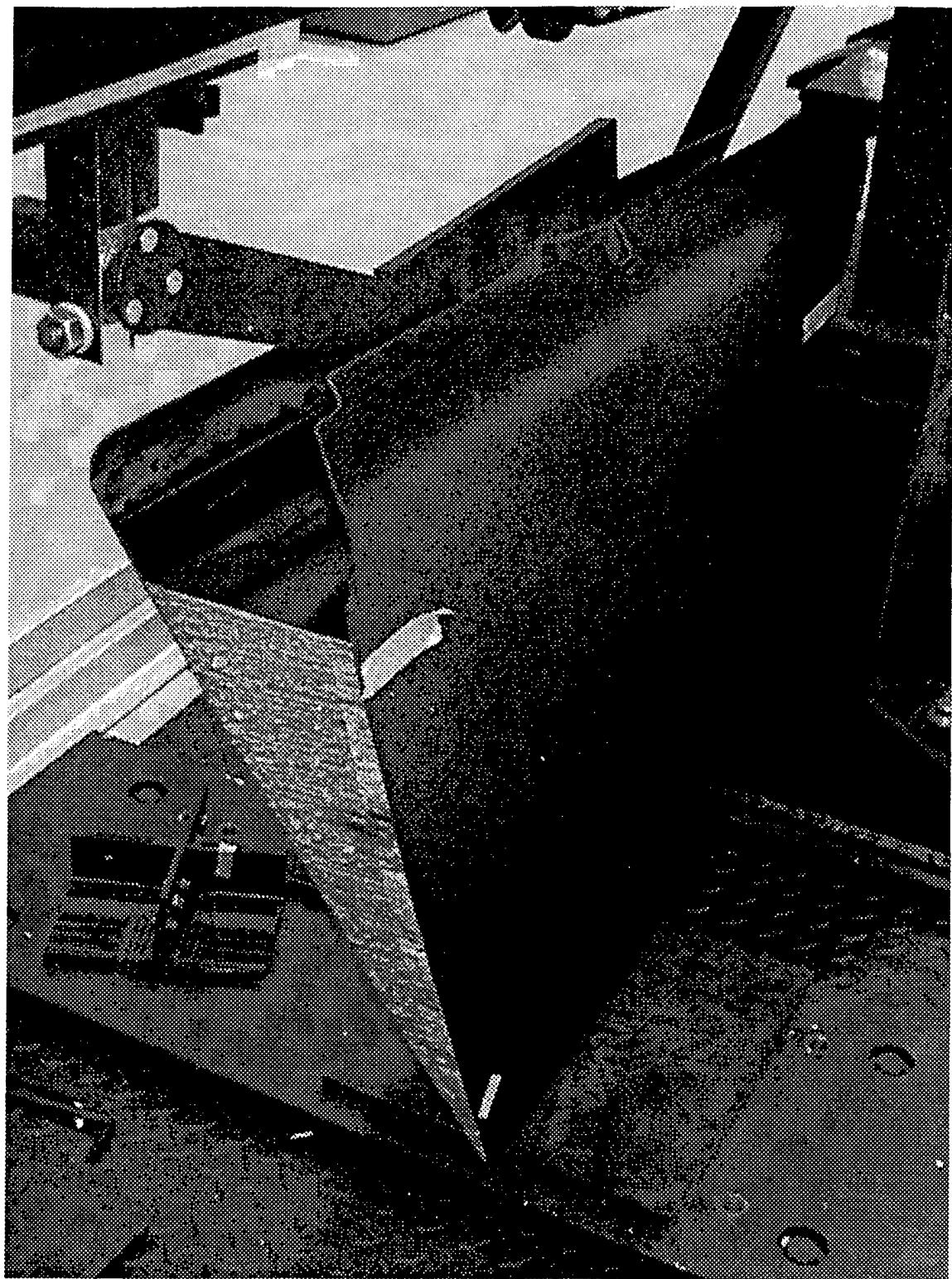


Figure 5.1.8-1. Photograph of leading edge of a short segment of a composite aileron

D950-10322-1

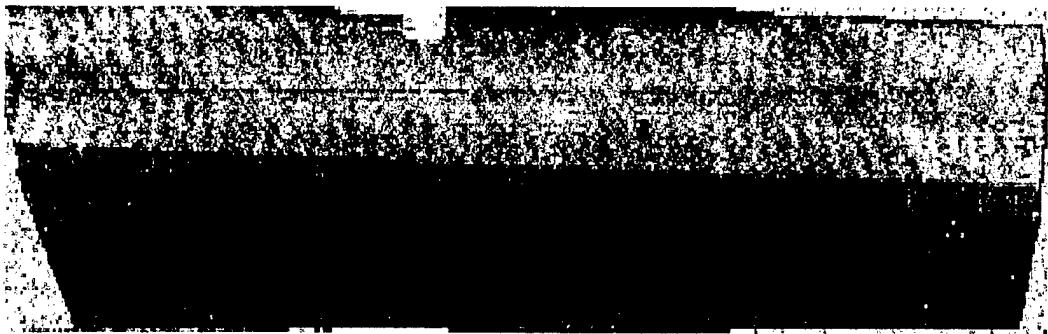


Figure 5.1.8-2. LUIS Peak Amplitude Image from Curved Leading Edge Laminate of Composite Aileron Segment



Figure 5.1.8-3. LUIS Time of Flight Image from Curved Leading Edge of Composite Aileron Segment

5.1.9 Graphite Composite Honeycomb Repair Panel R-10

This panel was prepared for a study of fault detection within repaired areas on honeycomb sandwich structures. The outer skins consisted of 12 plies of plain weave, prepreg fabric material bonded to nomex honeycomb core. After the panel was cured the upper skin and honeycomb core were removed from an eight inch circular area at the center of the panel on the tool-side surface. The skin plies surrounding the central region were tapered to allow new fabric to be added to the repaired skin. A circular 'plug' of core was machined to replace the core removed from the simulated damage area. The repair 'plug' was spliced to the original core and successively larger diameter circular fabric prepreg plies were added to bring the repaired thickness to the original 12 plies. Faults were simulated by one inch diameter inserts of graphite foil coated with Freekote parting agent. These were placed at various depths as shown in the drawing in Figure 5.1.9-1. The designation P3, for example, means an insert that is in the third ply above the honeycomb core, and there are nine plies above this insert. Circular holes were cut in the prepreg cloth to accommodate the inserts at each depth. Inserts were placed at all depths from 1 to 11 plies beneath the tool-side surface. Two additional circular areas were prepared near the center of the panel in which the core was machined to produce an air gap between the replacement skin and the core. In the center of the panel a one inch diameter plug of potting material was added to the core. Potted areas are often used to provide reinforcement for fasteners, and this central plug did not represent a fault.

Conventional Test Results

Repairs of this type are typically inspected by water jet through transmission ultrasonics (TTU) at 1 MHz. A TTU image of the repair panel may be seen in Figure 5.1.9-2. The image is oriented to match the drawing showing the graphite inserts. The central plug of potting material is clearly seen, as are the two areas of machined core. The machined core indication to the left of the central potting plug is between the core and the tool-side skin. The indication directly below the central potting plug is a gap machined between the bag-side skin and the core. There are indications from all of the inserts labeled P1 through P11; however, P2 and P3 are largely obscured by the core splice between the circular core repair plug and the surrounding core. The indications for P5 and P6 are smaller than the actual area of these inserts.

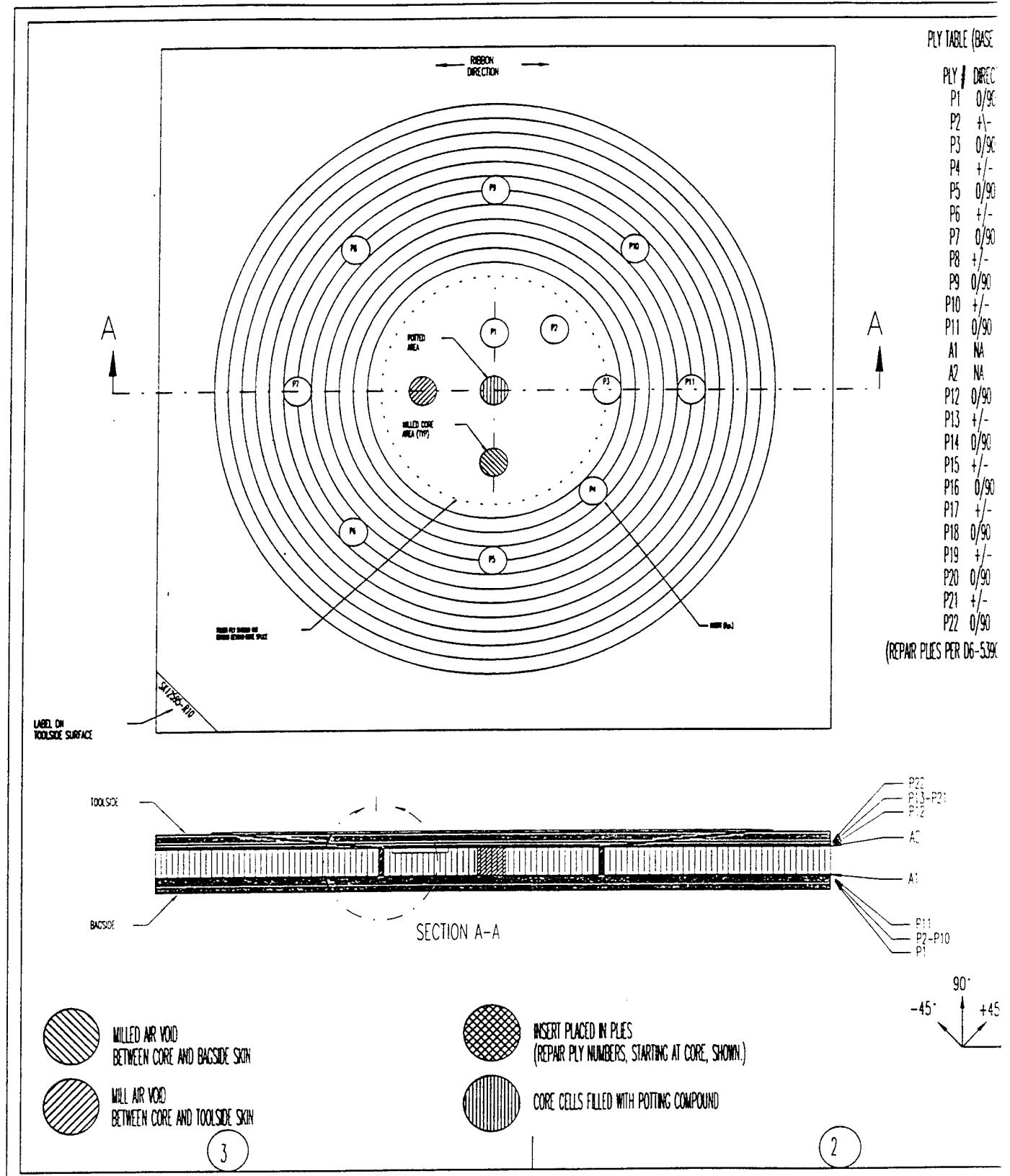


Figure 5.1.9-1 Honeycomb Repair Panel R-10

| | | | | |
|-----------|---------|--------------------|--------------------|---------------------|
| REV LR | REASONS | CHANGED BY/DATE | CHECKED BY/DATE | APPROVED BY/DATE |
|-----------|---------|--------------------|--------------------|---------------------|

PLY TABLE (BASE PANEL)

| PLY | DIRECTION |
|-----|-----------|
| P1 | 0/90 |
| P2 | +/- |
| P3 | 0/90 |
| P4 | +/- |
| P5 | 0/90 |
| P6 | +/- |
| P7 | 0/90 |
| P8 | +/- |
| P9 | 0/90 |
| P10 | +/- |
| P11 | 0/90 |
| A1 | NA |
| A2 | NA |
| P12 | 0/90 |
| P13 | +/- |
| P14 | 0/90 |
| P15 | +/- |
| P16 | 0/90 |
| P17 | +/- |
| P18 | 0/90 |
| P19 | +/- |
| P20 | 0/90 |
| P21 | +/- |
| P22 | 0/90 |

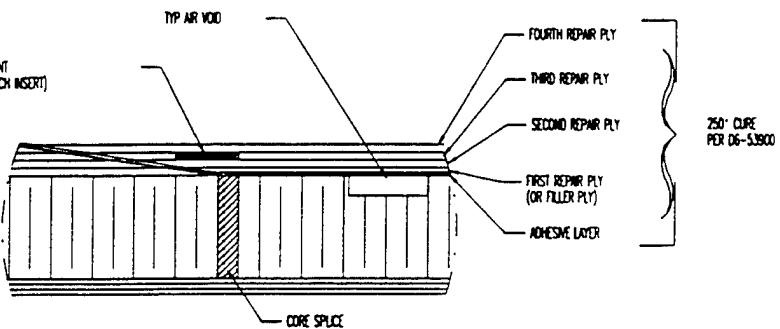
NOTES:

1. ALL INSERTS ARE MADE FROM GRAPHITE FOIL (PROVIDED)
 - DIP INSERTS IN FREEKOTE BEFORE POSITIONING THEM IN PANEL.
 - TRIM CIRCULAR AREAS FROM THE PREPREG TO MATCH DEFECT LOCATIONS
2. USE BMS 5-28 TYPE 7 FOR POTTED AREA IN CENTER OF PANEL.
PRE-CURE CORE DETAIL WITH POTTING TO PREVENT POTTING VODS.
3. BASE MATERIAL SKIN IS BMS 8-256 TYPE II CLASS 2 3K-70-PW
4. CURE BASE MATERIAL SKINS AT 350 DEGREES, 45 psi PER BAC 5317-4
5. REPAIR PER D6-53900, 250 DEGREE CURE, AFTER PLACEMENT OF INSERTS
6. CURE REPAIR MATERIAL AT 10.5 psi IN AN AUTOCLAVE OR VACUUM BAG IN AN OVEN
7. CORE MATERIAL: BMS 8-124, TYPE V, CLASS 4, GRADE 3
8. IDENTIFY PANEL IN LOWER LEFT CORNER AS SHOWN.
9. ALIGN REPLACEMENT CURE RIBBON DIRECTION WITH
BASE PANEL RIBBON DIRECTION

A

(REPAIR PLES PER D6-53900)

TOP INSERT PLACEMENT



DETAIL I
PLACEMENT OF DEFECTS
SCALE : NONE

2

A 3.5 MHz pulse echo bubbler was also used to scan the repaired honeycomb panel. Figures 5.1.9-3 and 5.1.9-4 are peak amplitude images made on the tool-side surface of the panel. The inserts labeled P4 through P11 are easily visible in Figure 5.1.9-3. These inserts range from 1 ply beneath the tool-side surface (P11) to 8 plies beneath this surface (P4). A later gate setting was used to prepare Figure 5.1.9-4 and inserts 11 plies beneath the tool-side (P1) to 9 plies (P3) were readily seen. The machined core between the tool-side surface was also detected to the left of center of Figure 5.1.9-4. The potted plug was not seen in the pulse echo scans as it is bonded to the face sheet. The machined core between the bag-side skin would, of course, not be visible to pulse echo from the tool-side surface.

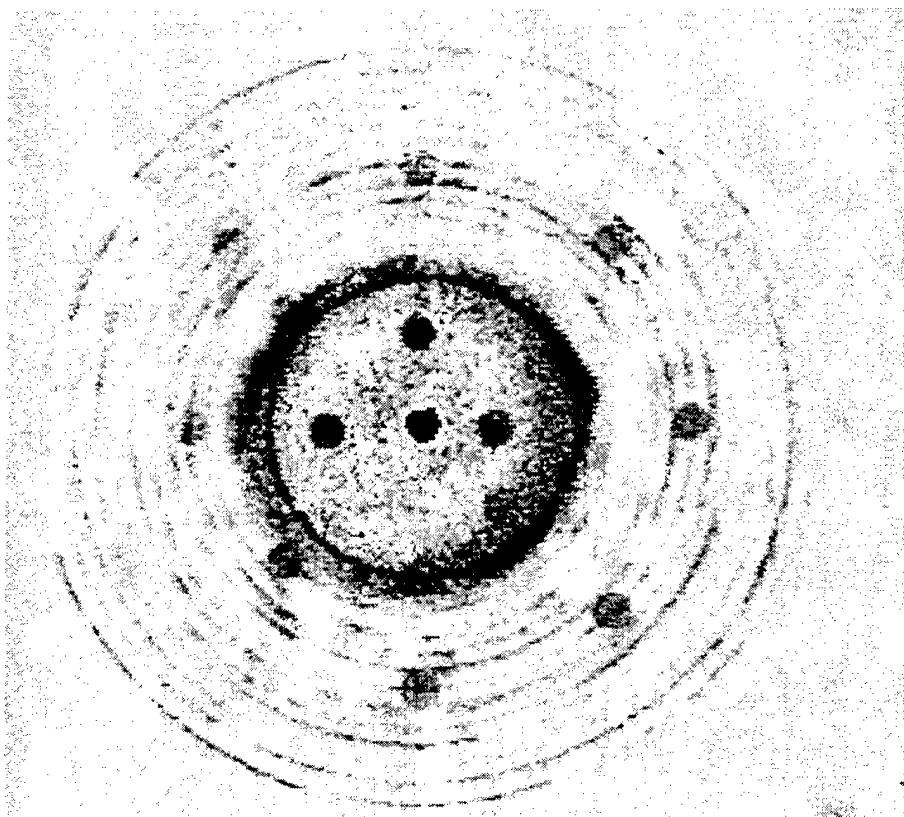


Figure 5.1.9-2. 1 MHz TTU image of Honeycomb Composite Repair panel R-10.

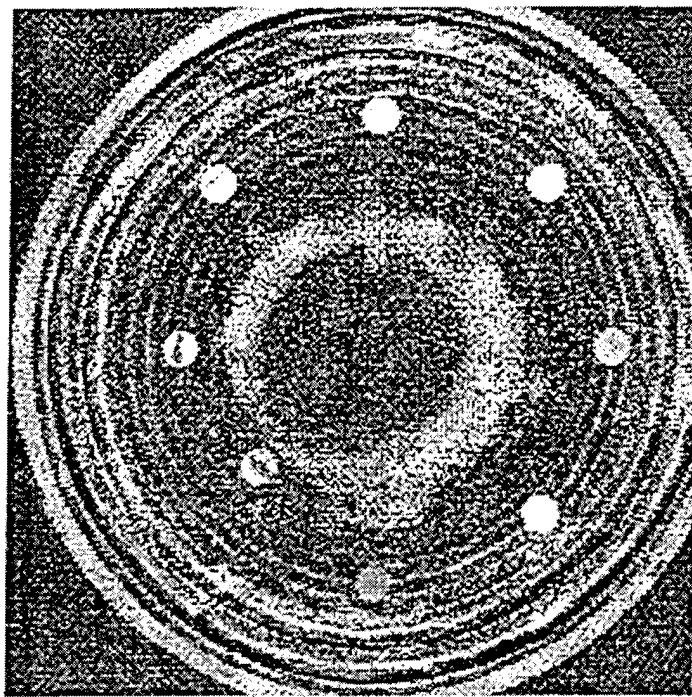


Figure 5.1.9-3. 3.5 MHz Bubbler Pulse Echo Amplitude Image of Honeycomb Repair Panel R-10. Gating inserts nearer to tool-side surface.

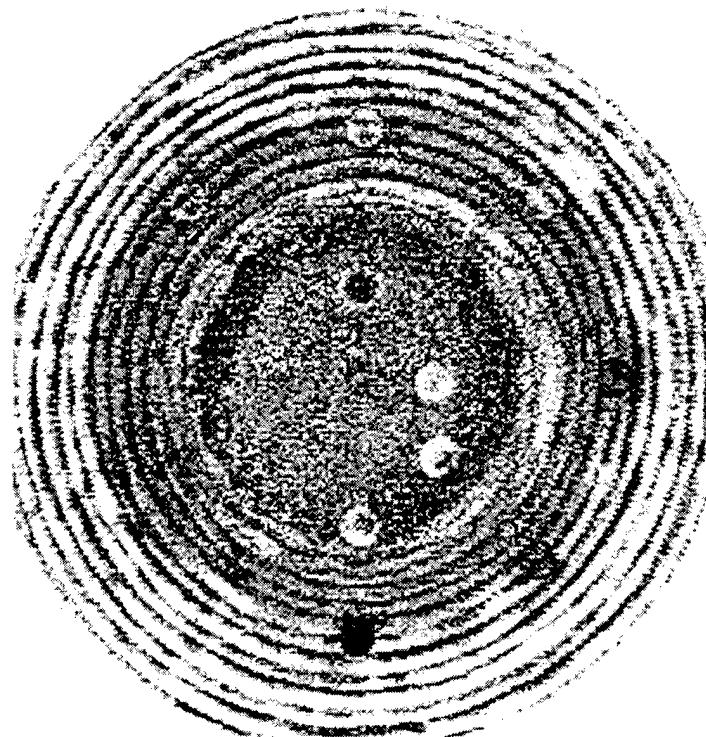


Figure 5.1.9-4. 3.5 MHz Bubbler Pulse Echo Amplitude Image of Honeycomb Repair Panel R-10. Gating inserts farther from tool-side surface.

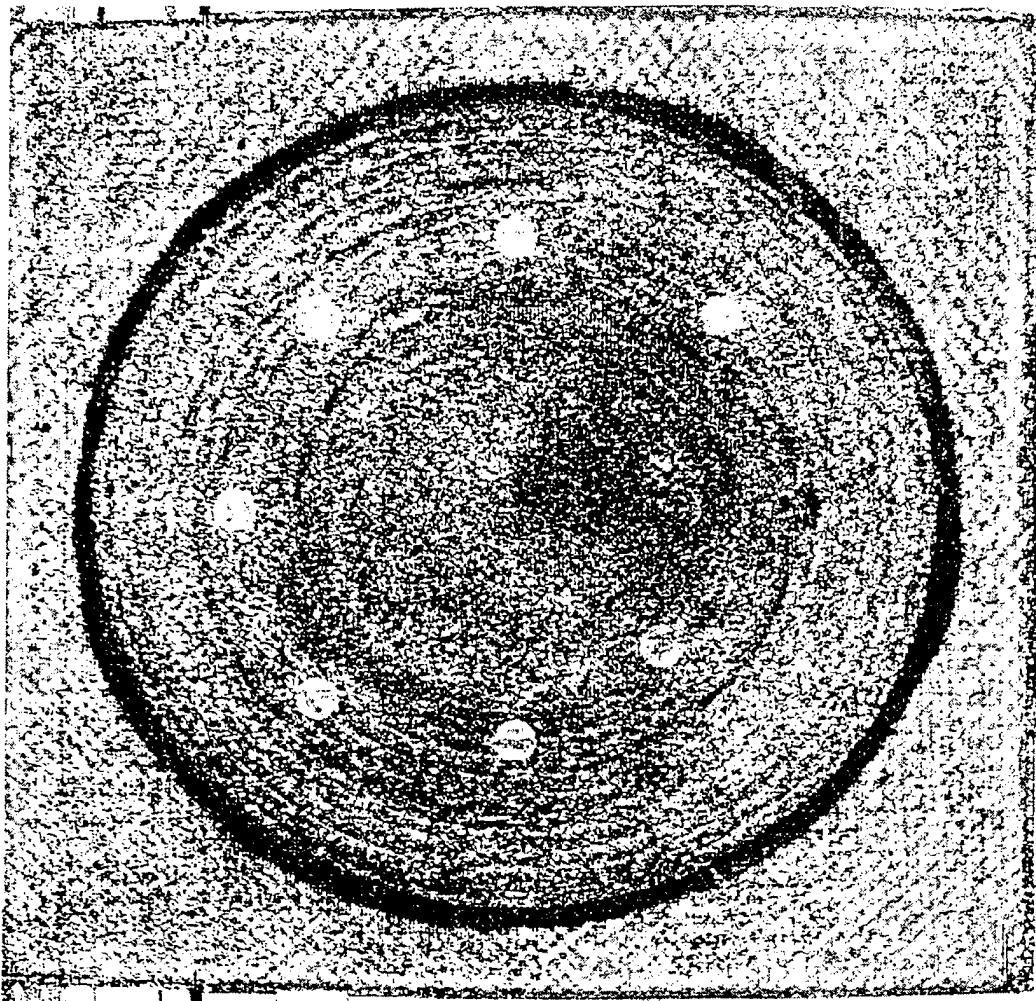


Figure 5.1.9-5. LUIS Pulse Echo Peak Amplitude Image of Honeycomb Repair Panel R-10. Inserts from 2 to 8 plies beneath the tool-side are lighter indications. The insert that is 1 ply beneath the tool-side is a dark indication at 3 o'clock from panel center.

LUIS Test Result

The peak amplitude image in Figure 5.1.9-5 clearly shows the inserts 2 to 8 plies beneath the tool-side surface as light indications owing to stronger echoes from these inserts. The insert that was 1 ply beneath the tool-side was difficult to image in the amplitude data. It was poorly detectable at the right of center of the panel as a dark indication. Several different time of flight images were also prepared with different gate settings to image the inserts at different depths. In Figure 5.1.9-6 those inserts ranging from 1 to 8 plies beneath the tool-side surface are seen easily. A wider gate was used in Figure 5.1.9-7 to image inserts from 5 to 11 plies beneath the tool-side surface. Detecting and correctly sizing these inserts is more difficult than for those inserts located

closer to the tool-side surface. The image in Figure 5.1.9-8 shows the insert 11 plies down slightly above the panel center and the insert 10 plies down is above and to the right of center. The inserts more than 8 plies beneath the tool-side surface could easily be lost in the noise if the LUIS TOF data were not evaluated very carefully.

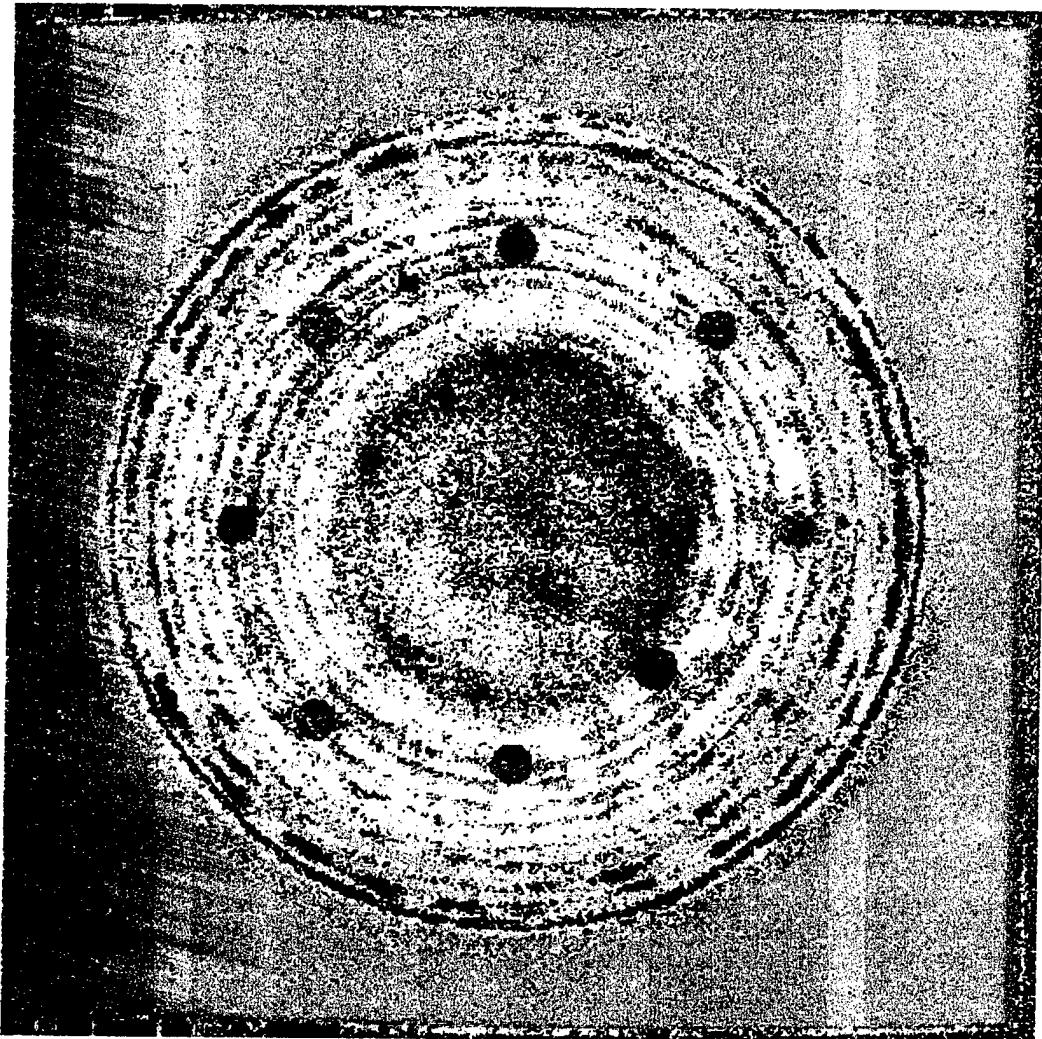


Figure 5.1.9-6. LUIS Time of Flight Image of Honeycomb Repair Panel R-10. Inserts that are from 1 to 8 plies beneath the tool-side are visible. The blue indication at 3 o'clock from the panel center is from a one-inch diameter graphite insert 1 ply below the tool-side surface.

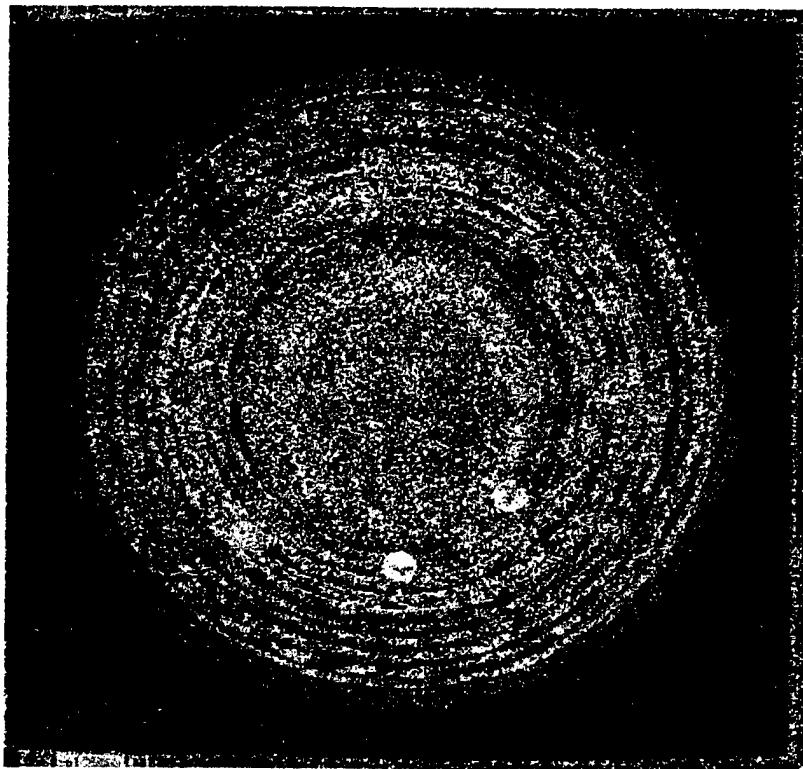


Figure 5.1.9-7. LUIS Time of Flight Image of Honeycomb Repair Panel R-10. Inserts that are from 5 to 11 plies beneath the tool-side surface are visible.

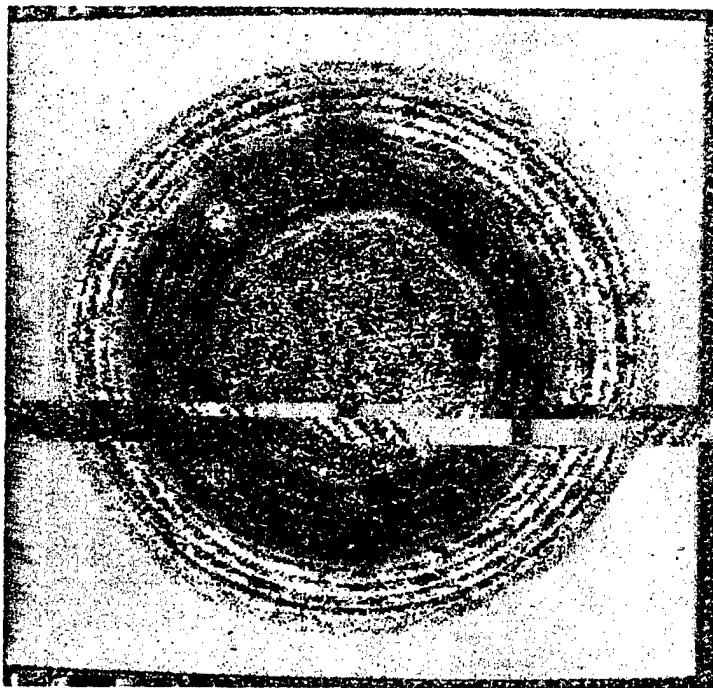


Figure 5.1.9-8. LUIS Time of Flight Image of Honeycomb Repair Panel R-10. The insert 11 plies beneath the tool-side are the orange circle at top center. The red indication to the right and slightly above this is 10 plies down from the tool-side surface.

D950-10322-1

Evaluation of Test Results

The TTU test detected or partially detected all of the inserts and areas of machined core adjacent to both the bag-side and tool-side surfaces. Inserts directly over the edges of the repair core plug, however, were difficult to see. If the inserts did not have a consistent shape these would have been missed. Also two of the inserts that were detected would not have been sized correctly from the TTU indications.

The bubbler pulse echo peak amplitude data required two different gate settings to enable visualization of all of the inserts. All of the inserts were clearly seen, as was the machined core beneath the tool-side surface. The indications at all depths were close to the actual sizes of the inserts or machined area.

The honeycomb panel was not painted prior to conducting the LUIS tests. Had the tool-side surface been painted, the detected signals would probably have been stronger and the flaw detectability improved. It was difficult to image the inserts that were greater than eight plies below the tool-side surface. Several iterations were required to generate the LUIS images of this panel, and the results were not impressive. It was not possible, for example, to detect the one-inch diameter area of machined core beneath the tool-side surface.

Owing to the greater sensitivity obtained with the water jet TTU and the bubbler tests and the ability to conduct these tests without application of a tool-side coating, the conventional tests would be the preferred means of inspecting this repair panel.

5.1.10 Horizontal Stabilizer Skin Panel 459

This graphite composite skin panel is the outboard portion of a 777 lower horizontal stabilizer skin. A photograph of the tool-side surface may be seen in Figure 5.1.10-1. The marks on the surface were to locate faults discovered during the conventional inspection. Figure 5.1.10-2 shows the tool-side surface following application of a strippable paint applied to improve the LUIS inspection results. The skin is stiffened by precured stiffeners, which are cobonded on the bag-side surface at the time the skin laminate is cured. It was scrapped owing to a leak in a lay-up tool vacuum port which resulted in inadequate compaction and resin flow as evidenced by numerous areas of excessive porosity and unfilled ply gaps. This panel is an attractive test article to evaluate the applicability of laser ultrasound to inspect a large composite structure containing natural faults.

Conventional Test Results

The production inspection of these parts is carried out by an eight-element, 3.5 MHz line-focus linear array transducer mounted in a rectangular bubbler. The bubbler is held by a gimbal attached to a vertical slider to enable the probe to follow the contour of the tool-side surface of the skin panels. The bubbler transmit signals are generated by separate pulsers coupled to individual piezo elements. The receive signals are sequentially detected by a USIP-20 instrument which provides distance amplitude correction and separate gate outputs for the peak amplitude and time of flight for the first echo exceeding a 10% threshold level. Data sampling takes place at 0.08" intervals in the scan direction (horizontal in the image) and the array element spacing of 0.12" sets the index increment.

The image in Figure 5.1.10-3 shows the peak amplitude and in Figure 5.1.10-4 the time of flight data collected with the bubbler array on this skin panel. The total scan time to collect this data was 6 minutes. The most notable features seen in the amplitude image are the exaggerated ply gap indications across the width of the panel and at $\pm 45^\circ$. Also, areas of porosity are seen as diffuse indications beneath the stringers. There is also a general increase in attenuation along the upper edge of the skin, which was near the site of the vacuum port leak. The time of flight image

also reveals the major sites of porosity and emphasizes the unfilled ply gaps at the upper edge of the skin.

LUIS Test Results

This panel was scanned twice with the LUIS. The first scan was made to yield a relatively high-resolution image (0.05" sampling and 0.05" index) for comparison with the bubbler amplitude image. Scan time was 64 minutes. As noted above, painting the tool-side surface with a strippable white paint improved the LUIS ultrasonic signal levels. Irregularities in the paint may have contributed to some of the variations seen in the LUIS amplitude images. The peak amplitude images in Figures 5.1.10-5 and 5.1.10-6 show lighter areas near the center of the panel, which may have been caused by variations in the paint thickness. The principal features seen in the high-resolution image closely match those in the bubbler peak amplitude image. The LUIS scan covered slightly more of the skin panel than is shown in the bubbler images.

A second scan was made with reduced data sampling (0.10" sampling and index increments) in order to increase the inspection rate. The scan time in this case was 19 minutes. By comparing the two LUIS images it is quite clear that all of the principal image features may be seen in the lower resolution data. This lead to a substantial increase in inspection speed.

Evaluation of Results

The need to paint the tool-side surface for LUIS tests is a drawback for the production environment. Inspection of in-service parts that are already painted would not require this step. In addition, the ability to scan a skin panel installed on an aircraft could be of great benefit. The use of arrays in conventional scanning systems coupled with the comparatively low cost of these systems make the bubbler scanners an attractive means of inspecting these parts in production. If a portable laser system with comparable performance was developed at a lower cost, this could be an attractive means of performing in-service tests of damaged structures.

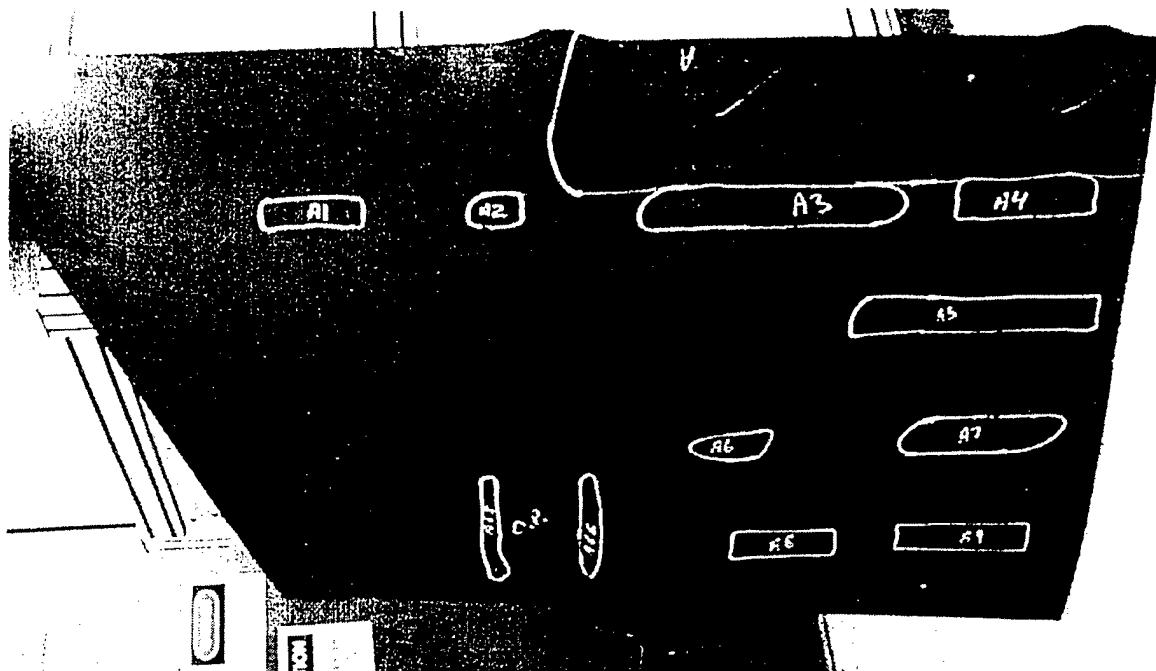


Figure 5.1.10-1. Photograph of tool-side surface of horizontal stabilizer skin panel 459

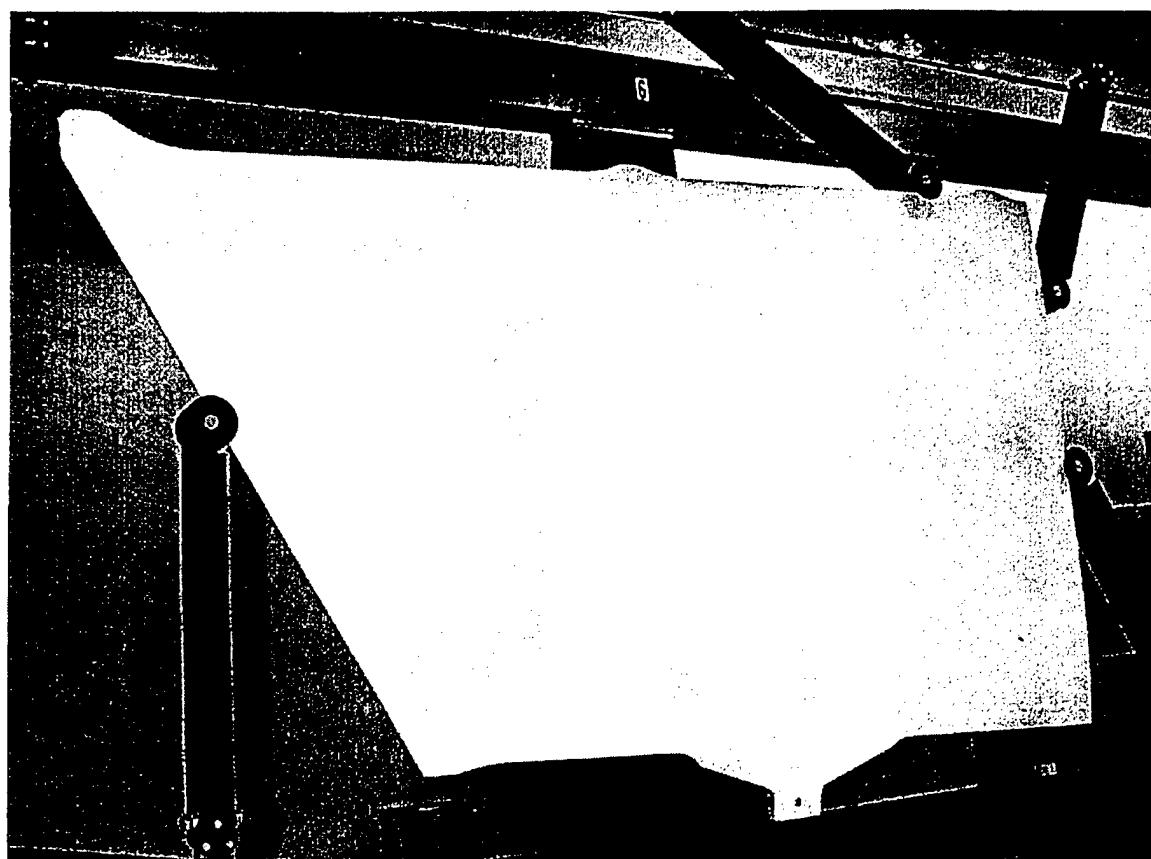


Figure 5.1.10-2. Photograph of painted tool-side surface of horizontal stabilizer skin panel

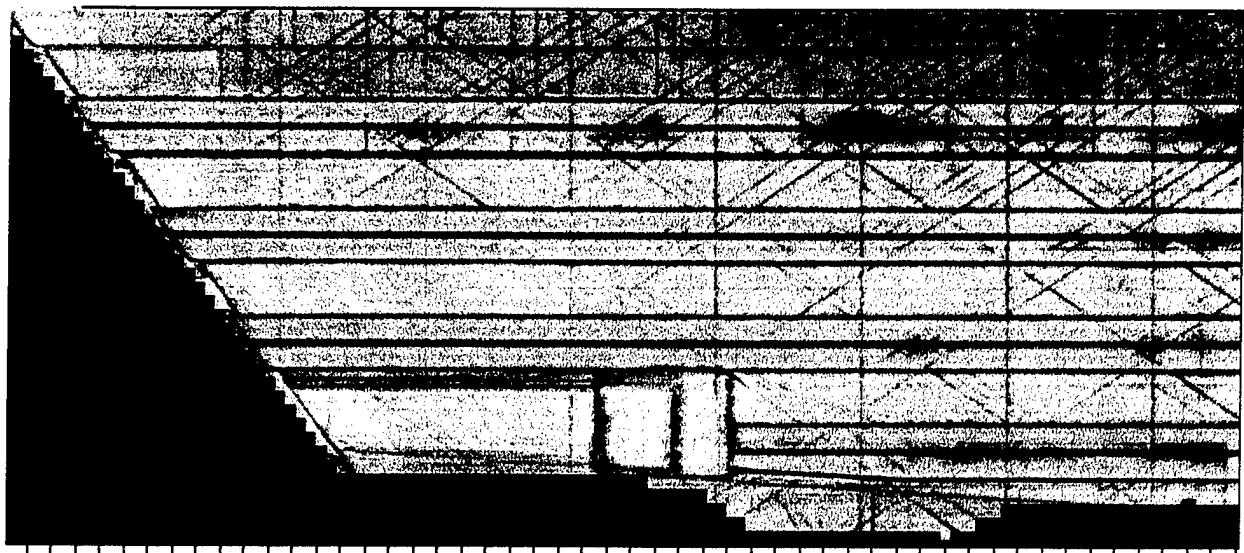


Figure 5.1.10-3. Peak amplitude image of horizontal skin panel 459. 3.5 MHz Pulse echo bubbler scan with 8-element array

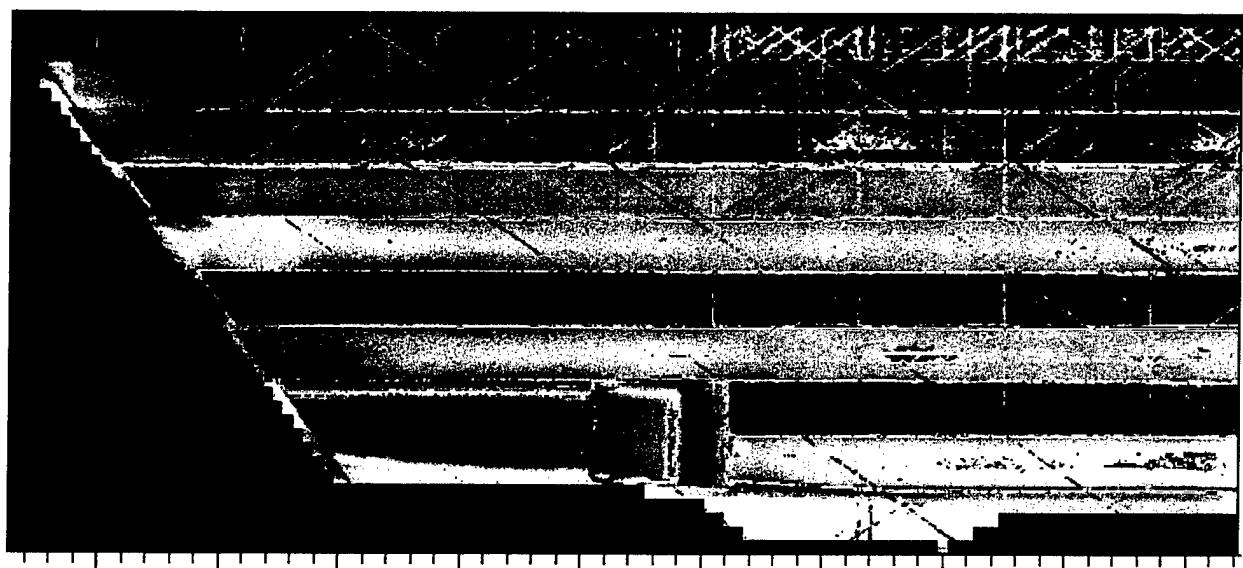


Figure 5.1.10-4. Time of flight image of horizontal skin panel. 3.5 MHz Pulse echo bubbler scan with 8-element

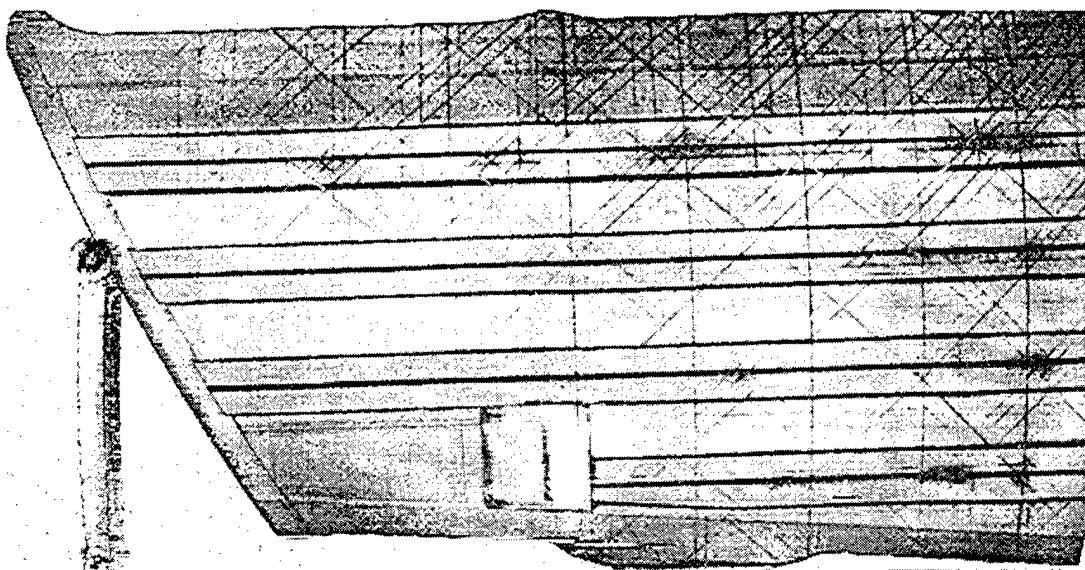


Figure 5.1.10-5. LUIS peak amplitude, high resolution image of skin panel

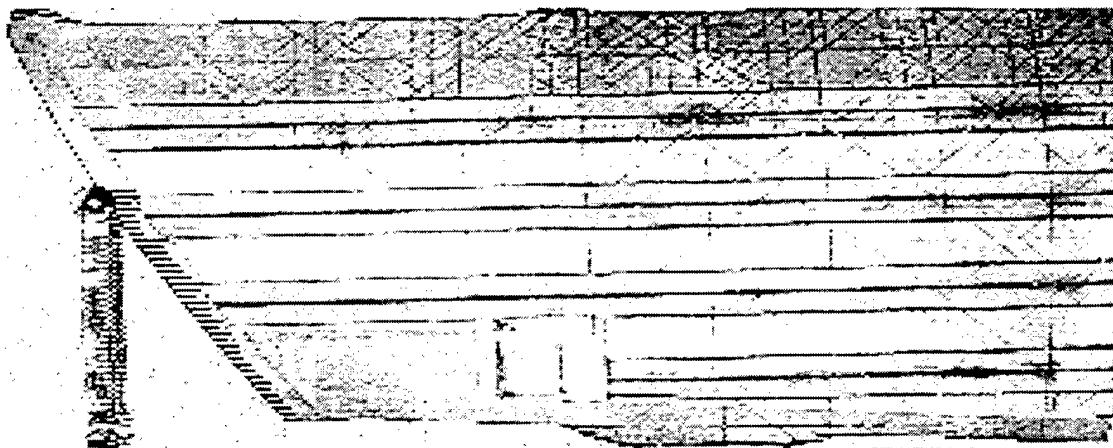


Figure 5.1.10-6. LUIS peak amplitude, reduced resolution image of skin panel 459

5.1.11 Complex Graphite Composite Component

This is a comparatively small graphite component shown in Figures 5.1.11-1 and 5.1.11-2. Its shape somewhat resembles an old-fashioned bicycle chain guard. The photograph in Figure 5.1.11-1 has been reversed left to right to match the picture from the concave surface. This part would be difficult to scan thoroughly with conventional pulse echo techniques, but the comparatively thin wall; composite construction seemed well suited for testing with LUIS. Only one end of the part was scanned. The portion tested contained the most difficult geometry, and it also contained some natural discontinuities.

Conventional Test Results

A laboratory, 3 MHz through transmission scan of the part was made with vertically opposed water jets. For this test the concave surface faced upward. The image obtained may be seen in Figure 5.1.11-3. Areas of increased attenuation may be seen in the radius on the right side of the image. These correspond to the markings in the radius area of the part that may be seen in Figure 5.1.11-2. The tape square used as an artificial flaw indicator seen in the photograph is also visible in the through transmission image.

LUIS Test Results

The LUIS scan was made from the convex or bag-side surface. As was often the case with composite parts, the LUIS ultrasonic signals obtained from the bag-side surface were better than from the tool-side surface. The peak amplitude image from the part may be seen in Figure 5.1.11-4 and the time of flight image is in Figure 5.1.11-5. The indications seen in the radius area with the peak amplitude data resemble those obtained in same area with the through transmission test. An indication was also seen corresponding to the tape attached to the tool-side surface. In addition, the time of flight data shows there are reflectors at discrete depths within the radius.

Evaluation of Test Results

The conventional and LUIS test data are in good agreement in locating the faults within the radius of this test article. The LUIS time of flight data also reveals the presence of reflecting surfaces in the radius suggesting areas of delamination are present. The depth information

pulse echo test is valuable in understanding the nature of the fault and it should also be useful in modifying the process by which these parts are made to eliminate these discontinuities.

Performing conventional pulse echo tests on this part geometry with a five axis scanner could be done, but it would require either training the system to tailor the motions to this complex part geometry or an accurate digital data description of the part would be required to control the scan motion. This was an excellent example of the ability of laser ultrasound to scan a complex part geometry quickly and to produce valuable information on the part. This part shows the potential use of LBU technology in rapid prototyping and process development. Complex shapes can be easily inspected without the need to build a jig or fixturing devices.

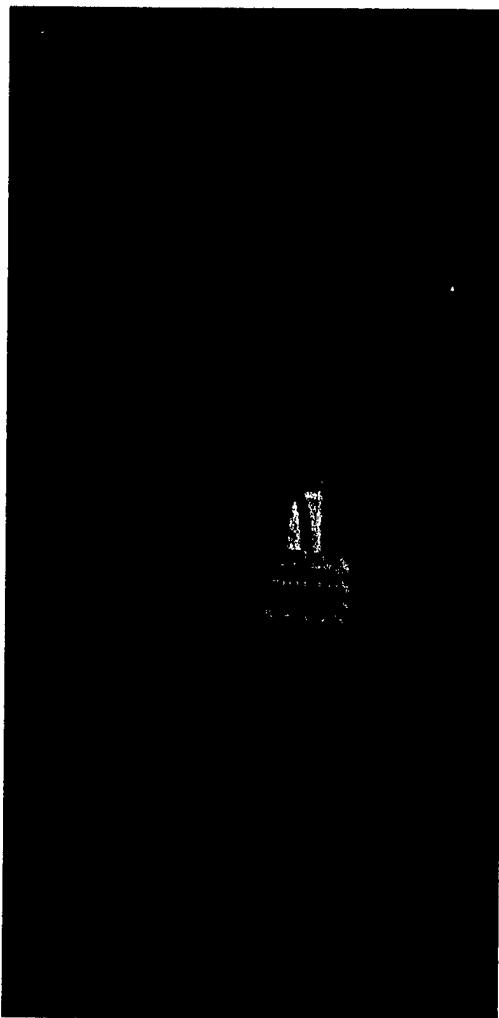


Figure 5.1.11-1. Photograph of convex surface



Figure 5.1.11-2. Photograph of concave surface



Figure 5.1.11-3. 3 MHz water jet through transmission ultrasonic image of "chainguard"



Figure 5.1.11-4. LUIS peak amplitude image from complex composite part

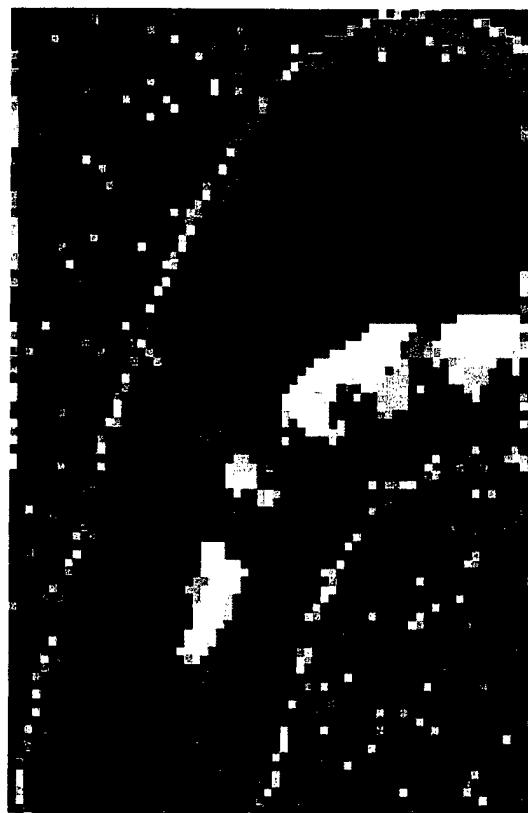


Figure 5.1.11-5. LUIS time of flight image from complex composite part

5.1.12 Graphite Composite Angle Test Standards

A number of angular components are manufactured from graphite composites for use in the horizontal stabilizer and vertical fin of the 777 aircraft. A series of standards were prepared for use in qualification and operational tests of the ultrasonic equipment developed for production inspection of the angular components. A variety of foreign materials were embedded in the standards at different depth to ensure the equipment would be sufficiently sensitive to detect the unwanted substances if they should mistakenly be placed in the laminates. Five of these standards ranging in thickness from 9 to 62 plies were used in the evaluation of the LUIS.

Drawings of standards 8A, 24, 25, 28, and 29 are given as Figure 5.1.12-2 through 5.1.12-6. The drawings show the location and depth of inserts within the radius and flange areas. The parts are pictured in Figure 5.1.12-1.

Conventional Test Results

The normal production inspection of the angular components is done with arrays of discrete transducers, which are used to achieve high inspection rates. Opposed pairs of transducers operate in through transmission mode to inspect both the flanges and radius portions of the angular components. The images produced by this system are not conveniently interpreted for comparison with the LUIS data. To provide more easily understood images from the standards; water jets were used to scan both flanges and radius areas of the standards. One flange would be scanned with indexing towards the radius. The standard was manually rotated as the jet indexed into the radius. This allowed the water jet data to be viewed in images that resembled the LUIS data. Since several different standards are to be shown in this section, the conventional and LUIS images for each standard will be shown together for comparison.

LUIS Test Results

As the LUIS was generally more effective in scanning test components from the bag-side surface, each of angle standards was scanned from this surface. In addition, the thickest standard 8A was also tested from the tool-side surface after it was painted with a strippable paint. The LUIS was quite effective in testing the angle standards. Except for the tool-side of 8A, none of the parts

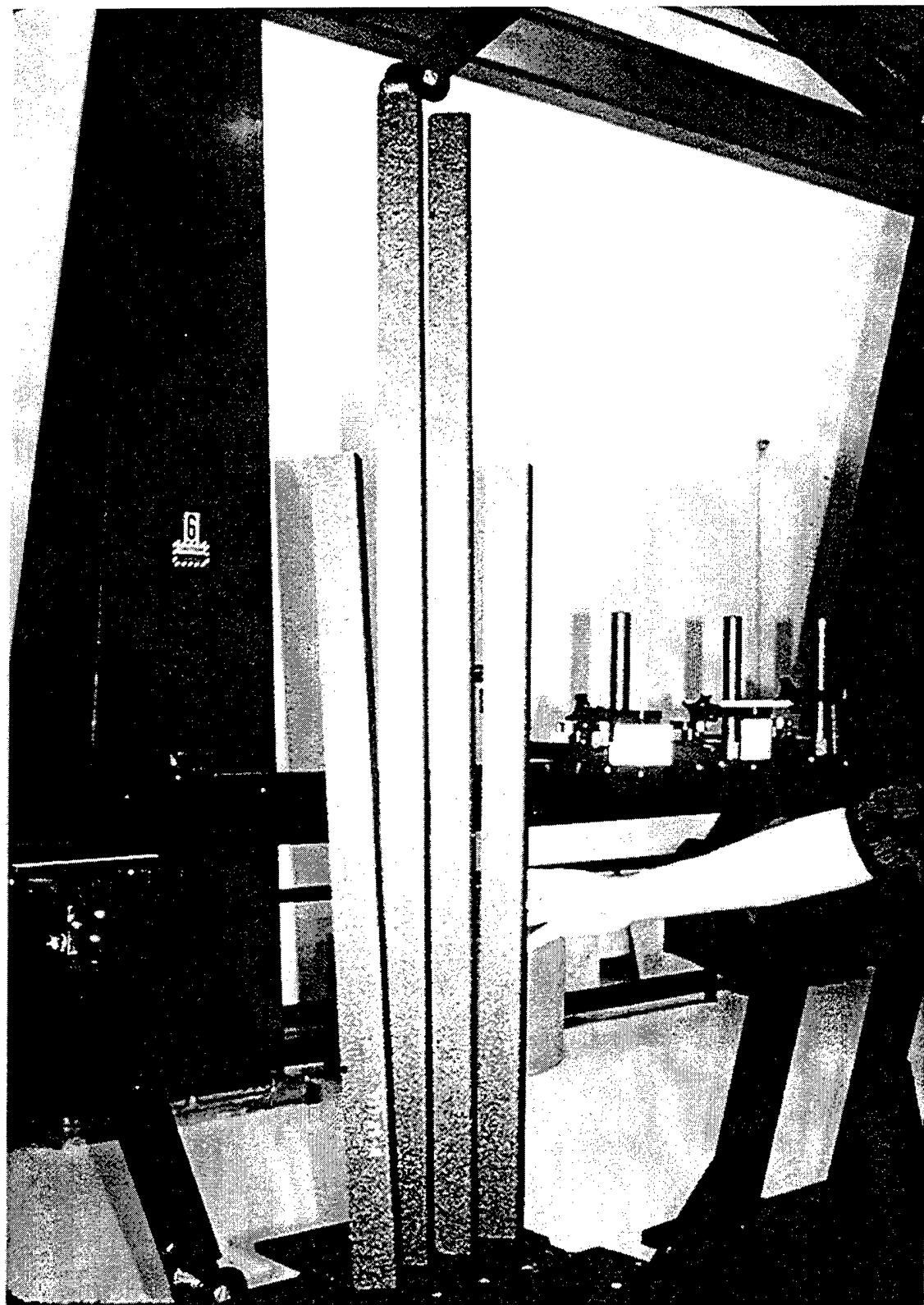
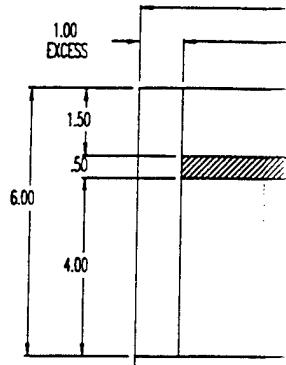


Figure 5.1.12-1. Photograph of angle standards

NOTES:

1. THIS IS NOT A CONTROLLED DRAWING(S)
2. BREAK ALL SHARP EDGES AND CORNERS EXCEPT AS NOTED
3. TOLERANCE: DECIMAL: $XX = \pm .010$
ANGULAR: $XX = \pm .02$
ANGULAR: $= \pm .5$
4. MATERIAL IS BMS 8-276 AND BMS 8-331
5. SPACING BETWEEN THE INSERTS IS GENERALLY 0.5".
6. TEXT NEAR INSERT DENOTES ITS MATERIAL TYPE AND PLY
DEPTH FROM THE TOOLSIDE SURFACE.
(F - RELEASE PLY, B - .001" BRASS FOIL, T - RELEASE EASE 234)
7. INSERTS LAY ON TOP OF PLY / INDICATED
8. PROCESS PER BAC 5578 (150 PSI CURE PRESSURE).
9. PLY-BY-PLY COMPACTION IS REQUIRED
(MINIMUM OF 1 MINUTE AT 25° TO 30° HG).
10. ALPHA DESIGNATOR SHALL BE ASSIGNED FOR UNIQUE IDENTITY.
NO CURRENT OR FUTURE STANDARD FABRICATED PER THIS DWG
WILL DUPLICATE THE ALPHA DESIGNATOR.

 = FREKOTED BRASS FOIL (0.001" THICK/25"X25")
 = FREKOTED BRASS FOIL (0.001" THICK/5"X5")
 = RELEASE EASE 234 TFP (0.003" THICK/5"X5")
 = RELEASE PLY "F" (0.005" THICK/7"X7")
 = IMAGE ANALYSIS SECTION



PLY TABLES

| PLY # | ORIENTATION | STEPS COVERED |
|-------|--------------|---------------|
| 1 | FABRIC (F/G) | A, B AND C |
| 2 | 0° (GR/EP) | A, B AND C |
| 3 | 0° (GR/EP) | A, B AND C |
| 4 | +45° (GR/EP) | A, B AND C |
| 5 | -45° (GR/EP) | A, B AND C |
| 6 | 90° (GR/EP) | A, B AND C |
| 7 | +45° (GR/EP) | A, B AND C |
| 8 | -45° (GR/EP) | A, B AND C |
| 9 | 90° (GR/EP) | A, B AND C |
| 10 | +45° (GR/EP) | A, B AND C |
| 11 | -45° (GR/EP) | A, B AND C |
| 12 | 90° (GR/EP) | A, B AND C |
| 13 | +45° (GR/EP) | A, B AND C |
| 14 | -45° (GR/EP) | A, B AND C |
| 15 | 90° (GR/EP) | A, B AND C |
| 16 | +45° (GR/EP) | A, B AND C |
| 17 | -45° (GR/EP) | A, B AND C |
| 18 | 0° (GR/EP) | A, B AND C |
| 19 | 0° (GR/EP) | A, B AND C |
| 20 | 0° (GR/EP) | B AND C |
| 21 | +45° (GR/EP) | B AND C |
| 22 | -45° (GR/EP) | B AND C |
| 23 | 90° (GR/EP) | B AND C |
| 24 | +45° (GR/EP) | B AND C |
| 25 | -45° (GR/EP) | B AND C |
| 26 | 90° (GR/EP) | B AND C |
| 27 | +45° (GR/EP) | B AND C |
| 28 | -45° (GR/EP) | B AND C |
| 29 | +45° (GR/EP) | B AND C |
| 30 | 0° (GR/EP) | B AND C |
| 31 | 0° (GR/EP) | B AND C |

| PLY # | ORIENTATION | STEPS COVERED |
|-------|--------------|---------------|
| 32 | 90° (GR/EP) | B AND C |
| 33 | -45° (GR/EP) | B AND C |
| 34 | +45° (GR/EP) | B AND C |
| 35 | -45° (GR/EP) | B AND C |
| 36 | 90° (GR/EP) | B AND C |
| 37 | +45° (GR/EP) | B AND C |
| 38 | -45° (GR/EP) | B AND C |
| 39 | 90° (GR/EP) | B AND C |
| 40 | 0° (GR/EP) | B AND C |
| 41 | 0° (GR/EP) | B AND C |
| 42 | 0° (GR/EP) | C |
| 43 | +45° (GR/EP) | C |
| 44 | -45° (GR/EP) | C |
| 45 | 90° (GR/EP) | C |
| 46 | +45° (GR/EP) | C |
| 47 | -45° (GR/EP) | C |
| 48 | 90° (GR/EP) | C |
| 49 | +45° (GR/EP) | C |
| 50 | -45° (GR/EP) | C |
| 51 | 0° (GR/EP) | C |
| 52 | 90° (GR/EP) | C |
| 53 | 0° (GR/EP) | C |
| 54 | +45° (GR/EP) | C |
| 55 | -45° (GR/EP) | C |
| 56 | 90° (GR/EP) | C |
| 57 | +45° (GR/EP) | C |
| 58 | -45° (GR/EP) | C |
| 59 | 90° (GR/EP) | C |
| 60 | 0° (GR/EP) | C |
| 61 | 0° (GR/EP) | C |
| 62 | FABRIC (F/G) | A, B AND C |

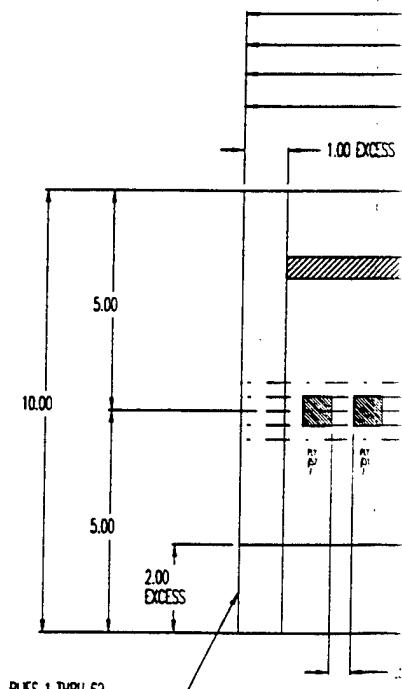


Figure 5.1.12-2 Angle Standard 8A

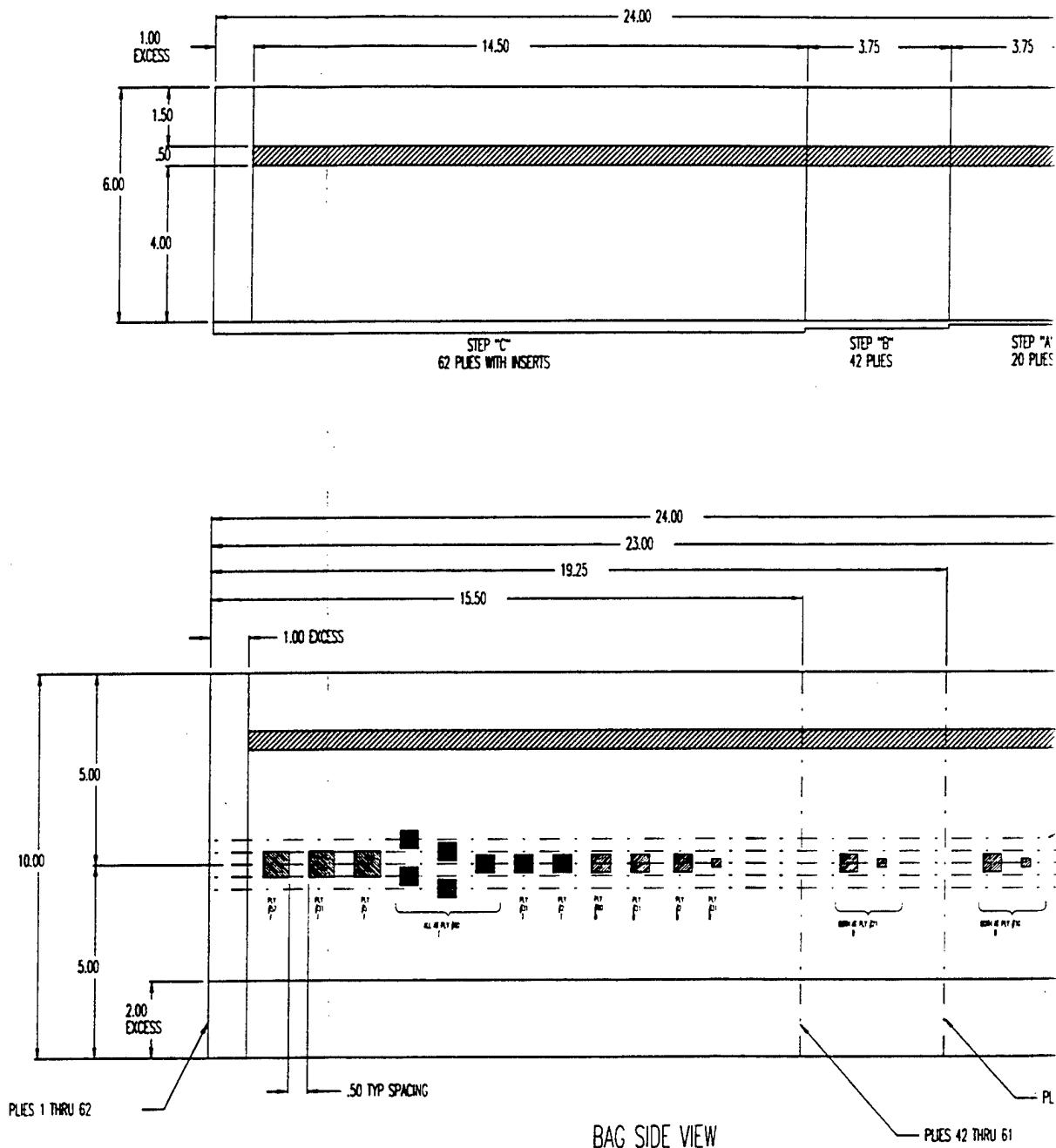
■ = FREKOTE BRASS FOIL (0.001" THICK/25'X25')

■ = FREKOTE BRASS FOIL (0.001" THICK/5'X5')

■ = RELEASE EASE 234 TFP (0.003" THICK/5'X5')

■ = RELEASE PLY "F" (0.005" THICK/7'X25')

■ = IMAGE ANALYSIS SECTION

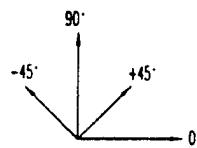
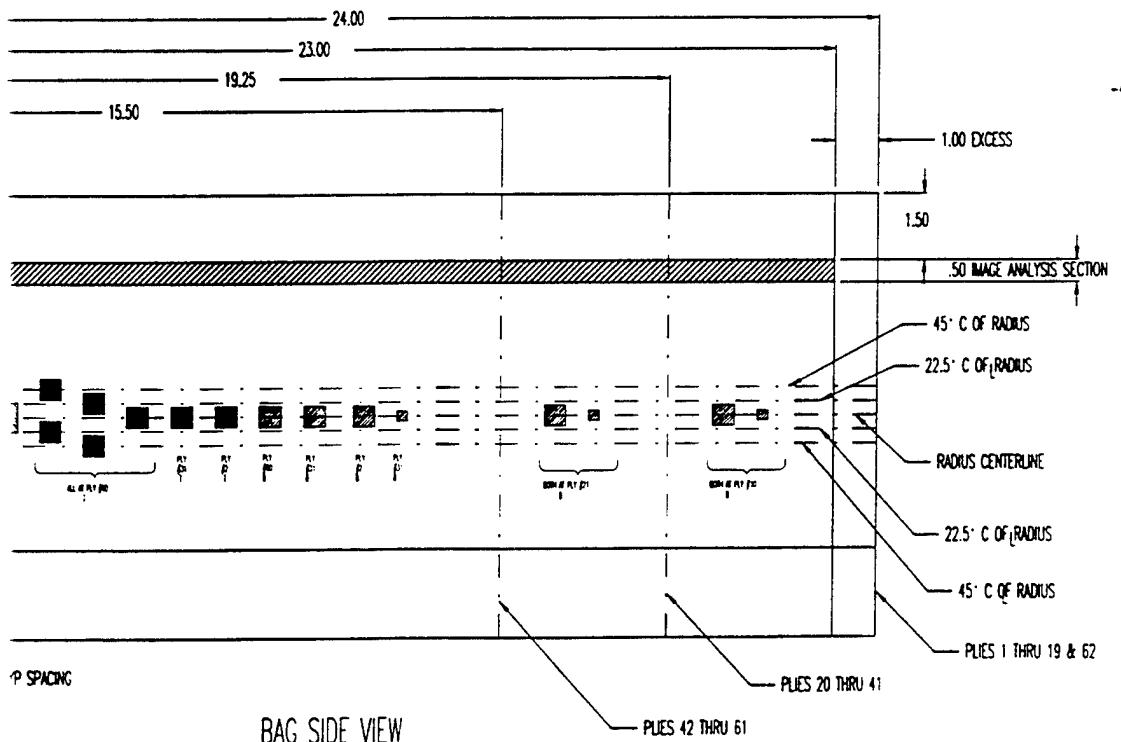
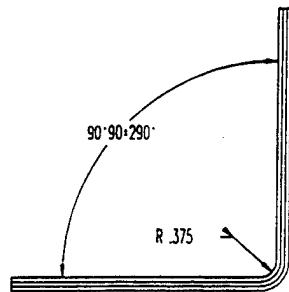
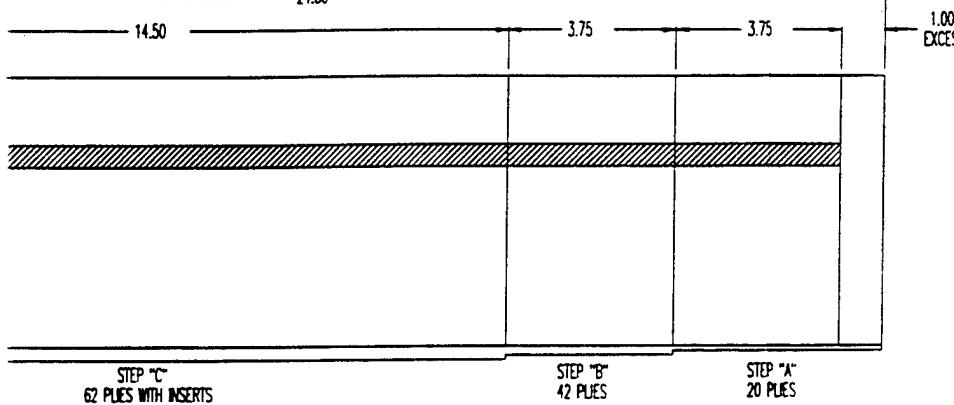


| |
|------------|
| TOLERANCE |
| |
| SCALE: 1/2 |

BOEING

| | |
|-------------|-------|
| DATE | TITLE |
| 08-31-83 | 777 E |
| CR C. MARES | |
| CR STICKNEY | |
| DR | |

Figure 5.1.12-2 Angle Standard 8A



| | | | | | | | | | |
|-------|----------|---------|------|---------------------------|----------|------|-----|----------|--------|
| RANGE | BOEING | | DATE | TITLE | 777-8-10 | SIZE | SH | 1 | 1 OF 1 |
| 3 | C.MARES | 8-31-83 | | 777 BMS 8-276 .375 RADIUS | | D | | | |
| E 1/2 | STICKNEY | | | STANDARD STEP BLOCK | | | | | |
| | | | | | | | NO. | SK7778-A | |

NOTES:

1. THIS IS NOT A CONTROLLED DRAWING(S).
2. BREAK ALL SHARP EDGES AND CORNERS EXCEPT AS NOTED
3. TOLERANCE: DECIMAL: $XXX = \pm .010$
ANGULAR: $XX = \pm .02$
ANGULAR: $= \pm .5$ ANGULAR: $= \pm .5$
4. MATERIAL IS BMS 8-276 TAPE / BMS 8-331

5. SPACING BETWEEN THE INSERTS IS GENERALLY 1.0".
6. TEXT NEAR INSERT DENOTES ITS MATERIAL TYPE AND PLY DEPTH FROM THE TOOLSIDE SURFACE. (T=AB 6782, F = RELEASE PLY F, B = BRASS).
7. AFTER TRIM, ALL EDGES MUST BE SEALED.
8. PROCESS PER BAC 5578 PSD 6-4 (150 PSI CURE PRESSURE).
9. PLY BY PLY COMPACTION IS REQUIRED (MINIMUM OF 1 MINUTE AT 25° TO 30° HG).

10. ALPHA DESIGNATOR SHALL BE ASSIGNED FOR UNIQUE IDENTITY. NO CURRENT OR FUTURE STANDARD FABRICATED PER THIS DWG WILL DUPLICATE THE ALPHA DESIGNATOR.

| PLY # | ANGLE | PLY TYPE |
|-------|-------|-----------|
| 1 | 0°/0° | BMS 8-331 |
| 2 | 0° | BMS 8-276 |
| 3 | +45° | BMS 8-276 |
| 4 | -45° | BMS 8-276 |
| 5 | 90° | BMS 8-276 |
| 6 | -45° | BMS 8-276 |
| 7 | +45° | BMS 8-276 |
| 8 | 0° | BMS 8-276 |
| 9 | 0°/0° | BMS 8-331 |

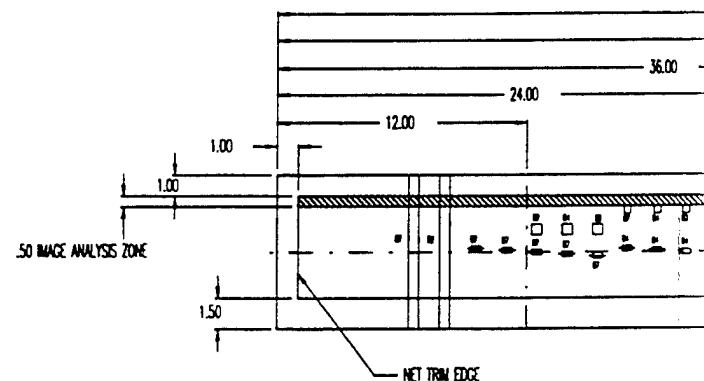
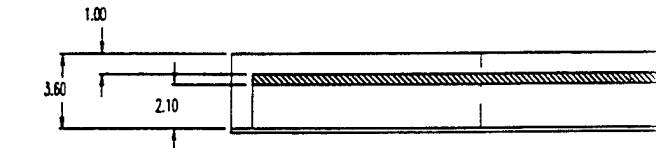


Figure 5.1.12-3 Angle St

TWEEN THE INSERTS IS GENERALLY 1.0".

INSERT DENOTES ITS MATERIAL TYPE AND PLY DEPTH FROM
DE SURFACE (T=AB 6782, F - RELEASE PLY F, B - BRASS).

ALL EDGES MUST BE SEALED.

TR BAC 5578 PSD 6-4 (150 PSI CURE PRESSURE).

COMPACTION IS REQUIRED

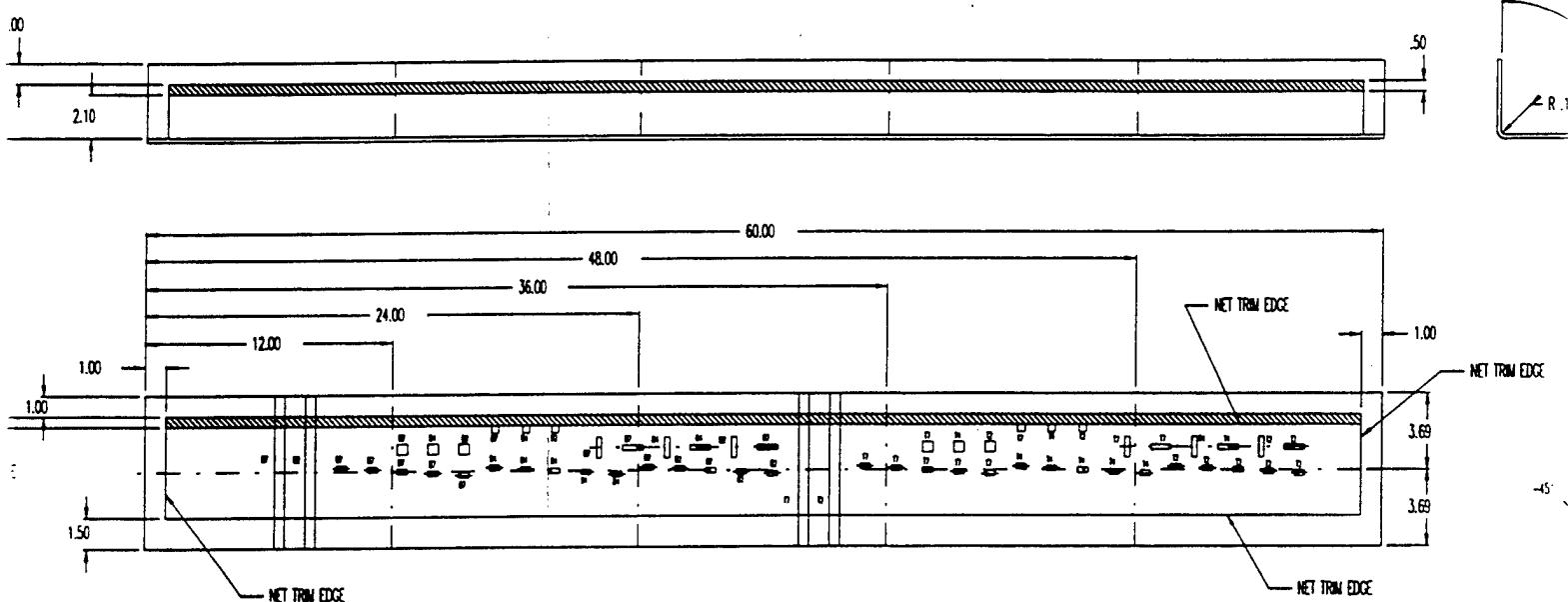
1 MINUTE AT 25° TO 30° Hz).

NATOR SHALL BE ASSIGNED FOR UNIQUE IDENTITY.
OR FUTURE STANDARD FABRICATED PER THIS Dwg
LE THE ALPHA DESIGNATOR.

KEY:

INSERT SIZES:

- $1" \times 1"$
- $0.50" \times 0.50"$
- $0.50" \times 0.375"$
- $0.50" \times 0.25"$
- $0.375" \times 0.375"$
- $0.25" \times 0.25"$
- = DCESS



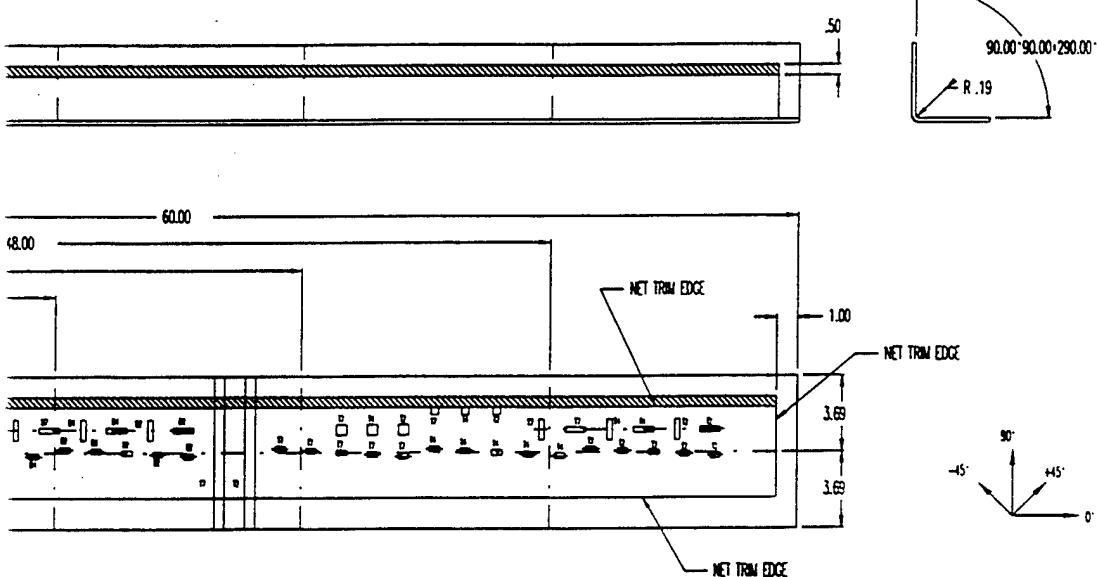
| | | | |
|-----------|------------|------------------|-----|
| REFERENCE | BOEING | DATE | 777 |
| SCALE 1/4 | C. MARES | EDGE SCANNER Dwg | |
| | C. STORNEY | STANDARD FOR 777 | |
| | 100 | | |

Figure 5.1.12-3 Angle Standard 24-A

KEY:

INSERT SIZES:

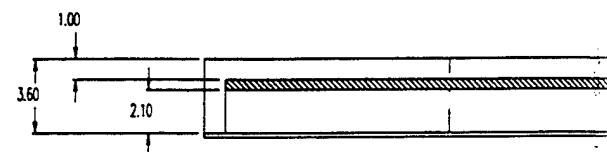
- 1.00" x 1.00"
- 0.50" x 0.50"
- 0.50" x 0.375"
- 0.375" x 0.25"
- 0.375" x 0.375"
- 0.25" x 0.25"
- = CROSS



| | | | | | | | | |
|------------|-------------------------|------|---------------------------|------|---------------------------|-----|---|---|
| REFERENCE | BOEING | DATE | 777-24- 15 | FILE | EDG SCANNER QUALIFICATION | SP | 1 | 1 |
| SCALE: 1/4 | C. MARES C. STOCKLEY | 100 | STANDARD FOR 777 EMPORIUM | D | SX77724 | NO. | | |

NOTES:

1. THIS IS NOT A CONTROLLED DRAWING(S).
2. BREAK ALL SHARP EDGES AND CORNERS EXCEPT AS NOTED
3. TOLERANCE: DECIMAL: XXX = $\pm .010$
XX = $\pm .02$
ANGULAR: $\pm .5$ ANGULAR: $\pm .5$
4. MATERIAL IS BMS 8-276 TAPE / BMS 8-331
5. SPACING BETWEEN THE INSERTS IS GENERALLY 1.0".
6. TEXT NEAR INSERT DENOTES ITS MATERIAL TYPE AND PLY DEPTH FROM THE TOOLSIDE SURFACE. (I=AB 6782, F = RELEASE PLY F, B = BRASS).
7. AFTER TRIM, ALL EDGES MUST BE SEALED.
8. PROCESS PER BAC 5578 PSD 6-4 (150 PSI CURE PRESSURE).
9. PLY BY PLY COMPACTION IS REQUIRED (MINIMUM OF 1 MINUTE AT 25° TO 30° Hg).
10. ALPHA DESIGNATOR SHALL BE ASSIGNED FOR UNIQUE IDENTITY. NO CURRENT OR FUTURE STANDARD FABRICATED PER THIS DWG WILL DUPLICATE THE ALPHA DESIGNATOR.



PLY TABLE

| AT | DEPTH | PLY TYPE |
|----|----------|-----------|
| 1 | 0 / .007 | BMS 8-331 |
| 2 | 0 | BMS 8-276 |
| 3 | $\pm .5$ | BMS 8-276 |
| 4 | $\pm .5$ | BMS 8-276 |
| 5 | .97 | BMS 8-276 |
| 6 | $\pm .5$ | BMS 8-276 |
| 7 | $\pm .5$ | BMS 8-276 |
| 8 | 0 | BMS 8-276 |
| 9 | 0 / .007 | BMS 8-331 |

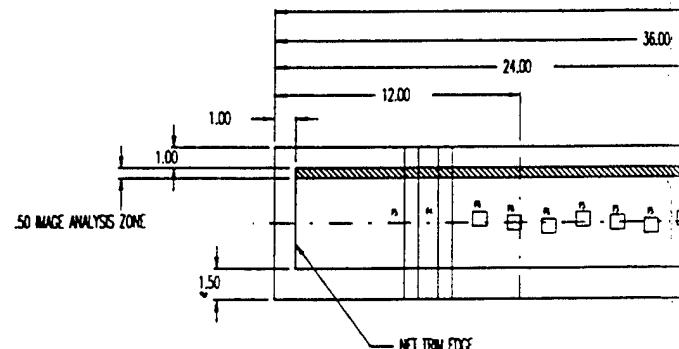


Figure 5.1.12-4 Angle

BETWEEN THE INSERTS IS GENERALLY 1.0".

2. INSERT DENOTES ITS MATERIAL TYPE AND PLY DEPTH FROM SIDE SURFACE. (T=AB 6782, F = RELEASE PLY F, B = BRASS).

1. ALL EDGES MUST BE SEALED.

PER BAC 5578 PSD 6-4 (150 PSI CURE PRESSURE).

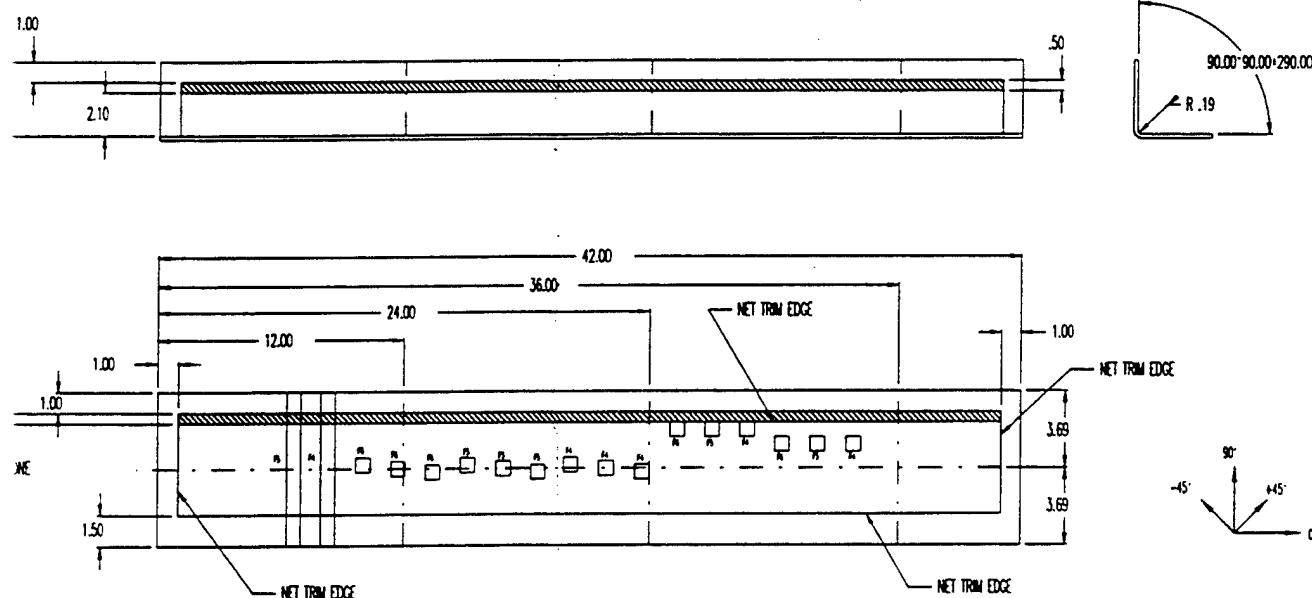
Y COMPACTION IS REQUIRED
OF 1 MINUTE AT 25° TO 30° HG.

MANUFACTURER SHALL BE ASSIGNED FOR UNIQUE IDENTITY.
IT OR FUTURE STANDARD FABRICATED PER THIS DWG
CATE THE ALPHA DESIGNATOR.

KEY:

INSERT SIZES:

- 1.00" x .70"
- 0.50" x 0.50"
- 0.50" x 0.375"
- 0.50" x 0.25"
- 0.375" x 0.375"
- 0.25" x 0.25"
- = EXCESS



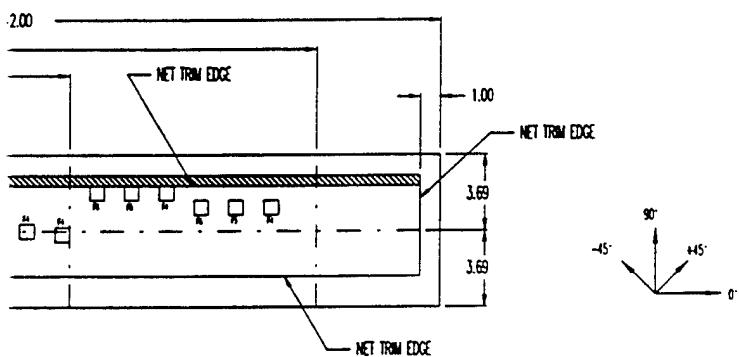
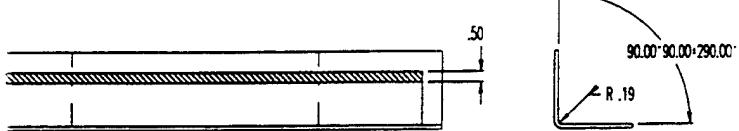
| | | | |
|-----------|--|------------------------------------|----|
| TOLERANCE | BOEING | DATE | 77 |
| SCALE 1/4 | G. MARES C. M. STOCKNEY D. M. F. | EDGE SCANNER DR STANDARD FOR 77 | |

Figure 5.1.12-4 Angle Standard 25-A

KEY:

INSERT SIZES

- .75" x .75"
- .50" x .50"
- .50" x .375"
- .50" x .25"
- .375" x .375"
- .25" x .25"
- DCESS



| | | | | |
|-----------------------|--------|--|--|---------------|
| REVISION SCALE 1/4 | BOEING | DATE C. MARES C. STOCKNEY DRAFT | FILE 777-75- EDGE SCANNER QUALIFICATION STANDARD FOR 777 EXPERIENCE | SR 1 0 |
| | | | | D NO. SK77725 |

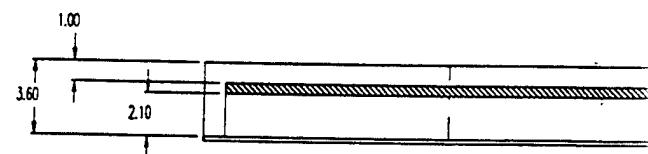
SOFTWARE: CADKEY 4.0 FILE: SK77725.PRT

NOTES:

1. THIS IS NOT A CONTROLLED DRAWING(S).
2. BREAK ALL SHARP EDGES AND CORNERS EXCEPT AS NOTED
3. TOLERANCE: DECIMAL: $XXX \pm .010$
ANGULAR: $\pm .02$
ANGULAR: $\pm .5$ ANGULAR: $\pm .5$
4. MATERIAL IS BMS B-276 TAPE / BMS 8-331

5. SPACING BETWEEN THE INSERTS IS GENERALLY 1.0".
6. TEXT NEAR INSERT DENOTES ITS MATERIAL TYPE AND PLY DEPTH FROM THE TOOLSIDE SURFACE. (T=AB 6782, F = RELEASE PLY, B = BRASS).
7. AFTER TRIM, ALL EDGES MUST BE SEALED.
8. PROCESS PER BAC 5578 PSD 6-4 (150 PSI CURE PRESSURE).
9. PLY BY PLY COMPACTION IS REQUIRED (MINIMUM OF 1 MINUTE AT 25° TO 30° Hg).

10. ALPHA DESIGNATOR SHALL BE ASSIGNED FOR UNIQUE IDENTITY. NO CURRENT OR FUTURE STANDARD FABRICATED PER THIS Dwg WILL DUPLICATE THE ALPHA DESIGNATOR.



PLY TABLE

| PLY | ANGLE | TYPE |
|-----|-------|-----------|
| 1 | 0°/0° | BMS 8-131 |
| 2 | 0° | BMS 8-276 |
| 3 | +45° | BMS 8-276 |
| 4 | -45° | BMS 8-276 |
| 5 | 90° | BMS 8-276 |
| 6 | 0° | BMS 8-276 |
| 7 | 0° | BMS 8-276 |
| 8 | +45° | BMS 8-276 |
| 9 | 90° | BMS 8-276 |
| 10 | -45° | BMS 8-276 |
| 11 | 0° | BMS 8-276 |
| 12 | +45° | BMS 8-276 |
| 13 | 90° | BMS 8-276 |
| 14 | 0° | BMS 8-276 |
| 15 | -45° | BMS 8-276 |
| 16 | 0° | BMS 8-276 |
| 17 | -45° | BMS 8-276 |
| 18 | 90° | BMS 8-276 |
| 19 | +45° | BMS 8-276 |
| 20 | 0° | BMS 8-276 |
| 21 | 0° | BMS 8-276 |
| 22 | 90° | BMS 8-276 |
| 23 | -45° | BMS 8-276 |
| 24 | +45° | BMS 8-276 |
| 25 | 0° | BMS 8-276 |
| 26 | 0°/0° | BMS 8-331 |

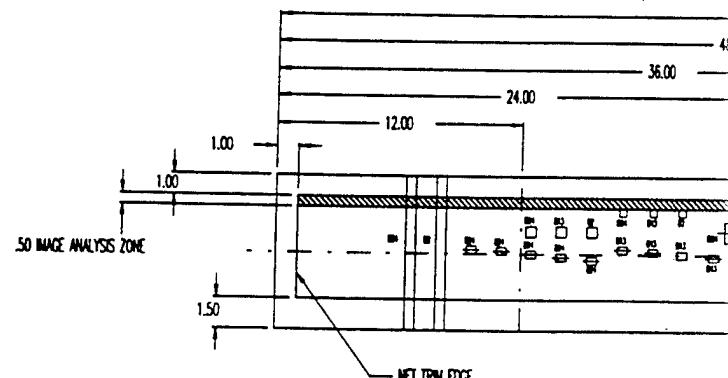


Figure 5.1.12-5 Angle St

5. SPACING BETWEEN THE INSERTS IS GENERALLY 1.0".
 6. TEXT NEAR INSERT DENOTES ITS MATERIAL TYPE AND PLY DEPTH FROM
 THE TOOLSIDE SURFACE. (T=AB 6782, F = RELEASE PLY, B = BRASS).
 7. AFTER TRIM, ALL EDGES MUST BE SEALED.
 8. PROCESS PER BAC 5578 PSD 6-4 (150 PSI CURE PRESSURE).
 9. PLY BY PLY COMPACTION IS REQUIRED
 (MINIMUM OF 1 MINUTE AT 25° TO 30° Hz).
 10. ALPHA DESIGNATOR SHALL BE ASSIGNED FOR UNIQUE IDENTITY.
 NO CURRENT OR FUTURE STANDARD FABRICATED PER THIS DNG
 WILL DUPLICATE THE ALPHA DESIGNATOR.

| KEY: | |
|---|-----------------|
| | INSERT SIZES: |
| <input type="checkbox"/> | 1.0" x 1.0" |
| <input type="checkbox"/> | 0.50" x 0.50" |
| <input type="checkbox"/> | 0.50" x 0.375" |
| <input type="checkbox"/> | 0.50" x 0.25" |
| <input type="checkbox"/> | 0.375" x 0.375" |
| <input type="checkbox"/> | 0.25" x 0.25" |
| ■ | = EXCESS |

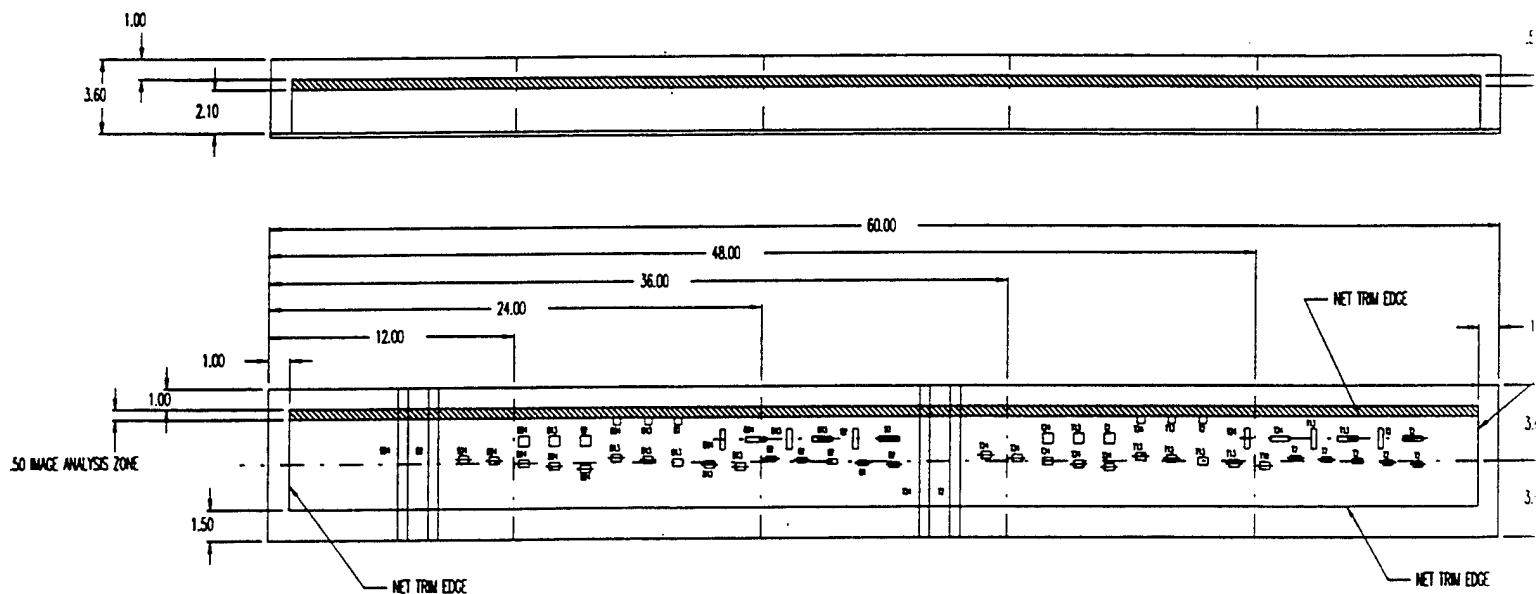
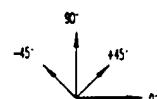
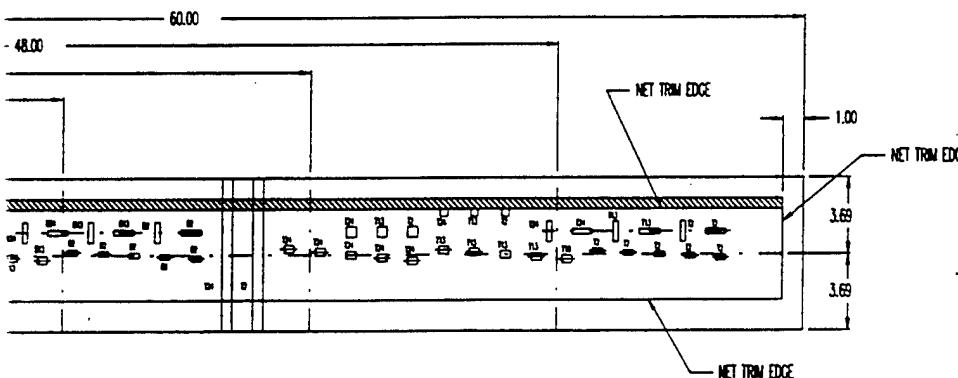
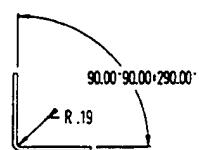


Figure 5.1.12-5 Angle Standard 28-A

KEY:

INSERT SIZES:

- 1" x 1"
- 0.50" x 0.50"
- 0.50" x 0.375"
- 0.50" x 0.25"
- 0.375" x 0.375"
- 0.25" x 0.25"
- = EXCESS



| | | | | | | |
|---------------|--------|----------------|--|--------------|---------|-------------|
| TOLERANCE | BOEING | DATE 7/7/28 | TITLE 777-28- EDGE SCANNER QUALIFICATION STANDARD FOR 777 FAIRING | SCALE 1/4 | SH 1 | 1 |
| | | | | | D | NO. SK77728 |

NOTES:

1. THIS IS NOT A CONTROLLED DRAWING(S).
2. BREAK ALL SHARP EDGES AND CORNERS EXCEPT AS NOTED
3. TOLERANCE: DECIMAL: $XXX \pm .010$
ANGULAR: $XX \pm .02$
ANGULAR: $= \pm .5$ ANGULAR: $= \pm .5$
4. MATERIAL IS BMS 8-276 TAPE / BMS 8-331

5. SPACING BETWEEN THE INSERTS IS GENERALLY 1.0".
6. TEXT NEAR INSERT DENOTES ITS MATERIAL TYPE AND PLY DEPTH FROM THE TOOLSIDE SURFACE. (T=AB 6782, F - RELEASE PLY, B - BRASS).
7. AFTER TRIM, ALL EDGES MUST BE SEALED.
8. PROCESS PER BAC 5578 PSD 6-4 (150 PSI CURE PRESSURE).
9. PLY BY PLY COMPACTION IS REQUIRED (MINIMUM OF 1 MINUTE AT 25° TO 30° HG).

10. ALPHA DESIGNATOR SHALL BE ASSIGNED FOR UNIQUE IDENTITY. NO CURRENT OR FUTURE STANDARD FABRICATED PER THIS DWG WILL DUPLICATE THE ALPHA DESIGNATOR.

| PLY # | ORIENTATION | MATERIAL TYPE |
|-------|-------------|---------------|
| 1 | 0°/000 | BMS 8-331 |
| 2 | 0° | BMS 8-276 |
| 3 | +45 | BMS 8-276 |
| 4 | -45 | BMS 8-276 |
| 5 | 90° | BMS 8-276 |
| 6 | 0° | BMS 8-276 |
| 7 | 0° | BMS 8-276 |
| 8 | +45 | BMS 8-276 |
| 9 | 90° | BMS 8-276 |
| 10 | -45 | BMS 8-276 |
| 11 | 0° | BMS 8-276 |
| 12 | +45 | BMS 8-276 |
| 13 | 0° | BMS 8-276 |
| 14 | 0° | BMS 8-276 |
| 15 | -45 | BMS 8-276 |
| 16 | 0° | BMS 8-276 |
| 17 | -45 | BMS 8-276 |
| 18 | 90° | BMS 8-276 |
| 19 | +45 | BMS 8-276 |
| 20 | 0° | BMS 8-276 |
| 21 | 0° | BMS 8-276 |
| 22 | 90° | BMS 8-276 |
| 23 | -45 | BMS 8-276 |
| 24 | +45 | BMS 8-276 |
| 25 | 0° | BMS 8-276 |
| 26 | 0°/000 | BMS 8-331 |

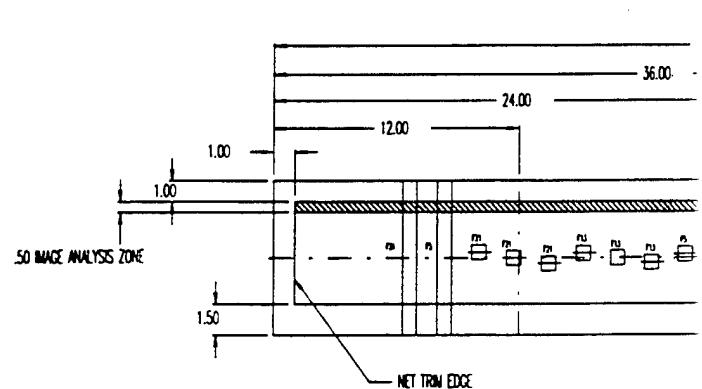
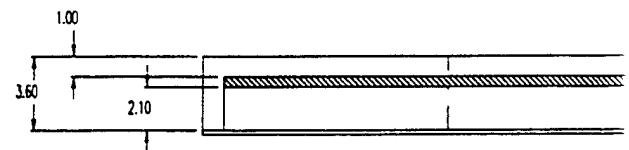
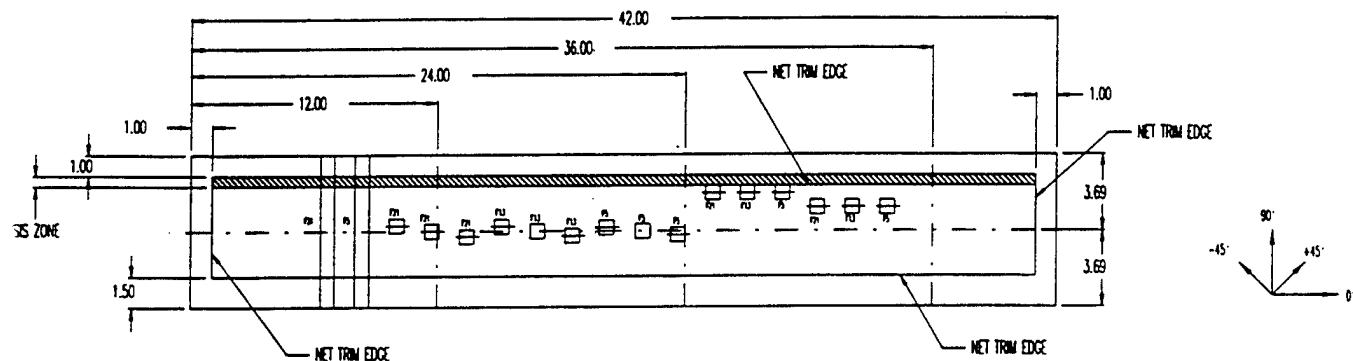
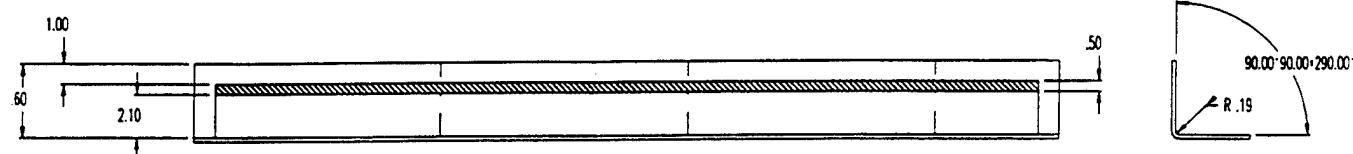


Figure 5.1.12-6 Angle St

ING BETWEEN THE INSERTS IS GENERALLY 1.0".
 NEAR INSERT DENOTES ITS MATERIAL TYPE AND PLY DEPTH FROM
 TOOLSIDE SURFACE. (T=AB 6782, F - RELEASE PLY F, B - BRASS).
 2 TRIM, ALL EDGES MUST BE SEALED.
 LESS PER BAC 5578 PSD 6-4 (150 PSI CURE PRESSURE).
 3Y PLY COMPACTION IS REQUIRED
 (MIN OF 1 MINUTE AT 25° TO 30° HG).
 4 DESIGNATOR SHALL BE ASSIGNED FOR UNIQUE IDENTITY.
 CURRENT OR FUTURE STANDARD FABRICATED PER THIS DWG
 DUPLICATE THE ALPHA DESIGNATOR.

KEY: INSERT SIZES:

- 70" x 70"
- 0.50" x 0.50"
- 0.50" x 0.375"
- 0.50" x 0.25"
- 0.375" x 0.375"
- 0.25" x 0.25"
- = EXCESS



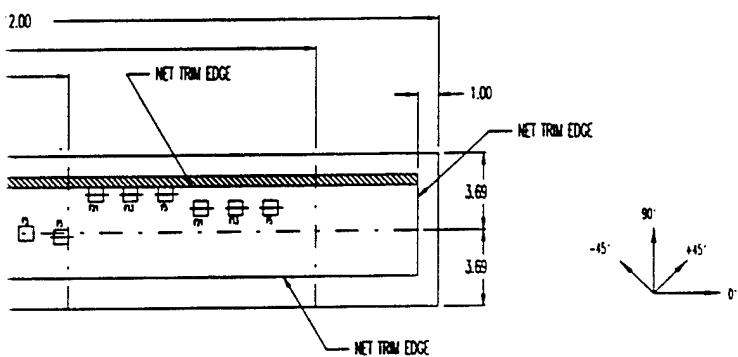
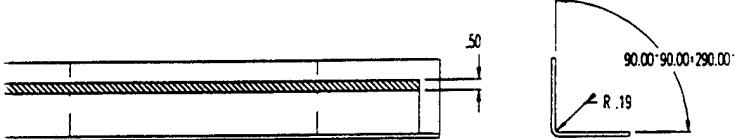
| | |
|-----------|----------------|
| TOLERANCE | DATE |
| SCALE 1/4 | BY C. MARES |
| | IN STOCKHOLM |
| | 1984 |
| | EDGE STANDARDS |

Figure 5.1.12-6 Angle Standard 29-A

KEY:

INSERT SIZES:

- .70" x .70"
- 0.50" x 0.50"
- 0.50" x 0.375"
- 0.50" x 0.25"
- 0.375" x 0.375"
- 0.25" x 0.25"
- DRESS



| | | | | |
|---------------|----------------------|---|--|---|
| REFERENCE | BOEING SCALE: 1/4 | DATE 10/22/77-29- TMR C.MARES TMR STICKNEY TMR | REF. E EDGE SCANNER CALIBRATION STANDARD FOR 777 EQUIPMENT | SIZE D SH 1 1 1 NO. SK77729 |
|---------------|----------------------|---|--|---|

were painted and excellent images were obtained from both the flanges and radius portions of the standards.

Evaluation of test results.

The LUIS was clearly more effective than water jet through transmission tests in revealing the majority of inserts in both radius and flange areas from five graphite composite angle standards ranging in thickness from 9 to 62 plies. The greater sensitivity of pulse echo ultrasound in detecting the foreign materials explains much of the difference in detection of the inserts. An additional benefit of the LUIS is the ability to image both the flanges and radius with a single setup. The ability to perform pulse echo tests without being normal to the inspection surface is a very attractive feature of laser ultrasound.

Angle Standard 25-A.

This part is shown in Figure 5.1.12-4. It was made with two plies of Fiberglas fabric and seven plies of graphite tape. The radius was 0.19" All of the inserts were a material termed "Release Ply F." This is moderately difficult to detect as can be seen in the 5 MHz through transmission ultrasonic results on this part. All of the inserts were detected in the LUIS images in Figure 5.1.12-7. The LUIS image is shown in two sections since the part required two separate scans. The conventional test was not effective in detecting the inserts as shown in Figure 5.1.12-8.

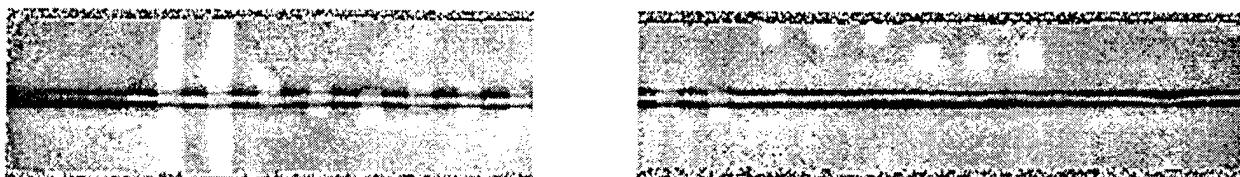


Figure 5.1.12-7. LUIS Time of flight images of angle standard 25-A.

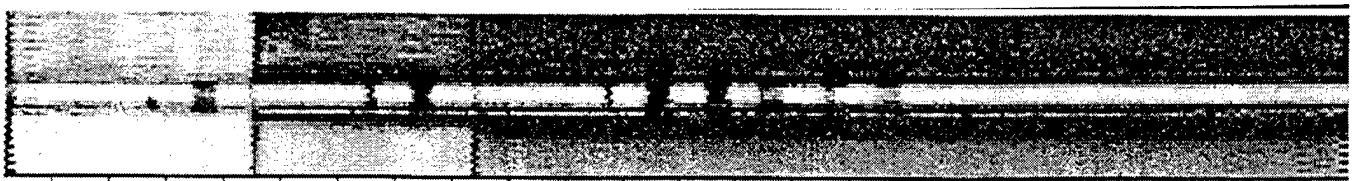


Figure 5.1.12-8. 5 MHz Water jet through transmission ultrasonic test of angle standard 25-A.

Angle Standard 24-A

This part is shown in Figure 5.1.12-3. This standard was comprised of two plies of Fiberglas fabric and seven plies of graphite tape. The radius was 0.19". The inserts were either 0.001" thick brass foil or a tape AB 6782. The brass inserts were detected in both the water jet data and the LUIS images. The LUIS was much more successful in detecting the tape inserts. Comparing the right side of Figure 5.1.12-9 to the right side of Figure 5.1.12-10, the advantages of the LUIS in detecting the tape inserts is clear.



<= Brass foil =>



<=Brass foil => <= Tape inserts =>

Figure 5.1.12-9. LUIS peak amplitude image of angle standard 24-A



Figure 5.1.12-10. Water jet 5 MHz through transmission image on angle standard 24-A. Gray

scale range 14 dB

Angle Standard 28-A

This part is shown in Figure 5.1.12-5. This standard was prepared with 2 plies of Fiberglas fabric and 24 plies of graphite tape. The inserts were brass foil (0.001" thick) and tape. The radius was 0.19" The LUIS was successful in detecting both types of inserts. Water jet through transmission at 5 MHz detected many of the brass inserts and a few of the tape inserts.

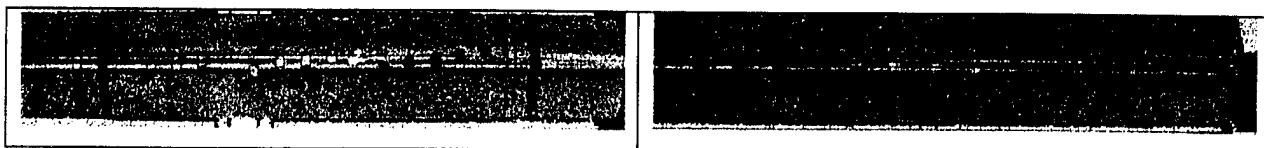


Figure 5.1.12-11. LUIS peak amplitude image of angle standard 28-A.



Figure 5.1.12-12. 5 MHz water jet through transmission image of angle standard 28-A

Angle Standard 29-A

This part is shown in Figure 5.1.12-6. This standard was prepared with 2 plies of Fiberglas fabric and 24 plies of graphite tape. The inserts were Release ply F (0.005" thick). The radius was 0.19. The inserts were detectable in either the peak amplitude or time of flight images from the LUIS. Inserts in both flanges and radius were detectable by the LUIS as shown in Figure 5.1.12-13. Water jet through transmission at 5 MHz was unable to detect these inserts as shown in Figure 5.1.12-14.

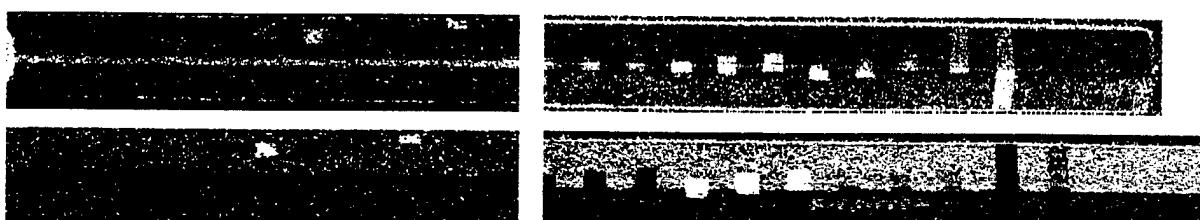


Figure 5.1.12-13. LUIS peak amplitude (upper) and time of flight (lower) images of angle standard 29-A

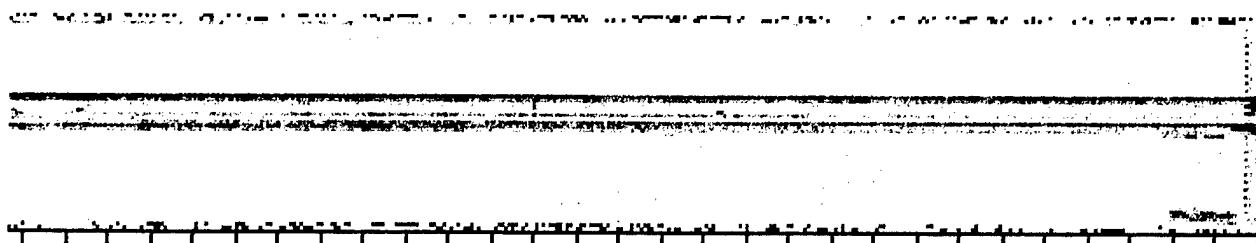


Figure 5.1.12-14. 5 MHz water jet through transmission image of angle standard 29-A

Angle standard 8-A

This part is shown in Figure 5.1.12-2. This standard had three different thicknesses, 20, 42, and 62 plies. In the ultrasonic scan image figures, the 20-ply region is on the left. Two plies were Fiberglas fabric in each section and the remainder was graphite tape. All of the inserts were placed at different depths within the radius. The LUIS data gave at least marginal indications to 16 of 18 inserts. Water jet through transmission data at 3 MHz gave indications for 10 of the 18 inserts.

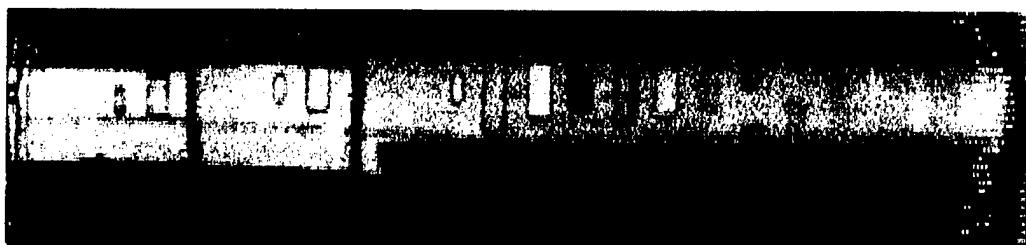


Figure 5.1.12-15. LUIS peak amplitude image of angle standard 8A

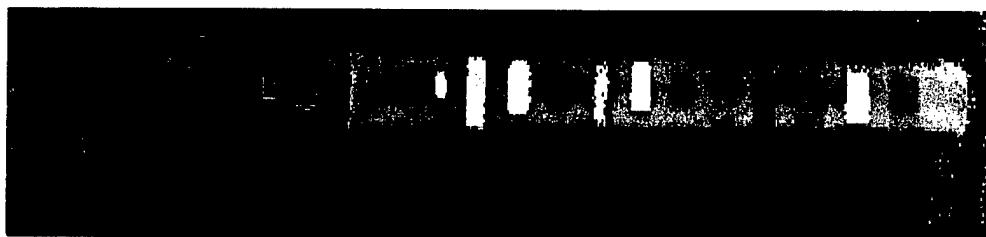


Figure 5.1.12-16. LUIS time of flight image of angle standard 8A

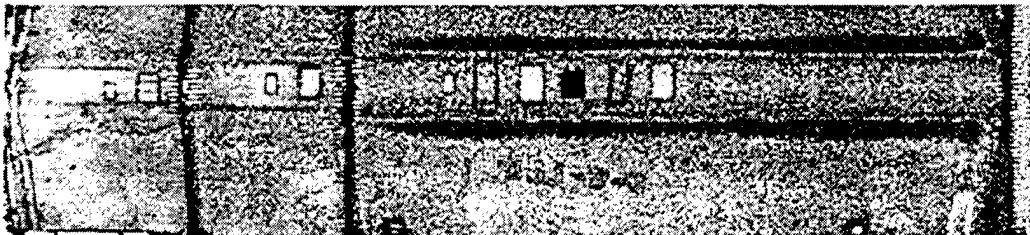


Figure 5.1.12-17. LUIS peak amplitude image of angle standard 8A of radius and adjacent flanges



Figure 5.1.12-18. 3 MHz through transmission ultrasonic image of standard 8A

As the LUIS was generally more effective in scanning the test components from the bag-side surface, each of angle standards was scanned from this surface. In addition, the thickest standard 8A was also tested from the tool-side surface after it was painted with a strippable paint. The LUIS was quite effective in testing the angle standards. Except for the tool-side of 8A, none of the parts were painted and excellent images were obtained from both the flanges and radius portions of the standards.

Evaluation of test results.

The LUIS was clearly more effective than water jet through transmission tests in revealing the majority of inserts in both radius and flange areas from five graphite composite angle standards ranging in thickness from 9 to 62 plies. The greater sensitivity of pulse echo ultrasound in detecting the foreign materials explains much of the difference in detection of the inserts. An additional benefit of the LUIS is the ability to image both the flanges and radius with a single setup with no subsequent moving of the part required. The ability to perform pulse echo tests without being normal to the inspection surface is a very attractive feature of laser ultrasound.

5.1.13 Porosity Standards

Pulse-echo ultrasonic C-scans were made for graphite laminate porosity standards to compare the porosity sensitivity of LUIS to the sensitivity of conventional UT. Nine samples were scanned, with porosity levels ranging from 1 to 4 percent, as determined from photomicrographs of polished cross sections. All the pieces were roughly 4" X 4" squares. Five samples were 32 plies thick, and the other four samples were 24 plies thick. All nine samples were scanned with the same fixed conditions. A gate was set on the back surface reflection, wide enough to cover both thickness. The displayed signal represents detection of the back surface echo remaining after signal loss due to the porosity.

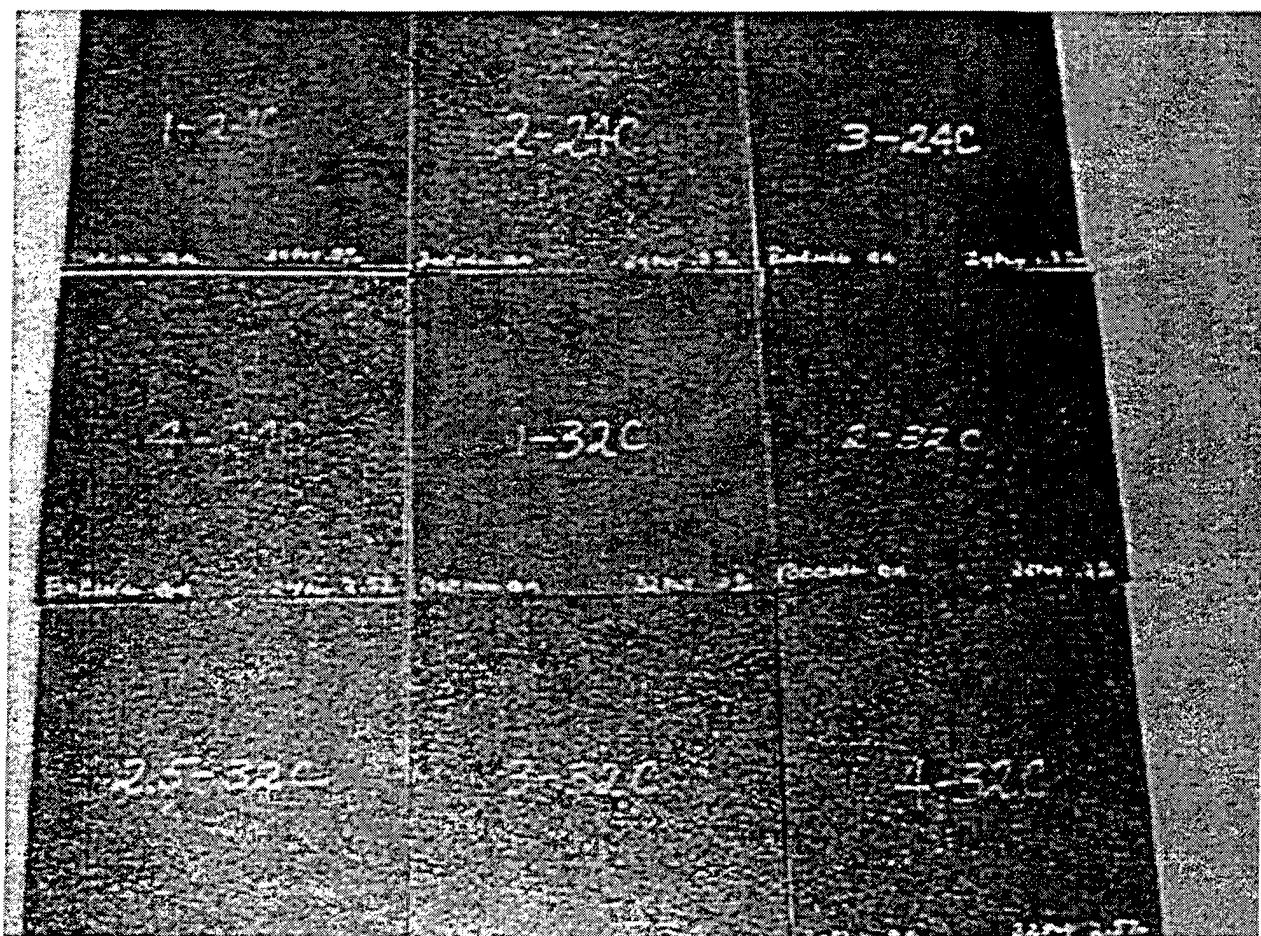


Figure 5.1.13-1. Porosity Standards

The layout of the samples as tested at McClellan AFB is seen in Figure 5.1.13-1. In the top row, from left to right, the samples had porosity levels of 1%, 2% and 3%. The left-most sample in the middle row had 4% porosity. These first four samples were 24 plies thick. The remaining five samples were 32 plies thick. Porosity levels, starting with the middle sample in the second row and moving left to right, were 1%, 2%, 2.5%, 3%, and 4%.

The LUIS image of the porosity standards in Figure 5.1.13-2 was extracted from the full waveform data. The image in Figure 5.1.13-3 was prepared using a Gaussian filter centered at 3 MHz with 1MHz bandwidth. Another image was prepared using a Gaussian filter centered at 5 MHz with 1 MHz bandwidth. Sampling interval in the LUIS scans is about .120 inch.

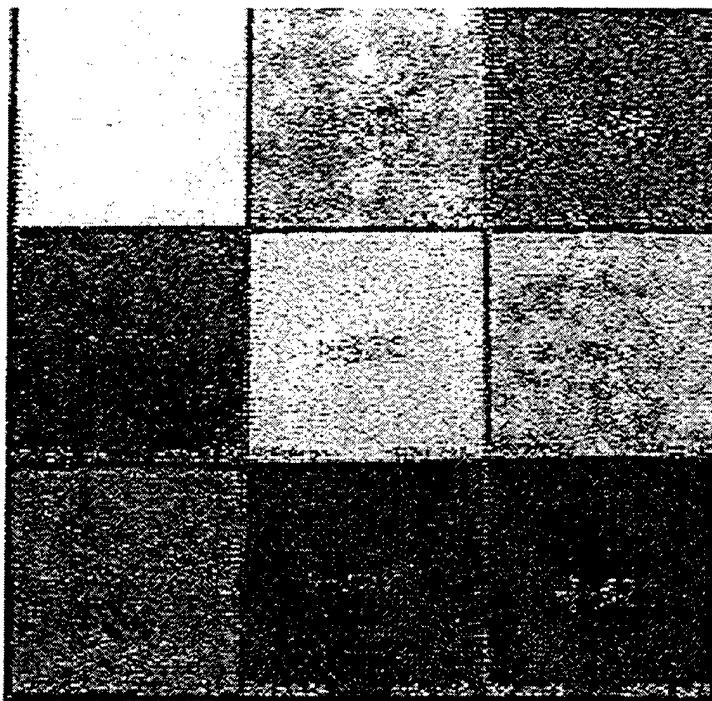


Figure 5.1.13-2. LUIS image using the full filtered waveform bandwidth

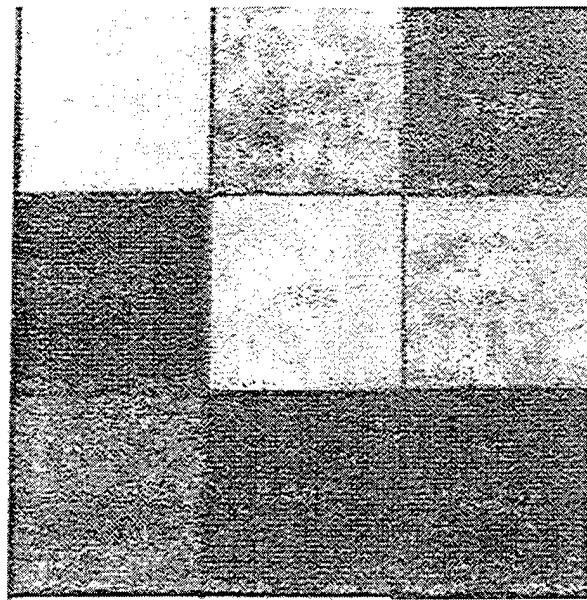


Figure 5.1.13-3. LUIS image filtered to 3 MHz center frequency

In the conventional scans, a 3.5 MHz transducer was used, with the gain set to 80% full screen height on the sample with the greatest signal. The index and scan intervals were 0.080 inches.

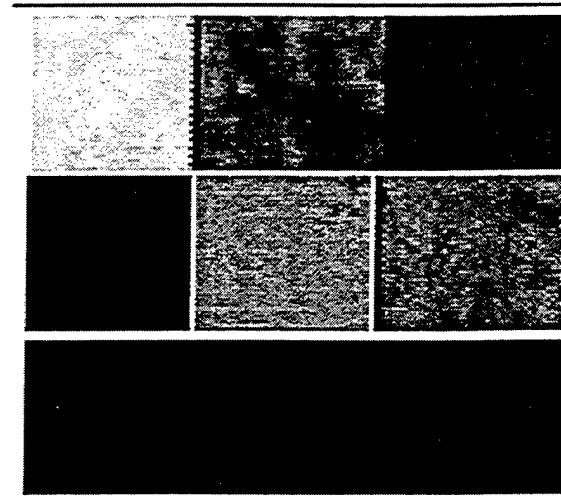


Figure 5.1.13-4. Conventional pulse-echo C-scan image taken at 3.5 MHz.

For the conventional pulse-echo image, the samples were arranged side-by-side in the scanner. The data displayed in Figures 5.1.13-4 and 5.1.13-6 were edited into 3X3 images for comparison

to the LUIS image. Once the LUIS and conventional images were produced, the U.S. government software application NIH Image was used to count the number of gray scale levels in each panel image.

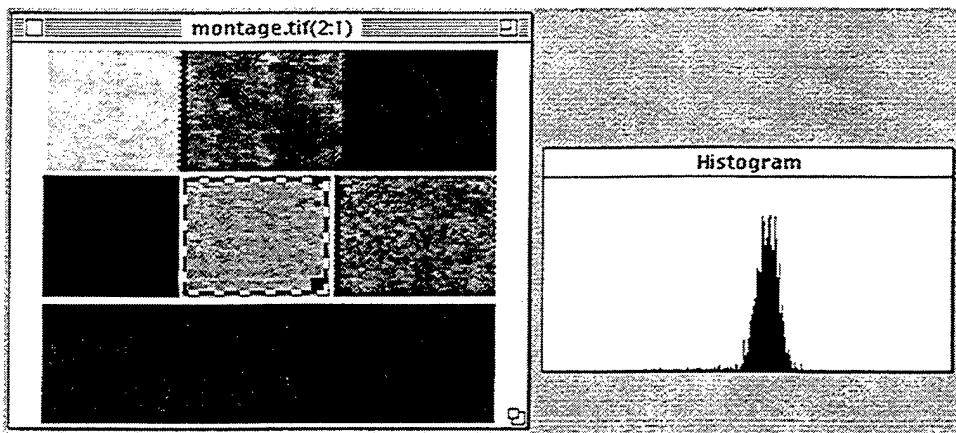


Figure 5.1.13-5. Conventional pulse-echo image and histogram of values in the center panel

Figure 5.1.13-5 shows an example histogram of counts per gray scale value for an area of the center sample, a 32 ply, 1% porosity sample. A “marquee” cursor is seen in Figure 5.1.13-5 marking an area to be measured by NIH Image for gray scale counts. Each panel was measured separately. Figure 5.1.13-5 shows the conventional system data for the center panel. A 3.5 MHz transducer was used for this scan. The LUIS image in Figure 5.1.13-6 is extracted from the full bandwidth A-scan data, filtered to 3MHz center frequency with 1MHz bandwidth.

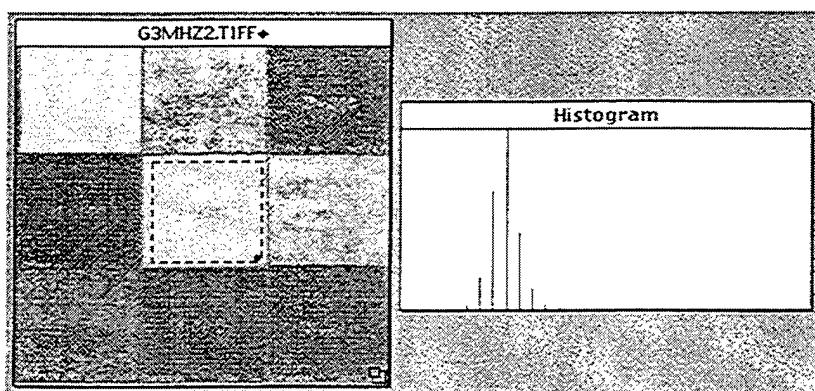


Figure 5.1.13-6. LUIS image of porosity samples and histogram of values in the center panel

The conventional ultrasonic instrument was set up relative to the back surface signal, so the digitizer's full 8 bits of dynamic range were applied to the signal. This allowed more values to be recorded and so the conventional histogram is denser than the LUIS data histogram. Since the LUIS digitizer was scaled to record the large front-surface echo, and devotes fewer bits of resolution to the small signal from the back surface of the sample, the LUIS histogram is sparser than the conventional histogram.

The peak in the conventional data histogram appears farther to the left than the peak in the LUIS data histogram because the scales in the histograms are reversed from each other. One scale shows minimum on the left and maximum on the right while the other shows maximum on the left and minimum on the right.

Comparison of the C-scans is somewhat complicated by different thresholds, gray levels and ranges in the data. After NIH Image computed the counts per gray scale level for each panel, the average gray scale value was computed for each set of data conditions and for each panel. That is, an average value was computed for the LUIS full bandwidth data and the 1 MHz bandwidth results. The results are shown in charts for 24 ply panels and 32 ply panels as percentages of a computed full, unattenuated signal amplitude.

All 9 panels were scanned at the same set-up conditions. For conventional scans, the instrument gain was set to make the strongest received signal roughly 80% of full screen. For LUIS images, software gates were set to achieve the same purpose.

Software thresholds were set so that the signal from the 1% porosity, 24-ply panel was roughly 90% of "full screen." The same settings were used throughout, resulting in somewhat lower values for the 3 and 5 MHz filtered LUIS images.

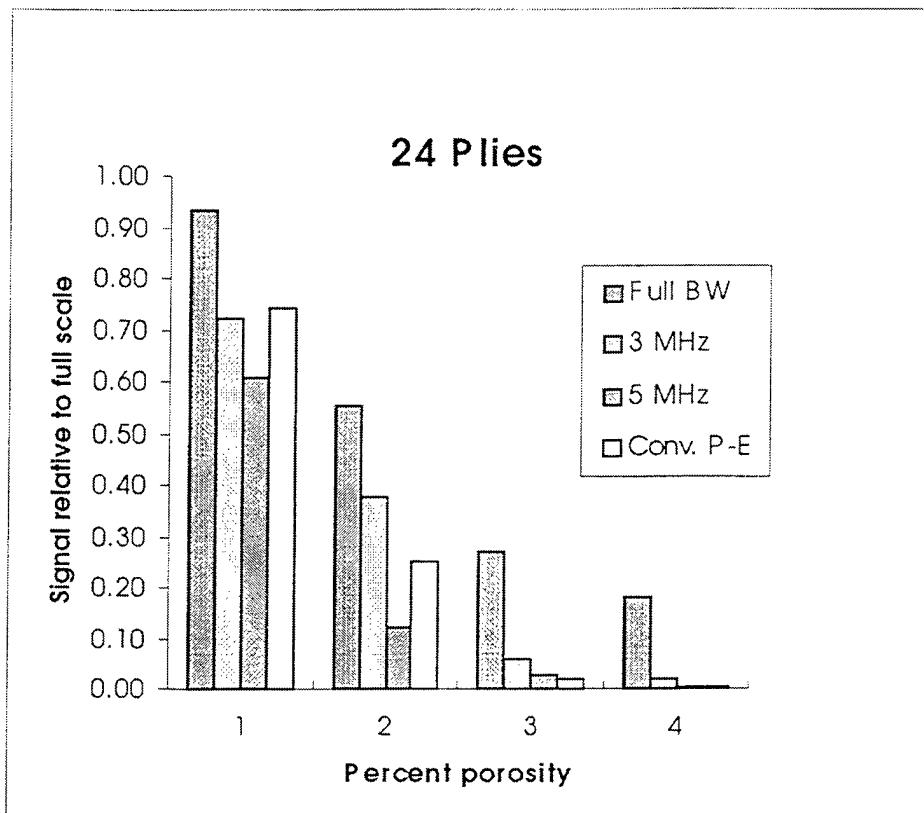


Figure 5.1.13-7. Signal levels for 24-ply thick composite panels with varying levels of porosity

In general, Figures 5.1.13-7 and 5.1.13-8 show that the signal for all bandwidth cases falls with increasing porosity as expected. Signal levels for the LUIS data are consistent with data from the 3.5 MHz conventional transducer. The LUIS 3 MHz centered signal has reasonable correlation to the conventional 3.5 MHz signal, at least at low porosity values. The LUIS full bandwidth signal provides a consistently greater return signal out to the highest porosity values sampled.

These results provide confidence that the LUIS can provide reasonable and reliable porosity indications.

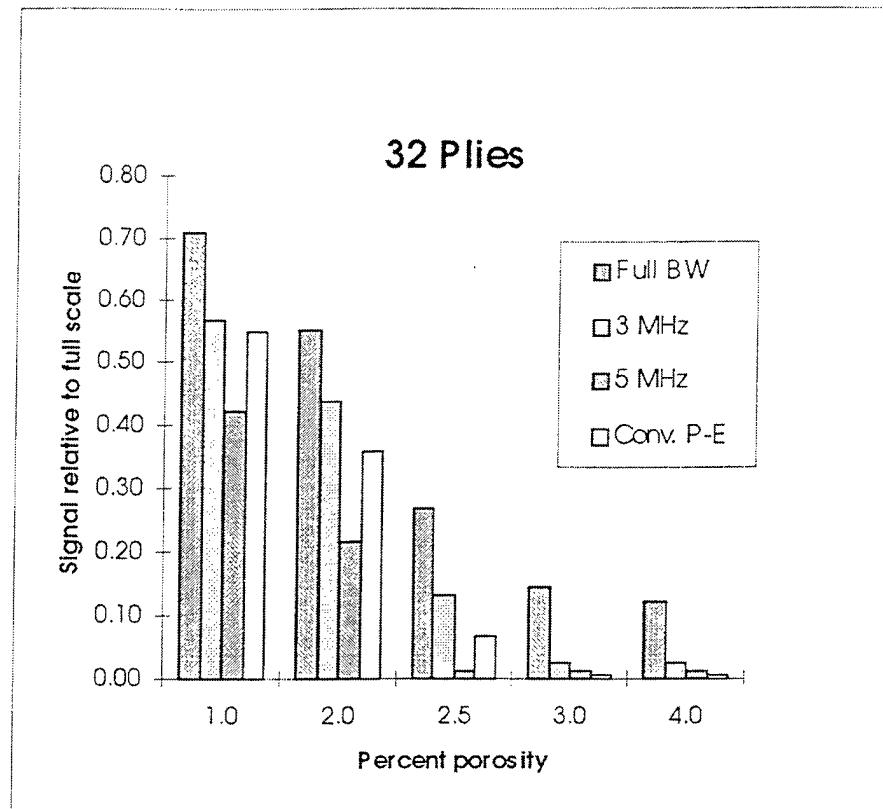


Figure 5.1.13-8. Signal levels for 32-ply thick composite panels with varying levels of porosity.

5.2 Military Aircraft Composite Parts

This section contains data from the inspection of composite parts and standards produced by Boeing for a variety of military aircraft.

5.2.1 A-6 Ply Drop Standard

This standard was used to establish NDE sensitivity for scanning associated with the A-6 re-wing program. The part is shown in Figure 5.2.1-1. It consists of two levels of composite, one 41 plies thick, and the other 83 plies. The transition area between the two levels has two rows of five 0.5" by 0.5" inserts made from five different materials. The inserts are located a number of plies from each of the sides of the panel, with one row being parallel to the flat tool side, and the other parallel to the slanted transition area on the bag side. It is normally reasonably difficult to detect the inserts that are not parallel to the surface from which the scan is taken.

The amplitude C-scan taken with the LUIS shown in figure 5.2.1-2 provides a good "picture" of the standard. The bottom portion of the figure is the thinner region. The transition is easily seen, with 4 of the 5 inserts parallel to the sloped transition (bag side) surface detected. The words "test aid" are easily seen on both of the plateaus, demonstrating the ease with which the LUIS can "see" surface discontinuities, even if they are very thin. This is due to the fact that different types of surface materials have different UT generation efficiencies. This scan does not pick up the inserts that lie deeper and are parallel to the opposite tool side. These inserts are not parallel to the scan surface, and hence are more difficult. A TOF image which is shown in figure 5.2.1-3 however, "hints" at least at one of these lowers inserts. This is located between the two inserts at the right side of the figure. It also detects all five near side inserts.



Figure 5.2.1-1. A-6 Ply Drop Standard

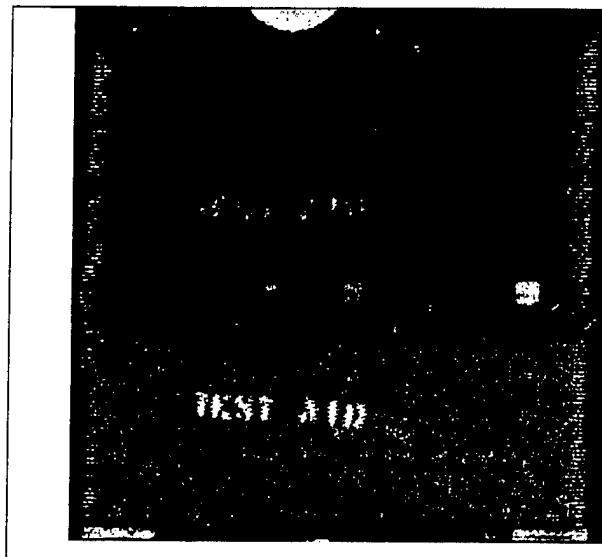


Figure 5.2.1-2. LUIS bag-side amplitude C-scan

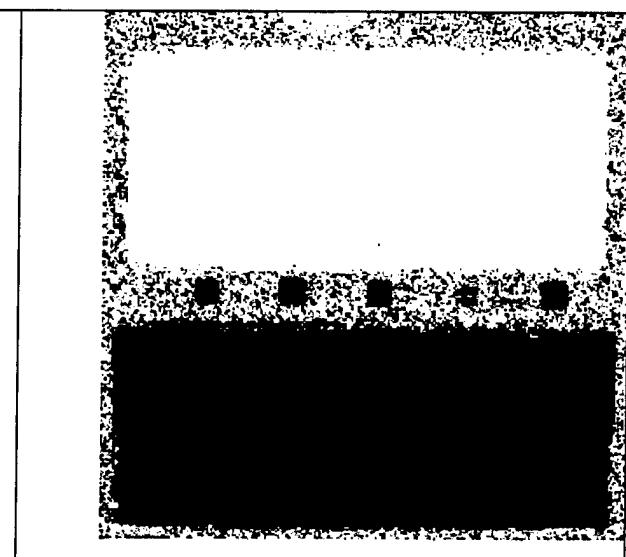


Figure 5.2.1-3. LUIS TOF bag side image

Scans taken with the Boeing production scanners from the bag side are shown in figures 5.2.1-4 and 5.2.1-5. It is easy to see all of the near side inserts in the amplitude scan, which is figure 5.2.1-4. The TOF scan shown in Figure 5.2.1-5 also shows about 4 of the inserts that lie deeper, and are sloped with respect to the scan surface. There is actually evidence of 8 out of the 10 total

D950-10322-1

126

inserts in this particular image. This panel is good for demonstrating the ability of the LUIS to "reach deep" into composite materials. Its realistic limit is somewhere in the 60 to 80-ply depth range.

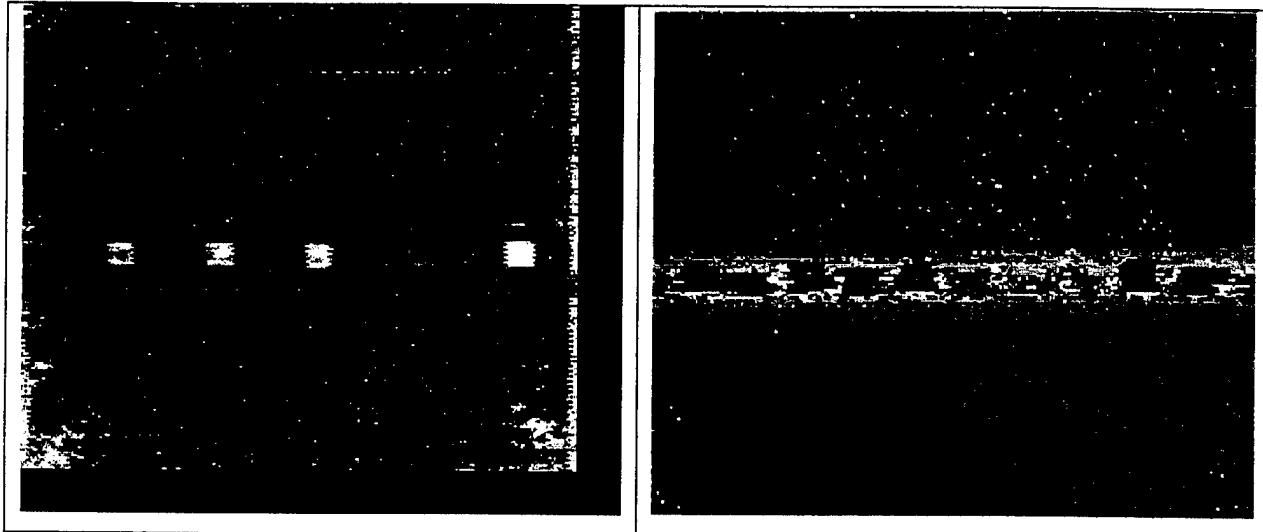


Figure 5.2.1-4. Boeing production amplitude C-scan of bag-side

Figure 5.2.1-5. Production TOF image of bag-side

Scans taken with the LUIS from the opposite flat tool side are shown in the next two figures.

Figure 5.2.1-6 is an amplitude C-scan, and Figure 5.2.1-7 is TOF. The amplitude scan shows four of the five near side inserts, and does not see any of the others. A narrow gate containing the depth of the inserts was used to generate the TOF image in figure 5.2.1-7. This figure gives an indication of the fifth insert, but certainly not its square shape.

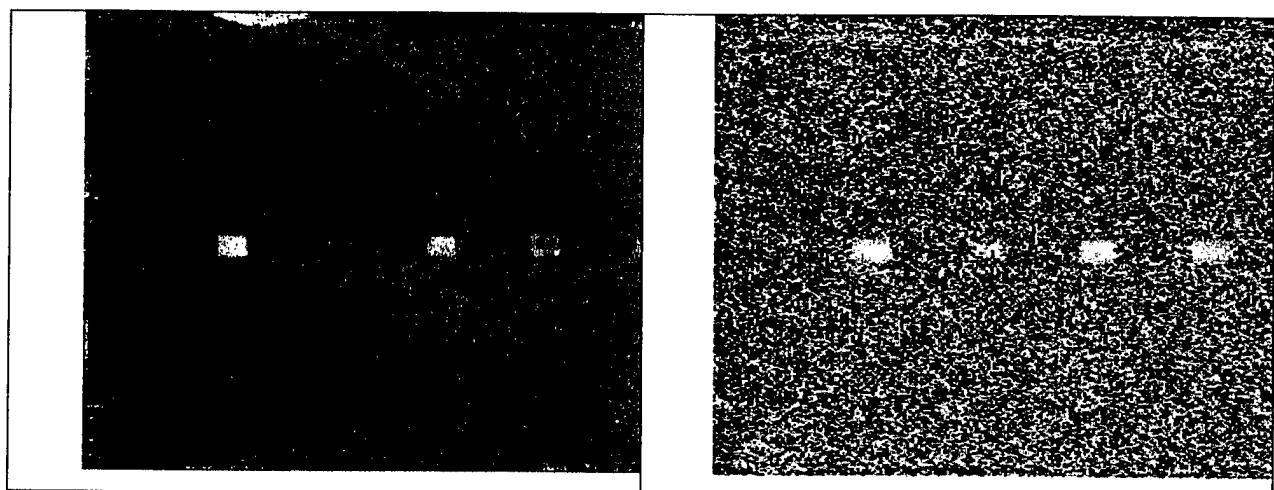


Figure 5.2.1-6. Tool-side LUIS amplitude C-scan

Figure 5.2.1-7. LUIS TOF of tool-side

The corresponding Boeing production scans are shown in figures 5.2.1-8 and -9. The amplitude image (figure 5.2.1-8) shows four of the five near side inserts, with indications of three of those on the far side. The TOF image (figure 5.2.1-9) shows all five of the near side inserts.

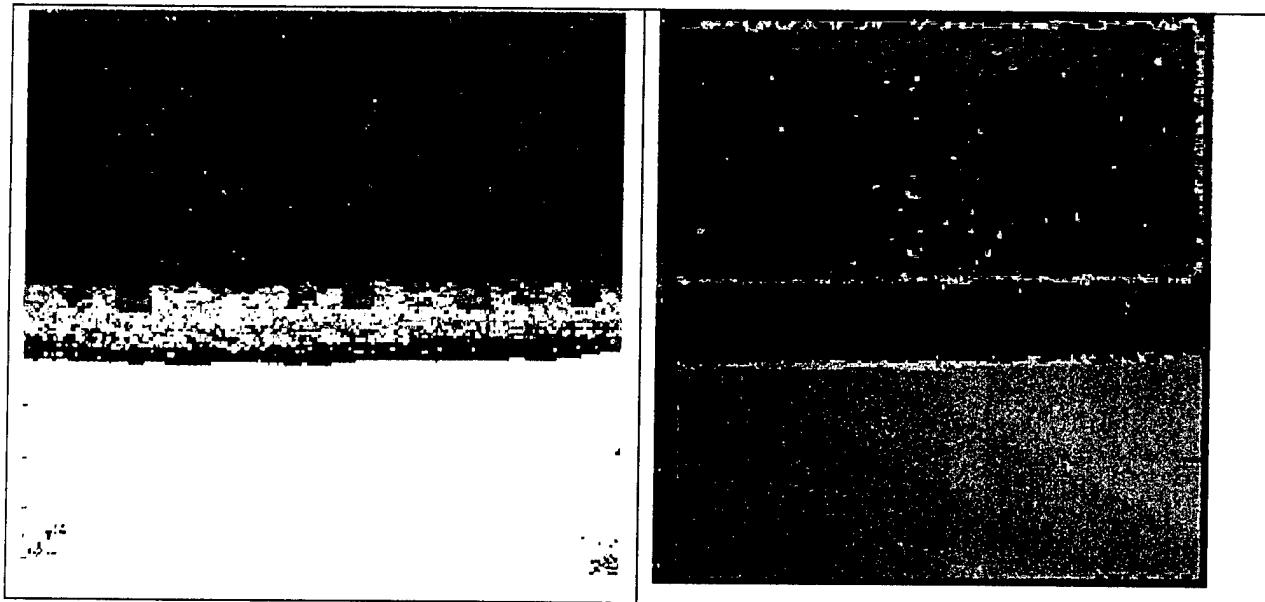


Figure 5.2.1-8. Tool-side production
amplitude C-scan

Figure 5.2.1-9. Production TOF image of
tool-side

5.2.2 A-6 Near/Far Surface Resolution Panel

The part is shown in Figure 5.2.2-1. This panel is constructed of 128 plies, and is 1.004 inch thick. It is approximately square, and contains a 23 x 23 square array of 529 0.5" x 0.5" inserts. The inserts are of 23 different materials that might be found in a production-manufacturing environment. The inserts are at depths of 1, 2, 3, 4, 5, 6, 7, 8, 9, 10, and 11 plies from each of the surfaces, (hence the name near/far surface resolution panel) and one series in the middle between the 64th and 65th ply.

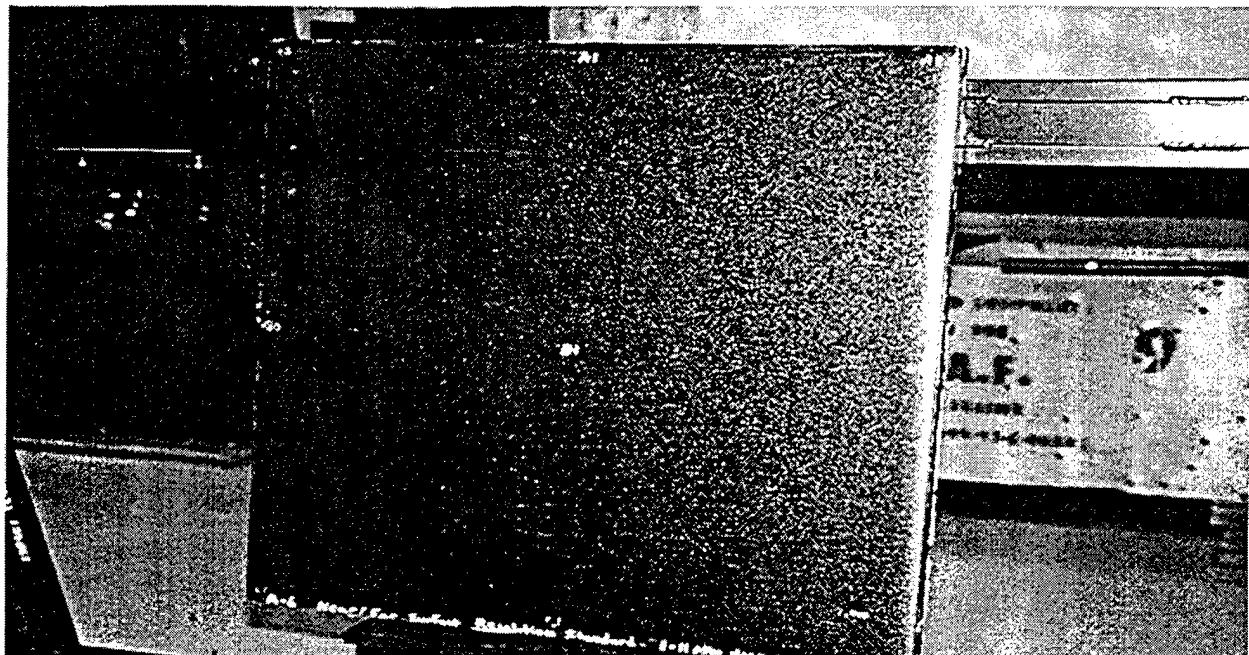


Figure 5.2.2-1. A-6 Near/Far Resolution Panel

The panel is flat on both sides, and as such is not a good candidate to demonstrate the LUIS's capability to scan complicated surfaces. In addition since it is flat, it can be scanned very quickly and with a minimum of set up time on a conventional production scanner. It does, however provide good opportunity for evaluation of the sensitivity of LUIS compared with production scanners in that there are many inserts, and thus it is easy to "poll" images from the LUIS scans and from production scans to compare how many of what type of insert at what depth each can detect.

The panel was scanned with the LUIS from both sides. The tool side required painting to reduce the specular reflection. The tool side scan did not have as good a signal to noise ratio as the bag side scan, and was therefore only usable for the inserts near the tool side. There were also scans made from the bag side that were cut short in the time domain, and thus only included the closer, near side inserts. Finally, some scans were made from the bag side at reduced resolution.

Amplitude C-scans are shown below for LUIS and Boeing production scanner data. The Boeing data were obtained with a 3.5 MHz bubbler "surface rider" transducer. Boeing images are not from full wave data, but are made by simply detecting the largest echo occurring within a gate which commences immediately after the front surface echo. The amplitude gate width is set to be sufficient to detect echoes arising from the full range of thickness of this panel. A second time of flight (TOF) gate commences immediately after the front surface echo, and it covers the same interval as the amplitude gate. The threshold of the TOF gate is set to 10-15% of the full-scale amplitude range to enable detection of weak echoes arising from poorly reflecting materials such as nylon bagging. Back surface echoes over the full range of part thickness are equalized by means of distance amplitude correction (DAC) circuitry in the ultrasonic instrument. It required approximately 10 minutes to scan and obtain the resultant images with the Boeing production scanner.

Figure 5.2.2-2 shows an amplitude C-scan image from the Boeing scanner and Figure 5.2.2-3 shows an amplitude C-scan image for LUIS. The LUIS scan was processed for maximum signal-to-noise ratio (SNR) by National Research Council personnel. The scans are roughly equivalent.

Figure 5.2.2-4 shows the Boeing scanner TOF scan image and Figure 5.2.2-5 shows TOF scan image for LUIS. As in the previous case, the LUIS image was made by optimizing the SNR.

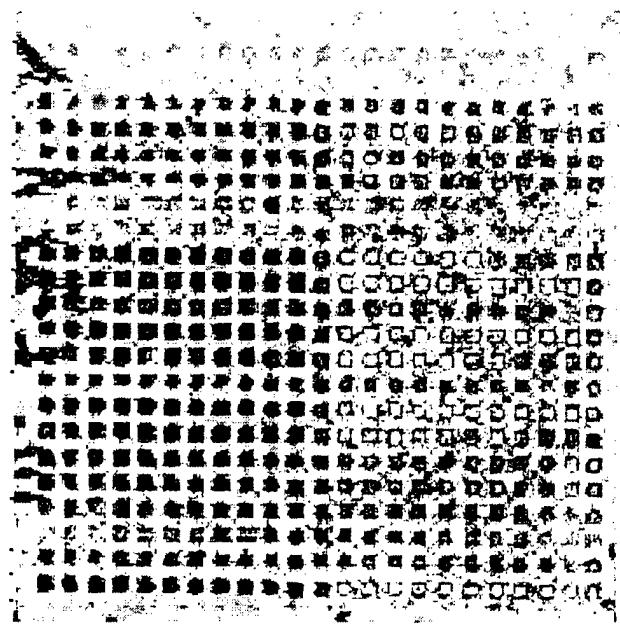


Figure 5.2.2-2. Amplitude C-scan taken by Boeing production scanner

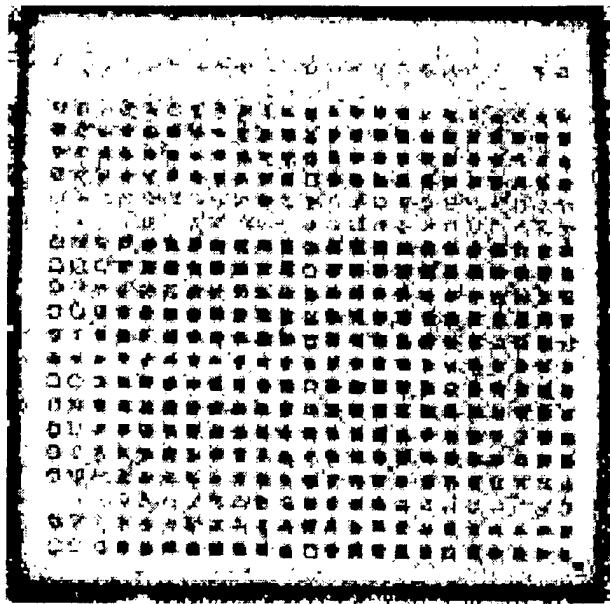


Figure 5.2.2-3. Amplitude C-scan taken with LUIS

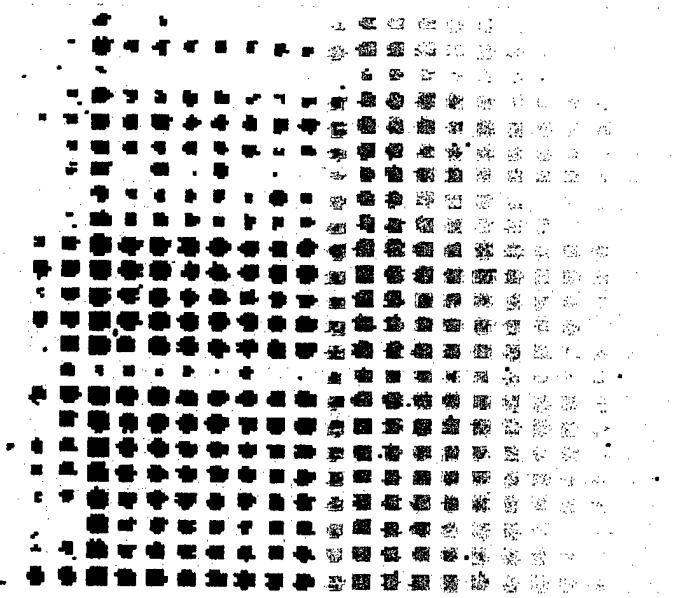


Figure 5.2.2-4. TOF image taken with Boeing scanner

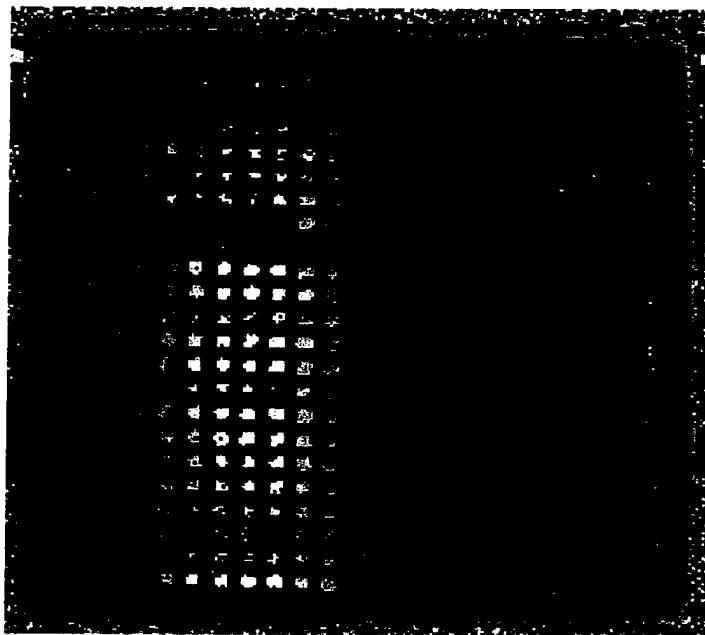


Figure 5.2.2-5. TOF image taken with LUIS

In order to see the echoes at the far surface of the panel, a gate was defined near the back surface. This results in seeing far surface echoes and near surface "shadows". A B-scan taken with the LUIS at line number 251, which passes through the row of inserts made of "black poly", is shown in figure 5.2.2-6. The far surface inserts are not well seen, whereas those on the near surface, (in

surface, (in this case the bag side), are very prominent. This typical B-scan is serves to demonstrate the usefulness of this panel in evaluating the sensitivity of a single side pulse-echo system such as LUIS to known flaws over a wide range of known depths, including near surface, far surface, and one in the center of the panel.

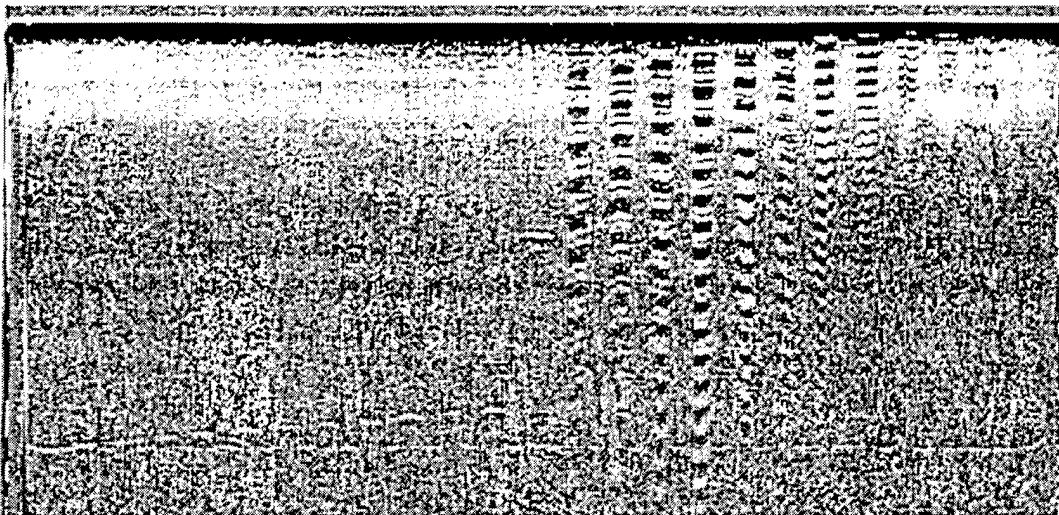


Figure 5.2.2-6. B-scan of A6 Near/Far Surface Resolution Panel taken with LUIS

To compare the sensitivity of LUIS scans of this part with conventional scans, score cards showing detection or nondetection of each of the 529 inserts were developed. Each score card shows an "X" or a blank in each of the 529 positions to indicate whether the insert was detected or not. Three different scorecards are shown. These include Table 5.2.2-1, the Boeing 3.5 MHz surface riding bubbler, Table 5.2.2-2, a composite of several images derived from two scans made by the LUIS (one from each side), and Table 5.2.2-3, one from only the bag side made by the LUIS. The scan taken by the Boeing scanner was done from the tool side, which is normal production procedure, but is displayed viewed from the bag side. This makes it directly comparable with the scan taken from the bag side with the LUIS. It is taken from the two images in figures 5.2.2-2 and 5.2.2-4. The scorecard for the single bag side LUIS scan is from the image used in figure 5.2.2-3 and its corresponding TOF image which is shown in figure 5.2.2-5. This scan has been processed for maximum SNR.

Table 5.2.2-1. Flaws Detected with 3.5 MHz Bubbler (Toolside Scan)
(Bagside View)

Panel 26" x 26", Inserts 0.5" x 0.5"

| Flaws Detected | 128 Plies - 1.004" Thick | | | | | | | | | | | | Distance from Bagside (Plies) | | | | | | | | | | | | |
|-------------------|--------------------------------|---|---|---|---|---|---|---|---|----|----|----|-------------------------------|----|---|---|---|---|---|---|---|---|---|---------------------|---------------------|
| | 1 | 2 | 3 | 4 | 5 | 6 | 7 | 8 | 9 | 10 | 11 | 64 | 11 | 10 | 9 | 8 | 7 | 6 | 5 | 4 | 3 | 2 | 1 | | |
| 11 | | | X | X | | | | | | X | X | X | X | X | X | X | X | X | X | | | | | Green Bag | |
| 17 | | X | X | X | X | X | X | X | X | X | X | X | X | X | X | X | X | X | X | | | | | Soft Bag | |
| 8 | | X | | | | | | | | X | X | X | X | X | X | X | X | X | X | | | | | Smoked Bag | |
| 23 | X | X | X | X | X | X | X | X | X | X | X | X | X | X | X | X | X | X | X | X | X | X | X | Tacky Tape Backing | |
| 23 | X | X | X | X | X | X | X | X | X | X | X | X | X | X | X | X | X | X | X | X | X | X | X | Thin Paper | |
| 23 | X | X | X | X | X | X | X | X | X | X | X | X | X | X | X | X | X | X | X | X | X | X | X | Heavy Paper | |
| 23 | X | X | X | X | X | X | X | X | X | X | X | X | X | X | X | X | X | X | X | X | X | X | X | New Brwn Drwg Paper | |
| 23 | X | X | X | X | X | X | X | X | X | X | X | X | X | X | X | X | X | X | X | X | X | X | X | Paper Part Label | |
| 17 | | X | X | X | X | X | X | X | X | X | X | X | X | X | X | X | X | X | X | X | X | X | X | Plastic Part Label | |
| 18 | | X | X | X | X | X | X | X | X | X | X | X | X | X | X | X | X | X | X | X | X | X | X | X | Blue Poly |
| 23 | X | X | X | X | X | X | X | X | X | X | X | X | X | X | X | X | X | X | X | X | X | X | X | X | Red Poly |
| 23 | X | X | X | X | X | X | X | X | X | X | X | X | X | X | X | X | X | X | X | X | X | X | X | X | Green Poly |
| 23 | X | X | X | X | X | X | X | X | X | X | X | X | X | X | X | X | X | X | X | X | X | X | X | X | Black Poly |
| 23 | X | X | X | X | X | X | X | X | X | X | X | X | X | X | X | X | X | X | X | X | X | X | X | X | Yellow Poly |
| 23 | X | X | X | X | X | X | X | X | X | X | X | X | X | X | X | X | X | X | X | X | X | X | X | X | White Backing Paper |
| 23 | X | X | X | X | X | X | X | X | X | X | X | X | X | X | X | X | X | X | X | X | X | X | X | X | Solid FEP |
| 23 | X | X | X | X | X | X | X | X | X | X | X | X | X | X | X | X | X | X | X | X | X | X | X | X | Perforated FEP |
| 23 | X | X | X | X | X | X | X | X | X | X | X | X | X | X | X | X | X | X | X | X | X | X | X | X | Blue Roll Tape |
| 23 | X | X | X | X | X | X | X | X | X | X | X | X | X | X | X | X | X | X | X | X | X | X | X | X | Red Roll Tape |
| 23 | X | X | X | X | X | X | X | X | X | X | X | X | X | X | X | X | X | X | X | X | X | X | X | X | Clear Vinyl Tape |
| 23 | X | X | X | X | X | X | X | X | X | X | X | X | X | X | X | X | X | X | X | X | X | X | X | X | White Vinyl Tape |
| 18 | | X | X | X | X | X | X | X | X | X | X | X | X | X | X | X | X | X | X | X | X | X | X | X | Masking Tape |
| 23 | X | X | X | X | X | X | X | X | X | X | X | X | X | X | X | X | X | X | X | X | X | X | X | X | Armalon |
| 23 | 1 | 2 | 3 | 4 | 5 | 6 | 7 | 8 | 9 | 10 | 11 | 64 | 11 | 10 | 9 | 8 | 7 | 6 | 5 | 4 | 3 | 2 | 1 | | |
| | Distance from Toolside (Plies) | | | | | | | | | | | | Distance from Bagside (Plies) | | | | | | | | | | | | |

Flaws detected marked with
X
480 Total Flaws Detected of 529 Possible
91% Per Cent Flaws Detected

Table 5.2.2-2. Flaws Detected with LUIS
(Composite of Bagside & Toolside Views)

Panel 26" x 26", Inserts 0.5" x 0.5"

128 Plies - 1.004" Thick

| Flaws Detected | Distance from Toolside (Plies) | | | | | | | | | | | | Distance from Bagside (Plies) | | | | | | | | | | | |
|-------------------|--------------------------------|---|---|---|---|---|---|---|---|----|----|----|-------------------------------|----|---|---|---|---|---|---|---|---|-----------------------|--|
| | 1 | 2 | 3 | 4 | 5 | 6 | 7 | 8 | 9 | 10 | 11 | 64 | 11 | 10 | 9 | 8 | 7 | 6 | 5 | 4 | 3 | 2 | 1 | |
| 17 | | | | X | X | X | X | X | X | X | X | X | X | X | X | X | X | X | X | X | | | Green Bag | |
| 20 | X | X | X | X | X | X | X | X | X | X | X | X | X | X | X | X | X | X | X | X | X | X | Soft Bag | |
| 15 | X | X | X | X | X | X | X | X | X | X | X | X | X | X | X | X | X | X | X | X | | | Smoked Bag | |
| 18 | X | X | X | X | X | X | X | X | X | X | X | X | X | X | X | X | X | X | X | X | X | X | Tacky Tape Backing | |
| 22 | X | X | X | X | X | X | X | X | X | X | X | X | X | X | X | X | X | X | X | X | X | X | Thin Paper | |
| 20 | X | X | X | X | X | X | X | X | X | X | X | X | X | X | X | X | X | X | X | X | X | X | Heavy Paper | |
| 21 | X | X | X | X | X | X | X | X | X | X | X | X | X | X | X | X | X | X | X | X | X | X | New Brown Drwg Paper | |
| 19 | X | X | X | X | X | X | X | X | X | X | X | X | X | X | X | X | X | X | X | X | X | X | Paper Part Label | |
| 18 | X | X | X | X | X | X | X | X | X | X | X | X | X | X | X | X | X | X | X | X | X | X | Plastic Part Label | |
| 22 | X | X | X | X | X | X | X | X | X | X | X | X | X | X | X | X | X | X | X | X | X | X | Blue Poly | |
| 23 | X | X | X | X | X | X | X | X | X | X | X | X | X | X | X | X | X | X | X | X | X | X | X Red Poly | |
| 21 | X | X | X | X | X | X | X | X | X | X | X | X | X | X | X | X | X | X | X | X | X | X | Green Poly | |
| 23 | X | X | X | X | X | X | X | X | X | X | X | X | X | X | X | X | X | X | X | X | X | X | X Black Poly | |
| 21 | X | X | X | X | X | X | X | X | X | X | X | X | X | X | X | X | X | X | X | X | X | X | Yellow Poly | |
| 23 | X | X | X | X | X | X | X | X | X | X | X | X | X | X | X | X | X | X | X | X | X | X | X White Backing Paper | |
| 23 | X | X | X | X | X | X | X | X | X | X | X | X | X | X | X | X | X | X | X | X | X | X | X Solid FEP | |
| 22 | X | X | X | X | X | X | X | X | X | X | X | X | X | X | X | X | X | X | X | X | X | X | X Perforated FEP | |
| 22 | X | X | X | X | X | X | X | X | X | X | X | X | X | X | X | X | X | X | X | X | X | X | X Blue Roll Tape | |
| 22 | X | X | X | X | X | X | X | X | X | X | X | X | X | X | X | X | X | X | X | X | X | X | X Red Roll Tape | |
| 22 | X | X | X | X | X | X | X | X | X | X | X | X | X | X | X | X | X | X | X | X | X | X | X Clear Vinyl Tape | |
| 20 | X | X | X | X | X | X | X | X | X | X | X | X | X | X | X | X | X | X | X | X | X | X | X White Vinyl Tape | |
| 23 | X | X | X | X | X | X | X | X | X | X | X | X | X | X | X | X | X | X | X | X | X | X | X Masking Tape | |
| 23 | X | X | X | X | X | X | X | X | X | X | X | X | X | X | X | X | X | X | X | X | X | X | X Armalon | |
| | 1 | 2 | 3 | 4 | 5 | 6 | 7 | 8 | 9 | 10 | 11 | 64 | 11 | 10 | 9 | 8 | 7 | 6 | 5 | 4 | 3 | 2 | 1 | |
| | Distance from Toolside (Plies) | | | | | | | | | | | | Distance from Bagside (Plies) | | | | | | | | | | | |

Flaws detected are marked with
X

480 Total Flaws Detected of 529 Possible
91% Per Cent Flaws Detected

Table 5.2.2-3. Flaws Detected with LUIS (Bagside Scan)
(Bagside View)

Panel 26" x 26", Inserts 0.5" x 0.5"

| Flaws Detected | 128 Plies - 1.004" Thick | | | | | | | | | | | | | | Distance from Bagside (Plies) | | | | | | | | | | |
|-------------------|--------------------------------|---|---|---|---|---|---|---|---|----|----|----|----|----|-------------------------------|---|---|---|---|---|---|---|---|---------------------|--------------------|
| | 1 | 2 | 3 | 4 | 5 | 6 | 7 | 8 | 9 | 10 | 11 | 64 | 11 | 10 | 9 | 8 | 7 | 6 | 5 | 4 | 3 | 2 | 1 | | |
| 3 | | | | | | | | | | | | | | | X | X | X | | | | | | | | Green Bag |
| 7 | | | | | | | | | | | | | | | X | X | X | X | X | X | | | | | Soft Bag |
| 1 | | | | | | | | | | | | | | | | | X | | | | | | | | Smoked Bag |
| 19 | | | X | X | | X | X | X | X | X | X | X | X | X | X | X | X | X | X | X | X | X | X | Tacky Tape Backing | |
| 23 | X | X | X | X | X | X | X | X | X | X | X | X | X | X | X | X | X | X | X | X | X | X | X | Thin Paper | |
| 23 | X | X | X | X | X | X | X | X | X | X | X | X | X | X | X | X | X | X | X | X | X | X | X | Heavy Paper | |
| 21 | | X | X | X | X | X | X | X | X | X | X | X | X | X | X | X | X | X | X | X | X | X | X | New Brown Drwg Pa | |
| 10 | | | | | | | | | | | | | | | X | X | X | X | X | X | X | X | X | | Paper Part Label |
| 9 | | | | | | | | | | | | | | | X | X | X | X | X | X | X | X | X | | Plastic Part Label |
| 23 | X | X | X | X | X | X | X | X | X | X | X | X | X | X | X | X | X | X | X | X | X | X | X | Blue Poly | |
| 23 | X | X | X | X | X | X | X | X | X | X | X | X | X | X | X | X | X | X | X | X | X | X | X | Red Poly | |
| 20 | | X | X | X | X | X | X | X | X | X | X | X | X | X | X | X | X | X | X | X | X | X | X | Green Poly | |
| 23 | X | X | X | X | X | X | X | X | X | X | X | X | X | X | X | X | X | X | X | X | X | X | X | Black Poly | |
| 22 | X | X | X | X | X | X | X | X | X | X | X | X | X | X | X | X | X | X | X | X | X | X | X | Yellow Poly | |
| 23 | X | X | X | X | X | X | X | X | X | X | X | X | X | X | X | X | X | X | X | X | X | X | X | White Backing Paper | |
| 23 | X | X | X | X | X | X | X | X | X | X | X | X | X | X | X | X | X | X | X | X | X | X | X | Solid FEP | |
| 23 | X | X | X | X | X | X | X | X | X | X | X | X | X | X | X | X | X | X | X | X | X | X | X | Perforated FEP | |
| 23 | X | X | X | X | X | X | X | X | X | X | X | X | X | X | X | X | X | X | X | X | X | X | X | Blue Roll Tape | |
| 23 | X | X | X | X | X | X | X | X | X | X | X | X | X | X | X | X | X | X | X | X | X | X | X | Red Roll Tape | |
| 22 | X | X | X | X | X | X | X | X | X | X | X | X | X | X | X | X | X | X | X | X | X | X | X | Clear Vinyl Tape | |
| 20 | | X | X | X | X | X | X | X | X | X | X | X | X | X | X | X | X | X | X | X | X | X | X | White Vinyl Tape | |
| 15 | | | X | X | X | X | X | X | X | X | X | X | X | X | X | X | X | X | X | X | X | X | X | Masking Tape | |
| 21 | X | | X | X | X | X | X | X | X | X | X | X | X | X | X | X | X | X | X | X | X | X | X | Armalon | |
| 23 | X | X | X | X | X | X | X | X | X | X | X | X | X | X | X | X | X | X | X | X | X | X | X | | |
| 420 | 1 | 2 | 3 | 4 | 5 | 6 | 7 | 8 | 9 | 10 | 11 | 64 | 11 | 10 | 9 | 8 | 7 | 6 | 5 | 4 | 3 | 2 | 1 | | |
| | Distance from Toolside (Plies) | | | | | | | | | | | | | | Distance from Bagside (Plies) | | | | | | | | | | |

Flaws detected are marked with

X

420 Total Flaws Detected of 529

Possible

79% Per Cent Flaws Detected

For this part, scans were done with the LUIS at a lower resolution. That is, the scan and step index were two times as large as the “high” resolution values used for most of the LUIS scans. This makes the data files somewhat more manageable, at 35.4MB instead of 142MB. The effect of resolution changes on image quality can be seen by comparing high resolution and low resolution scan images. Below are shown two LUIS scan taken from the bag-side. One is taken at high resolution and the other with a lower resolution scan. The set of images amplitude C-scans, in figure 5.2.2-7, and figure 5.2.2-8 are gated to the near (bag side) surface of the panel. The second set of images is time of flight scan images, in figure 5.2.2-9 and 5.2.2-10, which were gated to the back (tool side) surface of the panel.

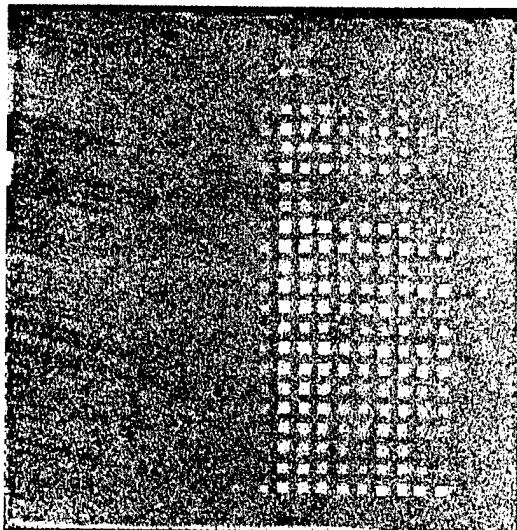


Figure 5.2.2-7. Amplitude C-scan gated to near the front surface taken with high resolution

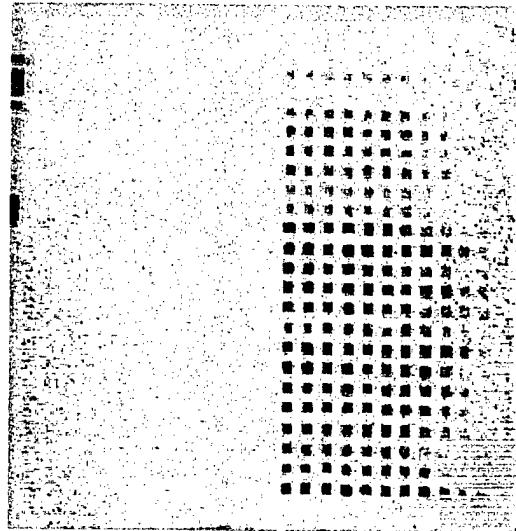


Figure 5.2.2-8. Amplitude C-scan gated to near the front surface taken at reduced resolution

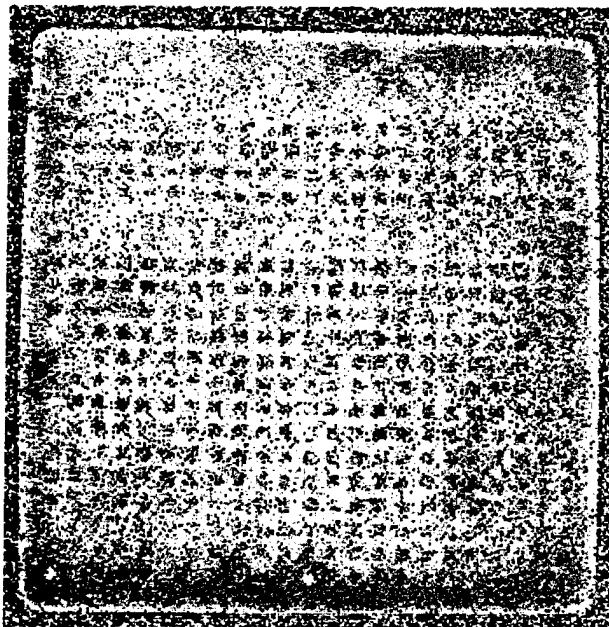


Figure 5.2.2-9. Time-of-Flight C-scan gated to near the back surface, taken with high resolution

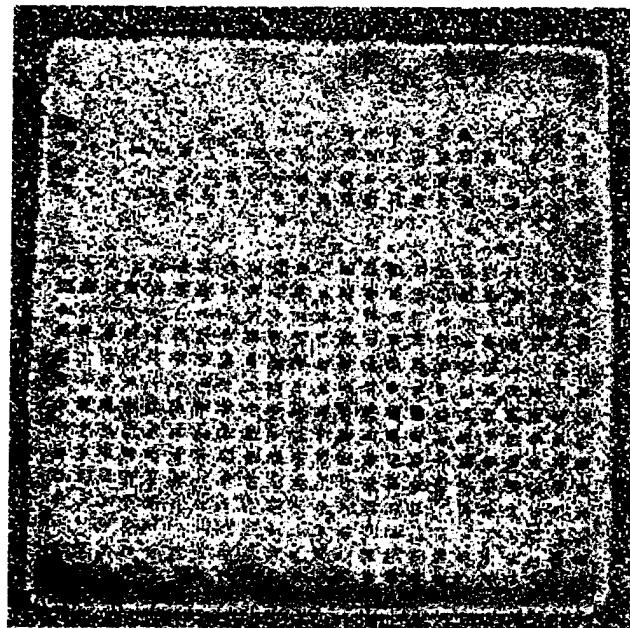
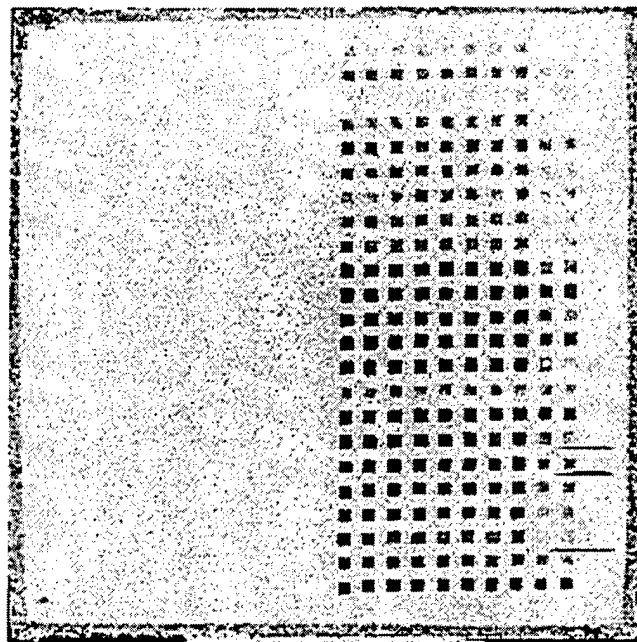


Figure 5.2.2-10. Time-of-Flight C-scan gated to near the back surface, taken with reduced resolution

Finally, “short gated” scans were made of both sides of the panel that went only to about 5 microseconds. This is only enough time to allow ultrasound transmission through about one quarter of the thickness of the panel, hence only the near side inserts could be detected.

Amplitude C-scans of each side of the panel are shown below in figure 5.2.2-11 and figure 5.2.2-12. The smoother appearance of the tool side image is noteworthy.



5.2.2-11. Short gated amplitude C-scan taken from tool side

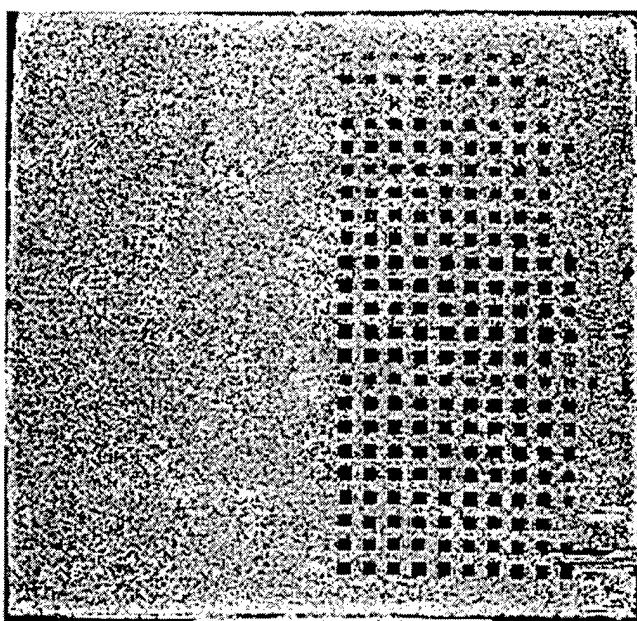


Figure 5.2.2-12. Short gated amplitude C-scan from bag side

The production scanner detected 91% of the flaws. If scans from both sides of the sample are included, the LUIS matched the production scanner with 91% detection. The LUIS was better at scanning from the bagside of the sample, whereas the production scanner excelled at scanning the toolside. For scanning from one side only, the LUIS had a more difficult time seeing the deeply located flaws, and required expert signal processing to be able to see them as well as the production scanner could.

A number of attempts were made at calculating the signal to noise ration of a LUIS scan. It was not possible to come up with a consistent calculation that was directly comparable to calculated SNR values for the production scanner. For this reason no SNR information is reported.

5.2.3 Foreign Material Panel #3

This panel is somewhat similar to the A-6 near/far surface resolution panel. This part is shown in Figure 5.2.3-1. It permits a sensitivity comparison between the Boeing production scanner and the LUIS for finding flaws. The LUIS would in general not be the system of choice for simple planar parts like this one since it can not scan them as quickly and can not process the data as quickly as the Boeing production scanner. For the Boeing squirter, the entire process took about 40 minutes from set up until the image was in hand.

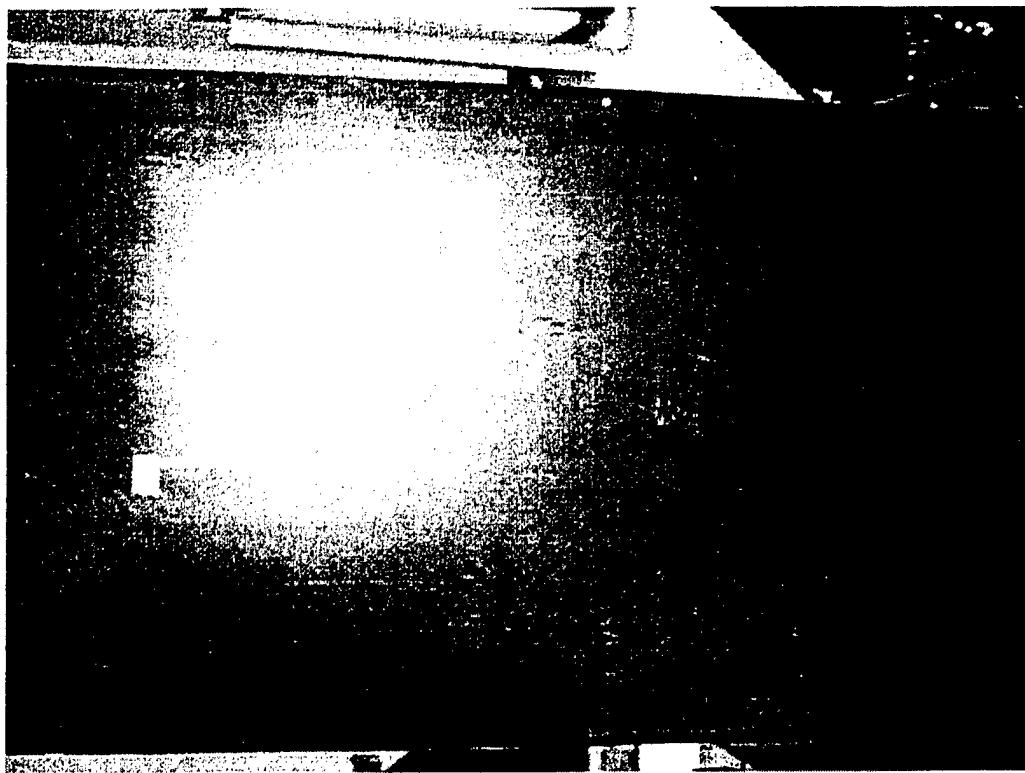


Figure 5.2.3-1. A-6 Foreign Material Standard

The panel consists of a rectangular array of 0.5" x 0.5" inserts of various materials at various depths from the surfaces, much like the A-6 near/far surface resolution panel. This panel however is thinner (only 46 plies total) and has each material repeated in two adjacent columns. The first two columns are B-276 backing, the next two are Mylar tape, and so on. From the bag side, each row of inserts is at 2, 4, 6, 8.up to 44 plies deep. The panel was scanned from the bag side with both the LUIS and the Boeing production scanner. Since the LUIS captures the full

the scan may be examined later to extract features. With the production scanner, the operator checks at several points on the part and then chooses the time gate and filtering appropriately according to his best estimate for the part. The scan is then commenced, with the results are dependent on the operator's skill and experience, and determined by the initial settings he selects at the start of the scan.

Figures 5.2.3-2 shows a LUIS TOF image. All told, the number of inserts detected was 727 out of 748. Figure 5.2.3-3 shows an amplitude C-scan taken with the Boeing production scanner which detects 735 out of 748 total inserts. In each case, the image was chosen that detected the most inserts, and then the corresponding image (whether amplitude or TOF) was checked to make sure that no inserts were left out of the total count.

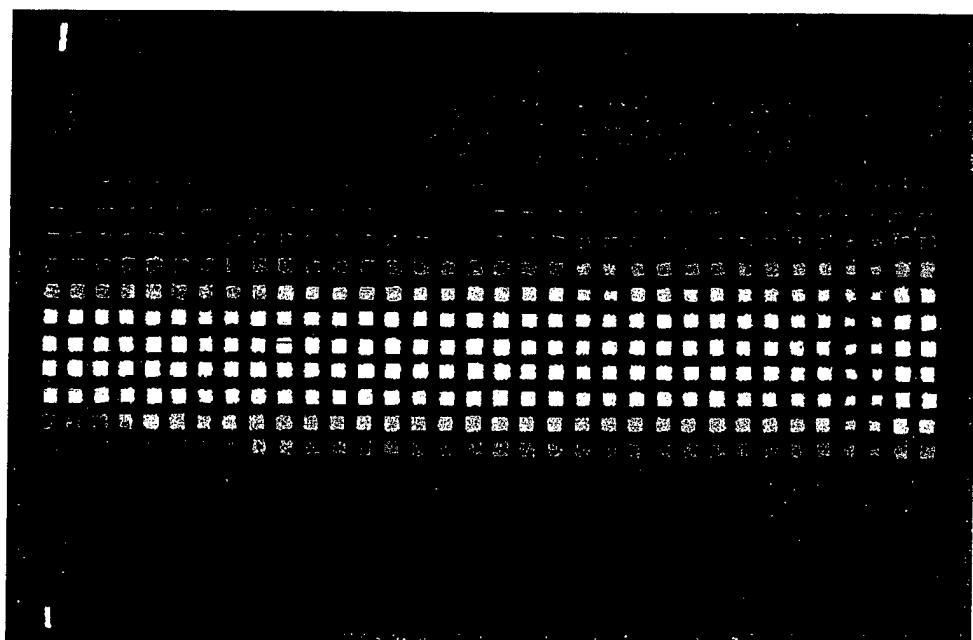


Figure 5.2.3-2. LUIS TOF image

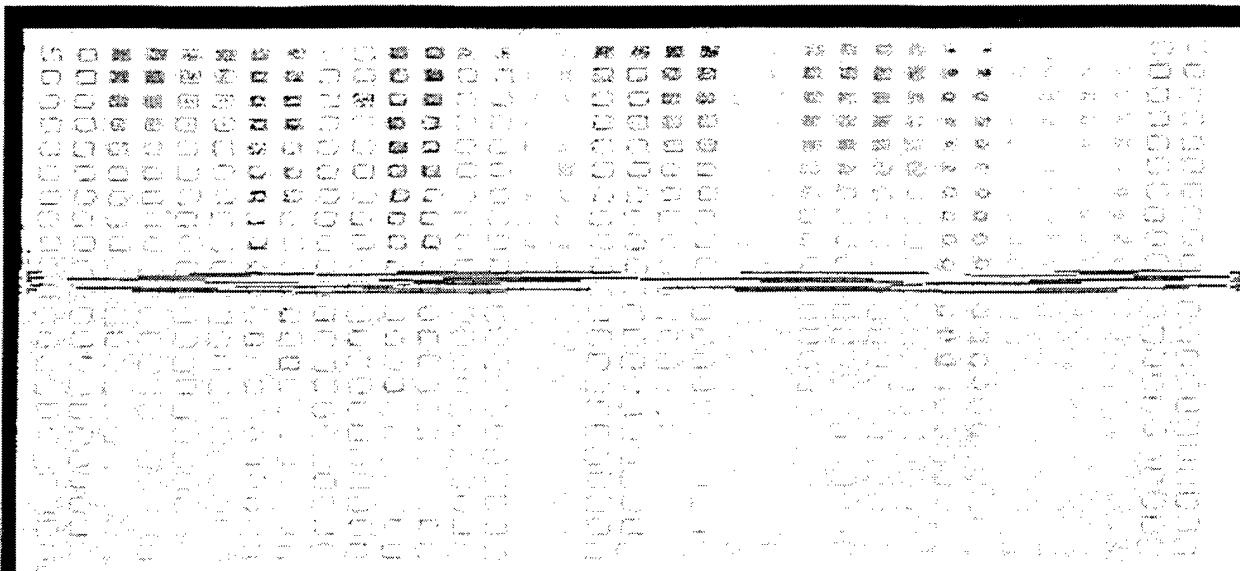


Figure 5.2.3-3. Production amplitude C-scan

5.2.4 Impact Test Panel

This panel is a solid laminate panel reinforced with "c" shaped stiffeners on one side. The panel was impacted with a spectrum of different weighted projectiles at varying energies, for the purpose of inspecting and evaluating the resultant damage. A photograph of the panel is shown in figure 5.2.4-1. The hand drawn circles indicate the locations of the various impacts. The three impacts down the center of the panel are directly over a stiffener. UT investigation of the panel and the center stiffener by hand held probe revealed that some damage was experienced by the underlying stiffener. Boeing used the LUIS to scan this area, with the hope of demonstrating the capability of the LUIS to show damage in two orthogonal planes. Figure 5.2.4-2 shows a photograph of the other side of the panel, with a rectangular region including part of the panel and part of the center stiffener denoted by masking tape. This is the region that was scanned with the LUIS.

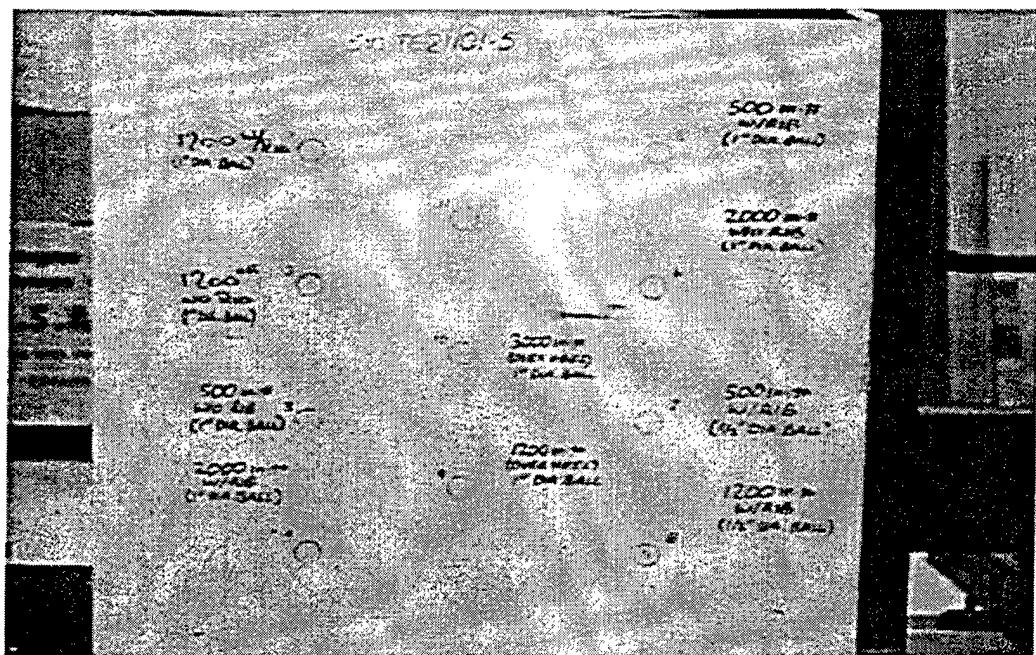


Figure 5.2.4-1. Impact panel



Figure 5.2.4-2. Backside of impact panel marked and ready for LUIS scanning

A TOF image taken with the LUIS is shown in figure 5.2.4-3. In this image it is easy to see the three damaged regions along the bond between the panel and the stiffener. It is also clear that the impacts did affect the stiffener. Spalling of some of the panel material may also be seen in the amplitude C-scan shown in figure 5.2.4-4. This spalling matches that of a previous production scan of the panel taken from the flat side. The flat side of the panel was not scanned with the LUIS. Since there is no way of effectively scanning the two-plane region shown in figure 5.2.4-2 easily with a production scanner, no production data are shown. This type of geometry is particularly well disposed for exploiting the unique capabilities of the LUIS.

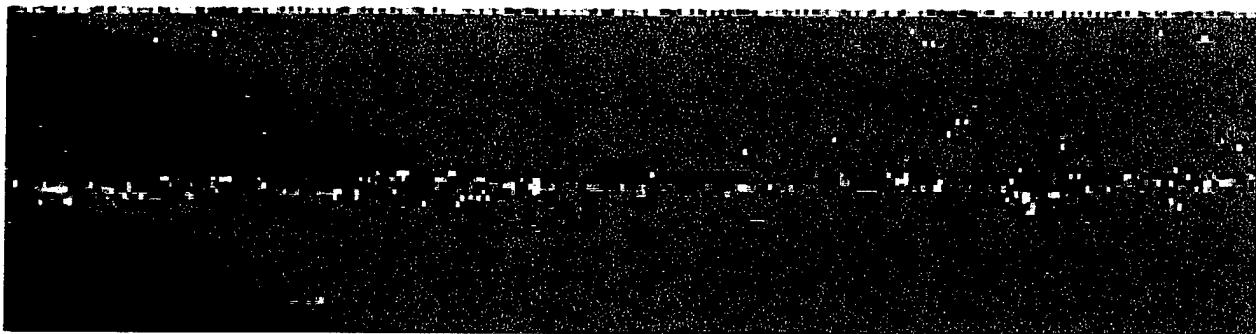


Figure 5.2.4-3. LUIS TOF scan



Figure 5.2.4-4. LUIS amplitude scan

5.2.5 F-22 Radius Standards

These standards are ninety-degree angles with three different bending radii, one at 0.13", one at 0.25", and the last at 0.38". Each of the standards has several thickness regions, resulting from differing numbers of plies in the regions. There are 0.25" x 0.25" and 0.5" x 0.5" inserts along the vertices of the standards at varying depths. The three standards are shown placed in position for scanning with the LUIS in the photograph in figure 5.2.5-1. In each case, the thickest region of the standard is at the bottom. The view is towards the interior angles of the standards. The standards have been painted white for better UT generation into the composite material.

An amplitude C-scan image taken with the LUIS is shown in figure 5.2.5-2. In the image, there is a white stripe going along the vertex of each of the standards. This stripe is due to the increase echo in the vicinity of the radius. The standard on the left is the 0.25" radius standard, that in the middle is the 0.38" radius standard, and the one on the right is the 0.13" radius standard. The width of the stripes is proportional to the curvature radius of each respective standard. This type of information could not be obtained with a surface-riding probe, no matter how much care is taken to arrange the transducers. This scan finds 33 out of the 36 inserts in the vertices of the standards. When the TOF image in figure 5.2.5-3 is inspected, two more inserts are detected, leaving a single insert remaining as not detected. This is extremely good given the depth, size, and difficult location of the inserts in the tight vertices. There is essentially no quick way of scanning these standards from either side with any surface riding arrangement or any TTU squirter.



Figure 5.2.5-1. Photograph of F-22 angle standards

D950-10322-1

148

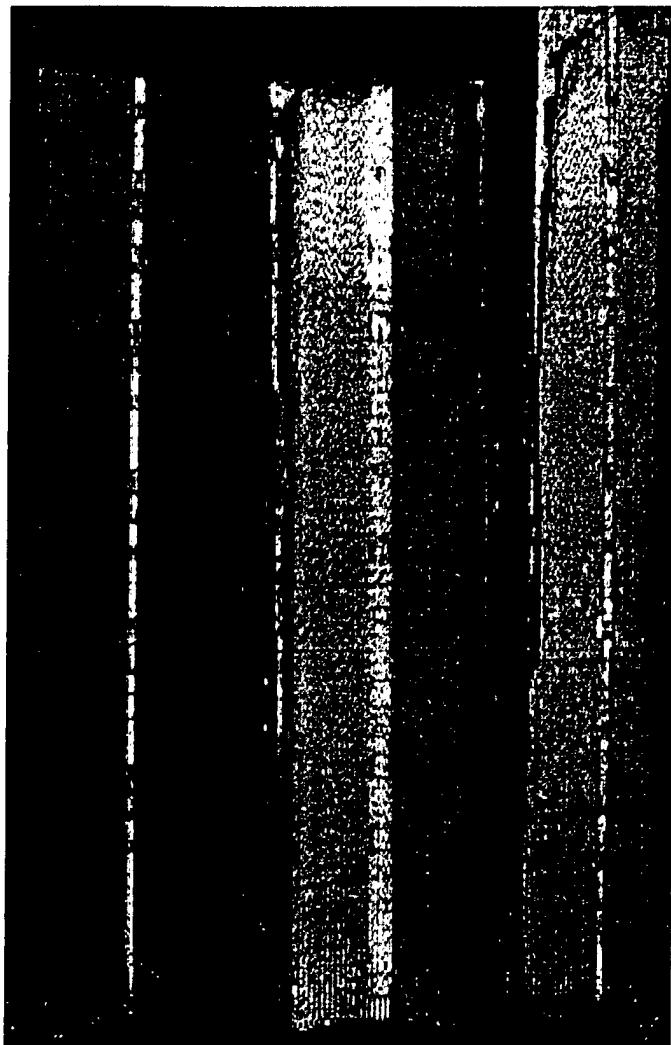


Figure 5.2.5-2. LUIS amplitude C-scan of angle standards



Figure 5.2.5-3. LUIS TOF scan of angle standards

5.2.6 Acute Angle Standards

Composite angle standards of 80° and 110° were inspected with the LUIS. The 110° parts are shown in Figure 5.2.6-1. There were various inserts at the vertex of the bend in the parts. The geometry was much like that of the radius standards for F-22 or 777. The F-22 standards were scanned along the inside of the vertices of their ninety-degree angles. The 80° standards, which have a tighter bend, were scanned along the exterior vertices. There is no other way to so easily inspect acute angles such as this with UT. The LUIS did an excellent job of finding all of the flaws. An amplitude C-scan of one of the 80° standards appears in Figure 5.2.6-2. This scan was made from the flange side of the vertex, but the offset angle of the LUIS scan axis still allowed access to the web side. All of the inserted flaws are easily seen, and it will be appreciated from the entire view that the external angle is easily scanned, with no discontinuity or apparent problems in the vertex area.



Figure 5.2.6-1. Angle Standard

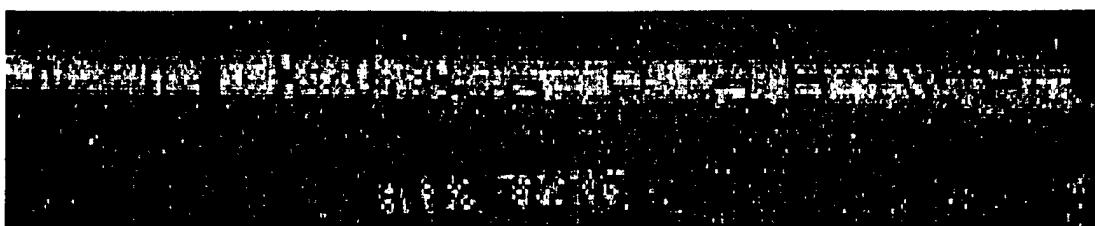


Figure 5.2.6-2. LUIS amplitude image of 80° standard

Figure 5.2.6-3 shows a TOF image of a scan taken directly above the vertex of the 80° part. It is done in such a way that the scan axis is normal to the midpoint of the angle's vertex, and thus the view is symmetric with respect to web and flange. The two figures together show that the quality of the scan is reasonably independent of the scanning view aspect, even when scanning a difficult acute exterior angle such as this.

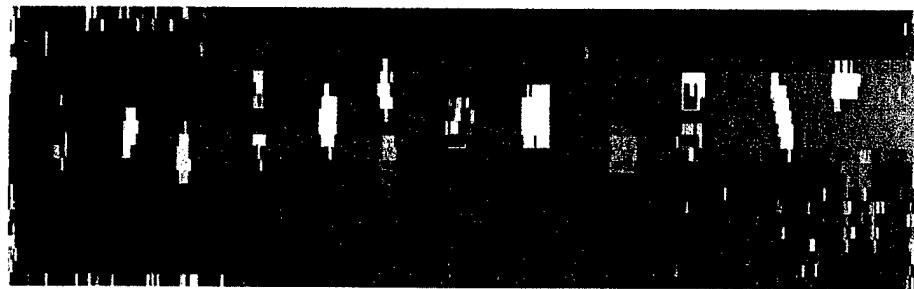


Figure 5.2.6-3. LUIS TOF image of 80° standard

A one hundred-ten degree external angle standard was scanned in the same orientation as that in Figure 5.2.6-3. A TOF scan for this slightly obtuse angle is shown in figure 5.2.6-4. It is easy to see all of the flaws along the vertex, as well as their relative depths.

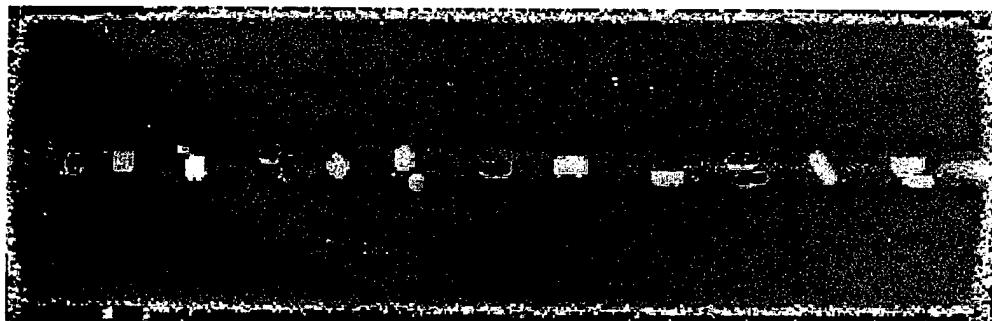


Figure 5.2.6-4. LUIS TOF image of 110° standard

5.2.7 F-22 Ply Drop Standard

The F-22 Ply Drop Standard is shown in the photographs in figures 5.2.7-1 and 5.2.7-2. This panel was chosen because it possesses a number of characteristics that make it suitable for inspection with the LUIS. Some of the characteristics serve to showcase the capabilities of LUIS. It contains known flaws at various depths and orientations with respect to each surface. It contains flaws in the plateau regions as well as in the transition regions. The flaws are of two different sizes, namely 0.5" x 0.5" and 0.25" x 0.25".

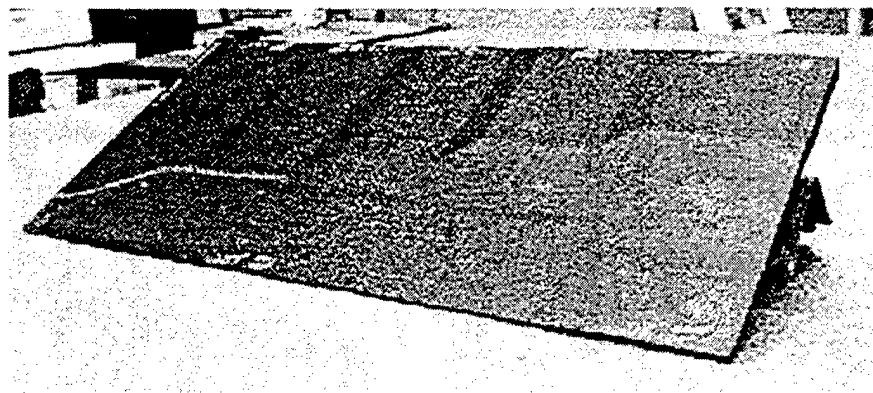


Figure 5.2.7-1. Photo of F-22 ply drop standard from bag side, showing plateaus and transitions

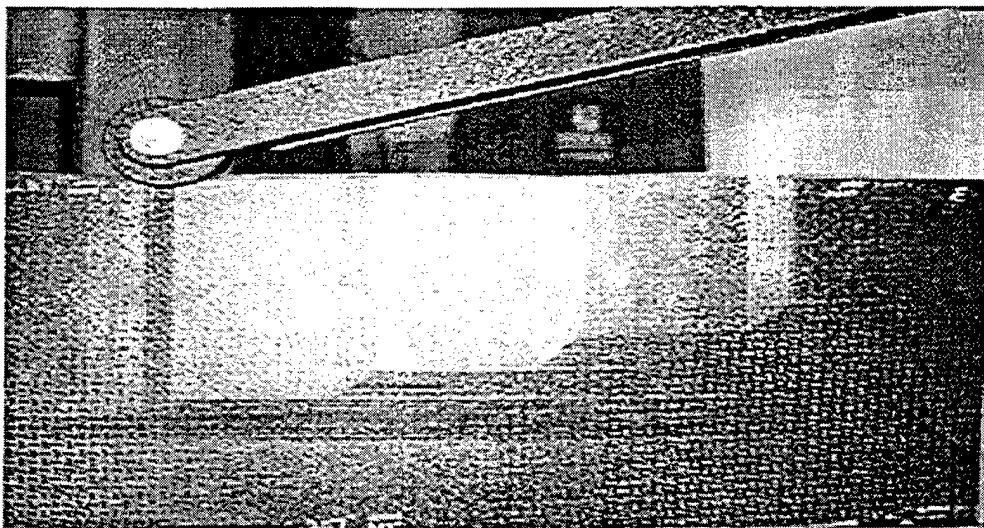


Figure 5.2.7-2. Close up of F-22 ply drop standard bag side, mounted for LUIS scanning

The bag side of the panel is difficult to scan with a surface rider because of the large amount of sloping surface, which can be in two planes for some scan lines. In addition, the bag side of any composite is commonly rougher than the tool side, which possibly results in adding noise to contact transducer data.

Boeing scanned the panel from both sides with the LUIS. The bag side was easier to scan than the tool side. The shiny tool side was too reflective and therefore had to be painted. The bag side scans were particularly good. A plan drawing of the panel is shown in figure 5.2.7-3. The numbers indicate the number of plies from the tool side corresponding to the plateaus, and the depth of the flaw locations.

An amplitude C-scan image obtained with the LUIS from the tool side of the part is shown in figure 5.2.7-4. Figure 5.2.7-5 shows a tool side amplitude C-scan image from a Boeing production scanner for comparison. Both scans acquired full wave data, which were processed after the data were acquired to produce the images. These two images are very comparable in that they are from the same side with full wave pulse-echo data. The results are roughly equivalent. However the Boeing scanner finds the two 0.25" inserts on the 54 ply plateau (second from the left). The LUIS misses these, as well as one of the 0.25" inch inserts at the next plateau (44 plies). Both scans pick up the one ply difference at the lower left-hand corner of the panel. The Boeing scan successfully detects 5 of the 6 inserts in the 64 to 25 ply region, while the LUIS detects only one of these.

Time-of-flight C scans are shown in figures 5.2.7-6 and 5.2.7-7. Figure 5.2.7-6 is the LUIS scan and figure 5.2.7-7 is the scan at Boeing. The LUIS TOF scan provides for the detection of an additional 0.25" inch insert in the 54 ply plateau, as well as the insert in the 64 ply to 54 ply transition in comparison to the LUIS amplitude scan. It also provides for the detection of an additional insert in the 64-ply plateau, for 3 additional inserts in 64 to 25 ply transition region, and for the small insert in the 54 to 24 ply transition. The Boeing TOF scan provides detection of the insert in the 64 to 54 ply transition in comparison to the conventional Boeing amplitude scan.

When combining for both amplitude and time-of-flight data, the LUIS successfully detects 37 out of 40 inserts and the Boeing conventional scans detect 38 out of 40.

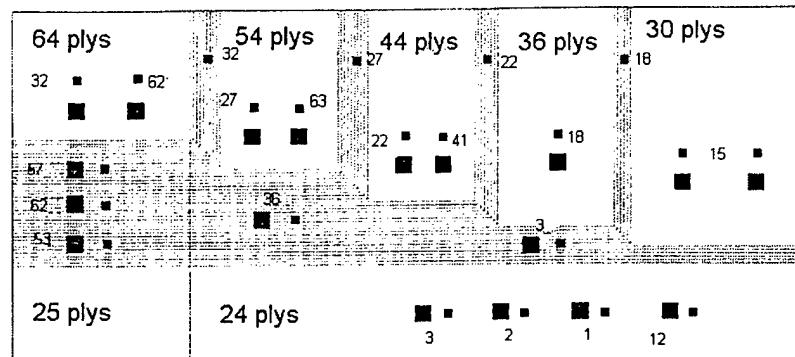


Figure 5.2.7-3. Plan Drawing of the Ply Drop Standard

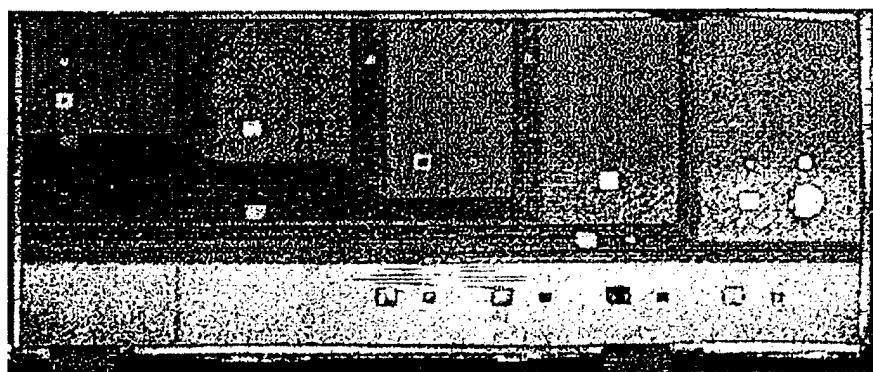


Figure 5.2.7-4. Amplitude C-scan taken from tool side by LUIS

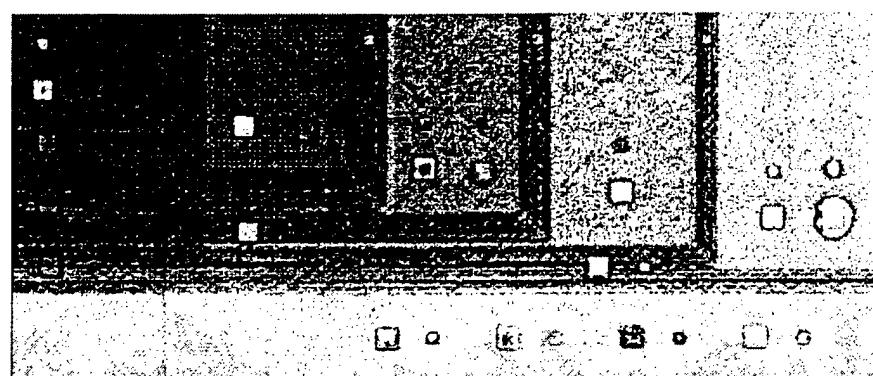


Figure 5.2.7-5. Conventional amplitude C-scan taken from tool side

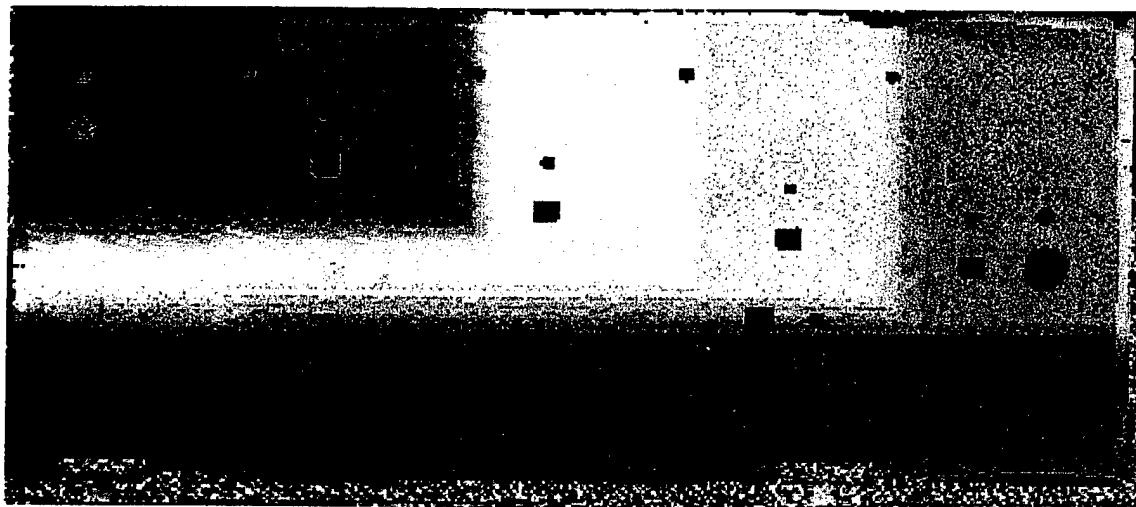


Figure 5.2.7-6. Time-of-flight C scan taken with LUIS

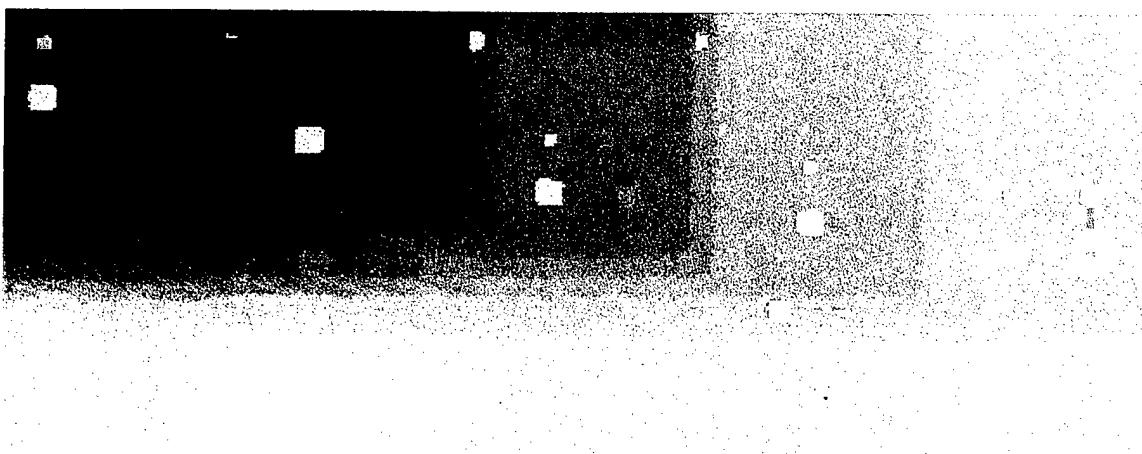


Figure 5.2.7-7. Time-of-flight C scan taken at Boeing

A Boeing production scan using UltraImage IV is shown in figure 5.2.7-8. This is an example of routine production scan that does not acquire full wave data. This amplitude scan detects 33 out of 40 inserts. The accompanying time-of-flight scan (not shown) identifies an additional 3 inserts.

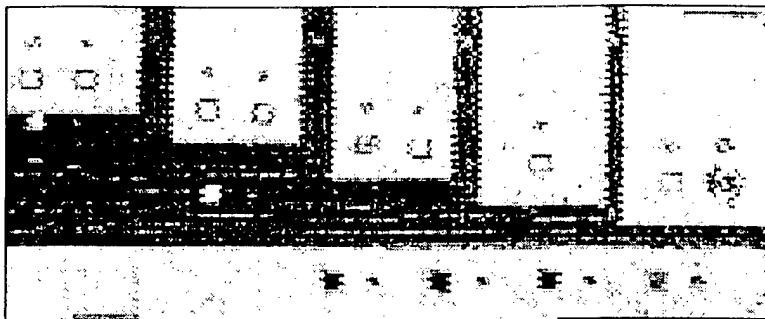


Figure 5.2.7-8. Boeing Production UltraImage IV Amplitude C-scan of tool side of standard

As mentioned earlier, the LUIS is remarkably successful at scanning the bag side of composite parts. Although there is usually no opportunity for this, it is none the less a very valuable asset, especially in the scanning of components where the bag side is available. Figure 5.2.7-9 shows amplitude scans and figure 5.2.7-10 shows time of flight C scans taken with LUIS, in which 40 out of 40 inserts were detected. In all fairness, the flaws were closer to the bag (scanned) side in the transition region from 64 to 25 plies. The inserts in the transitions from 36 to 24 plies, 54 to 24 plies, and 54 to 64 plies not detected by the amplitude scans are picked up by the time-of-flight scans.

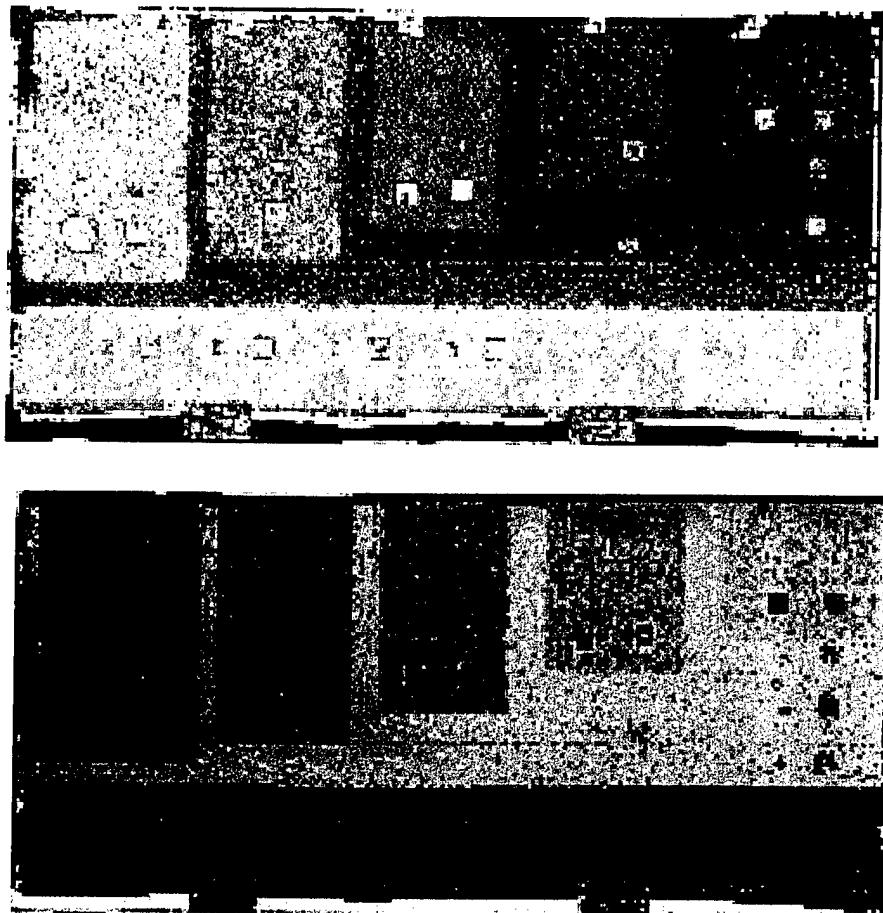


Figure 5.2.7-9. Bag side C-scans taken with the LUIS: Amplitude

D950-10322-1

158

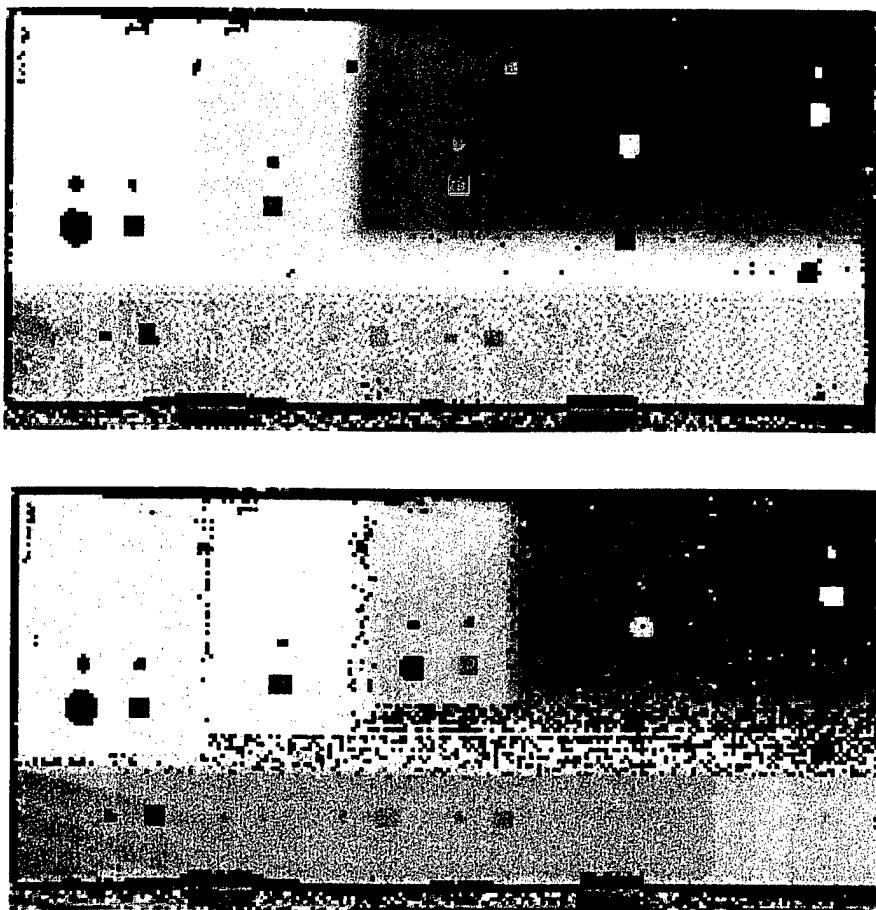


Figure 5.2.7-10. Bag side C-scans taken with the LUIS: Time-of-Flight

Typical LUIS B scans from both sides of the panel are shown figures 5.2.7-11 and 5.2.7-12. The B scans show a cross section of the part along a line intersecting the centers of the inserts located in the four horizontal transitions. These scans are included as an extra example of routine LUIS data acquisition. They show that the inserts are parallel to the tool side of the panel rather than the slanted bag side.

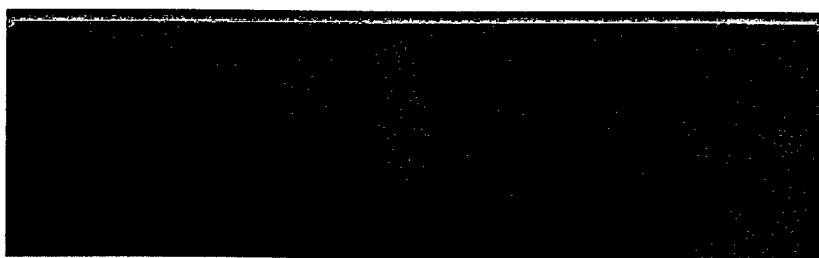


Figure 5.2.7-11. LUIS B-Scan taken from bag side

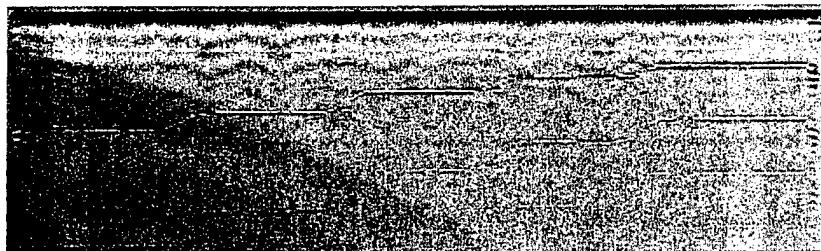


Figure 5.2.7-12. LUIS B-Scan taken from Tool Side

Figure 5.2.7-13 is a B-scan taken with the LUIS from the tool side along a line through the inserts in the long horizontal plateau at the top of figure 5.2.7-3(after a rotation of 180 degrees in the plane of the paper). This shows the inserts in the 24-ply plateau located at 12 plies, 23 plies, 22 plies and 21 plies respectively from the bag side. It also shows the transition from 24 plies to 25 plies at the right side of the figure. This is representative of a typical LUIS B-scan.

Inserts at: 12 plies 23plies 22 plies 21 plies transition: 24 plies 25 plies

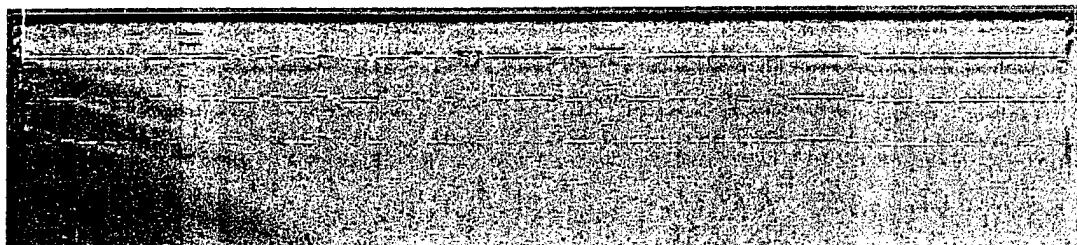


Fig 5.2.7-13. LUIS B-scan

5.2.8 B-2 Stiffened Wing Panels

These panels are NDE standard flaw panels for the B-2 program. They are curved leading edge panels with stiffeners. The stiffeners are placed as "U" sections on the inner surface of the curved panels, and a second cure process bonds them to the curved panel. This process results in each of the stiffeners being assembled from the vertical portions of two adjacent "U" sections, with the horizontal portions in contact with the inner surface of the panels. A photograph of the toolside such a panel is shown in Figure 5.2.8-1. Figure 5.2.8-2 shows the stiffeners on the bagside of the panel. There are a number of 0.25" x 0.25" and 0.5" x 0.5" teflon inserts. These occur both under the stiffeners, as well as across the joint between the curved panel surface and the space between the adjacent "U" sections.



Figure 5.2.8-1. B-2 Wing panel tool-side.

Figure 5.2.8-3 shows an amplitude C-scan image taken with the LUIS. In it, three .25 inch and three .5 inch inserts are seen along the edge of the upper stiffener. These inserts are between the curved surface and the "U" sections. In the central stiffener, there are two .5 inch inserts that are partially under the "U" sections and partly between them, as well as one .25 inch insert. Along the bottom stiffener in the image there are three .25 inch inserts along, next to, and under the stiffener. A TOF image from the same scan is shown in Figure 5.2.8-4, showing the same inserts detected.

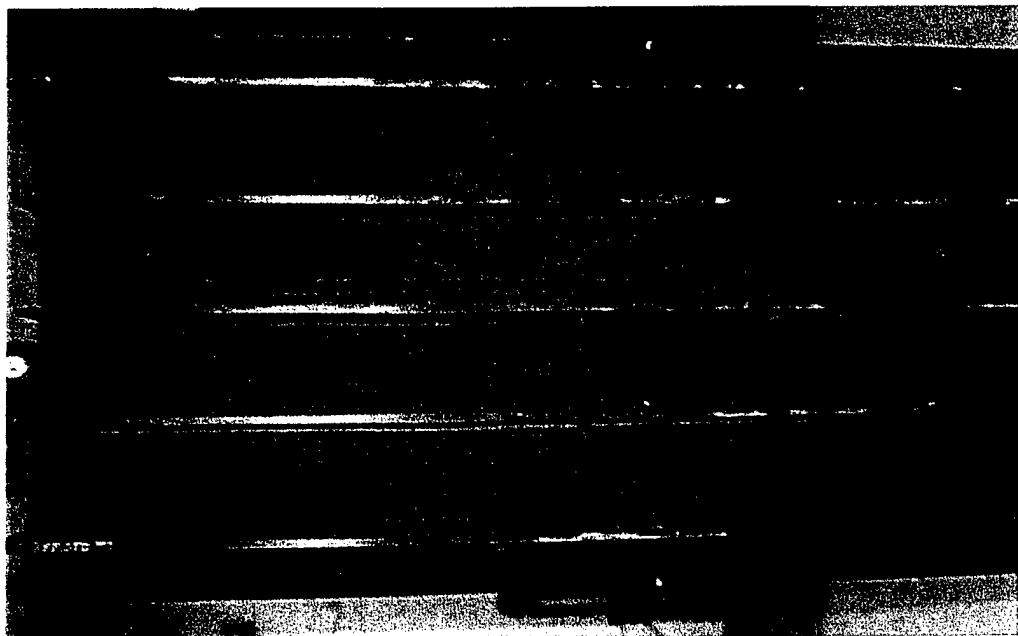


Figure 5.2.8-2. B-2 Wing panel bagside and stiffener

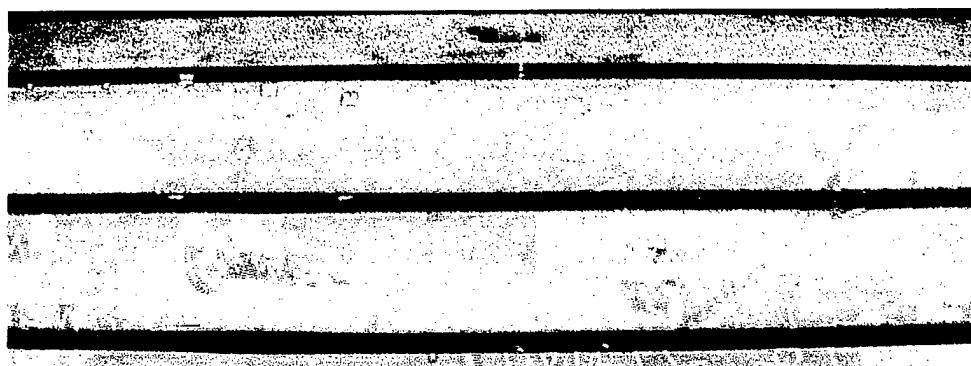


Figure 5.2.8-3. LUIS amplitude scan



Figure 5.2.8-4. LUIS TOF image

An amplitude C-scan taken with the Boeing production scanner, a surface riding 5 MHz bubbler, is shown in Figure 5.2.8-5. It essentially detects all of the inserts detected by the LUIS. The production scanner does not acquire full wave data, but simply operates with preset gates, looking for the maximum echo value in the gate.



Figure 5.2.8-5. Boeing 5MHz bubbler amplitude C-scan

5.2.9 Titanium Stiffened Composite "T" Section

This composite part is in the shape of a "T", and stiffened with a titanium insert. The insert extends the entire width of the flange, and about halfway up the web. Also, the insert decreases in thickness at a point about halfway up its vertical dimension into the web. There are a number of small holes in the web, all of which are above the region containing the titanium. In addition, there are three large holes drilled in each of the halves of the flange. A photograph of one end of the part ready for scanning in the LUIS facility appears in figure 5.2.9-1. The photo was taken to show the titanium insert, but the shadowing makes it somewhat hard to see.

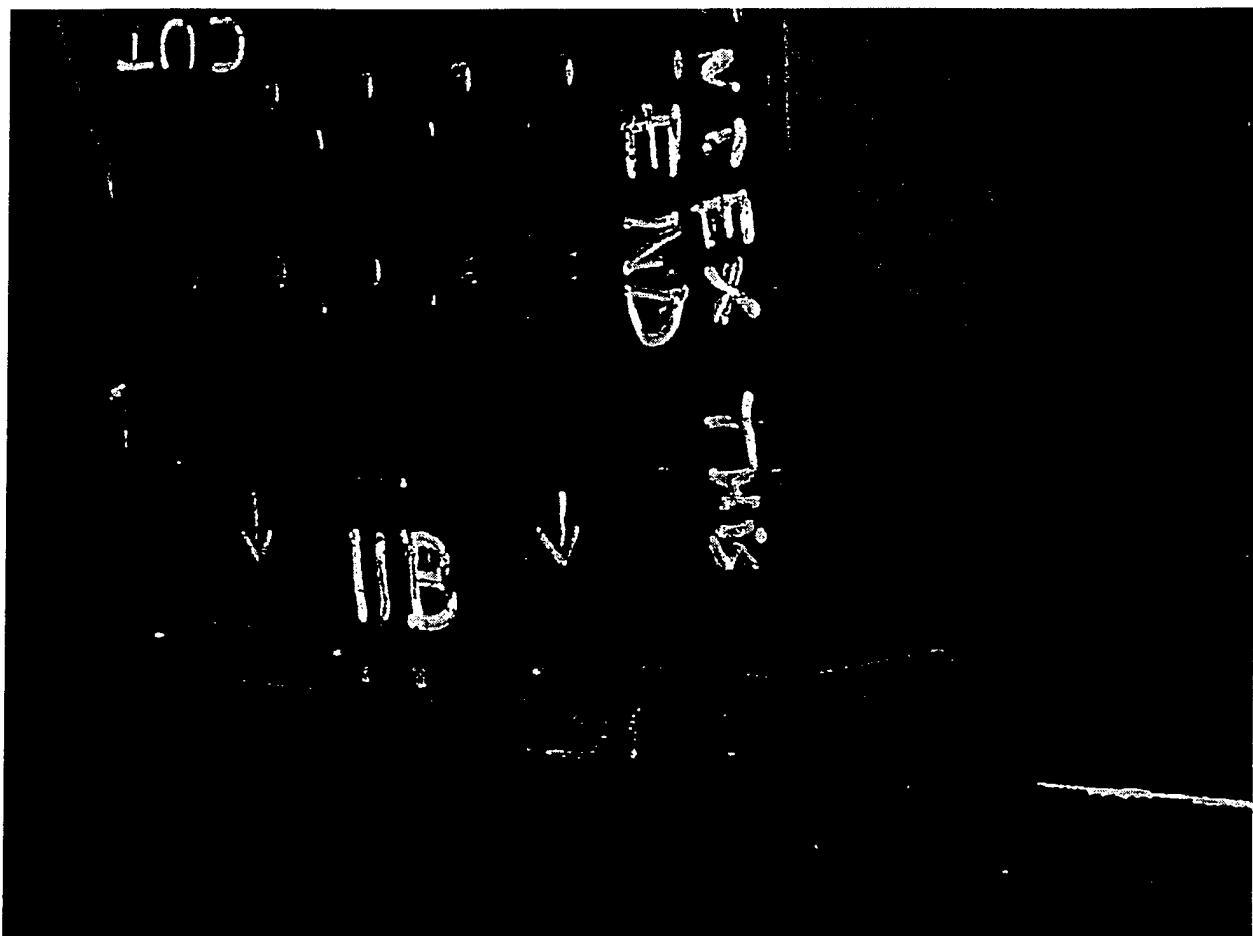


Figure 5.2.9-1. Photograph of stiffened "T" section

Figure 5.2.9-2 shows an amplitude C-scan image of the part taken with the LUIS. It is easy to see the internal spalling of the material arising from the drilling process around the three large holes

in the base of the part. This damage is not observable visually. This damage appears to extend right up to the radius bend, and possibly even go partially into the skin of the web. Even though it may be possible to detect the fact that there is spalling with standard scanning means, its extent would be impossible to detect unless some sort of a custom “shoe” holding a transducer were made.

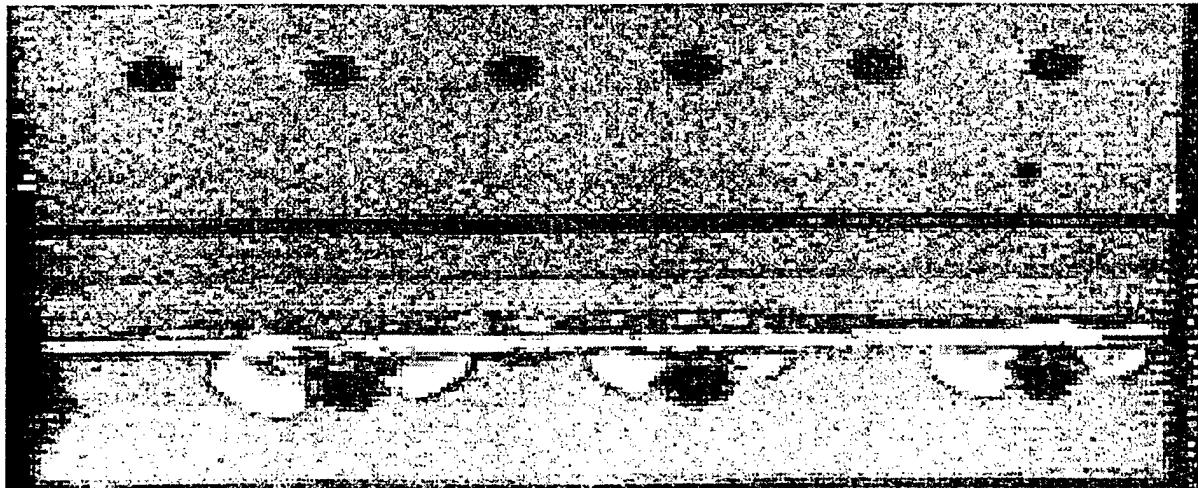


Figure 5.2.9-2. LUIS amplitude C-scan

There appears to be either delamination or disbonds extending up into the web from the bend. This is made more strongly suggested in the TOF image shown in figure 5.2.9-3. Subsequent inspection with a hand held probe was able to confirm that there was some disbonding between GREP layers, and some disbonding between the skin and the titanium insert. It would be quite difficult and time consuming to map the extent of the flaws by a hand held probe, whereas the LUIS does it readily for both flange and web in the same scan.

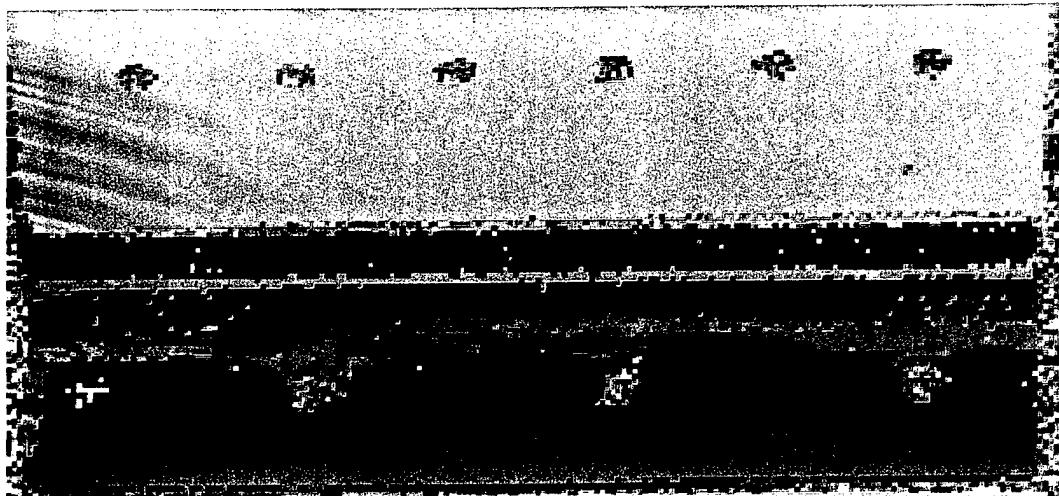


Figure 5.2.9-3. LUIS TOF image

D950-10322-1
166

5.2.10 "Hat" Stiffened Panel

This panel has a raised stiffening section, in the shape of a hat, hence its name. This stiffener prevents easy scanning with any type of surface rider. A photograph of the panel is shown in figure 5.2.10-1.

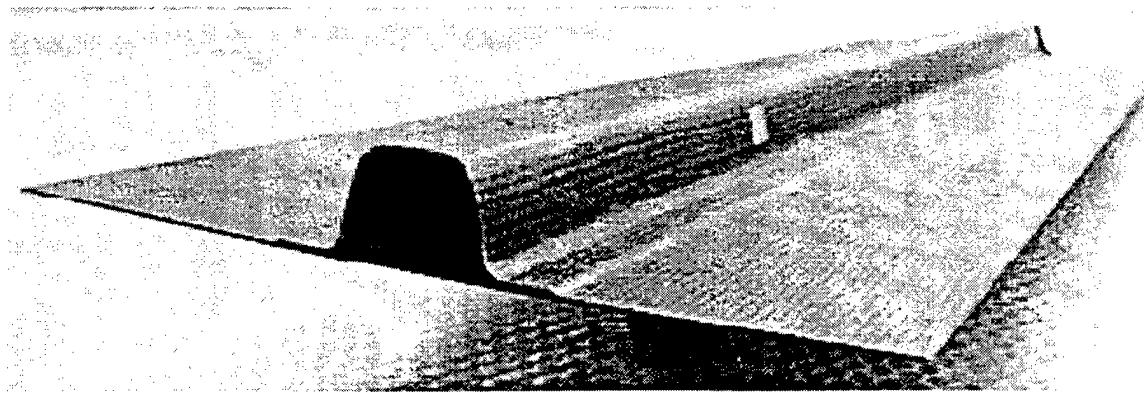


Figure 5.2.10-1. Hat stiffened Panel

An amplitude C-scan taken with the LUIS is shown if figure 5.2.10-2. This scan was performed, with the scan line parallel to the long axis of the panel, and includes a little more than one half of the panel. There are no apparent flaws in the panel, which is easily confirmed with a cursory check of the scan

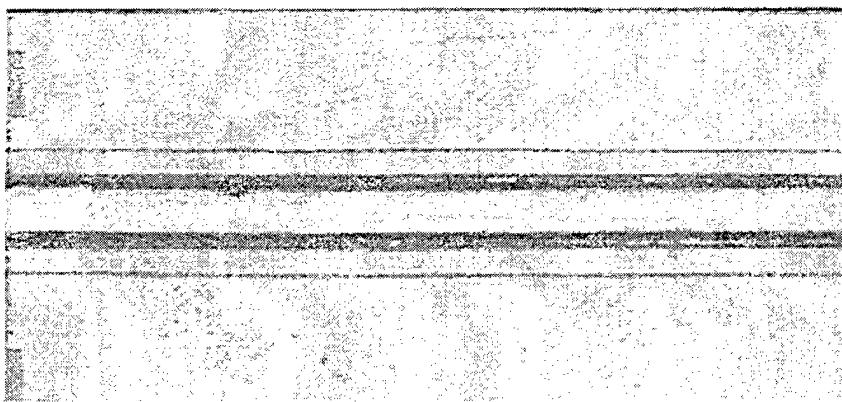


Figure 5.2.10-2. LUIS amplitude C-scan of hat stiffened panel

5.2.11 Seven Ply Composite Repair Test Standard

This standard is a scarf patch repair made in the tool side of a composite made of graphite epoxy with a honeycomb core. It is shown in Figure 5.2.11-1. The patch has seven plies, and contains several simulated flaws that may be detected from the tool side by pulse echo UT. These include core cells filled with potting compound located at the center of the patch, inserts placed between the core and the tool side skin, and inserts placed on the scarf between the base material and the repair plies. All inserts are circular and made of pre-cured adhesive film, which are then dipped in freekote. The panel was scanned with the LUIS, and several images processed from the scan are shown.

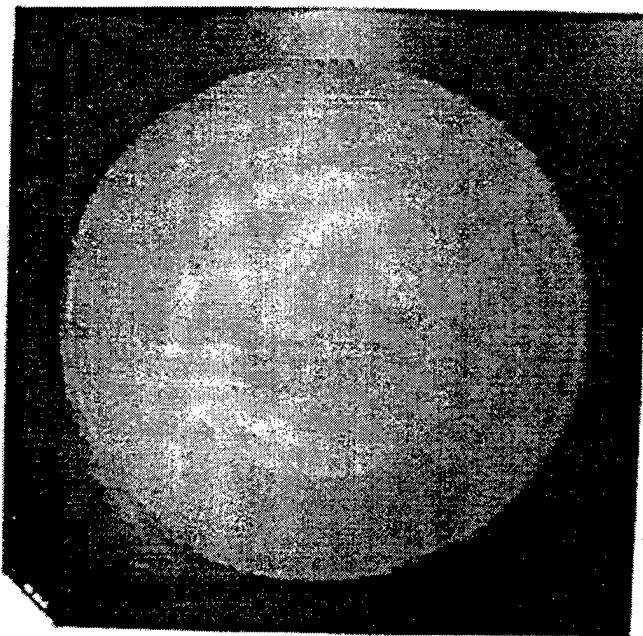


Figure 5.2.11-1. Photograph of repair standard

Figure 5.2.11-2 shows an amplitude C-scan of the standard. This scan clearly resolves all seven of the repair plies, as well as the potting at the center of the scarf and an insert on the scarf at roughly “2 o’clock” in the figure.

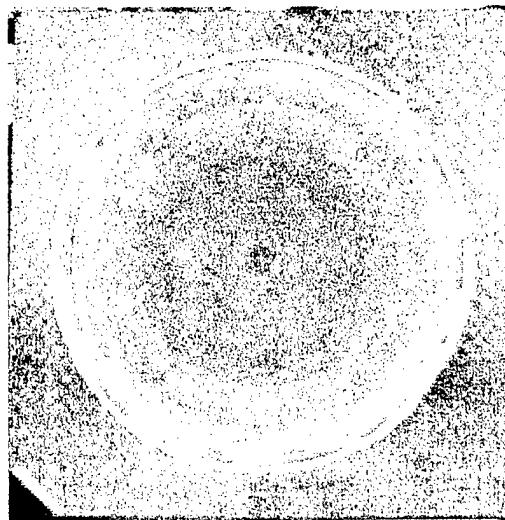


Figure 5.2.11-2. LUIS amplitude C-scan of repair standard

Figure 5.2.11-3 is a TOF image of the standard. This image shows the large insert placed at roughly 9 o'clock between the core and the tool side skin, as well as a smaller one at 6 o'clock. In addition, it shows a small flaw at 8 o'clock, of the same size as the one at 2 o'clock shown in figure 1, which may also be seen in this figure as well. Two larger inserts on the scarf are seen at 4 o'clock and 10 o'clock.



Figure 5.2.11-3. LUIS TOF image of repair standard

A Boeing production TTU scan is shown in figure 5.2.11-4. It shows all of the above flaws, in addition to 2 inserts located at 12 o'clock and 3 o'clock which are between the core and the bag

side skin, and therefore not detectable from the tool side with pulse echo. It will be quickly appreciated what a good job is done by the LUIS in seeing each of the repair plies.

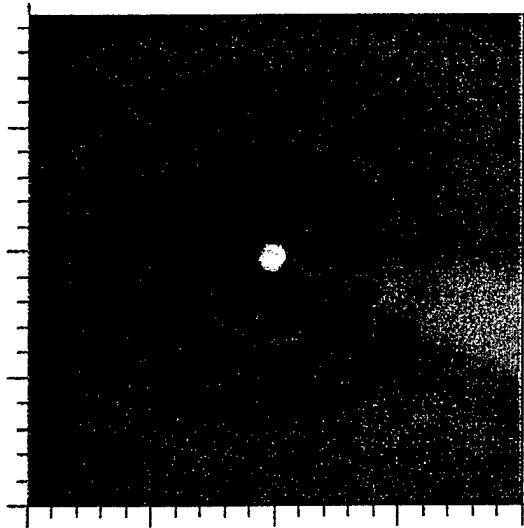


Figure 5.2.11-4. Conventional TTU scan

Finally, in Figure 5.2.11-5, another TOF image is shown. This one serves to demonstrate the ease with which the LUIS "sees" three of the inserts on the scarf that overlap two plies. These are located at 10 o'clock, 4 o'clock, and 8 o'clock respectively. The TOF properly picks up the fact that the inserts are on the slanted surface.

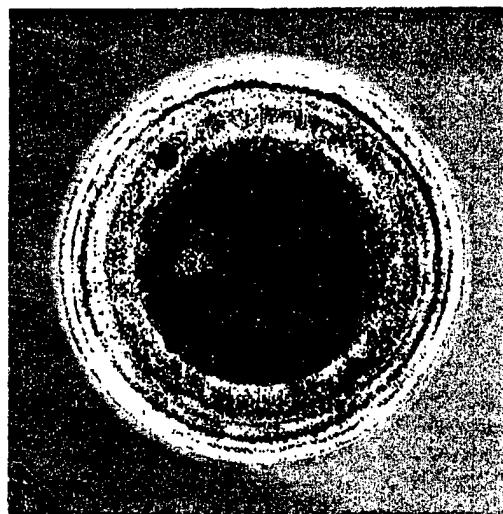


Figure 5.2.11-5. LUIS TOF image of repair standard

5.2.12 Aluminum Honeycomb Repair Panel K1

This panel was made up with a one inch diameter circular skin-to-core “disbond” simulated by a teflon insert. It is pictured in Figure 5.2.12-1. The LUIS scanned the panel, and found the insert, along with possibly a smear of adhesive on top of an adjacent section of the repair. Figure 5.2.12-2 shows an amplitude C-scan taken with the LUIS. The one-inch insert is detected in the left bay of the repair at 6 o'clock. A hint of a smear of adhesive or something else is seen in the left side of the bay on the right. The TOF scan shown in Figure 5.2.12-3 more clearly shows this flaw. Figure 5.2.12-4 is a Boeing production TTU scan of the repair. The conventional TTU inspection is preferred in this case.

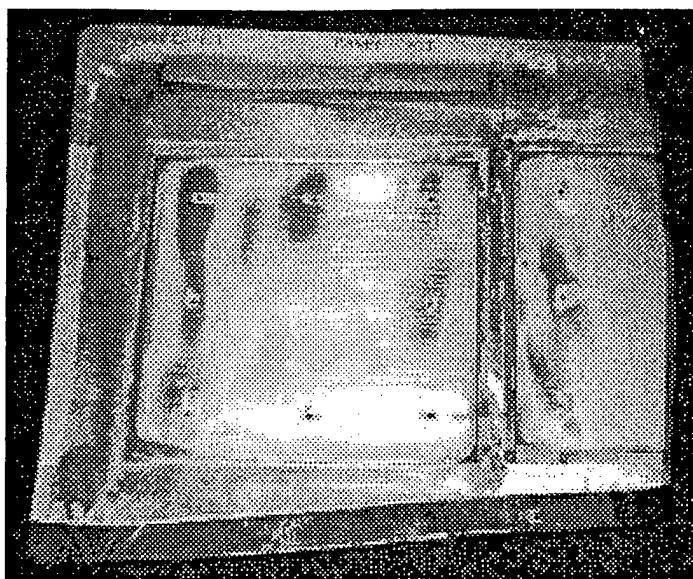


Figure 5.2.12-1. Photograph of panel K1

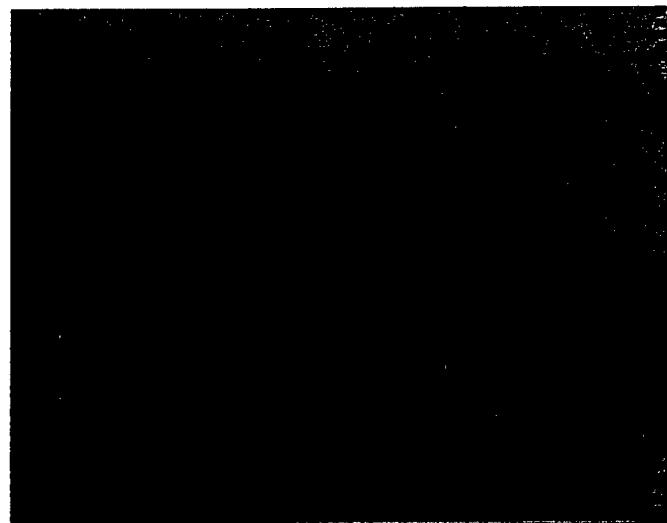


Figure 5.2.12-2. LUIS amplitude C-scan image of panel K1

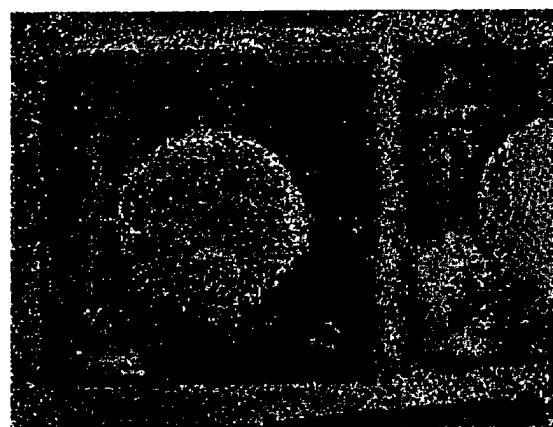


Figure 5.2.12-3. LUIS TOF image of panel K1

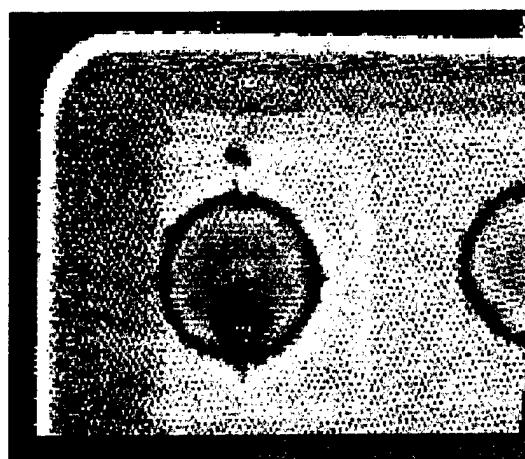


Figure 5.2.12-4. Conventional TTU image of panel K1

5.2.13 Aluminum Honeycomb Repair Panel K2

This panel contains inserts and a natural disbond. A photograph of the part is shown in Figure 5.2.13-1. The LUIS image is shown in figure 5.2.13-2, which detects two inserts as well as the natural disbond on the right. The Boeing production TTU scan is shown in figure 5.2.13-3, which also detects the same flaws. Note the LUIS's capability to see the cells of the honeycomb core.

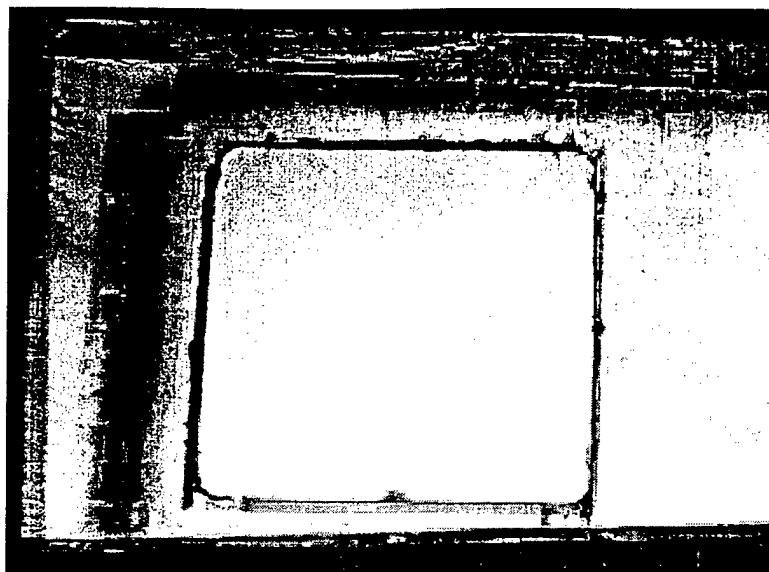


Figure 5.2.13-1. Photograph of panel K2

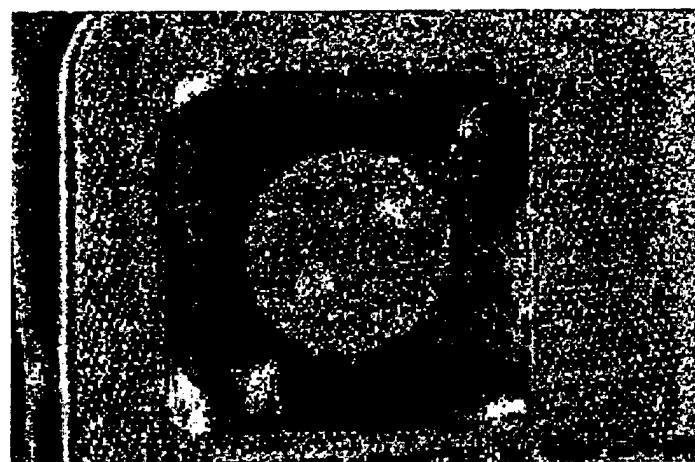


Figure 5.2.13-2. LUIS TOF image of panel K2

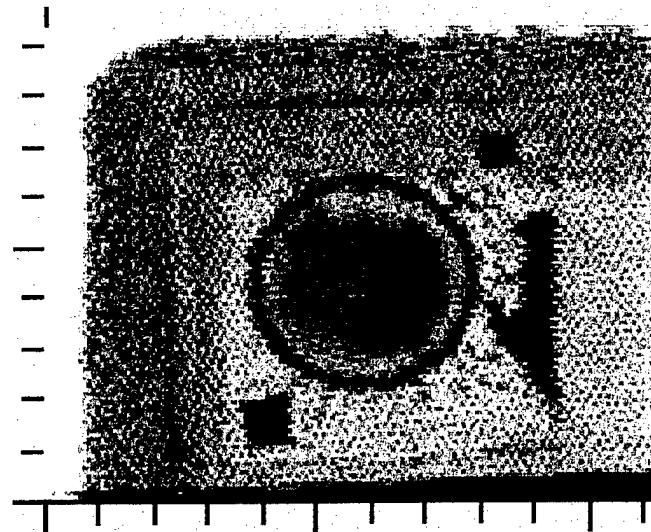


Figure 5.2.13-3. Conventional TTU scan of panel K2

5.2.14 Composite Repair Calibration Standard for Skin-To-Core Disbonds

This standard is used for calibration of detection of skin-to-core disbonds through various thicknesses of composite skin. The idea is to simulate typical composite structures with honeycomb cores. The panel consists of four skin thickness regions of three, six, nine and twelve plies respectively. The standard is 4 inches by 16 inches, making each of the regions nominally 4 inches by 4 inches. In the center of each region, at the skin-to-core interface, there is a one-inch diameter precured adhesive insert, simulating a disbond between the skin and core. A B-scan taken with the LUIS along the central axis of the standard is shown in figure 5.2.14-1. This image clearly shows the successively thicker skin regions, each on having an insert at its bottom.

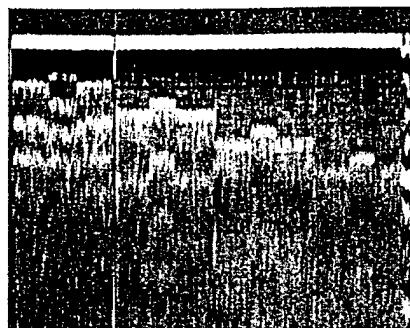


Figure 5.2.14-1. LUIS B-scan of composite repair calibration standard

Figure 5.2.14-2 shows an amplitude C-scan of the standard taken with the LUIS. It is easy to see the four inserts at the skin-to-core interface. The accompanying TOF image shown in Figure 5.2.14-3 also shows the various depths corresponding to the regions of differing skin thickness. The small triangular region in the lower left-hand corner is an identifying mark for orientation and flaw description.

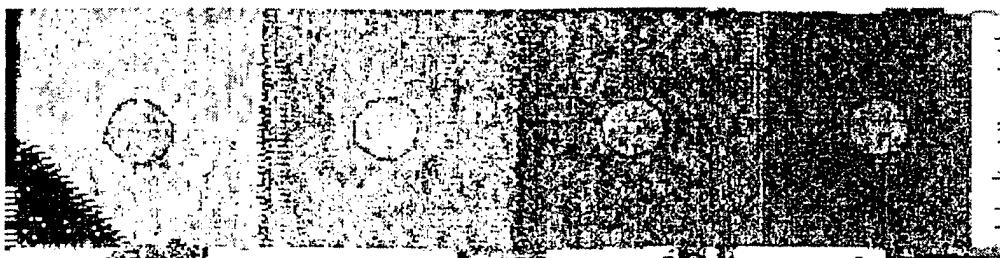


Figure 5.2.14-2. LUIS amplitude C-scan of composite repair calibration standard

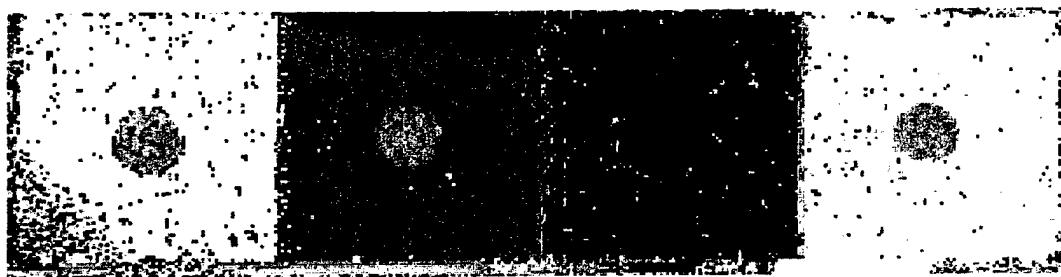


Figure 5.2.14-3. LUIS TOF image

Normally, a standard with honeycomb core would be scanned with through-transmission ultrasound (TTU), instead of pulse echo. Comparison images from production scans are shown for this standard in the next section, where this standard appears as part of a “matrix” with three other similar standards.

5.2.15 Honey Comb Cored Composite Repair Standard Matrix

This test sample consists of four standards, each similar to the one described in the previous section, but also designed to calibrate the NDE capability to detect different types of flaws and features. The four standards were taped together, and then scanned as a single part as shown in figure 5.2.15-1. All four of the honeycomb core standards are the same nominal size, each with four thickness regions of three, six, nine, and twelve plies. The skin-to-core disbond standard described in the previous section is shown along the top of the images of the matrix.

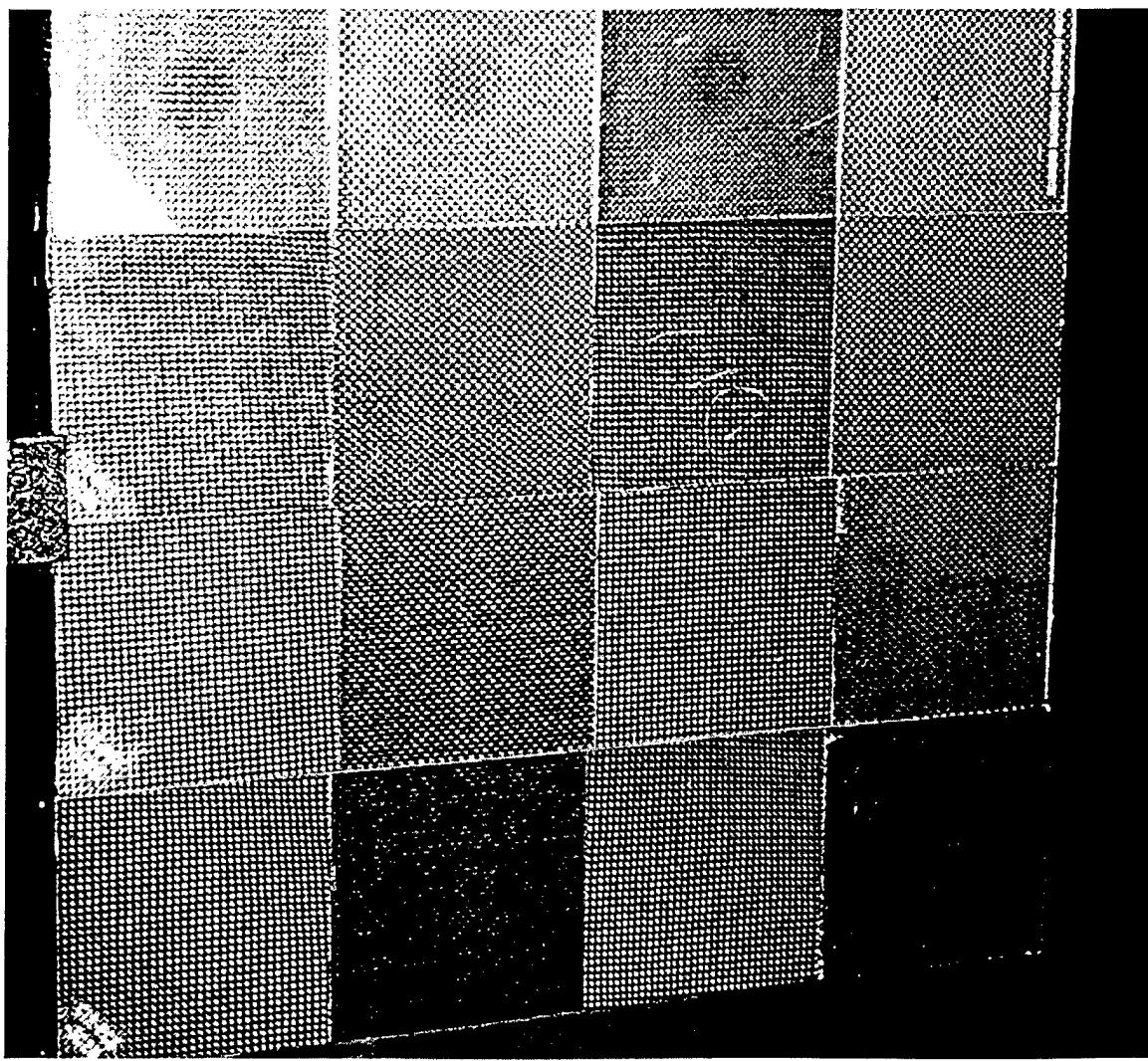


Figure 5.2.15-1. Photograph of standards.

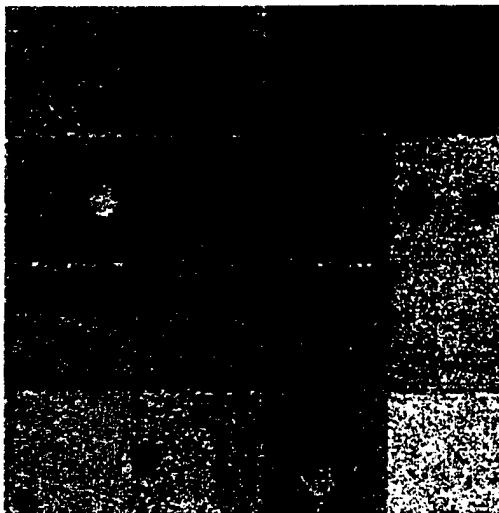


Figure 5.2.15-2. LUIS TOF image of matrix composite standards showing graphite inserts

The next standard is constructed to permit calibration of detection capability of air voids in potting in the core. A two-inch section of the core parallel to the long axis of the standard is potted all the way through. Each of the sections has a one-inch circular void milled into the core 0.2 inch deep. A B-scan through the center of each of the circular voids in the potted portion is shown in Figure 5.2.15-3. It will be appreciated how difficult to see these types of flaws is with pulse echo, as there are only the slightest "hints" of the flaws in the two sections with the thicker skins, that are on the right.

The final standard, which is located along the bottom of the matrix, is designed to permit calibration of NDE of core repair. All along the long axis of the standard is a core splice. In addition, each section has a hole milled all the way through the core, which is then potted. There is no potting in the remainder of the standard.

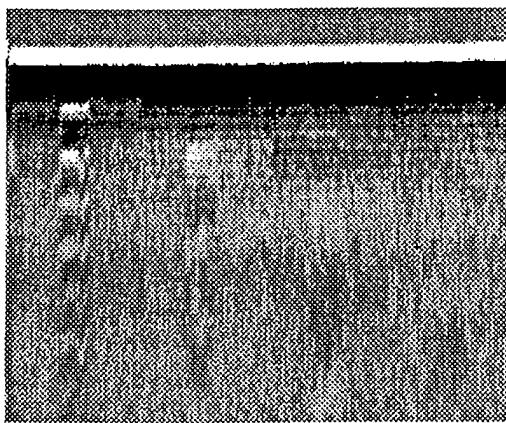
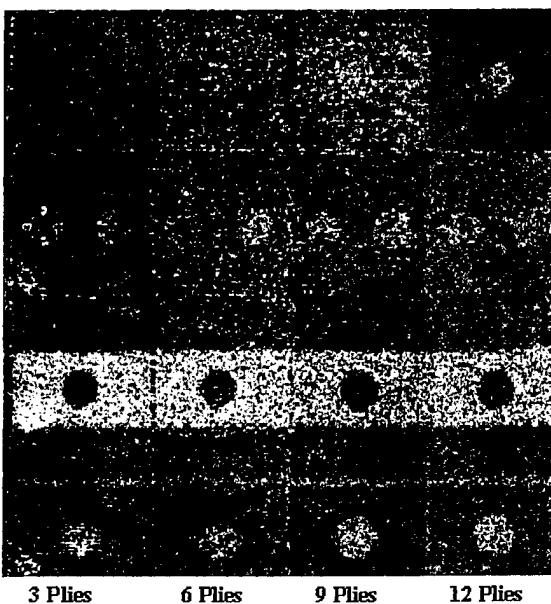


Figure 5.2.15-3. LUIS B scan of composite standard for potting with air voids

Figure 5.2.15-4 shows a LUIS TOF scan of the entire matrix. The image has been processed to show all flaws simultaneously, which in itself is a remarkable feat for any pulse echo scan. A pulse echo scan taken with the Boeing production scanner is shown in Figure 5.2.15-5. As has already been explained, this scanner requires that the gate and filters be chosen before the scan starts. It would therefore take a large number of tries to set the gate and filters correctly to detect all of the flaws in a single scan. It will be readily appreciated that the LUIS scan better detects all of the flaws, but in all honesty, it is much easier to find flaws or features already known to exist. In this case, since full wave data are available, the gate, filtering, and other signal processing can be experimented with until as many flaws show up as possible. This is a distinct asset of acquiring full wave data. The normal method for scanning a honey comb core sample is with TTU. A TTU image taken with the Boeing production scanner is shown in Figure 5.2.15-6. TTU provides the best image in this case and is preferred.

Matrix of Honeycomb Cored Repair Standards

Each Standard Has Four Skin Thickness Regions



Legend

Pre-Cured Adhesive Inserts in Skin-to-Core Layer

Graphite Inserts Placed in Plies Just above Skin-to-Core Layer

No Potting In Core

Potted Core Section with Voids Milled in Core

Core Splice

Potted Holes through Core, Remainder of Core without Potting

Figure 5.2.15-4. LUIS TOF image of composite standards

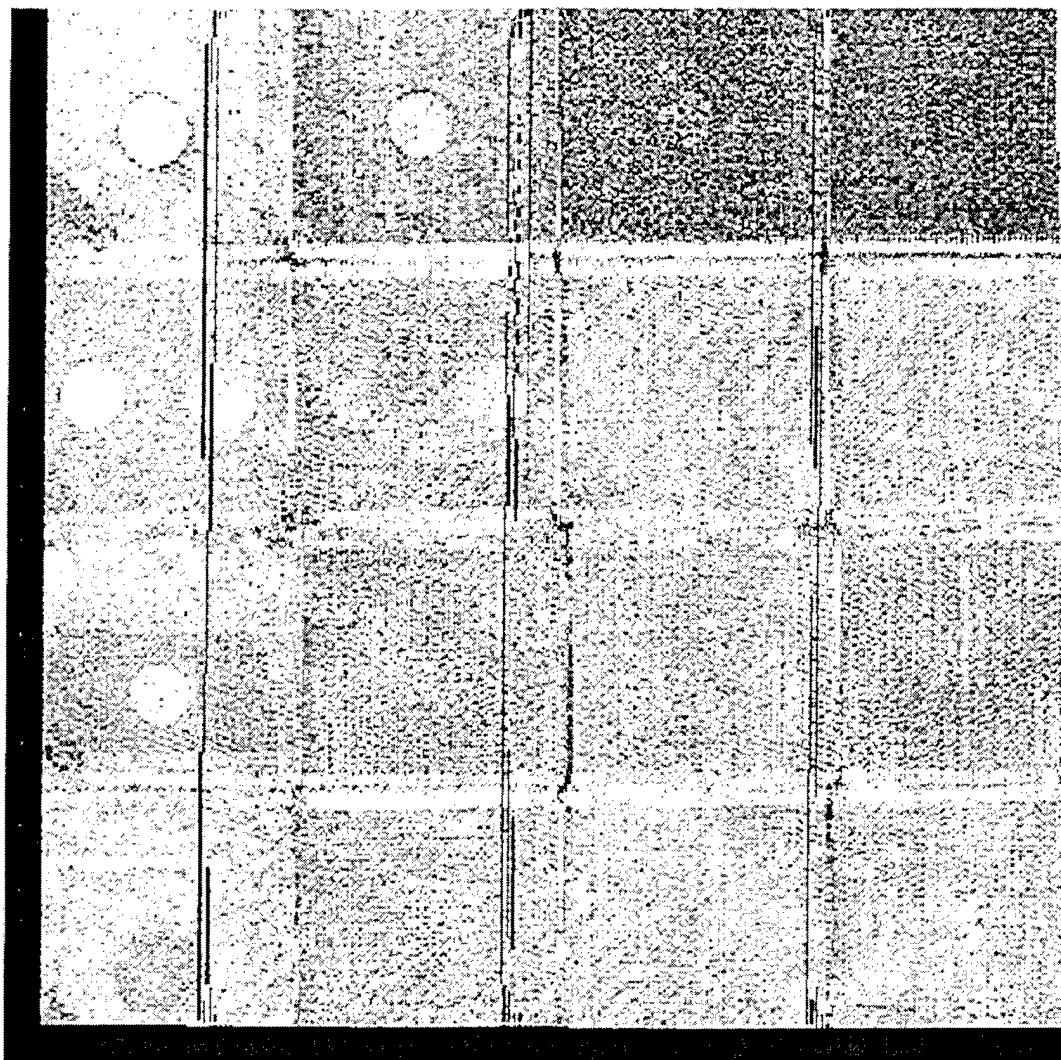


Figure 5.2.15-5. Boeing pulse echo amplitude C-scan

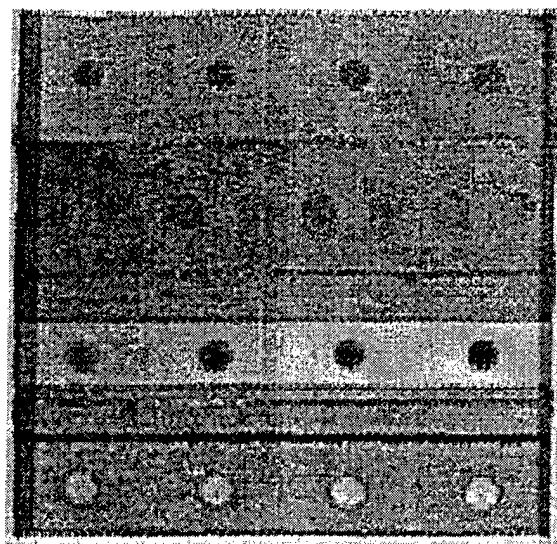


Figure 5.2.15-6. Boeing production TTU scan

5.2.16 Composite Flywheel

This part was constructed for purposes of storing energy on spacecraft. It is an annular ring approximately 16 inches in diameter, 5 inches in length, and $\frac{3}{4}$ inch thick. It is made up like a roll of tape as one continuous piece of prepreg material, which is cured as it is rolled. This particular specimen showed several regions of delamination when inspected by computed tomography. A photograph of the flywheel positioned for scanning with the LUIS flywheel is shown in Figure 5.2.16-1.

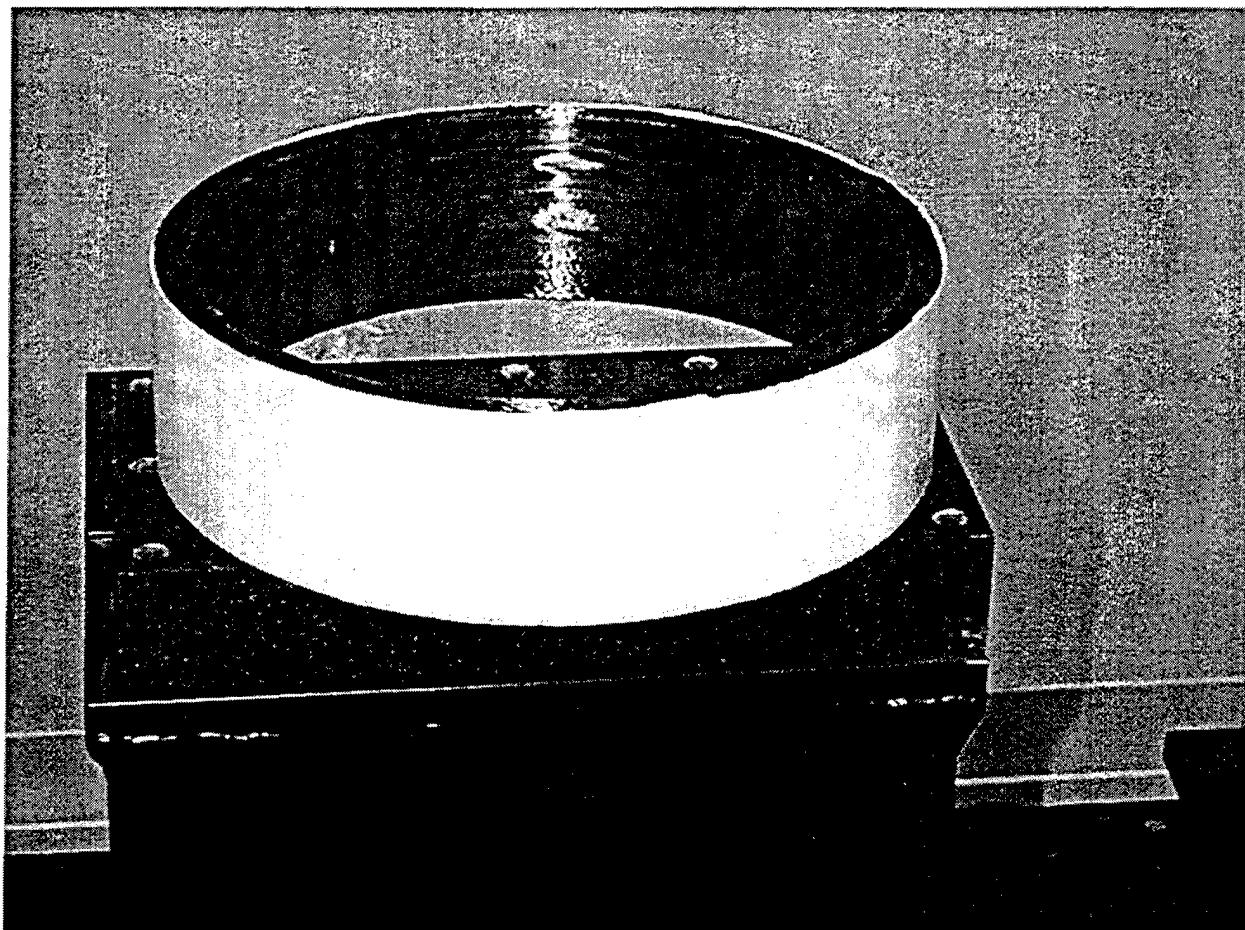


Figure 5.2.16-1 Composite Flywheel

An initial scan of the ring showed that the LUIS provided poor UT generation efficiency for this part. Despite this fact, scanning was completed to demonstrate the geometric versatility of the LUIS. As seen in the photograph, it is possible to scan the outer surface of the near portion of the

wheel and the inner surface of the far portion of the ring in a single scan. An amplitude C-Scan showing this appears in Figure 5.2.16-2. Some of the data have dropped out in the scan resulting in horizontal line "artifacts", but the geometric capability is easily seen. The parallel strands in the prepreg material make it difficult to inspect especially when the scan is parallel to these lines. Subsequent attempts at a better scan with the outer surface painted were attempted, but the UT generating efficiency was insufficient on this particular material to result in an acceptable signal to noise ratio. This is clearly a difficult part to inspect. No conventional data were available for comparison. Further work needs to be done to identify a preferred inspection method for this part.

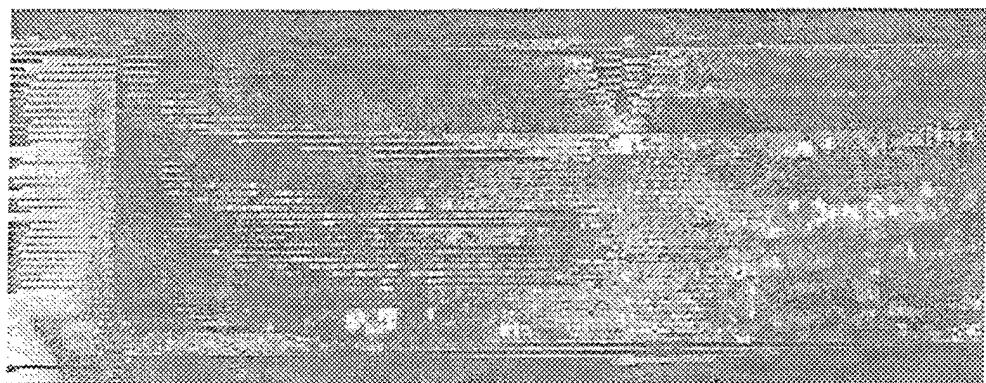


Figure 5.2.16-2. Flywheel amplitude C-scan

5.2.17 Sine Wave Spar

This part is a spar made up of sine wave webbing between two parallel planar end caps. It is shown in figure 5.2.17-1. The part was scanned normal to the webbing, and then a portion of the intersection of the webbing and one of the end caps was done close up. The only known flaw in the part was in the flat portion at the end of the webbing, which is not particularly difficult to detect with TTU or even pulse echo UT with hand held probes.

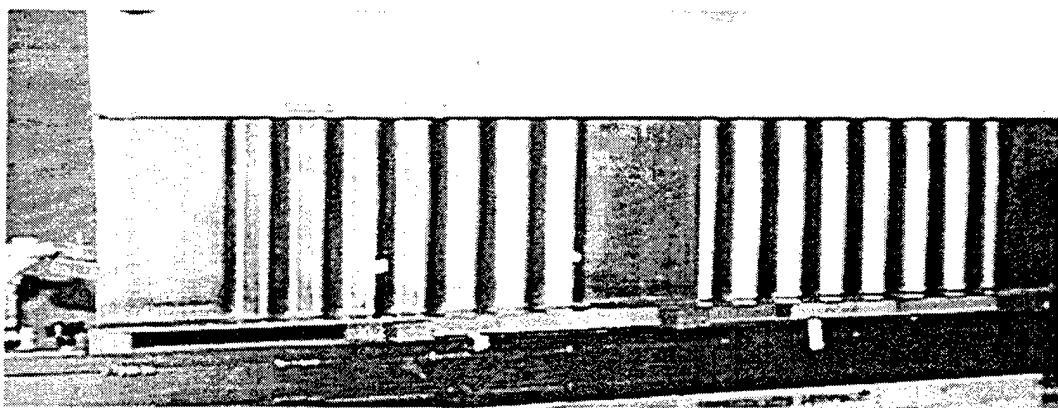


Figure 5.2.17-1. Photograph of sine wave spar

The part was scanned both vertically and horizontally as shown in the figure, with the same applying to the close up scan of the intersection. In the next four figures, C-scan images showing the difference in the horizontal and the vertical arrangements. In the horizontally oriented configurations, each scan line goes through all “phases” of all sine wave cycles of the webbing. In the images which are oriented so that the long axis of the part is vertical, each scan line goes through a constant “phase” of the sine wave, and therefore the ranging information is not constantly changing, and as a result, more smooth. This difference can be seen between the two amplitude C-scans (figures 5.2.17-2 and 5.2.17-3). Figure 5.2.17-2 does not show the same degree of gradation in the sine wave webbing as does Figure 5.2.17-3, which was scanned across the webbing so that each scan line was at the same “phase”. The same holds true for figures 5.2.17-4 and 5.2.17-5, which are TOF images.

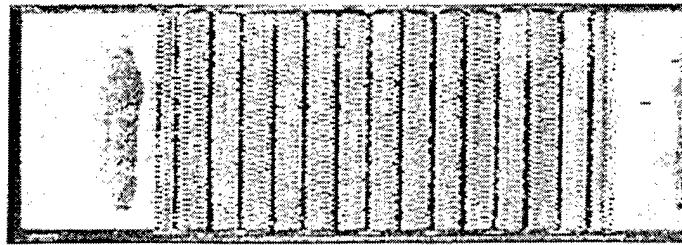


Figure 5.2.17-2. LUIS C-scan

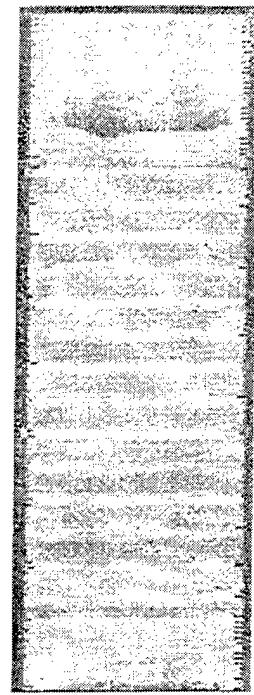


Figure 5.2.17-3. LUIS C-scan

Finally, a portion of the part was scanned to look more closely at the intersection of the webbing with one of the end caps. Two amplitude scans are shown, with the first one (fig 5.2.17-6) corresponding to the scan direction to be along all of the phases of the sine wave, and the second one (fig 5.2.17-7) scanned across the sine wave so that each scan line was at a constant phase of the sine wave webbing. The scan performed along constant phase lines reveals more of the information than the other, just as was the case above. LBU is the recommended inspection method for this part because there is basically no other way to inspect such an intersection line. For this reason there are no conventional data presented in comparison. This inspection is a good example of one, which exploits the LUIS's unique capabilities, and is a good warm up for the F-22 bulkhead and the bulkhead section.

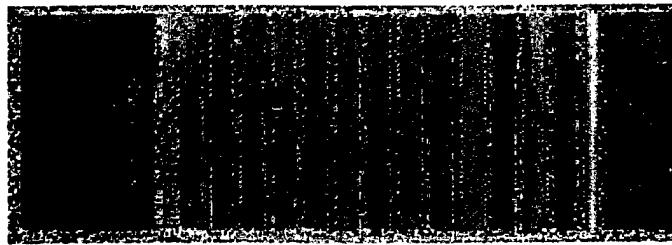


Figure 5.2.17-4. LUIS TOF image



Figure 5.2.17-5. LUIS TOF image

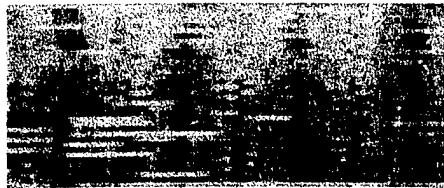


Figure 5.2.17-6. LUIS amplitude scan along sine wave phase

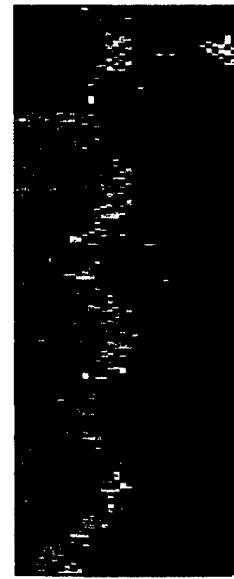


Figure 5.2.17-7. Scan across sine wave phase

5.2.18 F-22 Fuselage Bulkhead

This part is one of the more (if not the most) complex of the composite parts scanned during the program. Besides being very complex, it offers a great many opportunities for the LUIS to scan a part which is difficult at best and impossible at worst with normal production means. A photograph of the part is shown in figure 5.2.18-1. It is easy to see the wide range of challenges for UT scanning of any sort. This part is a good example of one that causes inspectors to dream

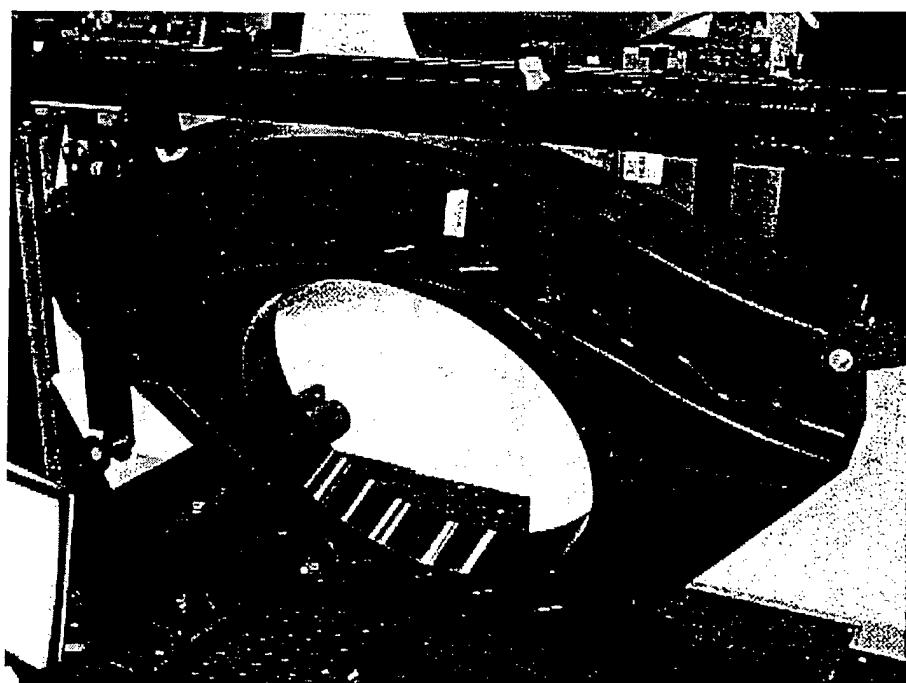


Figure 5.2.18-1. F-22 Fuselage Bulkhead

about non-contact scanning systems, simply due to its complexity and the large number of different types of shapes to be scanned. A comprehensive scan of this part with contact scanners whether pulse echo or through transmission (TTU), would be complicated, expensive and time consuming.

The part is of odd shape and contains varying thickness. It has complicated curved and cusped borders associated with the various regions. To further complicate things, parts of the webbing are "sine wave" surfaces. There are places where this sine wave webbing is contained inside flanges that are curved, and these curves themselves even contain inflection points. An example

of such a region is found in the upper right hand section of the part shown in the photograph above. Inspection of the intersection of the sine wave webbing with such curved flanges in such a section is particularly challenging.

An amplitude C-scan taken with the LUIS for the entire part is shown in figure 5.2.18-2. The part was scanned in six different sections and the images were later merged together. The software that allows three dimensional renderings is useful especially where parts are scanned in a number of sections, but the inspector needs to see the whole part at once. 3D geometry is acquired by the ranging system. This is potentially very useful in applications of reverse engineering or to confirm "as built" or "as tested" configurations in cases where modest resolution is required. It is useful in this capacity since it acquires data far more rapidly than computed tomography or coordinate measuring machines. Multiple scans requires more time, of course, but there is no other way to do the job with any kind of resolution. The six-part scan required about 1 hour and 42 minutes to set up, and then another 2 hours and 10 minutes to do the actual scanning. The recurring time for this type of part would be considerably less, as the setup would already be contained in the computer. It would only require removing the previous part and putting in the next part on the fixture, a job requiring 15 minutes, before moving the robot and laser to a reference point already predetermined from the original setup work.

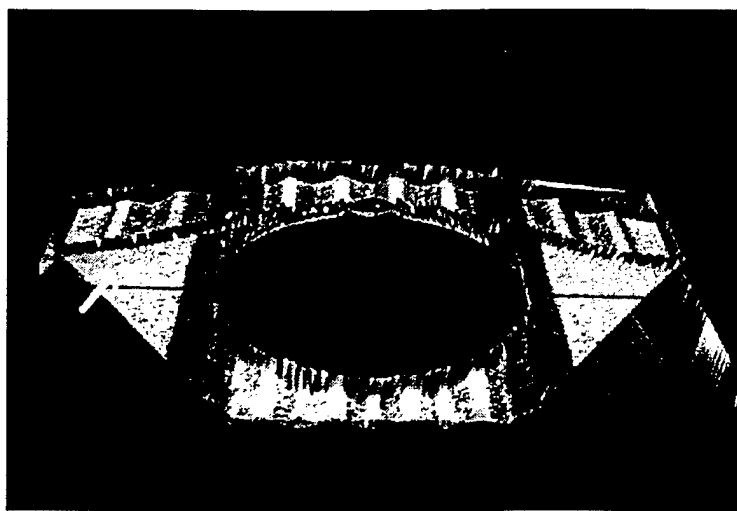


Figure 5.2.18-2. Amplitude C-scan with flaw indicated

The small dark spot in the trapezoid-shaped section on the left side, indicated by the arrow, is a flaw, as is confirmed on the next TOF scan of the three left hand sections shown in Figure 5.2.18-3. Although no major flaws show up on these scans, there is no other way of scanning a number of parts such as this with any speed or consistency. The numerous surface orientations of the part are all scanned in one shot. The part can be rotated through 15 or 20 degrees about the vertical axis to permit scanning of all of the vertical intersections on the left or right sides of the sections, and then rotated back through the same angle in the opposite direction to scan the intersections on the remaining sides of the sections. In this way the entire part can be scanned in 6 to 8 segments per side to inspect all intersection lines between each webbing section and its respective borders.

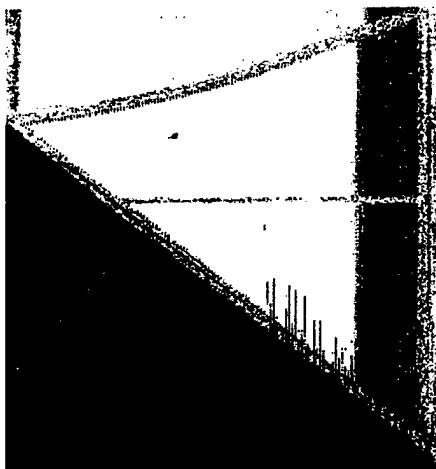


Figure 5.2.18-3. TOF image of left side of part

Figure 5.2.18-4 shows a close up amplitude C-scan of such an intersection, taken after slightly rotating the part about its vertical axis as stated in the above paragraph. This is an image of the section in the upper right hand corner of the part in the photograph shown in Figure 5.2.18-1. The scan does not appear to show any serious problems along the intersection. There is no other way of getting information from an intersection segment this complicated unless it is with a hand held probe, which has its associated difficulties and will not produce an image of anywhere near the quality shown in the figure. For this reason, LBU is the preferred method of inspecting a part like this.

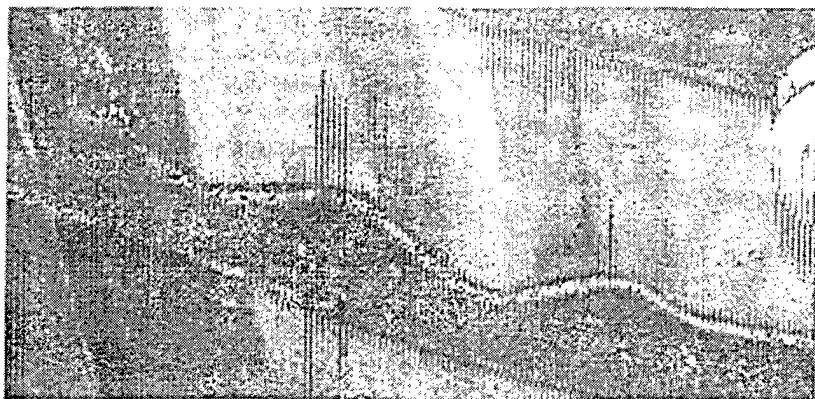


Figure 5.2.18-4. Amplitude C-scan of upper right side of part

5.2.19 Composite "Crow's Foot" Section

This highly unique part is shown in Figure 5.2.19-1. It is a section of a larger prototype structure for the F-22 program. A quick glance shows the complication of scanning such a part with any sort of device. Only a non-contact method such as Laser UT has a chance of scanning the whole part. There are widely varying thicknesses, two different thicknesses of sine wave webbing, various angles, complex bond lines, and at least two tight vertices of about 30 degrees.



Figure 5.2.19-1. A section of a larger prototype structure for the F-22 program

Both sides of the part were scanned as single scans with the LUIS. A scan of the thick edge portions of the part was not attempted. Those areas would be scannable with an appropriately designed conventional surface rider. Amplitude C-scans images derived from both of these scans are shown in figures 5.2.19-2 and 5.2.19-3. Since such complicated parts would require custom ultrasonic transducer fixturing, there are no production scans provided for comparison. It will be quickly appreciated that high quality images such as this would not be possible without a non-contact inspection method.

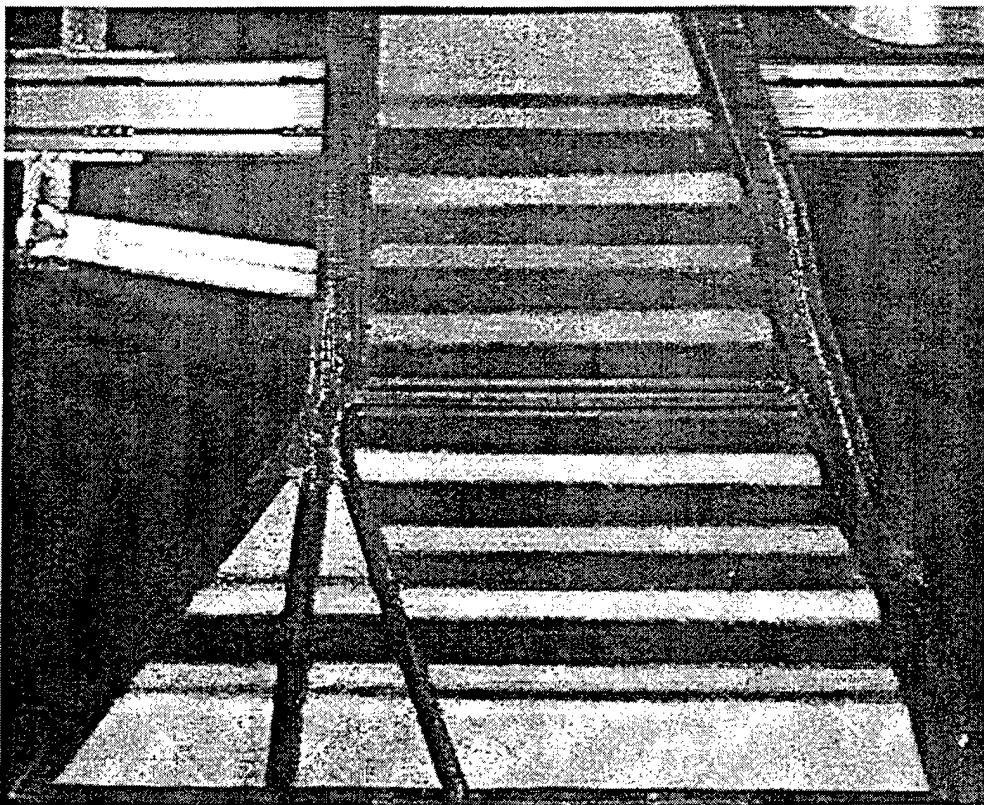


Figure 5.2.19-2. Amplitude C-scan frontside

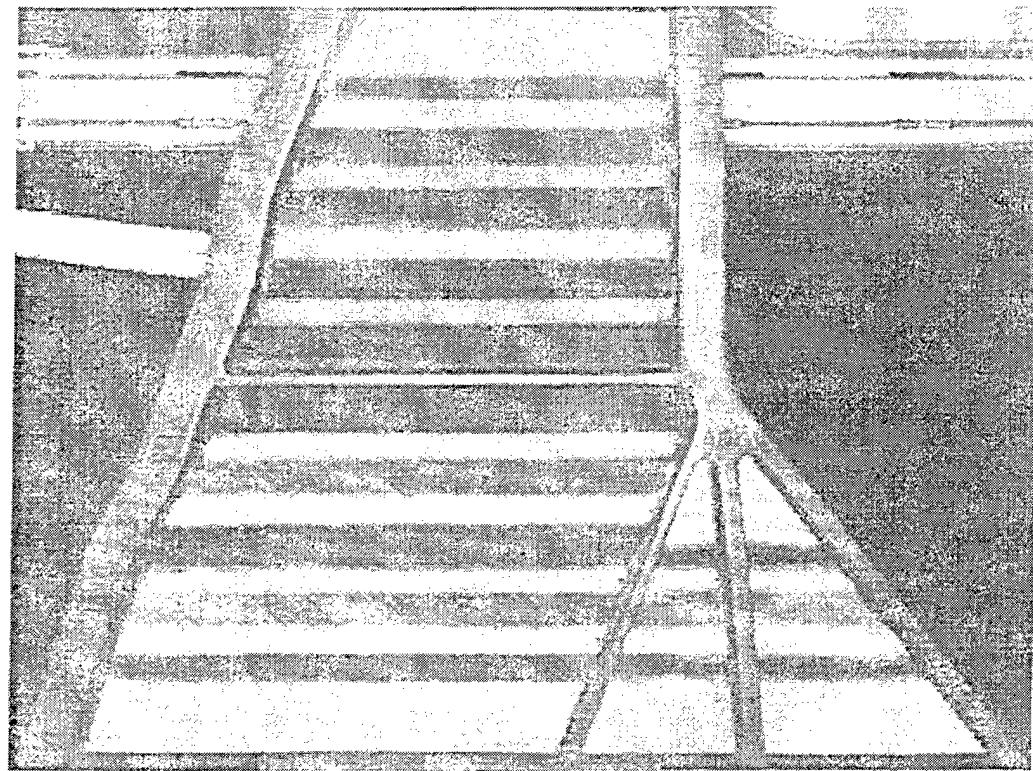


Figure 5.2.19-3. Amplitude C-scan backside

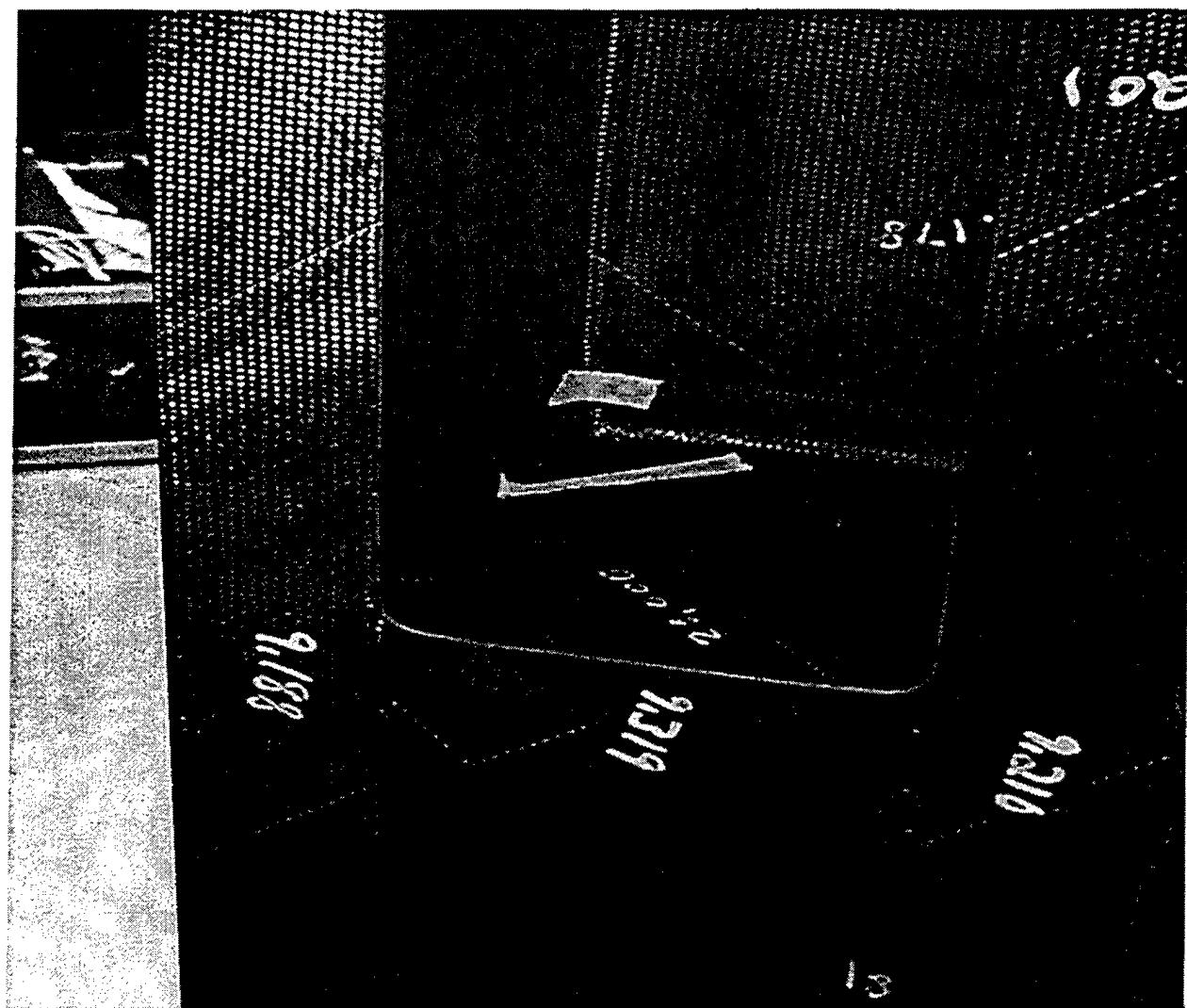
5.2.20 One Piece Wing Box

Current trends are towards making larger and larger composite portions of airframes. The prototype one piece wing box pictured in figure 5.2.20-1 is a good example demonstrating this trend. The entire part is cured as one piece. This of course causes more dependence on quick and comprehensive NDE. It is easy to see the large number of scans required of a hand held or robotically controlled scanner. There are 48 interior three-dimensional corners, 48 interior right angle intersection lines, 11 panels, and the back surface that would need to be inspected.



Figure 5.2.20-1. Integral wing box prototype

The wing box has a known flaw in the rib shown in the close up in figure 5.2.20-2. The surface of the rib is rough to the touch, which is easy to find simply by visual inspection. This surface roughness does not necessarily fail the part. The scan of interest is the section between the three dimensional corner and the diagonal marked by the masking tape. This surface roughness requires the scanning of the region containing the three dimensional corner which can't be scanned any other way. It was necessary to paint this region, and the painted close up of the corner is shown in Figure 5.2.20-3.



Figures 5.2.20-2. Close-up of wing box corner

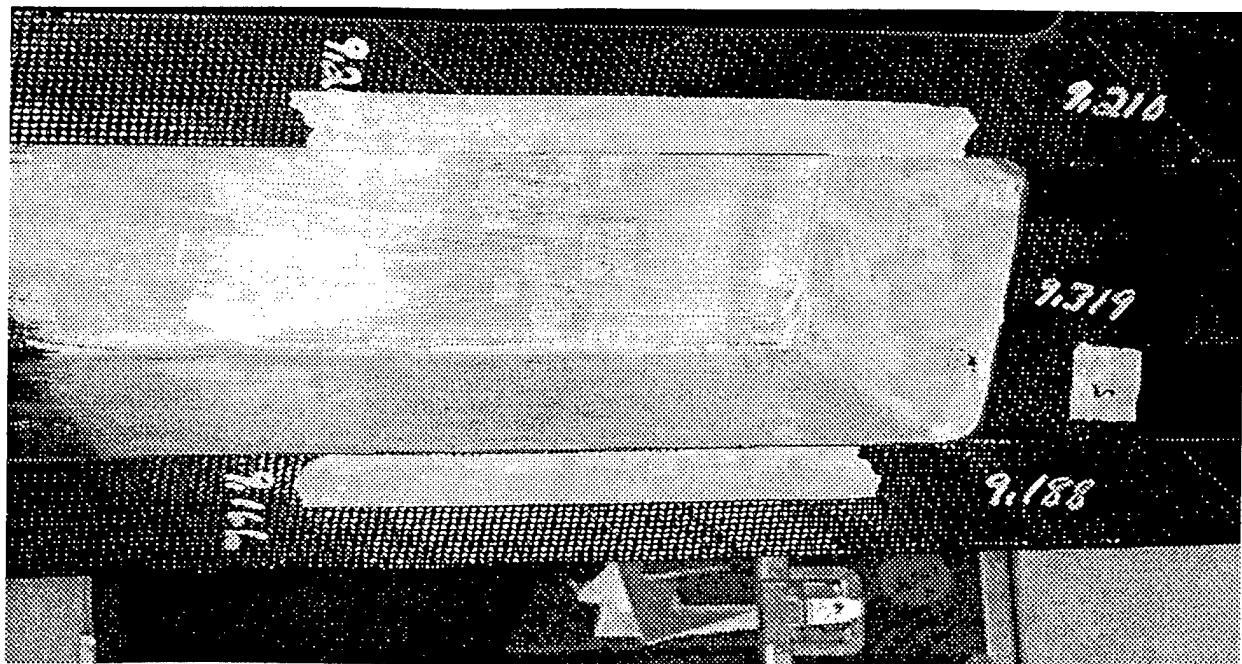


Figure 5.2.20-3. Wing box corner painted

Amplitude and TOF scans are shown in Figures 5.2.20-4 and 5.2.20-5 respectively. Figure 5.2.20-5 shows sufficient information to fail the part. The amplitude scan image shows an unusual pattern that is probably due to poor laser coupling because of the surface roughness already mentioned. The amplitude signal variations do not appear to be caused by internal flaws or defects. The TOF scan image shows variation in the time domain which is interpreted as a region of low density which can affect the strength of the rib. This is not seen by visual inspection or in the amplitude scan, but causes the part to be rejected. Because of the difficulty in conventionally inspecting this part, automated LBU inspection is very likely to be the preferred method. Further work would be necessary to establish the preferred procedure.



Figure 5.2.20-4. Amplitude scan of wingbox corner

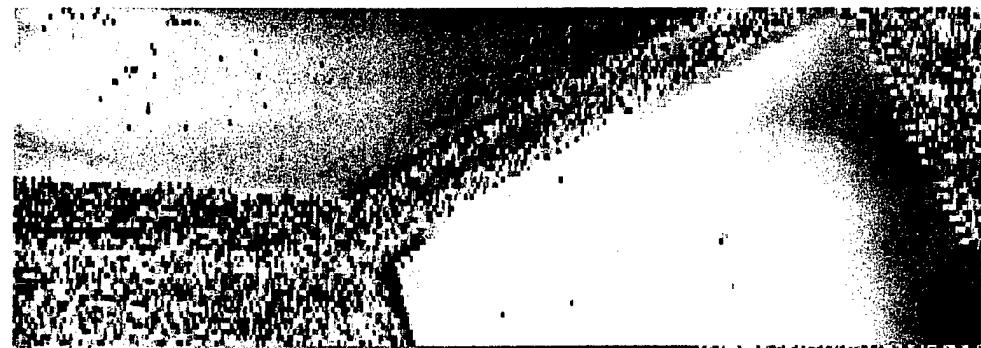


Figure 5.2.20-5. TOF image of wing box corner

5.2.21 F-22 Landing Gear Door

This part is a good example of a complex shape, including curvature in two orthogonal planes. The door is made of graphite epoxy skin over fiberglass honeycomb. A photograph of the bag side of the part is shown in figure 5.2.21-1. The portion of the door in the lower right hand corner of figure 5.2.21-1 was scanned with the LUIS. The door mounted in the fixture for scanning is shown in figure 5.2.21-2. In figure 5.2.21-2 the portion in the lower left hand corner is the surface that was actually scanned.

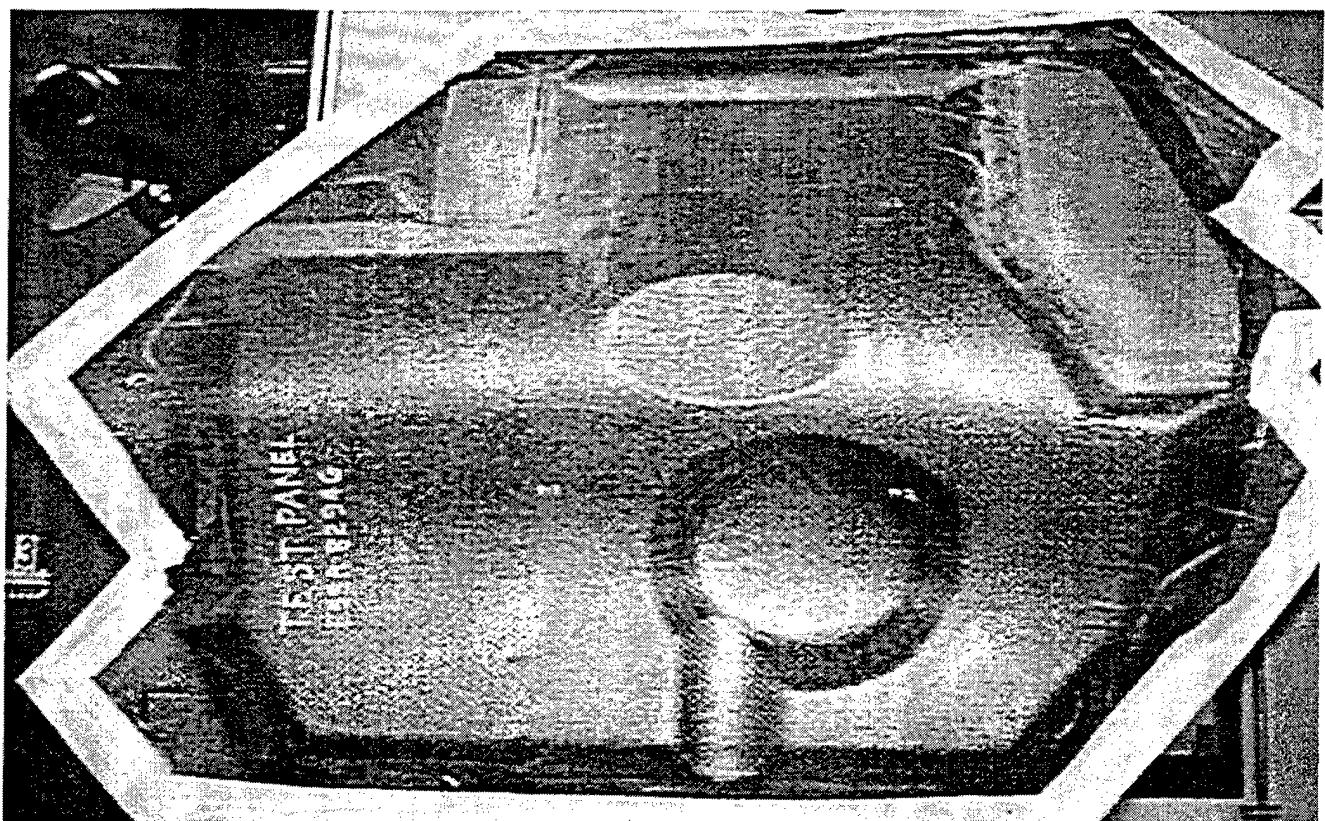


Figure 5.2.21-1. F-22 landing gear door bag side view



Figure 5.2.21-2. F-22 landing gear door mounted for tool side scan

Figure 5.2.21-3 shows the amplitude C-scan taken with the LUIS. It is easy to see internal features, including the honeycomb cell pattern. There are several regions where resin has been forced into the core; they appear as dark "splotches". Some wrinkling of the separators of the opposite side skin fabric or bunching of the resin is seen running along the upper portion of the image. It will be appreciated that this image was processed from the full wave data without doing any signal processing other than choosing an appropriate gate corresponding to the back surface of the front skin. Figure 5.2.21-4 is a Boeing production amplitude pulse echo scan of the same part. This scan was done in about 25 minutes and shows most of the same features. It does not extend quite high enough to include the wrinkling. Normal procedure would only call for inspecting such a part with TTU, but it was scanned in pulse echo mode to be able to strictly compare the image with that from the LUIS.

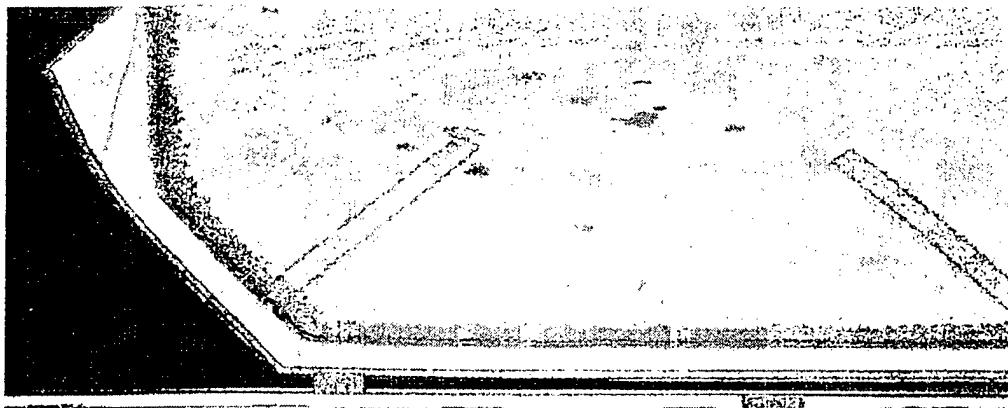


Figure 5.2.21-3. LUIS amplitude C-scan

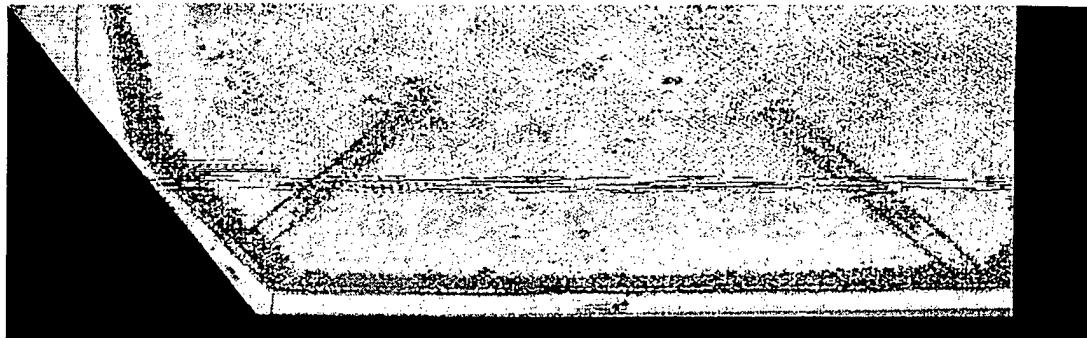


Figure 5.2.21-4. Boeing amplitude C-scan

TOF images from the LUIS and the Boeing production scanner appear as figures 5.2.21-5 and 5.2.21-6 respectively. The circular beveled depression in the opposite bag side is easily picked up with both scans. The streaks through the lower portion of the production scans are missing data. The LUIS scan is done at increments of 0.050" in both x and y. The production scans are done at 0.02" in x and 0.06" in y. Both of the scans detect the vertical splice in the skin on the opposite side of the door located at the extreme left portion of the image. The LUIS image is definitely superior to the production scan, which is as it should be for having been processed from the full waveforms. The cursory scan taken with the LUIS is very helpful in allowing a quick inspection of this part. It reveals the number, type and distribution of the flaws. If the setup time could be reduced by a factor of two or three, LBU would be the inspection method of choice over the current TTU for this honeycomb part. Despite the complexity of the part, it is thin enough to detect the interface at the back side. If there were a requirement for inspecting from the bagside

of the part it would be cost effective to use LBU even if the setup and scan times could not be reduced.

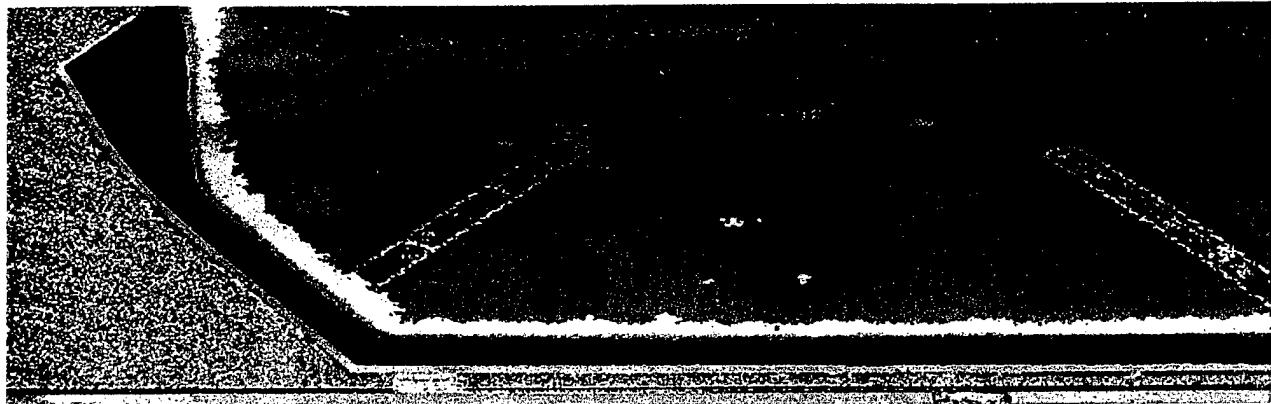


Figure 5.2.21-5. LUIS TOF image

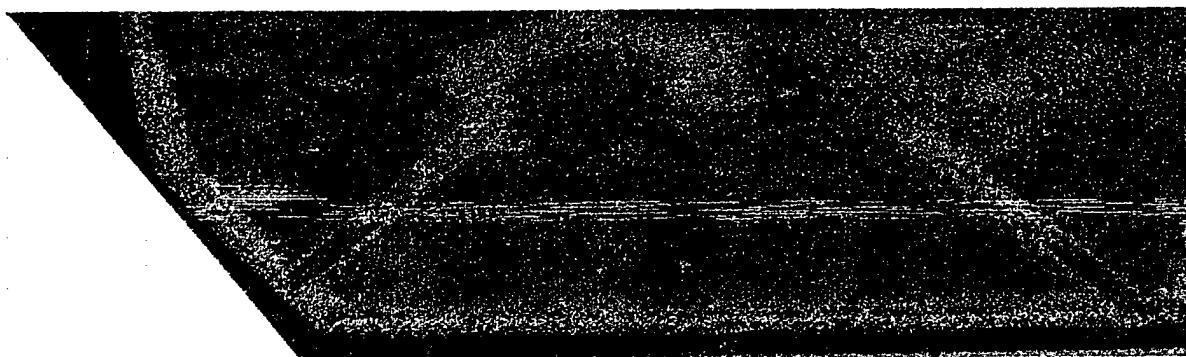


Figure 5.2.21-6. Boeing production TOF image

5.2.22 Foam Filled AWACS Instrument Panel Section

This section is made from a composite skin over a very tight foam. It is a good example for inspection of the interface of the foam and a typical adjoining skin. For pulse echo inspection, it would not be expected that full penetration could be achieved. However, images processed from the scans made by the LUIS proved very informative. An amplitude scan and the corresponding time of flight TOF image of the panel section are shown in figures 5.2.22-1 and 5.2.22-2 respectively. Note the vertical lines appearing along the bottom. These are at the interface between the skin and the foam core. It is possible that a subsurface ply in the skin has tows that are vertical and some sort of wicking occurred. It is also possible that for some reason the foam core was either scribed or assembled in sections. Foam section assembly is definitely the case for the slanted nearly vertical mark on the left, which separate two sections of the core, and could be seen from a side view (in the plane of the paper) with simple visual inspection. The section line appears dark in both of the scans and the unknown vertical lines appear light in the TOF scan.

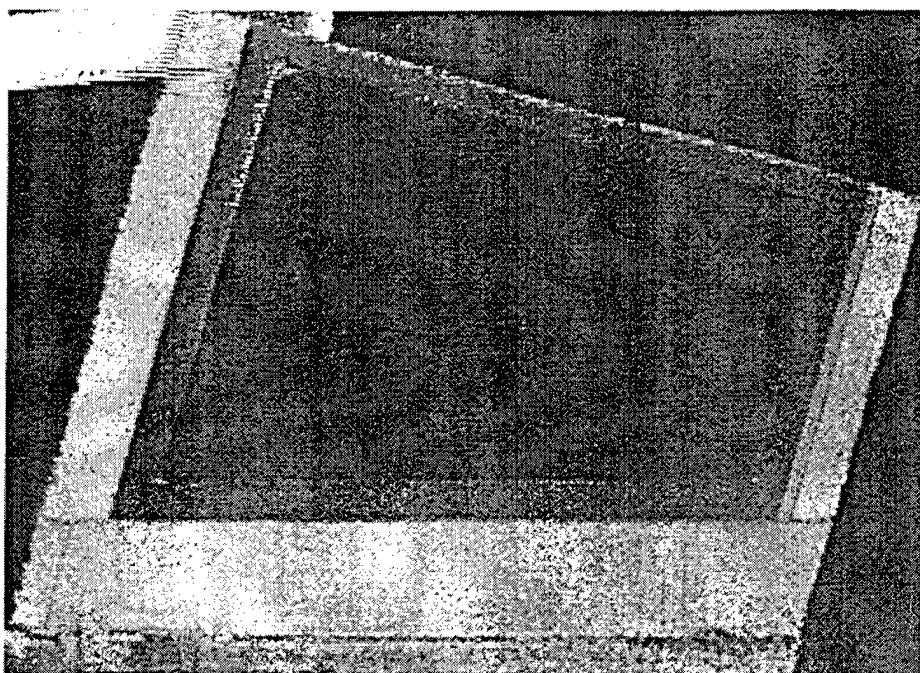


Figure 5.2.22-1 LUIS Amplitude Image

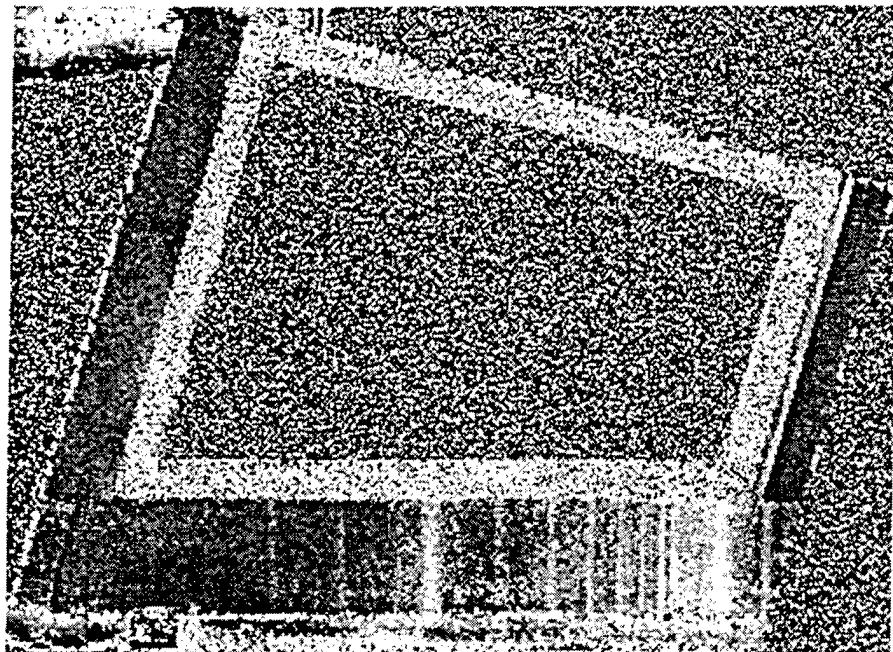


Figure 5.2.22-2 LUIS TOF Image

Another TOF image with a slightly wider time gate appears in figure 5.2.22-3. In this image it does appear that the foam core is not consistently adhered with the back surface of the near side skin. This is seen again in the production TTU scan shown in figure 5.2.22-4.

The LUIS did remarkably well in this case providing detail concerning the interface between the skin and the foam core. The LUIS is viable for quick scanning of large areas with a foam core and graphite epoxy skins of modest thickness. For large parts, where both sides of the part are not available, LUIS would be preferred over surface riding, conventional scanners. This is especially true when surfaces are stepped, curved or have unusual contours.

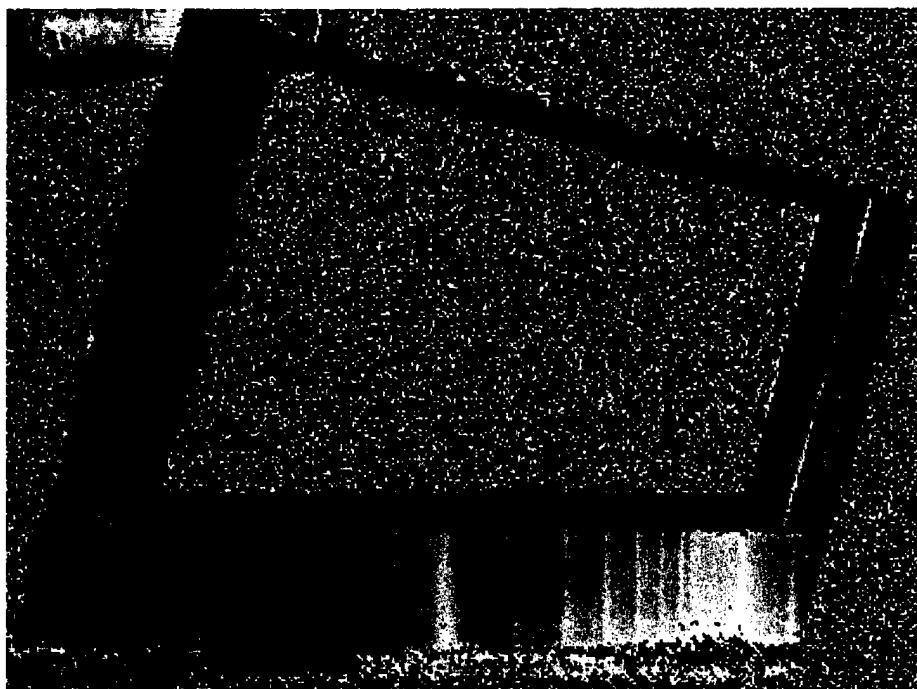


Figure 5.2.22-3 TOF Image

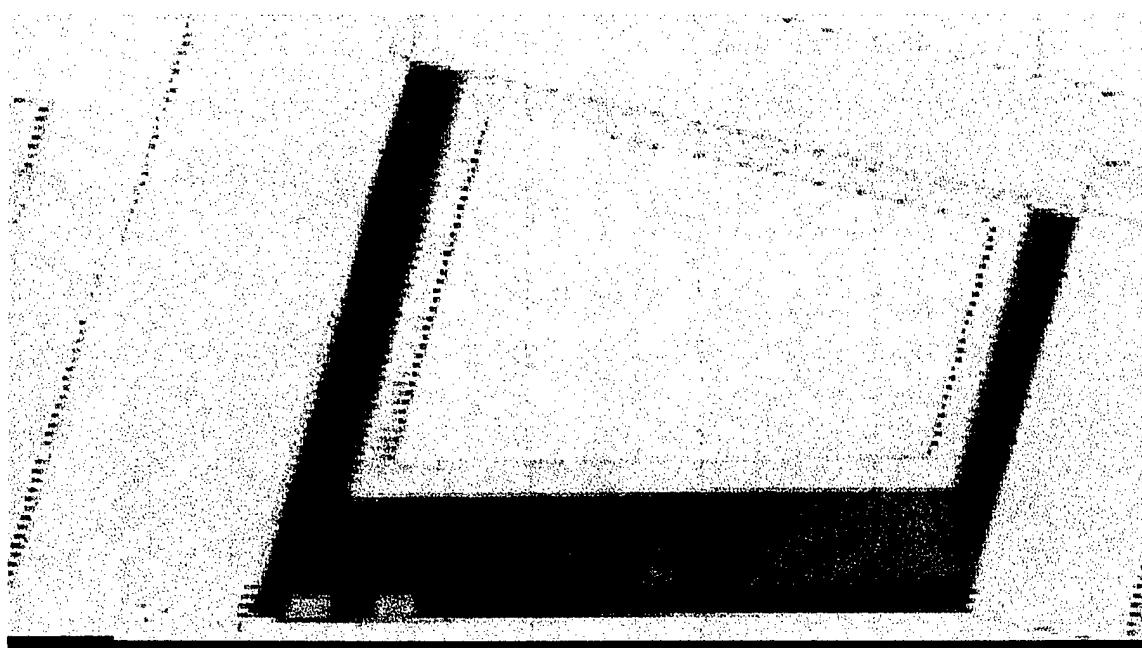


Figure 5.2.22-4 Production TTU Scan

5.2.23 Milstar Radome Sample

This sample is a “half pipe” section of a cylinder about three feet in diameter, and one and one half feet high. It is made of fiberglass skin about one eighth inch thick, with a special honeycomb core made of a brittle glass-like material called “e glass. The section was given two different types of damage. In one place it was hit with a hammer and in another it was subjected to compression through its thickness with a C-clamp. An amplitude C-scan of the area including the damage is shown in figure 5.2.23-1. It is easy to see the larger hammer blow, which is the lower of the two features. Around this blow is a dashed line made of marking chalk. This has been picked up also in the LUIS scan, as the chalk has a different ultrasound generation efficiency than the fiberglass skin. Figure 5.2.23-2 is a Boeing production scan of the same damage area for comparison.

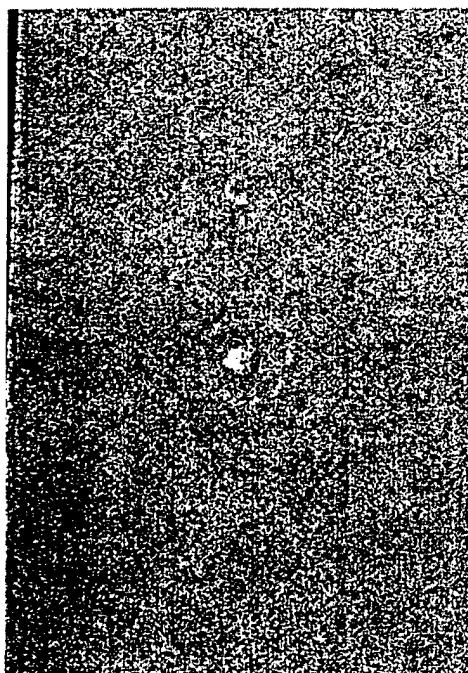


Figure 5.2.23-1. LUIS amplitude C-scan

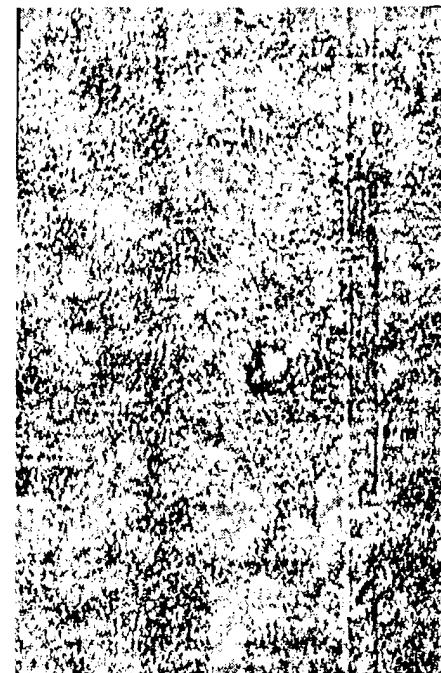


Figure 5.2.23-2. production amplitude C-scan

The upper feature is really the chalk mark around the supposed damage resulting from the compression with the c-clamp. It appears to possibly be damage. However, when the B-scans are inspected, it is clear that all that is seen is the chalk marks. This can be seen by inspecting a series of B-scans shown as figures 5.2.23-3, 5.2.23-4, and 5.2.23-5. Figure 5.2.23-3 is a scan

taken across the sample just tangent to the bottom of the chalk marked circle. Notice the single white "blip" at the top of the scan a little to the right of center. This is actually the thickness of the chalk. Figure 5.2.23-4 shows a B-scan taken one line up. In this figure, the scan cuts through the chalk marked circle leaving two distinct points of intersection. These can be seen at the top. Finally, in figure 5.2.23-5 a B-scan along a line near to the center of the circle is shown. Here the marks are further apart, and there does not appear to be any indication of a signal in the region between the two marks. This would tend to indicate that the clamp damage was either non-existent, or was too small to sufficiently alter the material to permit detection.

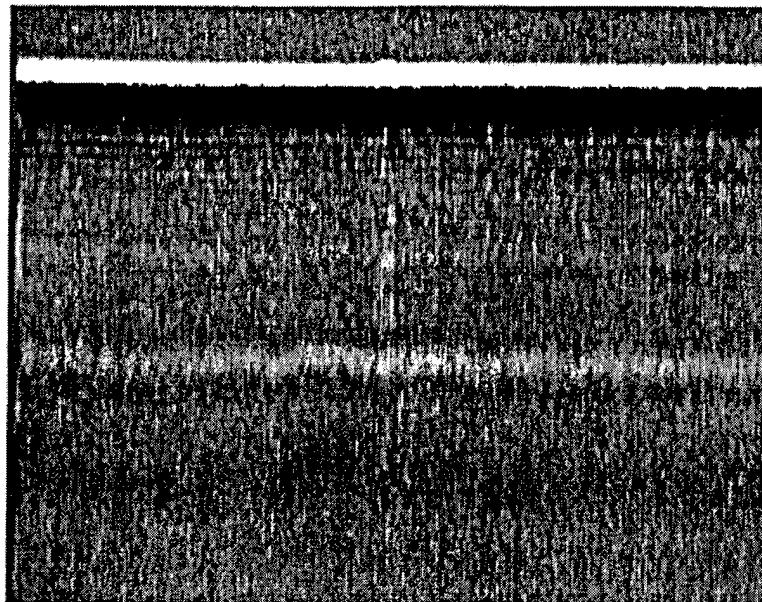


Figure 5.2.23-3. LUIS B-scan tangent to bottom of upper feature

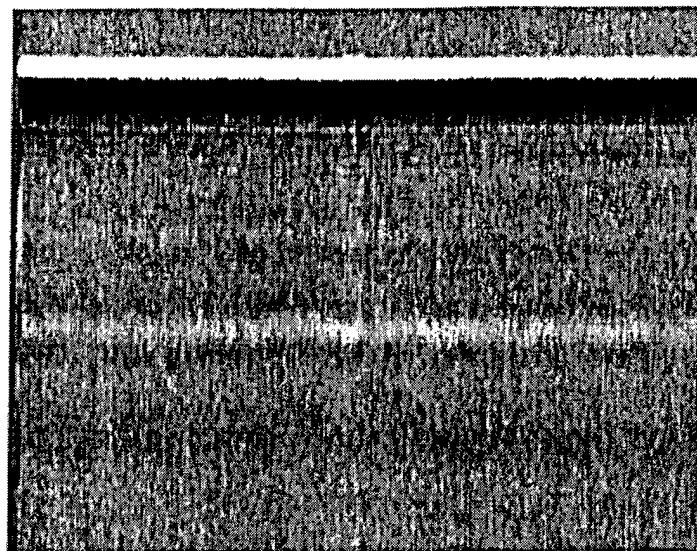


Figure 5.2.23-4. LUIS B-scan one line up from scan in figure -4

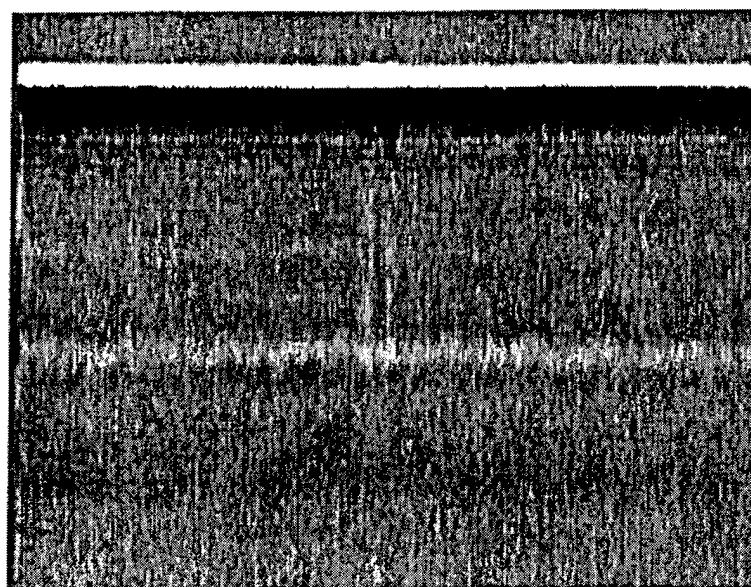


Figure 5.2.23-5. LUIS B-scan near center of upper feature

Finally, figure 5.2.23-6 shows a B-scan taken along a line through a point near the middle of the hammer blow damage (the lower feature in figure 5.2.23-1). This also clearly shows the chalk mark “blips” at the top of the figure.

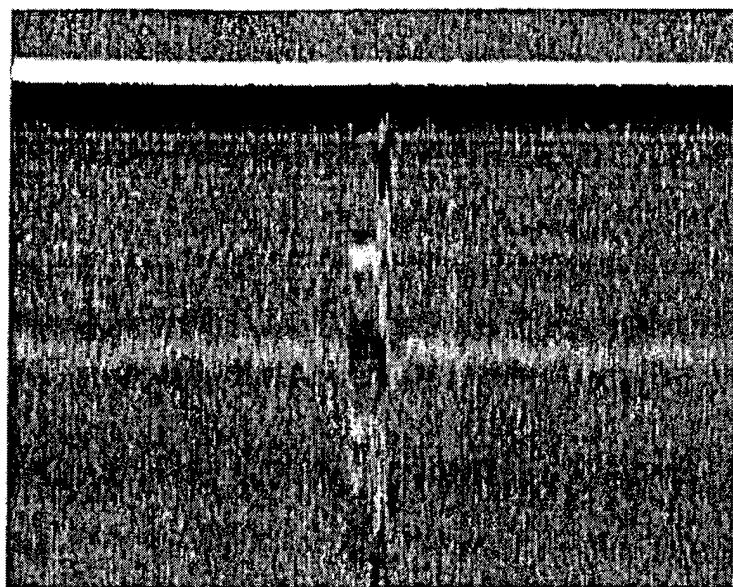


Figure 5.2.23-6. LUIS B-scan near center of hammer blow

5.2.24 Three Stage Cured Repair on Stiffened Solid Laminate Panel

This panel is a good example of a type of repair that is routinely encountered and is readily inspected by the LUIS. The panel is solid laminate and has stiffening members on one side. On the other side, a three-stage patch is applied to a scarfed hole, which is located over one of the stiffeners. Each of the cure stages is 6 plies thick. Inserts of brass were placed into the repair, as well as some contamination. The large blob at roughly 10 o'clock is an intentionally applied bit of contamination, between the deepest two plies of the third cure. The smaller blob at about 5 o'clock is the same simulated contamination between the two repair plies closest to the surface of the panel. A brass foil insert is located in the center of the repair, as well as one at 2 o'clock between the 4th and 5th repair plies and one at 8 o'clock in the adhesive film of the third cure.

An amplitude C-Scan taken with the LUIS is shown in figure 5.2.24-1. A pulse echo amplitude C-scan image taken with a Boeing production scanner is shown as figure 5.2.24-2. This production scan acquired full wave data, and is therefore more closely comparable with the LUIS scans.

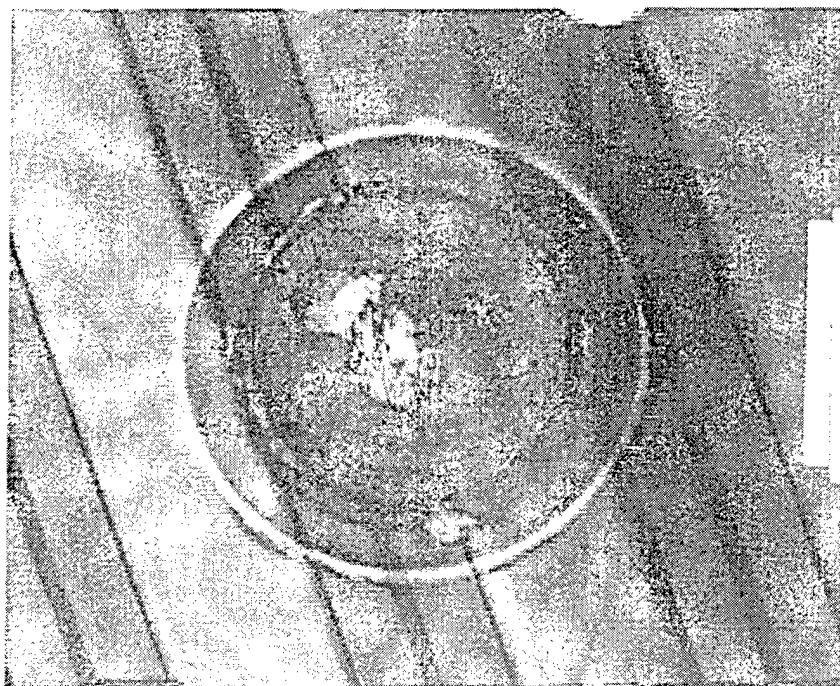


Figure 5.2.24-1. LUIS amplitude C-scan

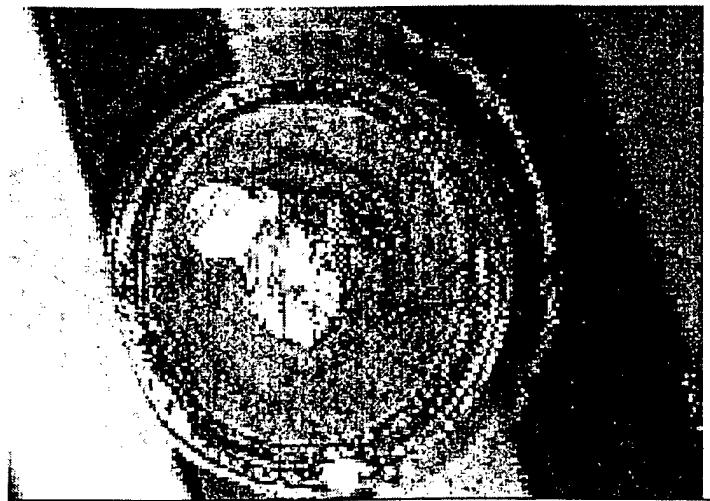


Figure 5.2.24-2. Boeing production amplitude C-scan processed from full wave data

Each of the simulated contamination areas is seen on both of the scans. The contamination is simulated by a substance that releases gas when heated in the curing process. This gas can then permeate the region between plies. It caused the large smear from the center of the circular boundary of the region at 10 o'clock down towards the center of the patch. The LUIS scan seems to be a little better in detecting the actual boundary of these two flaws. The gas released by the smaller contamination area at 5 o'clock seems to have been more evenly distributed in direction.

TOF images taken with the LUIS and TTU taken with a Boeing production scanner are shown in figure 5.2.24-3 and 5.2.24-4 respectively. The brass foil inserts at 2 o'clock and possibly a hint of the one at the center are seen in these two images. It is not clear that the insert in the center is actually detected. The insert at 8 o'clock is closer to the surface than that at 2 o'clock, but neither of the techniques was able to detect the simulated defect. It is obscured by the porosity in the plies just above it due to the gas released from the contamination region at 10 o'clock.

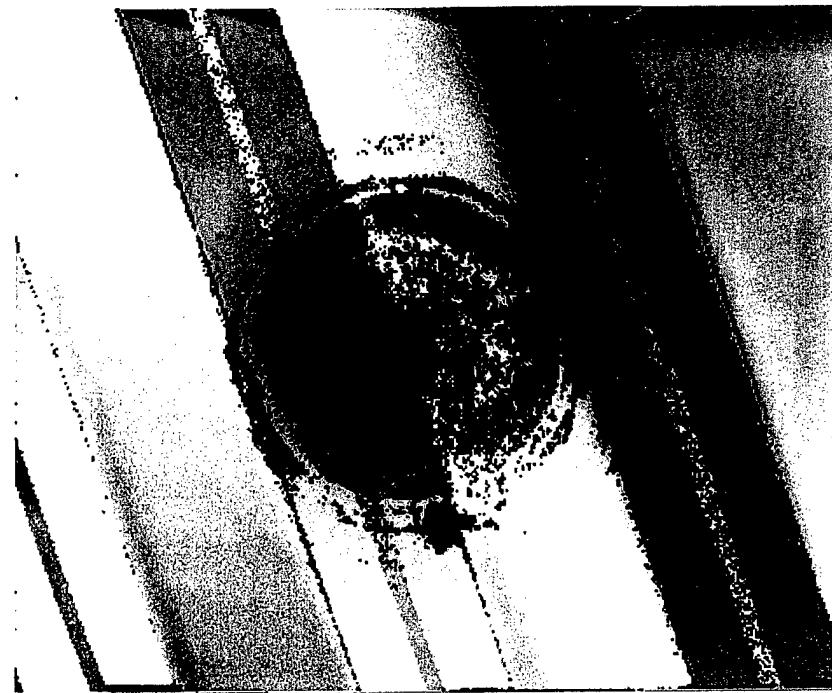


Figure 5.2.24-3. LUIS TOF image

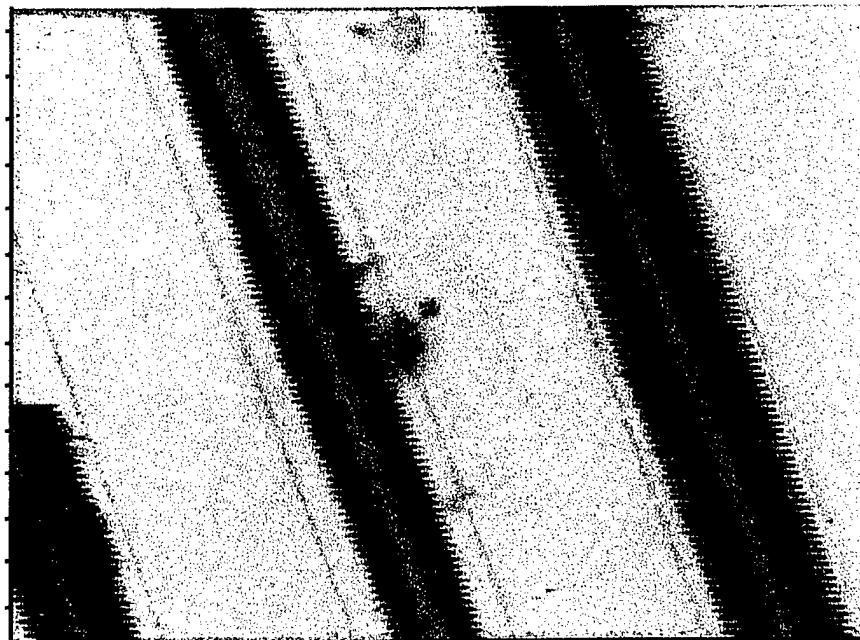


Figure 5.2.24-4. Boeing production TTU image

5.2.25 Fiberglass/Honeycomb Repair Panel K-4

This panel, made of fiberglass with a honeycomb core, has a repair over a transition region between honeycomb cored bays. Figure 5.2.25-1 contains a photograph of this part. The production TTU scan is shown in figure 5.2.25-2 and a LUIS amplitude C-scan is shown in figure 5.2.25-3. The TTU scan found a disbond in the center of the circular patch. LUIS scanned only the smooth skin tool side of the repair, and displayed considerable detail, but did not find the disbond. It could be that the disbond was between the core and the far surface, in which case the LUIS would never see it. Also, there is a small chance that the damage is in the interior of the core. Since the core is sloped in this region, though, it is hard to imagine that the damage is only internal to the core. The dark region in the center of the TTU scan shows where no energy is transmitted and is therefore a disbond discontinuity. This disbond is the only flaw in the panel. TTU is the recommended method for scanning this panel, as the LUIS cannot see disbonds if they are on the far side of the repair.

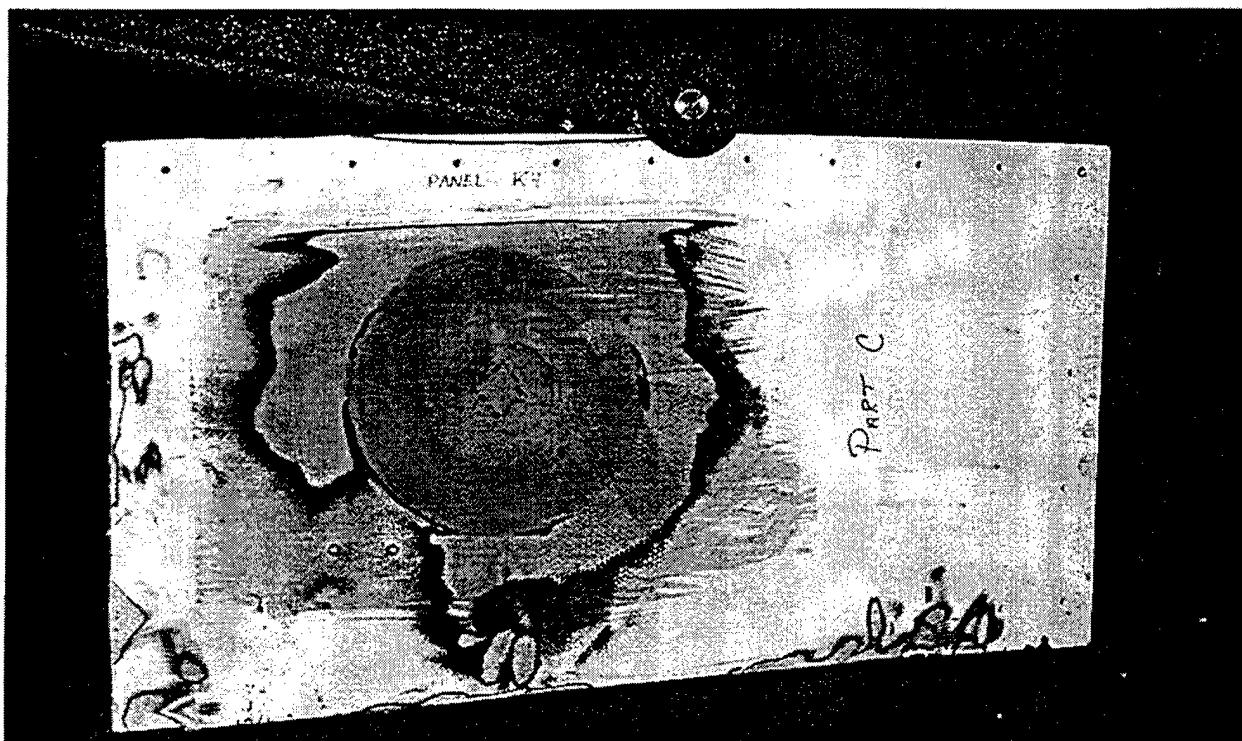


Figure 5.2.25-1. Repair Panel K-4

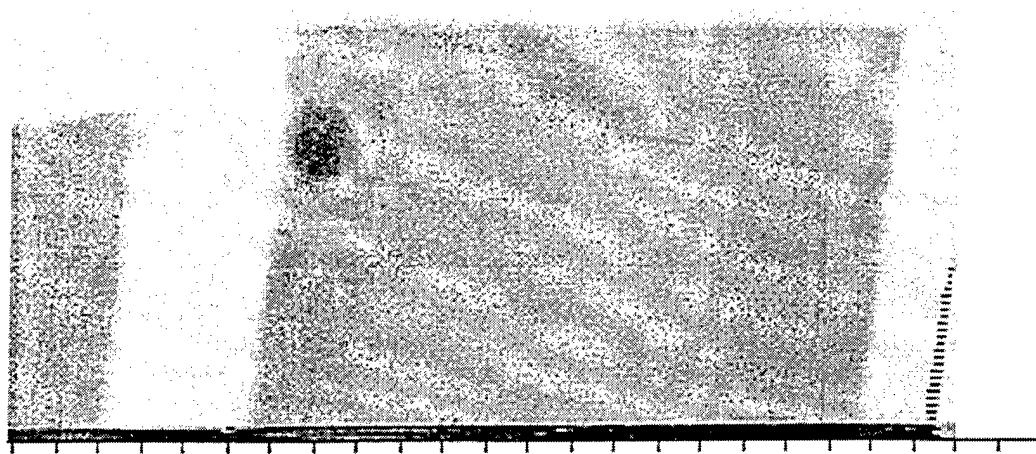


Figure 5.2.25-2. Boeing TTU image of panel K-4



Figure 5.2.25-3. LUIS amplitude C-scan of panel K-4

5.3 Miscellaneous LUIS Data

This section contains LUIS data that were not developed as part of this contract. However, the parts inspected are of interest to the Air Force or Boeing and are included here to build as complete a record as possible of LUIS information.

In 1996 the Advanced NonDestructive Technologies Engineering Laboratories of Rockwell International at Downey, CA, which is now a part of Boeing Information, Space and Defense Systems, performed a study of advanced NDE methods for inspection of spacecraft thermal protection systems. The study included conventional immersion ultrasound, AirScan ultrasound, LBU at both the LUIS 747 and Rockwell Science Center LBU laboratory, and several other NDE methods such as shearography and Computed Tomography. The entire study is recorded in document ANDTEL 96033, Thermal Protection System Advanced NonDestructive Testing, dated July 29, 1996. Selected results from that study are reproduced here. Several NDE methods were used to inspect panel SHM-8, a 12 inch by 12-inch graphite-epoxy 16-ply panel backed with Rohacell foam in honeycomb. Figures 5.3-1 and 5.3-2 show the honeycomb structure on the backside of the panel. Figure 5.3-3 shows the front of the panel.

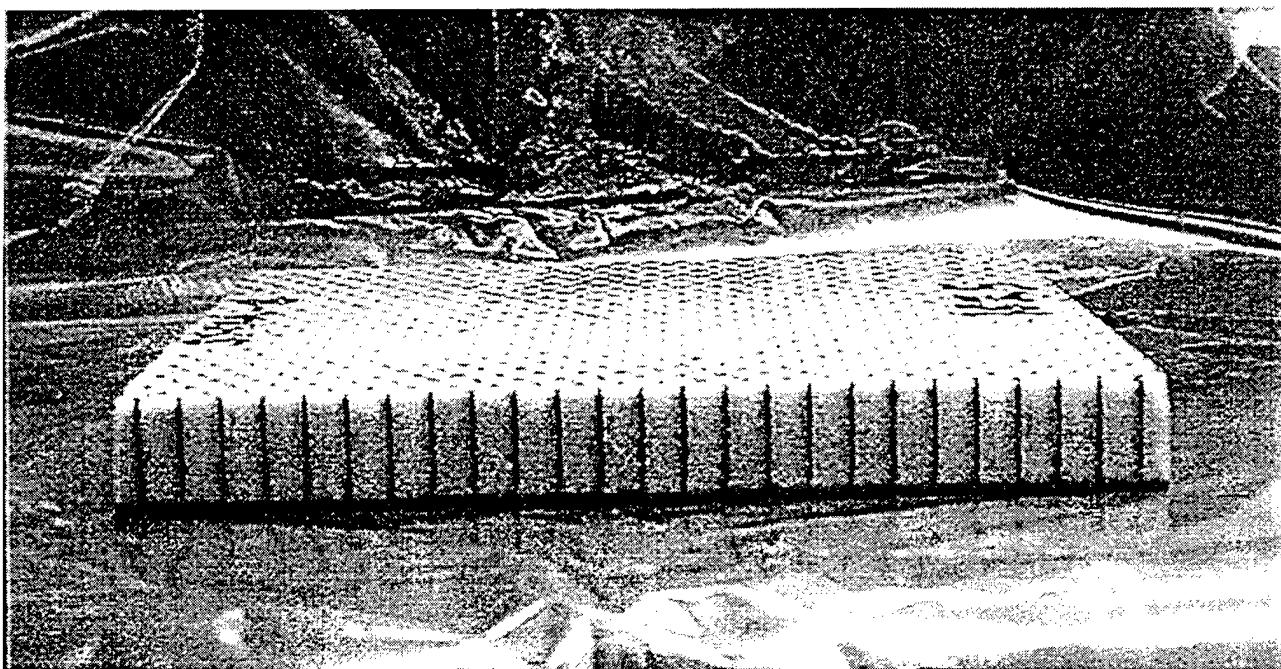


Figure 5.3-1. Edge view of panel SHM-8

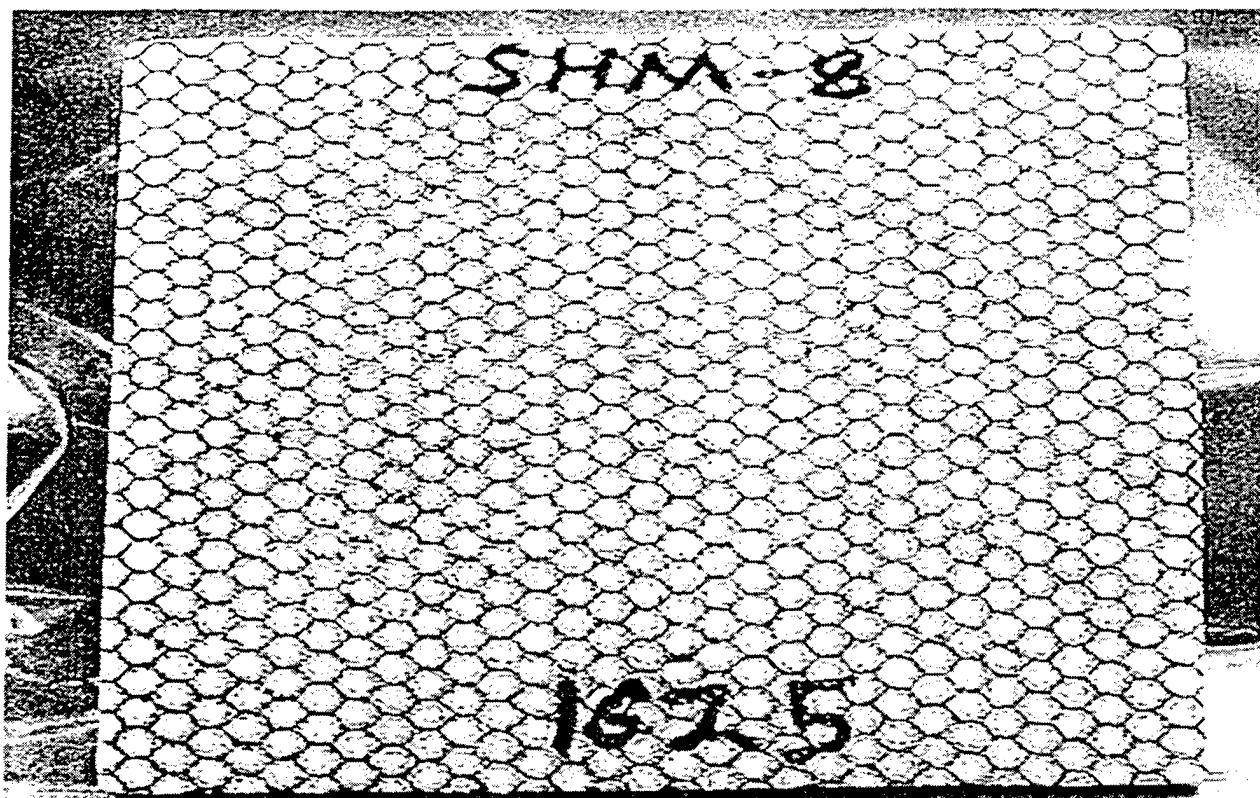


Figure 5.3-2. Backside of panel SHM-8

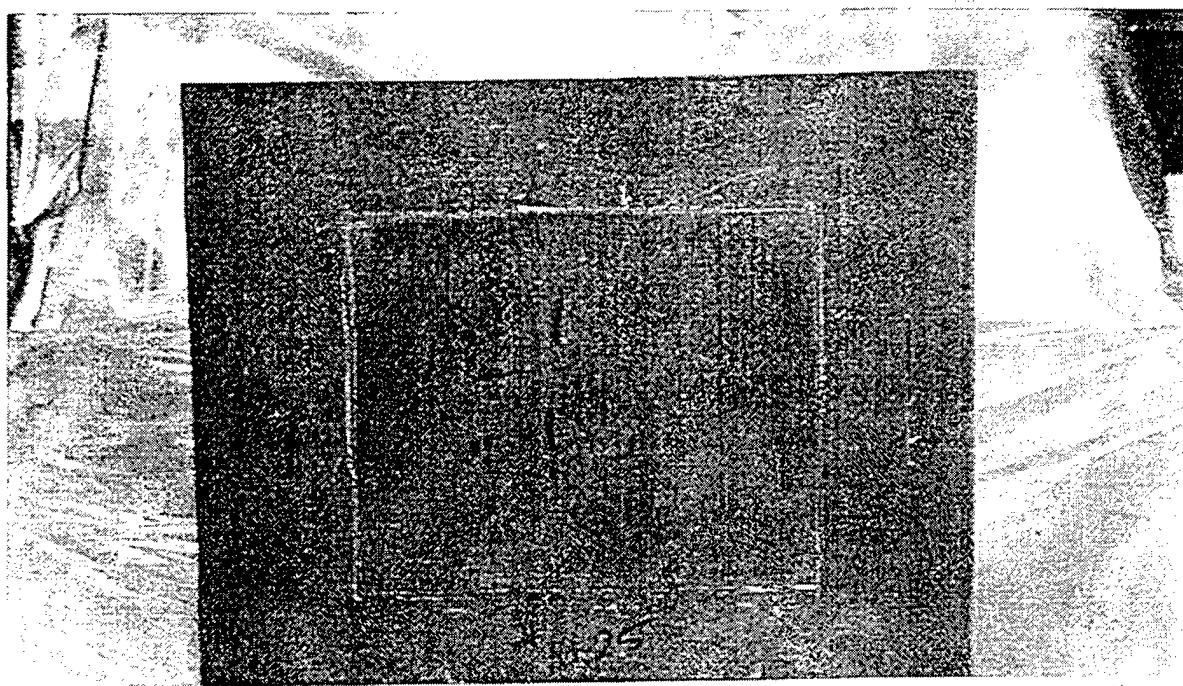


Figure 5.3-3. Frontside of Panel SHM-8

The panel sustained internal damage, not visible to the naked eye, during an impact test. Figure 5.3-4 shows an ultrasonic C-scan of the panel from a standard immersion system using a 5 MHz, 3 inch focus transducer. The primary damage site from an impact in the center of the panel is clearly visible. Additional damage is visible on the edge of the panel in a pair of nearly mirror image shapes. This damage was assumed to be "cantilever damage" caused by the clamp holding the panel during impact. Figure 5.3-5 shows an AirScan of the panel. An AirScan is a noncontact ultrasonic inspection, which uses spherically focused 50-mm focal length piezoelectric elements in a toneburst mode with a center frequency of 400 kHz to produce an acoustic signal of wavelength of .85 mm in air. The signal couples to the part and excites an ultrasonic signal in the part. AirScan model XP-12 used in the test was manufactured by Quality Material Inspection, Inc. of Costa Mesa, CA. The AirScan image replicates the main features of the conventional C-scan. Figure 5.3-6 shows a C-scan of the panel taken at the Rockwell Science Center LBU laboratory. The Rockwell LBU C-scan matches the primary details of the conventional system. Figure 5.3-7 is a LUIS 747 C-scan of the panel, which is also comparable to the conventional C-scan.

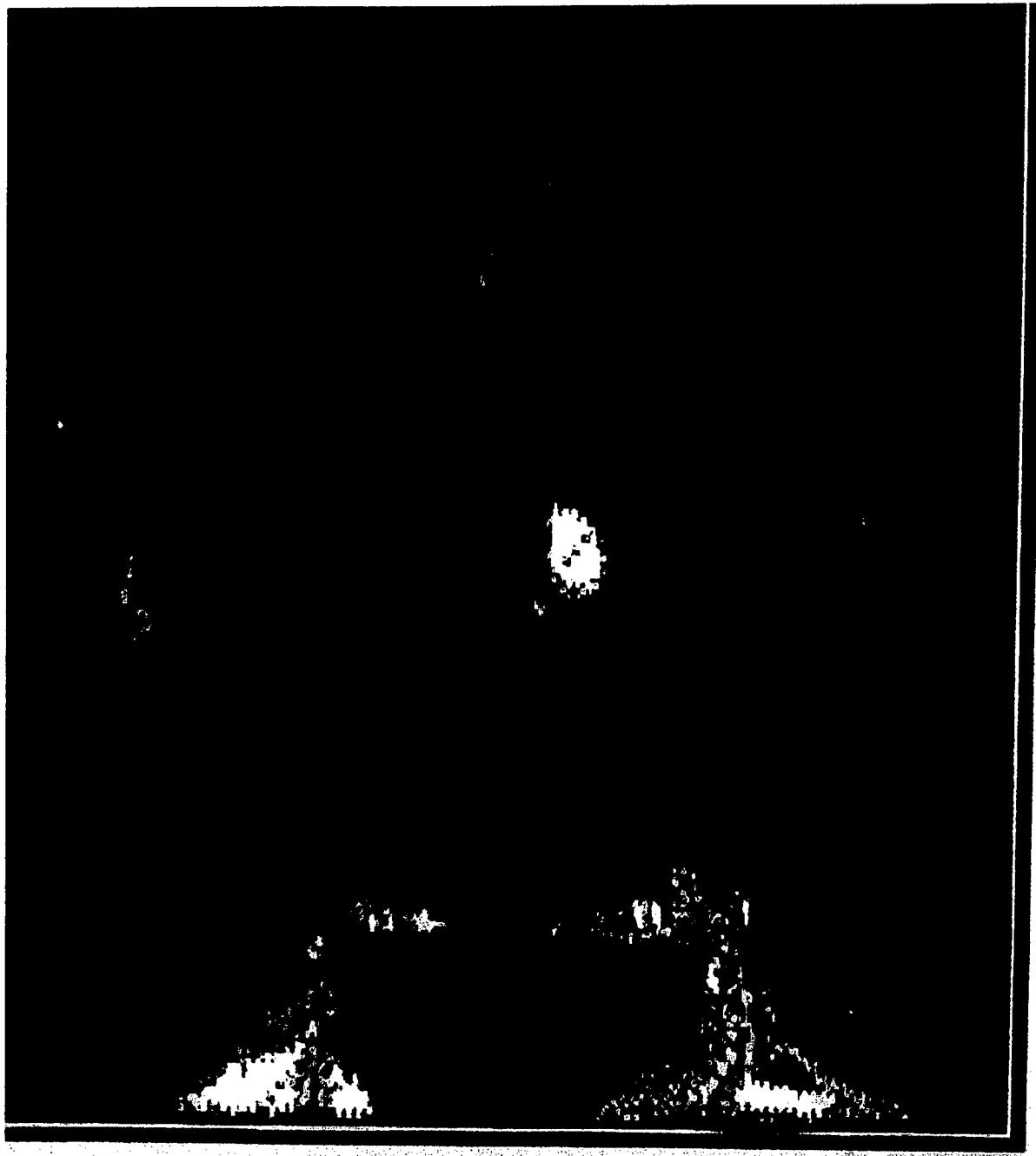


Figure 5.3-4. Conventional C-scan of Panel SHM-8

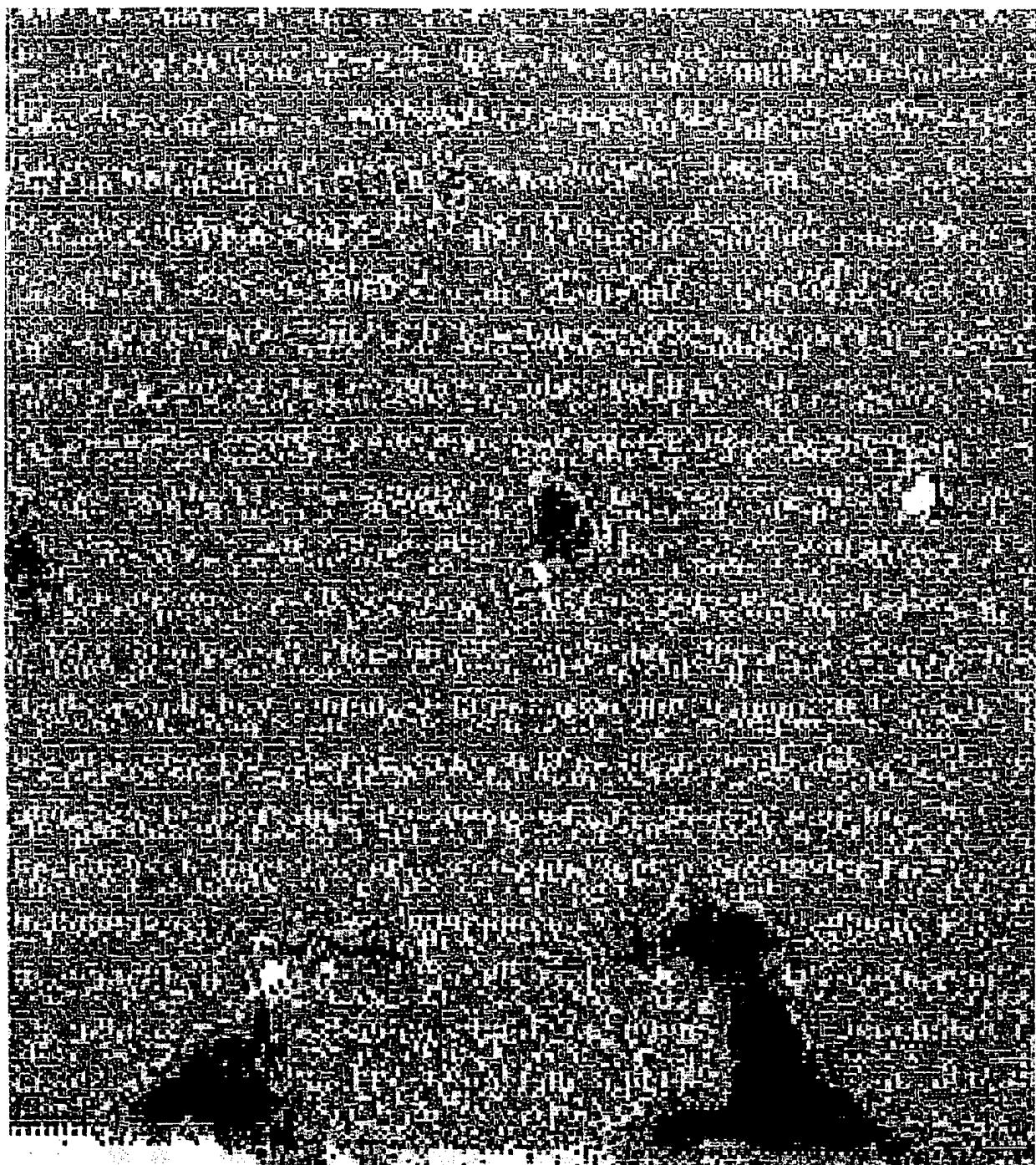


Figure 5.3-5. AirScan C-scan of Panel SHM-8

D950-10322-1

219



Figure 5.3-6. Rockwell Science Center LBU C-scan of Panel SHM-8

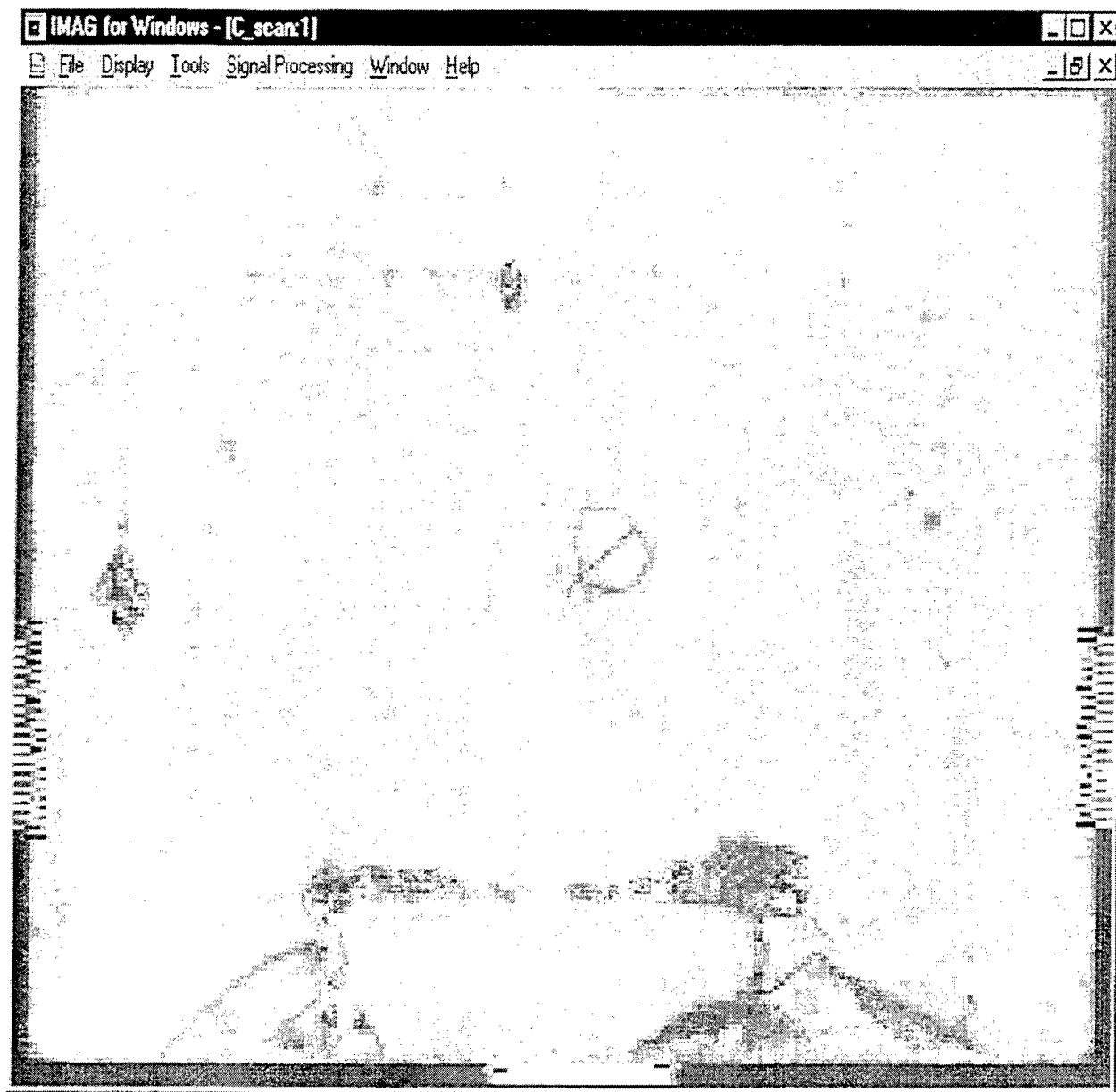


Figure 5.3-7. LUIS 747 C-scan of Panel SHM-8

At the time of this report, no information was available on the details of testing such as scan speed or setup time for the ultrasonic systems used. Only qualitative comparison of the images can be made. Visual comparison of the images shows that each method displays similar features of the panel.

Two LUIS data sets from Air Force studies of Boeing aircraft were made available for this report. The first was from a short study of the C-17. Figure 5.3-8 shows the LUIS C-scan image. No conventional data are available for comparison with this image.

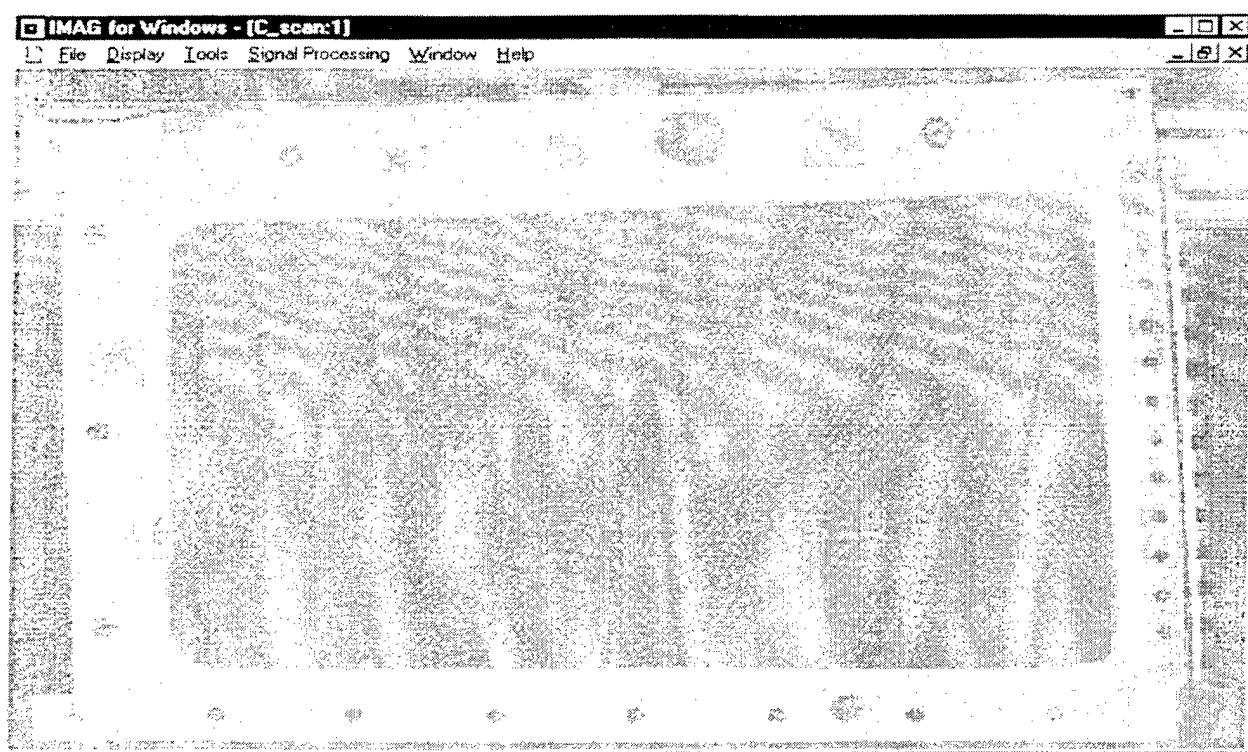


Figure 5.3-8. LUIS 747 C-scan C-17 part

The second set of LUIS data was taken as part of a large Air Force study of NDE data, which is currently underway. The study uses the left and right horizontal stabilizers from a US Marine Corps AV-8B. Since the stabilizers are too large to inspect completely in a single LUIS scan plan, each stabilizer was conceptually divided into a number of scan areas. Figure 5.3-9 shows a C-scan collage made from separate scans of the stabilizers.

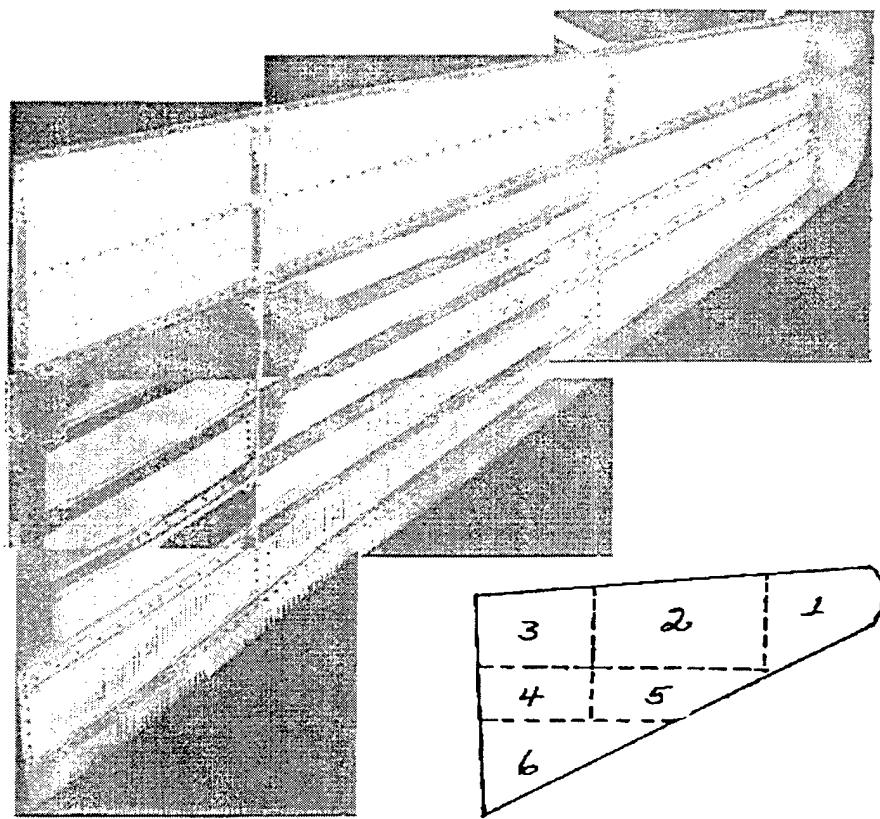


Figure 5.3-9. AV-8B stabilizer collage C-scan and scan plan

No conventional data are available for comparison to the AV-8 images. Current quality assurance guidelines in place at Boeing's St. Louis operation require only through-transmission ultrasonic inspection of the stabilizer skins before assembly.

6.0 SPECIAL STUDIES

Several specialized tests and studies were conducted as part of this contract. They are discussed in this section.

6.1 LUIS System Variability

Time features of ultrasonic pulse echo waveforms are relatively insensitive to variations in either the front face coupling or in the spectral content of the ultrasonic pulse. In contrast, amplitude features, such as signal attenuation, cannot be measured accurately in the presence of input pulse variability. While time features are useful for metallic structures with discrete defects, evaluation of composite structures with continuous property variations often requires precision amplitude measurements.

Amplitude measurements on systems with high input pulse variability may require careful normalization and spectral content correction algorithms. For conventional pulse echo ultrasound amplitude measurements, it is common practice to normalize the amplitude of echo signals to the front face amplitude to eliminate surface coupling variations (due to changes in acoustic impedance, roughness, and/or beam incidence angle) and to model both the frequency dependent signal attenuation and beam divergence by an empirical correction model, referred to as a DAC (distance amplitude correction). This approach depends on the assumption that the incident signal is highly repeatable, particularly in spectral content. Nonconventional signal generation, such as laser generation, will require different data reduction models if the variability of certain input pulse features is high.

In order to assess the initial pulse variability of LUIS, six 70mm x 70mm x 12mm solid hexahedral test panels were inspected over one face. The test panels are shown in figure 6.1-1.

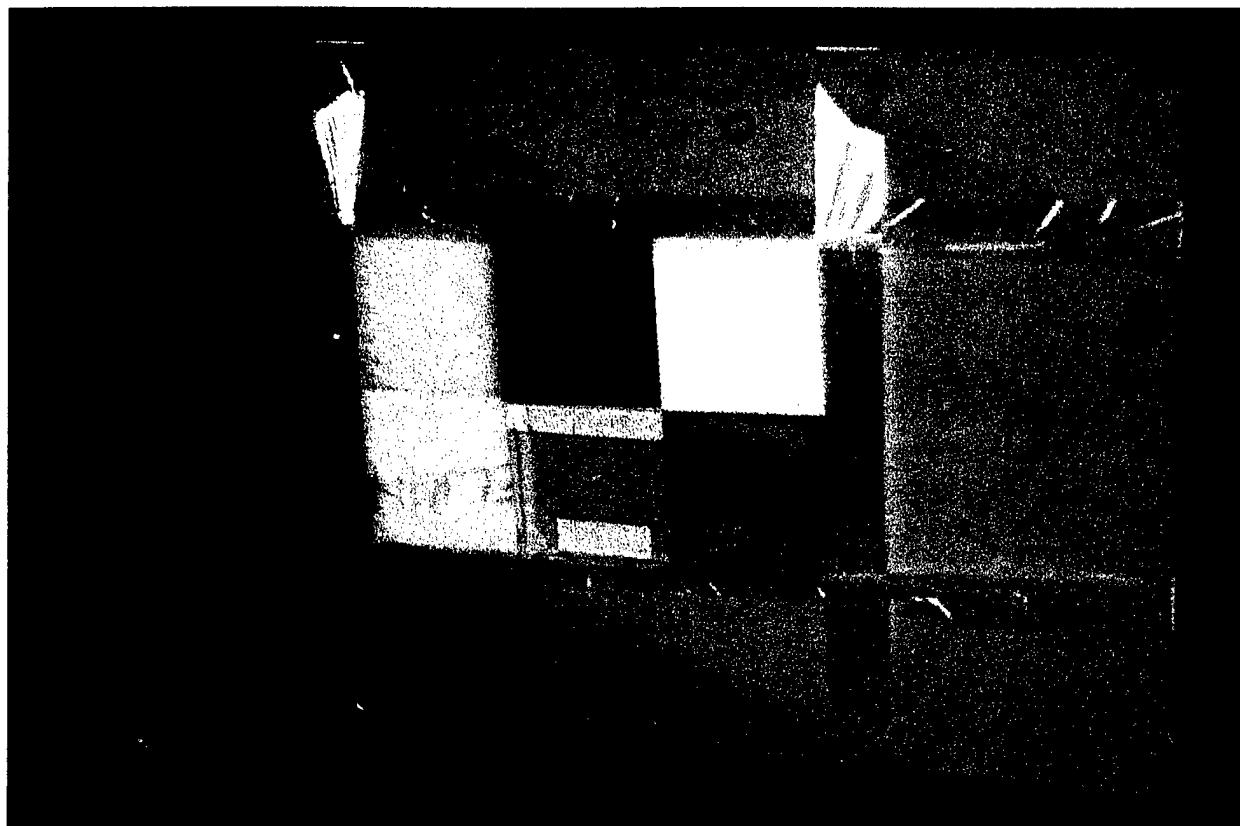


Figure 6.1-1. Variability Test Samples

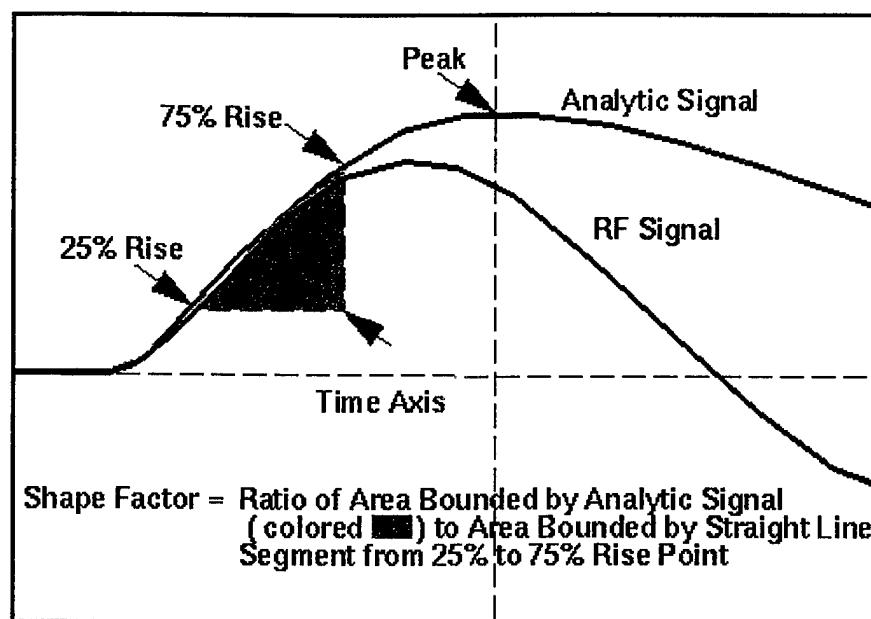


Figure 6.1-2. Shape Definition

The six panels are identified in sequence by material type: 001=Polypropelene, 002=ABS Plastic, 003=Teflon, 004=Delrin, 005=Plexiglass, and 006=Lexan. The test was designed to permit the determination of the variability of the initial ultrasonic pulse ("front face" response) for the ultrasonic imaging system being evaluated, and to partition that variability into point-to-point (i.e. surface condition dependent) and time-to-time (i.e. environmental and optical/electronic) variability components. Digitized full waveform RF data were collected for each material, incidence angle, and environmental condition. The filenames are provided in Table 6.1-1. The designations "cold", "warm" and "hot" do not refer to temperature, but rather the duration for which the LUIS system had been operating. "Cold" refers to a test conducted immediately after system switch-on and calibration in the morning, "warm" to a period after approximately four hours of operation, and "hot" to a test performed at the limit of the vendors recommended continuous operating period (about 11 hours).

The amplitude and shape of the initial pulses were determined by calculating the analytic signal (by standard Hilbert Transform convolution method) and applying well established feature extraction algorithms for peak detection and shape. The shape of the incident pulse's leading edge was defined by the ratio of the area under the interval from the 25% rise time to the 75% rise time to the area of the corresponding triangle (as if the leading edge were linear between these two points). This is illustrated in figure 6.1-2. This signal feature is intended to capture variations in the pulse spectral content.



Figure 6.1-3. Spatial Variation of Pulse Amplitude

Maps of the feature values over the inspected parts are provided in figures 6.1-3 and 6.1-4. These provide a check that the variations are representative of the measurement system's true variability, because they show variations which appear to be randomly distributed over the inspection areas.

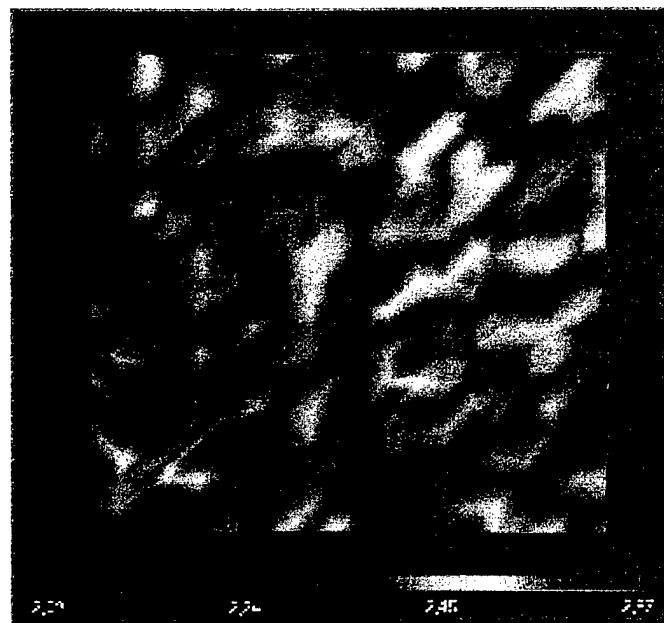


Figure 6.1-4. Spatial Variation of Shape Factor

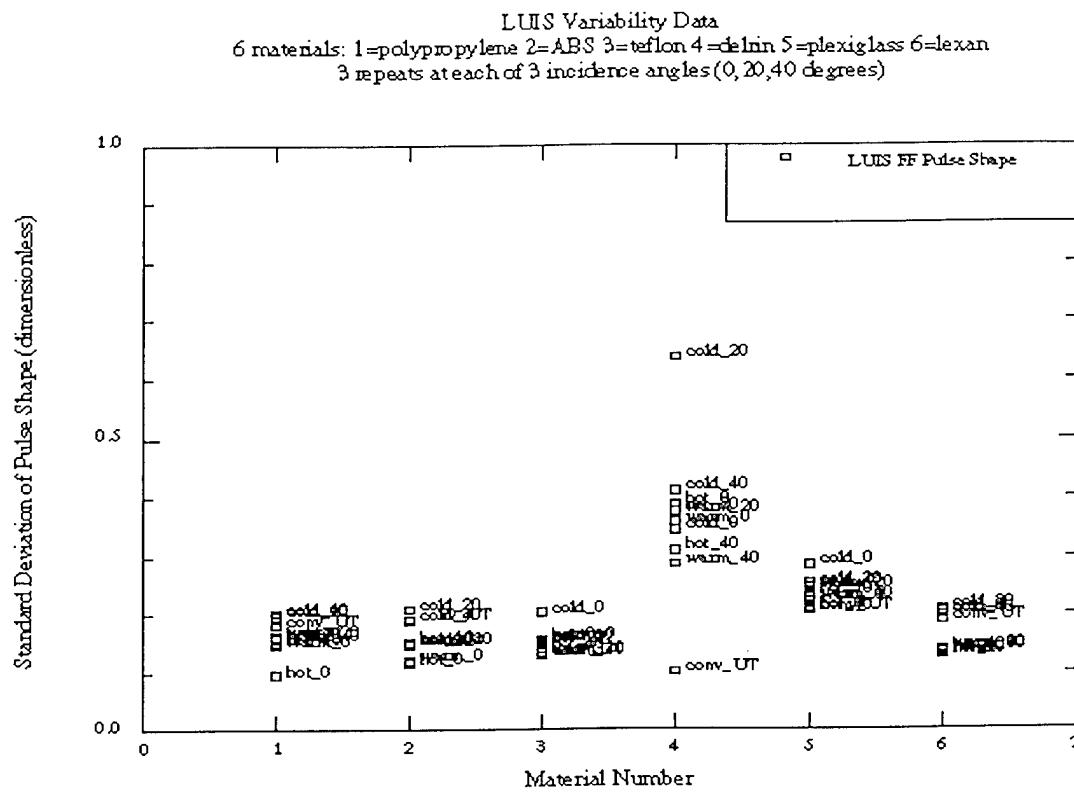


Figure 6.1-5. Variability in Pulse Shape

The results are summarized in figures 6.1-5 and 6.1-6. These figures include data from testing of the same six test panels in a Boeing conventional immersion scanner at normal incidence angle (labeled conv_UT). With the exception of the delrin panel, LUIS amplitude variability generally was similar to conventional ultrasonic expectations. A possible explanation is that the optical coupling variability of the test panel (i.e. thermoelastic property variation) was higher than acoustic variability (i.e. surface roughness). The LUIS data showed large variability in pulse shapes within a single test for cases where the laser system had been just started or was near the end of its operating cycle. In the worst case, LUIS demonstrated six times the variability in initial pulse shape of the corresponding conventional ultrasonic measurement system. Providing these operating conditions are avoided, LUIS' capability for measuring amplitude features appears to be on par with conventional ultrasonic systems.

LUIS Variability Data
 6 materials: 1=polypropylene 2=ABS 3=teflon 4=delrin 5=plexiglass 6=lexan
 3 repeats at each of 3 incidence angles (0,20,40 degrees)

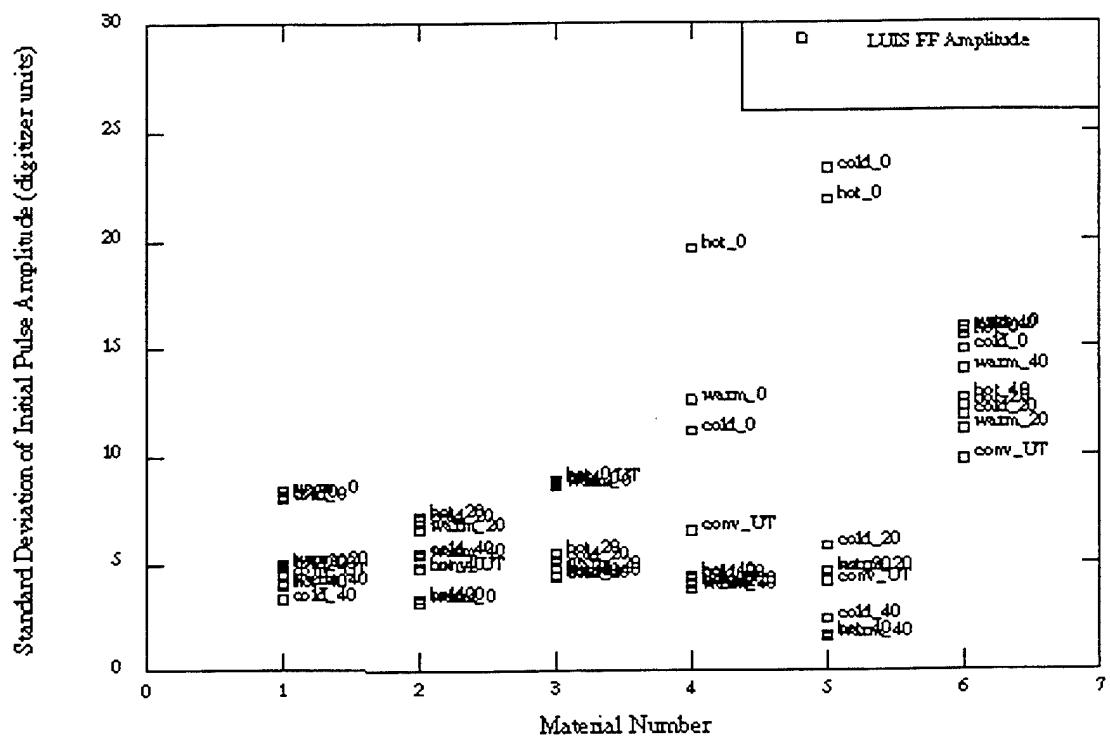


Figure 6.1-6. Variability in Pulse Amplitude

Table 6.1-1. Listing of Data Files and Conditions for Variability Study

| Filename | Material | Angle | Condition |
|--------------|----------|-------|-----------|
| 0065b001.wav | poly | 0 | cold |
| 00633001.wav | poly | 0 | warm |
| 00655001.wav | poly | 0 | hot |
| 00661001.wav | poly | 20 | cold |
| 00639001.wav | poly | 20 | warm |
| 0064f001.wav | poly | 20 | hot |
| 00667001.wav | poly | 40 | cold |
| 0063f001.wav | poly | 40 | warm |
| 00649001.wav | poly | 40 | hot |
| 00650001.wav | ABS | 20 | hot |
| 00668001.wav | ABS | 40 | cold |
| 00640001.wav | ABS | 40 | warm |
| 0064a001.wav | ABS | 40 | hot |
| 00656001.wav | ABS | 0 | hot |
| 00662001.wav | ABS | 20 | cold |
| 0063a001.wav | ABS | 20 | warm |
| 0065c001.wav | ABS | 0 | cold |
| 00634001.wav | ABS | 0 | warm |
| 0065d001.wav | teflon | 0 | cold |
| 00635001.wav | teflon | 0 | warm |
| 00657001.wav | teflon | 0 | hot |
| 00663001.wav | teflon | 20 | cold |
| 0063b001.wav | teflon | 20 | warm |
| 00651001.wav | teflon | 20 | hot |
| 00669001.wav | teflon | 40 | cold |
| 00641001.wav | teflon | 40 | warm |
| 0064b001.wav | teflon | 40 | hot |
| 0065e001.wav | delrin | 0 | cold |
| 00636001.wav | delrin | 0 | warm |
| 00658001.wav | delrin | 0 | hot |
| 00664001.wav | delrin | 20 | cold |
| 0063c001.wav | delrin | 20 | warm |
| 00652001.wav | delrin | 20 | hot |
| 0066a001.wav | delrin | 40 | cold |
| 00642001.wav | delrin | 40 | warm |
| 0064c001.wav | delrin | 40 | hot |
| 0065f001.wav | plexigl | 0 | cold |
| 00637001.wav | plexigl | 0 | warm |
| 00659001.wav | plexigl | 0 | hot |
| 00665001.wav | plexigl | 20 | cold |
| 0063d001.wav | plexigl | 20 | warm |
| 00653001.wav | plexigl | 20 | hot |

Table 6.1-1. Listing of Data Files and Conditions for Variability Study (Continued)

| Filename | Material | Angle | Condition |
|--------------|----------|-------|-----------|
| 0066b001.wav | plexigl | 40 | cold |
| 00643001.wav | plexigl | 40 | warm |
| 0064d001.wav | plexigl | 40 | hot |
| 00660001.wav | lexan | 0 | cold |
| 00638001.wav | lexan | 0 | warm |
| 0065a001.wav | lexan | 0 | hot |
| 00666001.wav | lexan | 20 | cold |
| 0063e001.wav | lexan | 20 | warm |
| 00654001.wav | lexan | 20 | hot |
| 0066c001.wav | lexan | 40 | cold |
| 00644001.wav | lexan | 40 | warm |
| 0064e001.wav | lexan | 40 | hot |

6.2 Determination of Modulation Transfer Function for LUIS

This inspection was designed to permit the measurement of the edge response function and the subsequent computation of the line spread function and modulation transfer function of the ultrasonic imaging system being evaluated.

A graphite step wedge with four steps was inspected from the flat side in pulse echo mode. RF data from the digitized full waveform was captured for analysis. Figure 6.2-1 shows the C-scan generated from the data.

Calculation of the line spread function and subsequent modulation transfer function (MTF) provide for an accurate assessment of image resolution as distinct from image sensitivity. By scanning a discrete reflector edge and normalizing the image response across the edge (averaged laterally), the line spread function is estimated. The discrete Fourier transform of the derivative of the edge response is the MTF. MTF image resolution is typically stated as "X line pairs per millimeter at Y percent modulation". Figures 6.2-2 shows a typical edge response, it shows density along a line segment sampled averaged laterally over the width of the step wedge. Figure 6.2-3 shows the MTF for each step. The LUIS scan of the graphite steps provided an MTF resolution of approximately 1 line pair per millimeter at 10% modulation.

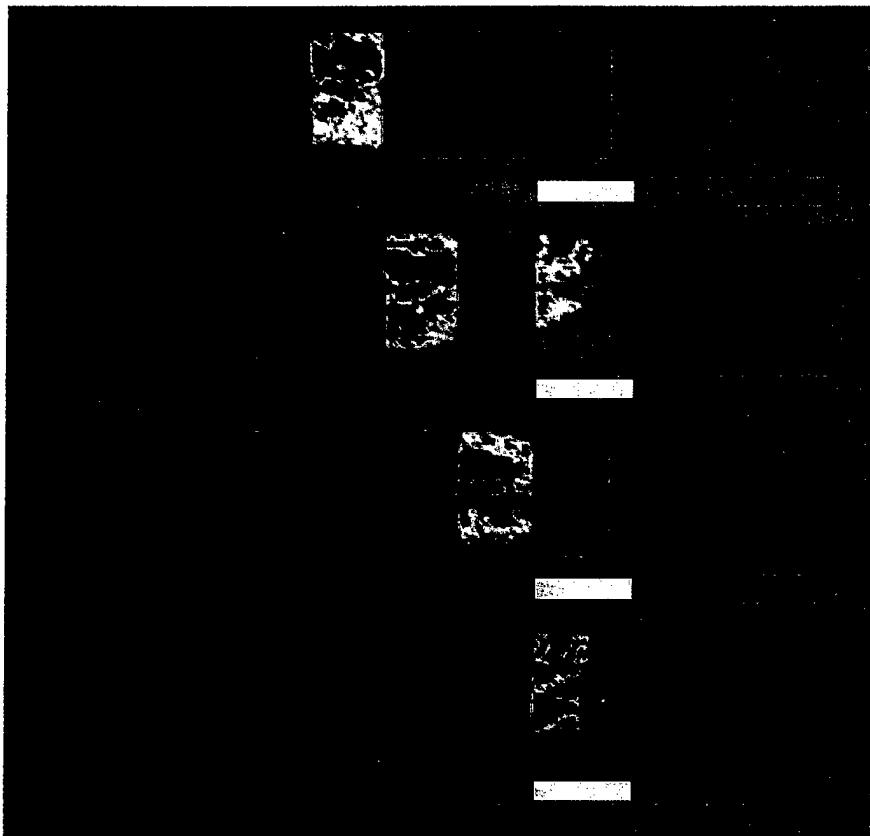


Figure 6.2-1. C-scan views of gated echo amplitude at each of four steps in graphite step wedge

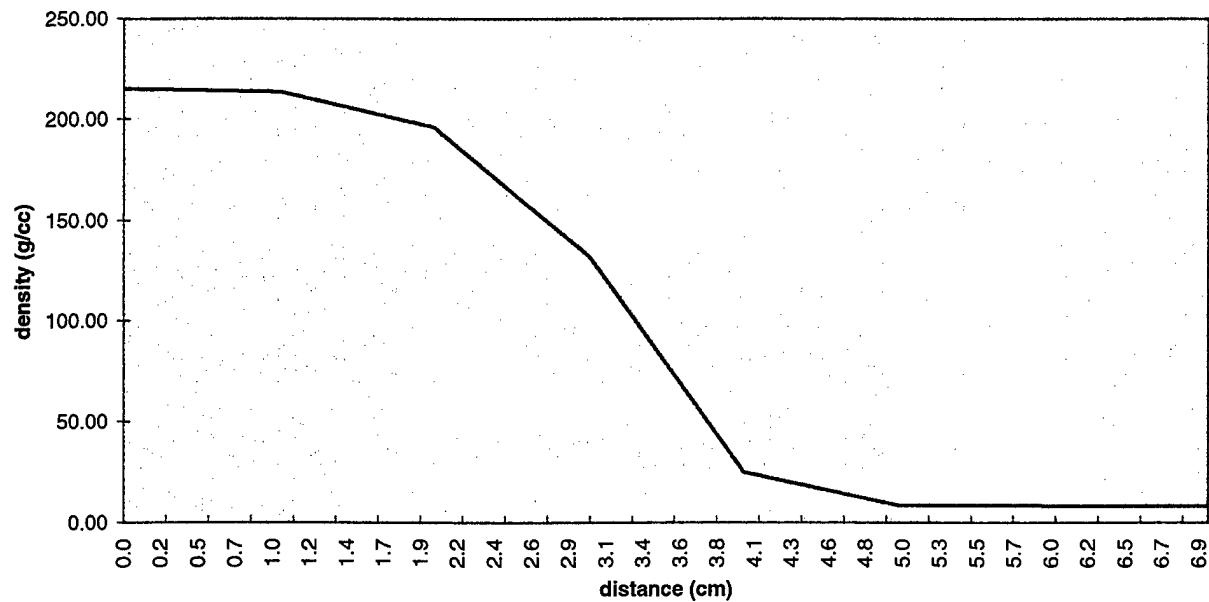


Figure 6.2-2. LUIS ultrasonic edge response from back face echo

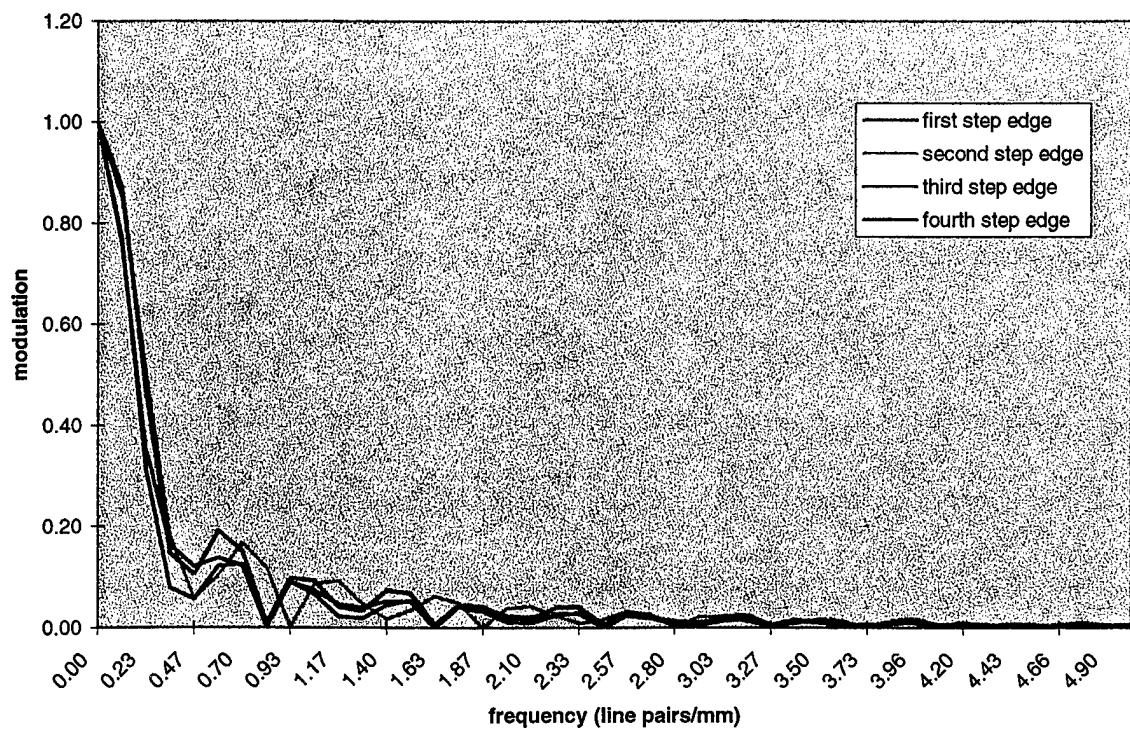


Figure 6.2-3. Modulation Transfer Function Measurement for each of four steps

6.3 Production Testing Simulation

To simulate production testing and to evaluate the repeatability of defect detection and imaging, a single part was inspected multiple times. The 7J7 test panel discussed in section 5.1.4 was chosen for this study. This study does not report on comparisons between LUIS and conventional inspections for the 7J7 panel, those comparisons are in section 5.1.4. In this study, the panel was set up in the fixture for LUIS scanning. It was scanned, removed, replaced into the fixture and scanned over the same portion of it again, as if it were a second identical part. This was done a total of five times, simulating the testing of five such panels. This allowed evaluation of two characteristics of the LUIS. The first of these is the time taken for both recurring and non-recurring activities associated with each of the scan events.

6.3.1 Time Evaluation

The time taken to scan the selected portion of the panel was as follows:

1. 8 minutes--- To set the part up on the cart.
2. 6 minutes--- To fill in the ME (Material Editor).
3. 13 minutes--- To fill in the PSE (Part Setup Editor).
4. 20 minutes--- To fill in the APE (Acquisition Parameters Editor). In addition to other steps this is where the damage threshold of the part to laser energy is determined. Two inspectors are required to accomplish this.
5. 4 minutes--- To fill in the IPE (Inspection Plan Editor). A large and or a complex part shape could increase this time by a factor of 4 to 6.
6. 5 minutes--- To fill in the IPC (Inspection Process Control).
7. 59 minutes--- Time to scan this particular portion of this part.

Total time needed to set up and inspect this part was 1 hour and 55 minutes.

Items 3 through 6 are non-recurring for the same part/portion. Adding up the time required for items 1, 2, and 7 yields the total time needed for each subsequent inspection of the same part of 1 hr and 9 minutes. This length of time is typical of the setup time required for parts inspected on this contract.

As a comparison the following set up times are typical for a conventional bubbler used at Boeing for inspecting 195 sq. ft. 777 skin panels. The panels are inspected in 5 segments. A manual "teach" to describe the part to the bubbler system would require 15 minutes for each segment or 75 minutes total for each scan of an example skin panel. To speed up the production process and avoid this 75-minute setup for each panel, the part geometries were extracted once from a CAD data set and then permanently saved in the system memory. This process required about 16 hours per part type. Once the geometry data are available, the operator enters the part type and a serial number into a file header and position the bubbler at a referenced start point to begin scanning.

Times required for painting and other processes are not included in the LUIS figures. However, times required for several adjunct operations were noted over the course of the contract tasks. A typical time for painting a 3 X 5-foot part was about 45 minutes. Hand stripping took anywhere from minutes to hours depending on the complexity and roughness of part surfaces. No attempt was made to optimize these times. Mechanization of painting and stripping processes would likely result in increases in speed. The time to transfer collected data files from the acquisition system to the analysis system was also noted. A typical 600-MB file required about 12 minutes for transfer.

6.3.2 Repeatability Evaluation

The second characteristic revealed by this study is the consistency between successive scans of the same part. The degree of consistency may be used as a measure of system repeatability. Amplitude C-scan images from the five scans are shown below as figures 6.3-1 through 6.3-5. Each of the images is taken from one of each of the five full wave data sets acquired with the

LUIS. The images are all processed from the data with the same time and amplitude gates, and with no filtering or other signal processing. They appear to be remarkably equivalent.

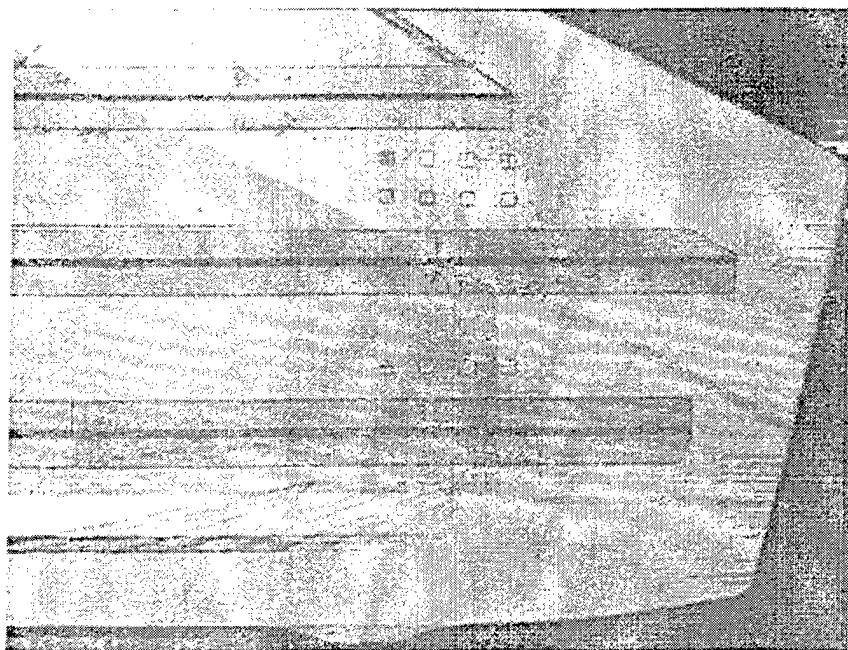


Figure 6.3-1. First scan

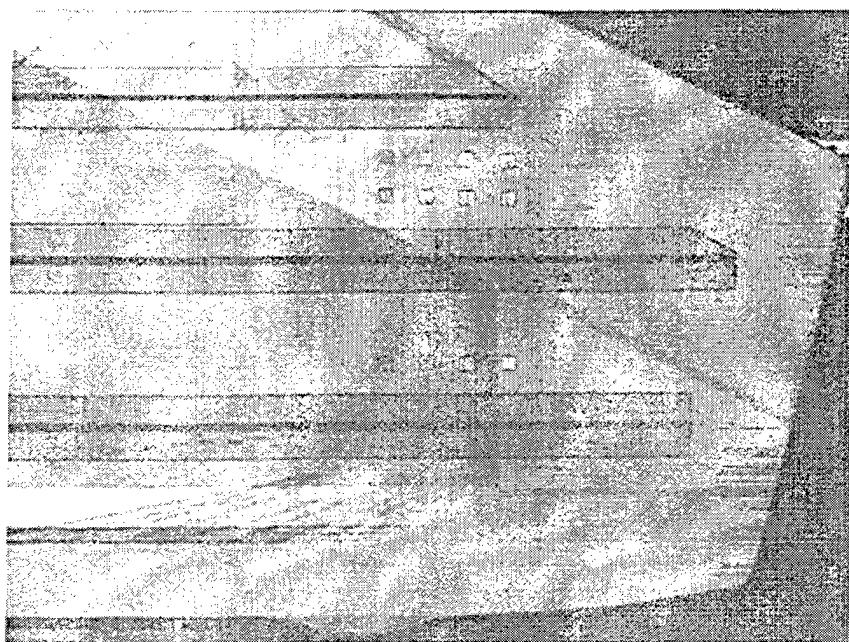


Figure 6.3-2. Second scan

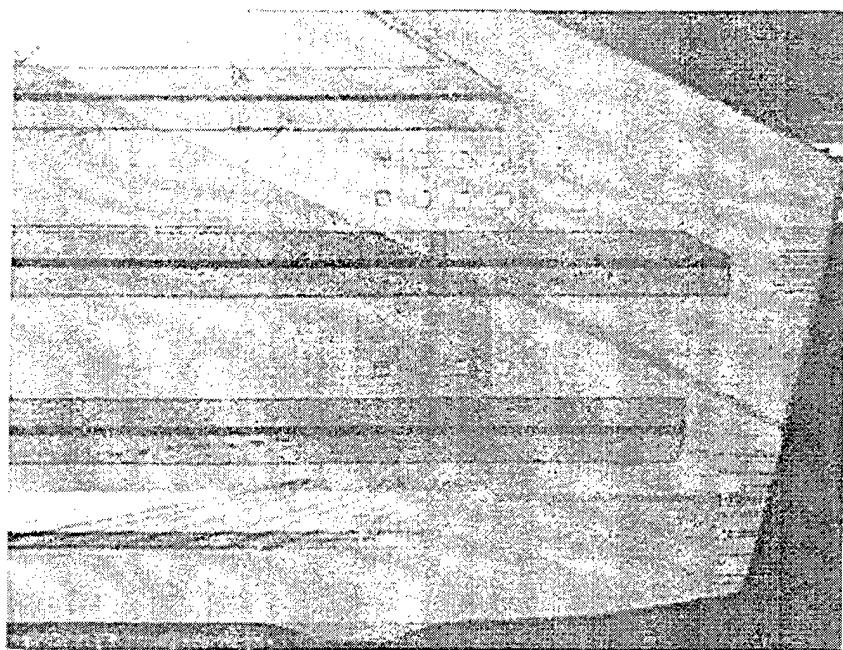


Figure 6.3-3. Third scan

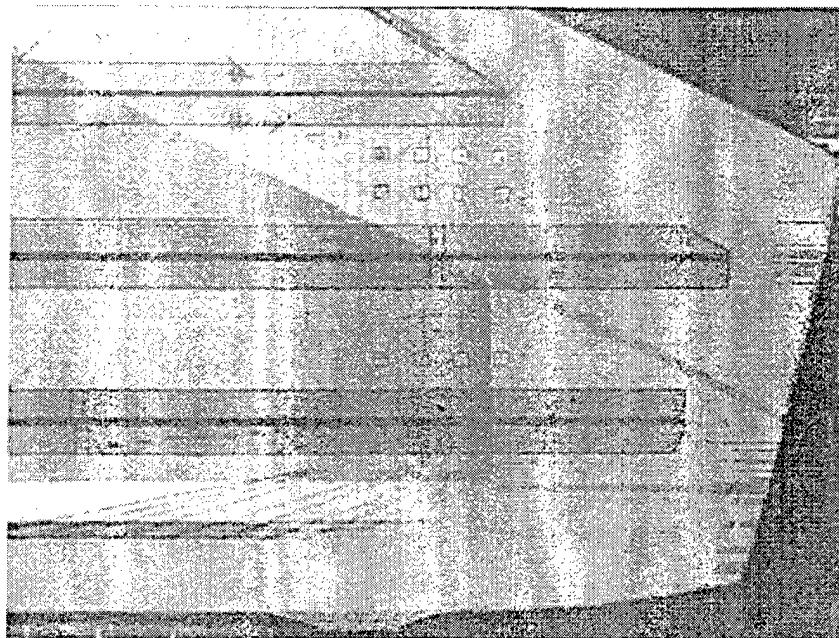


Figure 6.3-4. Fourth scan

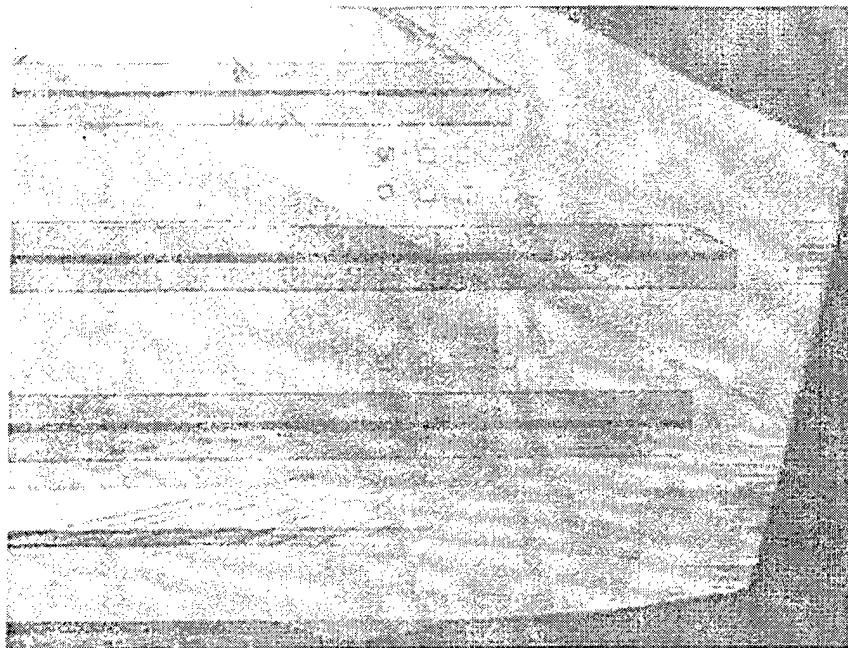


Figure 6.3-5. Fifth scan

The eye can pick out some differences in the images in figures 6.3-1 through 6.3-5, but further processing can assist this evaluation. The U.S. Government program NIH Image was used to evaluate the LUIS data images in the figures. NIH Image uses a 256 level gray scale image. The software version employed for this evaluation uses a value of 0 to indicate white and a value of 255 to indicate black. NIH Image provides the ability to count the number of pixels in each gray scale level. This count was taken for each of the 5 images and the gray scale count for each is plotted in Figure 6.3-6. Figure 6.3-6 shows that the gray scale counts are very similar to one another. Although the gray scale of NIH Image extends from 0 to 255, the LUIS images included gray scale values only up to 134 as seen in Figure 6.3-6. This means that no data were taken that were represented by very dark pixels.

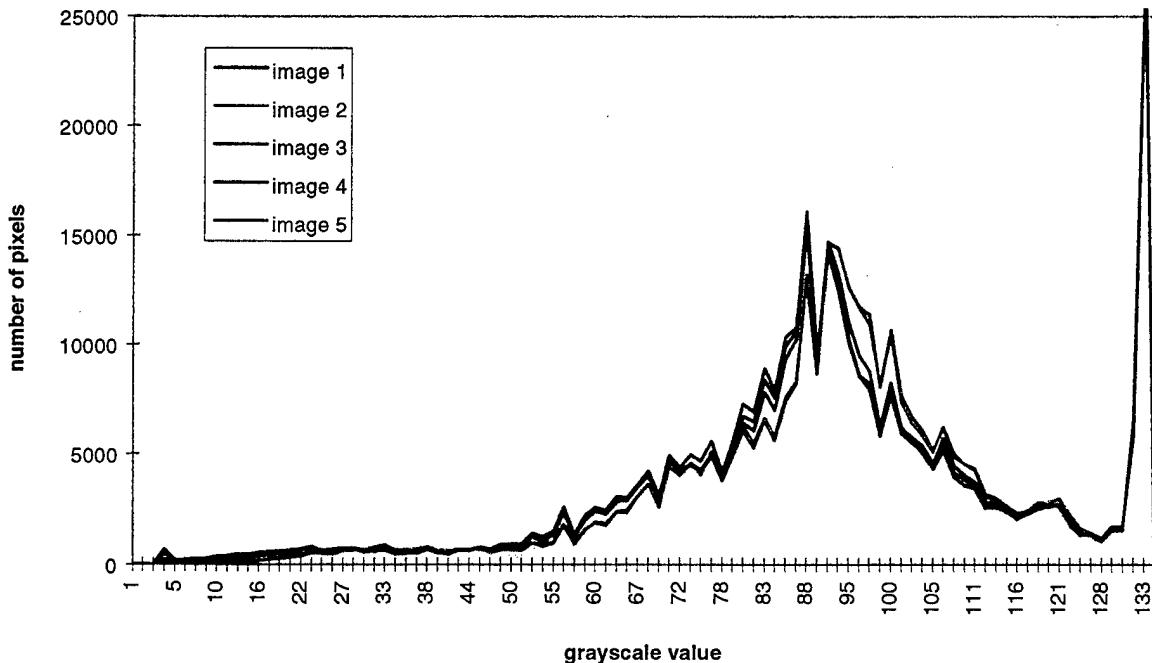


Figure 6.3-6. Histogram of Pixel Gray Scales for Figures 6.3-1 through -5

The large peak at 133 is due to the large number of pixels representing the dark background outside of the scanned part in the images. Table 6.3-1 shows the mean, standard deviation and range of gray scale counts for each image. These comparisons show that the data collected were remarkably similar, at least in terms of the response for raw numbers of pixels. While this fact is interesting, it is meaningless unless the comparison is among corresponding pixels in each image.

Table 6.3-1. Gray Level Ranges for LUIS Images

| image | gray level mean | gray level std dev | min gray level | max gray level |
|-------|-----------------|--------------------|----------------|----------------|
| 1 | 90.39 | 24.75 | 3 | 198 |
| 2 | 92.0 | 23.44 | 3 | 187 |
| 3 | 92.7 | 23.76 | 3 | 192 |
| 4 | 90.26 | 25.21 | 3 | 196 |
| 5 | 90.65 | 25.29 | 3 | 202 |

NIH Image revealed that each LUIS image had exactly equivalent dimensions and number of pixels. A basic comparison of the C-scan images was made by finding the pixel by pixel difference between the images. Using NIH Image functions, the differences between the images were

difference between the images. Using NIH Image functions, the differences between the images were computed and displayed using the same gray scale as the original images. These difference images are shown in figures 6.3-7 through 6.3-16. The captions of the figures indicate the original images compared.

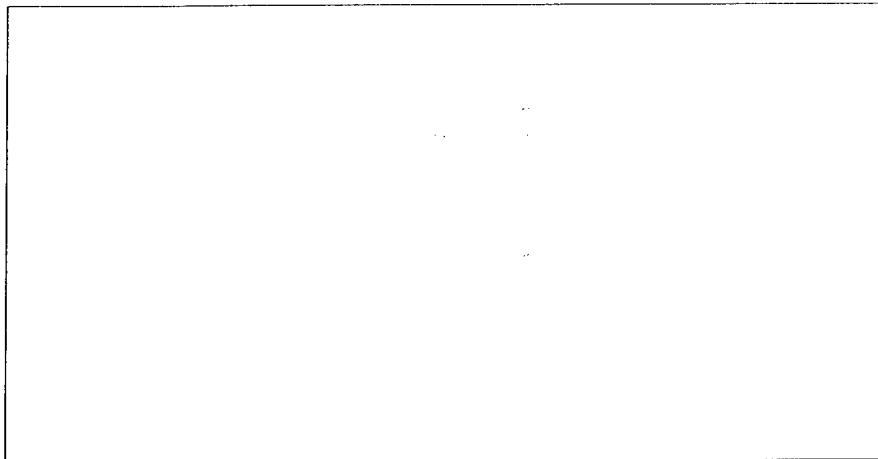


Figure 6.3-7. Pixel Gray Scale Difference between Figures 6.3-1 and 6.3-2

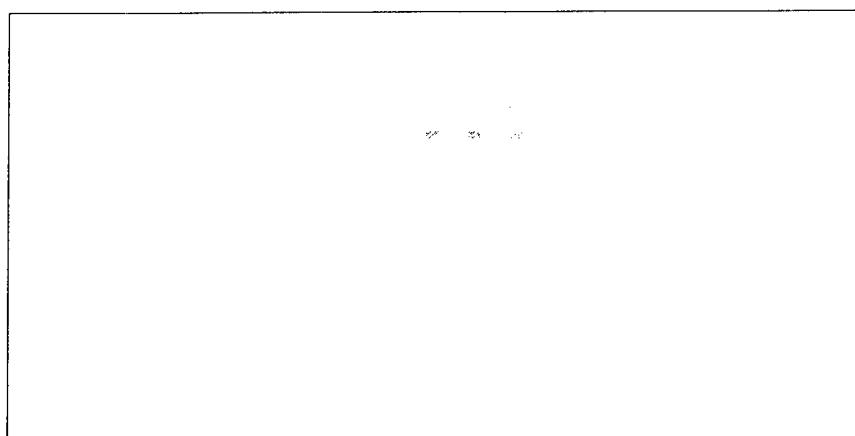


Figure 6.3-8. Pixel Grayscale Difference between Figures 6.3-1 and 6.3-3

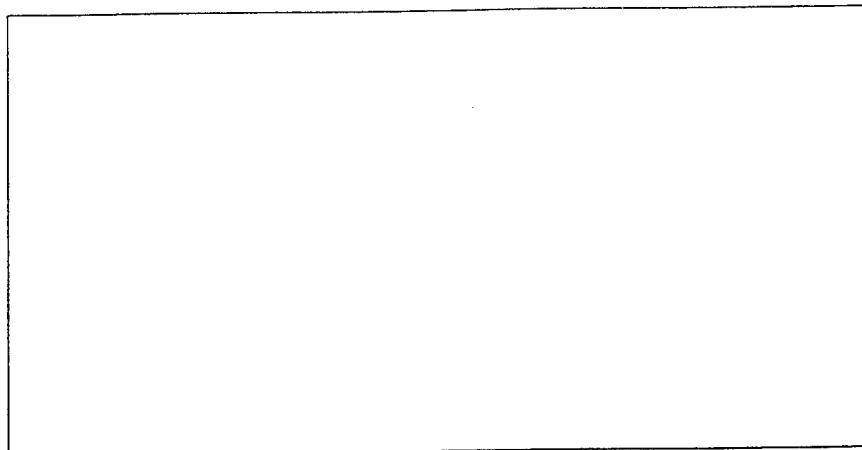


Figure 6.3-9. Pixel Gray Scale Difference between Figures 6.3-1 and 6.3-4

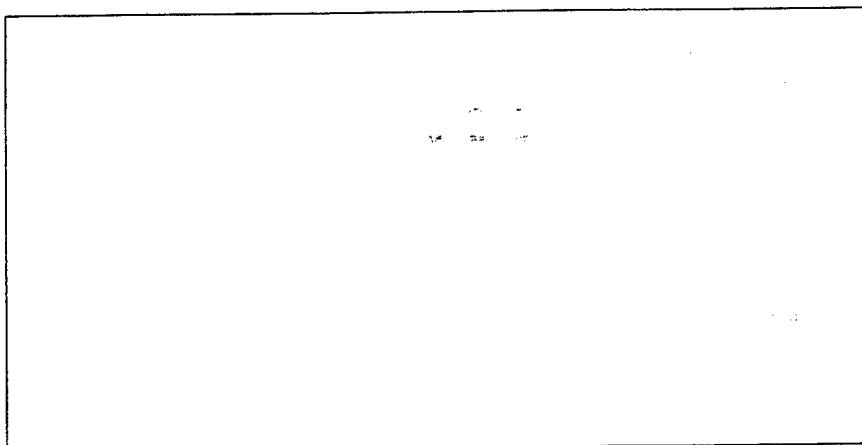


Figure 6.3-10. Pixel Gray Scale Difference between Figures 6.3-1 and 6.3-5

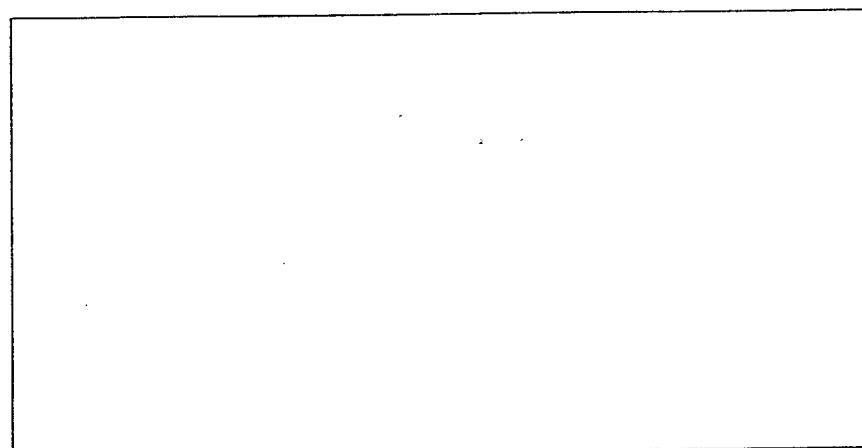


Figure 6.3-11. Pixel Gray Scale Difference between Figures 6.3-2 and 6.3-3

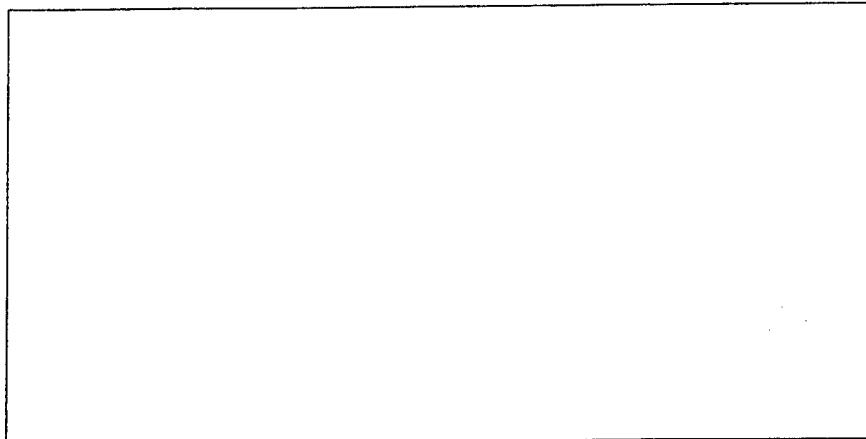


Figure 6.3-12. Pixel Gray Scale Difference between Figures 6.3-2 and 6.3-4

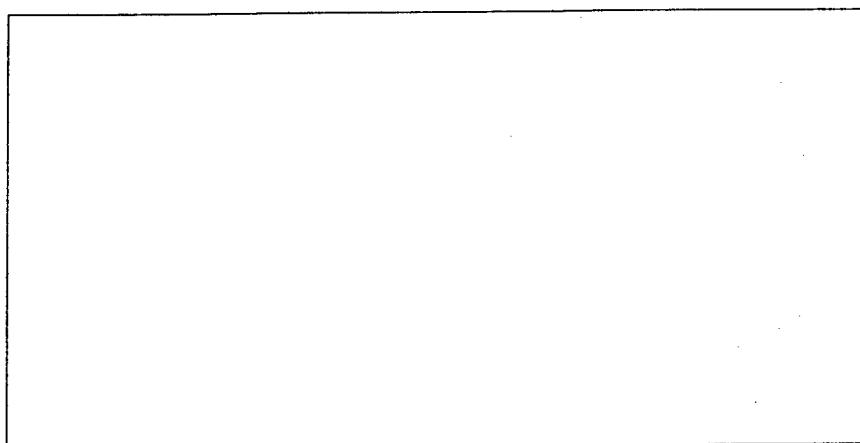


Figure 6.3-13. Pixel Gray Scale Difference between Figures 6.3-2 and 6.3-5

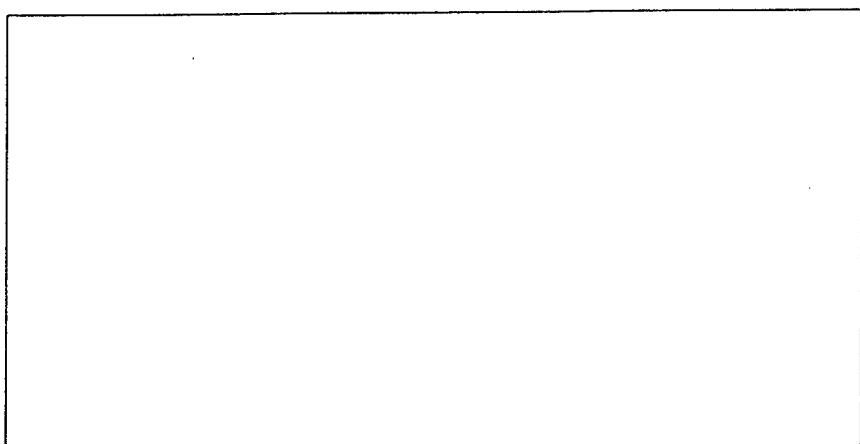


Figure 6.3-14. Pixel Gray Scale Difference between Figures 6.3-3 and 6.3-4

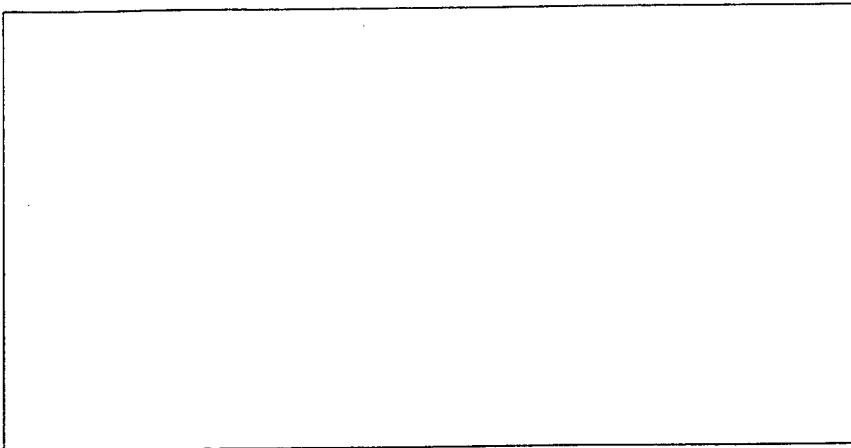


Figure 6.3-15. Pixel Gray Scale Difference between Figures 6.3-3 and 6.3-5

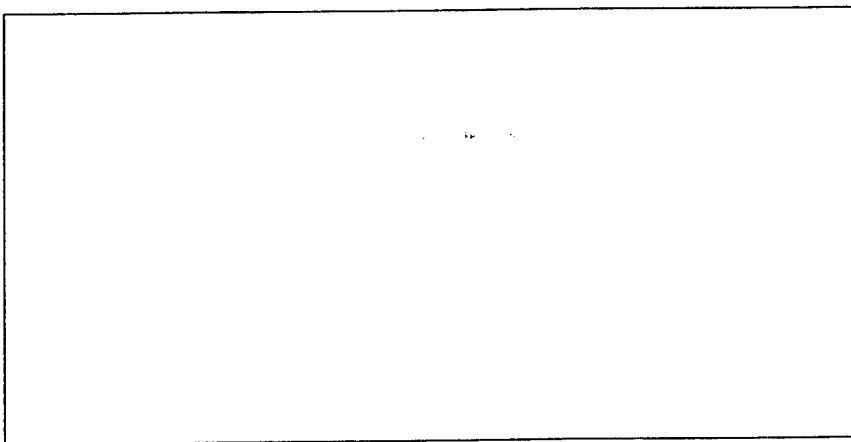


Figure 6.3-16. Pixel Gray Scale Difference between Figures 6.3-4 and 6.3-5

The very light gray images in the figures indicate only small differences in the equivalent pixels for the data from one scan to the next. Table 6.3-2 indicates pixel count information for the differences between images. The statistics on the difference images are all very similar.

Table 6.3-2 . Gray Level Ranges for Differences between LUIS Images

| difference image | gray level mean | gray level std dev | min gray level | max gray level |
|------------------|-----------------|--------------------|----------------|----------------|
| 1-2 | 1.47 | 3.69 | 0 | 88 |
| 1-3 | 1.57 | 4.11 | 0 | 121 |
| 1-4 | 2.61 | 4.64 | 0 | 90 |
| 1-5 | 2.53 | 4.97 | 0 | 98 |
| 2-3 | 2.5 | 4.45 | 0 | 114 |
| 2-4 | 4.01 | 5.5 | 0 | 95 |
| 2-5 | 3.81 | 5.54 | 0 | 91 |
| 3-4 | 3.86 | 5.26 | 0 | 85 |
| 3-5 | 3.63 | 5.2 | 0 | 85 |
| 4-5 | 2.21 | 4.16 | 0 | 91 |

A comparison histogram is shown in Figure 6.3-17. It shows that the vast majority of pixels in the difference images are at the lowest gray scale levels. Numerical analysis of the data shows that 72% of the pixels in all 10 different images have a gray scale level of 0. These white pixels in the difference images correspond to zero difference between pixels in the base images compared. Thus, 72% of all the pixel by pixel comparisons showed no difference. 90% of the difference image pixels have a gray scale level of 5 or under. This means that 90% of the base image pixel by pixel comparisons show a gray scale difference of no more than 5/256, which is under 2%. 99.5 % of pixel comparisons show a gray scale difference of 7% or less. Based on these values, the total differences between the LUIS responses for the 5 scans are clearly very small, on the order of a few percent. This small difference in system response between scans indicates that system variability is small.

Pixel Count per Grayscale in Difference Images

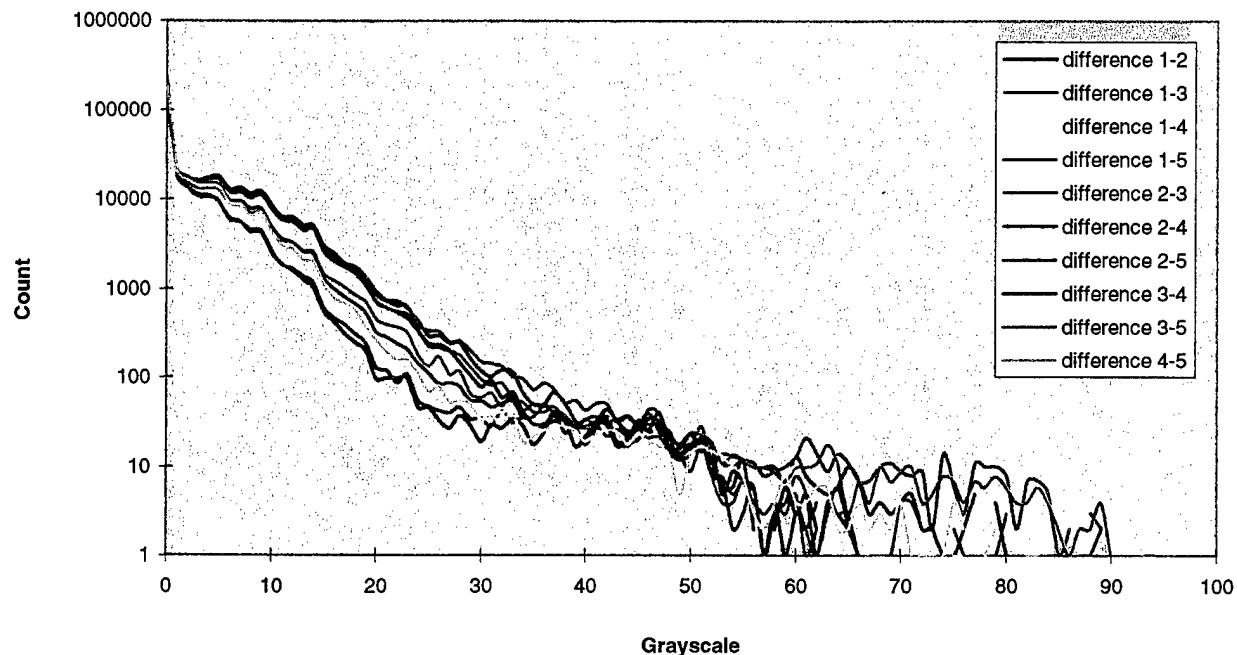


Figure 6.3-17. Histogram of Pixel Gray Scale Differences

While total variation in system response is important, the variation in system sensitivity to features of interest (“flaws”) is much more important. That is, a user needs to know that the LUIS will provide detection of the same feature each time a part is inspected. Within amplitude C scan images, detection is dependent on spatial contrast. To measure the variation in feature detection, the change in contrast in the 5 images was evaluated for a particular feature. The feature chosen is indicated in figure 6.3-18. This insert showed a wide range of pixel value representation in the 5 datasets. As seen in the image differences in figures 6.3-7 through 6.3-16, it is one of the features that appeared most frequently after image comparison.

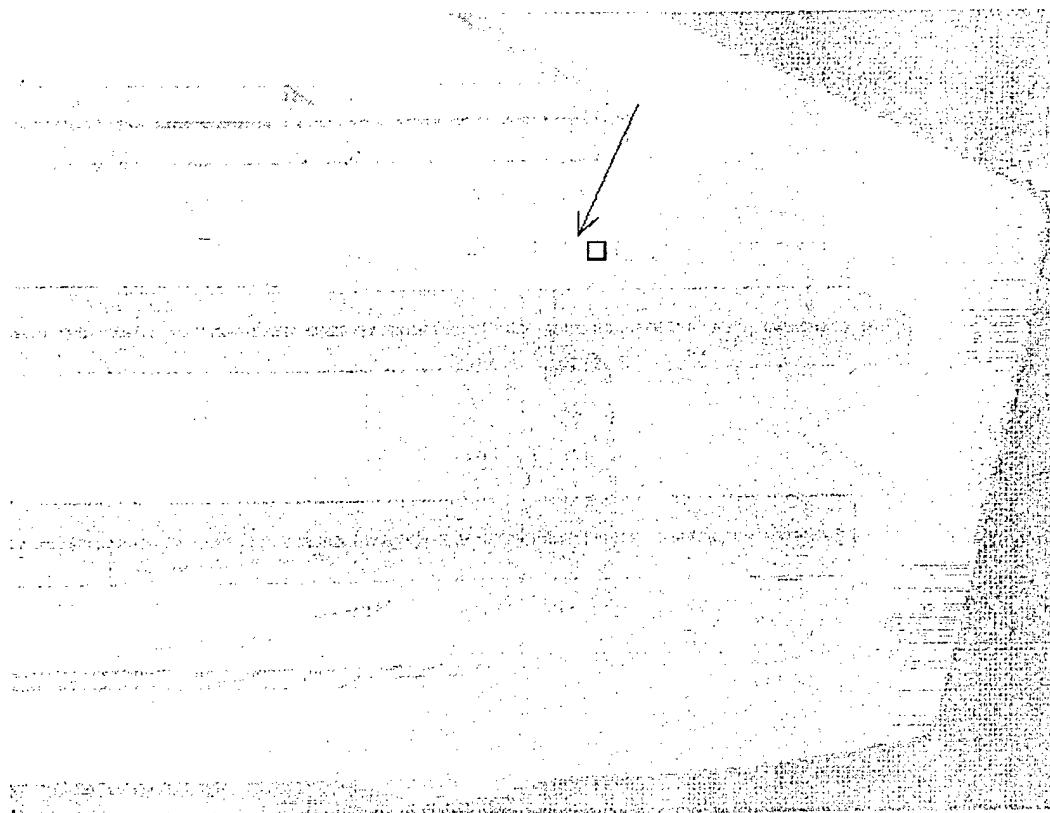


Figure 6.3-18. Contrast Comparison Feature

Again using NIH Image, the average gray scale level of the pixels in the feature was measured and compared to the average gray scale level of an area of the same size immediately to the right of the feature. The average gray scale of the feature and comparison areas are shown in Table 6.3-3.

Table 6.3-3. Average Gray Scale Values

| test number | Feature Average Gray Scale | Comparison Average Gray Scale | % Difference |
|-------------|----------------------------|-------------------------------|--------------|
| 1 | 96.15 | 90.6 | 6.1 |
| 2 | 75.96 | 93.74 | 19 |
| 3 | 54.33 | 94.23 | 42 |
| 4 | 88.28 | 91.17 | 3.1 |
| 5 | 59.9 | 91.93 | 53 |

The average gray scale value in the comparison area changes very little from scan to scan. The difference is only a few percent as discussed above. The gray scale value for the feature changes from scan to scan by range of almost 200%. The difference between the average gray scale in the feature and in the comparison area ranges from a low of 3% to a high of 53%. This quantifies the fact apparent to the eye when looking at the scan images in Figures 6.3-1 through 6.3-5, there is a marked difference in feature contrast from one scan to the next. It is interesting that the variability in contrast is mainly in the system response to the insert. It may be speculated that the increase variability for the insert is caused by the saturation of the laser-ultrasonic signal at the insert. If the laser-ultrasonic response of an insert is near saturation of the digitizer or of the gate used to produce the C-scan image, the shot-to-shot variability of the generation and detection lasers will cause the pixels to "switch" from a saturated to a non-saturated states (and vice-versa). Comparing images between saturated and non-saturated states would produce a sharp variation in the contrast between images.

While some amount of variation is present in the total LUIS process of data acquisition, based on all results shown here, the system repeatability appears adequate.

6.4 Inspection of Metal Parts

Although the main focus of the contract was on composite parts, a few specialized metal parts were inspected with the LUIS to explore possible niche uses of the system and to gain some understanding of methods needed to inspect metal parts with this LBU system. Very little effort was expended on metal parts. Metal parts were included in the LUIS test sequence to gain a simple understanding of whether metal objects could be easily inspected with the LUIS, to understand the best way to prepare metal parts for LUIS inspection and to compare LUIS data on specialized metal parts to data from other systems.

An Inconel metal alloy rocket nozzle being developed at the Rocketdyne division of Boeing was inspected to evaluate the usefulness of the LUIS for that application. A photo of the rocket nozzle is shown in figure 6.4-1. A portion of the nozzle has been cut away to allow scanning of the inside surface. The inspected surface contains a variable radius of curvature ranging from about 23 mm to about 37 mm. The adjoining LUIS scan of the inside of the nozzle clearly shows the cooling channels which are on backside of the surface that was scanned.

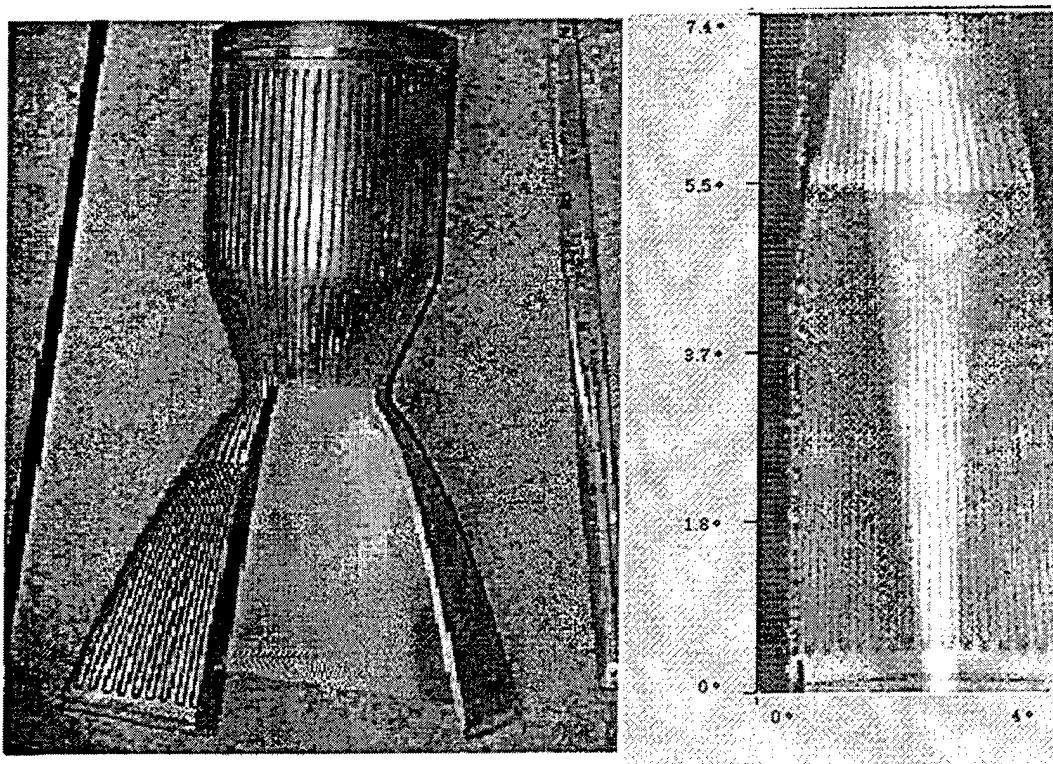


Figure 6.4-1. Rocket Nozzle Photograph and LUIS scan

As a comparison to the typical LUIS scan of this part, figure 6.4-2 shows a scan from another LBU system. The Rockwell Science Center has spent 10 years investigating the capabilities of LBU and has developed a very flexible, brassboard-type laboratory LBU system. The same rocket nozzle was scanned at this LBU laboratory. The nozzle was painted and inspected using a 10.6 um CO₂ generation laser and a long pulse 1.064 um Nd:YAG detection laser. The Rockwell Science Center LBU image resolution is 200 x 345 pixels and smaller laser spot size was used than on LUIS. This is somewhat greater resolution than available from the fixed resolution of the LUIS as is evident from comparing the images. This difference points out the desirability of designing LBU systems to allow easy changes in resolution and other system parameters. It is important to remember that LUIS parameters such as spot size were specified values and do not represent fundamental limitations on LBU technology.



Figure 6.4-2. Rockwell Science Center LBU scan of rocket nozzle

A titanium nozzle seal for the F-22 program was inspected to evaluate whether LBU can provide faster measurement of part thickness that is needed as feedback in the chemical milling process used for manufacturing the part. The current method uses a handheld ultrasonic system that requires several days of effort to create a detailed map of part thickness. Figure 6.4-3 shows a typical titanium seal for F-22.

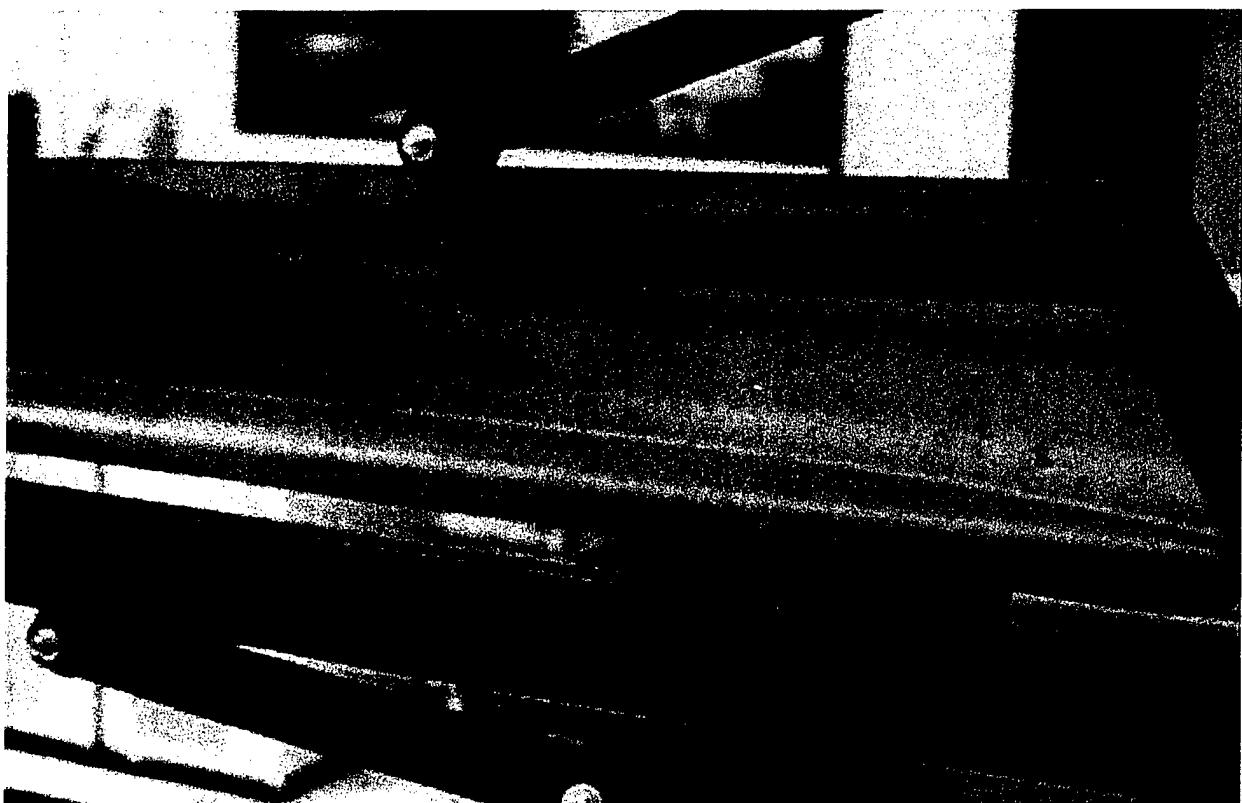


Figure 6.4-3. F-22 Titanium Seal

The LUIS data from the F-22 titanium seal was processed to create a mapping of the thickness of the part. The mapping is shown in Figure 6.4-4.

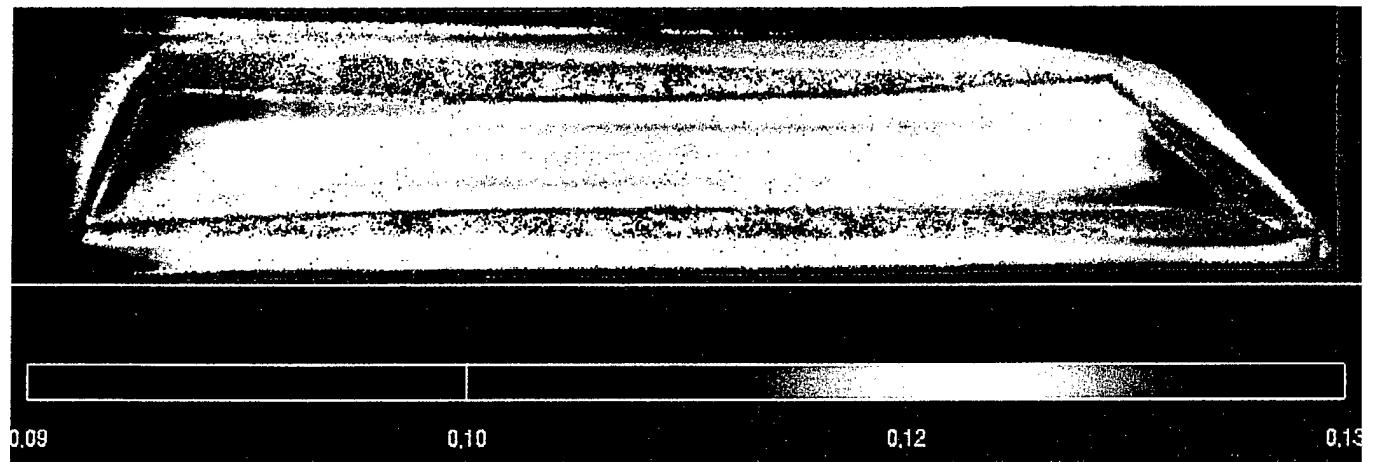


Figure 6.4-4. F-22 Titanium Seal Thickness Mapping

The setup and scanning of this part took about 1 ½ hours. The data were converted into a different format via a batch job in a several hour period overnight. The re-formatted data was displayed using software developed under the Data Fusion contract (-C5234) to create the image in Figure 6.4-4. This process is a very large time saving compared to the existing method of using a handheld ultrasonic unit, which requires several days to generate a thickness map of acceptable resolution. Scanning the seal with the LUIS did require the painting of the back side of the seal. This step is not required by the present method. Painting does not interfere with the subsequent chemical milling of this part which takes place only on the front side. An attempt was made to compare LUIS scanning of the seal with scanning by a conventional, semi-automated UT system. The seal was provided to the operator of a UT immersion system, with a request to scan the part to obtain thickness data. After considering the part geometry and trying some initial set up parameters, the operator decided that a complete set up would require 40 hours or more to complete because of the curvature of the part. The set up was not pursued. Based on this experience it appears that the LUIS has some real benefits in saving set up time for parts with moderate amounts of surface curvature, compared to conventional systems.

6.5 Paint Study

In the effort to identify high value niche applications for the LUIS, consideration was given to uses for various LBU systems currently marketed. An overview of LBU vendors led to a vendor named Autospect, Inc. which has developed a laser based system for measuring paint thickness for the automotive industry. Several aircraft paint systems are of interest in the aerospace industry. AWACS radome paint is of continuing interest to the Air Force. Periodic refurbishment of AWACS radomes requires close attention to the repainting process since paint thickness directly affects the dielectric properties of the radome and can make significant differences in radar propagation. The current labor expenditure per radome could be substantially decreased if repainted radomes could be quickly inspected for precise measurement of paint thickness. Evaluation of standard fuselage paints are of interest to the Air Force and airlines because of weight and maintainability considerations. In an attempt to determine the suitability of the LUIS for precision measurement of paint thickness, several painted samples were scanned. Painted samples included a section of the AWACS radome, AWACS radome

paint on plastic substrates, commercial aircraft paint on aluminum and commercial aircraft paint on graphite epoxy. The painted samples were scanned by the LUIS in a manner similar to inspection of other parts. Instead of evaluating the results for indications of defects, the captured waveforms were analyzed to determine whether information regarding paint thickness could be readily extracted from the LUIS data.

Paint samples on aluminum and graphite/epoxy substrates were inspected to establish capability of the facility for thin layer measurement. Preliminary evaluations of data have been completed in both time and frequency domains, using the Winimag software. Some evaluation has also been done using the Boeing developed INDERS software, which generally allows greater sophistication in the analysis because, as the developers, we are able to provide feature extraction algorithms tailored to the part response. Based on results from Winimag software, paint measurement with the LUIS scanner does not look promising for films of 4 mils and less. The principal reason for this is that the ultrasonic response from the front surface of the paint is too long to provide unambiguous separation of the response from the paint/substrate interface. The echo, which should be observed no more than about 100 nanosecs from the onset of front surface excitation, occurs within the high amplitude front surface echo. It is somewhat unclear from the data what the prompt response of the painted surface is. Compared to the subsequent substrate ringing, data from Autospect Inc. shows that the excitation response is at approximately 4 MHz or higher. This compares with approximately 2 MHz for LUIS. The difference is that the Autospect system produces a laser excitation pulse of 5 nsec duration while the LUIS produces a 130 nsec pulse. The front surface response of a laser excited sample is determined by both the absorption depth in the surface and the length of the laser pulse. Absorption depth establishes the thickness of the heated layer whose stress relaxation is governed by the acoustic transit time across the layer. This provides a fundamental lower limit on excitation pulse length and is the value that dominates when the laser pulse is very short. If the laser pulse is long with respect to the characteristic stress relaxation time, then the pulse length is determined by the laser. With Autospect, it appears that relaxation dominates. For a paint film 4 mils thick, the round trip sonic transit time is roughly $2*0.1/C$, where C is approximately 2 mm/microsec for typical paints and liquids. This gives a back surface echo response about 100 nsec after the onset of the front

surface response, and corresponds to a 10 MHz response frequency. The time domain response is therefore probably also obscured by the front surface response with Autospect. It appears that thickness estimation with Autospect relies on the resonance response of the substrate which is modified by mass loading by the overlying paint. This phenomenon was also observed with aircraft paint on aluminum with LUIS. Unfortunately, it requires a substrate that supports resonance with low acoustic loss. It also requires knowledge of the substrate thickness, either by measurements on the bare substrate with the laser system, or from a priori information. We conclude that LUIS can not measure paint thickness in the range required for aircraft paint, except in special circumstances where substrate resonance occurs. This does not mean that LBU technology cannot be used for such purposes, but rather that the LUIS is not appropriate for such a task. It is likely that Autospect systems will suffer the same limitations and be unsuitable for measurements on composite substrates.

7.0 CONCLUSIONS

The LUIS 747 is a remarkable example of a LBU system. It provides the capability of inspecting a very wide variety of composite parts in an industrial setting. The LUIS showed some distinctively positive characteristics and some notable negative characteristics. As it stands today, the LUIS 747 is an excellent device for supporting the rapid prototyping of composite parts with complicated geometries, as well as a testbed for developing LBU inspection concepts. Operation of the LUIS showed that it is not currently the best device for inspecting large numbers of standard production parts. The work did show the flexibility of the LUIS to scan a variety of different parts with a limited amount of preparation or fixturing. This flexibility could be an asset in a maintenance area where it would not be affordable to acquire a dedicated inspection system for different kinds of parts. With some modifications to hardware and software the existing LUIS unit can be made faster and easier to use. The LUIS is a valuable resource as a testbed for composite manufacturing process development, as well as being a stepping stone to new LBU systems.

7.1 Notable Successes

Scanning of thin, angled radius standards with flaws in the vertex, web and flange was very successful. The scans did not take long, they were scanned from the bagside, they generally did not require painting, and the results appear to be good. Flaws were detected by the LUIS that were not seen in conventional inspections of these part types and the LUIS demonstrated the utility of being able to scan continuously from the web and flange across the vertex without changes in part orientation.

On parts such as skin panels, LUIS demonstrated the desirable ability to scan right up to the edge of the part. In conventional systems, an extra edge scanning transducer may be needed to inspect the part periphery. On oddly shaped parts such as the "crowsfoot" the F-22 bulkhead and the aileron leading edge, LUIS demonstrated the ability to inspect difficult geometry that conventional systems cannot handle at all.

7.2 Notable Limitations

In many of the parts inspected during this contract, the LUIS did not detect flaws as well as the conventional systems that are optimized for particular parts. The detection limit is inherent to the laser-ultrasonic technology within the LUIS but could be enhanced by using novel laser-ultrasonic detection devices (e.g. photorefractive detection devices). Since most of the parts inspected in the contract were analyzed for the first time with the LUIS, a large amount of post-processing time by highly skilled individuals was needed. In some cases, the post-processing would still be required on a daily basis to enhance the detectability of defects. However, this post-processing could be avoided by addition of suitable hardware that would allow a broad range of filters and electronic distance amplitude correction (DAC) of the laser ultrasonic signal. Nearly every conventional scan was accomplished considerably faster than the LUIS scan of the same part. These factors of detection capability, time and speed limit the broad application of the LUIS in cases where conventional systems already excel.

7.3 Specific Positive and Negative Factors

In operating the system, various features and characteristics of the LUIS 747 were noted as being especially beneficial or especially difficult. Changes to the LUIS that correct or ameliorate the problems listed in this section would increase the value of the system.

7.3.1 Data Files

The LUIS 747 captures and stores complete waveforms for each point scanned which are currently digitized with an 8 bit A/D. This means that the range of the signals detected is limited to 256 discrete values per scan position, bounding the sensitivity. The current LUIS 747 records each data point as a 16 bit “unsigned short” value. So the system is already capable of storing data from a 16 bit digitizer. The current 8 bit limitation is due to technology available at the time the LUIS 747 was designed. An upgrade from 8 to 12 bits is feasible as demonstrated in a LBU system in operation at the National Research Council of Canada.

The capture and storage of complete waveforms has both positive and negative implications for use of the LUIS. Full waveforms can be very valuable to have for detailed investigation of

unusual results. However, on a daily production basis, storage of the complete waveforms can lead to time-consuming manipulations of large data files. Real-time images can be produced with the LUIS but they must be transferred to a workstation with visualization software to perform any manipulation on the image. In most production systems the operator sees the final image on a monitor as the scan is performed and can manipulate the images to enhance features (through color palette control, for example). Hence, simple tools such as color palette control and image processing should be added to the primary LUIS acquisition and display software. In some cases, signal processing would still be required to enhance the detectability of defects. In such cases, post-processing, and therefore storage, of the full waveform would be needed. However, if more hardware processing of the signal prior to digitization were added to the LUIS, there would be no need to store the full waveforms. For such purpose, commercial UT analog signal processing modules could be incorporated into the LUIS. At this point in time, the LUIS has a few band pass filters in hardware but the acquisition DAC and most other functions are numerical. A broader range of hardware functions would be helpful.

7.3.2 Resolution

Spatial resolution in the parts inspected is limited by the scanning step size. Values of either .1 or .05 inch may be chosen by the operator. In some cases, these figures prevent the LUIS from providing sufficient resolution. For the Rocketdyne nozzle that was inspected, the step size of .05 inch was too large to supply the resolution desired. It should be noted, however, that the LUIS was never intended for use with very small step sizes. The present step sizes were specifications set by the USAF. Smaller step sizes could be made with the LUIS with some modifications of the scanner control software. A reduction of the smallest step size of the LUIS by a factor of two could easily be achieved.

While the existing LUIS step size may be inadequate for small parts with fine details, for a large part .05 inch step size will result in rather large data files that are difficult to manipulate. At .05 inch per step, 1 square inch will contain 400 scanned points of 2048 values each or 81,920 values. Scanning one square foot will require storage of nearly 118 million values. While the system can mechanically scan parts up to 6 X 6 feet in size, the file generated is rather unwieldy

with current computers. In addition, large part scanning becomes quite time consuming. Parts scanned at using the .05 inch step size require 4 seconds per square inch, which is 576 seconds or 9.6 minutes per square foot. Scanning dozens of square feet requires hours. This does not compare favorably with modern conventional transducer array systems such as one installed at Boeing Commercial Airplane Group which can scan about 200 square feet per hour.

Changing the step size to .1 inch reduces scan time and data collected by a factor of 4 with an attendant loss of resolution, of course. These facts indicate that for general usage, the LUIS needs the capability to easily set small step sizes for small parts with high resolution needs and large step sizes for large parts with low resolution needs. Importantly, operators must recognize the trade-offs. Practical use of the LUIS for large parts with high resolution will require an increase in the data acquisition rate, which is fundamentally determined by the 100 Hz rate of the current laser.

7.3.3 Scan Size and Ranging

Ultimately, the maximum scan size area is determined by the scattering power of the surface of the inspected parts and the generation efficiency of the surface material. The sensitivity of a laser-ultrasonic system is directly determined by the amount of light collected by the signal photo detector of the detection unit. The signal to noise ratio, if shot noise limited, is proportional to the square root of the intensity of light on the photo detector. As the angle of incidence to the part's surface increases, the back scattered light decreases and therefore, the light collected at the photo detector also decreases. To compensate such loss in collected light, the LUIS system uses a feedback loop on the detection laser's output. At a given angle, depending on the back scattering efficiency of the part's surface, the laser's output will be unable to compensate for the loss in signal. Such angles will determine a boundary within which the signal-to-noise ratio will be relatively constant. Hence, for a flat panel, the maximum scan area is determined by the maximum angle of incidence to the surface for which an appropriate signal to noise ratio is obtained. The auto-focus system of the LUIS and the dynamic output range of the detection laser provide a certain amount of compensation to the loss of light that significantly increases the maximum scan area. For example, with the auto-focus system deactivated, the LUIS has a static

depth of field of about 10 cm. So without the auto-focus feature, the maximum scan area would be 2 ft x 2 ft for a flat surface at 5 ft.

The scanning mirror ultimately limits the scan area. The maximum angle for which the scanning mirror does not significantly “mask” part of the collected light is the ultimate limit. This limit corresponds to the 6'x6' at 5' quoted in the specifications of the system. Note that the size of the scan area does not significantly affect the time it takes to inspect a part. A large scan area is a good thing since it enables visualization of a large part in a single image. Software modifications to the LUIS display modules could allow for a better 2D picture of a multiple scan image, instead of using the 3D visualization software.

The maximum scan area can also be limited by the shape of the part. To inspect a section of a part, there must be a line of sight between the generation unit scanner mirror and the target area. The slopes of the part will limit the maximum extent of scan. This does not mean that a part with large curvatures cannot be scanned, but that the generation unit must be moved between the scans of different sections of the part.

Although the system can scan areas up to 6' X 6', the data points are not at constant spacing on a flat surface. UltraOptec recommends that the gantry head be moved and smaller scan areas such as 3' X 3' be used. There is a trade-off between some time needed for repositioning the head and the elimination of distortion. UltraOptec calculations showed that scan areas of 3'x3' were the optimum conditions even though the gain in time is relatively small for average parts, such as an 8' x 4' parts. The gain is noticeable only for large parts such as a wing of 32' x 16'.

An optical auto-ranging system determines the distance from the scanning head to the part surface. This information is used to adjust the lenses that focus the generation and detection lasers. It also generates a map of the part surface. An example is shown in figure 7.3.3-1. The figure shows a portion of the ranging data for the F-22 titanium seal pictured in Figure 6.3-3. This is a useful feature because C-scan images can then be plotted directly on a 3-dimensional rendering of the part. An example of this is Figure 7.3.3-2 which shows the autoranging data and

part time of flight data processed to represent part thickness of the F-22 seal. This is a 3 dimensional analog to the data shown in figure 6.3-4.

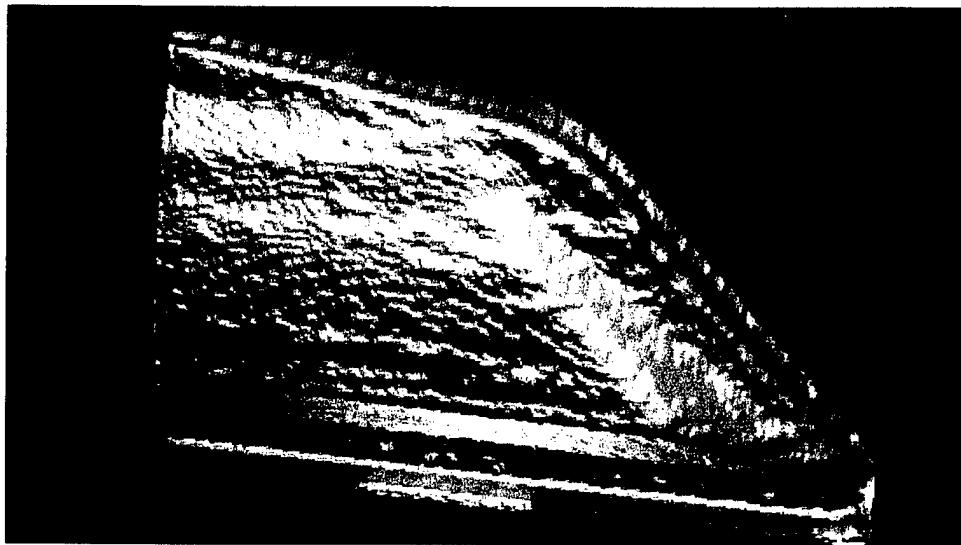


Figure 7.3.3-1. LUIS Autoranging Data

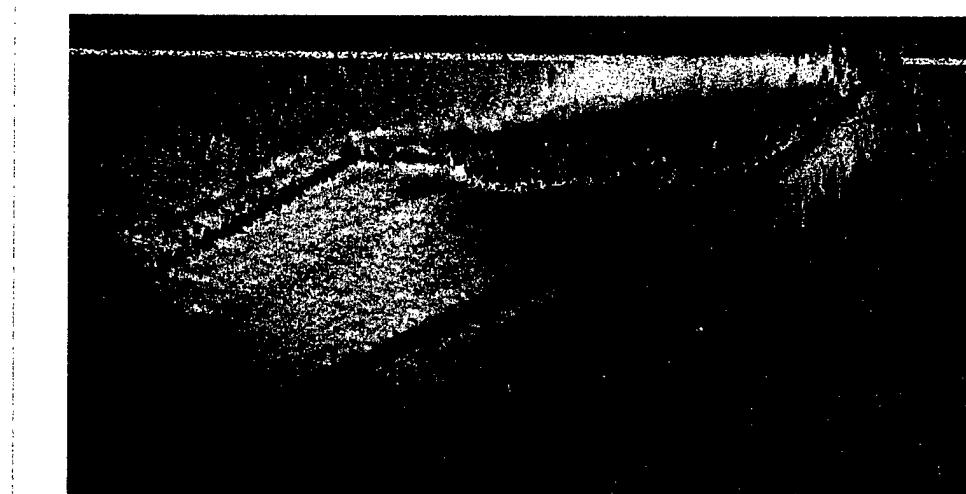


Figure 7.3.3-2. LUIS Autoranging and Time of Flight Data Combined

This mapping feature is simply an added bonus of having the autofocus system, which is required to let the LUIS operate within its 4 to 8 foot depth of field. As such there is no “added cost” attributable to the feature. Its value is a matter of speculation depending on particular uses. The example shown indicates that it may be useful as a very quick, one sided geometry capture

mechanism. It operates much faster but with much less resolution than Computed Tomography (CT) reverse engineering systems currently in use in industry.

One negative of the auto-ranging system is that it does not always follow complex surfaces in a single scan even though the ultrasonic portions of the system are still producing useful data.

Two circumstances can lead to ranging system problems: direct beam reflection onto the ranging camera and insufficient light received by the ranging camera. The measurement of the ranging distance is based on a simple optical triangulation of the image of the detection laser on the surface of the part. If a specular reflection is detected by the ranging system camera, the position calculated by the ranging software may be wrong and causes a defocusing of the laser beams on the target's surface. This can also occur when inspecting the inner section of a tight radius. In this case, the multiple reflections from the inner walls of the parts could lead to an erroneous ranging measurement. If the erroneous ranging measurement is out-of-range of the focusing optics, an error is sent to the LUIS control software and the focusing system stays at its present location until a new valid ranging measurement is given. For a highly reflective surface, the amount of light received by the ranging camera may be insufficient to get a ranging measurement. In this case, the ranging system sends an error message to the LUIS control software and the focusing system stays at its present position until a new valid ranging measurement is given.

Unfortunately, although a ranging error is not a critical error, the LUIS control software terminates a scan if a ranging error is received. To improve the LUIS 747, this would have to be modified in a new version of the software. A ranging error will, at most, cause a slight defocusing of the detection and generation lasers. A warning should be given to the operator and a warning map should be displayed and saved, so that the operator could discriminate between defects and possible features solely caused by focusing problems.

In the meantime, conditions leading to ranging error can be eliminated by a proper orientation of the part with respect to the generation unit. The problem areas can be identified by making a pre-scan of the part and corrected by modifying either the scan plans or the orientation of the part

mounting on the inspection cart.

There are practical limits to the part complexity that can be scanned due to the obliquity of the surface to the laser beam. The generation efficiency is dependent on the energy density delivered to the surface, not the pulse energy. Hence, as the spot size becomes more and more elliptical, the energy density decreases rapidly and, therefore, the generation efficiency also decreases. Also, as explained earlier, as the angle of incidence to the part's surface increases, the amount of light collected decreases as well as the signal-to-noise ratio. The maximum allowable angle of incidence is dependent on the part's surface material. A good test for obliquity limitations is to present multiple scans of a flat panel at different angle of inclinations with respect to the generation unit.

One of the advantages of laser-ultrasonic is the relaxed normalcy requirement as compared to conventional ultrasonic techniques (UT). Although the maximum angle of incidence is limited by the physical characteristics of the part's materials, this maximum angle is generally much greater than what is tolerated by conventional UT systems.

7.3.4 Preparation and Setup

Software interface and controls for set up were found to be cumbersome and time-consuming. A significant amount of time was required to define and start each scan. Some typical setup times are discussed in Section 6.3. Since LBU has a relaxed normalcy requirement, a feature should be added to the control software to allow a quick scan of the part. This would quickly define the start and end point of the scan using the tracer beam. Creation of a database scan plan would only be needed when repeated scans of given part type was required.

Tool-side surfaces of composite parts can produce "glare" of specular reflection when the lasers strike the surface straight on. These reflections can overwhelm both the autoranging system and the detection system. This produces a characteristic artifact in the initial image that appears as a set of dark stripes. Painting the surface reduces this problem, as would careful alignment of the part in its holding fixture. Both of these precautions limit one presumed benefit of LUIS - which

was minimal set-up effort and no part preparation.

The inspections of composite parts showed that rougher bagside surfaces of composite parts seemed to be better suited for efficient generation of ultrasound than the smoother, toolside surfaces. In order to inspect parts from the toolside, most of the parts needed painting with a water-based, strippable paint. Typically more than an hour was required for painting and drying each coat. Removal of paint is also time consuming. Subsequent operations on inspected surfaces would require very thorough removal of paint. This would not be desirable in a production environment. In general, painting of parts solely for inspection during production would be considered a non-value added process. While there are composite parts that can be tested from the bagside, many aircraft structure applications have the toolside exposed and the need to paint these surfaces is time consuming. Of course, in a maintenance environment with parts that are already painted this may not be an issue.

The decision to coat a part depends on a large number of parameters such as: generation efficiency of the surface materials, ultrasonic attenuation in the materials, size and type of the defect, and shape of the part. The decision is generally made during the setup procedure while determining the laser power settings, or after a pre-scan of the part. The LUIS operation is based on the assumption that a small set of part types would be inspected repetitively. Hence, once a type of part has been identified as requiring a coating, all parts of this type would be coated before scanning.

Figures 7.3.4-1 and 7.3.4-2 present data that are indicative of the magnitude of the signal increase due to painting. Figure 7.3.4-1 shows a maximum amplitude C scan image of the 7J7 panel before painting with the associated waveform at a particular spot on the surface marked by the cursor crosshairs. Note that the area around the cursor is quite dark and the return signal is very low. Figure 7.3.4-2 shows a subsequent scan of the same part after painting. The part was rotated 90 degrees, but the same point on the surface is represented by the waveform plot. Notice that the area around the cursor is much lighter. Inserts and stiffeners can be seen and the return signal is apparently much higher than in the previous figure. Unfortunately, saturation of the

front surface peak makes it impossible to quantify the exact difference in signal received before and after painting. Boeing did not attempt to quantify the effect of painted surfaces for correlation to signal strength during this contract. It was simply noted that some parts scanned from the toolside showed a substantial increase in the back surface echo and returns from inserts after painting.

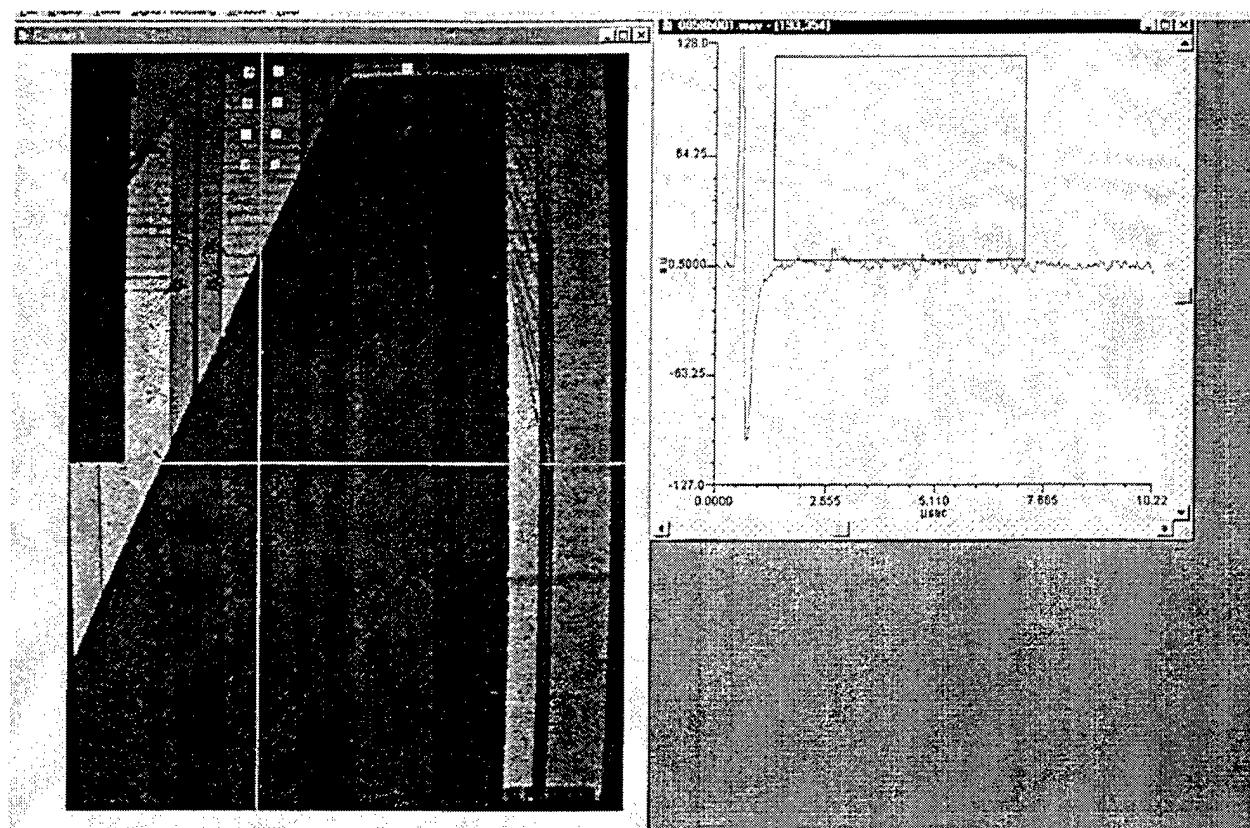


Figure 7.3.4-1. 7J7 panel LUIS data without paint

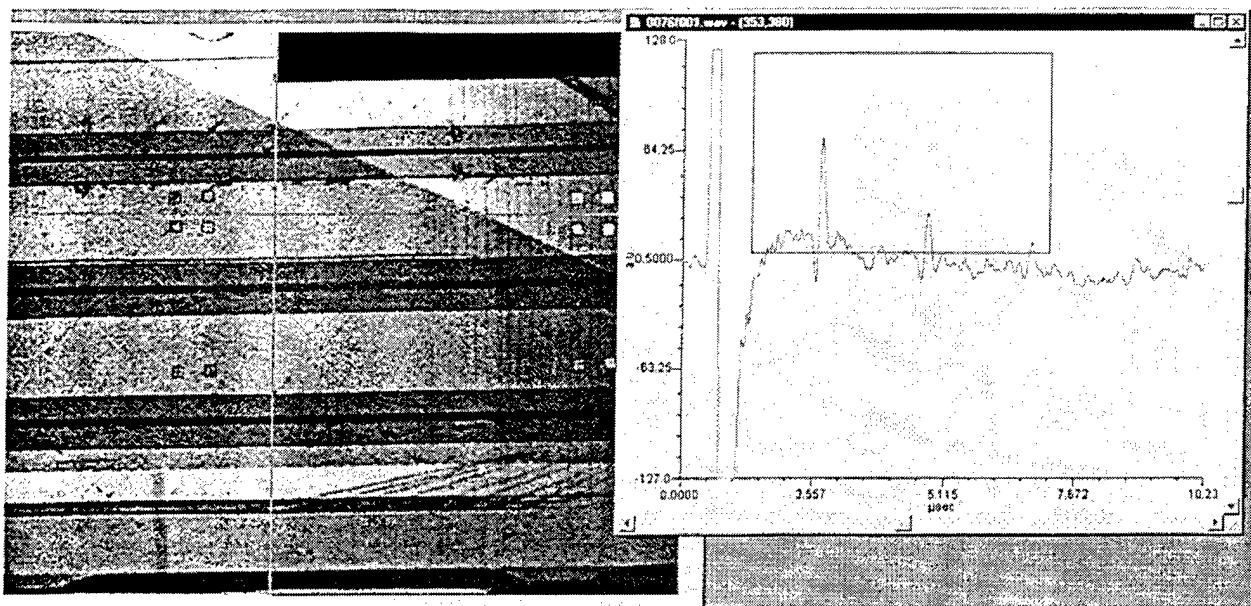


Figure 7.3.4-2. 7J7 panel LUIS data with paint

Some research data is available on the benefit of painting parts to increase signal strength. Personnel from the Rockwell Science Center have reported on laser generated ultrasonic signals obtained with white paint on aluminum in "Laser Based Ultrasonic Inspection of Complexly Contoured Rocket Engine Components", A.D. McKie and R.C. Addison, Jr., QNDE, 1997, San Diego. Paint was applied in single layers over a range of .5 mil to 1.7 mils and in multiple layers from 1.5 mil to 2.8 mils. They report amplitude increases by factors of 8X to 18X compared to uncoated aluminum. In private communications, the Rockwell Science Center has also reported increases of 14X with painted graphite epoxy compared to unpainted graphite epoxy surfaces. Rockwell reported that the increase in signal is strongly dependent on the thickness of the applied paint.

7.3.5 Penetration Depth

With conventional UT, the frequency is chosen by the operator to provide sufficient penetration for the material being tested. With LBU however, the frequency is determined by the response of the material to the generating laser pulse. The detection system must have acceptable response in the range of frequencies generated in the material. The frequencies generated by LBU can be too high to permit sufficient signal penetration into the object being inspected. The only way to

increase penetration is to increase the pulse power delivered by the laser to the part surface. This is possible only to the point where damage occurs. These factors tend to limit the effective penetration depth of LBU in general. Specifically for the types of composites inspected during this contract, the effective penetration depth of the LUIS was limited to between 60 and 80 plies.

It is possible to change the frequency response of the optical demodulator to increase its responsivity to lower frequencies. The current interferometer has a peak responsivity near 5 MHz. This could be lowered by increasing the reflectivity of the mirrors. However, this would reduce optical throughput and reduce the useful amount of light collected from the sample surface. A better solution for a newly developed LBU system might be to use one of the new photoreactive devices that have been shown to have a low cutoff frequency around 100 kHz. This should increase detection depth in thick composites.

7.3.6 Speed

The goal of the LUIS was to allow the use of a slow robot coupled to a fast mirror scanning system, in order to rapidly inspect large areas. With the McClellan AFB LUIS, once the settings of a type of part are in the database, the scan time is not limited by the robot motion or the size of the scan but by the maximum 100 Hz acquisition rate of the system which is limited by the maximum firing rate of the lasers. Cutting the number of scans would not significantly decrease the total scan time of a part since the robot motion is not a significant portion of the total scan time. It should be noted that laser ultrasonics does not require the use of a robotics arm. The choice of the present configuration is a design choice based on the required specifications of the USAF at the time of the negotiation of the LUIS purchase contract.

The LUIS software currently flushes the data if a scan is interrupted. This should be changed. Unless a system error causes damage to the system or the inspected part, the operator should be able to reset the system and continue the scan from where the error was reported or to kill the scan in process. The choice should be left to the operator. The errors that do not significantly influence the operation of the system, such as low light on the ranging system, should be indicated as a warning either on the screen of the control workstation and/or in a scan log file

associated to the data.

7.3.7 Data Processing

Data processing appears to be effective in bringing out the known flaws with regular geometry at different depths in Boeing standards. The following approach can be used to process data from complex parts with varying thickness and flaws with irregular shapes.

With full wave form data, defects can be better identified using B-scan and Z-scan images rather than C-scan images. Z-scans are C-scans with very narrow gates, i.e. amplitude C-scans for a set time T. Pre-scans and test panels can be used to determine typical settings for image processing to identify some class of defects with C-scans. However, for unknown or complex shaped components, by “flipping through” the B-scans or (with faster PCs) the Z-scans, an operator can better determine the presence of defects.

This process is impressive in its far reaching ability for data analysis. The downside is that it is time intensive. In a production environment, it is not possible to devote such resources economically to inspection. In a developmental environment such ability may be very important. The LUIS also has the ability to display real time gathering of gated data for what amounts to conventional amplitude and time of flight scans. This amounts to recording only the largest signal within a time gate, and the time at which the signal exceeds a preset threshold. The scans are built and displayed line by line as the scan progresses. Unfortunately, few tools are currently available in the LUIS to manipulate these images once they have been acquired. Modifications to the LUIS acquisition and display software show allow a better use of this real time data. With these images, a direct feedback can be given to the operator and small areas of interest could be rescanned to capture the full waveform data for postprocessing and detailed inspection.

7.4 LBU Benefit Analysis

An economic comparison of the LUIS and non-LBU ultrasonic inspection systems is difficult to perform for a number of reasons. First, in general there is not a one-to-one hardware correspondence between the LUIS and a non LBU system. Some conventional systems are highly adapted for each particular application. In addition, the inspection capabilities of the LUIS in terms of data collection and part throughput speed do not closely match the capabilities of many existing systems. In order to understand some of the differences and similarities between the LUIS 747 and conventional systems, the following two subsections discuss some of the characteristics of two conventional systems in use at Boeing

7.4.1 Customized Conventional System

A pulse echo bubbler skin panel system is described here. This system was developed for \$350,000 as a comparatively inexpensive means to test graphite composite laminate structures for the 777 program at high production rates. There are four large composite skins for the horizontal stabilizer and two for the vertical fin on each Boeing 777 aircraft. Each skin is about 50 ft. long, 6 ft. wide at the root, and about 3 ft. wide at the tip. The approximate area of each of the skins is 195 square feet. The expected production rate was 7 airplanes per month. The necessity to detect weakly reflecting foreign materials in these skins dictated that a pulse echo technique be used. These skins are contoured both spanwise and chordwise. Although the curvature is relatively small, in order to remain normal to the test surface a more costly multiaxis scanning system would have been required if testing were done by non-contact immersion.

In earlier composite aircraft programs Boeing had developed surface-riding pulse echo inspection techniques that seemed appropriate for these skins. Owing to the slight curvature of the skins, it was possible to limit the scan motion to X and Y axes and to rely on the gimbal mounted transducer to conform to the local surface contour. A vertical slider to which the gimbal was attached enabled the probe to follow surface height variations. A photograph in Figure 1-2 in Section 1 shows a bubbler with a single transducer attached to a gimbal and positioned on a composite test article with varying laminate thickness and four adhesively bonded graphite I-stiffeners. The bubbler has been a very reliable means of scanning on the toolside surface of

composite laminates at speeds of 20 inches/second. A small amount of water leaks from the base of the bubbler, but this is easily replenished with a water supply with a low flow rate.

The ultrasonic signals are detected with a Krautkramer-Branson USIP-20 ultrasonic test instrument employing separate peak amplitude and time of flight gates. The peak amplitude gate commences immediately after the toolside front surface echo and spans the time for echoes to return from the thickest portions of the skin panels. A digital peak value is stored for the largest echo that occurs within the gate interval at the time data sampling is triggered. This is normally the back surface echo. A DAC within the USIP-20 enables correction for the greater attenuation in the thicker portions of the panel. This results in a relatively constant back surface echo over the full range of skin thickness. The time of flight gate covers the same time span, but it is set to 10% of the full scale response on the USIP-20 CRT display. The first signal that exceeds the 10% threshold is detected and stored as a depth or thickness value. Data sampling takes place at 0.08" increments in the scan direction, and the array is indexed by 0.84." Two images are generated simultaneously during part scanning. The peak amplitude image shows the location of stiffener flanges and centerlines. Ply gaps at 90 degrees and plus and minus 45 degrees are often visible. The time of flight image shows the thickness of the skins and foreign materials that are inadvertently built into the skins.

The USIP-20 ultrasonic instrument has stored setup programs, which simplify daily production operations. Prior to scanning each skin panel, a "daily use standard" is scanned to confirm the detection of foreign materials at different depths within the laminate. The mechanical scanner is pictured in Figure 1-1 in Section 1. The scanner was built from modular drives and supporting members. Use of these components substantially reduced both the design time and construction costs of this scanner. As the scan stroke is 10 feet, the frame is moved stepwise along the part to cover successive segments over the full length of the part. The ultrasonic electronics, motion control hardware, and data acquisition and display computer are mounted on a table on the cart, which is attached to the scanner. One of the wheels of the cart is powered by a motor to propel the scanner and equipment cart. Guide tracks set flush in the floor ensure the scanner remains aligned with the test part.

The skins are brought to the scanner by an overhead "Lowervator" system that suspends them from an edge. They are lowered onto a pivoting tool with removable headers which supports the skin panels. Three sets of headers were prepared to accommodate the upper horizontal, lower horizontal, and vertical skins. Left and right skins are handled by reversing the headers in the tool. The stiffener caps from the bagside of the skin panels contact the headers. The toolside surface is positioned to provide minimum vertical height differences over the extent of the part. The maximum vertical excursion required by the bubbler is about 12 inches.

Identifying marks are painted on the skins by the automated ply lay-up machine. These marks are used to define the scan segments, and they also serve as the initial points for positioning the probe to commence a scan segment. In order to scan the irregular shapes in each skin, scan definition files are stored for each of the five segments for each type of skin. For the 6 skins there are 30 different scan definition files that control the scan motions. The appropriate scan definition file is automatically selected after the operator enters the part number and the segment identifier which is a portion of the data file name. The irregular shape to be scanned is displayed and the path to be moved from the reference point (the painted locators described earlier) to the scan start point is shown on the display. After moving to the scan start point the operator can request that the probe move to each of the vertices which define the scan definition envelope. Upon completion of a scan, with one key stroke the operator can display an overlay on the ultrasonic image. The overlay includes laminate ply drops, ply drops in the stiffener, rib centerlines, and stiffener flange footprints. The overlays are very useful aids in reporting the location of faults within the skin to others involved in their design and manufacture.

An eight-element, linear, line-focus, 3.5 MHz array is mounted in a rectangular bubbler. The bubbler scans at speeds up to 20 ips. The time required to scan a skin panel, excluding part positioning and movement between scan segments, typically ranges from 1.1 to 1.5 hours. A skin can be inspected and the data evaluated in four hours. Scan rates measured on five lower horizontal stabilizer production skins ranged from about 100 sq. ft/hour. up to nearly 200 sq. ft./hour. The total area scanned with each skin was 195 sq.ft.

The pulse echo bubbler inspection system has proven to be a reliable means of testing graphite composite laminate skin panels with modest curvature. It is a comparatively low-cost means of achieving high inspection rate pulse echo scanning of complex structures with a simple, two-axis modular mechanical system. Use of bubblers with linear arrays has made it possible to scan each 195 sq.ft. skin panel in slightly more than one hour. The initial requirement was to inspect one skin per eight hour shift. Normal skins with few faults can be mounted on the tool, completely scanned, and evaluated in half that time with this technique.

7.4.2 Flexible Conventional System

The AUSS family of ultrasonic systems developed and marketed by Boeing St. Louis comes closer to approximating the LUIS in terms of hardware configuration and part flexibility. The AUSS family features multi-processor computer controlled, contour-following ultrasonic inspection systems, which have been specifically designed for the UT inspection of adhesively bonded, composite assemblies having complex, contoured shapes. The systems are designed to perform through-transmission and pulse-echo test using water squirters for UT coupling between the scanner and the part. The systems use UT frequencies in the 0.2-30 MHz range to inspect for delaminations, porosity, voids, ply slippage and foreign materials.

Providing a description of part contours to the modern motion control hardware and software allows the AUSS units to scan parts with compound curvature. Data is acquired from the three dimensions of the structural parts and translated into two dimensional data image media with a minimum of surface distortion. A broad dynamic range of UT data is acquired, digitized and stored for each data point.

The data is processed and displayed, in near real-time, in operator selectable windows on a high performance workstation in color or shades of gray. Support hardware including optical disk storage, color plotters, Ethernet connections, etc. are available on the AUSS systems.

The AUSS mechanical configuration is tailored to meet the specific customers' requirements.

The standard nine-axis system has multiple additional axes supplementing subsystems such as a turntable or automated parts positioner. Other configurations include dual five axes opposing (either vertical or horizontal) mechanical arrangements.

As seen in Figure 7.4.2-1 and 7.4.2-2, AUSS systems are physically similar to the LUIS. They have extensive robotics with multiple degrees of freedom. AUSS installations are comparable in price to the LUIS 747 and offer similarities in flexibility of part types and shapes that can be accommodated. Depending on the model and exact features ordered, AUSS systems cost from \$1.75 M to \$2.5 M.

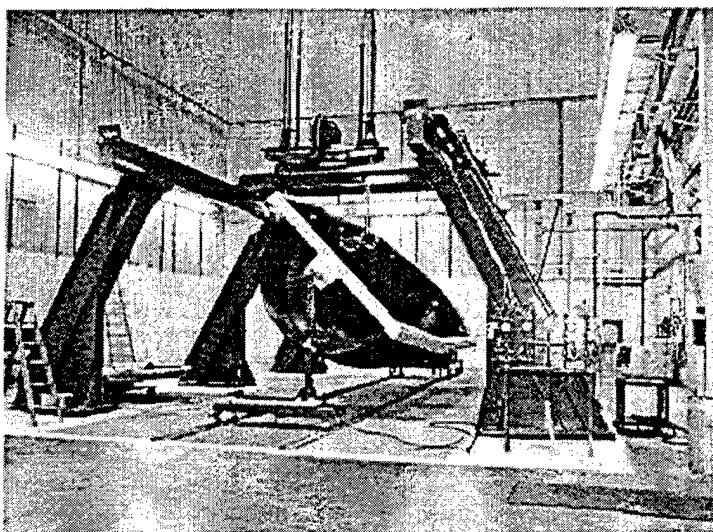


Figure 7.4.2-1. AUSS

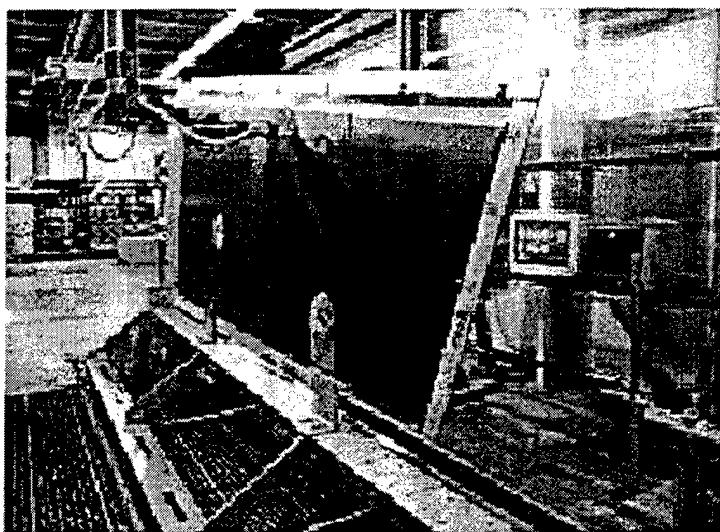


Figure 7.4.2-2. AUSS Closeup

7.4.3 System Scanning Comparisons

The Boeing experiences presented in Section 5 of this document indicate that in many cases, use of the LUIS to inspect the parts used in this contract would not be a benefit in speed, throughput or cost compared to conventional inspection systems currently in use. The LUIS is very flexible and can accommodate an astonishing variety of part sizes and shapes, but it is not optimized for any of them. The cost of a customized conventional UT system is far less than the cost of the LUIS. The added cost for flexibility may not be warranted in a production environment. However for complex parts, a flexible system is the best alternative. Table 7.4.3-1 shows a system parameter comparison for AUSS, LUIS and optimized UT systems.

Table 7.4.3-1. System Comparisons

| System | AUSS V | AUSS X | bubbler | LUIS | units |
|--------------------------|-----------------------------------|------------------------------------|------------------------|-----------------|---------------------|
| Inspection type | TTU/PE | TTU/PE | PE | PE | |
| Detects impact damage | yes | yes | yes | yes | |
| Detects delaminations | yes | yes | yes | yes | |
| Detects disbonds | yes | yes | yes | yes | |
| Dynamic range TTU | 130 ¹ | 130 | na | na | dB |
| Dynamic range PE | 35 ² | 35 ² | 35 ² | 40 | dB |
| Frequency range PE | .5-15 | .5-25 | 1 - 7.5 | 1.5-15.5 | MHz |
| Resolution | 10 | 10 | 8 - 11 ⁸ | 8 | bits |
| Max sampling rate | 70 | 70 | | 160 | MHz |
| Inspection spot size | .08, .187, .25, .35 ³ | .08, .187, .25, .35 ³ | .08 | .1, .2 | In. |
| Data display | A,B,C | A,B,C | A,B,C | A,B,C, 3D | scans |
| Inspection speed | 42 ⁴ , 78 ⁵ | 56 ⁴ , 105 ⁵ | 200 ⁷ | 25 | Ft ² /hr |
| Cost | 1.75-2.5 | 2.5 | .25 - .35 ⁹ | 2 ¹⁰ | \$M |
| Couplant | water | water | Water | none | |
| Inspect sharp radii | slowly | yes | No | yes | |
| Inspect thick composites | yes | yes | Yes | no | |
| Inspect parts on AC | no | no | No | no | |
| Inspect on flightline | no | no | No | no | |
| Points/sec | | | | 100 | |
| Step size | .04 X .08 ⁶ | .04 X .08 ⁶ | .08 X .12 | .1 | In. |
| Max travel speed | 30 | 40 | 20 | 40 | In/sec |
| Resolution | .02 | .0005 | .02 | .01 | In. |
| Inspection envelope | 20 X 8 | 20 X 10 | 6 X 50 | 40 X 11 | Ft. |

Notes

1. for newest models

2. additional 30 to 60 dB of Time Corrected Gain for increasing thickness parts

3. waterstream diameter, .35 used in applications where transducer focused on surface. Spot size determined by transducer.

4. single nozzle

5. dual nozzle

6. max resolution

7. 8 bits amplitude, 11 bits time of flight

8. eight element linear array

9. \$350K development cost, \$250K subsequent units

10. does not include shielded bay and other infrastructure

The cost of the LUIS is comparable to the cost of an AUSS installation, depending on exact configuration. However, the LUIS again suffers in comparing capabilities. AUSS offers similar complex contour following capabilities to the LUIS, but offers both pulse echo and TTU modes of inspection. In addition, the AUSS supports a very broad range of UT inspection frequencies which provides greater flexibility in optimizing inspections for parts characteristics such as thickness and material type. Excepting cases with extremely complex geometries, the AUSS is a better all-around inspection tool.

The LUIS is not competitive in situations where conventional systems already work very well. As an example, the inspection of the 7J7 test panel can be considered. This panel was inspected in 38 minutes with a single surface riding bubbler while the LUIS scan took 106 minutes. A production system dedicated to such parts would probably make use of multiple transducers, which would reduce the inspection time significantly. Using 4 transducers would reduce the conventional scan time to under 10 minutes. The LUIS also suffers from other time comparisons since a significant amount of labor intensive post-processing of the full waveform data must be accomplished. The LUIS images presented in this report typically required 1 to 2 hours of time for a highly trained analyst to produce. This contrasts with the seconds or minutes required for a technician to create the conventional scan images shown in this report. To be fair, it must be pointed out that if the LUIS could be dedicated to the inspection of a limited number of part types, full wave digitization would not be used frequently. The LUIS process of full wave digitization and subsequent data reduction is expensive compared the conventional process of retrieving only the data desired through dedicated, optimized processing hardware and software. If such dedicated hardware and software could be added to the LUIS, we could expect a significant reduction in the time to produce the images. Since the data from the LUIS is nothing more than ultrasonic signal, the time to produce the images should then be identical to conventional UT systems.

The LUIS scan of the 7J7 part was superior in one respect, the laser system can scan up to the edge of the part. The surface riding bubbler was unable to reach the outside 1 inch around the periphery of the part. The images presented for several of the parts in Section 5 show this slight

reduction in conventional data compared to the LUIS data. In the Boeing production system, a specialized transducer to handle part edges is used. This eliminates the advantages of the LUIS. Since the quality of data from the two systems is comparable in terms of features detected, the LUIS does not present compelling economic advantages for this part. The same arguments can be made for many of the other production part types inspected where a conventional solution is available.

7.4.4 Best LBU Applications

The simple parts types for which the LUIS made the best showing versus conventional inspection were for the various angle standards and the composite aileron leading edge. Manual scanning of the leading edge of the aileron takes about 2 hours. The LUIS can scan this part in about 20 minutes. The angle standards tests in Section 5.1 clearly showed the superiority of the LUIS compared to the usual TTU test. The TTU inspection was very poor at detecting tape inserts. The pulse echo LUIS scans were able to find most or all of the tape inserts. In addition the LUIS was able to scan the web, vertex and flange in a single scan setup. While this is somewhat of an "apples and oranges" comparison, it is factual. The TTU method compared is currently used because it is much easier to implement than a conventional pulse echo system. The LUIS results indicate that a LBU pulse echo system could provide results that are superior to conventional TTU at a cost less than conventional pulse echo. In other cases where geometry does not permit use of automated conventional scanning, the LUIS presents opportunity for improvement over manual methods.

New systems which are optimized in hardware and software to inspect particular problem areas while taking advantage of LBU capabilities with curved surfaces are likely to be the best usage of LBU. A non-aerospace example of optimization to particular situations is the CLUES system developed by Hughes Research Lab as a prototype LBU weld inspection system for General Motors. The CLUES device was designed for a specific inspection of a specific part and enjoys the benefits of small size, limited volume of laser shielding, optimized generation and detection of ultrasound and tight integration to a particular industrial process which would translate to low cost. It presents a different model for the future of LBU instruments than the LUIS.

Besides inspection of large quantities of particular part shapes like angled spars or composite leading edges where LBU has a decided advantage, utility is evident for a non part-specific system like the LUIS in a developmental role. There are no optimized inspection systems for new and unusual parts like the integral wingbox, the F-22 bulkhead and the "crowsfoot". For such parts, the versatility of a system like the LUIS is a positive factor. A flexible, developmental system like the LUIS is able to be configured to inspect odd geometries and unusual shapes. The knowledge gained from this type of work can be important in the timely, rapid prototyping development of new parts and processes including inspection methods and techniques.

Access to a system like the LUIS can pave the way for development of new qualification standards for new part types. As an example, the integral wingbox type of structure is very important in reducing costs and weight since it reduces the number of manufacturing steps and uses no fasteners. However, the structure is difficult to inspect with conventional ultrasonic scanning methods. An array of piezoelectric transducers might be built to scan all the flat internal surfaces, but corners would be difficult to handle. In this contract, the LUIS demonstrated the ability of LBU systems to handle inspection of radii. Further work could show that an optimized LBU system is capable of inspecting this structure quickly enough to support production use of LBU inspections. In this regard, the LUIS 747 can point the way for future production LBU systems.

It is important for a developmental activity to have access to the LUIS or a similar system where new inspection techniques and prototypes can be investigated and proven for transition to production. It is the opinion of the Boeing researchers who performed this contract that this is where the greatest value of the current LUIS 747 installation lies.

7.4.5 Economic Analysis

There is difficulty in putting a price tag on LBU capabilities. To be successful, a LBU system must deliver performance that cannot be met with conventional systems like those described above. The value is likely to be specific to particular programs and parts. The clearest cases are

situations in which large numbers of a given part can be inspected with an advantage. Figure 7.4.4-1 shows a drawing of a typical composite L cross section 90 degree vertex part with scalloped edges. The F-22 program uses numbers of parts similar to this as fairing attach brackets and spar rib posts. These parts are currently inspected with a manual, non-imaging ultrasonic system at a rate of about 2 manhours per part. Based on Boeing experience on this contract, it is estimated that a LBU system customized to handle such parts could cut the inspection time to 20 minutes per part with added benefits of superior detection of flaws in the vertex, repeatability of measurements and automatic storage of digital data records. This represents savings of about 1.6 manhours per part. At an assumed labor rate of \$150/ hour, this saves \$240 per part while increasing the overall quality and usefulness of the inspection procedure. Boeing estimates that with continued development, a small LBU system customized for such parts could be fielded for about \$500,000. The break even point is then the inspection of about 2000 parts. Numbers such as these make sense for high volume situations such as commercial aircraft and for military systems with a reasonable production run such as F-22 and especially JSF.

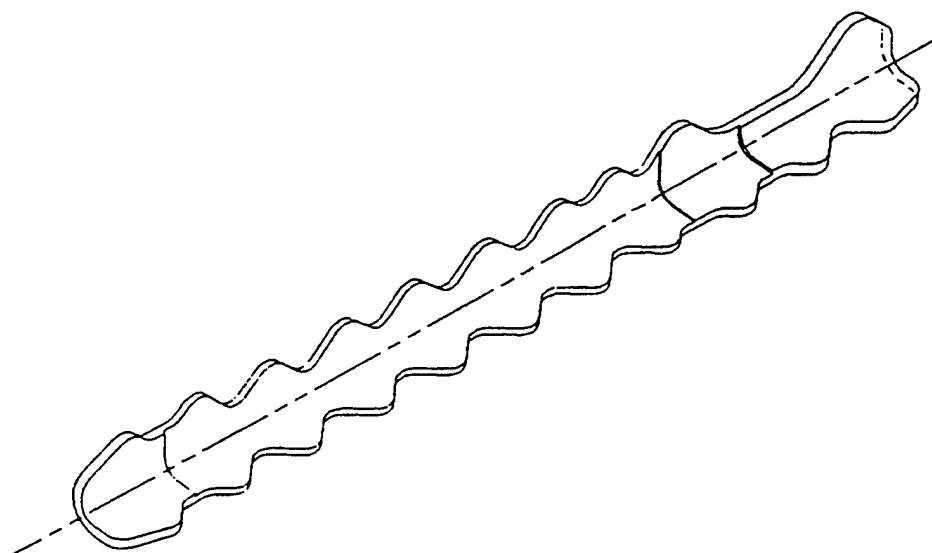


Figure 7.4.5-1. F-22 Rib Post

The value of LBU for development may be much greater, but is more difficult to quantify. For example, a program may place great value on a LBU inspection system that can qualify an integral wingbox and allow the part to be made from material that is thinner than otherwise

possible. Weights engineers working on B-2 wing structures at Boeing estimated that every pound saved had a value of \$17,500 in non recurring costs over the 21 aircraft buy for that program. For JSF, suppose that the estimated the value of weight saved is about \$500 per pound. If use of LBU can save only 2 pounds of structural weight per aircraft on the JSF, a saving of \$3 million will accrue during the estimated production of 3000 airplanes.

7.5 Recommendations

Based on contract experiences, Boeing offers the following recommendations.

7.5.1 Short term

There are numerous scenarios for the possible disposition of the LUIS during the transfer of facilities at McClellan AFB to the County of Sacramento. Among all the scenarios possible there are several that most likely. The LUIS could remain Air Force property within the privatized base, the LUIS could be moved to another Air Force base, an outside agency such as a national laboratory or university could manage the LUIS as a LBU lab, the LUIS could be operated by a contractor under the County ownership, or the County could surplus and sell the equipment. In Boeing's view, the Air Force is committed to leaving equipment in place. Since there is not a pressing Air Force requirement for LUIS, the Air Force is not likely to retain ownership of the site or move the equipment elsewhere. Although Boeing would prefer to see the system managed by a national lab or university willing to foot the bill for keeping the LUIS running as a public facility, there appears to be no interested parties for such a scenario. Boeing believes that the LUIS 747 will become the property of Sacramento County and the County will attempt to market the services of the system within DoD and industry. Boeing recommendations for the LUIS installation are based on this scenario.

Since the Air Force will likely not continue to own the LUIS, Boeing recommends that no U.S. Government efforts be expended to upgrade, change or improve the system for its own enhancement before it is turned over to the County. Boeing recommends that the U.S. Government strongly encourage the continued use of the LUIS 747, after change of ownership, as

a testbed for development of new LBU concepts. With the concurrence of Sacramento County, the U. S. Government should allow expenditures for modification of the LUIS system by contractors pursuing new concepts in LBU development.

As long as the LUIS is in good working order it will be a valuable laboratory. The money that could be realized by scrapping the equipment is a fraction of the real value of the system. Boeing recommends that Sacramento County return any revenue generated by the LUIS directly back into maintaining the system to keep it useful. There are a number of possible changes identified during this contract that would enhance the operation and use of the LUIS. Boeing recommends that the first two be strongly considered since they are relatively minor and would prevent some very annoying situations. The enhancements are shown along with a very rough, order-of-magnitude estimate of the task. The estimates are based on Boeing's limited understanding of the LUIS. Since Boeing is not a LBU vendor, the estimates should not be viewed as authoritative in any way. Actual contracted costs for performing the work could vary widely from the estimates and Ultra-Optec, Inc. should be contacted for realistic estimates of the costs involved.

In recommended priority order the changes are:

1. Fix software bug in APE that causes crashes. Estimated at 6 man weeks.
2. Modify control software to generate warning instead of terminating scan when ranging error detected. Estimated at 3 man weeks.
3. Provide control console with color palette control and image processing software. Estimated at 6 man months.
4. Addition of DAC, filtering and other signal processing in hardware. Depends on the exact hardware and functions used, no estimate.
5. Upgrade detector A/D from 8 to 12 bits. Estimated at 3 man months plus \$10K. Could be incorporated into number 4.
6. Modify scanner control software to allow wider operator choice of step sizes. Estimated at 4 man weeks.
7. Modify software to allow better display of multiple scans. Estimated at 6 man weeks, if appropriate commercial software is available.
8. Modify control software to allow quick scan of part without creation of scan plan. Estimated

at 6 man months.

9. Add low frequency detector, e.g. photorefractive detector. Estimated at \$ 60K plus 4 man months.
10. Modify scanner control software to allow scanning of irregular areas instead of rectangular areas. Cannot be done without major changes to system, no estimate.

Boeing recommends that the LUIS or a system like it be used for rapid prototyping of composite parts with complex geometries. This includes both the quick look inspection of such parts during the initial prototyping process, as well as the development of the appropriate inspection methods and techniques, once the parts are in production. Such prototyping could be very valuable to new developments, but Boeing is unable to quantify a likely workload for the LUIS.

Turning attention to the development of technology, Boeing recommends that the U.S. Government pursue specific short term development of LBU technology by focusing on developing a cost effective, prototype system capable of inspection of parts in a production environment. The real benefits of LBU to the U.S. aerospace industry will be realized only if there is widespread awareness, acceptance and use of LBU. Widespread acceptance will occur only if LBU demonstrates real economic advantages. The best chance to demonstrate the real advantages will be to inspect parts for which LBU has known advantages, as shown in this contract. The demonstration will be most effective in an environment where LBU can inspect a large number of production parts and be critically compared to current inspection processes.

7.5.2 Long term

Technological innovation can enhance the cost effectiveness of LBU systems by driving down the cost of expensive hardware. The U.S. Government should continue to encourage and fund research efforts with this aim. Lasers with higher repetition rates can lead to faster inspections. In general, university or industrial research into development of lasers with higher repetition rates will support LBU. A repetition rate of 1000 Hz is an excellent goal, it would provide a sampling rate closer to that of today's piezoelectric transducers. Generation lasers with suitable power and

spectral characteristics that can be carried over fiber optics can reduce the need for large, costly robotics systems. Fiber-capable lasers may also provide the capability of penetrating deeply into complex structures. Researchers should focus on development of fiber-capable lasers for these reasons. Replacement of expensive, complex interferometers with simpler detectors may reduce cost, system complexity and maintenance issues. In addition, new detectors could work at lower frequencies, this would allow inspection of thicker parts where high frequencies are attenuated. A LBU detector with peak responsivity near 1 MHz is a useful goal. Items such as these should be carried on as pertinent elements of future research that the Air Force funds.

APPENDIX A. TABLE OF SCANS

| Wisard Inspection # | File # | Part Description | Part marking | Notes |
|---------------------------|-----------|--------------------------------------|--------------------------------------|----------------------------------|
| 1403 | #0057b001 | F22 Ply drop standard | | Bag side of part |
| 1406 | #0057e001 | F22 Ply drop standard | | Tool side of part |
| 1407 | #0057f001 | 777 qualification standard | 777-1-A | Tool side of part |
| 1408 | #00580001 | 777 qualification standard | 777-3-A | Tool side of part |
| 1415 | #00587001 | A-6 ply drop standard | | Inspection of bag side of part |
| 1417 | #00589001 | A-6 ply drop standard | | Inspection of tools side of part |
| 1419 | #0058b001 | 7J7 test stiffener & skin | 65C32501-7 | Bottom of part/tool side of part |
| 1419 | #0058b002 | 7J7 test stiffener & skin | 65C32501-7 | Top of part/tool side of part |
| 1421 | #0058d001 | F22 Ply drop standard | | Painted tool side of part |
| 1422 | #0058e001 | curved wing panel with stiffeners | REF STD #1 | Tool side of part/left side |
| 1424 | #00590001 | curved wing panel with stiffeners | REF STD #1 | Tool side of part/right side |
| 1428 | #00594001 | curved wing panel with stiffeners | LO STR A 0428-2 | Tool side of part/left side |
| 1429 | #00595001 | 777 qualification standard | 777-3-A | Painted tool side of part |
| 1430 | #00596001 | BD&SG radius std 80 deg-2 | X157153 | 80 deg angle corner |
| 1432 | #00598001 | BD&SG radius std 80 deg-1 | X157153 | 80 deg angle corner |
| 1437 | #0059d001 | 777 skin panel | | 1/3 scans |
| 1437 | #0059d002 | 777 skin panel | | 2/3 scans |
| 1437 | #0059d003 | 777 skin panel | | 3/3 scans |
| 1438 | #0059e001 | F22 door panel | ESSR 82946 | Exterior surface |
| 1441 | #005a1001 | hat stiffened panel | L74-223 | Panel side 1/2 |
| 1441 | #005a1002 | hat stiffened panel | L74-223 | Panel side 2/2 |
| 1442 | #005a4001 | BCAG porosity std matrix | | |
| 1445 | #005a5001 | Sine wave spar | 96LCW5010-1-B5- 1 | |
| 1446 | #005a6001 | Sine wave spar | 96LCW5010-1-B5- 1 | |
| 1447 | #005a7001 | Sine wave spar | 96LCW5010-1-B5- Bad scan 1 | |
| 1448 | #005a8001 | Sine wave spar | 96LCW5010-1-B5- Horizontal scan 1 | |
| 1449 | #005a9001 | Sine wave spar | 96LCW5010-1-B5- Vertical scan 1 | |
| 1450 | #005aa001 | Composite fly wheel | #6 CT scanned | |
| 1451 | #005ab001 | 777 rib with foreign material | 172W5101-2 | |
| 1452 | #005ac001 | 747 Krueger flap | | |
| 1454 | #005ae001 | 777 qualification standard | 777-3-A | Painted surface (second scan) |
| 1455 | #005af001 | 777 rib with foreign material | 172W5101-2 | Flat section of rib |
| 1456 | #005b0001 | Impact test panel with spars | | |
| 1457 | #005b1001 | BD&SG radius std 110 deg- | X157154 1 | |
| 1458 | #005b2001 | BD&SG radius std 110 deg | X157154 -2 | |
| 1459 | #005b3001 | BD&SG radius std 110 deg- | X157154 1 | |

Appendix A. Table of Scans (Continued)

| Wisard Inspection # | File # | Part Description | Part marking | Notes |
|---------------------------|------------|---------------------------------|--------------|--------------------------------------|
| 1460 | #005b4001 | A-6 near/far surface test panel | | bag side repeat because of data loss |
| 1473 | #005c1001 | Foreign material test panel | | |
| 1493 | #005d5001 | back surface step wedge | | |
| 1494 | #005d6001 | back surface step wedge | | |
| 1495 | #005d7001 | back surface step wedge | | |
| 1500 | #005dc001 | back surface step wedge | | |
| 1506 | #005e2001 | honeycomb repair | | |
| 1508 | #005e4001 | A-6 near/far surface test panel | | |
| 1509 | #005e5001 | A-6 near/far surface test panel | | |
| 1510 | #005e6001 | A-6 near/far surface test panel | | |
| 1524 | #005f4001 | B-2 vent tube | | |
| 1524 | #005f4002 | B-2 vent tube | | |
| 1539 | #00603001 | honeycomb standard | SKA1A1A1 | |
| 1540 | #00604001 | honeycomb standard | | |
| 1541 | #00605001 | ?? | | Not Milstar Radome - unknown part |
| 1542 | #00606001 | ?? | | Not Milstar Radome - unknown part |
| 1553 | #00611001 | Paint test matrix | | |
| 1554 | #00612001 | Paint test matrix | | |
| 1556 | #00614001 | Paint test matrix | | |
| 1557 | #00615001 | Paint test matrix | | |
| 1558 | #00616001 | honeycomb standard | SKA1A1A1 | |
| 1559 | #00617001 | Panel K-4 | | |
| 1561 | #00619001 | Repair patch | R-5,95-24-A | |
| 1563 | #0061b 001 | 777 test part | 777-8-A | |
| 1564 | #0061c001 | 777 test part | 777-8-A | |
| 1565 | #0061d001 | Panel K-2 | | |
| 1566 | #0061e001 | Panel K-2 | | |
| 1551 | #0060f001 | A6 near/far panel | | Scan of painted side - bad file |
| 1567 | #0061f001 | 777 qualification standard | 777-3-A | Demonstration of low resolution scan |
| | #00620001 | 777 qualification standard | 777-3-A | Same as above with different gate |
| | #00621001 | 777 qualification standard | 777-3-A | Same as above with different gate |
| | #00622001 | 777 qualification standard | 777-3-A | Same as above with different gate |
| 1587 | #00633001 | Signal processing sample 1 | | Repeatability samples:(0 deg) |
| 1588 | #00634001 | Signal processing sample 2 | | Repeatability samples (0 deg) |
| 1589 | #00635001 | Signal processing sample 3 | | Repeatability samples (0 deg) |
| 1590 | #00636001 | Signal processing sample 4 | | Repeatability samples (0 deg) |
| 1591 | #00637001 | Signal processing sample 5 | | Repeatability samples (0 deg) |
| 1592 | #00638001 | Signal processing sample 6 | | Repeatability samples (0 deg) |
| 1593 | #00639001 | Signal processing sample 1 | | Repeatability samples (20 deg) |
| 1594 | #0063a001 | Signal processing sample 2 | | Repeatability samples (20 deg) |

Appendix A. Table of Scans (Continued)

| Wisard Inspection # | File # | Part Description | Part marking | Notes |
|---------------------------|-----------|----------------------------|--------------|------------------------------------|
| 1595 | #0063b001 | Signal processing sample 3 | | Repeatability samples (20 deg) |
| 1596 | #0063c001 | Signal processing sample 4 | | Repeatability samples (20 deg) |
| 1597 | #0063d001 | Signal processing sample 5 | | Repeatability samples (20 deg) |
| 1598 | #0063e001 | Signal processing sample 6 | | Repeatability samples (20 deg) |
| 1599 | #0063f001 | Signal processing sample 1 | | Repeatability samples (40 deg) |
| 1600 | #00640001 | Signal processing sample 2 | | Repeatability samples (40 deg) |
| 1601 | #00641001 | Signal processing sample 3 | | Repeatability samples (40 deg) |
| 1602 | #00642001 | Signal processing sample 4 | | Repeatability samples (40 deg) |
| 1603 | #00643001 | Signal processing sample 5 | | Repeatability samples (40 deg) |
| 1604 | #00644001 | Signal processing sample 6 | | Repeatability samples (40 deg) |
| 1609 | #00649001 | Signal processing sample 1 | | Repeatability samples (40 deg) - 2 |
| 1610 | #0064a001 | Signal processing sample 2 | | Repeatability samples (40 deg) - 2 |
| 1611 | #0064b001 | Signal processing sample 3 | | Repeatability samples (40 deg) - 2 |
| 1612 | #0064c001 | Signal processing sample 4 | | Repeatability samples (40 deg) - 2 |
| 1613 | #0064d001 | Signal processing sample 5 | | Repeatability samples (40 deg) - 2 |
| 1614 | #0064e001 | Signal processing sample 6 | | Repeatability samples (40 deg) - 2 |
| 1615 | #0064f001 | Signal processing sample 1 | | Repeatability samples (20 deg) - 2 |
| 1616 | #00650001 | Signal processing sample 2 | | Repeatability samples (20 deg) - 2 |
| 1617 | #00651001 | Signal processing sample 3 | | Repeatability samples (20 deg) - 2 |
| 1618 | #00652001 | Signal processing sample 4 | | Repeatability samples (20 deg) - 2 |
| 1619 | #00653001 | Signal processing sample 5 | | Repeatability samples (20 deg) - 2 |
| 1620 | #00654001 | Signal processing sample 6 | | Repeatability samples (20 deg) - 2 |
| 1621 | #00655001 | Signal processing sample 1 | | Repeatability samples (0 deg) - 2 |
| 1622 | #00656001 | Signal processing sample 2 | | Repeatability samples (0 deg) - 2 |
| 1623 | #00657001 | Signal processing sample 3 | | Repeatability samples (0 deg) - 2 |
| 1624 | #00658001 | Signal processing sample 4 | | Repeatability samples (0 deg) - 2 |
| 1625 | #00659001 | Signal processing sample 5 | | Repeatability samples (0 deg) - 2 |
| 1626 | #0065a001 | Signal processing sample 6 | | Repeatability samples (0 deg) - 2 |
| 1576 | #00628001 | stringer 172W3118-2 | 412528J | |
| 1577 | #00629001 | 777-8-A test part | | Left half of part |
| 1578 | #0062a001 | 777-8-A test part | | Right half of part |
| 1579 | #0062b001 | 777-8-A test part | | Radius of part |
| 1584 | #00630001 | 777-25-A | | |
| 1584 | #00630002 | 777-25-A | | |
| 1627 | #0065b001 | Signal processing sample 1 | | Repeatability samples (0 deg) - 3 |
| 1628 | #0065c001 | Signal processing sample 2 | | Repeatability samples (0 deg) - 3 |
| 1629 | #0065d001 | Signal processing sample 3 | | Repeatability samples (0 deg) - 3 |
| 1630 | #0065e001 | Signal processing sample 4 | | Repeatability samples (0 deg) - 3 |
| 1631 | #0065f001 | Signal processing sample 5 | | Repeatability samples (0 deg) - 3 |
| 1632 | #00660001 | Signal processing sample 6 | | Repeatability samples (0 deg) - 3 |
| 1633 | #00661001 | Signal processing sample 1 | | Repeatability samples (20 deg) - 3 |
| 1634 | #00662001 | Signal processing sample 2 | | Repeatability samples (20 deg) - 3 |
| 1635 | #00663001 | Signal processing sample 3 | | Repeatability samples (20 deg) - 3 |

Appendix A. Table of Scans (Continued)

| Wisard Inspection # | File # | Part Description | Part marking | Notes |
|---------------------------|-----------|-------------------------------|--------------|------------------------------------|
| 1636 | #00664001 | Signal processing sample 4 | | Repeatability samples (20 deg) - 3 |
| 1637 | #00665001 | Signal processing sample 5 | | Repeatability samples (20 deg) - 3 |
| 1638 | #00666001 | Signal processing sample 6 | | Repeatability samples (20 deg) - 3 |
| 1639 | #00667001 | Signal processing sample 1 | | Repeatability samples (40 deg) - 3 |
| 1640 | #00668001 | Signal processing sample 2 | | Repeatability samples (40 deg) - 3 |
| 1641 | #00669001 | Signal processing sample 3 | | Repeatability samples (40 deg) - 3 |
| 1642 | #0066a001 | Signal processing sample 4 | | Repeatability samples (40 deg) - 3 |
| 1643 | #0066b001 | Signal processing sample 5 | | Repeatability samples (40 deg) - 3 |
| 1644 | #0066c001 | Signal processing sample 6 | | Repeatability samples (40 deg) - 3 |
| 1645 | #0066d001 | 777-29-A | | |
| 1645 | #0066d002 | 777-29-A | | |
| 1646 | #0066e001 | 777-29-A BW gate | | |
| 1646 | #0066e002 | 777-29-A BW gate | | |
| 1647 | #0066f001 | 777-8-A test part | | Painted surface |
| 1648 | #00670001 | 777-8-A test part | | Painted surface - different gate |
| 1653 | #00675001 | Patch 3 | | |
| 1654 | #00676001 | A6 near/far panel | | Medium resolution |
| 1655 | #00677001 | A6 near/far panel | | Medium resolution |
| 1657 | #00679001 | paint sample white 51-92 | | |
| 1658 | #0067a001 | paint sample red 51-110 | | |
| 1659 | #0067b001 | paint sample red 51-102 | | |
| 1660 | #0067c001 | paint sample white 51-100 | | |
| 1661 | #0067d001 | paint sample blue 51-112 | | |
| 1662 | #0067e001 | paint sample blue 51-120 | | |
| 1605 | #00645001 | Boeing plexi-laminate | | Unknown sample ? |
| 1606 | #00646001 | Boeing plexi-laminate | | Unknown sample ? |
| 1607 | #00647001 | Boeing steel | | Unknown sample ? |
| 1608 | #00648001 | Boeing stiffener #1 | | |
| 1663 | #0067f001 | AWACS Black surface paint | | |
| 1664 | #00680001 | AWACS surface paint ID 12 | | |
| 1665 | #00681001 | AWACS surface paint ID 14 | | |
| 1666 | #00682001 | AWACS surface paint ID 140 | | |
| 1668 | #00684001 | 777 28-A angle part | | Scan 1/2 |
| 1668 | #00684002 | 777 28-A angle part | | Scan 2/2 |
| 1669 | #00685001 | 777 24-A angle part | | Scan 1/2 |
| 1669 | #00685002 | 777 24-A angle part | | Scan 2/2 |
| 1672 | #00688001 | Boeing demo wing box | | |
| 1673 | #00689001 | F22 bulkhead | | Error in file/Bad file |
| | #0068b001 | | | |
| 1676 | #0068c001 | F-22 bulkhead | | Scan 1/6 |
| 1676 | #0068c002 | F-22 bulkhead | | Scan 2/6 |
| 1676 | #0068c003 | F-22 bulkhead | | Scan 3/6 |

Appendix A. Table of Scans (Continued)

| Wisard Inspection # | File # | Part Description | Part marking | Notes |
|---------------------------|-----------|------------------------------------|--------------|----------------------|
| 1676 | #0068c004 | F-22 bulkhead | | Scan 4/6 |
| 1676 | #0068c005 | F-22 bulkhead | | Scan 5/6 |
| 1676 | #0068c006 | F-22 bulkhead | | Scan 6/6 |
| 1580 | #0062c001 | stringer 172W3118-2 | | Scan of lower flange |
| 1581 | #0062d001 | stringer 172W3118-2 | | Scan of upper flange |
| 1583 | #0062f001 | 777-8-A test part | | Scan from bag side |
| 1746 | #006d2001 | 777 block #2 | STD-9-4882 | Unpainted |
| 1747 | #006d3001 | "Chain guard" | | |
| 1748 | #006d4001 | "Chain guard" | | |
| 1750 | #006d6001 | Paint coating - Boeing_51 | | |
| 1751 | #006d7001 | Paint coating - Boeing_52 | | |
| 1752 | #006d8001 | Paint coating - Boeing_53 | | |
| 1753 | #006d9001 | Paint coating - Boeing_51 | | |
| 1754 | #006da001 | Paint coating - Boeing_52 | | |
| 1755 | #006db001 | Paint coating - Boeing_53 | | |
| 1756 | #006dc001 | AWACS "golf ball" - Boeing_70 | | |
| 1757 | #006dd001 | AWACS "golf ball" - Boeing_70 | | |
| 1758 | #006de001 | AWACS coating - Boeing_71 | | |
| 1759 | #006df001 | AWACS coating - Boeing_72 | | |
| 1760 | #006e0001 | Panel window - Boeing_58 | | |
| 1761 | #006e1001 | T-shape part - Boeing_73 | | |
| 1762 | #006e2001 | T-shape part - Boeing_73 | | |
| 1763 | #006e3001 | T-shape part - Boeing_73 | | |
| 1764 | #006e4001 | Patch sample - Boeing_59 | | |
| 1765 | #006e5001 | Patch sample - Boeing_59 | | |
| 1766 | #006e6001 | HSCT - Boeing_74 | | |
| 1767 | #006e7001 | 777 block #2 | STD-9-4882 | Painted |
| 1768 | #006e8001 | Radii standards - Boeing_75 | | |
| 1769 | #006e9001 | 777 horiz stab skin - Boeing_76 | | Fast scan |
| 1770 | #006ea001 | 777 horiz stab skin - Boeing_76 | | |
| 1771 | #006eb001 | Aileron - Boeing_81 | | |
| 1772 | #006ec001 | Aileron - Boeing_81 | | |
| 1773 | #006ed001 | MacDac T-shape std - Boeing_77 | | |
| 1774 | #006ee001 | MacDac T-shape std - Boeing_78 | | |
| 1775 | #006ef001 | MacDac T-shape std - Boeing_79 | | |
| 1776 | #006f0001 | T-shape part - Boeing_73 | | |

Appendix A. Table of Scans (Continued)

| Wisard Inspection # | File # | Part Description | Part marking | Notes |
|---------------------------|-----------|------------------------------------|--------------|-----------------|
| 1777 | #006f1001 | Boeing Wingbox - Boeing_test_64 | | |
| 1778 | #006f2001 | Paint sample - Boeing_54 | | |
| 1779 | #006f3001 | Paint sample - Boeing_54 | | |
| 1782 | #006f6001 | Paint sample - Boeing_55 | | |
| 1783 | #006f7001 | Paint sample - Boeing_56 | | |
| 1784 | #006f8001 | Paint sample - Boeing_57 | | |
| 1786 | #006fa001 | damaged honeycomb Boeing_82 | | |
| 1787 | #006fb001 | F22 Bulkhead - Boeing_38b | | |
| 1788 | #006fc001 | F22 Bulkhead - Boeing_38b | | |
| 1789 | #006fd001 | MacDac T-shape std - Boeing_77 | | Scan radius |
| 1790 | #006fe001 | MacDac T-shape std - Boeing_78 | | Scan radius |
| 1791 | #006ff001 | MacDac T-shape std - Boeing_79 | | Scan radius |
| 1792 | #00700001 | Fly wheel - Boeing_test_24 | | Painted surface |
| 1793 | #00701001 | Fly wheel - Boeing_test_24 | | Painted surface |
| 1794 | #00702001 | Fly wheel - Boeing_test_24 | | Painted surface |
| 1795 | #00703001 | Fly wheel - Boeing_test_24 | | Painted surface |